

Design and Synthesis of Stereogenic-at-Iron Complexes with Multidentate Ligands and Application in Asymmetric Catalysis

Dissertation

zur Erlangung des Doktorgrades

der Naturwissenschaften

(Dr. rer. nat.)

dem Fachbereich Chemie

der Philipps-Universität Marburg

vorgelegt von

Philipp Stefan Steinlandt

aus Wehrda (Marburg)

Marburg/Lahn 2023

Die vorliegende Dissertation wurde in der Zeit von Mai 2019 bis März 2023 am Fachbereich Chemie der Philipps-Universität Marburg unter der Anleitung von Prof. Dr. Eric Meggers angefertigt.

Vom Fachbereich Chemie der Philipps-Universität Marburg (Hochschulkennziffer: 1180) als Dissertation angenommen am: _____

Erstgutachter: Prof. Dr. Eric Meggers

Zweitgutachter: Prof. Dr. Armin Geyer

Eingereicht am: 28.03.2023

Tag der mündlichen Prüfung: 05.05.2023

Philipp Stefan Steinlandt

born 7.11.1991 in Wehrda (Marburg), Germany

List of Publications:

1. F. Weber, P. S. Steinlandt, M. Ballmann, G. Hilt, Structure-Dependent Nickel-Catalysed Transposition of *N*-Allylamides to *E*- or *Z*-Enamides. *Synthesis* **2017**, *49*, 440-450.
2. P. S. Steinlandt, W. Zuo, K. Harms, E. Meggers, Bis-Cyclometalated Indazole Chiral-at-Rhodium Catalyst of Asymmetric Photoredox Cyanoalkylation. *Chem. Eur. J.* **2019**, *25*, 15333-15340 (“Hot Paper”).
3. S. Brunen, Y. Grell, P. S. Steinlandt, K. Harms, E. Meggers, Bis-Cyclometalated Indazole and Benzimidazole Chiral-at-Iridium Complexes: Synthesis and Asymmetric Catalysis. *Molecules* **2021**, *26*, 1822.
4. P. S. Steinlandt, X. Xie, S. Ivlev, E. Meggers, Stereogenic-at-Iron Catalysts with a Chiral Tripodal Pentadentate Ligand. *ACS Catal.* **2021**, *11*, 7467-7476.
5. H. Jung, M. Hong, M. Marchini, M. Villa, P. S. Steinlandt, X. Huang, M. Hemming, E. Meggers, P. Ceroni, J. Park, M.-H. Baik, *Chem. Sci.* **2021**, *12*, 9673-9681 (part of “Most popular 2021 catalysis articles” and “2021 Chemical Science HOT Article Collection”).
6. P. S. Steinlandt, L. Zhang, E. Meggers, Metal Stereogenicity in Asymmetric Transition Metal Catalysis. *Chem. Rev.* **2023**, DOI: 10.1021/acs.chemrev.2c00724.
7. P. S. Steinlandt, M. Hemming, X. Xie, S. I. Ivlev, E. Meggers, Trading Symmetry for Stereinduction in Tetradentate, non-*C*₂-Symmetric Fe(II)-Complexes for Asymmetric Catalysis. *Chem. Eur. J.* **2023**, *accepted*.

Acknowledgements

First and foremost, I would like to thank Prof. Dr. Eric Meggers for the opportunity to work under his excellent supervision for the past four years. Thank you for your support and motivating spirit and for providing a work environment of comfort that has given me the chance to pursue the projects of my choice. Your open door and ear have been a great amenity for any problems that I encountered in my time here, for which I am very grateful. Moreover, I'd like to thank you for your insights into all areas of chemistry and your valuable feedback. Without the fruitful discussions, I would not have been able to accomplish the things I've envisioned. I also want to thank you for the possibility of writing our elaborate and valuable review together and the chemical questions we encountered on the way. All these experiences helped me become a better scientist; inside and outside of the lab.

Secondly, I would like to thank Prof. Dr. Armin Geyer and Prof. Dr. Jörg Sundermeyer for their readiness to participate as members of the examination commission and for evaluating this thesis. Additionally, I'd like to thank Prof. Dr. Geyer for his kind acceptance of acting as the second assessor for this work.

Due to their invaluable contributions and services, I want to thank all service departments of the Philipps-Universität Marburg. The reliability of their work and the fast results have been of great significance to me while the willingness of listening to any questions and problems provided a nice and fruitful environment.

Especially, I would like to thank Dr. Xiulan Xie for her help with all problems that involve NMR spectroscopic measurements. I am very grateful for all the insights you were able to gain during our collaborations. I am still impressed by all the in-depth knowledge you have about chemistry.

Moreover, I am grateful for the support and work of Ina Pinnschmidt and Dr. Lili Zhang. You are at the heart of our working group and keep the business running. Thank you for handling all organizational matters and concerns that we are not able to solve. You give us the chance to focus on the scientific part of our work.

In addition to that, I want to thank Marcel Hemming for handling all sorts of miscellaneous laboratory work. Your kind spirit and helping hand in the lab are much appreciated and I will always remember all the laughs we shared in the last few years. I also want to thank Tim F. Ohlenburger for his help and the discussions about football, although you chose the wrong team to support.

I would like to express a special thanks to Yvonne Grell. You introduced me to this working group and its chemistry. And I will always be thankful for your chemical feedback, the discussions about

any challenges we encountered here, and all the laughs we shared. And for always keeping a humble mindset, despite our stargazing and high hopes sometimes being bigger than our possibilities. I couldn't have wished for a better lab partner! But much more important, I am very grateful for our friendship outside of the lab that has always given me great comfort and delight. And of course, for the shared interest and love of movies, series, angry rappers, and much more.

Furthermore, I would like to thank Erik Winterling for the time we shared in the Meggers group and his kind helpfulness without hesitation when it came to any problems with soft- or hardware. I'd also like to thank Frank Abendroth for contributing to the collegial work environment in our lab. Your knowledge about the animal kingdom has always provided a fruitful ground for some much-appreciated discussions. Additionally, I want to thank Nemrud Demirel and Dominik Baran for their contributions to the good atmosphere. While one of you demonstrated to me the advantages of big scale brominations, the other showed me the benefits of keeping a clear desk (especially regarding drawings). Moreover, you have been a good audience for all sorts of jokes.

I also want to express my gratitude towards all other former and current members of the Meggers laboratory, including Xin Nie, Peng Xiong, Suyang Yao, Chen-Xi Ye, Kuan Yin, Bing Zhou, Tianjiao Cui, Jordan Thelemann, Xiang Shen, Han Feng, Zijun Zhou, Yubiao Hong, Chenhao Zhang, Lucie Jarrige, Sebastian Brunen, Long Li, Guanghui Wang, Tatsuya Jamahira, Kenichi Endo, Nikita Ankudinov, Takuya Mochizuki, Yuqi Tan, Jie Qin, Jiajia Ma, and Qi Zhang. I am very grateful for the warm and kind atmosphere you all provided and the countless things I learned from all of you. In addition, I specifically would like to thank Xiaoqiang Huang for his help and insight into photochemistry. I enjoyed all of our discussions and your feedback has always been very helpful, especially during my master thesis.

Additionally, I want to appreciate all the students I had the pleasure to work with including Ruth Esther Pessi Kenmogne, Paul H. Moths, and Alena Ahrens. Your dedicated work and enthusiasm have been of great value to me. I also like to thank Raquel Hernández Ruiz for her contributions and the work we accomplished together. I appreciate all the talks about music and thank you for showing me that Spanish is not that difficult to learn.

Furthermore, I am very grateful for all the people I was able to meet during my time here. I want to thank Matthias Tripp and Oliver Pilgram for all the gaming sessions and for showing me that you can also have fun when you are not good at something, Jannick Meinecke for always being in my debt because of one relocation, Philipp Hofmann for expanding my cultural horizon, Juliane Gaß for all the nice meals and talks we shared, Veronika Schmalz for all the discussions about basically

everything, Stefan Gerstenecker for making my dentist rich, and many people more. I am thankful for all the experiences I was able to share with you.

Moreover, I want to thank Yvonne Grell, Veronika Schmalz, Matthias Tripp, Frank Abendroth, Dominik Baran, and Nemrud Demirel for the fast and thorough proofreading of this thesis.

Special thanks go out to all my friends that have nothing to do with chemistry, especially Franziska Steinhoff and Sebastian Goos and. The readiness and willingness to listen to all my struggles is very much appreciated.

Finally, I want to express my deepest gratitude towards my mother and my sister, who both supported me unconditionally throughout my whole time here in Marburg and without whom I would not have been able to achieve this.

“It’s been a ride“

–Marshall Bruce Mathers III– “Not Afraid”

Parts of the research presented in this dissertation have been published:

- P. S. Steinlandt, X. Xie, S. Ivlev, E. Meggers, Stereogenic-at-Iron Catalysts with a Chiral Tripodal Pentadentate Ligand. *ACS Catal.* **2021**, *11*, 7467-7476.
- P. S. Steinlandt, M. Hemming, X. Xie, S. I. Ivlev, E. Meggers, Trading Symmetry for Stereinduction in Tetradentate, non- C_2 -Symmetric Fe(II)-Complexes for Asymmetric Catalysis. *Chem. Eur. J.* **2023**, *accepted*.

Abstract

Asymmetric catalysis is an indispensable tool of great importance for the economic and sustainable synthesis of non-racemic chiral molecules. In addition to organic compounds and biomolecules, chiral transition metal complexes represent a pivotal pillar for generating enantiomerically pure products. The design and development of metal complexes for the transfer of stereochemical information form the very foundation of creating a sophisticated chiral environment to achieve sufficient enantioselectivities. Often, the applied catalysts comprise a stereogenic metal center that gives rise to a distinct chiral topology. Therefore, considerations regarding the metal-centered chirality are crucial in the composition of novel catalysts. In recent years, the Meggers group demonstrated the potential of emphasizing the absolute configuration at the metal with numerous iridium(III), rhodium(III), ruthenium(II), and iron(II) complexes and their applicability in asymmetric transition metal catalysis.

Chapter 3.1. A synthetic access to furnish pentadentate, achiral ligands that give rise to iron(II) complexes comprising metal-centered stereogenicity upon coordination (chiral-at-metal) is described. A ligand scaffold containing a mesityl substituted dipicolylamine moiety connected to a quinoline ring by an amido tether is shown to provide a paramagnetic complex without the required feasibility of extensive NMR spectroscopic analysis. By substitution of the 8-amido quinoline motif with a 2,2'-bipyridyl group, the corresponding racemic iron(II) complex exhibits diamagnetic properties, hence facilitating NMR measurements. A subsequent chiral auxiliary mediated separation of the enantiomeric mixture of complexes with chiral oxazolines, sulfoxides, and carboxylic acids is demonstrated to give insufficient results.

Chapter 3.2 and 3.3. The modular synthesis of pentadentate, chiral ligands comprising a central dipicolylamine motif generating metal-centered chirality upon complexation (stereogenic-at-metal) is depicted. Incorporation of a methyl group into the ligand framework results in a diastereomeric mixture of iron complexes after reaction with Fe(II)-perchlorate. The necessity of a laborious separation is prevented by exploiting the different thermodynamic stabilities of the diastereomers. The ligand centered chirality can act as a chiral lever enabling a subsequent isomerization to furnish the diastereomerically pure iron(II) complex. The rate of this interconversion is significantly influenced by the steric demand of the chiral lever and is demonstrated to improve with the incorporation of a bulkier isopropyl motif. A following structural elucidation via NMR spectroscopic measurements and X-ray crystallographic analysis confirms the overall topology and coordination mode. The modular synthetic approach of the ligand synthesis provides the convenient possibility of derivatization which is shown by incorporation of a mesitylene and a benzimidazole group. The efficiency of the obtained catalysts is then demonstrated for a ring contraction of isoxazoles under

open flask conditions to afford chiral *2H*-azirines with high enantioselectivities (up to 93% ee) and an exceptional activity affording turnover numbers (TON) of up to 10,000.

Chapter 3.4. The design and synthesis of novel non- C_2 -symmetric, tetradentate chiral ligands to obtain octahedral complexes with heterotopic reaction sites is demonstrated. The central stereogenic motif of this ligand scaffold is represented by a proline-derived chiral diamine backbone that enables a convenient synthetic access to the final ligands. Moreover, this backbone provides a high selectivity towards a *cis- α* topology of the corresponding Fe(II)-complexes while evincing a Λ -configuration at the metal center. Pyridyl, benzimidazolyl, and benzothiazolyl groups are incorporated as terminal coordinating groups and all nine possible combinations of the dichloro complexes are synthesized. The influence of the catalyst symmetry in regard to the steric and electronic environment is evaluated with the asymmetric ring contraction of isoxazoles to furnish enantiomerically enriched *2H*-azirines. A catalyst comprising a terminal pyridine and a benzothiazole group provides the best results and is applied in a substrate scope of 19 different isoxazoles. The corresponding *2H*-azirines are obtained with high enantioselectivities (up to 92% ee) and excellent yields (up to >99%) under open flask conditions. A subsequent survey of the versatility of the chiral products showcases their usefulness as synthetic intermediates without loss of enantioselectivity in the synthesis of several α -amino acid derivatives. Additionally, an unprecedented transformation of *2H*-azirines to directly access a racemic β -amino acid derivative is shown.

Zusammenfassung

Asymmetrische Katalyse stellt ein unverzichtbares Werkzeug von großer Bedeutung für die ökonomische und nachhaltige Synthese nicht racemischer, chiraler Moleküle dar. Neben organischen und biologischen Katalysatoren bilden chirale Übergangsmetallkomplexe eine tragende Säule bei der Erzeugung enantiomerenreiner Produkte. Das Design und die Entwicklung solcher Metallkomplexe, die stereochemische Informationen übertragen können, bilden die Grundlage für die Schaffung einer definierten chiralen Umgebung und das Realisieren von hohen Enantioselektivitäten. Häufig enthalten die verwendeten Katalysatoren ein stereogenes Metallzentrum, welches zu einer einzigartigen Topologie führt. Daher ist das Berücksichtigen dieser metallzentrierten Chiralität entscheidend für die Zusammensetzung neuartiger Katalysatoren. In den letzten Jahren hat die Meggers-Gruppe gezeigt, welches Potenzial in der genauen Betrachtung der absoluten Konfiguration am Metall steckt und dies mit zahlreichen Iridium(III)-, Rhodium(III)-, Ruthenium(II)-, und Eisen(II)-Komplexen sowie deren Anwendung in asymmetrischer Übergangsmetallkatalyse demonstriert.

Kapitel 3.1. Ein synthetischer Zugang zu fünfzähligen, achiralen Liganden ist beschrieben, die zu Eisen(II)-Komplexen mit metallzentrierter Chiralität nach Koordination führen (*chiral-at-metal*). Das Liganden-Gerüst besteht aus einer Mesityl-substituierten Dipicolylamin-Einheit, die über einen Amid-Linker mit einem Chinolinring verbunden ist. Wie gezeigt wird, erlaubt der resultierende paramagnetische Komplex jedoch nicht eine nötige umfassende NMR-spektroskopische Analyse. Nach Ersetzen der 8-Amidochinolin-Einheit durch ein 2,2'-Bipyridin-Motiv wird ein racemischer Eisen(II)-Komplex mit diamagnetischen Eigenschaften erhalten, der eine Charakterisierung über NMR-Messungen ermöglicht. Eine nachfolgende Auftrennung der Enantiomere mittels chiraler Auxiliare unter Verwendung von chiralen Oxazolinen, Sulfoxiden und Carbonsäuren zeigt unzureichende Ergebnisse.

Kapitel 3.2 und 3.3. Es wird die modulare Synthese fünfzähliger, chiraler Liganden mit einem zentralen Dipicolylamin-Motiv gezeigt, die bei der Komplexbildung zu metallzentrierter Chiralität führen (*stereogenic-at-metal*). Der Einbau einer Methylgruppe in das Ligandengerüst führt nach Reaktion mit Eisen(II)-Perchlorat zu einem Diastereomeren-Gemisch von Eisenkomplexen. Die Notwendigkeit einer aufwendigen Trennung wird durch das Ausnutzen der unterschiedlichen thermodynamischen Stabilitäten der Diastereomere vermieden. Die ligandenzentrierte Chiralität kann als chiraler Hebel dienen, der eine Isomerisierung zu einem diastereomerenreinen Eisen(II)-Komplex ermöglicht. Die Geschwindigkeit dieser Umwandlung wird maßgeblich durch den sterischen Anspruch des chiralen Hebels beeinflusst und erhöht sich nachweislich durch den Einbau eines

größeren Isopropylrests. Eine anschließende Strukturaufklärung durch NMR-spektroskopische Messungen und röntgenkristallographische Analyse bestätigt die Topologie und den Koordinationsmodus. Der modulare synthetische Aufbau der Liganden bietet die praktische Möglichkeit der Derivatisierung, welche durch den Einbau einer Mesitylen- und einer Benzimidazolgruppe gezeigt wird. Die Effizienz der erhaltenen Katalysatoren ist für eine Ringkontraktion von Isoxazolen unter Luft gezeigt, um chirale *2H*-Azirine mit hohen Enantioselektivitäten (bis zu 93% ee) und einer außergewöhnlichen Aktivität zu erhalten. Dabei werden katalytische Produktivitäten (engl. *turnover numbers*, TON) von bis zu 10,000 beobachtet.

Kapitel 3.4. Das Design und die Synthese neuartiger, nicht- C_2 -symmetrischer, vierzähliger chiraler Liganden zur Herstellung von oktaedrischen Komplexen mit heterotopen reaktiven Koordinationsstellen werden präsentiert. Das zentrale stereogene Motiv dieses Ligandengerüsts wird von einer chiralen Diamin-Einheit dargestellt, die von Prolin abgeleitet ist und einen praktischen Zugang zu den finalen Liganden ermöglicht. Darüber hinaus bietet dieses Ligandenrückgrat eine hohe Selektivität für eine *cis*- α -Topologie der entsprechenden Fe(II)-Komplexe, die eine Λ -Konfiguration am Metall aufweisen. Pyridyl-, Benzimidazolyl- und Benzothiazolylgruppen werden als endständig koordinierende Einheiten in den Liganden eingebaut und die Synthese aller neun möglichen Kombinationen der Dichlorokomplexe gezeigt. Der Einfluss der Katalysatorsymmetrie auf die sterische und elektronische Umgebung wird anhand der asymmetrischen Ringkontraktion von Isoxazolen zu enantiomerenangereicherten *2H*-Azirinen bewertet. Ein Katalysator, der eine endständige Pyridin- und eine Benzothiazolgruppe enthält, ermöglicht die besten Ergebnisse und wird für 19 verschiedene Isoxazol-Substrate verwendet. Die erhaltenen *2H*-Azirine können unter Luft mit hohen Enantioselektivitäten (bis zu 92% ee) und hervorragenden Ausbeuten (bis zu >99%) gebildet werden. Die Nützlichkeit und Vielseitigkeit der chiralen Produkte als synthetische Intermediate wird daraufhin demonstriert, indem mehrere α -Aminosäurederivate ohne Verlust der Enantiomerenreinheit synthetisiert werden. Darüber hinaus wird ein neuartiger, direkter Zugang zu einem racemischen β -Aminosäurederivat ausgehend von *2H*-Azirinen gezeigt.

Table of Contents

1. Iron Complexes in Asymmetric Transition Metal Catalysis.....	1
1.1 Introduction.....	1
1.2 Asymmetric Iron Catalysis.....	2
1.2.1 Asymmetric Iron Catalysis with Bidentate Ligands	4
1.2.2 Asymmetric Iron Catalysis with Tridentate Ligands	8
1.2.3 Asymmetric Iron Catalysis with Tetradentate Ligands	16
1.3 Concluding Remarks	23
2. Aim of this Work	25
3. Results and Discussion	28
3.1 Development of Chiral-at-Metal Iron(II) Complexes with a Pentadentate Ligand...28	
3.1.1 Chiral Iron Complexes with Pentadentate Ligands in Asymmetric Catalysis	28
3.1.2 Initial Design of a Chiral-at-Iron Complex.....	30
3.1.3 Design and Synthesis of a Diamagnetic Chiral-at-Iron Complex.....	33
3.1.4 Concluding Remarks	39
3.2 Stereogenic-at-Iron Complexes with a Chiral Tripodal Pentadentate Ligand	40
3.2.1 Considerations for a Stereogenic-at-Iron Complex with a Chiral Pentadentate Ligand.....	40
3.2.2 Synthesis and Complexation of Chiral Pentadentate Ligands	41
3.2.3 Structural Elucidation of the Diastereopure Stereogenic-at-Iron Complex.....	48
3.2.4 Modifications of the Pentadentate Ligand Scaffold.....	52
3.2.5 Concluding Remarks	55
3.3 Application of Iron Complexes with a Chiral Pentadentate Ligand in Asymmetric Catalysis.....	56
3.3.1 Initial Survey of Application in Asymmetric Catalysis	56
3.3.2 Asymmetric 2 <i>H</i> -Azirine Synthesis via Ring Contraction of Isoxazoles.....	58
3.3.3 Concluding Remarks	66
3.4 Expanding the Family of non-<i>C</i>₂-Symmetric, Linear, Tetradentate Ligands for Fe(II)-Catalysts	68
3.4.1 Base Metal Catalysts Comprising Tetradentate, Linear, <i>C</i> ₁ -Symmetric Ligands	68
3.4.2 Synthesis of non- <i>C</i> ₂ -Symmetric Ligands for Fe(II)-Catalysts.....	72
3.4.3 Asymmetric Catalysis with the Non- <i>C</i> ₂ -Symmetric Iron Complexes.....	80

Table of Contents

3.4.4	Concluding Remarks	94
4.	Summary and Outlook.....	96
4.1	Summary.....	96
4.2	Outlook.....	100
5.	Experimental Part	103
5.1	General Methods	103
5.2	Materials and Instruments.....	103
5.3	Synthesis of Pentadentate Ligands	106
5.3.1	Synthesis of Pentadentate Amide Ligand 101 and Complex 108	106
5.3.2	Synthesis of Pentadentate Ligand 115 and Complex 121	110
5.3.3	Synthesis of Chiral Pentadentate Ligands.....	115
5.3.4	Synthesis of Fe(II) Complexes with Chiral Pentadentate Ligands	129
5.4	Synthesis of Tetradentate Complexes	141
5.4.1	Synthesis of Chiral Tetradentate Ligands.....	141
5.4.2	Synthesis of Complexes with Tetradentate Ligand Scaffold 189	159
5.5	Asymmetric Ring Contraction of Isoxazoles towards Chiral <i>2H</i> -Azirines.....	167
5.5.1	Synthesis of Substrates and Analytical Data	167
5.5.2	Asymmetric Ring Contraction Catalyzed by Fe(II)-Complexes with a Chiral Pentadentate Ligand and Product Characterization	179
5.5.3	Asymmetric Ring Contraction with Tetradentate Complexes and Product Characterization..	190
5.5.4	Follow-Up Conversion of <i>2H</i> -Azirines	207
6.	Appendix.....	218
6.1	Representative NMR Spectra	218
6.2	Chiral HPLC Traces.....	241
6.3	X-Ray Crystallographic Data	246
7.	Abbreviations and Symbols	256
8.	References.....	258

1. Iron Complexes in Asymmetric Transition Metal Catalysis

1.1 Introduction

Transition metal catalysis represents an essential pillar in the toolbox of modern chemistry for the ongoing pursuit of exploring chemical space by the synthesis of novel compounds. Accordingly, transition metal catalysts have become an imperative and fundamental tool for not only realizing this endeavor of pushing the boundaries in research, but also for meeting the increasing demand for crucial molecules in the fields of medicinal and material chemistry on an industrial scale.^[1-3] In addition of providing indispensable possibilities for the exploration of new synthetic pathways, transition metal catalysis also contributes significantly to humanity's ongoing efforts of improving effectiveness and sustainability as catalysis itself is a fundamental principle of "Green Chemistry".^[4] Yet, many catalysts still require the application of rare, expensive, and noble transition metals and today's chemists are faced with the challenge of combining the general advantages of transition metal catalysis with the advantages of earth-abundant 3d-transition metals regarding economic, environmental, and toxicity aspects.^[5] Hence, the development and design of novel, catalytically active complexes relying on cheap and earth-abundant base metals presents a challenging yet intriguing field of research.^[6]

This enticing task becomes all the more ambitious regarding the area of asymmetric transition metal catalysis in which the predominance of noble metals is even more noticeable. Since its beginnings in the late 1960's, enantioselective catalysis with transition metal complexes has evolved into an important tool for the transfer and implementation of chirality into prochiral molecules to furnish enantioenriched products. Therefore, its pivotal impact was honored in 2001 when William S. Knowles, Ryoji Noyori, and K. Barry Sharpless were awarded the Nobel Prize (Figure 1).^[7]

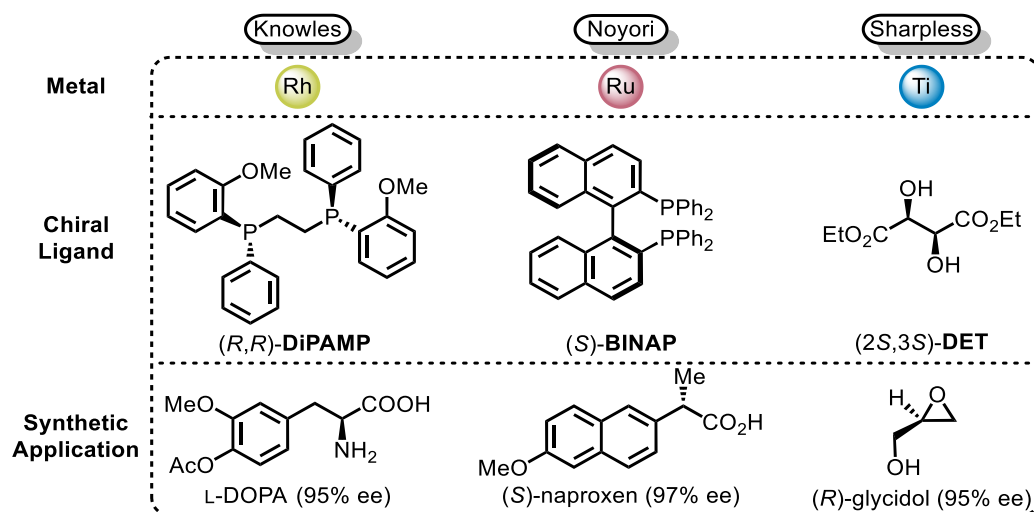


Figure 1: Representative examples of catalytic systems invented by Knowles, Noyori, and Sharpless, and synthetic application.^[7]

Prior to asymmetric catalysis, the synthesis of enantiopure compounds mostly relied either on using precursors from the chiral pool or on the separation of a racemic mixture of enantiomers. Both approaches suffer from the drawback that stoichiometric amounts of chiral precursors or ancillary molecules are necessary.^[8] In contrast, enantioselective transition metal catalysis requires only sub-stoichiometric amounts of chiral information to invoke chirality in achiral precursors. The optically active products of such conversions are crucial for many industrial branches, including the agrochemical, food, and pharmaceutical industry.^[8,9] Consequently, the development and application of new catalysts is of high interest, especially regarding aspects of environmentally-friendly chemistry. In particular, recent research on catalytically active transition metal systems based on 3d-metals has attracted a lot of attention.^[10]

Since the groundbreaking work of Knowles,^[11] Noyori,^[12] Sharpless,^[13] Kagan,^[14] and others, much effort and progress has been made towards the application of 3d-metal complexes in asymmetric catalysis to provide a broad variety of chiral molecules while following a more sustainable path. Many of such examples show that 3d-metal catalysts are not only capable to substitute their noble congeners, but can also exhibit distinct mechanistic pathways that open up possibilities for novel synthetic routes to further expand the limits of chemical space.^[10]

1.2 Asymmetric Iron Catalysis

In terms of sustainability, especially iron stands out as a suitable candidate as its abundance in earth's crust (5.63%)^[15] is significantly higher than that of other 3d- or 4d-transition metals as depicted in Figure 2.

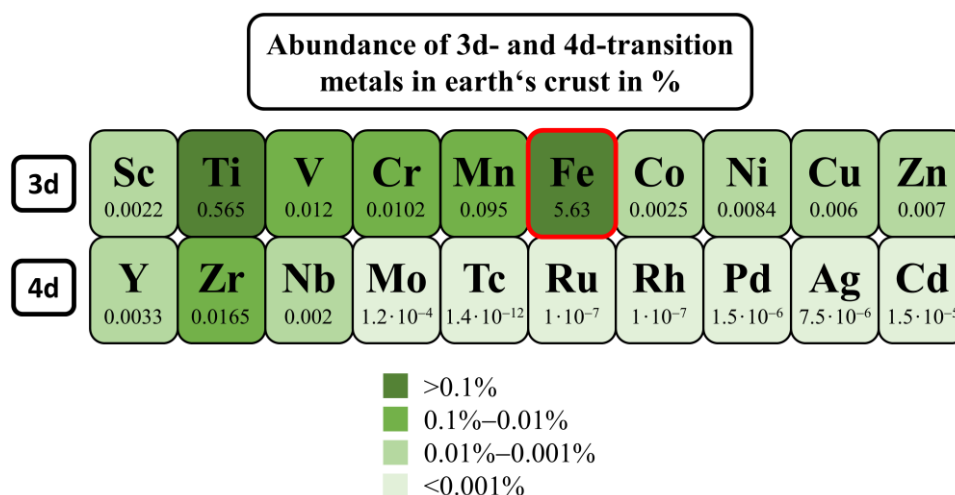


Figure 2: Relative abundance of 3d- and 4d-transition metals in earth's crust.^[15]

Consequently, it is not surprising that nature makes extensive use of iron and its catalytic properties in countless proteins and enzymes making it an essential element for virtually every living

organism.^[16,17] A prominent example of an iron-containing enzyme that is ubiquitously found in nature is the superfamily Cytochrome P450, a monooxygenase that serves as a natural catalyst for the oxidation of numerous molecules.^[18] It has been extensively researched in the last decades and employed as a powerful tool for the realization of using enzymes in reactions involving non-natural substrates.^[19] Moreover, its subvariants have been redesigned and modified to function as efficient catalysts in enantioselective reactions by research groups like Retz,^[20] Arnold,^[21] and many more.^[22] The method of developing such artificial enzymes for specific targets is commonly known as “*Directed Evolution*” and was awarded 2018 with the Nobel Prize in chemistry. Although its importance for asymmetric catalysis is indisputable, enzymatically catalyzed asymmetric reactions involving iron are beyond the scope of this introduction.

The following sections will provide a concise survey of selected representative examples of asymmetric homogeneous catalysis with iron complexes comprising multidentate ligands that coordinate to the central metal exclusively via nitrogen atoms. Due to its rich coordination chemistry, many chiral iron catalysts have been reported in the last decades with a broad variety of different, multidentate ligand scaffolds.^[23–25] An overview of the presented ligand scaffolds discussed in this introduction is depicted in Figure 3.

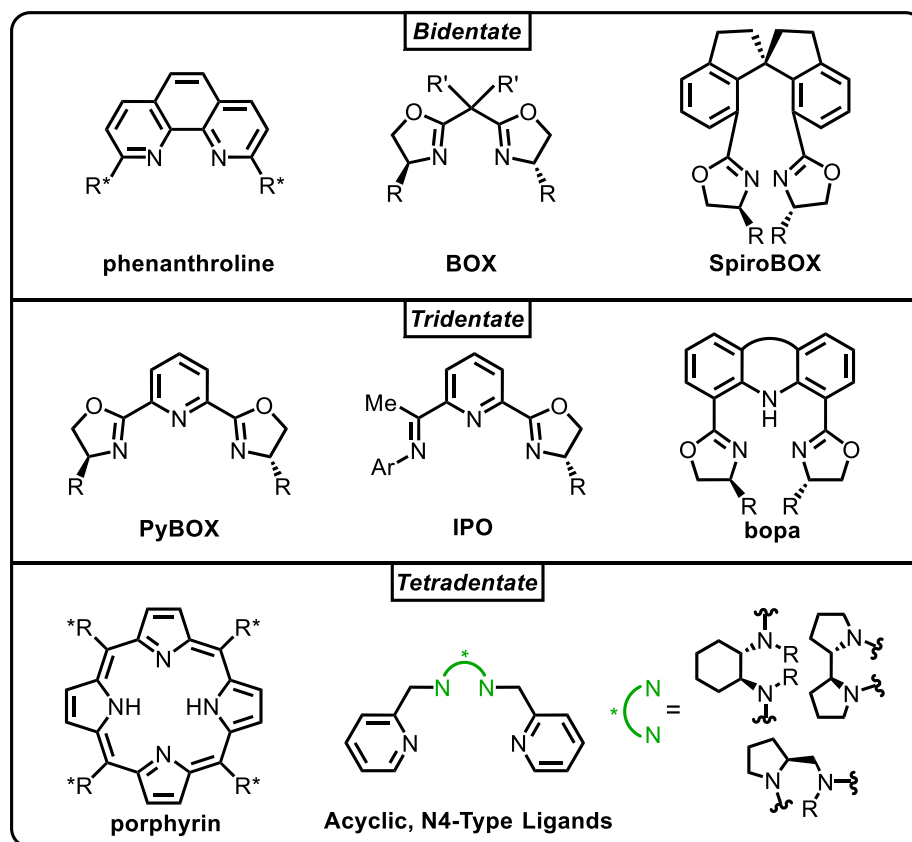
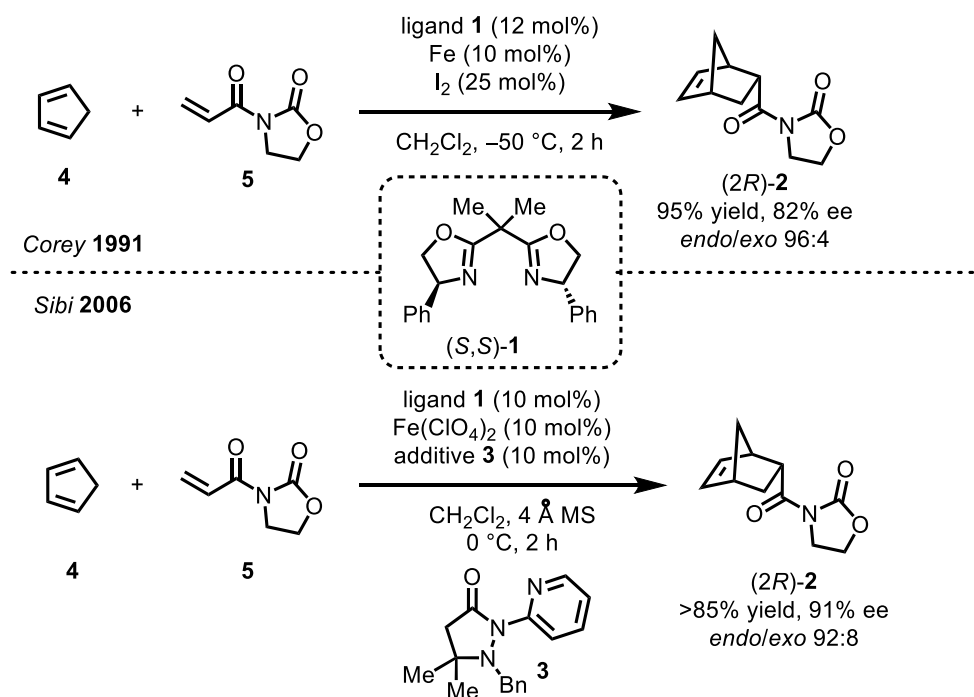


Figure 3: Overview of multidentate chiral ligand scaffolds for asymmetric iron catalysis presented in this chapter. An emphasis is made on ligands that exclusively coordinate to the central iron atom via nitrogen atoms.

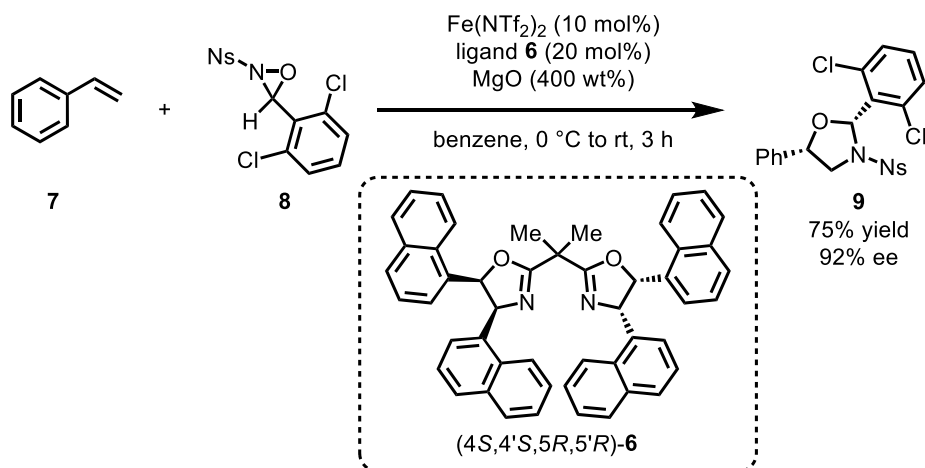
1.2.1 Asymmetric Iron Catalysis with Bidentate Ligands

The application of bidentate chiral ligands for asymmetric transition metal catalysis has been scrutinized since the very beginning of this field of chemistry in 1968.^[26] In the following decades, numerous chiral bidentate ligand systems were developed with imine moieties being a prominent structural motif. In 1989, the group of Masamune first reported the application of a chiral bidentate bisoxazoline (BOX) ligand for an asymmetric, copper-catalyzed cyclopropanation.^[27] The BOX scaffold has since become a privileged ligand system and has been applied in a broad variety of asymmetric catalytic reactions.^[28] Due to its overall C_2 -symmetric topology, this ligand class usually gives rise to catalytically active species exhibiting homotopic reaction sites, hence reducing the number of possible reaction intermediates or transition states when compared to C_1 -symmetric catalyst-ligand systems.^[29] Regarding enantioselective iron catalysis with chiral BOX-derivatives, seminal work has been achieved by Corey *et al.* in 1991. An enantioselective Diels-Alder addition was conducted by *in situ* generation of the active Fe-complex from elemental iron and chiral BOX-ligand **1** in the presence of I_2 . With CH_2Cl_2 as solvent at $-50\text{ }^\circ\text{C}$, full conversion was observed after 2 h and the product (*R*)-**2** was obtained in 95% yield with a high selectivity towards the *endo*-isomer (*endo/exo* 96:4) and an enantioselectivity of 82% ee (Scheme 1).^[30] Inspired by these promising results, the group of Sibi later reported the same reaction with BOX-analogue **1**, $Fe(ClO_4)_2$ as a precursor, and pyrazolidine-3-one **3** as an additive to furnish Diels-Alder product **2** with an improved enantioselectivity of 91% ee (Scheme 1).^[31]



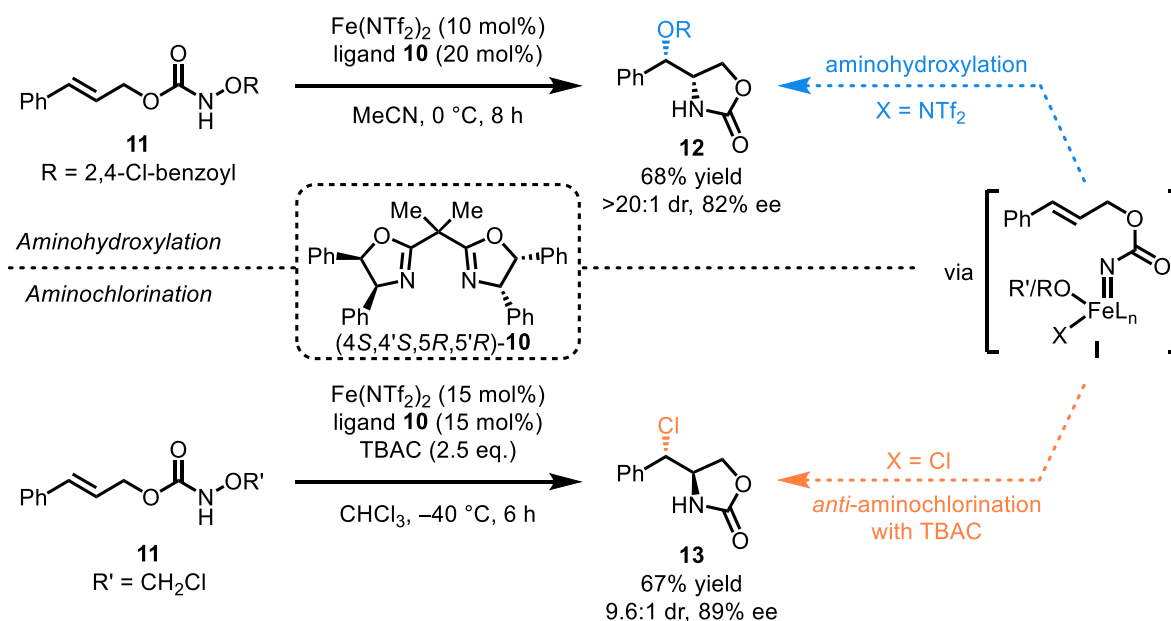
Scheme 1: Top: Enantioselective, Fe-catalyzed Diels-Alder reaction with chiral BOX-ligand **1**.^[30] Bottom: Improvement of Corey's system by Sibi for the enantioselective Diels-Alder reaction by using additive **3**.^[31]

In addition to their application in asymmetric Diels-Alder reactions, BOX-derived compounds have been proven to be suitable ligands for an enantioselective, Fe-catalyzed oxyamination as reported by the group of Yoon in 2012. By synthesizing the bulky, 1-naphthyl-substituted, chiral BOX-ligand **6**, they were able to convert styrene (**7**) and *N*-sulfonyl oxaziridine **8** with Fe(NTf₂)₂ as precursor and MgO as drying agent to the corresponding oxyamination product **9** in 75% yield with a high enantioselectivity of 92% ee (Scheme 2).^[32]



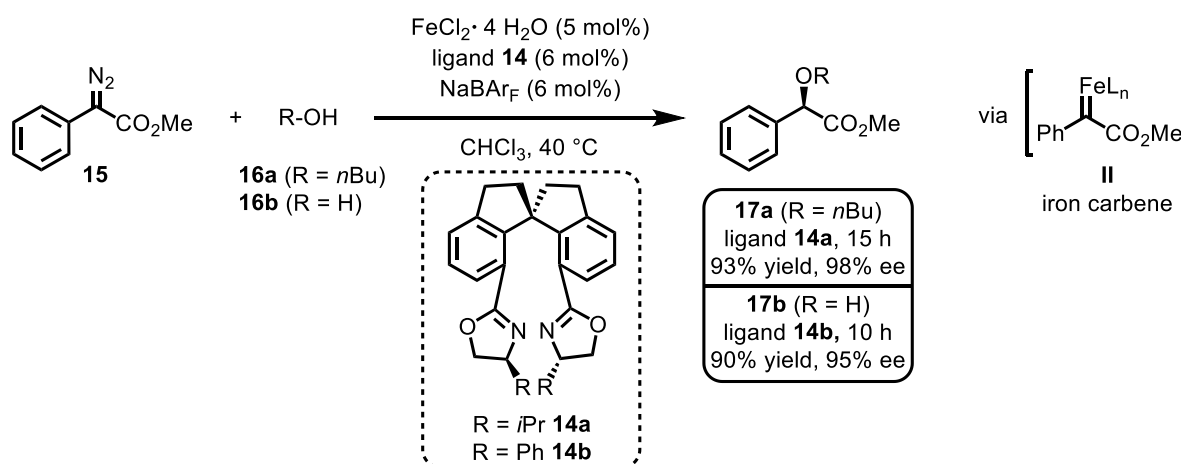
Scheme 2: Enantioselective oxyamination of styrene (**7**) with chiral BOX-ligand **6** by Yoon.^[32]

Following the report by Yoon, the group of Xu achieved an intramolecular functionalization of double bonds via an aminohydroxylation by using a catalyst system comprising BOX-analogue **10** and iron(II)-bis(trifluoromethylsulfonyl)azanide as metal precursor. When this catalytic system was employed in a reaction with *N*-benzoyloxycarbamate **11**, cyclic carbamate *syn*-**12** was obtained in 68% yield with high diastereoselectivity (>20:1 dr) and good enantioselectivity (82% ee) as shown in Scheme 3.^[33] In 2015, the same group was able to exploit the mechanism of this reaction by the addition of chlorinating agent tetrabutylammonium chloride (TBAC) to furnish the *anti*-isomer of aminochlorination product **13** in 67% yield. Though the diastereoselectivity of this conversion was lower compared to the aminohydroxylation, a higher enantioselectivity of 89% ee was achieved (Scheme 3).^[34] Both reactions are supposed to proceed via the crucial intermediate **I**. Upon cleavage of the N-O bond by the iron catalyst, nitrenoid species **I** is formed that can subsequently initiate a cycloamination. Depending on the counterion coordinated to the iron-center (when TBAC is present, X = Cl), either aminohydroxylation product **12** or aminochlorination product **13** can be obtained.^[33,34]



Scheme 3: Enantioselective, Fe-catalyzed aminohydroxylation (top) and aminochlorination (bottom) with BOX-ligand **10** as reported by Xu.^[33,34]

A more rigid, BOX-derived ligand system containing a chiral spirobiindane backbone was first introduced in 2006 by Zhou *et al.* and is commonly abbreviated as SpiroBOX.^[35] This scaffold was shown to be a competent ligand for highly enantioselective, iron-catalyzed O-H bond insertion reactions outperforming classical BOX-ligands in terms of stereoselection.^[36] For example, Zhou and coworkers were able to apply SpiroBOX ligand **14** in combination with an iron-salt for a highly stereoselective O-H bond insertion with diazocompounds **15** (Scheme 4).^[37] For this reaction system, iron proved to be most suitable with regard to activity and selectivity, while other metals gave inferior results. Intriguingly, this system exhibited excellent applicability towards a broad variety of different alcohols **16** in terms of enantioselectivity and also tolerates allylic alcohols and H₂O as suitable substrates.^[37]



Scheme 4: Asymmetric O-H bond insertion of diazocompounds **15** via iron carbene **II** with SpiroBOX-ligands **14** by Zhou.^[37]

In contrast to the previously described examples, in which presumably a single chiral bidentate ligand coordinates to one iron center, a 2+2-topology of two bidentate ligands surrounding a central iron atom can be feasible. This topology gives rise to a stereogenic metal center that can either result in the Λ -(left-handed propeller) or Δ -(right-handed propeller) isomer when the resulting complex exhibits an octahedral coordination sphere (Figure 4).

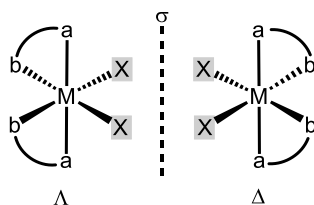
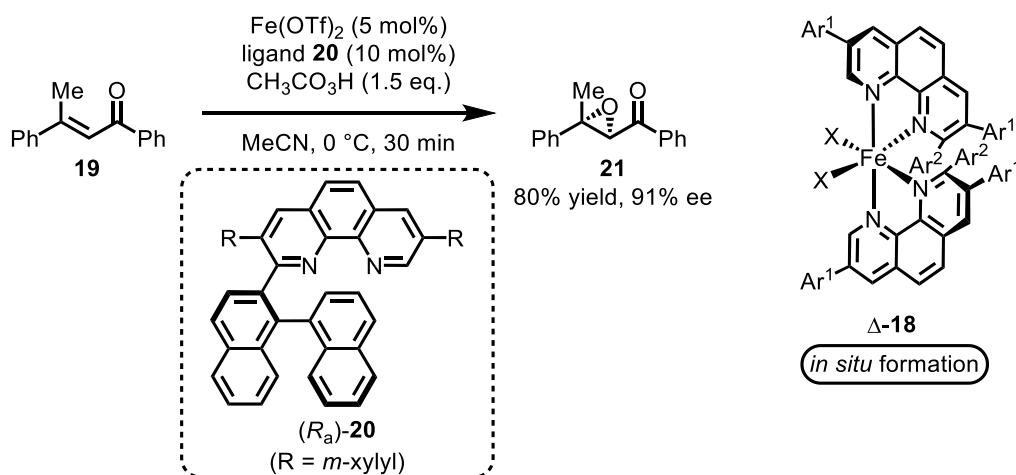


Figure 4: Topology of octahedral complexes with helical chirality (X = labile ligands).

Consequently, the isomers have to be separated in order to facilitate an enantioselective conversion or a well-tailored chiral ligand system has to be applied to control the resulting diastereoselectivity during the formation of the catalytically active species. Furthermore, the application of C_1 -symmetric bidentate ligands can lead to several possible diastereomers. In a very elegant approach, by using a chiral 1,10-phenanthroline ligand comprising a chiral (R_{ax})-binaphthyl moiety, Yamamoto *et al.* were able to achieve the *in situ* formation of an iron catalyst with a high diastereoselectivity towards an overall *cis*-topology, affording a C_2 -symmetric catalyst (complex **18** in Scheme 5).^[38] The selectivity of the coordination was investigated by X-ray analysis of the isolated complex confirming the ligand's ability to exclusively induce the aforementioned configuration, presumably due to π - π interactions between the naphthyl groups and the diphenylphenanthroline residue. Notably, due to a limited configurational stability of 3d-metal complexes, the chiral ligands must coordinate under thermodynamic control, thus fixing the absolute configuration at the metal center which is suggested to be the main contributor during the asymmetric stereoinduction. The efficacy of this system was shown for an enantioselective epoxidation of challenging β,β -disubstituted enones **19** with chiral ligand **20** to afford enantioenriched epoxides **21** in good yields with high enantioselectivities of mostly >90% ee.^[38] A representative example is depicted in Scheme 5.

Remarkably, such a complex topology can even be apt for asymmetric iron catalysis when the bidentate ligands are devoid of any chirality as was shown in 2019 by Meggers *et al.* with a chiral-at-iron complex comprising *N*-heterocyclic carbene ligands for enantioselective Nazarov cyclization and Cannizzaro reactions.^[39]



Scheme 5: Enantioselective epoxidation with chiral phenanthroline derivative **20** by Yamamoto.^[38]

Since their first applications in asymmetric transition metal catalysis, chiral bidentate ligands have become an essential tool for realizing various asymmetric transformations and the last decades have given birth to countless novel chiral bidentate frameworks for enantioselective, metal-catalyzed reactions. In terms of iron, the BOX-ligand scaffold in particular has proven to be effective for a wide variety of different reaction pathways providing access to sufficient stereoselectivities. Due to their well-established synthesis and their convenient application by *in situ* formation of the catalytically active species, there are many reports of successfully conducted reactions with this class of ligands.^[36]

1.2.2 Asymmetric Iron Catalysis with Tridentate Ligands

In contrast to the unambiguous coordination mode of bidentate ligand scaffolds, tridentate ligands can surround a central metal atom either in a facial or meridional fashion resulting in different overall topologies of the complexes (Figure 5). Generally, a meridional coordination mode is realized when a more rigid scaffold is applied. Consequently, tridentate ligands with all donor-atoms arranged in a single plane are only able to coordinate meridionally to a metal center.

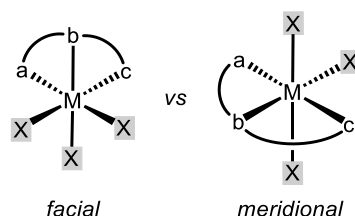
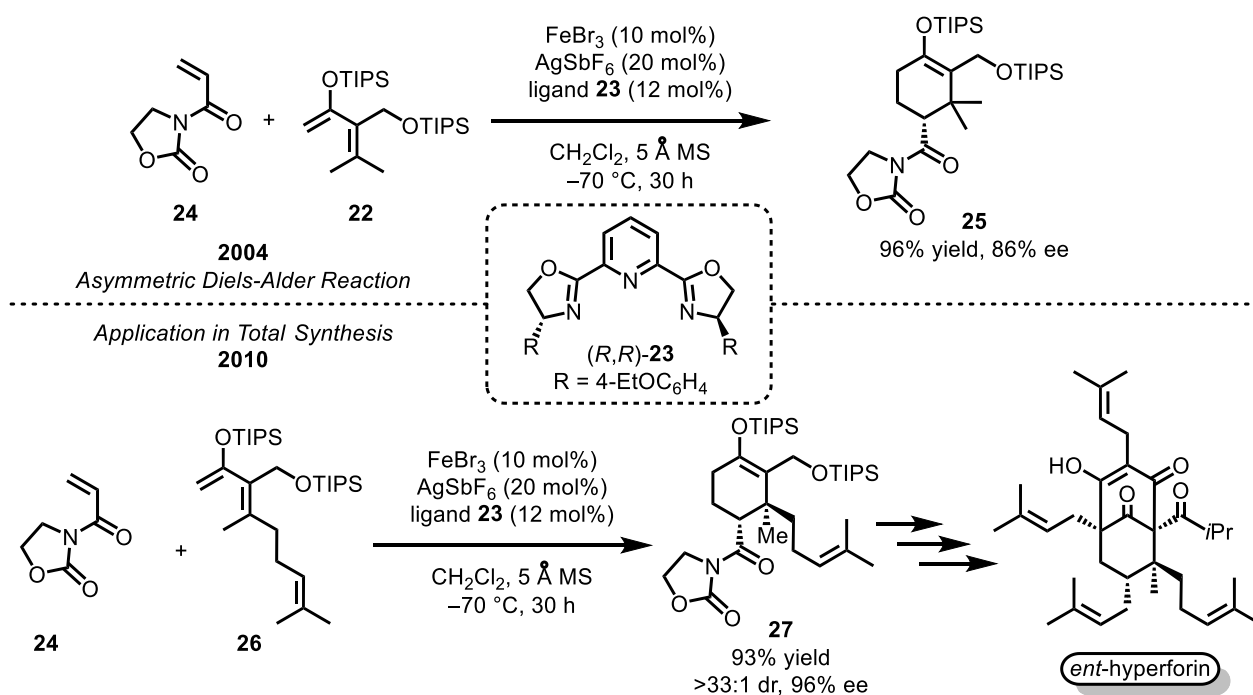


Figure 5: Facial and meridional coordination mode of a tridentate ligand in an octahedral complex.

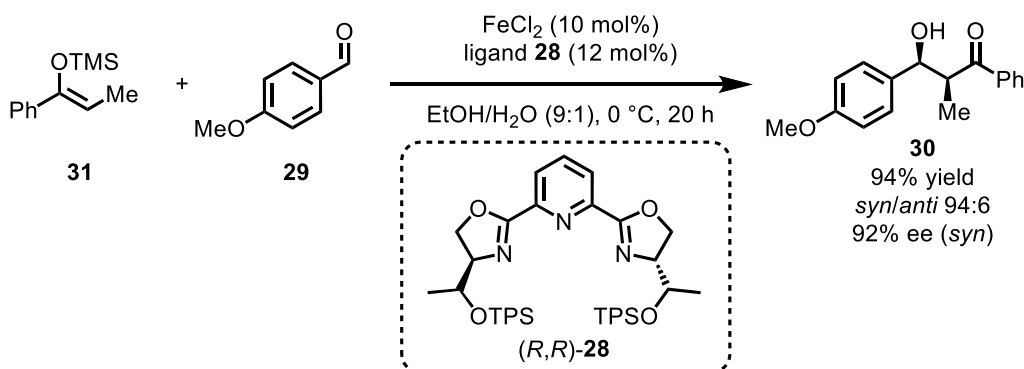
A prevalent, tridentate ligand system prominently used in asymmetric iron catalysis is represented by the pyridine bis(oxazoline) (PyBOX) motif. This scaffold was first reported by Nishiyama *et al.* in

1989 for an asymmetric, rhodium-catalyzed hydrosilylation of ketones even before the previously described BOX-ligands were introduced.^[40] As a consequence of their rigid arrangement of coordinating atoms, PyBOX-ligands surround a metal center exclusively in a meridional fashion. An early report of an iron-catalyzed asymmetric reaction involving the employment of a PyBOX-ligand scaffold was published in 2004 by the group of Shibasaki.^[41] This catalysis represents the first asymmetric, catalyzed Diels-Alder reaction of an acyclic tetrasubstituted 1,3-diene **22**. In the presence of FeBr₃, aryl-substituted PyBOX-derivative **23**, AgSbF₆ as activating additive, and dienophile **24** Diels-Alder product **25** was formed in 96% yield with 86% ee.^[41] Interestingly, the group was able to exploit this catalytic system later for the total synthesis of biologically active *ent*-hyperforin (Scheme 6).^[42]



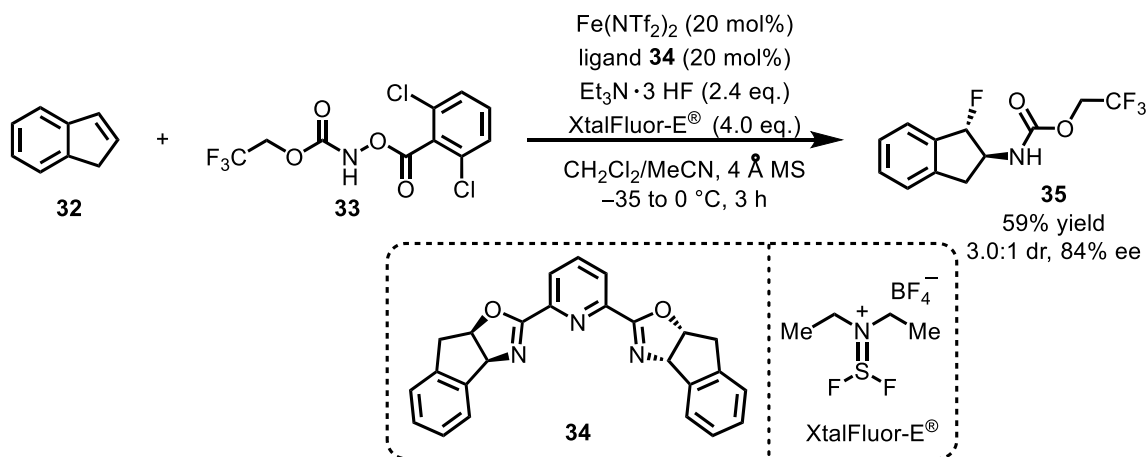
Scheme 6: Asymmetric, Fe-catalyzed Diels-Alder reaction with PyBOX-ligand **23** and application of the catalytic system in the total synthesis of *ent*-hyperforin.^[41,42]

In 2006, the group of Mlynarski reported the application of an iron catalyst for an enantioselective Mukaiyama-aldol reaction. The employed FeCl₂/PyBOX-catalyst system provided the corresponding ketones with high diastereoselectivities and moderate enantioselectivities of up to 75% ee.^[43] By a thorough screening of different PyBOX-derivatives, they were able to improve the enantioselectivity.^[44] When sterically bulky *O*-*tert*-butyldiphenylsilyl(TPS)-hydroxyethyl-substituted PyBOX analogue **28** in combination with FeCl₂ was used, *para*-methoxy benzaldehyde (**29**) could be converted into β -hydroxyketone **30** in 94% yield with a high dr of 94:6 and an ee of 92% for the major diastereomer (Scheme 7). Remarkably, for several substrates the corresponding Zn(II)-catalyst gave significantly higher enantioselectivities.^[44]



Scheme 7: Stereoselective Mukaiyama-aldol reaction with bulky PyBOX-ligand **28** as reported by Mlynarski *et al.* 2007.^[44]

In order to expand the scope of their developed asymmetric aminohalogenation reaction (Scheme 3), Xu *et al.* scrutinized the advantages of using PyBOX-ligands for the realization of a stereoselective intermolecular aminofluorination in 2016.^[45] In a proof of concept study, indene (**32**) was reacted with carbamate **33** in the presence of Fe(NTf₂)₂, chiral PyBOX-ligand **34**, Et₃N · 3 HF, and XtalFluor-E[®] to furnish aminofluorination product **35** with a modest diastereoselectivity of 3:1 while both diastereomers were formed with an ee of 84% (Scheme 8). The reaction is supposed to proceed via an iron-nitrenoid species (see intermediate **I** in Scheme 3). Noteworthy, the electrophilic fluorination agent XtalFluor-E[®] was crucial for the prevention of a competing olefin aminohydroxylation as it is assumed to sequester the anionic benzoate leaving group, thus acting as a trapping reagent.^[46] The reaction is depicted in Scheme 8.



Scheme 8: Intermolecular aminofluorination of indene (**32**) with a chiral Fe(II)/PyBOX-catalyst by Xu.^[45]

In addition to the examples shown here, chiral PyBOX-ligands have been demonstrated to be suitable ligands regarding activity and selectivity for other iron-catalyzed, asymmetric transformations.^[36]

Although the majority of oxazoline-based scaffolds exhibit C₂-symmetry due to the convenient synthesis and the advantages mentioned previously, there are examples showing that a C₁-symmetric

topology can be beneficial for the outcome of a reaction and even outperform related ligands with C_2 -symmetry. In 2014, the groups of Huang and Lu almost simultaneously introduced a novel iminopyridine-oxazoline (IPO, sometimes also abbreviated as OIP, Figure 6) scaffold for a copper-catalyzed enantioselective hydroboration of disubstituted aryl alkenes.^[47,48] Interestingly, a related PyBOX-ligand showed a significantly lower yield for this catalysis implying that the imine moiety is crucial for an enhanced activity of the catalyst.

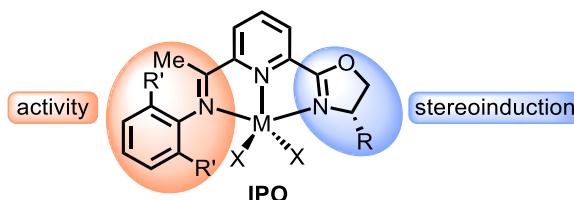
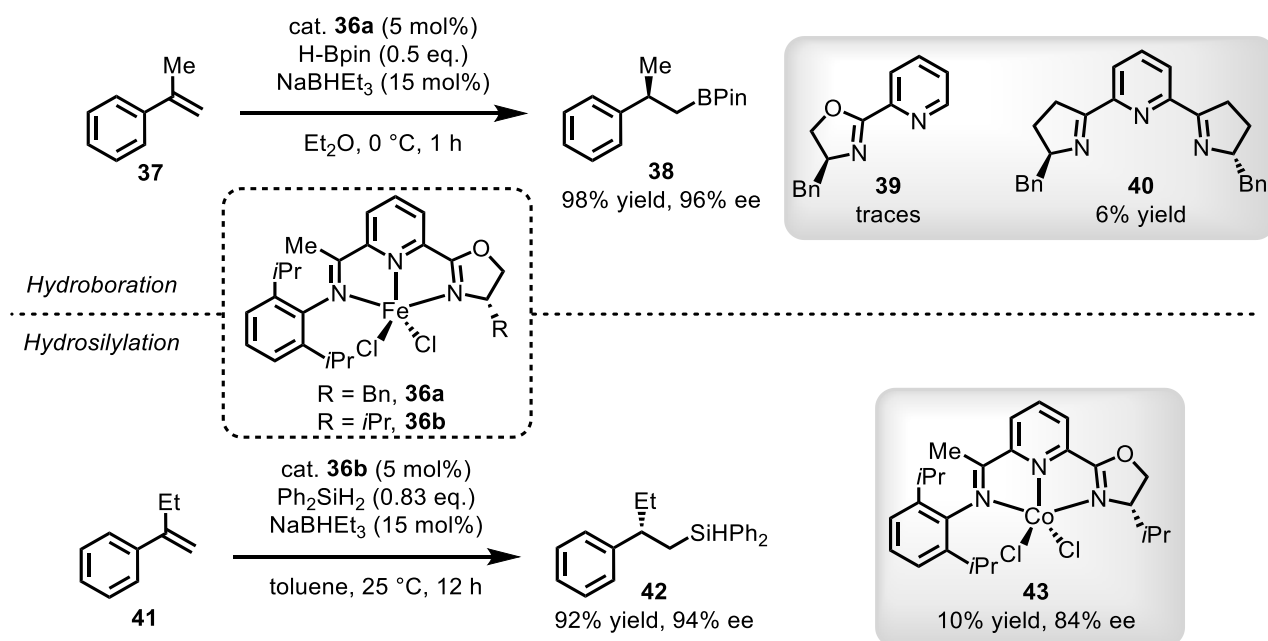


Figure 6: General structure of catalysts comprising the C_1 -symmetric IPO ligand. The oxazoline moiety is supposedly steering the stereoselection during reactions while the imine motif enhances the activity as well as stability of the obtained complexes.^[47,48]

Subsequently, the IPO-scaffold proved to be a competent ligand for asymmetric catalysis, especially in reactions involving 3d-metals such as iron, cobalt, or nickel.^[49] Moreover, the convenient synthesis (as demonstrated by Lu with a ten gram-scale synthetic protocol)^[50] and possibility to implement modifications on both terminal coordinating moieties render it a promising ligand system for asymmetric transition metal catalysis.

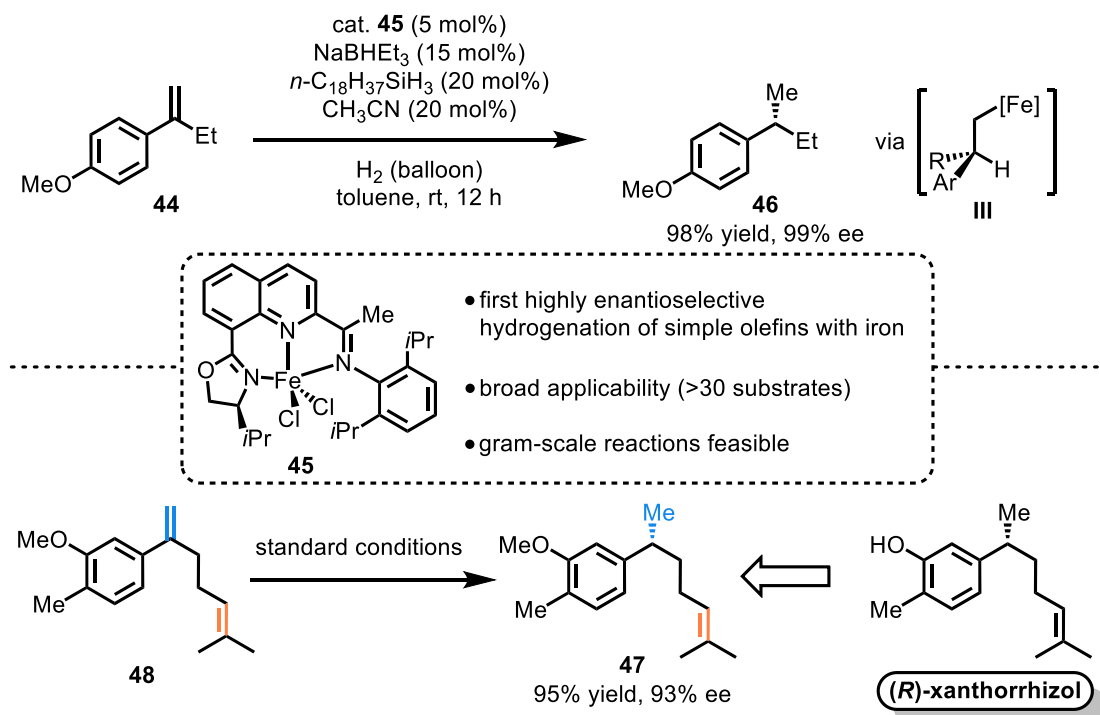
Regarding asymmetric iron catalysis, Lu *et al.* reported in 2014 that Fe-complex **36** comprising an IPO-ligand was capable of promoting an enantioselective hydroboration of 1,1-disubstituted aryl alkenes.^[51] For example, olefin **37** was converted in the presence of pinacolborane (H-Bpin), catalyst **36a** (5 mol%), and NaBHET₃ as reductant to obtain chiral hydroboration product **38** in excellent yield (98%) and with excellent stereoselectivity (96% ee, Scheme 9). A subsequent substrate scope emphasized the efficiency of this catalyst system for the presented reaction with the possibility of obtaining a variety of electronically different products in high yields with mostly excellent enantioselectivities. Notably, employment of a chiral bidentate pyridino-oxazoline ligand **39** or chiral PyBOX-derivative **40** gave significantly lower activity and provided product **38** only in traces or in 6% yield, respectively.^[51] In 2015, the same group reported a successful asymmetric hydrosilylation of 1,1-disubstituted alkenes for the synthesis of optically pure organosilanes.^[52] Specifically, iron complex **36b**, bearing an *i*Pr-motif on the oxazoline moiety, was shown to be an apt catalyst for the conversion of α -ethyl styrene (**41**) towards chiral silane **42** in 92% yield with 94% ee. When cobalt congener **43** was applied as a catalyst, a drastic decline in activity but only a slight decrease in enantioselectivity to 84% ee was observed (Scheme 9).^[52]

Iron Complexes in Asymmetric Transition Metal Catalysis



Scheme 9: Top: Enantioselective hydroboration catalyzed by complex **36a**. Chiral bidentate ligand **39** and PyBOX-ligand **40** in combination with FeCl₂ as catalytic system gave product **38** in low yields.^[51] Bottom: Asymmetric iron-catalyzed hydrosilylation in the presence of chiral complex **36b** to furnish enantiopure organosilane **42**. A cobalt-derivative **43** of the catalyst provided the product in low yield with decreased enantioselectivity.^[52]

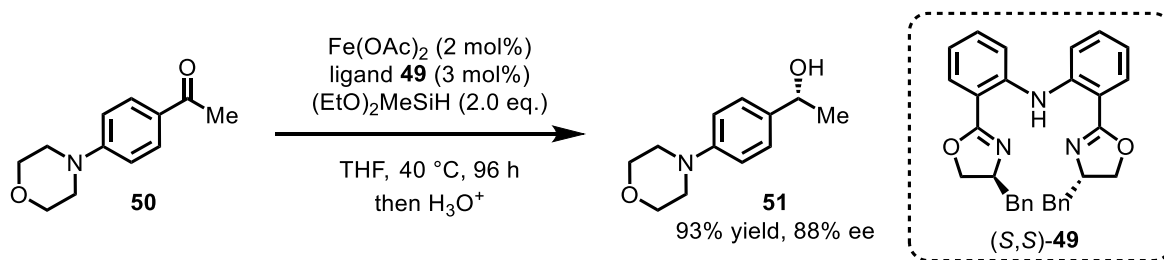
In the following years, Lu and coworkers succeeded in using the IPO-ligand scaffold in combination with cobalt or iron for several asymmetric functionalizations of olefins.^[53] In an impressive more recent study, the group was able to achieve a highly enantioselective iron-catalyzed hydrogenation of minimally functionalized alkenes. The incorporation of a central quinoline motif instead of a pyridine into the scaffold lead to significantly better results with respect to activity and selectivity for this catalytic transformation.^[54] Accordingly, olefinic substrate **44** was hydrogenated by employing iron catalyst **45** in the presence of NaBHET₃, a long chained hydrosilane, and acetonitrile as an additive. After 12 h under mild conditions and an atmosphere of hydrogen gas, chiral product **46** was furnished in excellent yield (>99%) and with excellent enantioselectivity (99% ee, Scheme 10).^[54] Strikingly, this marked the first report of a highly enantioselective iron-catalyzed hydrogenation of minimally functionalized alkenes and is an impressive contribution to the concept of using more benign metals for reactions that have been predominantly performed with noble metals. Mechanistically, the catalytic cycle commences with the formation of an iron-hydride species that can insert into the double bond forming iron alkyl species **III**. Afterwards, intermediate **III** can participate in σ -bond metathesis with the hydrosilane to afford optically active product **46**. Furthermore, the system was shown to tolerate other olefinic bonds and was subsequently applied for the synthesis of enantiopure **47**, a compound that can be converted to biologically active (*R*)-xanthorrhizol in one step (Scheme 10).^[54,55]



Scheme 10: Top: Iron catalyzed hydrogenation of styrene derivative **44** with catalyst **45**. Bottom: Showcase of tolerance towards other double bonds for substrate **48**. Hydrogenation product **47** can be converted to the sesquiterpenoid (*R*)-xanthorrhizol in one step. Xanthorrhizol possesses a variety of biological activities.^[54–56]

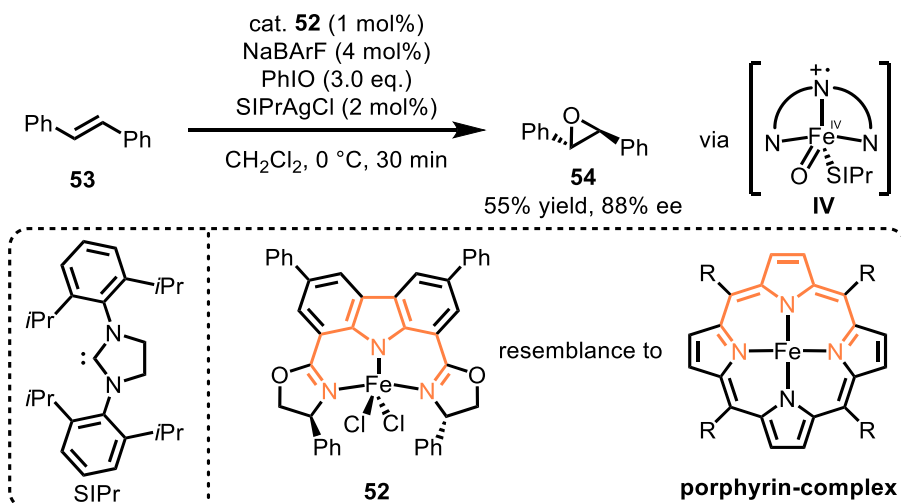
Another class of tridentate bis(oxazoline) ligands is represented by compounds containing a bis(oxazolinyphenyl)amine (bopa) motif. This type of scaffold was first introduced by Guiry and McManus in 2002 for an asymmetric transfer hydrogenation of acetophenone.^[57] Although initial experiments exhibited low enantioselectivities, the group was able to improve the selectivity for a ruthenium catalyzed transfer hydrogenation in a subsequent study.^[58] First attempts of employing this ligand scaffold in asymmetric iron catalysis were reported in 2007 by the group of Nishiyama for the hydrosilylation of ketones. Although the majority of the presented substrate scope was conducted with achiral ligands, the feasibility of asymmetric catalysis was scrutinized for selected examples with chiral bopa-derivatives providing a stereinduction of up to 79% ee. Remarkably, a chiral PyBOX-ligand provided a significantly lower enantioselectivity.^[59] Following these promising results, the group further explored the efficacy of the bopa-framework for enantioselective iron catalysis. In 2010, they presented the iron-catalyzed asymmetric hydrosilylation in the presence of chiral ligand **49** (Scheme 11). Through *in situ* formation of the catalytically active species by employing 2 mol% of Fe(OAc)₂, 3 mol% of chiral ligand **49**, and (EtO)₂MeSiH as reducing agent, ketone **50** was converted to (*R*)-**51** in 93% yield with 88% ee.^[60] A substrate scope of various ketones which was performed with iron- and cobalt-salts indicates a better stereinduction of the cobalt-congener providing higher enantioselectivities for most substrates. Furthermore, a structural elucidation of the active catalyst species was conducted by synthesizing and isolating the bopa-

complexes containing chloride counterions. Interestingly, the two oxazoline-moieties occupy apical positions in the iron-complex whereas X-ray analysis revealed the two oxazoline rings to be situated at equatorial positions for the cobalt congener.^[60]



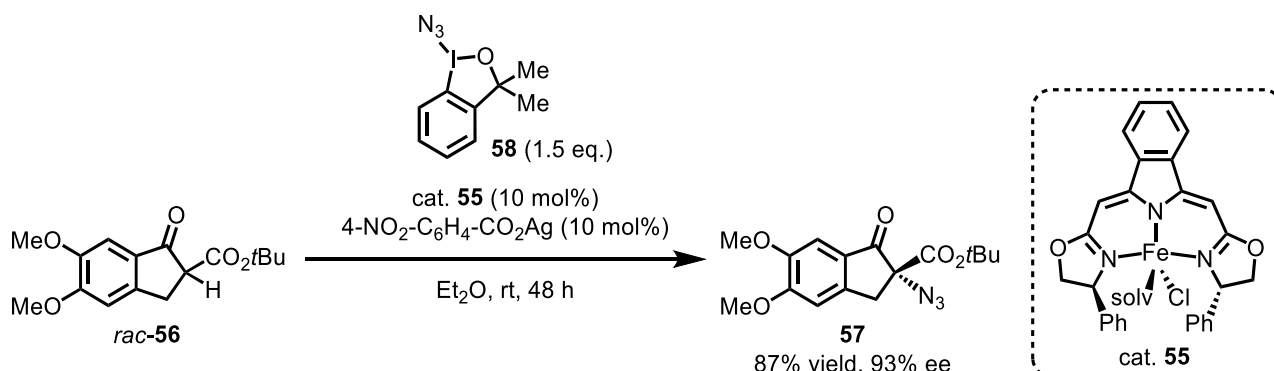
Scheme 11: Enantioselective hydrosilylation in the presence of chiral bopa-ligand **49** to furnish enantiopure alcohol **51** by Nishiyama.^[60]

In 2003, Nakada and colleagues introduced a structurally very similar scaffold comprising a fused carbazole backbone for an asymmetric Nozaki-Hiyama allylation and methallylation.^[61] This ligand as part of iron complex **52** was later presented to efficiently catalyze an enantioselective epoxidation of olefins.^[62] For example, alkene **53** could be converted to the (*S,S*)-epoxide **54** with PhIO as oxygen source and sodium tetrakis(3,5-bis(trifluoromethyl)-phenyl)borate (NaBARF) with an enantioselectivity of 83% ee. Addition of a silver-carbene salt (SIPrAgCl; SIPr = *N,N'*-bis(2,6-diisopropylphenyl)-4,5-dihydroimidazole-2-ylidene) as additive was shown to slightly improve the stereoselection (88% ee) as well as the yield. The catalysis is supposed to proceed via an iron(IV)-oxo species bearing a π -cation radical (intermediate **IV**) that is formed upon reaction of the catalyst with PhIO (Scheme 12).^[62]



Scheme 12: Enantioselective epoxidation reported by Nakada *et al.* in the presence of chiral iron catalyst **52** via iron-oxo intermediate **IV**. The carbazole ligand scaffold partially resembles the porphyrin scaffold.^[62]

A similar N,N,N-pincer ligand framework was introduced in 2011 by the group of Gade for enantioselective fluorinations and Nozaki-Hiyama-Kishi reactions with nickel- and chromium-catalysts.^[63] Two years later, the group proved this scaffold to be a suitable ligand to access chiral azides via an iron-catalyzed azidation of β -keto esters and oxindoles.^[64] In analogy to the previous examples, the developed bis(oxazolinylmethylidene)isoindoline (boxmi) also coordinates in a meridional fashion providing a suitable framework for the incorporation of a sophisticated stereodirecting environment. By application of catalyst **55** for the azidation of racemic compound **56**, optically pure azide **57** was furnished in 87% yield with 93% ee (Scheme 13).^[64]



Scheme 13: Enantioselective azidation of β -keto ester *rac*-**56** by employment of iron complex **55** developed by the group of Gade.^[64]

Conspicuously, when compared to bidentate ligand scaffolds, chiral catalyst systems comprising a tridentate ligand framework are more frequently applied as pre-isolated complexes in asymmetric transformations. The pre-isolation and, more importantly, characterization of these complexes can give valuable insight into the coordination enabling a better understanding of the mode of operation for the corresponding complexes during asymmetric catalysis. Notably, oxazolines are a prominent motif in many tridentate ligands for iron catalysts, again confirming their importance and usefulness for asymmetric iron-mediated transformations. Moreover, the possibility of altering these tridentate chelates in order to realize C_1 -symmetric frameworks (as for the IPO scaffold) provides chances for intriguing modifications on the ligands and, subsequently, on the formed iron catalysts. Noteworthy, the vast majority of applied tridentate systems exert a meridional complexation mode when coordinated to the central metal due to their high rigidity.

1.2.3 Asymmetric Iron Catalysis with Tetradentate Ligands

For the vast majority of chiral transition metal catalysts containing a tetradentate ligand scaffold, the coordinating donor atoms are arranged in a linear (or sequential) framework. In octahedral complexes, this framework can lead to the three different topologies *trans*, *cis- α* , and *cis- β* (Figure 7). Whereas complexes with *trans*-topology do not exhibit metal-centered stereogenicity, formation of *cis- α* or *cis- β* complexes is accompanied by the creation of a chiral center at the metal as shown in Figure 7.

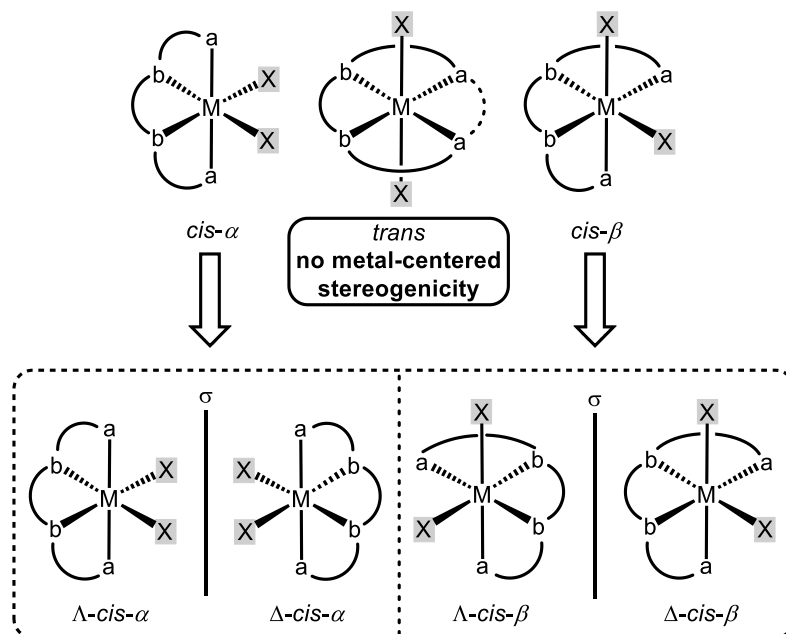
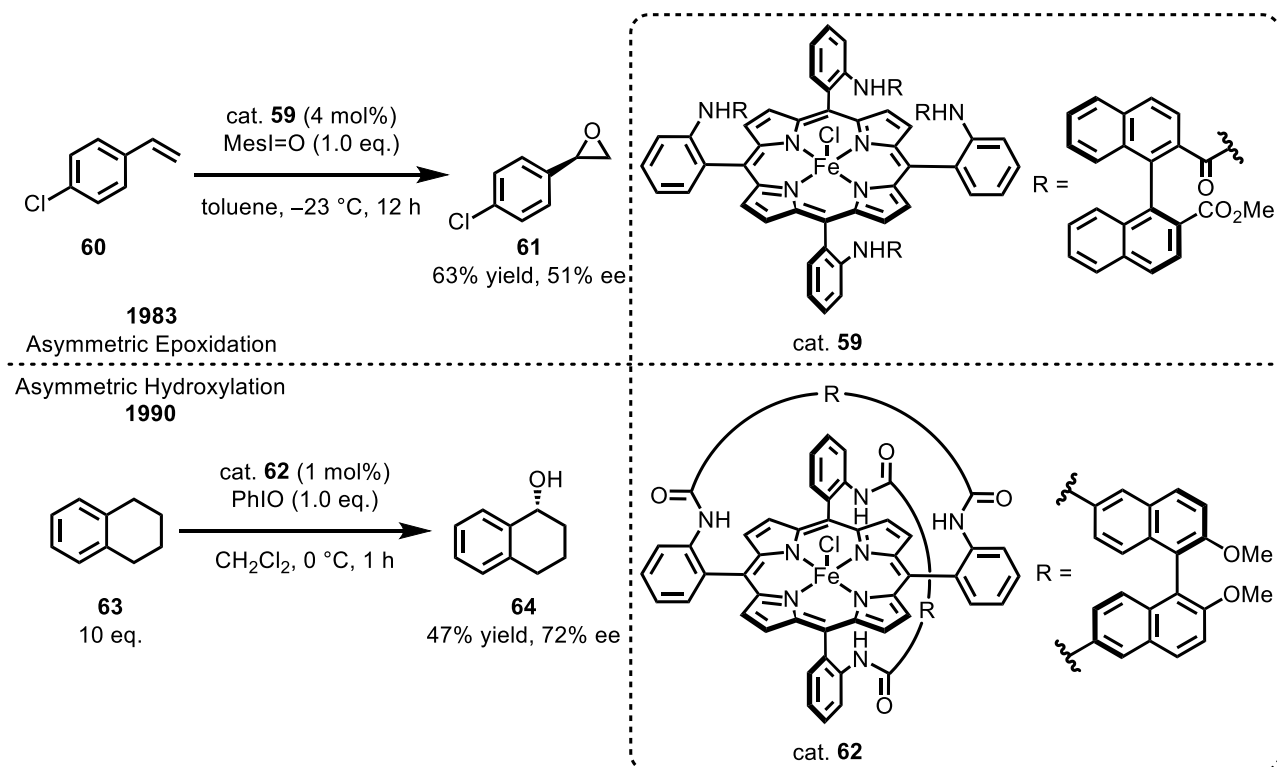


Figure 7: Coordination isomers for linear tetradentate ligands in an octahedral coordination sphere. Complexes exhibiting *cis- α* or *cis- β* lead to metal-centered stereogenicity (Λ - and Δ -isomer). The *trans*-configuration is devoid of a chiral metal-center.

In resemblance to a meridional coordination mode, the donor sites in tetradentate ligands giving rise to complexes with a *trans*-topology are aligned in equatorial positions. Usually, the coordination is complemented by one or two apical coordinating monodentate ligands. A non-cyclic privileged scaffold frequently applied to asymmetric iron catalysis that falls beyond the scope of this introduction are for example *N,N*-ethylenebis(salicylimine) (salen) derived ligands.^[65]

Another class of compounds that exclusively forms complexes with *trans*-topology when applied as ligands are porphyrins. Due to their strong ability to form stable iron complexes, nature makes extensive use of these compounds and exploits their complexation abilities in numerous metalloproteins such as hemoglobin or Cytochrome P450.^[66,67] Inspired by these biological systems, Groves and Myers achieved a pioneering and seminal accomplishment in 1983 regarding enantioselective iron catalysis following their research on iron-porphyrin complexes for racemic epoxidations and hydroxylations.^[68,69] By incorporation of chiral moieties into the central porphyrin

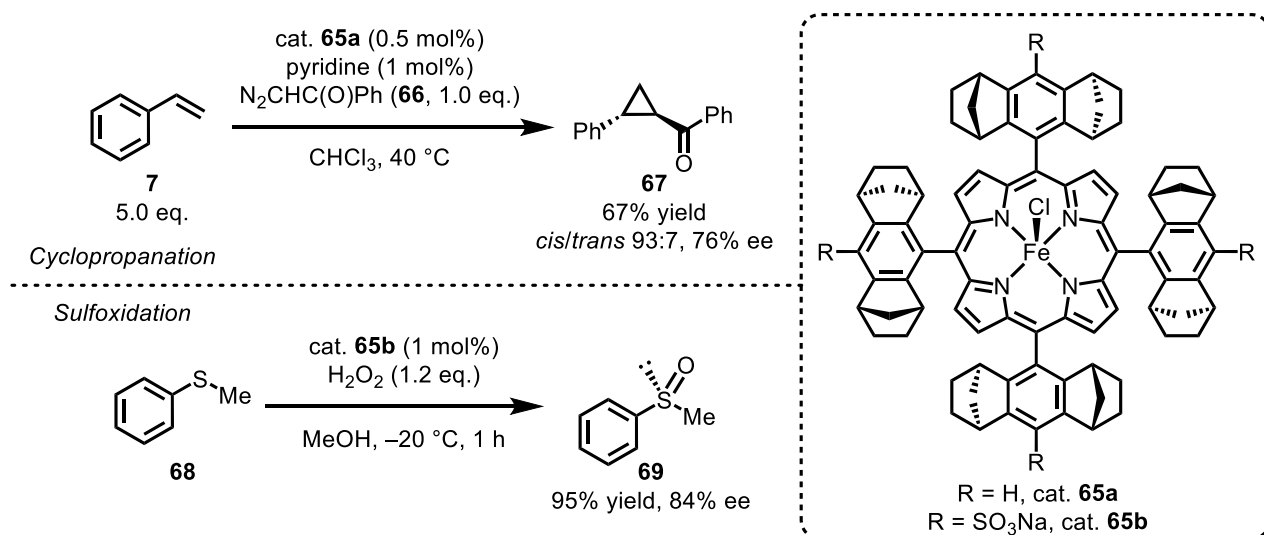
motif of iron complex **59**, they were able to attain a satisfying stereinduction for the epoxidation of prochiral olefinic bonds. Specifically, four chiral (*S*)-binaphthyl motifs connected to the porphyrin core via a phenyl-amido tether provide an overall chiral environment during catalysis. For example, *p*-chlorostyrene (**60**) was converted into chiral epoxide **61** in the presence of catalyst **59** (4 mol%) and iodosylmesitylene at $-23\text{ }^{\circ}\text{C}$ for 12 h providing the desired product in 63% yield with an enantiomeric excess of 51% (Scheme 14).^[68] This study represents a milestone due to it representing the first report of an artificially synthesized chiral iron-porphyrin complex successfully employed in asymmetric catalysis. Afterwards, the group envisioned to improve the efficiency of the porphyrin scaffold for asymmetric iron catalysis. In 1990, the vaulted iron-porphyrin complex **62** was introduced and its efficacy in oxygen-transfer reactions such as epoxidations, sulfoxidations, and hydroxylations was investigated. For instance, when tetrahydronaphthalene (**63**) was used as a substrate for an asymmetric hydroxylation in the presence of 1 mol% of catalyst **62** and PhIO as oxidizing agent, chiral alcohol **64** was provided in 47% yield with 72% ee (Scheme 14).^[70]



Scheme 14: Top: First enantioselective iron-catalyzed epoxidation as reported by Groves and Myers in 1983.^[68] Bottom: Asymmetric hydroxylation of tetrahydronaphthalene (**63**) by Groves.^[70]

Over the past decades, the porphyrin framework has been exploited as a scaffold for numerous different chiral ligand systems by implementation of various chiral moieties.^[66,71,72] Furthermore, in addition to their application in oxygen-transfer reactions, chiral iron-porphyrin complexes have also been shown to be competent catalysts for intermolecular cyclopropanations of alkenes via a metal-

carbenoid. In 2009, the group of Simonneaux presented such a catalytic transformation by employing iron-porphyrin complex **65a** bearing multiple norbornanes fused to central phenyl benzene rings, a ligand first introduced by Halterman *et al.* in 1991.^[73,74] By reacting styrene (**7**) with diazocompound **66** in the presence of catalyst **65a**, cyclopropane **67** was obtained in 67% with an ee of 76% and a good diastereoselectivity (*trans/cis* 93:7, Scheme 15).^[73] Interestingly, a concomitant formation of the dimeric by-product originating from the coupling of two carbene precursors was observed. By further modifying the porphyrin ligand via addition of four sulfonate moieties, the group later achieved an asymmetric sulfoxidation of thioanisole (**68**) with catalyst **65b** and H₂O₂ to obtain chiral sulfoxide **69** in an excellent yield with 84% ee (Scheme 15).^[75] Unsubstituted complex **65a** provided a significantly lower yield and stereoinduction when compared to complex **65b**. Initially, the modifications on the ligand of catalyst **65b** were conducted to provide better solubility in protic solvents; however, addition of major amounts of H₂O during the catalysis deteriorated the activity as well as selectivity.

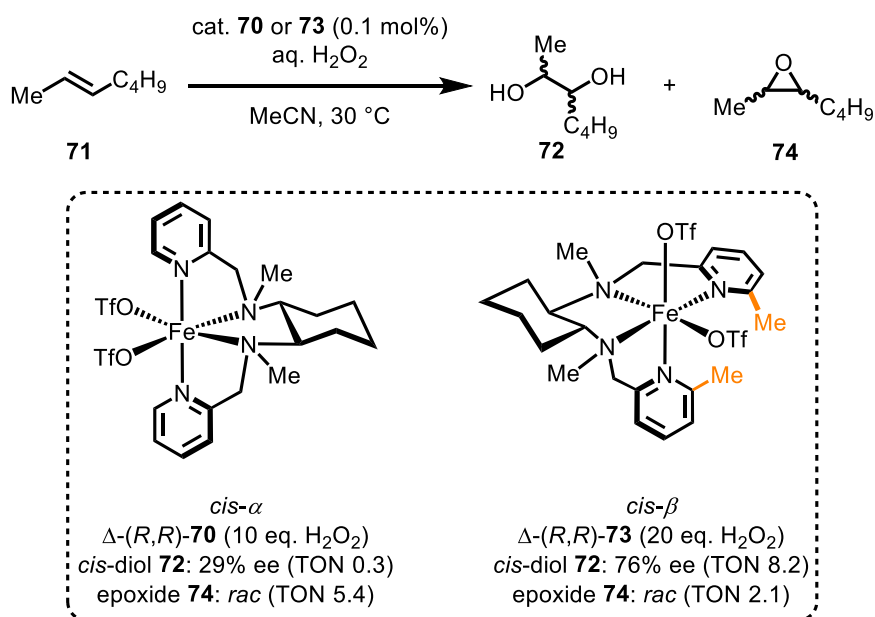


Scheme 15: Top: Enantioselective intermolecular cyclopropanation with iron porphyrin complex **65a** to furnish chiral cyclopropane derivative **67**.^[73] Bottom: Asymmetric sulfoxidation of thioanisole (**68**) in the presence of catalyst **65b** to obtain chiral sulfoxide **69**.^[75]

In contrast to the previously described porphyrin-based compounds, non-cyclic tetradentate ligands comprising a chiral and flexible diamino-backbone usually exhibit a *cis-α* or *cis-β* topology when coordinated to a complex in an octahedral coordination sphere (Figure 7). The derived complexes have emerged as a powerful class of catalysts for several asymmetric reactions, such as hydroxylations and epoxidations.^[76,77] These two topologies give rise to a metal-centered stereogenicity (Figure 7) and, thus, can theoretically result in a mixture of diastereomers when a stereogenic ligand is employed. However, the ligand-centered chirality can have a profound influence on the overall chiral topology of the complex and can even be exploited for the predetermination and

fixation of the metal-centered stereogenicity. For this purpose, usually a chiral backbone is applied that is complemented by two ancillary, terminally coordinating moieties whose rigidity can also have an impact on the overall topology of the resulting complex.^[76–78]

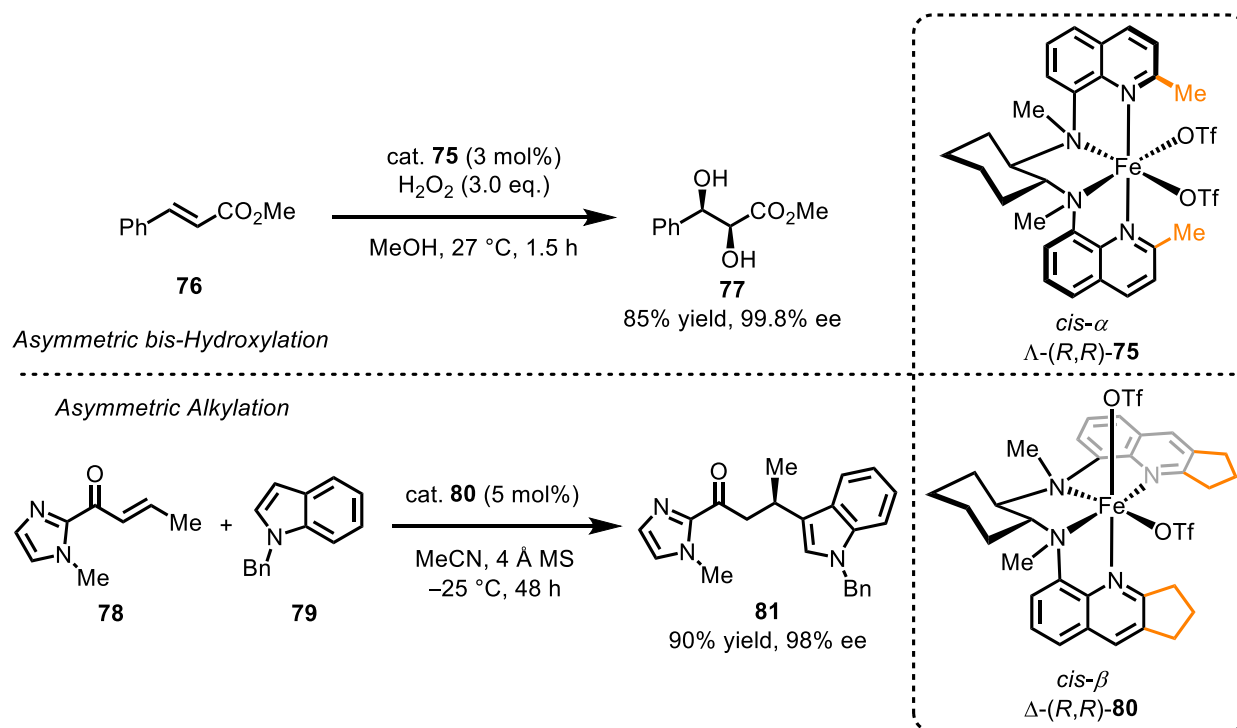
Especially iron- and manganese-complexes with such tetradentate, N₄-type ligands proved to be powerful catalysts for asymmetric transformations.^[79] A prominent backbone for these types of chelating compounds is represented by a chiral 1,2-diaminocyclohexyl motif. First reported by Vagg and coworkers in 1991, this ligand is complemented by two 2-pyridinyl groups that are connected to the backbone by a methylene-bridge.^[80] Gratifyingly, this scaffold exhibited a strong tendency towards a *cis-α* coordination when applied as a ligand for the synthesis of cobalt complexes. Furthermore, a selective complexation towards the Δ -isomer of the product was feasible by using the (*R,R*)-configured cyclohexyl-backbone.^[80] The predetermination of the overall topology of the obtained complexes by a finely tailored ligand framework is crucial for their application as chiral catalysts. Hence, the research and development of such coordinating compounds enabling the complete control over the chiral environment is of high interest. An early example of exploiting this coordination behavior for asymmetric iron catalysis was achieved by Que Jr. *et al.* in 2001 when they reported the first iron-catalyzed enantioselective *cis*-bis-hydroxylation.^[81] The iron-congener **70** of the previously described cobalt-complex by Vagg was shown to facilitate the conversion of *trans*-2-heptene (**71**) with H₂O₂ to furnish the corresponding diol **72**, albeit only with low activity (TON 0.3) and a modest ee of 29%. Moreover, the activity of the catalyst for the competing epoxidation was higher with a TON of 5.4. Noteworthy, the implementation of a methyl-group into the pyridines significantly improved the selectivity as well as activity towards the bis-hydroxylation. When the reaction was conducted with complex **73** as catalyst, product **72** was obtained with a significantly higher activity (TON 8.2) and 79% ee in a virtually diastereopure fashion while the formation of epoxide **74** was less favored with a TON of 2.1. Single crystals of both catalysts gave further insight into the influence of the additional methyl groups at the 6-position of the pyridyl-rings of complex **73**. Depending on this residue, the resulting complex can either be formed in a *cis-α*-topology (Δ -(*R,R*)-**70**) or can exhibit a *cis-β*-configuration (Δ -(*R,R*)-**73**). The results are depicted in Scheme 16. These structures clearly highlight the importance of the ligand design even regarding minor modifications and the effects that such alterations can have on the resulting overall chiral topology of the complex.^[81]



Scheme 16: Enantioselective bis-hydroxylation of olefin **71** with complexes **70** and **73** comprising a chiral, tetradentate linear N4-type ligand scaffold. For both catalysts, epoxide **74** was formed as a single diastereomer without any enantiomeric excess.^[81]

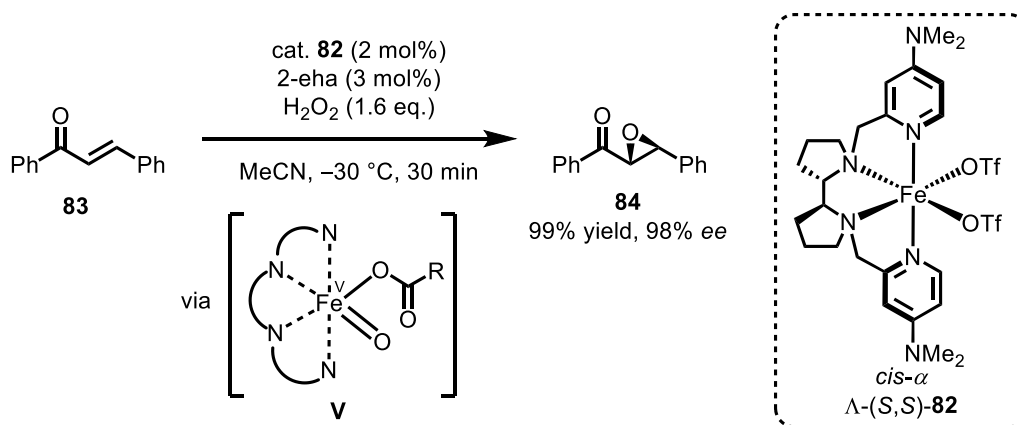
In 2016, the group of Che further scrutinized the feasibility of asymmetric bis-hydroxylations with an iron complex comprising a tetradentate, N4-type ligand with a cyclohexyl diamine backbone.^[82] The implementation of two 2-methyl quinoline-motifs as terminally coordinating groups and omission of a flexible methylene-bridge resulted in the formation of complex **75** exhibiting *cis- α* topology with a Λ -stereogenicity at the metal center if the (*R,R*)-configured ligand was used. When **75** was applied as catalyst for a bis-hydroxylation of methyl cinnamate (**76**) in the presence of H₂O₂, *cis*-diol **77** was obtained in 85% yield with an excellent enantioselectivity of 99.8% (Scheme 17).^[82] Interestingly, an in-depth evaluation of the X-ray crystallographic analysis of complex **75** shows that both, Λ and Δ , configurations at the metal center are possible with this ligand and observable in the unit cell. In addition to the oxidation of olefinic bonds, the group of Che showed the feasibility of employing a similar catalyst system as Lewis acid in the alkylation of *N*-heteroaromatic compounds.^[83] For example, 2-acylimidazole **78** and *N*-benzyl indole (**79**) were reacted with catalyst **80** to obtain alkylated product **81** in a very good yield and an enantioselectivity of 98% ee (Scheme 17). Regarding the relative and absolute configuration of complex **80**, a crystal structure with the (*R,R*)-configured cyclohexyl diamine motif proved the complex to comprise a Δ -chirality at the metal center with an overall *cis- β* -topology.^[83] Conspicuously, the implementation of fused cyclopentane rings into the quinoline moieties unexpectedly gave rise to this overall topology in contrast to catalyst Λ -(*R,R*)-**75**. Moreover, when unsubstituted quinoline groups are implemented into this ligand scaffold, the preferred coordination mode can even be influenced by the choice of the

counterion as shown by the groups of Shin and Nam.^[84] These examples illustrate the high flexibility of the cyclohexyl diamine backbone as it can give rise to different topologies and metal-centered stereogenicities, albeit exhibiting the same ligand-centered absolute configuration. Furthermore, they indicate the significance of even small modifications on the ligands regarding their preferred coordination mode and emphasize the relevance of a carefully tailored ligand design.



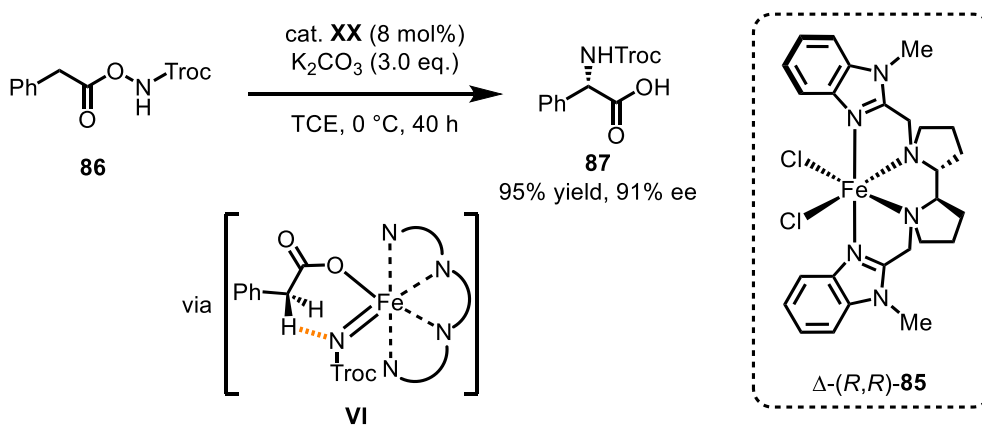
Scheme 17: Top: Enantioselective bis-hydroxylation of methyl cinnamate (**76**) to furnish optically pure *cis*-diols as reported by Che in 2016.^[82] Bottom: The same group reported in 2019 an asymmetric Lewis acid catalyzed alkylation of *N*-heteroaromatics **79** in the presence of complex Δ-(*R,R*)-**80**.^[83]

Another prominent chiral motif implemented into such tetradentate N₄-type ligands is represented by the 2-(2-pyrrolidinyl)pyrrolidine moiety. First introduced in 2007 by White *et al.*,^[85] this backbone exhibits a stronger tendency towards a *cis-α* topology of the corresponding complexes due its higher rigidity which was exploited by Que Jr. and coworkers for an iron-catalyzed asymmetric bis-hydroxylation of olefins in 2008.^[86] By addition of electron-donating NMe₂-groups to the coordinating pyridine rings, the group of Costas achieved a highly enantioselective epoxidation of double bonds as presented in 2013.^[87] When the reaction was conducted with catalyst **82**, chalcone (**83**) could be converted into epoxide **84** in the presence of H₂O₂ and 2-ethylhexanoic acid (2-eha) in quantitative yield with almost complete enantioselectivity of 98% (Scheme 18). This transformation is proposed to proceed via iron(V)-oxo intermediate **V** as the oxygen-transferring species.^[87,88]



Scheme 18: Asymmetric epoxidation of **83** with *cis*- α catalyst **82** via iron-oxo intermediate **V** by Costas.^[87]

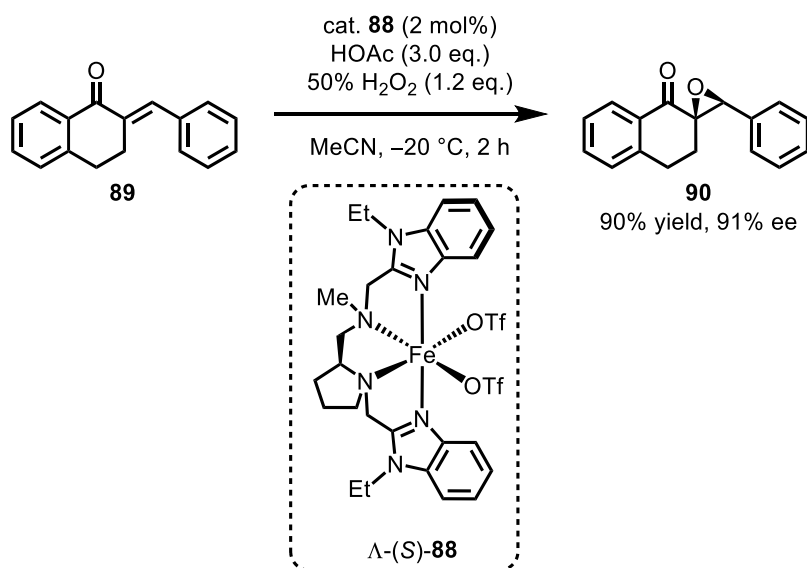
Beyond their application in oxidative transformations, this class of ligand scaffold is also suitable for nitrene-transfer reactions as shown by Meggers *et al.* in 2022.^[89] In an attempt of enhancing the bulkiness of the stereoregulating aryl-moieties, two *N*-methyl benzimidazole rings were incorporated into the ligand system to afford Δ -(*R,R*)-**85**. Notably, the bench stable complex **85** comprising two chloride ligands was directly applied in contrast to other similar catalysts depicted in this section that mostly contain triflate ligands. Ultimately, complex **85** facilitated the conversion of azanyl ester **86** to α -amino acid **87** in 95% yield with 91% ee. Mechanistically, formation of iron-nitrene intermediate **VI** and subsequent hydrogen-atom-transfer (HAT) are promoting this conversion as depicted in Scheme 19.



Scheme 19: Asymmetric synthesis of chiral α -amino acids **87** via iron-nitrene species **VI** and subsequent HAT (indicated by a dashed orange bond) as reported by the group of Meggers.^[89]

Another chiral motif applied in linear, tetradentate, N4-type frameworks showing a high selectivity towards a *cis*- α topology upon coordination is displayed by the aminomethylpyrrolidine moiety. This scaffold was first introduced by Vagg and Williams in 1992 for the synthesis of Co(III)-complexes enabling the predetermination of the metal-centered stereogenicity by the ligand-centered chirality.^[90]

In contrast to the previously described C_2 -symmetric ligands in this chapter, the corresponding complexes inherit C_1 -symmetry due to the non- C_2 -symmetric nature of the backbone. The first showcases of applying this proline-based scaffold in asymmetric catalysis were reported in 2012 by the group of Sun for manganese- and iron-complexes.^[91,92] Accordingly, the group presented the efficiency of this chiral backbone, complemented by two *N*-ethyl benzimidazole moieties, in an asymmetric epoxidation of multi-substituted enones to access a variety of different epoxyketones. For instance, complex Λ -(*S*)-**88** conveniently catalyzed the epoxidation of trisubstituted enone **89** in the presence of acetic acid and H_2O_2 furnishing the desired epoxyketone **90** in 90% yield with 91% ee (Scheme 20). Subsequently, the system was shown to provide enantioselectivities of up to 98% ee for several other enones.^[92] During the following years, the group of Sun explored the applicability of this scaffold in numerous reactions, mainly involving manganese complexes.^[79,93]



Scheme 20: Asymmetric epoxidation of trisubstituted enone **89** by complex Λ -(*S*)-**88** comprising a proline-derived chiral backbone.^[92]

1.3 Concluding Remarks

Since the pioneering work of Groves *et al.* in 1983 a lot of progress and efforts have been made to realize the application of iron catalyst systems in asymmetric transition metal catalysis. Initially, the complexes were mainly inspired by motifs found in nature, *i.e.* porphyrins. Starting in the early 1990s, the application of oxazoline moieties in ligands for enantioselective iron catalysis (BOX, PyBOX, IPO, etc.) became very popular with many examples of successfully facilitated transformations. The rich coordination chemistry of iron has furthermore been explored by employing linear, tetradentate scaffolds with a chiral central motif that give rise to *cis*- α or *cis*- β octahedral topologies, resulting in the creation of metal-centered stereogenicity. Especially these adaptive systems show that the rational

design of carefully tailored ligands is an essential part in the development of new catalysts to allow a satisfying transfer of chiral information for an access towards enantioenriched compounds. A brief overview of seminal work for iron-catalyst systems applied to asymmetric catalysis with ligands that are exclusively coordinating via nitrogen atoms and that have been depicted in this chapter is provided in Figure 8.

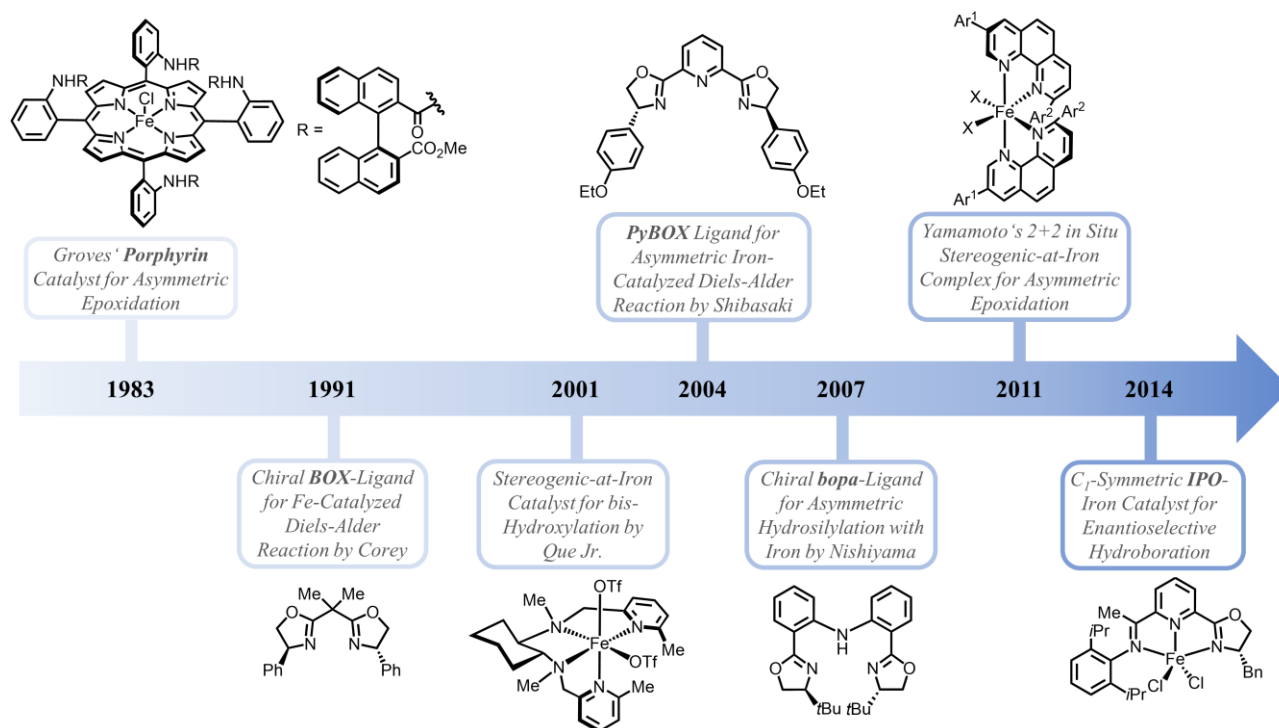


Figure 8: Timeline of selected seminal work regarding application of nitrogen-coordinating ligand systems in asymmetric iron catalysis.

Due to iron being the most earth-abundant transition metal in earth's crust, its low toxicity profile, and its environmental benignity, the development of new catalytically active complexes for highly stereoselective chemical transformations is a very timely and relevant endeavor. With aspects of sustainability becoming more and more important, the possibility of substituting rare and noble transition metals is of high interest and the past achievements in this field of chemistry imply, that iron is not only capable to substitute precious noble transition metals in many reactions but can also provide access towards novel synthetic pathways with distinct mechanisms.

2. Aim of this Work

The design and development of carefully tailored ligand systems to generate overall chiral transition metal complexes represents an essential pillar for the success of asymmetric transition metal catalysis for already half a century.^[94] Typically, the central metal is assigned the role of a reaction center while the ligand sphere is providing the sophisticated chiral environment for a satisfying stereinduction. Hence, the influence of the metal-centered chirality on the topology and, consequently, on the stereoiducing capabilities has been somewhat underappreciated.^[95] However, to acknowledge the stereogenicity of the metal is important for an expedient ligand design as well as for understanding the origin of the asymmetric induction in the course of enantioselective transformations.^[96]

These considerations become apparent for the tetradentate, acyclic N₄-type scaffolds discussed in Section 1.2.3. Such ligands give rise to complexes exhibiting metal-centered stereogenicity (termed stereogenic-at-metal) and contemplations about its influence on the overall chiral environment are pivotal to understand the source of stereoiduction. The chiral ligands provide a lever to determine the chirality and, as a consequence, the overall topology of the catalysts. Due to the carbon stereocenters being situated distant from the catalytically active site, ultimately, the metal-centered stereogenicity is responsible for the stereoiduction in asymmetric transformations.

Furthermore, a chiral complex can even be obtained when ligands devoid of any chirality are implemented (termed chiral-at-metal) as discovered and demonstrated by Alfred Werner in 1911.^[97] Remarkably, the concept of applying chiral-at-metal complexes for asymmetric transition metal catalysis was introduced by Fontecave in 2003 almost a century after Werner's discovery.^[98] However, the development of chiral-at-metal catalysts providing high enantioselectivities is only a recent development demonstrated in a pioneering work by the groups of Hartung and Grubbs in 2013.^[99] Following this first example, the Meggers group attained major contributions demonstrating the generality of this concept and the application to a variety of different metals and reactions.^[100–102] Subsequently, the groups of Gong, Kang, Xu, and Du further showed the versatility of the catalysts developed by the Meggers laboratory in numerous asymmetric transformations.^[103–106] These achievements emphasize the importance and potential of metal-centered stereogenicity in the course of asymmetric catalysis.

With these considerations in mind, the first aim of this work was the design and development of novel, iron-based complexes comprising a pentadentate ligand system. Despite bidentate, tridentate, and tetradentate N₄-type ligands being successfully applied in numerous reactions (see Chapter 1.2), reports on pentadentate coordination scaffolds for the synthesis of chiral complexes are scarce. Furthermore, by applying a properly designed ligand system, the possibility of forming a stereogenic metal center was set to be investigated. Importantly, the ligand system was supposed to enable the

Aim of this Work

formation of low-spin, diamagnetic Fe(II)-complexes to facilitate the feasibility of evaluating important characteristics via NMR-spectroscopic measurements. A report by Hitomi *et al.* from 2012 served as the initial inspiration for the design of a suitable ligand system to furnish a chiral Fe(II)-catalyst as depicted in Figure 9.^[107]

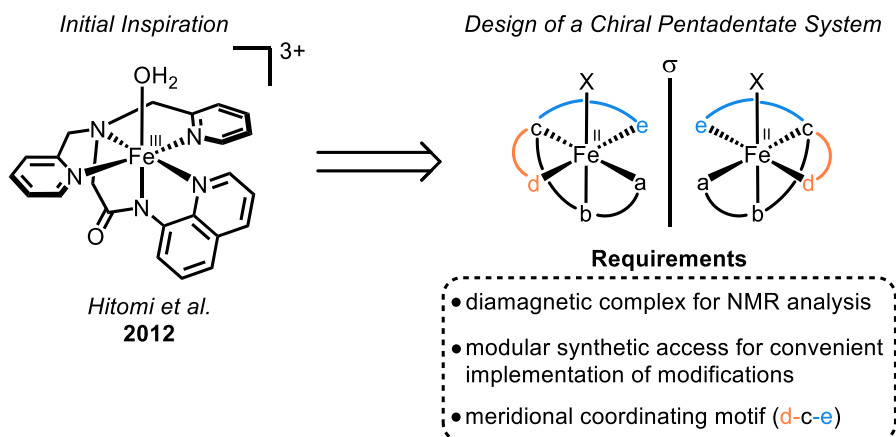


Figure 9: Inspiration and subsequent rational ligand design for chiral iron complexes containing a pentadentate ligand framework.^[107]

Very recently, the Meggers group showed that a decrease in symmetry of complexes can have beneficial effects on the outcome of a reaction. For example, C_1 -symmetric catalysts were proven to be superior for an asymmetric Ru(II)-catalyzed C-H-amidation of dioxazolones and for a Rh(III)-catalyzed enantioselective α -fluorination and α -chlorination of 2-acyl pyrazoles when compared to C_2 -symmetric analogues.^[108,109] Hence, the second aim of this work was an investigation of combining the advantages of lowering the overall symmetry with the advantages of the iron complexes containing a tetradentate, N4-type ligand regarding sustainability to create heterotopic reaction sites in the furnished catalysts (Figure 10).

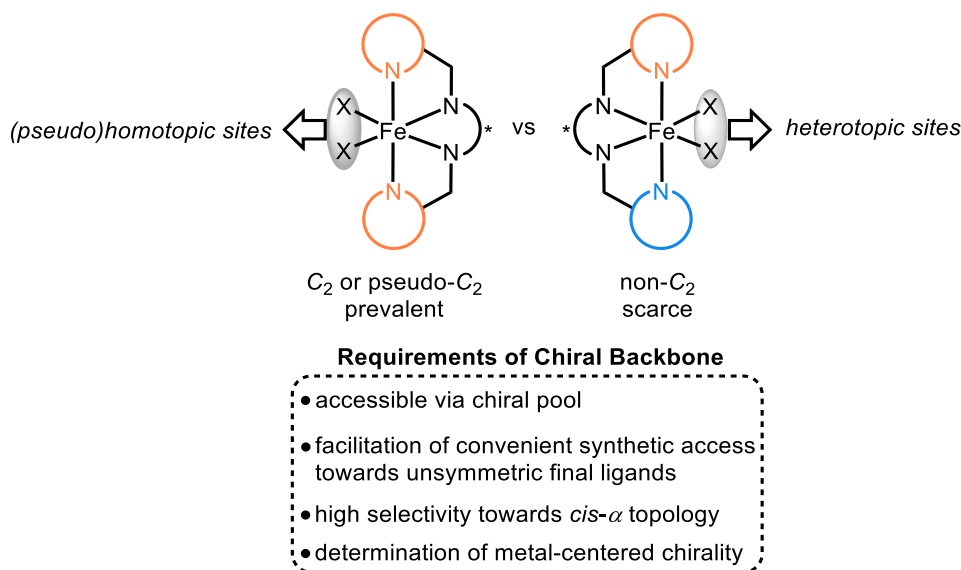


Figure 10: Concept of lowering the symmetry in octahedral complexes comprising a tetradentate N4-type ligand scaffold to furnish heterotopic reaction sites.

Aim of this Work

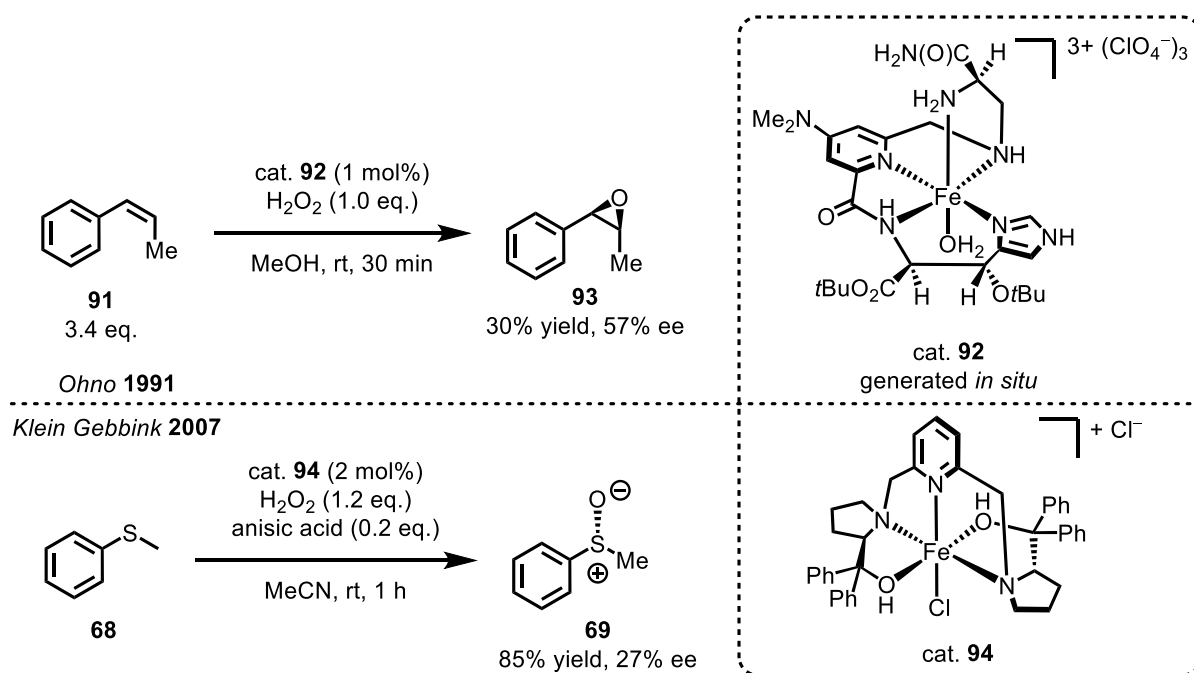
Furthermore, the potential application of both systems as competent catalysts for enantioselective transformations was set to be scrutinized. Due to a great number of reports about asymmetric iron-catalyzed oxidation reactions, an emphasis was made on catalytic transformations that do not involve the formation of C-O-bonds.

3. Results and Discussion

3.1 Development of Chiral-at-Metal Iron(II) Complexes with a Pentadentate Ligand

3.1.1 Chiral Iron Complexes with Pentadentate Ligands in Asymmetric Catalysis

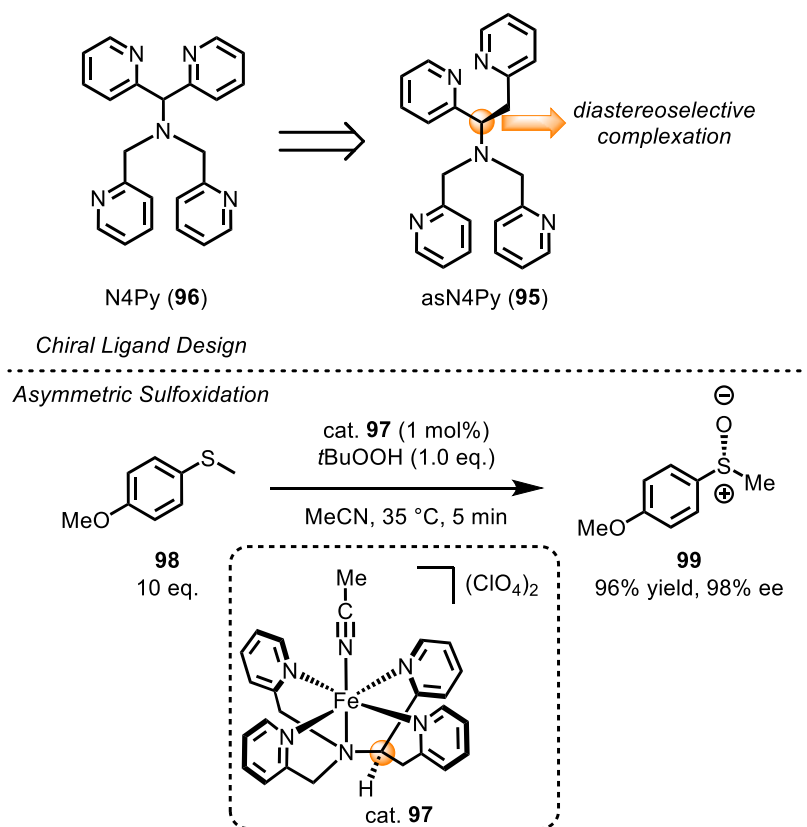
Multidentate ligand frameworks have been shown to offer a great number of possibilities for asymmetric iron catalysis and, thus, contribute a lot to its success. Despite this and many reports on a variety of different achiral pentadentate ligands and their corresponding iron complexes,^[110,111] there are surprisingly few reports on well-defined chiral iron complexes arising from pentadentate ligands. One of the first examples was introduced by the group of Ohno in 1991.^[112] A linear, pentadentate ligand mimicking the binding site of the antitumor antibiotic glycopeptide bleomycin was synthesized and applied in an iron-catalyzed epoxidation of *cis*-methyl styrene (**91**) with H₂O₂ in presence of *in situ* generated catalyst **92** to furnish chiral epoxide **93** in 30% yield with an enantioselectivity of 57% (Scheme 21, Top).^[112] Another linear, pentadentate framework for the synthesis of a stereogenic iron complex was reported by Klein Gebbink *et al.* in 2007.^[113] The group presented the synthesis of different ligands derived from a central bis-pyrrolidinyl pyridine pincer unit and their subsequent application for the complexation of iron. Accordingly, complex **94** was shown to catalyze an asymmetric sulfoxidation of thioanisole (**68**) with a high activity (85% yield), albeit only a modest enantioselectivity of 27% (Scheme 21, Bottom).^[113]



Scheme 21: Chiral iron complexes derived from linear, pentadentate ligands for asymmetric catalysis. Top: The Fe-catalyst **92** comprising a bleomycin inspired ligand was reported to facilitate an asymmetric epoxidation of styrene derivative **91** as reported by the Ohno group.^[112] Bottom: Asymmetric sulfoxidation of thioanisole (**68**) to furnish chiral sulfoxide **69** as presented by the group of Klein Gebbink.^[113]

Results and Discussion

Arguably, the most notable pentadentate scaffold for chiral iron complexes was developed by Kaizer and coworkers. In 2016, the group introduced the chiral ligand *N,N*-bis(2-pyridylmethyl)-1,2-di(2-pyridyl)ethylamine (asN4Py, **95**).^[114] This compound is derived from the well-established tetrapyridyl ligand *N,N*-bis(2-pyridylmethyl)-*N*-bis(2-pyridyl)methylamine (N4Py, **96**)^[115–119] by replacing one 2-pyridyl moiety with a 2-pyridylmethyl group, therefore creating a stereogenic carbon center in the backbone (Scheme 22, Top). Consequently, chiral ligand **95** facilitated a diastereoselective complexation when applied as a ligand to furnish iron complex **97** which was shown to be an apt catalyst for the enantioselective sulfoxidation of methoxythioanisole (**98**) to obtain chiral sulfoxide **99** in high yield with 98% ee (Scheme 22, Bottom). Subsequently, the group applied this scaffold to an enantioselective hydroxylation of ethylbenzene and other stoichiometric oxidation reactions.^[120–123]

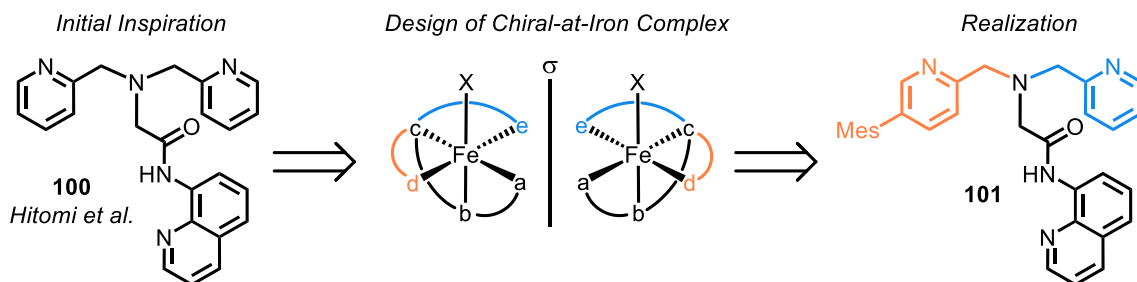


Scheme 22: Top: Design of chiral pentadentate asN4Py (**95**) inspired by achiral N4Py (**96**). Bottom: Application of asN4Py-derived complex **97** for a highly enantioselective sulfoxidation.^[114]

The depicted examples reveal that chiral iron complexes derived from pentadentate ligand frameworks can be suitable catalysts for the transfer of chirality into products. However, mainly oxidation reactions are reported and the presented enantioselectivities are mostly low to moderate with the exception of the sulfoxidation reported by Kaizer. Hence, the design and development of novel pentadentate systems and the derived chiral iron catalysts represents an enticing field that could comprise untapped opportunities for unique complexes evincing distinct catalytic properties.

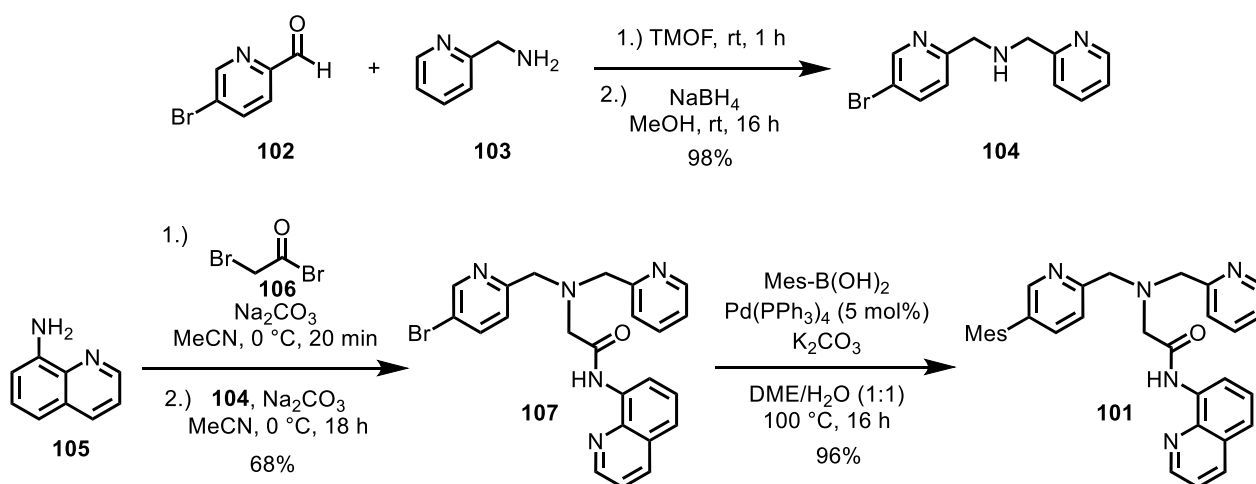
3.1.2 Initial Design of a Chiral-at-Iron Complex

Based on the pentadentate amido ligand **100** reported by Hitomi *et al.*,^[107] the design of a derivative that, upon complexation to iron, gives birth to a complex inheriting metal-centered stereogenicity is depicted in Scheme 23. By addition of a mesitylene-group to one of the two pyridyl rings of ligand **100**, the symmetry of the dipicolylamine motif is broken in **101**, consequently resulting in the possibility of forming two enantiomeric iron complexes when coordinated.



Scheme 23: Rational ligand design for the development of a chiral-at-iron complex. Pentadentate ligand **101** is inspired by the scaffold **100** reported by the Hitomi group in 2012.^[107]

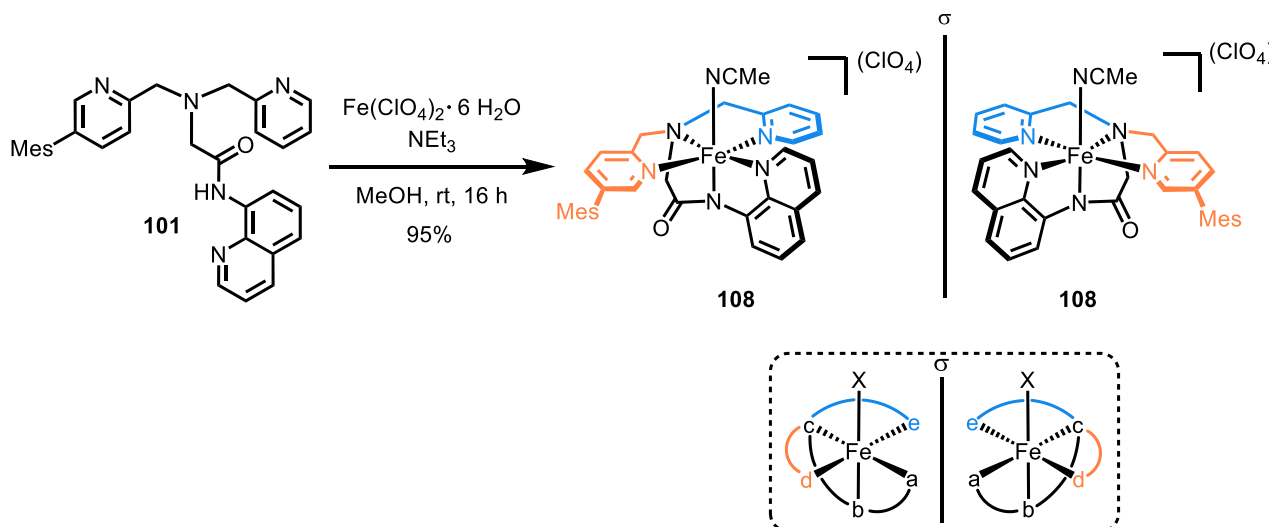
Synthetic access towards the novel pentadentate amido ligand **101** is illustrated in Scheme 24 and was realized via a three-step synthesis commencing with commercially available bromopyridine **102**. Following a slightly modified procedure by the group of Harbury,^[124] reductive amination of **102** with 2-picolylamine (**103**) provided dipicolylamine **104** in 98% yield. Subsequently, 8-aminoquinoline (**105**) was converted with 2-bromoacetyl bromide (**106**) to the corresponding amide followed by a nucleophilic substitution with dipicolylamine **104** in a one-pot procedure in analogy to the procedure by the Hitomi group to furnish **107** in 68% yield.^[107] Ultimately, a Suzuki-coupling with mesitylboronic acid provided the final ligand **101** in an excellent yield of 96% (Scheme 24).^[125]



Scheme 24: Synthetic pathway towards amido ligand **101** via three steps starting from commercially available 5-bromo-2-pyridinecarboxaldehyde (**102**).

Results and Discussion

Afterwards, ligand **101** was reacted with Fe(II)-perchlorate hexahydrate to conveniently furnish iron complex **108** as a mixture of enantiomers in 95% yield (Scheme 25).



Scheme 25: Complexation with tripodal, pentadentate ligand **101** to obtain a racemic mixture of iron complexes **108**. Conditions are according to Hitomi's reported procedure.^[107]

Analysis of the obtained mixture was first conducted by high resolution mass analysis (HRMS) and elemental analysis (CHN) which both confirmed the formation of the desired complex with a high purity. Apparently, subsequent NMR spectroscopic measurements indicated that **108** exhibits paramagnetic characteristics. All measured spectra show no conclusive and distinct signals in the diamagnetic region of 0 to 15 ppm (Figure 11) for complex **108**, thus impeding a thorough evaluation of the complexation by NMR spectroscopic methods. Furthermore, attempts of purifying the crude mixture by column chromatography on deactivated silica gel or alumina led to exclusive isolation of the free ligand, hence indicating decomposition during work-up. Due to the confirmation of the product by HRMS and its purity by elemental analysis, the possibility of a failed coordination was, however, discarded. Application of other bases besides NEt₃, such as di-isopropyl ethylamine (DIPEA) or 2,6-lutidine provided the same results.

Results and Discussion

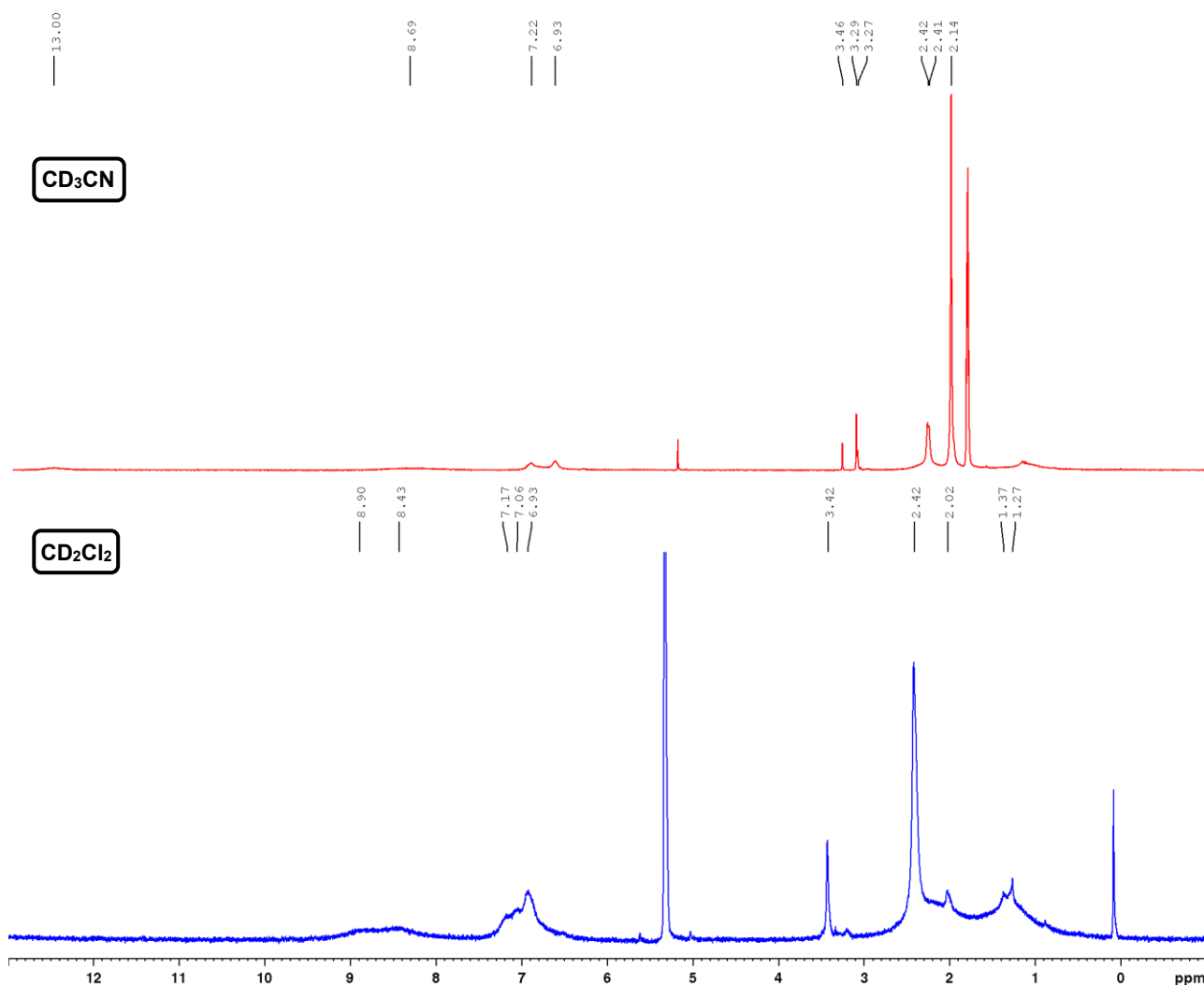


Figure 11: Representative ¹H NMR spectra of complex **108** in CD₃CN (top, 300 MHz, rt) and CD₂Cl₂ (bottom, 300 MHz, rt).

Possibly, these results could be explained by formation of a high-spin Fe(II)-complex rather than the desired low-spin complex resulting in a paramagnetic species. Additionally, a potential oxidative decomposition could lead to the formation of an Fe(III)-center resulting in paramagnetic properties. Reports of other pentadentate ligands show, that the nature of the ligand has a profound influence on the redox-potential of their derived iron complexes. The half wave potentials of selected pentadentate ligands applied to the synthesis of corresponding iron perchlorate complexes are depicted in Figure 12. Strikingly, ligands **100** and **109**, comprising a carboxamido nitrogen upon deprotonation and complexation, show significantly lower redox potentials when compared to other pentadentate scaffolds (**110-114**). A higher potential resembles a stronger tendency towards the Fe(II)-species of the derived complexes suggesting that the carboxamido ligands **100** and **109** are able to facilitate the formation of an Fe(III)-complex.^[107,126] In contrast, iron complexes derived from ligands **110-114** exhibit a relatively high half wave potential implying a higher affinity towards an iron(II) oxidation

state. For example, when ligand **113** was reacted with iron(III) perchlorate, a spontaneous reduction of the coordinated iron compound in MeCN was observed as reported by the group of Mascharak.^[127]

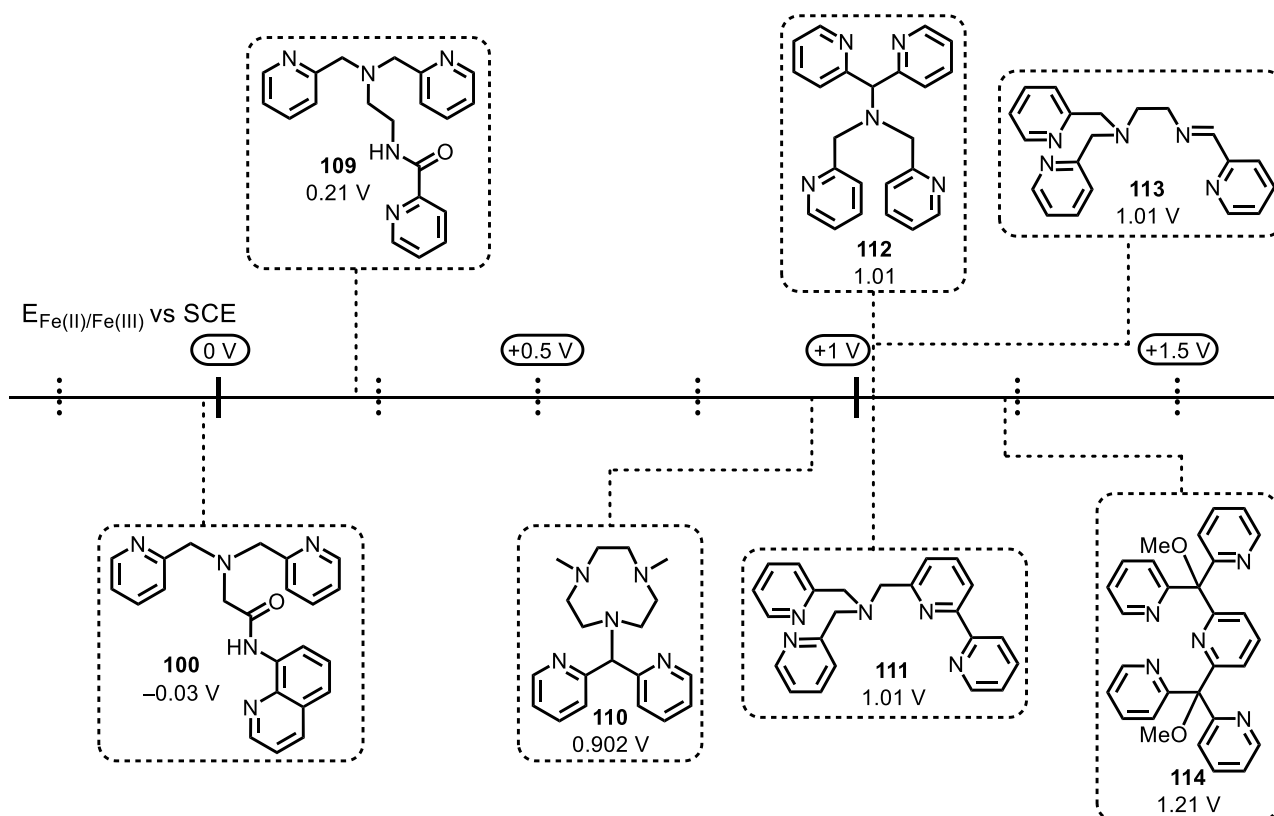


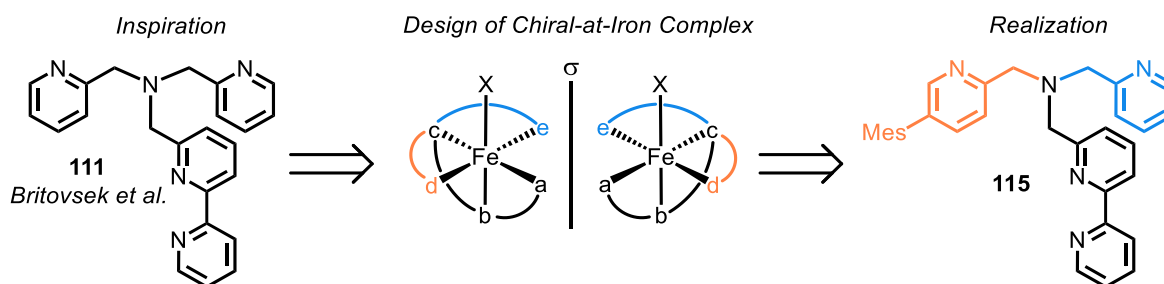
Figure 12: Half wave potentials ($E_{1/2}$) for the Fe(II)/Fe(III) redox couple (vs SCE) of the iron perchlorate complexes derived from the depicted ligands.^[107,126–131]

Considering these reports, a potential undesired and spontaneous oxidation of iron complex **108** could result in an isolation of the Fe(III)-complex, therefore emanating paramagnetic characteristics. The formation of an iron(III)-species during the complexation depicted in Scheme 25 was subsequently qualitatively conformed by HRMS of the fragment $[\text{Fe}(\mathbf{101})\text{H}_2\text{O}(\text{ClO}_4)]^{2+}$. Consequently, a different scaffold was chosen to realize the synthetic access towards novel diamagnetic iron complexes containing metal centered stereogenicity.

3.1.3 Design and Synthesis of a Diamagnetic Chiral-at-Iron Complex

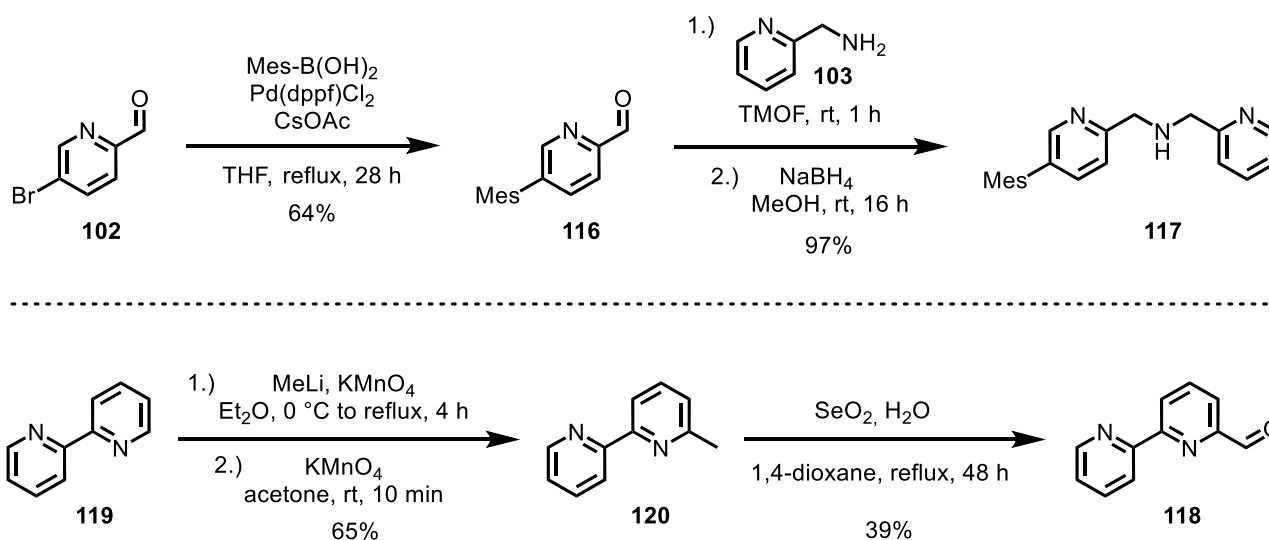
In 2013, the group of Britovsek introduced a strong-field pentadentate ligand for the synthesis of a low-spin iron(II) complex.^[128] Conveniently, the obtained complex could be analyzed and verified by ^1H NMR spectroscopy, thus implying to be a suitable scaffold for meeting the requirements for this work as stated in Chapter 2. In analogy to pentadentate ligand **101**, the addition of a mesityl group to one of the pyridine rings of the dipicolylamine substructure was planned to give rise to a stereogenic metal center upon complexation (Scheme 26).

Results and Discussion



Scheme 26: Modification of the ligand framework **111** reported by Britovsek *et al.* to obtain metal-centered chirality upon complexation.

To establish a synthetic access towards compound **115**, the target structure was divided into two parts; the 2,2'-bipyridyl substructure and the dipicolylamine motif. The synthesis of the two building blocks was realized as illustrated in Scheme 27 and commenced with the implementation of the mesityl-group into commercially available bromine **102** via a Suzuki-coupling providing aldehyde **116** in 64% yield.^[132] Subsequently, reductive amination (TMOF: trimethyl orthoformate) with NaBH₄ as reducing agent yielded the desired dipicolylamine **117** in 97%.^[124] Synthetic access towards 2,2'-bipyridine aldehyde **118** was achieved via literature-known procedures starting from 2,2'-bipyridine (**119**) in a two-step synthesis.^[133,134]

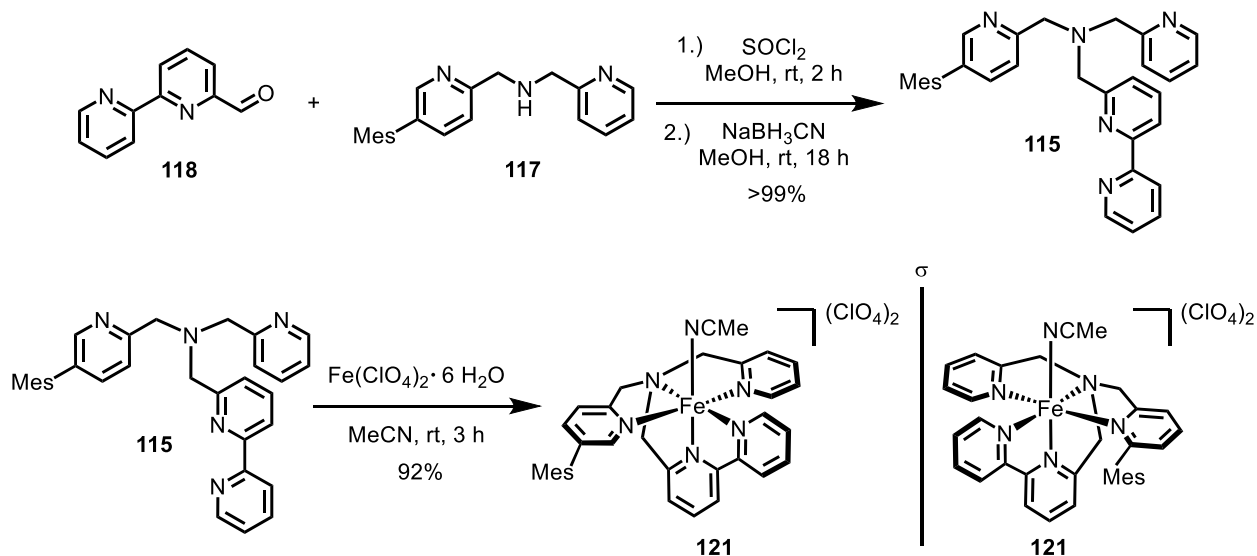


Scheme 27: Independent synthesis of building blocks **117** and **118**.

Ultimately, the desired ligand **115** was furnished by a final reductive amination in presence of thionyl chloride for the condensation step and NaBH₃CN as reducing agent during the second step to give **115** with quantitative yield.^[128] Conveniently, purity of the crude product was sufficient for the subsequent complexation eliminating the necessity of further purification. Notably, addition of activating thionyl chloride during the first step of this one-pot procedure was crucial as when it was omitted, the yield of **115** significantly dropped. With pure ligand **115** in hand, complexation with Fe(ClO₄)₂ · 6 H₂O in MeCN was conducted providing complex **121** as an enantiomeric mixture after

Results and Discussion

purification via precipitation in 92% yield (Scheme 28). The reaction conditions for the complexation were chosen in analogy to a procedure by the group of Britovsek with an exact 1:1 ratio of catalyst and ligand to prevent the formation of undesired side products such as paramagnetic eight-coordinated iron complexes as reported by the group.^[128]



Scheme 28: Reductive amination to furnish final pentadentate ligand **115** and subsequent complexation to obtain racemic Fe(II)-complex **121**.

Gratifyingly, the ^1H NMR spectrum of the obtained compound **121** exhibited a well resolved spectrum with distinct and sharp signals indicating the formation of a low-spin, diamagnetic species facilitating the possibility of NMR spectroscopic analysis (Figure 13).

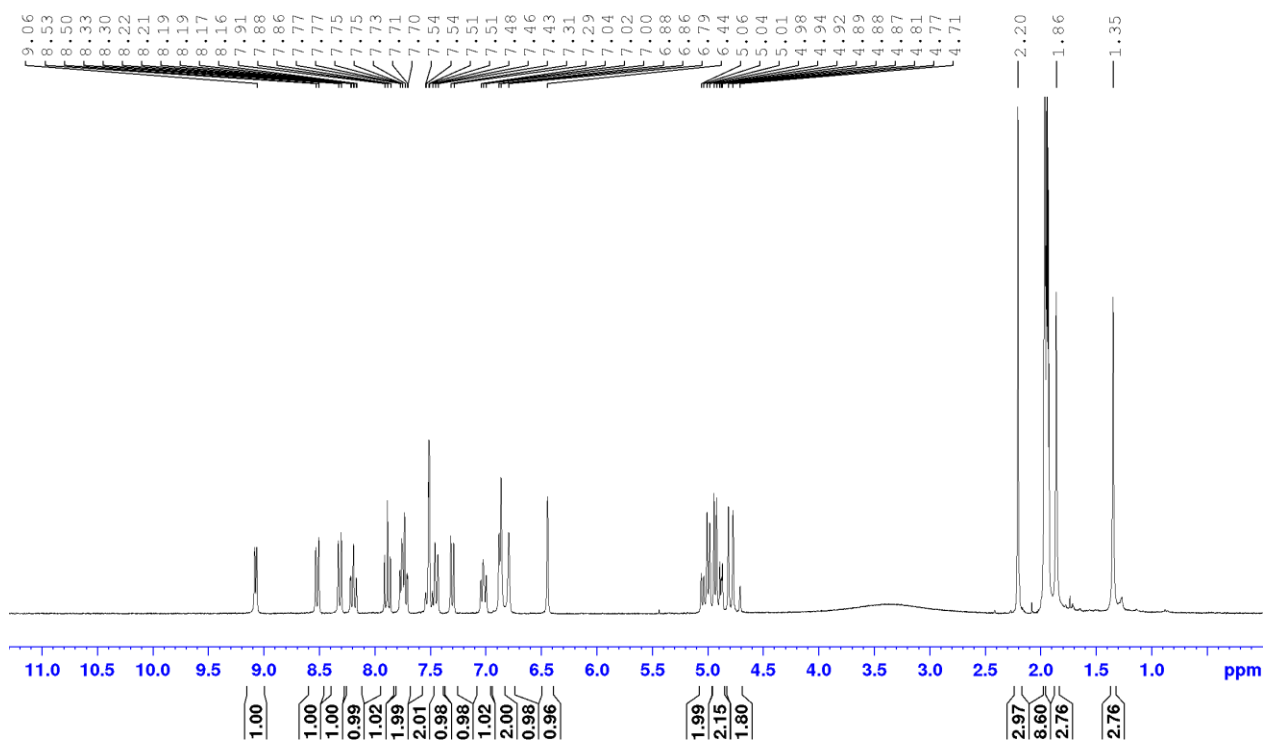


Figure 13: ^1H NMR (300 MHz, rt) spectrum of iron(II) complex **121** in CD_3CN .

Moreover, X-ray analysis of a single crystal of complex **121** confirmed the expected structure in the solid state and gave further insight into the coordination mode of ligand **115**. The crystal structure is depicted in Figure 14.

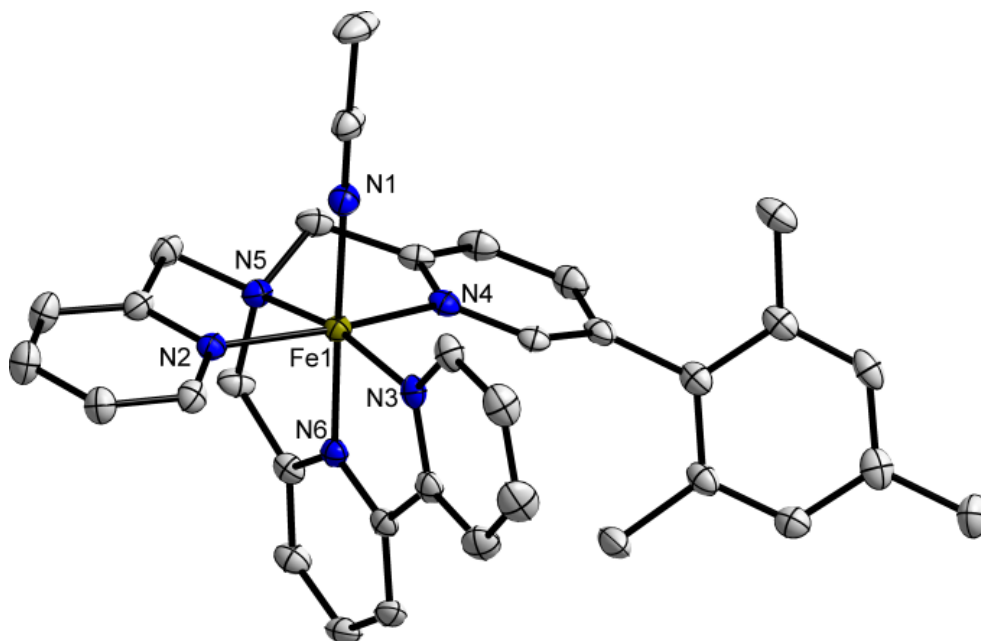
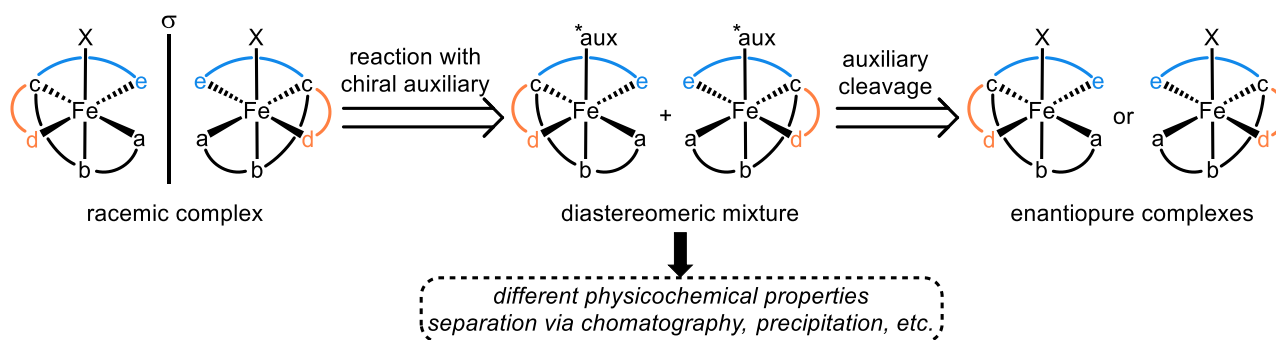


Figure 14: Crystal structure of *rac*-Fe(II)-complex **121** as an ORTEP drawing with 50% probability thermal ellipsoids. Solvent molecules and perchlorate counterions are omitted for clarity.

For the separation of enantiomers, a chiral auxiliary mediated approach was tested as established by the Meggers group.^[39,135–137] For this purpose, a chiral coordinating compound with a fixed configuration is reacted with the racemic complex, consequently giving rise to two diastereomers. Due to their different physicochemical properties, such diastereomers can subsequently be separated by methods such as chromatography or precipitation/recrystallization. Finally, by auxiliary cleavage of the diastereopure compound, an enantiopure complex can be obtained (Scheme 29).



Scheme 29: Concept of the auxiliary mediated separation of a racemic complex mixture to obtain enantiopure iron-compounds. Due to the different physicochemical properties of the diastereomers, they can be separated by conventional purification methods such as chromatography or precipitation.

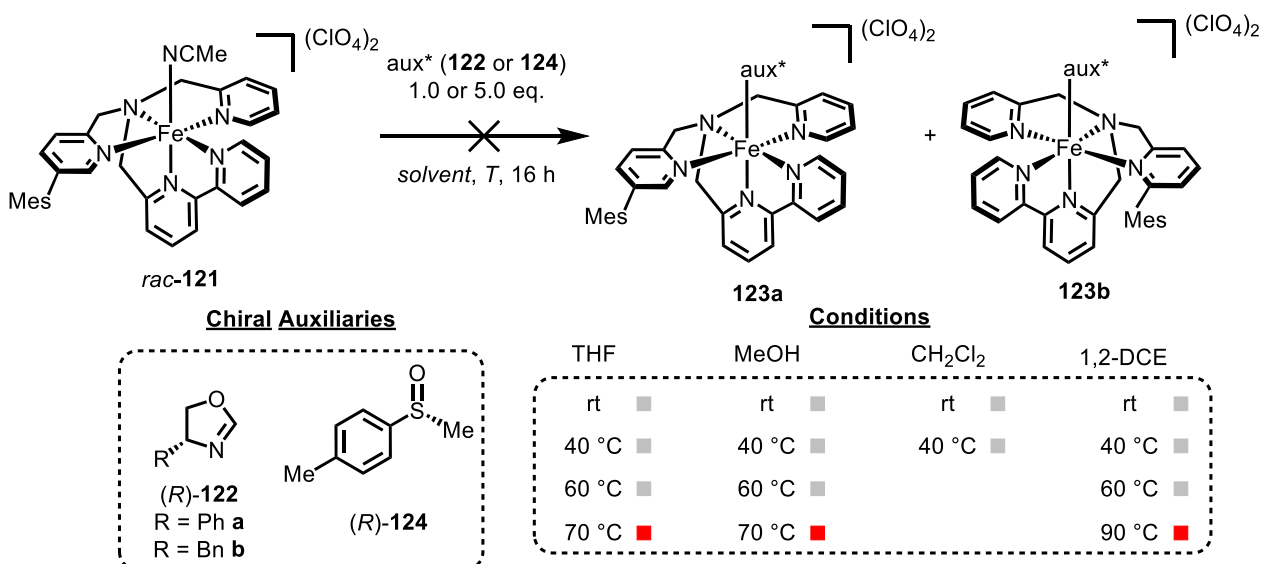
Results and Discussion

In 2019, the Meggers group introduced a chiral-at-iron complex comprising two bidentate NHC-pyridyl ligands to furnish octahedral complexes which are complemented by two labile acetonitrile ligands. Enantiomerically pure iron catalysts were accessed by the aforementioned chiral auxiliary mediated approach using a chiral bidentate salicyloxazoline.^[39] Due to a chelating effect of this ligand, the convenient separation of the diastereomers was feasible. In contrast, the here introduced complex **121** contains only one labile coordination site. Hence, a survey of finding a suitable monodentate chiral auxiliary was conducted. Furthermore, bidentate coordinating compounds were discarded due to a potentially competing coordination with one of the ligand donor atoms that could result in the agitation of the overall topology.

First, chiral oxazolines were scrutinized as they are a prominent motif in reported bidentate chiral auxiliaries.^[39,135–139] Accordingly, iron complex **121** was reacted with phenyl-substituted (*R*)-**122a** under several conditions as shown in Scheme 30. ¹H NMR spectroscopic analysis showed no conversion to the desired products **123a** and **123b** after conducting the reaction in THF, MeOH, CH₂Cl₂, or 1,2-dichloroethane (1,2-DCE) in presence of 1.0 eq. of (*R*)-**122a**. Instead, only starting material and free auxiliary **122a** were detected which was also confirmed by HRMS measurements. Likewise, applying elevated temperatures and/or increasing the amount of oxazoline **122a** did not facilitate the transformation and, starting at 70 °C, induced decomposition of the starting material. Next, benzyl-substituted chiral oxazoline (*R*)-**122b** was chosen due to the higher flexibility of the benzyl group compared to the phenyl-moiety of (*R*)-**122a** and, thus, a potentially higher possibility of giving rise to π -stacking with one of the pyridine rings. However, with the applied conditions, no conversion to the desired diastereomers or, at higher temperatures, decomposition of compound **121** was detected (Scheme 30), rendering the application of monodentate oxazoline auxiliaries insufficient for the separation of racemic complex **121**. Notably, a possible formation of the diastereomeric complexes could be occurring with the coordination exhibiting a high lability. This could result in a possible ligand exchange when NMR measurements in CD₃CN were conducted, ligand cleavage during mass spectroscopy, or ligand substitution by the reaction solvent.

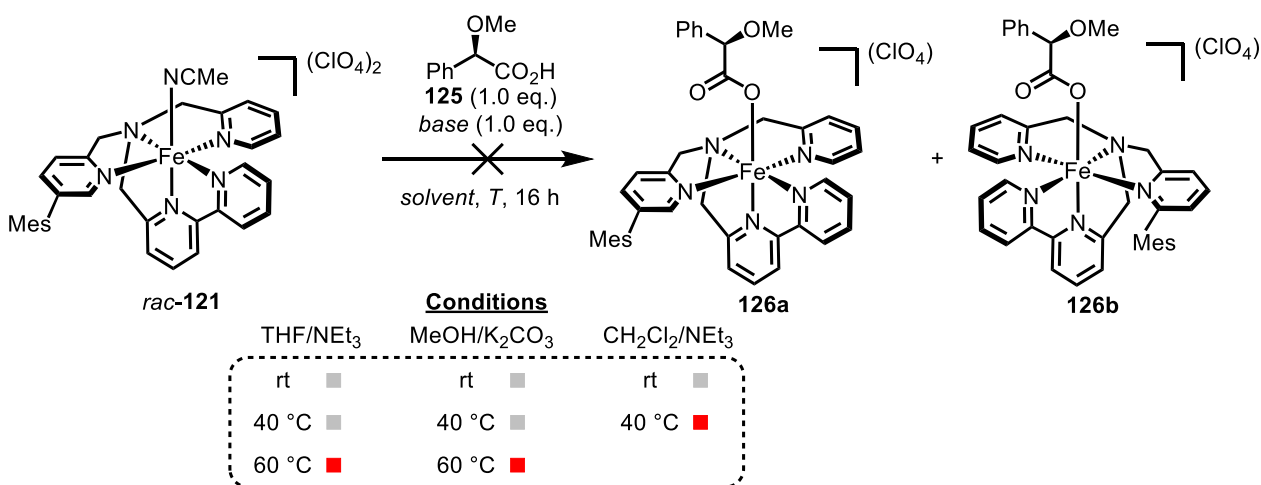
Because of its high affinity towards iron as displayed in numerous proteins,^[140–143] the possibility of using chiral sulfoxide **124** for the formation of a diastereomeric complex mixture was investigated. Similar to the above-described results for chiral oxazolines **122**, sulfoxide **124** proved to be insufficient for providing an access towards enantiopure complexes of **121**, either showing no conversion or leading to decomposition of the starting material like shown in Scheme 30. A detailed characterization of all decomposition products by NMR spectroscopic methods was not feasible due to presumably paramagnetic properties of these species.

Results and Discussion



Scheme 30: Temperature and solvent screening for the application of chiral oxazolines **122a** and **122b**, and chiral sulfoxide (*R*)-**124** to furnish diastereomeric complexes **123a** and **123b**. Conditions without any detectable conversion are indicated by a grey square (■); conditions that resulted in (partial) decomposition are indicated by a red square (■).

In contrast to the previous auxiliaries, monoanionic chiral α -methoxy phenylacetic acid (**125**) was tested as a potentially suitable candidate for the purpose of obtaining diastereomeric complexes. Consequently, racemic complex **121** was reacted with (*R*)-**125** in presence of NEt₃ or K₂CO₃ in THF, MeOH, or CH₂Cl₂ at different temperatures as illustrated in Scheme 31. All applied reaction conditions were insufficient to facilitate the formation of desired complexes **126a** and **126b**. When compared to the results depicted in Scheme 30, decomposition of the starting material was observed at lower temperatures, which could be explained by the presence of base destroying the complex or an agitation of the topology by the coordination of the carboxylate leading to the formation of a paramagnetic species.



Scheme 31: Temperature and solvent screening for the application of chiral carboxylic acid **125** to furnish diastereomeric complexes **126a** and **126b**. Conditions without any detectable conversion are indicated by a grey square (■); conditions that resulted in (partial) decomposition are indicated by a red square (■).

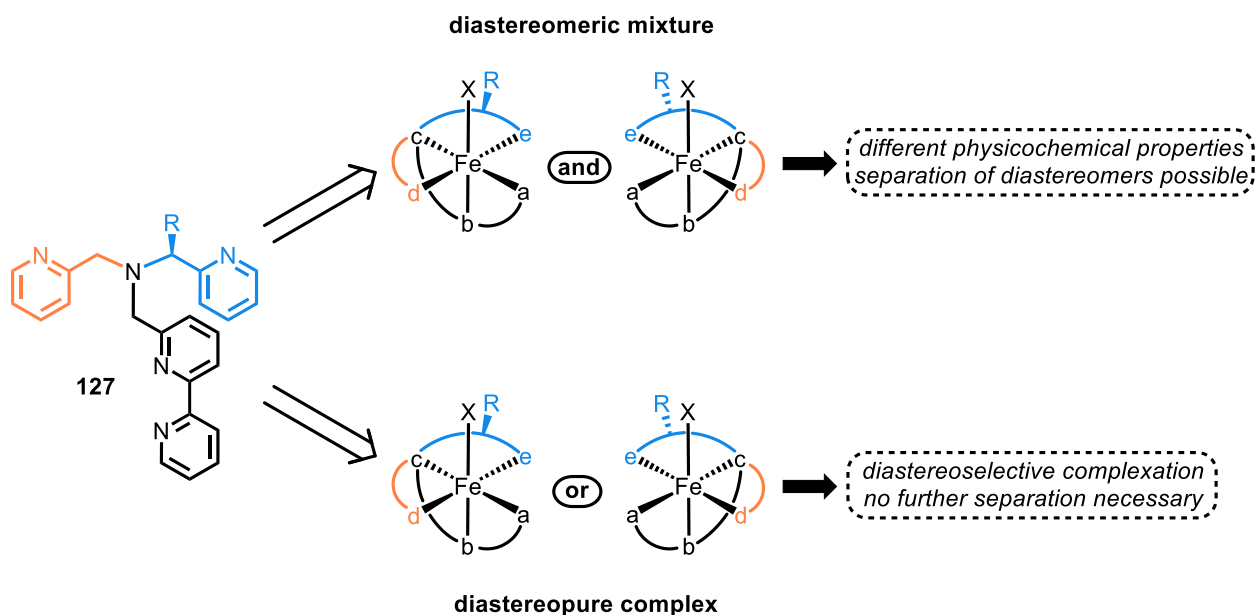
3.1.4 Concluding Remarks

In summary, the development and synthesis of chiral iron complexes comprising an achiral pentadentate ligand scaffold while exhibiting metal-centered stereogenicity was described. First attempts of applying an amido ligand provided a complex not meeting the requirement of facilitating a convenient characterization via NMR spectroscopic analysis. This could be rationalized by a potentially oxidative decomposition of the obtained iron compound due to the ligand framework implementing an insufficient redox stability. Therefore, the ligand framework was successfully modified to furnish diamagnetic complexes that inherit a stereogenic iron center upon coordination and enable NMR spectroscopic measurements. Subsequent approaches of separating the two enantiomers via a chiral auxiliary mediated approach to gain access towards enantiomerically pure chiral-at-metal iron complexes proved to be insufficient. All attempts of applying this method provided no conversion to the desired diastereomers or led to decomposition of the starting material. Possibly, the coordination of neutral monodentate chiral auxiliaries could be deficient, thus impeding an isolation of the diastereomeric complexes. Likewise, application of a monoanionic chiral carboxylate did not facilitate the conversion and more quickly led to decomposition of racemic complex **121** that could be explained by a destabilization of the overall coordination topology by the monodentate ligand. Considering these results, the auxiliary mediated separation of enantiomers was discarded and a different approach was chosen that will be discussed in the following section.

3.2 Stereogenic-at-Iron Complexes with a Chiral Tripodal Pentadentate Ligand

3.2.1 Considerations for a Stereogenic-at-Iron Complex with a Chiral Pentadentate Ligand

When the coordination of a chiral ligand is accompanied by the formation of metal-centered stereogenicity, the complexation provides a mixture of diastereomers that can be separated due their different physicochemical properties. Moreover, by selection of a suitable ligand, such systems can be exploited to provide a diastereoselective access to the desired complex, hence eliminating the necessity of a potentially laborious separation (Scheme 32). Thus, the implementation of a chiral moiety (*chiral lever*) into the ligand scaffold **127** was planned to obtain stereogenic-at-iron complexes that can either be separated or, more intriguingly, that form in a diastereoselective fashion (some examples have been discussed in Chapter 1).

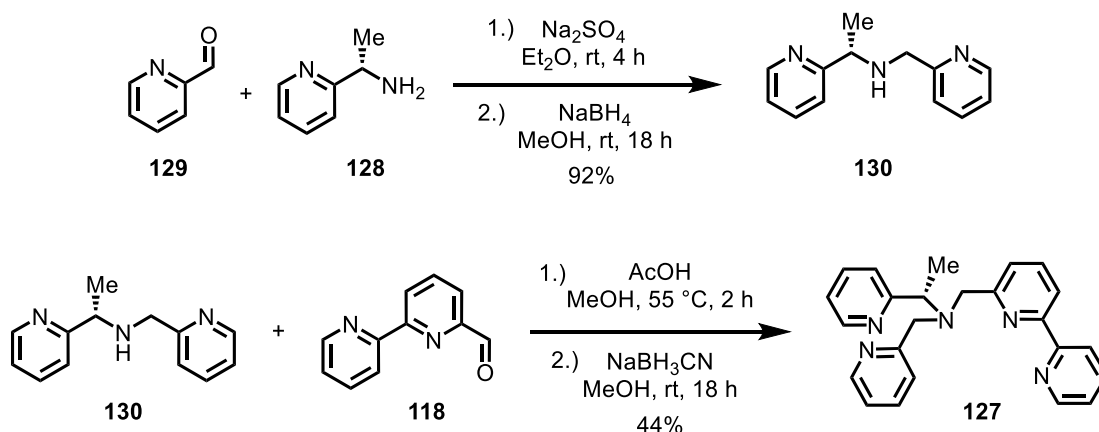


Scheme 32: Formation of stereogenic-at-metal complexes with a chiral pentadentate ligand. Complexation can either provide a mixture of diastereomers that can be separated (top) or the coordination proceeds in a diastereoselective fashion providing only one diastereomer (bottom).

The strategy to implement such a chiral lever into the ligand scaffold to obtain the possibility of a more convenient synthetic access towards stereogenic-at-metal complexes can furthermore rely on an improved thermodynamic control of the metal-centered stereogenicity as reported before by the group of Carmona.^[144–147]

3.2.2 Synthesis and Complexation of Chiral Pentadentate Ligands

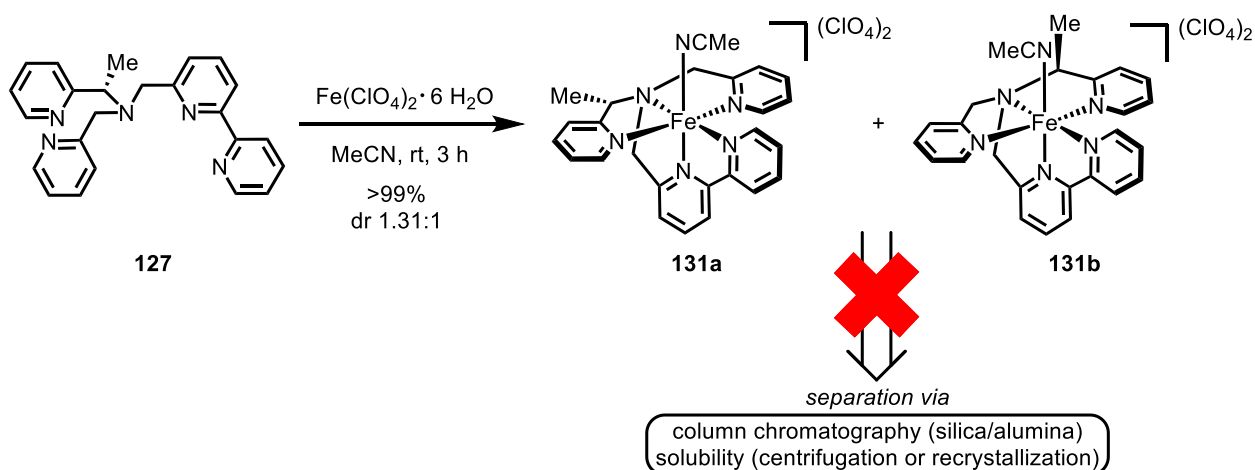
Gratifyingly, chiral picolyamine **128** comprising a methyl residue was commercially available and, therefore, chosen for first attempts of synthesizing stereogenic-at-metal iron complexes with chiral, pentadentate ligand scaffold **127**. Starting from pyridine aldehyde **129**, two consecutive reductive aminations were conducted to obtain desired compound **127**. Due to a higher yield and purity of the obtained product, dipicolylamine **130** was synthesized based on a procedure by the Brunner group^[148] instead of the conditions depicted in Scheme 27 providing **130** in 92% yield. Subsequently, a second reductive amination with AcOH as an activating reagent at an elevated temperature of 55 °C followed by reduction with NaBH₃CN provided pentadentate ligand **127** in 44% yield (Scheme 33).



Scheme 33: Synthesis of chiral pentadentate ligand **127** via two consecutive reductive aminations.

Afterwards, complexation with iron(II) perchlorate hexahydrate conveniently gave a mixture of **131a** and **131b** in quantitative yield after precipitation and filtration. The ¹H NMR spectrum of the obtained complex showed the formation of two separate species with a ratio of 1:1.31 implying that the two diastereomers exhibit significantly different thermodynamic stabilities or the coordination of ligand **127** occurs under kinetic control (Scheme 34). Next, separation of **131a** and **131b** by conventional methods was envisioned. However, attempts of purification by column chromatography on silica or alumina resulted in major decomposition of the complexes on all tested stationary phases. Even when deactivated silica gel or basic alumina was applied, only a decomposed species could be obtained as evaluated by ¹H NMR analysis. Segregation of the two complexes by exploitation of different solubilities was examined with various solvents, such as MeOH, EtOH, THF, CH₂Cl₂, CHCl₃, EtOAc, Et₂O, acetone, or toluene, leading either to a significant decomposition or an insufficient separation.

Results and Discussion



Scheme 34: Synthesis of diastereomeric stereogenic-at-iron complexes **131a** and **131b**.

Fortunately, when the complexation was conducted for a longer reaction time of 16 h, a change of the diastereomeric ratio could be observed. This was confirmed by dissolving the complex in CD_3CN to determine the ratio by ^1H NMR measurements followed by a second assessment after 24 h with the same sample. After 24 h at rt, the dr changed from 1:1.31 to 1:1.73 indicating that the diastereomers are interconvertible and one of them is thermodynamically more favored (Figure 15). Considering steric repulsion, complex **131a** with the methyl group pointing away from the labile coordination site was initially assumed to be thermodynamically more favored.

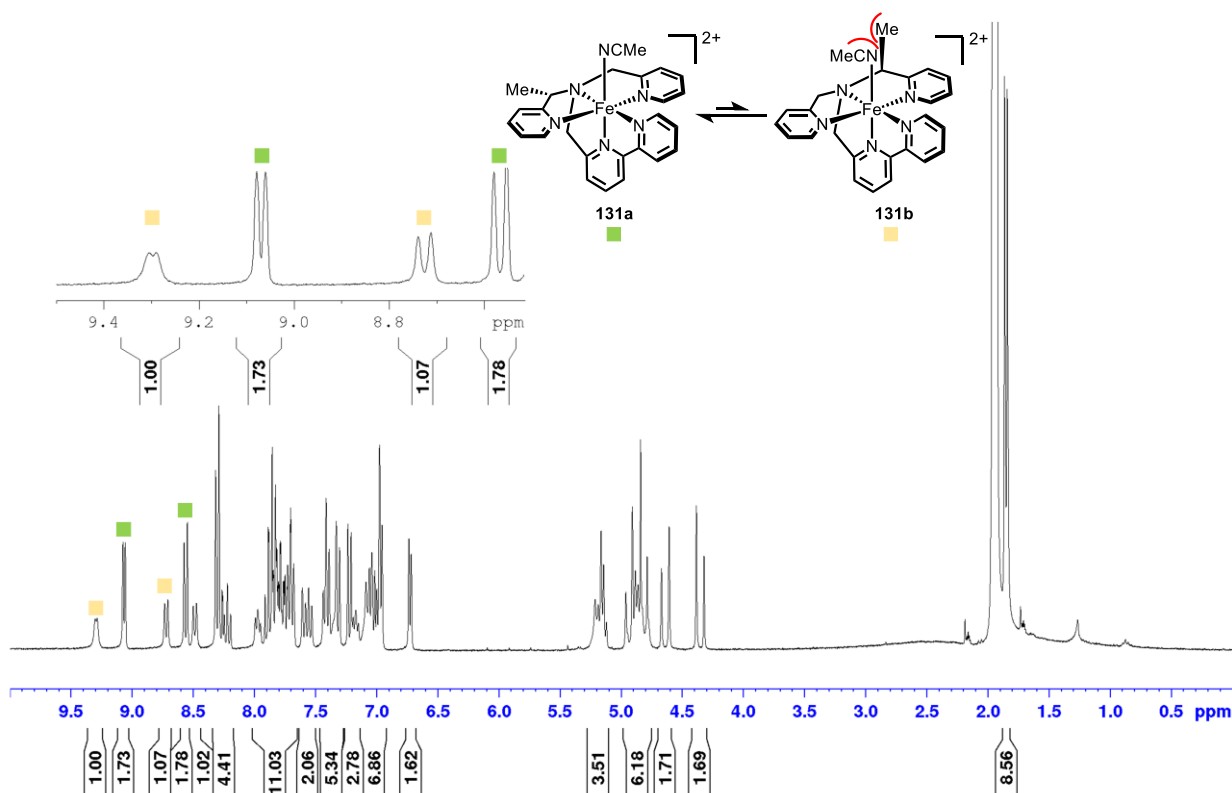


Figure 15: ^1H NMR spectrum (300 MHz, rt, CD_3CN) of the product mixture obtained after complexation. Conspicuously, the spectrum shows two sets of signals in a ratio of 1:1.73. Selected peaks used for ratio determination are highlighted with colored squares.

Results and Discussion

Subsequently, isomerization was quantified via ^1H NMR spectroscopic analysis after dissolving the complex mixture in MeCN and stirring at room temperature and $75\text{ }^\circ\text{C}$ to gain insight into the rate of conversion. As illustrated in Figure 16, dissolving the product in acetonitrile for 48 h provided a dr of 1:1.91 implying that higher temperatures are necessary in order to furnish a diastereomerically pure complex. Hence, the mixture was stirred at $75\text{ }^\circ\text{C}$ for several days providing a virtually pure compound with a high dr of $>20:1$. The possibility of one diastereomer decomposing during the process was discarded by addition of an internal standard (1,1,2,2-tetrachloroethane) that confirmed an isomerization occurring. Conveniently, the feasibility of converting the minor into the major diastereomer discards the necessity of a separation and, thus, grants a neat access towards a diastereomerically pure product.

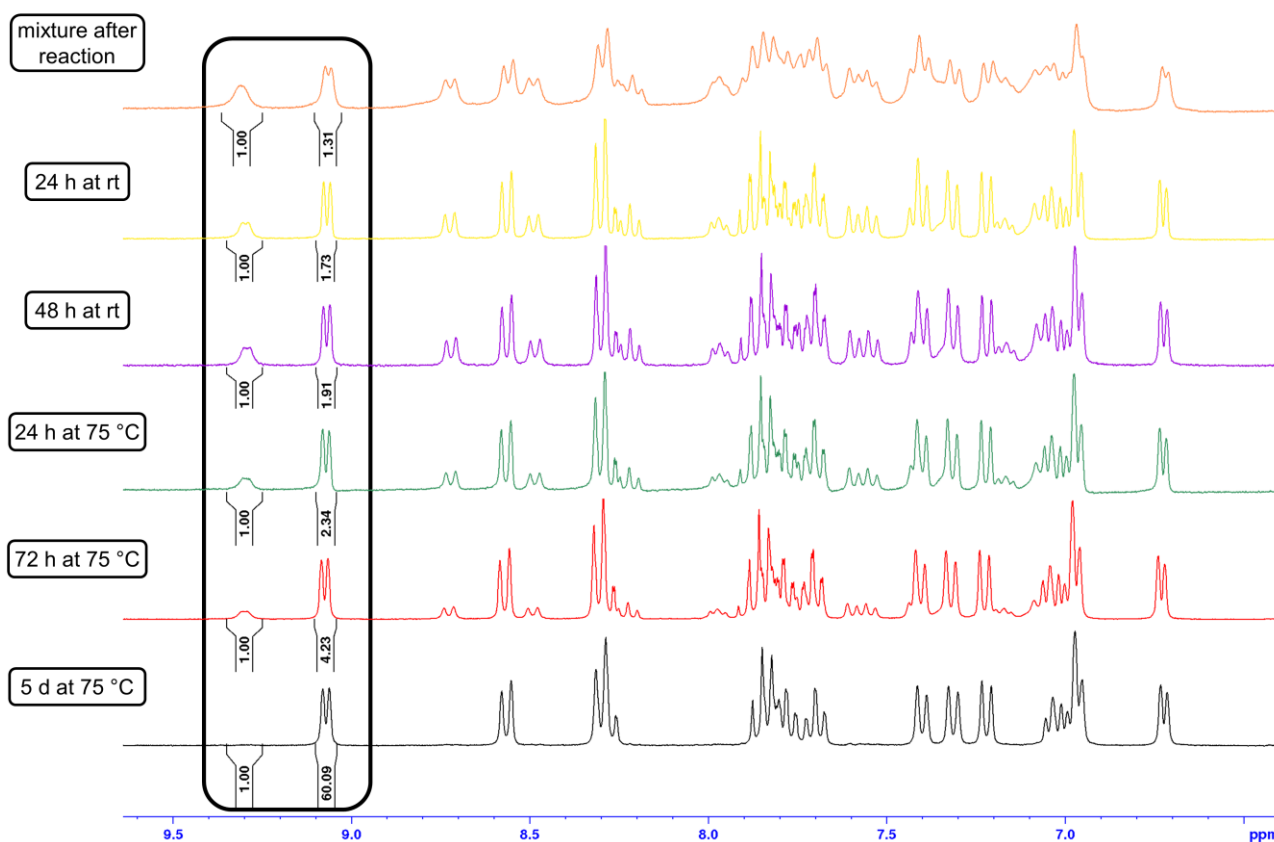
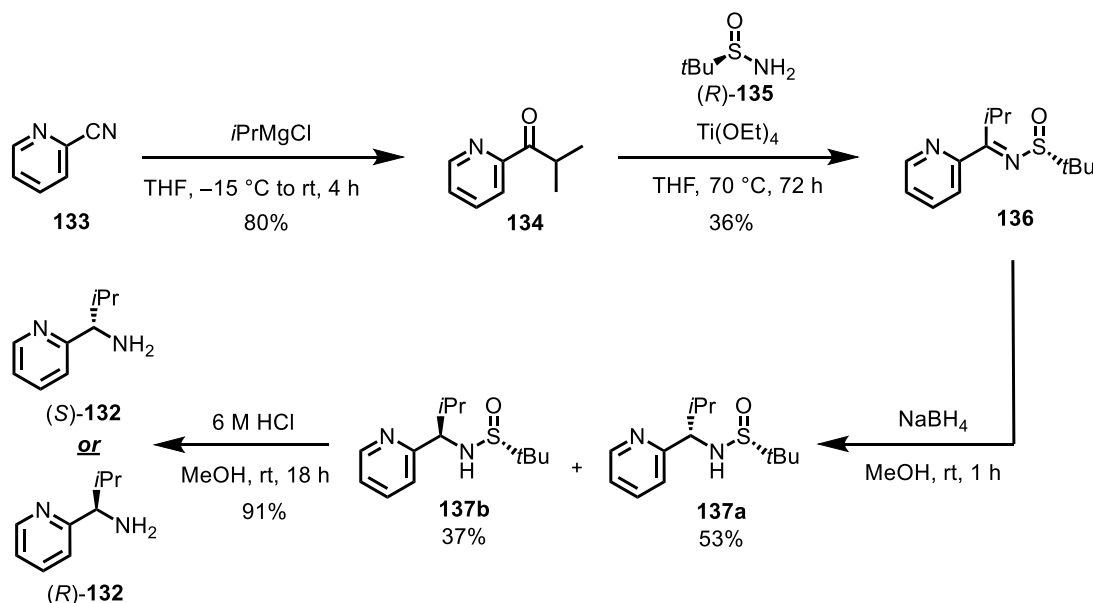


Figure 16: Aromatic region of ^1H NMR spectra (CD_3CN , 300 MHz, rt) of the diastereomeric mixture after stirring complexes **131a** and **131b** at the stated temperature. The signals used to determine the diastereomeric ratio are highlighted.

Next, the implementation of a bigger chiral lever into the ligand scaffold and its influence on the isomerization of the corresponding complex was investigated. Instead of a methyl residue, a sterically bulkier isopropyl group was chosen which supposedly could provide a more diastereoselective complexation or facilitate the subsequent isomerization. Due to the corresponding picolyamine **132** not being commercially available, a suitable synthetic pathway was examined to obtain the chiral

Results and Discussion

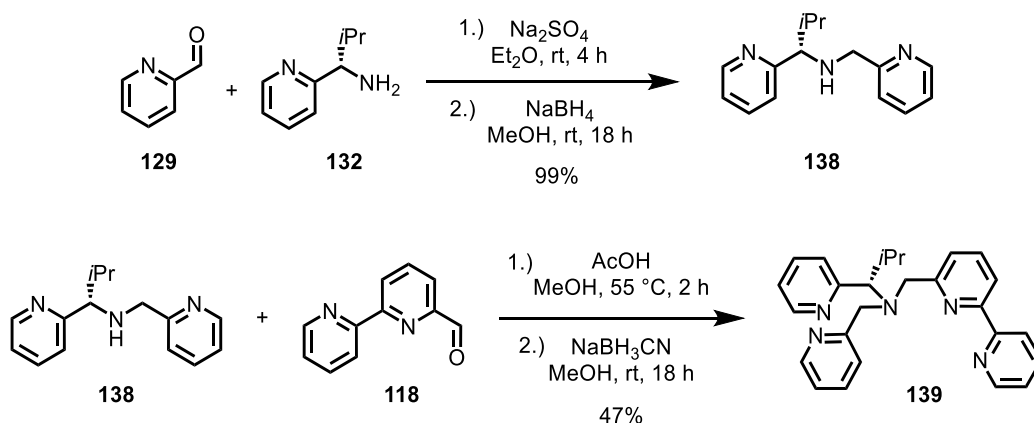
building block with high enantiopurity. A protocol reported by the group of Chelucci^[149] was chosen that commenced with a reaction of commercially available 2-cyano pyridine (**133**) with *i*PrMgCl yielding ketone **134** in 80%. Afterwards, condensation with enantiomerically pure Ellman's sulfinamide (**135**) in presence of activating reagent Ti(OEt)₄ gave imine **136** in a modest yield of 36%. Subsequent imine reduction with NaBH₄ provided a mixture of the two diastereomers **137a** and **137b** that could be separated by column chromatography on silica gel to furnish highly diastereomerically pure (dr >20:1) products. Ultimately, cleavage of the sulfinyl moiety under acidic conditions gave enantiomerically pure picolylamine **132**. The synthetic route is depicted in Scheme 35.



Scheme 35: Synthetic pathway to access chiral picolylamine building block **132** as reported by the Chelucci group.^[149]

With enantiomerically pure picolylamine (*S*)-**132** in hand, the pentadentate chiral ligand was synthesized in analogy to the synthesis of ligand **127**. Reductive amination with aldehyde **129** conveniently gave dipicolylamine **138** in quantitative yield. Subsequent reductive amination provided the final pentadentate ligand **139** in 47% yield after purification (Scheme 36). Notably, purification of desired compound **139** exhibited a strong dependency of the mobile phase during column chromatography on the furnished yield. For example, when silica gel was used, a significant drop of yield to 18% was observed possibly due to decomposition. Similar results and, furthermore, an adverse effect on the purity were obtained when neutral alumina was applied. Ultimately, column chromatography on basic alumina proved to be most efficient in regard to yield and purity.

Results and Discussion

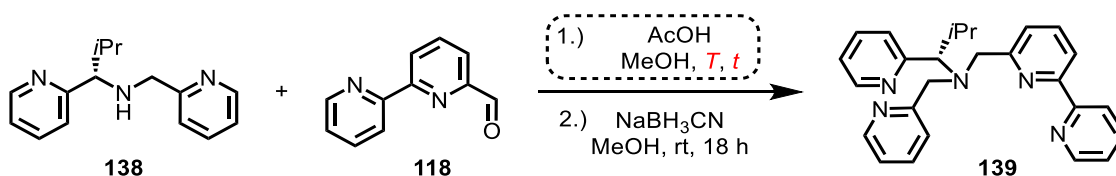


Scheme 36: Synthesis of pentadentate ligand **139** comprising an *i*Pr-moiety as chiral lever.

When the first step of the final reductive amination was conducted at higher temperatures and stirred for a prolonged time, the yield could be improved to 60%. However, due to a possible application of the complexes as catalysts for asymmetric transformations, the enantiomeric purity of the ligand and, consequently, of the iron complex is of high priority to ensure an efficient stereinduction. Accordingly, different temperatures were applied and their effect on the yield and the ee of compound **139** were determined (Table 1). Conspicuously, the conditions of the condensation can induce a significant racemization depending on the applied temperature and reaction time. With standard conditions, final compound **139** was obtained with an ee of 99% (Table 1, entry 1). Prolonging the reaction time from 2 h to 4 h was accompanied by a minor racemization with an enantiomeric excess of 98% (entry 2). When higher temperatures were applied, the optical purity significantly dropped while the yield could be increased up to 60% (entries 3–5). Furthermore, the effect of the activating agent was evaluated. When AcOH was omitted, the reaction proceeded at a slower rate while the enantioselectivity remained at 99% ee (entry 6). Increasing the amount of acid provoked a higher degree of epimerization giving desired compound **139** in 48% yield with 92% ee (entry 7) implying that acidic conditions accelerate the formation of the undesired enantiomer by racemization. The application of formic acid instead of acetic acid provided ligand **139** with 99% ee, however, a significant drop in yield was obtained (entry 8). Ultimately, the conditions stated in entry 1 were chosen as standard conditions due to a focus on enantioselectivity, albeit other conditions provided higher yields.^[150]

Results and Discussion

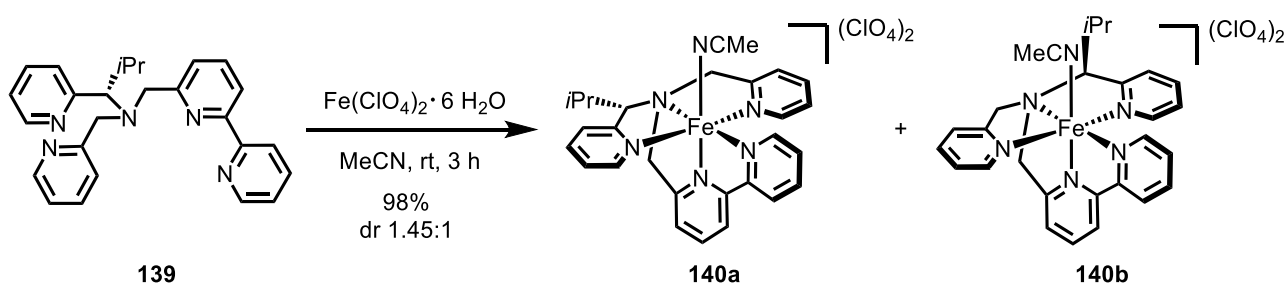
Table 1: Survey of Reaction Conditions for Final Reductive Amination.^a



entry	<i>T</i> (°C)	<i>t</i> (h)	yield (%) ^b	ee (%) ^c
1	55	2	47	99
2	55	4	50	98
3	70	2	52	97
4	70	4	60	94
5	65	2	48	98
6^d	70	4	20	99
7^e	55	2	55	92
8^f	55	2	30	99

^aReaction conditions: A flame dried Schlenk flask was charged with aldehyde **118** (1.00 eq.), dipicolylamine **138** (1.30 eq.), and MeOH (0.13 M) under inert gas atmosphere. Afterwards, AcOH (0.50 eq.) was added and the resulting mixture was stirred for the indicated time at the stated temperature. Subsequently, the reaction was treated with NaBH₃CN (6.00 eq.) and stirred for 18 h at rt. ^bIsolated yield. ^cEnantiomeric excess was established by HPLC analysis on a chiral stationary phase. ^dReaction was conducted without AcOH. ^eReaction was conducted with 1.00 eq. of AcOH. ^fReaction was conducted with formic acid (0.50 eq.) instead of AcOH.

After establishing the optimal conditions for the ligand synthesis, **139** was employed in a complexation reaction to obtain diastereomeric complexes **140a** and **140b** with a dr of 1:1.45 (Scheme 37).



Scheme 37: Complexation with chiral pentadentate ligand **139** to form diastereomeric complexes **140a** and **140b** with a dr of 1:1.45.

Again, analysis of the diastereomeric mixture was feasible via ¹H NMR spectroscopic measurements showing that a slightly increased diastereoselectivity during complexation is realized with the *i*Pr-moiety when compared to the complex comprising the methyl substituted ligand **127**. The ¹H NMR spectrum of the obtained product is depicted in Figure 17.

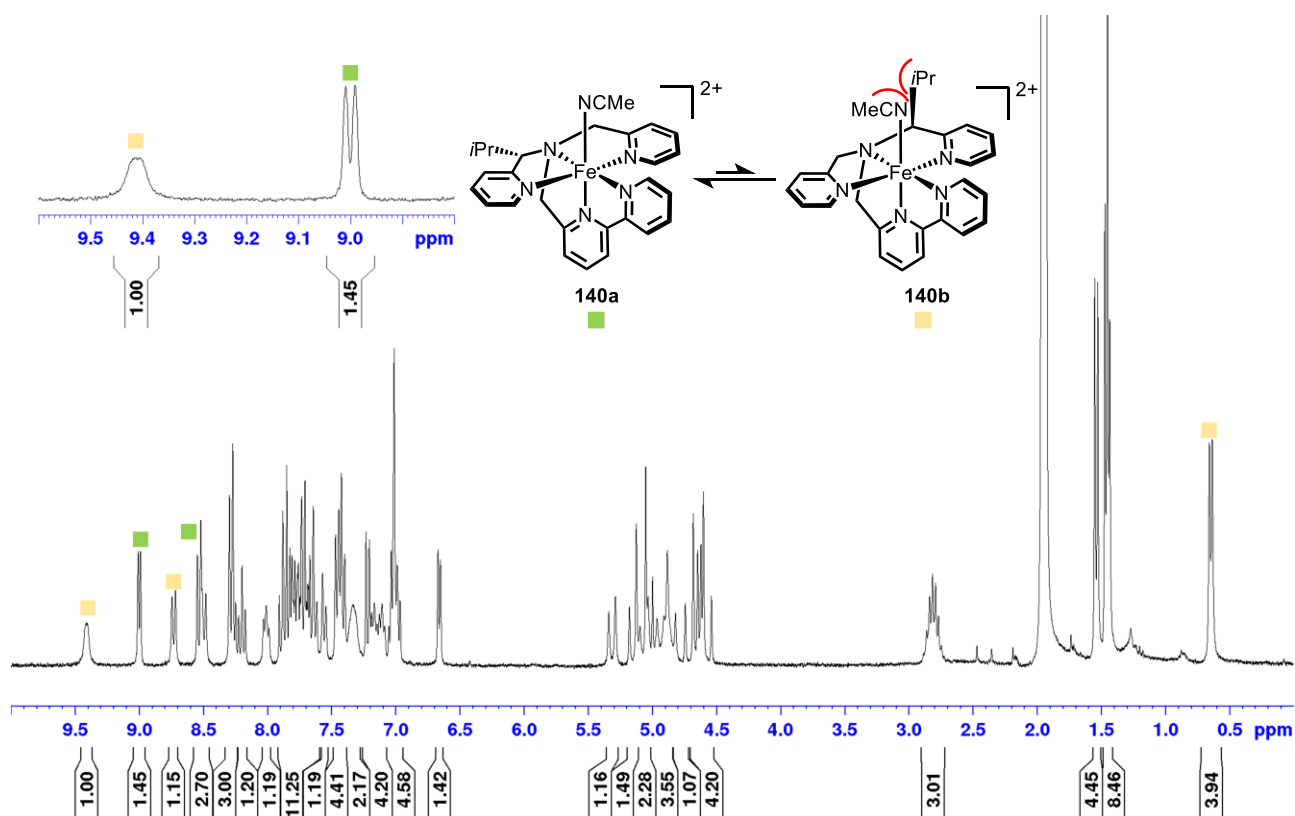


Figure 17: ^1H NMR spectrum (300 MHz, rt, CD_3CN) of the product mixture obtained after complexation.

Afterwards, isomerization of the diastereomeric mixture was realized by stirring in acetonitrile at rt and 70 °C. Diastereomeric ratios were determined by ^1H NMR measurements of the obtained product mixture to evaluate the effect of the bulkier *iPr*-group on this interconversion (Figure 18). Gratifyingly, implementation of the sterically more demanding chiral lever accelerated the rate of isomerization. After stirring for 24 h at rt, a dr of 1:3.72 was observed that improved to >20:1 after an additional 24 h, hence, providing a virtually diastereomerically pure complex mixture. Moreover, complete conversion to the desired thermodynamically more stable diastereomer could be achieved after 16 h when an elevated temperature of 70 °C was applied. Furthermore, a possible bypassing of complex isolation prior to the isomerization was tested by conducting the coordination at elevated temperatures for longer times. However, no complete isomerization after 48 h at 50 °C was detected and ^1H NMR analysis revealed minor formation of an unidentified species, indicating that these conditions could result in decomposition. Therefore, ancillary isolation of the diastereomeric mixture prior to isomerization was maintained to ensure a high purity without any decomposition products forming.

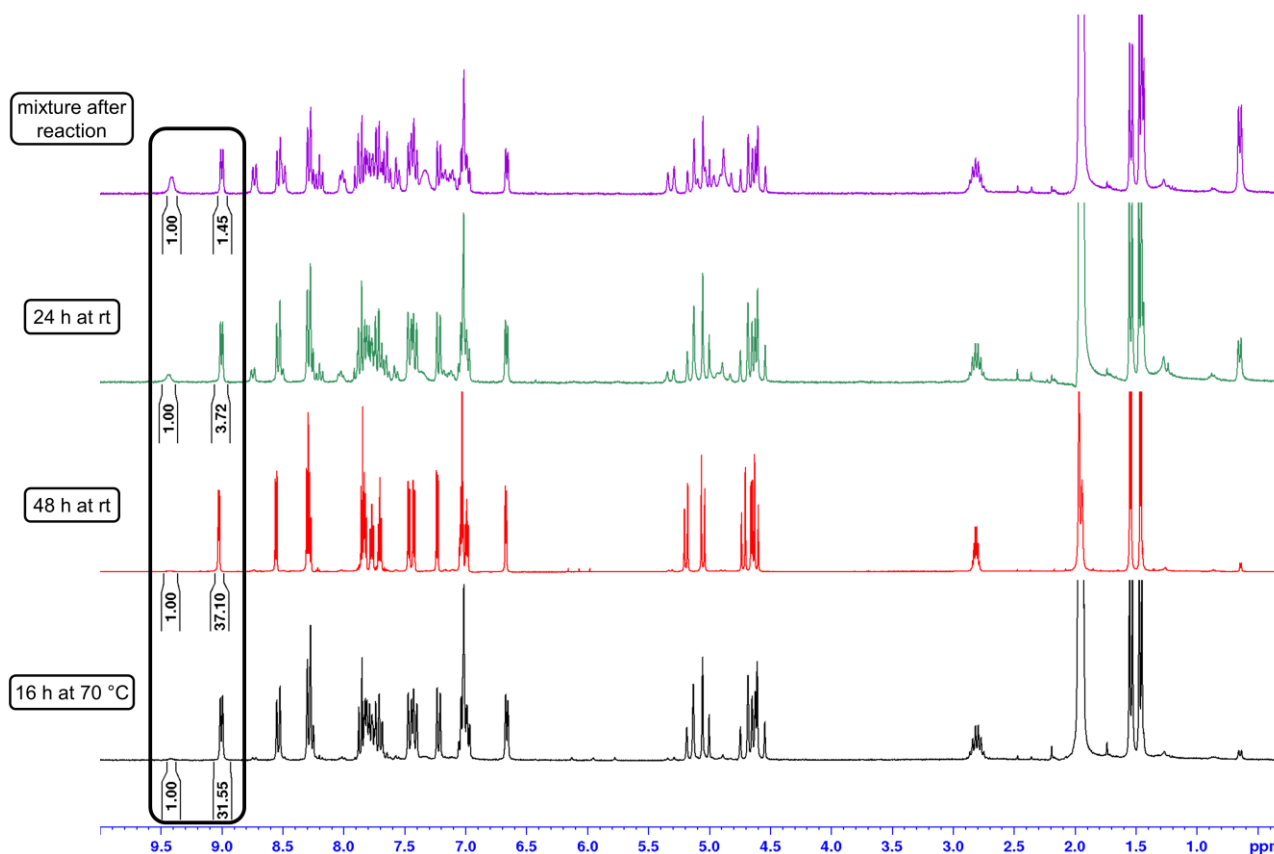


Figure 18: ^1H NMR spectra (CD_3CN , 300 MHz, rt) of the diastereomeric mixture after stirring complexes **140a** and **140b** at the stated temperature for the noted time. The signals used to determine the diastereomeric ratio are highlighted.

3.2.3 Structural Elucidation of the Diastereopure Stereogenic-at-Iron Complex

With diastereomerically pure complex in hand, a full NMR signal assignment for further insights into the kinetics and complexation of the ligand was performed in cooperation with Dr. Xiulan Xie from the Philipps-Universität Marburg. Furthermore, such measurements were supposed to provide a structural elucidation and verify the conformation of the isolated diastereomer. For this purpose, the tripodal pentadentate ligand **139** was divided into three segments as illustrated in Figure 19 by different colors. Analysis of DQF-COSY and TOCSY spectra exhibited spin systems and connection within the segments. The HMBC spectrum confirmed the long-range connectivity among them, ultimately providing the possibility to assign every signal in the ^1H NMR spectrum (Figure 19).

Results and Discussion

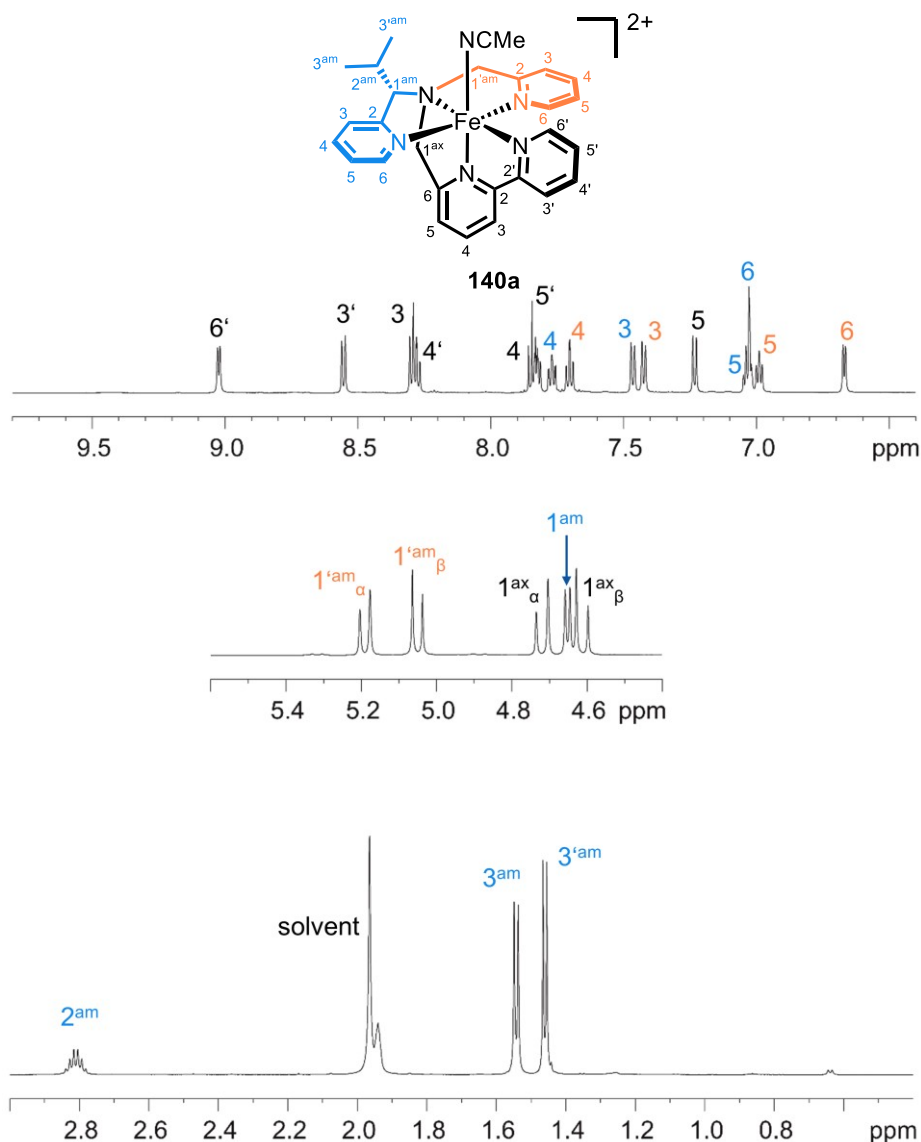


Figure 19: Significant excerpts of the ^1H NMR (CD_3CN , 600 MHz, rt) spectrum of iron complex **140a** and corresponding signal assignments.

On the basis of the complete assignment, unambiguous NOE interactions among the aliphatic protons of the isopropyl moiety of the ligand, the methine, and the methylene groups at the α -positions of the tertiary amine could be identified. The pattern of cross peaks and NOE interactions depicted in Figure 20 strongly indicates that the *i*Pr-group of the ligand is facing away from the labile MeCN ligand. NOE measurements of the diastereomeric mixture further confirmed the structure assignment (for further information, see Section 5.3.4.1).^[150]

Subsequently, a single crystal suitable for X-ray crystallographic analysis was obtained to confirm the structure of complex **140a**, hence, reassuring that the structures in solution and the solid state are identical. Additionally, the crystal structure confirmed that the dipicolylamine motif in the ligand framework is coordinating in a meridional fashion (Figure 21).

Results and Discussion

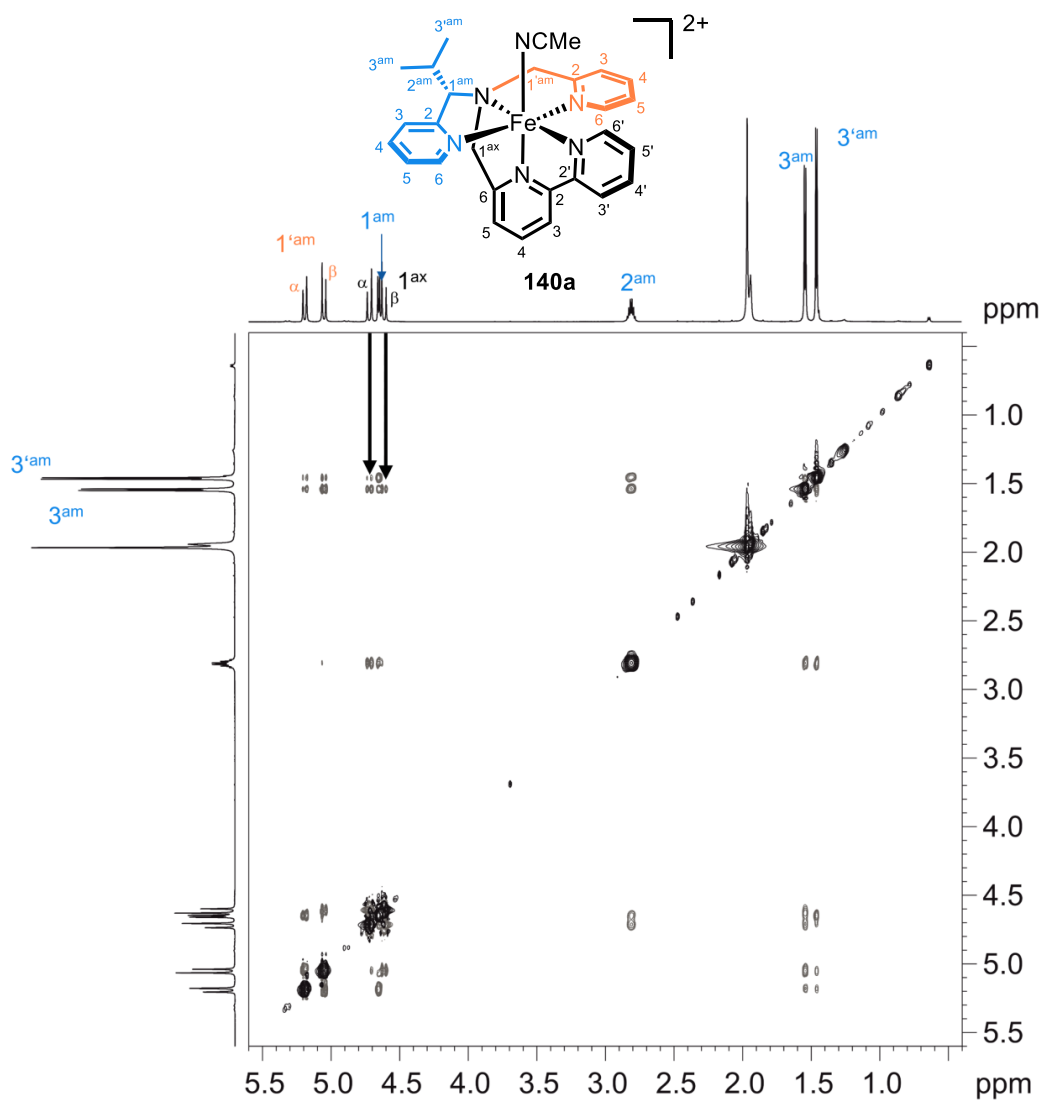


Figure 20: Section of the ^1H - ^1H NOESY spectrum of diastereomer **140a** showing interactions among the aliphatic fragments. The spectrum was recorded on an AVII 600 at rt with a mixing time of 0.5 s.

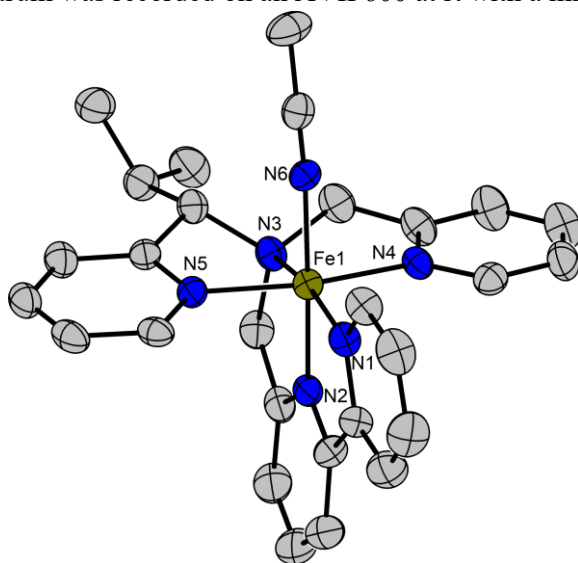


Figure 21: X-ray crystallographic structure of complex **140a** as an ORTEP drawing with 50% probability thermal ellipsoids. Perchlorate counterions and solvent molecules are omitted for clarity.

Results and Discussion

Next, studies in other solvents were conducted to gain additional insights into the coordination characteristics. Unfortunately, complex **140a** exhibited an insufficient solubility in various solvents besides acetonitrile for further NMR spectroscopic analysis. Gratifyingly, dichloromethane provided an ample solubility facilitating NMR measurements. At rt, the spectrum only showed broad peaks with no possibility of distinguishing between single signals. Interestingly, at 0 °C more defined peaks were observed and, accordingly, at -10 °C a well-defined spectrum was obtained. Such a temperature dependency could be explained by a more rigid coordination of the ligand to the metal center in methylene chloride at lower temperatures, indicating that the configurational stability is lower when compared to MeCN (Figure 22).^[150]

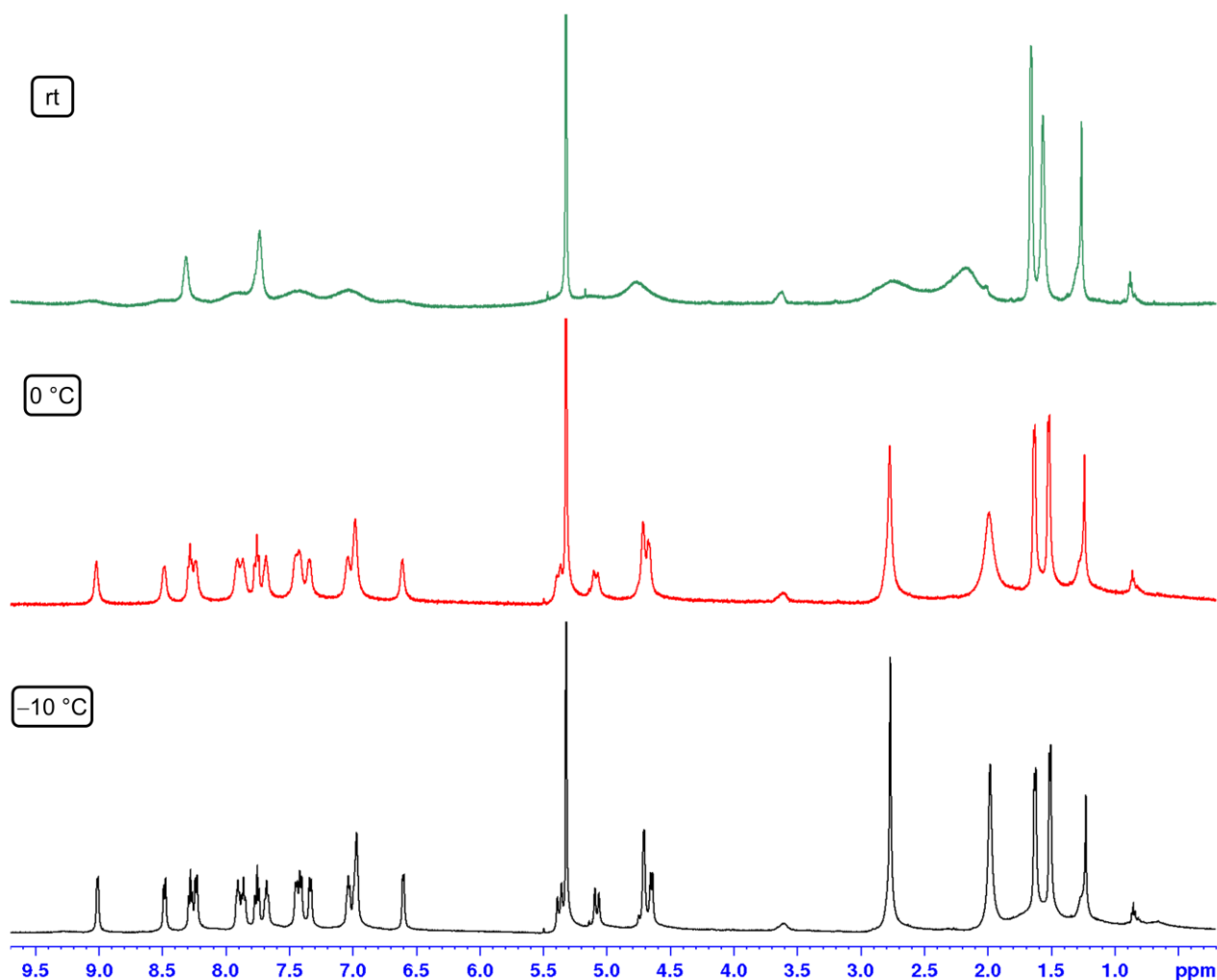


Figure 22: ¹H NMR (CD₂Cl₂, 600 MHz) of complex **140a** at different temperatures. The signals get more defined when measurements were conducted at lower temperatures implying a rather strong influence of the solvent on the configurational stability.

With the possibility of conducting NMR spectroscopic measurements in CD₂Cl₂, kinetic investigations concerning the lability of the acetonitrile ligand were feasible. By using a mixture of CD₂Cl₂ and MeCN (4% v/v of MeCN), ROESY measurements were performed to determine the

chemical exchange of metal-bound solvent molecules with “free” MeCN. The cross peaks illustrated in Figure 23 confirm this ligand to be the most labile site of the complex and EXSY experiments provided further insights into the exchange rate for complex **140a** which was determined to be 6 s^{-1} (see Section 5.3.4.1).

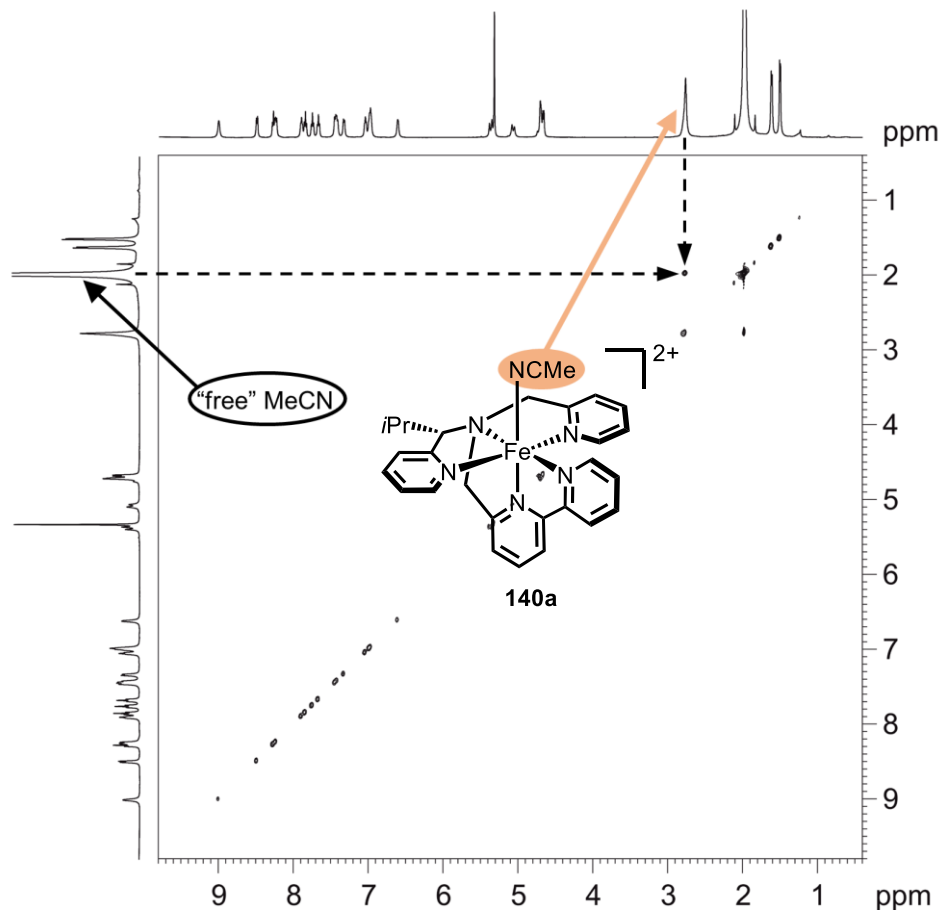


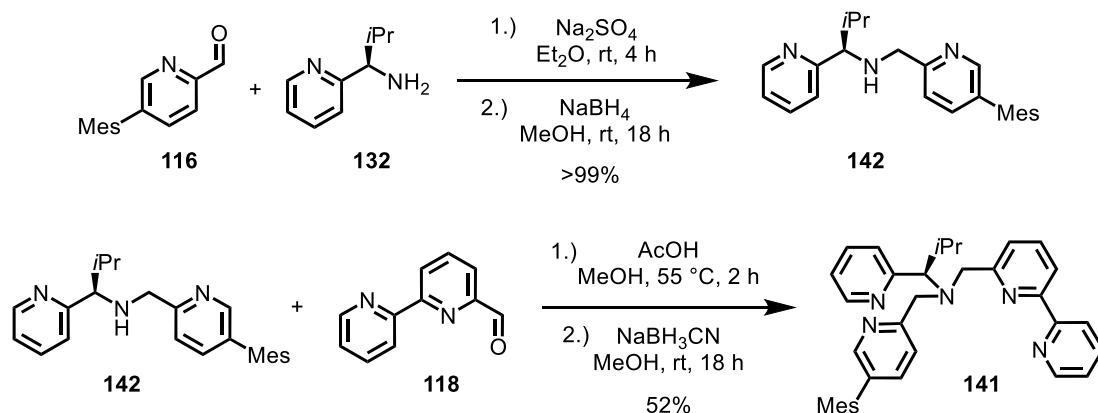
Figure 23: ROESY (500 MHz, 0 °C, mixing time 50 ms) spectrum of **140a** in CD₂Cl₂/MeCN (4% v/v of MeCN).

3.2.4 Modifications of the Pentadentate Ligand Scaffold

With the possibility of conveniently exploiting the chiral lever to furnish diastereomerically pure iron complexes and the structural elucidation by X-ray crystallographic and NMR spectroscopic analysis, possible modifications in the ligand scaffold were tested. Specifically, implementation of a sterically demanding mesityl group on one of the pyridine rings and application of a different bidentate coordinating aryl moiety instead of the 2,2'-bipyridine motif were set to be investigated. Considering a potential employment of the complexes as catalysts for asymmetric transformations, these diversifications of the framework can provide helpful information about their effects on the stereoinducing capabilities.

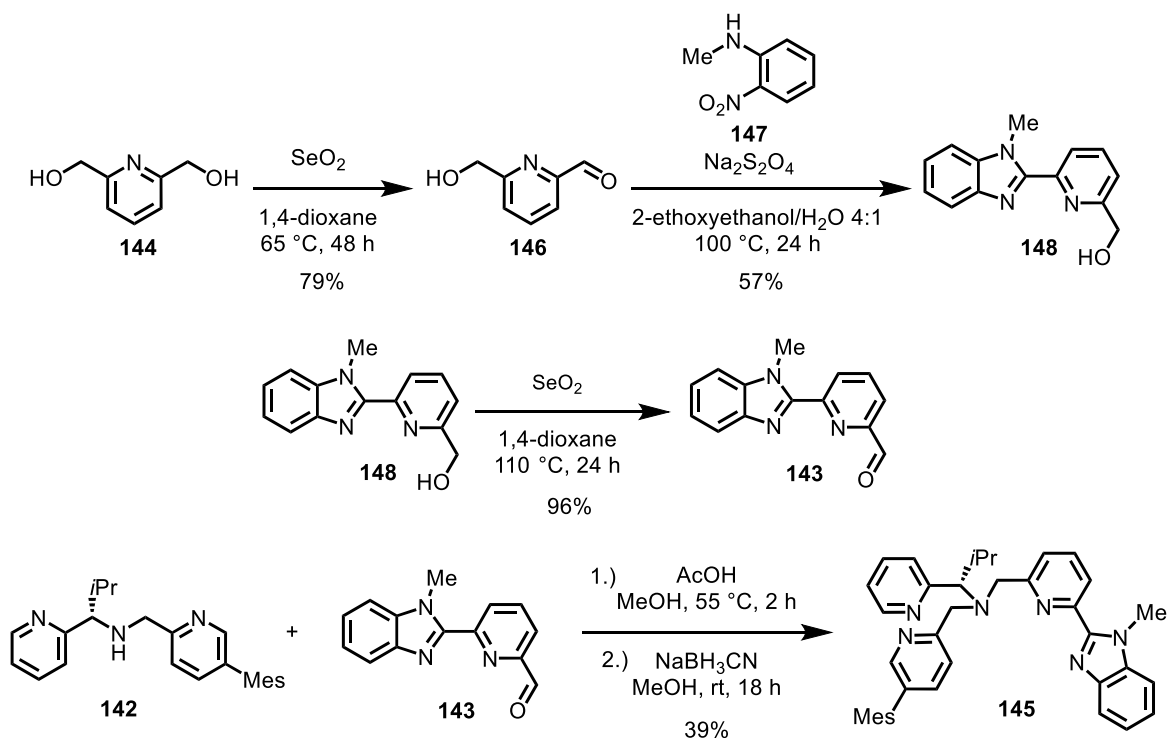
Results and Discussion

Accordingly, chiral pentadentate ligand **141** was synthesized via the established route by conducting two consecutive reductive aminations as illustrated in Scheme 38. Enantiomeric purity of the desired compound **141** was evaluated by HPLC analysis on a chiral stationary phase and determined to be 99%.



Scheme 38: Synthesis of mesityl substituted pentadentate chiral ligand **141** via the established synthetic route.

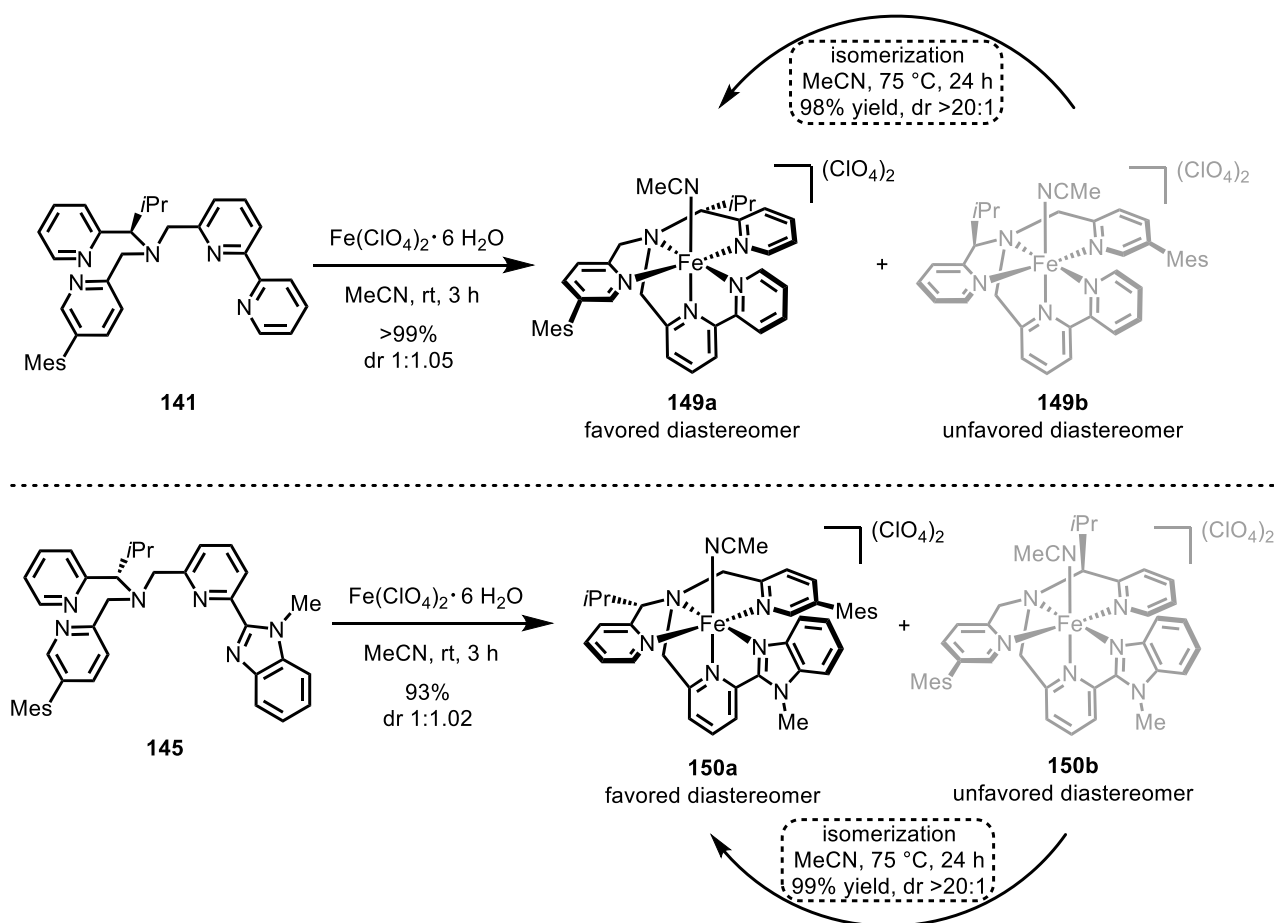
Next, implementation of a benzimidazole moiety into the scaffold was realized by synthesis of aldehyde building block **143** via a three-step procedure by the Beller group starting from commercially available pyridine-2,6-dimethanol (**144**).^[151] The obtained benzimidazole aldehyde **143** was subsequently converted to the desired chiral pentadentate ligand **145** via the established reductive amination in 39% yield. Determination of the enantiomeric purity of the furnished ligand confirmed an excellent optical purity with 99% ee (Scheme 39).



Scheme 39: Synthesis of benzimidazole building block **143** starting from commercially available pyridine-2,6-dimethanol (**144**) and subsequent conversion to final pentadentate ligand **145**.

Results and Discussion

With enantiomerically pure ligands **141** and **145** in hand, complexation with iron(II) perchlorate conveniently provided the desired iron complexes. Noteworthy, the diastereoselectivity was lower when compared to ligands **127** and **139**. When mesityl substituted compound **141** was applied, diastereomeric complexes **149a** and **149b** were formed with a dr of 1:1.04 (Scheme 40, top). Likewise, when benzimidazole ligand **145** was employed for complexation, almost no diastereoselectivity during the formation of **150a** and **150b** (1:1.02) was observed (Scheme 40, bottom). Notably, isomerization of both complex mixtures required prolonged reaction times of 24 h and a slightly increased temperature of 75 °C to furnish diastereomerically pure iron compounds **149a** and **150a** (dr >20:1) as determined via ¹H NMR analysis. The longer reaction time and higher activation barrier of the interconversion could be rationalized by the higher steric demand of the ligands impeding this transformation.



Scheme 40: Complexation and isomerization with ligand **141** (top) and ligand **145** (bottom) to furnish diastereomerically pure chiral Fe(II)-complexes **149a** (top) and **150a** (bottom).

Subsequently, a single crystal suitable for X-ray diffraction analysis of complex **149a** was obtained again confirming the favored structure to comprise a chiral *i*Pr-moiety pointing away from the catalytically active site as shown in Figure 24. Attempts of growing single crystals of benzimidazole iron compound **150a** were not successful, probably due to decomposition during crystalization.

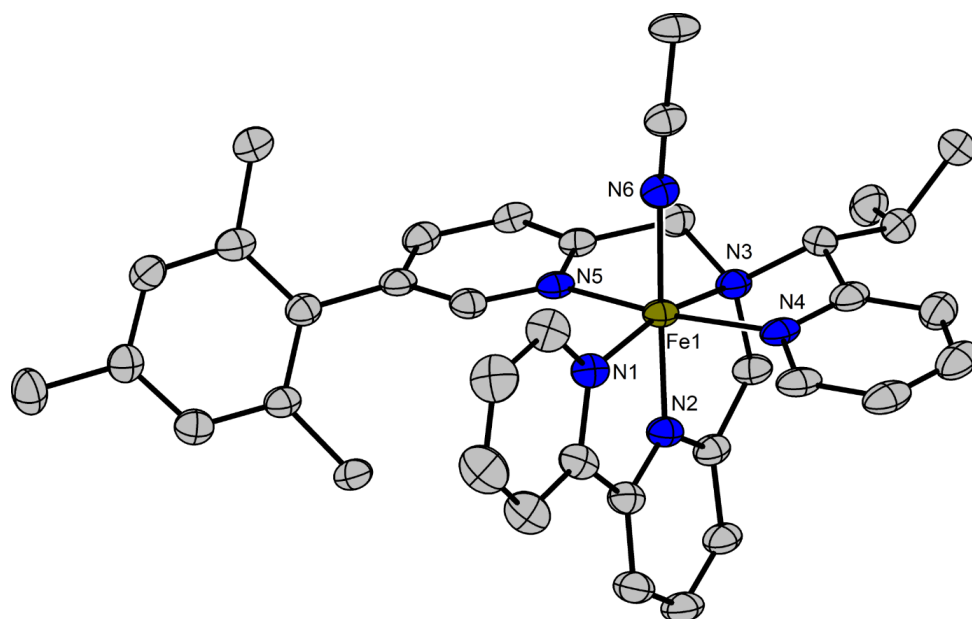


Figure 24: X-ray crystallographic structure of complex **149a** as an ORTEP drawing with 50% probability thermal ellipsoids. Perchlorate counterions and solvent molecules are omitted for clarity.

Having established a synthetic pathway to access diastereomerically pure stereogenic-at-iron complexes with chiral pentadentate ligands, next, their efficiency during asymmetric catalysis was planned to be scrutinized. The results of this survey will be discussed in the following chapter.

3.2.5 Concluding Remarks

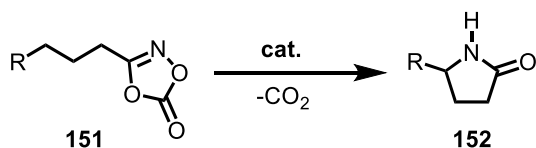
To summarize, a synthetic access towards diastereomerically pure stereogenic-at-iron complexes comprising chiral pentadentate ligands has been achieved. Incorporation of a chiral lever into the ligand framework conveniently granted the possibility of an isomerization to exclusively furnish a single diastereomer after interconversion. Subsequent modification of the chiral ligand showed that by choosing a sterically more demanding lever group, the isomerization can be improved in regards to reaction time, affording the desired pure complexes after stirring at elevated temperatures overnight. Moreover, a structural elucidation via NMR spectroscopic measurements granted further insights into the coordination topology of the ligand and provided crucial information about the kinetics of the Fe(II)-complexes. Analysis of X-ray crystallographic data of two complexes confirmed the structural proposal obtained by NMR measurements. Interestingly, upon complexation, the dipicolylamine motif of the ligand coordinates in a meridional fashion in contrast to the iron complexes introduced by the Kaizer group, that exhibit a facial coordinating dipicolylamine unit. As a consequence, this topology can potentially give birth to a unique sophisticated chiral environment beneficial during asymmetric catalytic transformations. The results of the application as chiral catalysts will be discussed in the following chapter.

3.3 Application of Iron Complexes with a Chiral Pentadentate Ligand in Asymmetric Catalysis

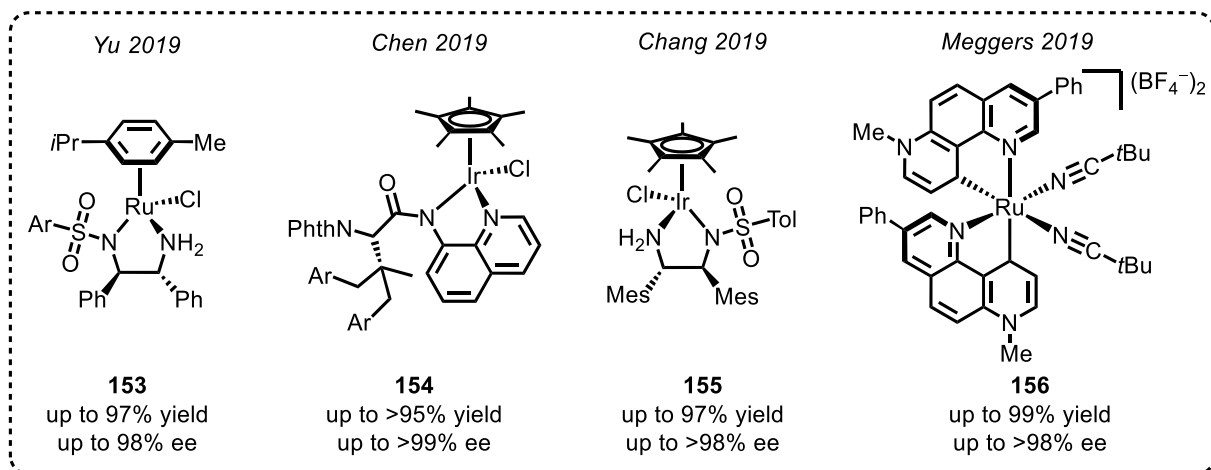
3.3.1 Initial Survey of Application in Asymmetric Catalysis

As discussed in Section 3.1.1, chiral iron complexes with pentadentate ligand frameworks have exclusively been applied to oxidation reactions as catalysts. Therefore, investigation of a possible application in other reaction types is an enticing endeavor due to the possibilities such a unique overall topology could provide in regard to activity and selectivity.

In recent years, the enantioselective formation of C-N bonds has specifically attracted a lot of attention due to nitrogen appearing in countless biologically active chiral compounds.^[152,153] Remarkably, transition metal nitrenes have lately been shown to provide a convenient access to chiral nitrogen-containing compounds.^[89,154–160] A prominent organic precursor for the formation of metal nitrenoid intermediates is represented by 1,4,2-dioxazol-5-ones **151** as intriguingly shown in 2018 by the group of Chang for an Ir-catalyzed C-H amidation to furnish γ -lactams **152**.^[161] Subsequently, catalytic enantioselective versions of this reaction have been reported emphasizing the versatility of this nitrene-precursor (Scheme 41).^[109,162–164]



Catalysts

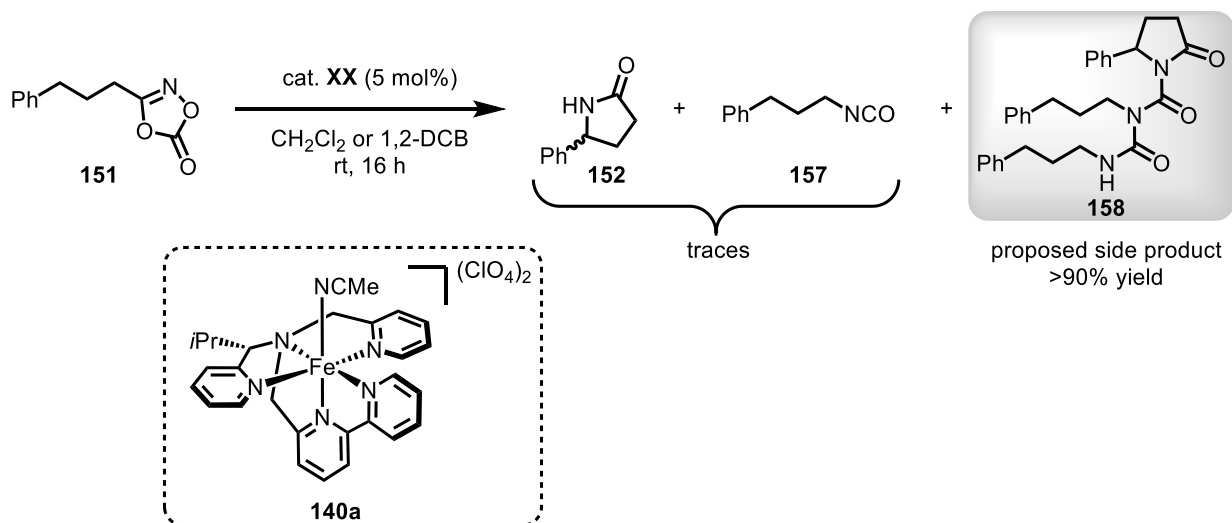


Scheme 41: Enantioselective, intramolecular C(sp³)-H amidation of 1,4,2-dioxazol-5-ones **151** and applied catalysts.^[109,162–164]

Due to numerous publications about iron-nitrene mediated reactions,^[165–167] the possibility of applying the complexes introduced in this work to an intramolecular C-H amidation with dioxazolones was investigated. Complex **140a** was chosen as the standard catalyst for initial

Results and Discussion

feasibility studies because of its established synthetic access, extensive structural elucidation, and more easily accessible catalytically active reaction site. Accordingly, based on a procedure by the Meggers group,^[109] substrate **151** was applied to a reaction in the presence of 5 mol% catalyst **140a** in methylene chloride or 1,2-dichlorobenzene as solvents. However, NMR spectroscopic analysis of the crude product revealed that desired γ -lactame **152** and undesired Curtius-rearrangement product **157** were formed only in traces while the conversion was complete. However, major amounts (>90% yield) of an undesired side product were detected. Further evaluation of the NMR spectra in combination with mass spectroscopic analysis suggests that upon product- and isocyanate-formation, a subsequent, iron-catalyzed hydroamination to form **158** would match the analytical data obtained during this reaction (Scheme 42). Furthermore, this assumption is supported by a report from 2019 by the groups of Geer and Kays about an iron(II)-catalyzed hydroamination of isocyanates.^[168]

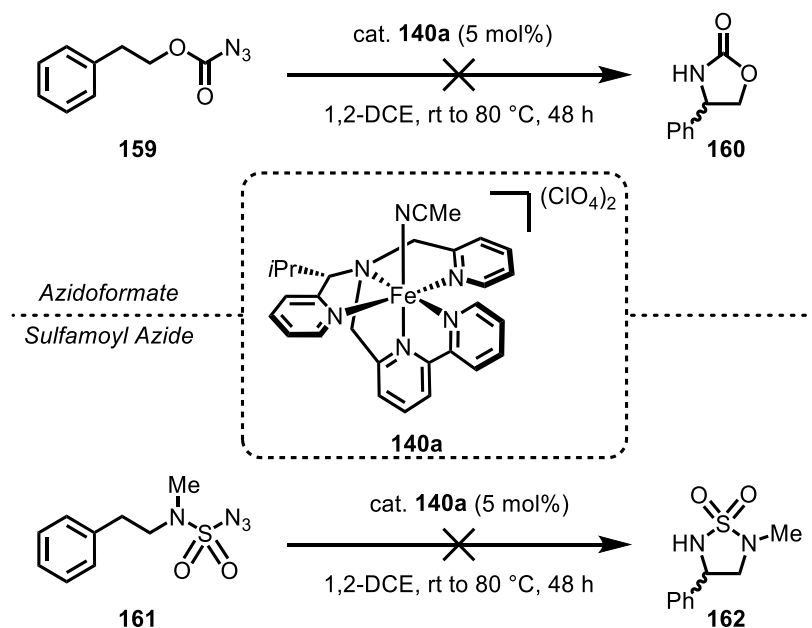


Scheme 42: Intramolecular C(sp³)-H amidation in presence of catalyst **140a**. Desired product **152** and Curtius rearrangement product **157** were only observed in traces. NMR and mass spectroscopic data lead to the proposed structure of hydroamination product **158**.

Another type of precursor for the formation of reactive transition metal nitrene intermediates is represented by azides.^[169] Previously, these compounds have been reported to form active iron-nitrene species suitable for C-N bond formation reactions.^[170–173] Therefore, preactivated azides^[169] were considered as potential precursors for the novel Fe(II)-complexes presented in this work. Initial experiments with catalyst **140a** and azidoformate **159** were conducted to evaluate the feasibility of an intramolecular C(sp³)-H amination to furnish cyclic carbamate **160**. When the reaction was performed in 1,2-DCE at rt, no conversion was observed after 24 h. Consequently, the reaction temperature was gradually increased due to similar reactions being achieved only at elevated temperatures.^[172] However, even at a higher temperature of 80 °C, no conversion was observed implying that complex **140a** is not capable of forming the nitrene species (Scheme 43, top). Higher

temperatures were not tested due to a potential decomposition of the catalyst system.

A different type of azide precursor for nitrene mediated transformations is depicted by sulfamoyl azides and sulfonyl azides. In previous reports, this class of compounds has proven to be a suitable precursor for an intramolecular C-H amination with various catalysts.^[174–178] Moreover, in 2019, the group of Arnold reported an enzymatic, iron-mediated version of this reaction showing that iron can serve as a suitable catalyst to facilitate this conversion.^[179] Hence, the reaction was conducted with complex **140a** in 1,2-DCE to convert sulfamoyl azide **161** to the desired product **162**. Again, no conversion was observed even when higher temperatures up to 80 °C were applied rendering the application of catalyst **140a** for this type of nitrene precursors not sufficient (Scheme 43, bottom).



Scheme 43: Intramolecular C(sp³)-H amination of azidoformate **159** (top) and sulfamoyl azide **161** (bottom) in presence of catalyst **140a**. Even at elevated reaction temperatures of 80 °C, no conversion was observed. Higher temperatures were not applied due to possible decomposition of complex **140a**.

3.3.2 Asymmetric 2*H*-Azirine Synthesis via Ring Contraction of Isoxazoles

In 2018, the Ohe group presented a rhodium- and iridium-catalyzed enantioselective synthesis of 2*H*-azirines via ring contraction of isoxazoles to furnish tetrasubstituted stereocenters with up to 94% ee.^[180] Following this report, Meggers *et al.* achieved a ruthenium-catalyzed version of this transformation in 2020 with a catalyst comprising a meridional coordinating tridentate PyBOX-motif and a cyclometalated bidentate NHC-ligand.^[174] This complex was shown to furnish chiral 2*H*-azirines with up to 97% ee while exhibiting an exceptional activity (turnover number (TON) up to 2000). The overall topology of ruthenium catalyst **163** is comparable to the coordination topology of

Results and Discussion

complex **140a** comprising a pentadentate ligand as illustrated in Figure 25. Moreover, with iron being the lighter congener of ruthenium, potentially a similar reactivity during this conversion could be expected.

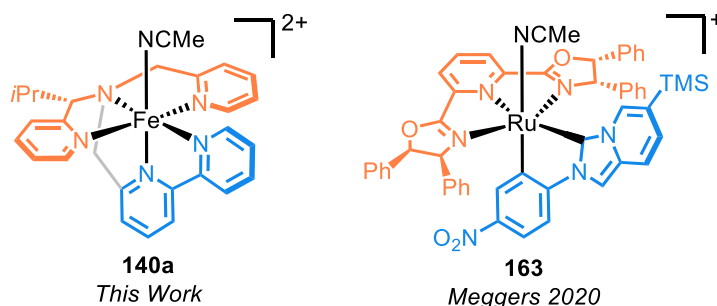
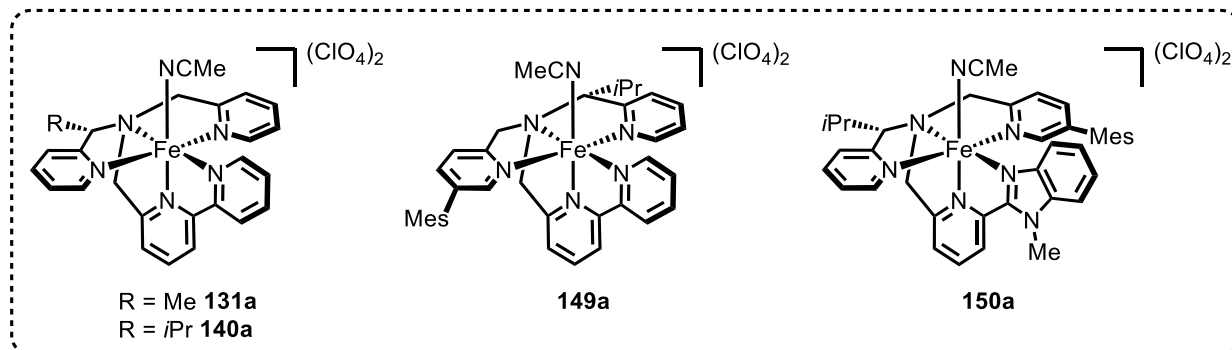
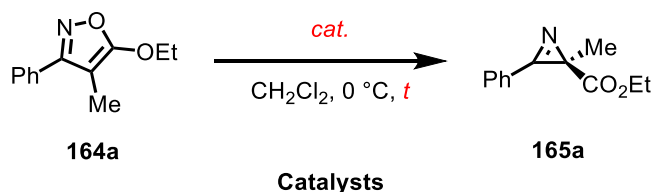


Figure 25: Structural resemblance of complex **140a** with a pentadentate ligand and ruthenium catalyst **163**.

Gratifyingly, an initial reaction with iron(II) complex **140a** as catalyst and isoxazole **164a** as substrate showed an exceptionally high activity of this catalytic system. Full conversion to the desired product was observed in under 1 min reaction time at rt in presence of 4 mol% catalyst when CH_2Cl_2 was used as solvent. A comparably high activity was observed for the other iron catalysts (Table 2). Furthermore, an evaluation of the enantioselectivity at a lowered temperature of 0 °C gave a first impression on the stereoinducing capabilities of the catalysts. When compound **131a** with a methyl group as chiral lever was applied, product **165a** was formed with a low selectivity of 6% ee (Table 2, entry 1). The stereoselectivity could be improved when the reaction was conducted in presence of catalyst **140a** providing quantitative yield with 16% ee. By implementation of sterically more demanding modifications on the ligand framework the enantioselectivity was further improved (entries 3 and 4). For example, iron complex **149a** comprising an additional mesityl group on the pyridine ring conveniently facilitated the asymmetric ring contraction, consequently granting 2*H*-azirine **165a** with an enantioselectivity of 32% (entry 3). Interestingly, substitution of the 2,2'-bipyridyl motif by a (1-methyl-1*H*-benzimidazol-2-yl)pyridine-2-yl unit significantly enhanced the stereoinduction, thus showing the importance of this position on the overall topology in order to achieve a sophisticated chiral environment for a satisfying stereoinduction. Accordingly, the desired product was obtained with 66% ee by application of complex **150a** as catalyst (entry 4). Due to the exceptionally high activity of these iron(II) systems, a decrease of the catalyst loading to 1 mol% for a subsequent optimization of reaction conditions was evaluated. Again, full conversion was observed in a very short reaction time of only 2 min (entry 5). This fast conversion conveniently granted the opportunity to further improve and optimize reaction conditions to enhance the stereoselectivity. Considering catalyst **150a** exhibiting the highest stereoinduction, this complex was chosen for further optimizations of this catalytic transformation.^[150]

Results and Discussion

Table 2: Initial Catalyst Screening for Ring Contraction of Isoxazoles **164a**.^a



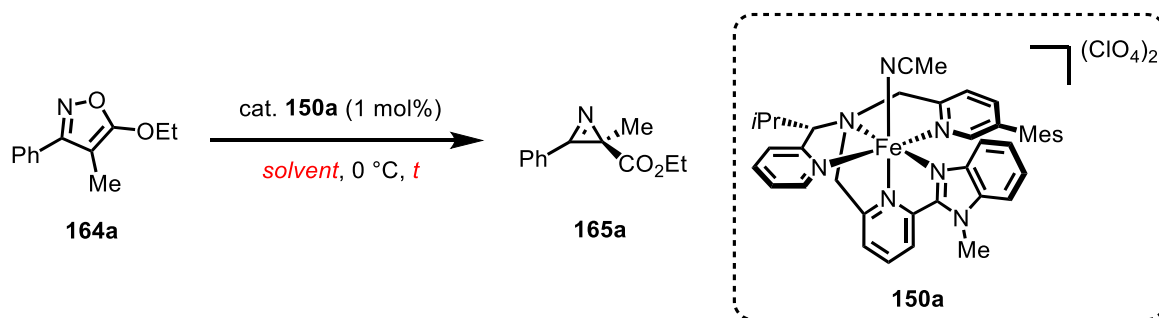
entry	catalyst (mol%)	<i>t</i> (min)	yield (%) ^b	ee (%) ^c
1	131a (4)	1	99	6
2	140a (4)	1	99	16
3	149a (4)	1	99	32 ^d
4	150a (4)	1	99	66
5	150a (1)	2	99	66

^aReaction conditions: Catalyst (1 or 4 mol%) was dissolved in CH₂Cl₂ (0.1 M, 0.5 mL) under inert gas atmosphere and the solution was cooled to 0 °C. Isoxazole **164a** (0.05 mmol) was added and the reaction was stirred until complete conversion of the starting material was observed. Afterwards, the solvent was removed under vacuum and crude ¹H NMR and HPLC were measured. ^bNMR yield with 1,1,2,2-tetrachloroethane as internal standard. ^cDetermined by HPLC analysis on a chiral stationary phase. ^dThe other enantiomer of the product was obtained due to the catalyst being composed of the ligand with (*R*)-configuration.

Afterwards, a survey of finding the most suitable solvent for the ring contraction was conducted (Table 3). When chloroform or MeOH were used, similar results could be obtained in regard to enantioselectivity with the latter solvent slightly retarding the reaction (Table 3, entries 2 and 3). Next, acetone and MeCN were tested (entries 4 and 5). In both solvents a decrease in stereoselection was observed and the desired azirine **165a** furnished with 48% and 49% ee, respectively. Moreover, a significantly lower conversion rate was detected with MeCN which can be rationalized by a competing coordination to the active site by solvent molecules hampering substrate complexation. In regard to enantioselectivity, a reaction set-up with 1,2-DCB as solvent provided the best result with 70% ee at 0 °C (entry 6). For an evaluation of further optimizing the reaction in 1,2-DCB, the catalysis was conducted at –15 °C resulting in an ee of 72%. Consequently, methylene chloride was chosen as solvent for subsequent reactions, albeit 1,2-DCB giving the highest enantioselectivity, due to the possibility of applying lower temperatures to improve the selectivity.

Results and Discussion

Table 3: Survey of Solvents for Asymmetric Ring Contraction.^a



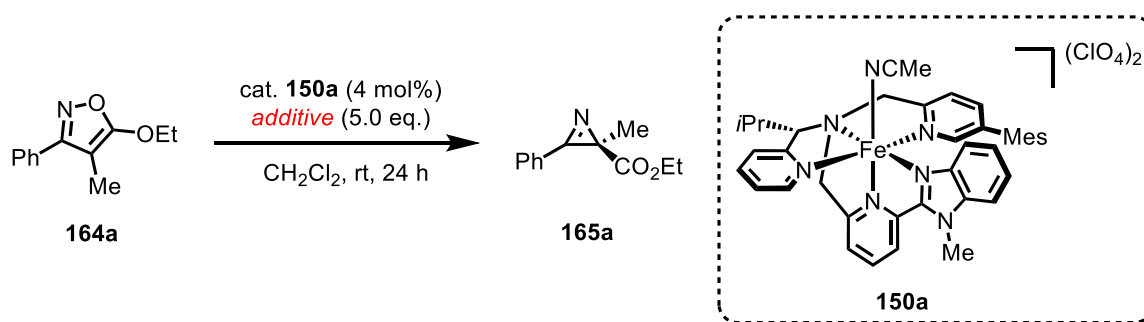
entry	solvent	t (min)	yield (%) ^b	ee (%) ^c
1	CH ₂ Cl ₂	2 min	99	66
2	CHCl ₃	2 min	99	63
3	MeOH	50 min	98	62
4	acetone	5 min	98	48
5	MeCN	180 min	96	49
6	1,2-DCB	8 min	98	70
7^d	1,2-DCB	45 min	97	72

^aReaction conditions: Catalyst **150a** (1 mol%) was dissolved in the indicated solvent (0.1 M, 0.5 mL) under inert gas atmosphere and the solution was cooled to 0 °C. Isoxazole **164a** (0.05 mmol) was added and the reaction was stirred until complete conversion of the starting material was observed. Afterwards, the solvent was removed under vacuum and crude ¹H NMR and HPLC were measured. ^bNMR yield with 1,1,2,2-tetrachloroethane as internal standard. ^cDetermined by HPLC analysis on a chiral stationary phase. ^dReaction was conducted at -15 °C.

As previously described and shown in Figure 22, NMR spectra of complex **140a** in CD₂Cl₂ imply that the chiral tripodal ligand is coordinated more tightly to the metal center at lower temperatures. Considering this indication, lower temperatures could substantially contribute to a more defined overall topology of the complex and, consequently, lead to significantly enhanced enantioselectivities. However, due to the exceptionally high activity of the presented iron catalysts in this reaction, a suitable procedure for an effective quenching of the transformation was set to be established beforehand. For this purpose, the catalysis was performed in presence of different quenching reagents (Table 4). When triethylamine, pyridine, or sodium benzoate were added to the reaction, a significantly lower conversion to the desired product **165a** was observed after 24 h at rt (Table 4, entries 1–3). However, to prevent undesired conversion with lower enantioselectivity during work-up, virtually complete prevention of the transformation was necessary. Gratifyingly, bidentate ligand 2,2'-bipyridine gave sufficient results completely impeding the reaction and was chosen as a suitable quenching reagent (entry 4).

Results and Discussion

Table 4: Screening of a Suitable Quenching Reagent.^a



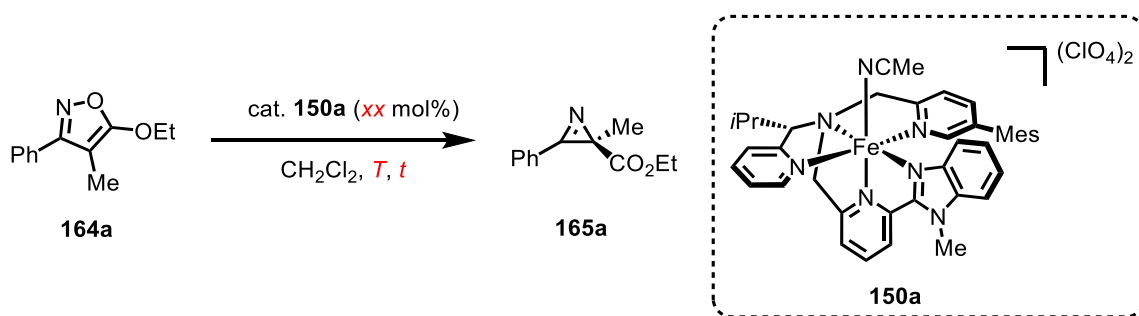
entry	additive	yield (%) ^b
1	NEt_3	53
2	pyridine	27
3	sodium benzoate	45
4	2,2'-bipyridine	no conversion

^aReaction conditions: Catalyst **150a** (4 mol%) and the indicated additive were dissolved in CH_2Cl_2 (0.1 M, 0.5 mL) under inert gas atmosphere at rt. Isoxazole **164a** (0.05 mmol) was added and the reaction was stirred for 24 h at rt. Afterwards, the solvent was removed under vacuum and crude ^1H NMR was measured. ^bNMR yield with 1,1,2,2-tetrachloroethane as internal standard.

With a convenient quenching procedure in hand, the catalysis was conducted at low temperatures for a potential improvement of enantioselectivity (Table 5). When the reaction was performed at $-50\text{ }^\circ\text{C}$, a significantly higher ee of 88% after a prolonged reaction time of 36 h could be achieved providing azirine **165a** in 74% yield (Table 5, entry 2). By further lowering the temperature to $-60\text{ }^\circ\text{C}$, a slightly improved stereoselection was detected (entry 3). To account for the reduced activity, the concentration was raised to 0.2 mol/L and the catalyst loading increased to 2 mol% granting quantitative yield after 20 h reaction time without loss of selectivity (entry 4). Subsequently, the stability of the catalyst in regard to hydrolysis or oxidative decomposition was evaluated (entries 5 and 6). Addition of H_2O showed no disadvantageous effect on the enantioselectivity, albeit the reaction proceeded slightly slower (94% yield) which can be rationalized by a competing complexation of H_2O by the catalyst (entry 5). Conveniently, the presence of air during the reaction neither effected activity nor selectivity, hence enabling a simpler reaction set-up with “open flask” conditions (entry 6). By setting up the catalysis at $-75\text{ }^\circ\text{C}$, a further enhancement of the enantioselectivity to 92% was feasible, however, the yield was significantly lower with 50%. Despite providing a slightly lower enantiomeric excess, the reaction parameters described in entry 6 were chosen as standard conditions for a following substrate scope.

Results and Discussion

Table 5: Concluding Optimization and Control Reactions.^a



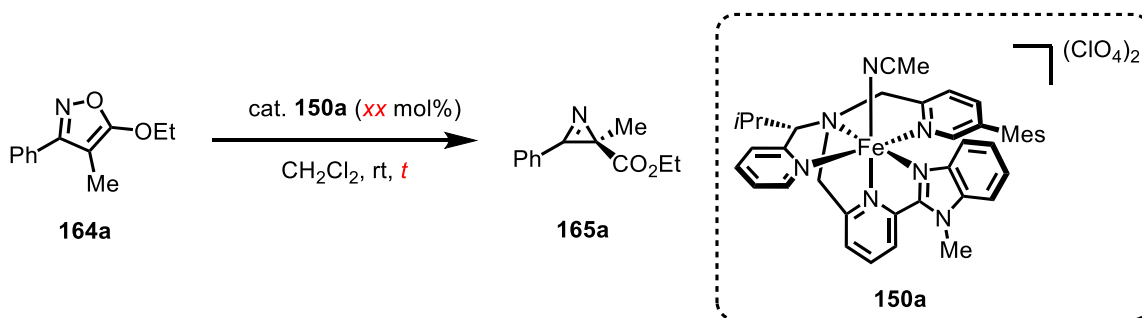
entry	<i>xx</i> (mol%)	concentration (mol/L)	T (°C)	t	yield (%) ^b	ee (%) ^c
1	1	0.1	0	2 min	99	66
2	1	0.1	-50	36 h	74	88
3	1	0.1	-60	36 h	48	89
4	2	0.2	-60	20 h	99	89
5^d	2	0.2	-60	20 h	94	89
6^e	2	0.2	-60	20 h	99	89
7^e	2	0.2	-75	20 h	50	92

^aReaction conditions: Catalyst **150a** (1 mol%) was dissolved in CH_2Cl_2 under inert gas atmosphere, cooled to the stated temperature, and prestirred for at least 15 min. Isoxazole **164a** (0.05 mmol) was added and the reaction was conducted for the stated time. For conditions at -50 °C or lower, the reaction was quenched with 2,2'-bipyridine (0.25 mmol) and stirred for another 30 min at low temperature. Subsequently, the solvent was removed under vacuum and crude ^1H NMR and HPLC were measured. ^bNMR yield with 1,1,2,2-tetrachloroethane as internal standard. ^cDetermined by HPLC analysis on a chiral stationary phase. ^d5.0 eq. of H_2O were added to the reaction. ^eReaction was conducted under air.

Prior to an evaluation of this catalyst system in a substrate scope, further investigations concerning the activity were performed (Table 6). In presence of 1 mol% catalyst **150a** the reaction provided desired azirine **165a** in quantitative yield with 60% ee after 2 min reaction time (Table 6, entry 1). Reducing the catalyst loading to 0.1 mol% gave complete conversion after 30 min while the enantioselectivity remained at 60% (entry 2). Entry 3 depicts a reaction set-up with 0.01 mol% of complex **150a** showing that a TON of up to 10,000 is feasible within reasonable reaction times. Notably, this catalysis was conducted under inert gas atmosphere to prevent a possible catalyst decomposition upon longer reaction times at rt under air.

Results and Discussion

Table 6: Survey of Catalyst Activity.^a



entry	<i>xx</i> (mol%)	<i>t</i>	yield (%) ^b	ee (%) ^c
1	1	2 min	99	60
2	0.1	30 min	99	60
3^d	0.01	18 h	99	59

^aReaction conditions: Catalyst **150a** (*xx* mol%) was dissolved in CH_2Cl_2 (0.1 M, 0.5 mL) under air at rt. Isoxazole **164a** (0.05 mmol) was added and the reaction was stirred for the indicated time at rt. Afterwards, the solvent was removed under vacuum and crude ¹H NMR and HPLC were measured. ^bNMR yield with 1,1,2,2-tetrachloroethane as internal standard. ^cDetermined by HPLC analysis on a chiral stationary phase. ^dReaction conducted under inert gas atmosphere.

The high activity of the novel iron(II) complexes towards this conversion shows that 3d-transition metals can exhibit unique properties for catalytic transformations and can even exceed the performance of noble transition metals in terms of reactivity. The rhodium catalyst **166** of the Ohe group exhibited a TON of about 40 at an elevated temperature of 40 °C over 17 h for this enantioselective ring contraction.^[180] Even the ruthenium catalyst **163** introduced by Meggers *et al.* with a high TON of 2,000 at 40 °C is surpassed by the here introduced Fe(II)-complex **150a** in terms of reactivity.^[174] The complexes applied to this catalytic reaction and their activities are displayed in Figure 26.

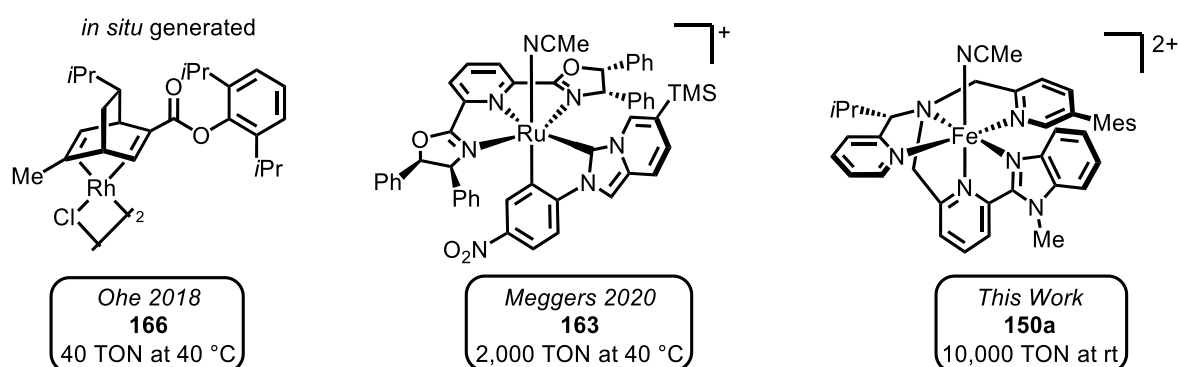
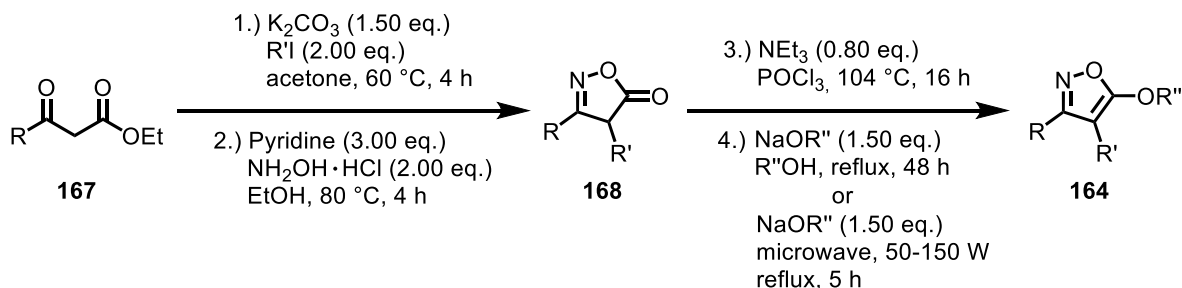


Figure 26: Chiral catalysts facilitating the asymmetric ring contraction of isoxazoles to furnish 2*H*-azirines. The maximum TONs are stated below each complex.^[174,180]

Results and Discussion

In order to explore the applicability and substrate dependency of the catalytic system, the reaction was conducted with various isoxazoles **164**. The general synthesis of the majority of substrates was conducted according to literature procedures and is depicted in Scheme 44 (for more information, see Section 5.5.1).^[174,180]

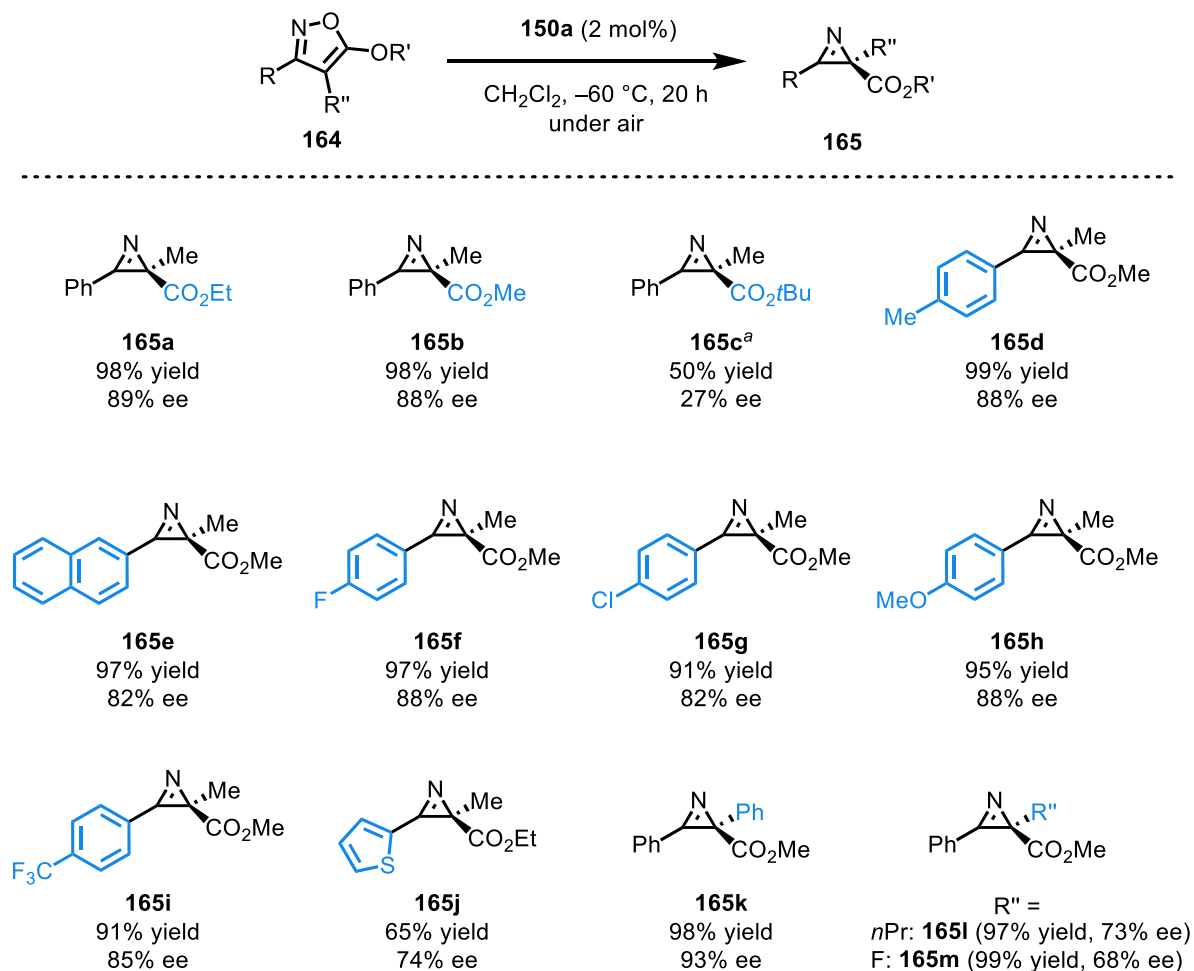


Scheme 44: Synthetic pathway towards the majority of isoxazole substrates **164**.

With a variety of different substrates in hand, the substrate scope was conducted as illustrated in Scheme 45. First, the influence of the alkoxy moiety on the substrate (**164a-c**) was investigated. When methoxy substituted isoxazole **164b** was used, corresponding *2H*-azirine **165b** could be isolated in a high yield of 98% with 88% ee. A significant drop in enantioselectivity and activity was observed when a sterically more demanding *Ot*Bu group was implemented. Product **165c** was obtained in 50% yield when 4 mol% of catalyst **150a** were applied with a low enantiomeric excess of 27%. This could be rationalized by a distorted complexation of substrate **165c** due to an interference of the bulky *Ot*Bu moiety impeding a sufficient stereinduction. In addition, different aryl substituted isoxazoles were synthesized and subsequently converted to the corresponding azirines (**165d-j**). Implementation of a *p*-tolyl group resulted in quantitative yield with a good ee of 88% (**165d**). *2H*-Azirine **165e** comprising a 2-naphthyl residue was formed in an excellent yield of 97%, albeit with a significantly lower enantioselectivity of 82% ee. The addition of a halogen atom in the *para*-position of the aryl ring provided the isolated azirines **165f** and **165g** in good yields with good enantioselectivities. Conspicuously, product **165g** was furnished with a significantly lower ee of 82% compared to **165f** (88% ee). Electron-donating (**165h**) and electron-withdrawing (**165i**) moieties on the phenyl substituent had no disadvantageous effect on the stereinduction and reactivity, accordingly furnishing the products in very good yields and good enantioselectivities. When **164j** with a 2-thiophenyl motif was applied to the catalysis, azirine **165j** exhibited a significantly lower yield and a moderate ee of 74% implying that a phenyl ring on this position of the substrates is essential for enabling high enantioselectivities. The decrease in reactivity could be explained by the low solubility of isoxazole **164j** at -60 °C in methylene chloride. Afterwards, the influence of the residue on the 4-position of isoxazoles **164** was tested. Intriguingly, by incorporation of a phenyl substituent at this

Results and Discussion

position, 2*H*-azirine **165k** was provided with an excellent yield of 98% and a very high ee of 93%. However, when the ring contraction was performed with a propyl group (**164l**) or a fluorine substituent (**164m**) on the same position, a considerable drop in enantioselectivity to 73% and 68% ee, respectively, was observed, albeit the reactivity remaining high with 97% and 99% yield. In summary, iron complex **150a** facilitated the ring contraction of isoxazoles **164** to chiral 2*H*-azirines **165** with generally high activities and mostly good to very high enantioselectivities of up to 93% ee.^[150]



Scheme 45: Substrate scope of the asymmetric ring contraction of isoxazoles **164** to furnish chiral 2*H*-azirines **165** catalyzed by complex **150a**. The stated yields refer to isolated yields. "Reaction was performed with 4 mol% of catalyst **150a**."

3.3.3 Concluding Remarks

In conclusion, the novel stereogenic-at-iron complexes developed and synthesized in the course of this work have proven to be suitable catalysts for enantioselective transformations. As discussed in Section 3.1.1, chiral iron catalysts being composed of a pentadentate ligand scaffold have exclusively been applied to enantioselective C-O bond formations, hence applying this overall class in other

Results and Discussion

reaction types represents an underdeveloped field. Considering these previous reports, the presented results of the here introduced system are unprecedented among complexes derived from chiral pentadentate ligands. Gratifyingly, the uncommon complexation of the dipicolylamine motif to the metal center in a meridional fashion enables a strong stereinduction during the asymmetric ring contraction which could be exploited in future work by incorporation of other, sterically more bulky shielding groups to enhance the enantioselectivity.

Furthermore, comparing the novel iron catalysts with previously applied rhodium and ruthenium complexes for the synthesis of *2H*-azirines reveals distinct properties in regard to reactivity for the here developed catalyst system. An exceptionally high activity could be achieved with turnover numbers of up to 10,000. This demonstrates that base metal complexes are not only suitable to replace precious 4d- and 5d-transition metal catalysts but can also surpass their efficiency. Moreover, the novel iron complexes represent the first 3d-transition metal catalysts facilitating the enantioselective ring contraction of isoxazoles to furnish chiral *2H*-azirines with an exceptionally high activity.

3.4 Expanding the Family of non- C_2 -Symmetric, Linear, Tetradentate Ligands for Fe(II)-Catalysts

3.4.1 Base Metal Catalysts Comprising Tetradentate, Linear, C_1 -Symmetric Ligands

Asymmetric transition metal catalysis has given birth to a large number of different chiral ligand scaffolds with many frameworks proven to be suitable for various metals and reaction types. Notably, a survey of many prominent and privileged ligands shows that the vast majority evinces an overall C_2 -symmetry.^[181] Accordingly, this observation also applies to linear, tetradentate N4-type scaffolds that have been established as powerful ligands for enantioselective transformations.^[76,79,81,83,86,87,89,182] The anchor of the aforementioned N4-type ligands is commonly represented by a chiral diamine backbone that implements the possibility of selectively steering the metal-centered stereogenicity for complexes exhibiting an octahedral topology. Moreover, the backbone is crucial for determining the selectivity towards a *cis- α* or *cis- β* coordination mode (see Section 1.2.3). Frequently used motifs are chiral 2-(2-pyrrolidinyl)pyrrolidine-,^[183–190] cyclohexyl-1,2-diamine-,^[191–196] and 1,2-diphenylethyl-1,2-diamine^[182,197–199]-units. All these examples usually give rise to C_2 -symmetric ligands and, hence, provide C_2 -symmetric catalysts. In contrast to these examples, the Sun group applied a C_1 -symmetric chiral 1-(pyrrolidine-2-yl)methanamine moiety as ligands to furnish complexes suitable for asymmetric transition metal catalysis.^[91] Ever since, this chiral, proline-derived backbone has been applied to numerous catalysts for asymmetric reactions.^[79,200–204] Due to the backbone not being situated near the catalytically active site, the resulting ligands and complexes can be referred to as pseudo- C_2 -symmetric when two identical ancillary terminal coordinating groups are implemented. Predominantly, such complexes with a N4-type ligand scaffold exhibit a C_2 - or pseudo- C_2 -symmetric overall topology and examples of non- C_2 -symmetric complexes comprising a lower symmetry with a higher catalytic performance are scarce (Figure 27).

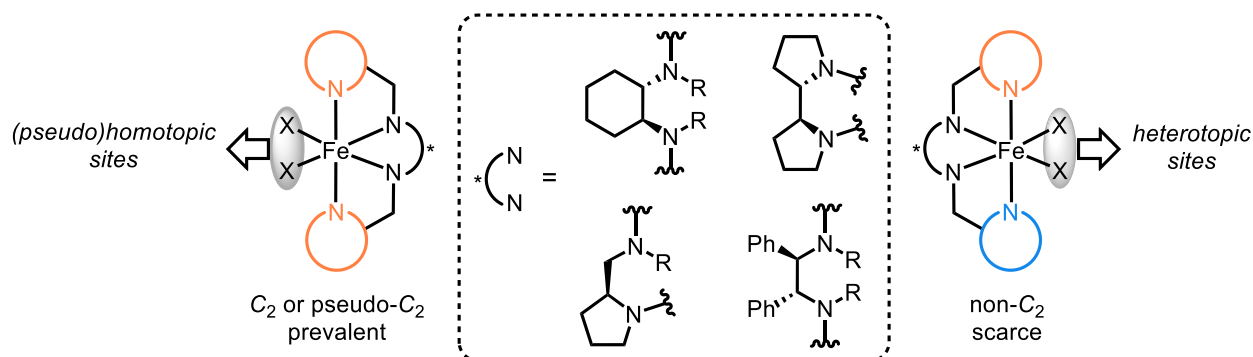
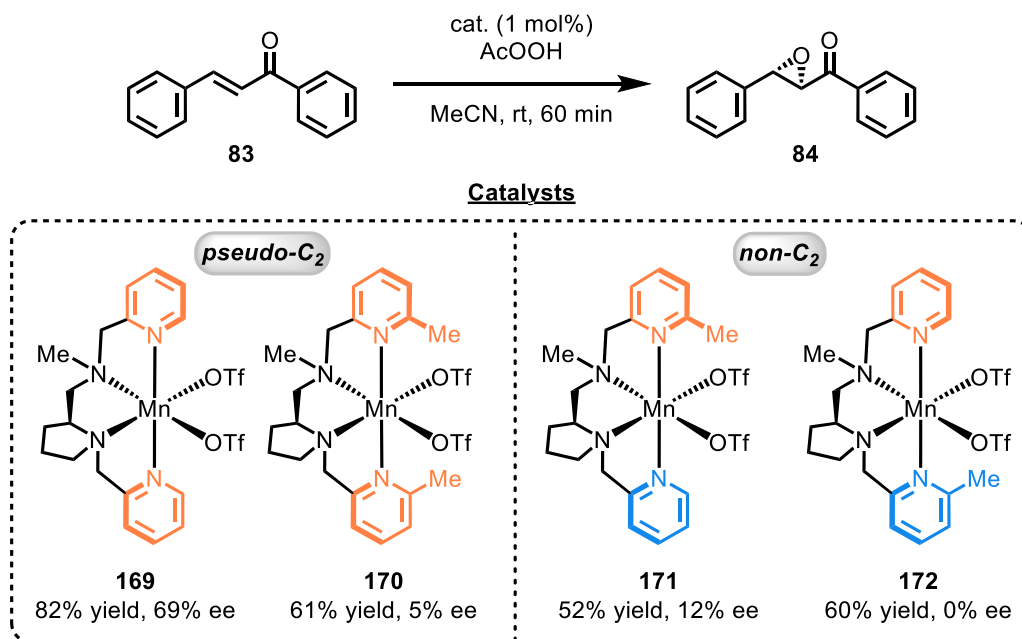


Figure 27: Comparison of (pseudo)- C_2 - and non- C_2 -symmetric complexes comprising a linear, tetradentate, N4-type ligand and frequently applied chiral diamine backbones. Reports of non- C_2 -symmetric catalysts with heterotopic reaction sites providing superior results are scarce.

Results and Discussion

Usually, the synthesis of C_2 - or pseudo- C_2 -symmetric ligands is more convenient and the related catalysts exhibit a better performance in regard to stereoselection and activity.^[79] For instance, the group of Sun reported the synthesis of Mn(II)-complexes with tetradentate, N4-type ligands that comprise a chiral, proline-based diamine backbone. The coordination scaffold was complemented by two terminal ancillary pyridine rings. By independent implementation of methyl residues on the 6-position of these aryl moieties, the group ultimately furnished the two pseudo- C_2 -symmetric complexes **169** and **170**, and complexes **171** and **172** evincing a non- C_2 -symmetric overall topology. Subsequently, the obtained catalysts were applied to an enantioselective epoxidation of chalcone (**83**) for the synthesis of chiral epoxide **84**. A juxtaposition of the pseudo- C_2 -symmetric derivatives with the non- C_2 -analogons showed that the latter were inferior in regard to activity and selectivity (Scheme 46).^[91] The slight difference of “inverted” complexes **171** and **172** in terms of enantioselectivity can be rationalized by the C_1 -symmetric backbone of the scaffold, thus creating a differentiation of the two labile reaction sites.

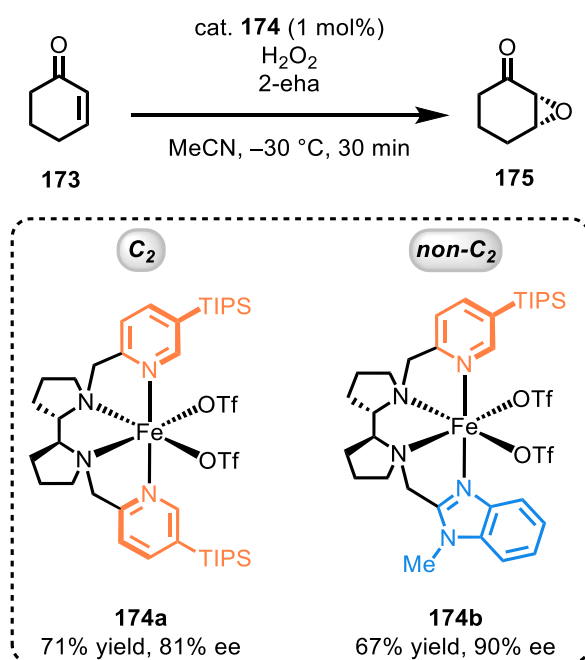


Scheme 46: Asymmetric epoxidation of chalcone (**83**) by Sun *et al.* in presence of pseudo- C_2 - and non- C_2 -symmetric Mn(II)-catalysts **169–172**.^[91]

The most alluring example of a systematic decrease of symmetry in tetradentate, N4-type ligands in order to improve the performance of the derived catalysts was reported in 2016 by the groups of Klein Gebbink and Costas.^[205] By applying a chiral bis-pyrrolidinyll backbone combined with two ancillary coordinating heterocycles, a variety of different catalyst systems was accessible. The catalytic efficacy of the corresponding iron complexes was scrutinized in a subsequent epoxidation of challenging cyclohex-2-enone (**173**). When the reaction was conducted in presence of 1 mol% **174a**, chiral epoxide **175** could be furnished in 71% yield exhibiting an enantiomeric excess of 81%.

Results and Discussion

Strikingly, by implementation of two different terminal coordinating motifs and, hence, application of a non- C_2 -symmetric catalyst **174b**, the enantioselectivity could be enhanced to 90% ee while the activity remained similar with 67% yield (Scheme 47). After optimizing the reaction conditions by using 3 mol% of catalyst **174b**, the yield could be improved to up to 86% while the enantiomeric excess of the furnished epoxide **175** remained unaltered.^[205] More recently, the Costas group was able to present the efficiency of a non- C_2 -symmetric Mn(II)-complex for a remote amino acid recognition and peroxide activation in order to facilitate an asymmetric epoxidation. Interestingly, the overall non- C_2 -symmetry was essential in order to obtain sufficient results.^[206]

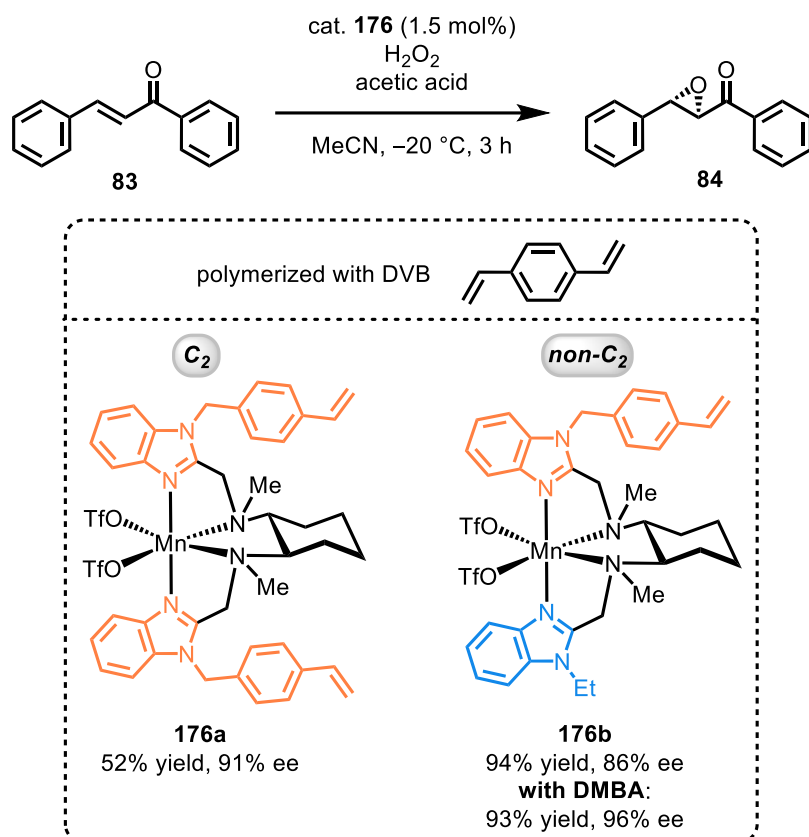


Scheme 47: Asymmetric epoxidation of cyclohex-2-enone (**173**) with a non- C_2 -symmetric iron(II) catalyst **174a** and the C_2 -symmetric derivative **174b** as reported by Klein Gebbink and Costas.^[205]

Another example of a lower symmetry exhibiting a higher catalytic efficacy in such tetradentate ligands was reported in 2021 by Sun *et al.* for a heterogenous manganese catalyst system.^[207] Different manganese complexes comprising a chiral cyclohexyldiamine backbone were synthesized. Olefinic sidechains were incorporated into the terminal coordinating aryl groups in order to embed the catalytic units in a skeleton of porous organic polymers by reaction with divinylbenzene (DVB). Subsequently, the heterogenous catalysts were shown to facilitate an enantioselective epoxidation of chalcone (**83**). For instance, polymers of the manganese complexes **176a** and **176b** promoted this asymmetric transformation yielding chiral epoxide **84** in high enantioselectivities of 91% ee and 86% ee, respectively (Scheme 48). However, non- C_2 -symmetric Mn(II)-catalyst **176b** exhibited a significantly higher activity (94% yield). After a subsequent optimization of reaction conditions by substituting acetic acid with 2,2-dimethylbutanoic acid (DMBA) chiral epoxide **84** could be afforded

Results and Discussion

in 93% yield with an excellent enantioselectivity of 96% ee. Additionally, the immobilized catalyst system was successfully recycled for numerous times without losing its efficiency regarding activity and stereoselectivity.^[207]



Scheme 48: Enantioselective epoxidation of chalcone (**83**) with manganese catalysts **176a** and **176b**. Prior to reaction, the complexes were polymerized with divinylbenzene (DVB) for application as heterogeneous catalysts.

The development of linear, tetradentate, N₄-type scaffolds has furnished a broad variety of different ligands that were successfully applied in many catalytic systems. However, like for other types of ligands, the design and application of ligands with lower symmetry (non-C₂-symmetry) represents an underdeveloped field possibly granting enticing possibilities in terms of application in asymmetric catalysis. Regarding homogenous enantioselective catalyst systems with a N₄-type scaffold, the only example of a significantly enhanced efficacy of a complex with a reduced symmetry has been reported by Klein Gebbink and Costas (Scheme 47). Thus, combining the advantages of this ligand framework with possible advantages of a decrease in symmetry could give rise to catalytic systems emanating unique properties in regard to the steric as well as the electronic environment.

3.4.2 Synthesis of non- C_2 -Symmetric Ligands for Fe(II)-Catalysts

In order to realize the feasibility of novel N4-type ligands and elaborate on a suitable framework for conveniently accessing Fe(II)-complexes, certain requirements for the chiral backbone were embraced. For the purpose of this work, several major considerations were taken into account as depicted in Figure 28. Accordingly, the chirality of the diamine backbone should be readily available, ideally by access via the chiral pool and its structure should facilitate a convenient, unsymmetric synthetic access towards the final tetradentate ligands. Furthermore, the chirality of the ligand is required to permit the complexation in a *cis- α* -selective fashion while simultaneously determining the absolute metal-centered stereogenicity. With these considerations in mind, the proline derived aminomethylpyrrolidine backbone was selected as the most suitable candidate for this endeavor as its C_1 -symmetric nature enables a convenient synthetic approach towards unsymmetric ligands. Moreover, its applicability as a sufficient backbone in tetradentate ligands for locking the metal-centered chirality and overall topology of corresponding 3d-metal complexes has been established by groups like Vagg,^[90] Sun,^[79,92,132,200,207–209] or Bryliakov.^[210]

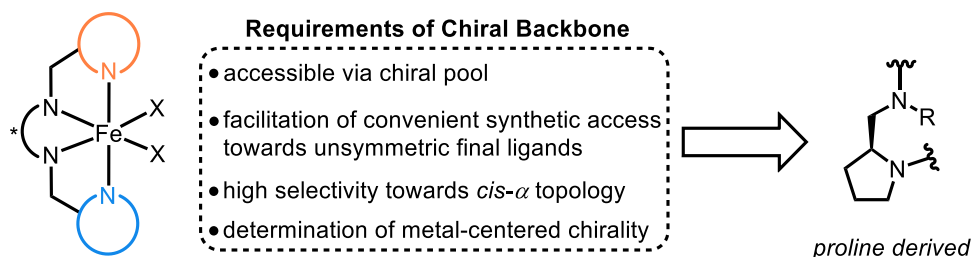
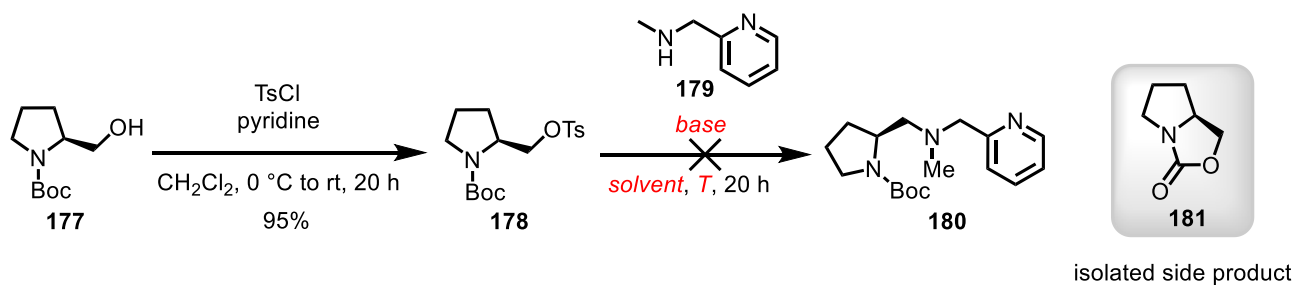


Figure 28: Initial design and requirements for novel tetradentate N4-type ligands for iron complexes with non- C_2 -symmetry.

Synthetic attempts commenced with commercially available Boc-protected (*S*)-prolinol (**177**). For accessing unsymmetric ligands, independent incorporation of the two coordinating aryl groups into the chiral backbone via nucleophilic substitutions was planned. Therefore, the hydroxy moiety of **177** was converted to a sufficient leaving group by tosylation with tosyl chloride in presence of base to afford product **178** in 95% yield. For an initial feasibility study, pyridine was chosen as the first terminal coordinating moiety. Nucleophilic substitution of tosylate **178** with *N*-methyl-1-(pyridine-2-yl)methanamine (**179**) was examined under different conditions (Table 7). Applying basic conditions for nucleophilic substitution in either MeCN (Table 7, entries 1–4) or dimethylformamide (DMF, entries 5–8) were not suitable and desired proline derivative **180** was only formed in traces at elevated temperatures. Instead, major formation of an undesired side product was observed, which could be identified as carbamate **181** resulting from an intramolecular cyclization as previously reported for similar proline derivatives.^[211,212]

Results and Discussion

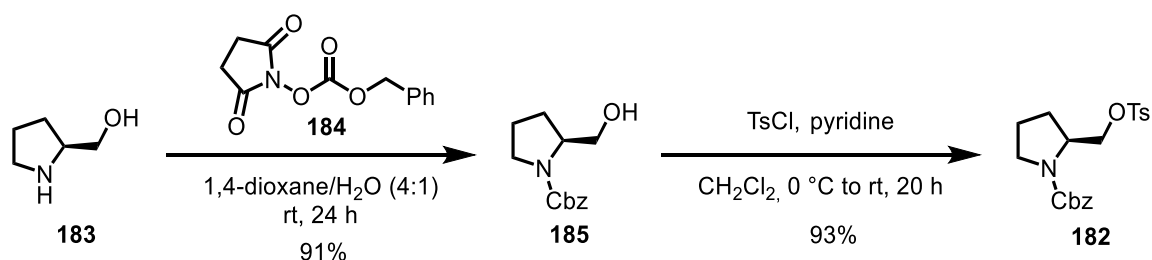
Table 7: Survey of Reaction Conditions for Nucleophilic Substitution with Amine **179a** to Afford **180**.



entry	base (eq.)	solvent	T (°C)	yield 180 (%) ^a	yield 181 (%) ^a
1	K ₂ CO ₃ (2.0)	MeCN	rt	none	none
2	K ₂ CO ₃ (2.0)	MeCN	80	traces	60
3	K ₂ CO ₃ (1.0)	MeCN	80	traces	58
4	NEt ₃ (2.0)	MeCN	80	traces	67
5	K ₂ CO ₃ (2.0)	DMF	rt	none	none
6	K ₂ CO ₃ (2.0)	DMF	50	none	30
7	K ₂ CO ₃ (2.0)	DMF	80	traces	69
8	NEt ₃	DMF	80	5	66

^aNMR yield with 1,1,2,2-tetrachloroethane as internal standard.

In order to impede the formation of undesired side product **181**, a different amine protecting group was chosen that should also facilitate a more convenient reaction monitoring by thin layer chromatography (TLC). Hence, a Cbz-protected proline derivative was appointed for further investigations. Protected and tosylated prolinol **182** was synthesized starting from commercially available (*S*)-prolinol (**183**) in a two-step synthesis as depicted in Scheme 49.



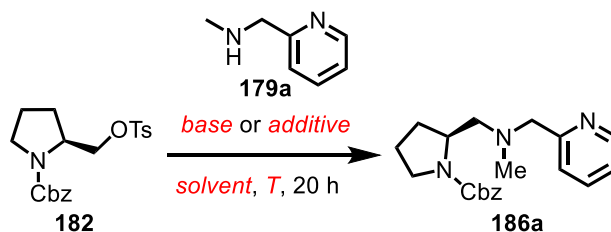
Scheme 49: Synthesis of Cbz-protected prolinol tosylate **182** starting from commercially available (*S*)-prolinol (**183**).

Next, nucleophilic substitution was attempted with secondary amine **179a** under various conditions to afford desired compound **186a** (Table 8). Apparently, conducting the reaction in MeCN or DMF with either NEt₃ or K₂CO₃ as base provided insufficient results and desired product **186a** could only be isolated in less than 10% yield (Table 8, entries 1–4). Gratifyingly, a procedure reported by the

Results and Discussion

Frederich group^[213] with sodium iodide as additive instead of base provided desired **186a** in higher yields. Ultimately, after optimizing the work-up conditions, Cbz-protected **186a** was furnished in 57% yield providing a sufficient access towards the desired ligands.

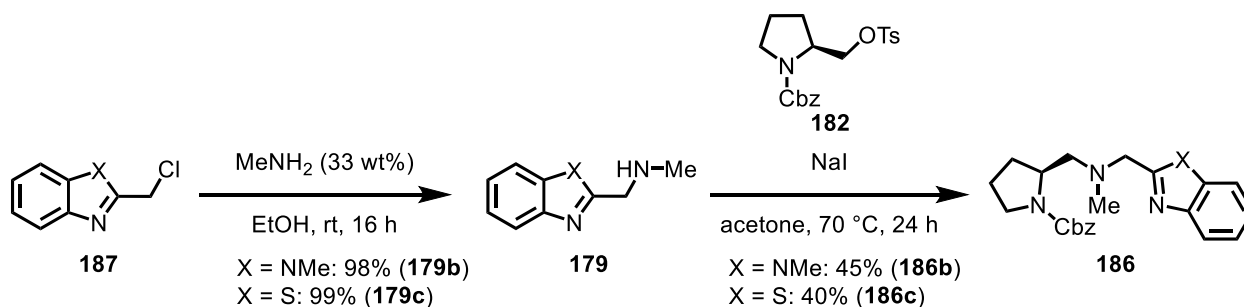
Table 8: Nucleophilic Substitution with Cbz-Protected Tosylate **182** and **179a** under Various Conditions.



entry	base or additive (eq.)	solvent	T (°C)	yield 186a (%) ^a
1	K ₂ CO ₃ (2.0)	MeCN	80	6
2	NEt ₃ (2.0)	MeCN	80	5
3	K ₂ CO ₃ (2.0)	DMF	100	8
4	NEt ₃ (2.0)	DMF	100	9
5^b	NaI (2.0)	acetone	70	57

^aIsolated yield. ^bReaction was stirred for 24 h.

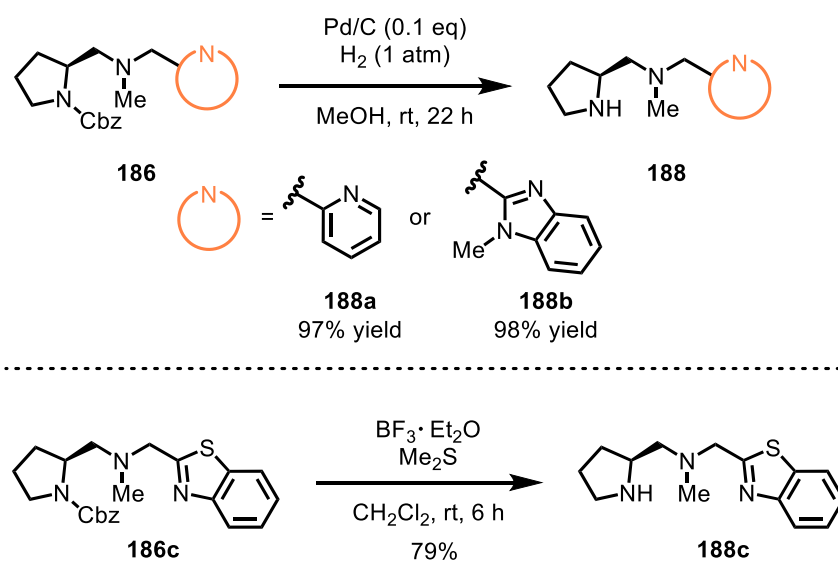
With these conditions in hand, the incorporation of other terminal coordinating aryl groups was envisioned. To provide the derived complexes with a diverse steric and electronic environment, benzothiazole and *N*-methyl benzimidazole moieties were chosen. The synthesis of the corresponding amines suitable for the nucleophilic substitution step was achieved by reaction of the commercially available chloride derivatives **187** in a methylamine solution (33 wt% in EtOH) to give the desired benzimidazole (**179b**) and benzothiazole (**179c**) amine in 98% and 99% yield, respectively (Scheme 50). Afterwards, nucleophilic substitution of amines **179** with tosylate **182** was performed with the conditions described in Table 8 to afford desired Cbz-protected prolinol derivatives **186** comprising a benzimidazole (**186b**) or benzothiazole (**186c**) motif in moderate yields.



Scheme 50: Synthesis of *N*-methyl heteroaromatic compounds **179** and subsequent nucleophilic substitution with tosylate **182**.

Results and Discussion

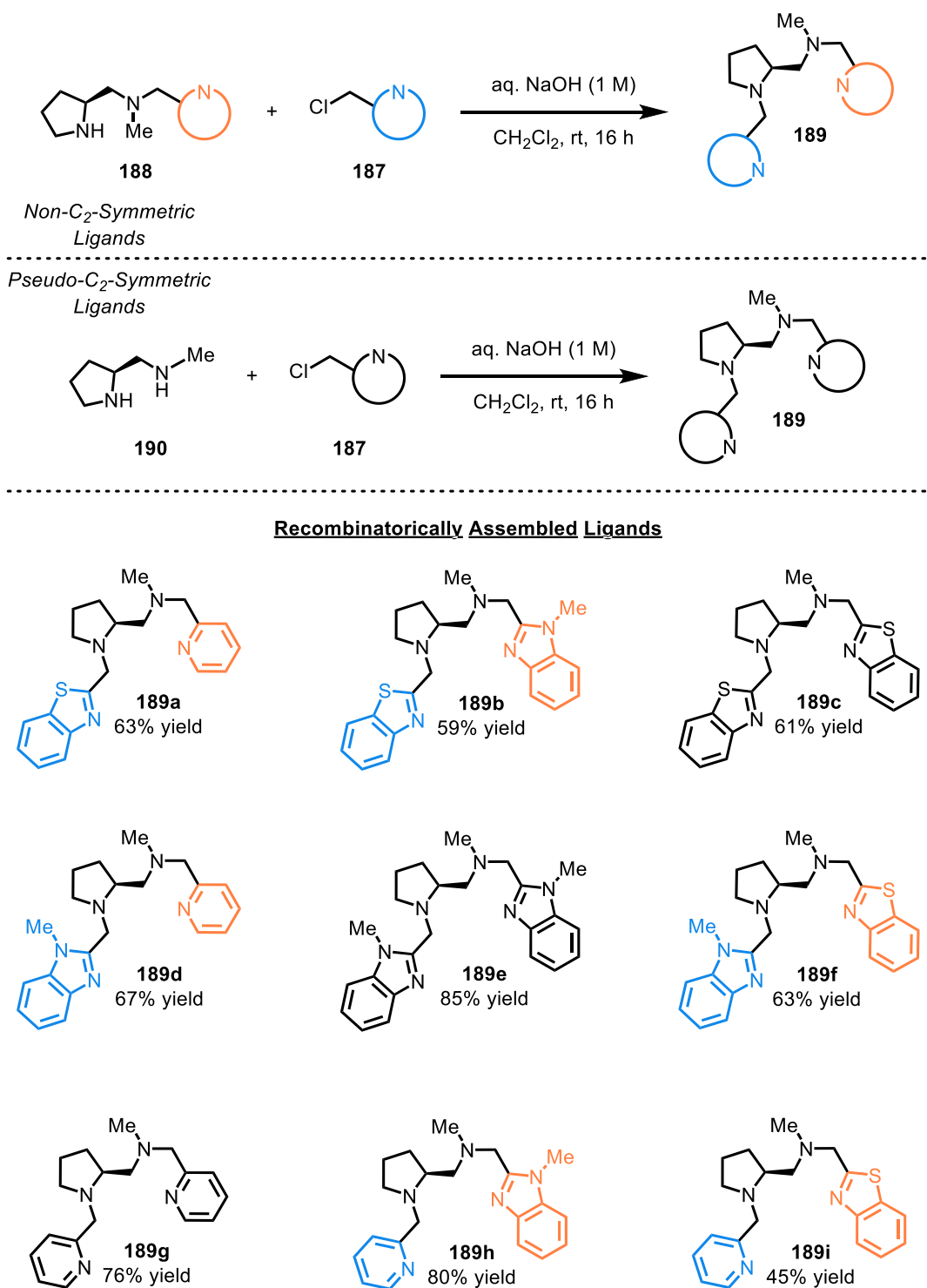
Next, deprotection of the Cbz-group followed by a second nucleophilic substitution was planned to ultimately afford the final tetradentate ligands. Deprotection via hydrogenation proceeded smoothly with compounds comprising a pyridine (**186a**) or a benzimidazole (**186b**) moiety, yielding the desired products **188a** and **188b** in quantitative yield. However, attempts of hydrogenolytic Cbz-cleavage with benzothiazole compound **186c** were not successful, most likely due to a catalyst poisoning by the sulfur. Gratifyingly, a deprotection procedure by the group of Andersson^[214] was successfully applied, providing desired compound **188c** in 79% yield. The deprotection reactions are depicted in Scheme 51.^[215]



Scheme 51: Cbz-deprotection of prolinol derivatives via hydrogenation (**186a** and **186b**). Benzothiazole derivative **186c** required a different procedure due to a potential catalyst poisoning by the benzothiazole.

Consequently, the last step towards the final non-*C*₂-symmetric ligands **189** was accomplished by a second nucleophilic substitution with free amines **188** and chloride compounds **187** by following a procedure reported by the Meggers group.^[89] Additionally, pseudo-*C*₂-symmetric ligands **189** were prepared for a subsequent investigation of the different chiral environments that accompany these two topologies in the derived iron(II) complexes. Conveniently, the pseudo-*C*₂-symmetric derivatives could be accessed in one step by nucleophilic substitution with commercially available (*S*)-**190**. The general synthetic approach towards the final ligands is depicted in Scheme 52 for both types. Due to the *C*₁-symmetric chiral diamine backbone of this framework and three selected terminal coordinating aryl moieties, overall nine combinations are possible. Accordingly, all nine ligands were synthesized and are shown in Scheme 52.

Results and Discussion

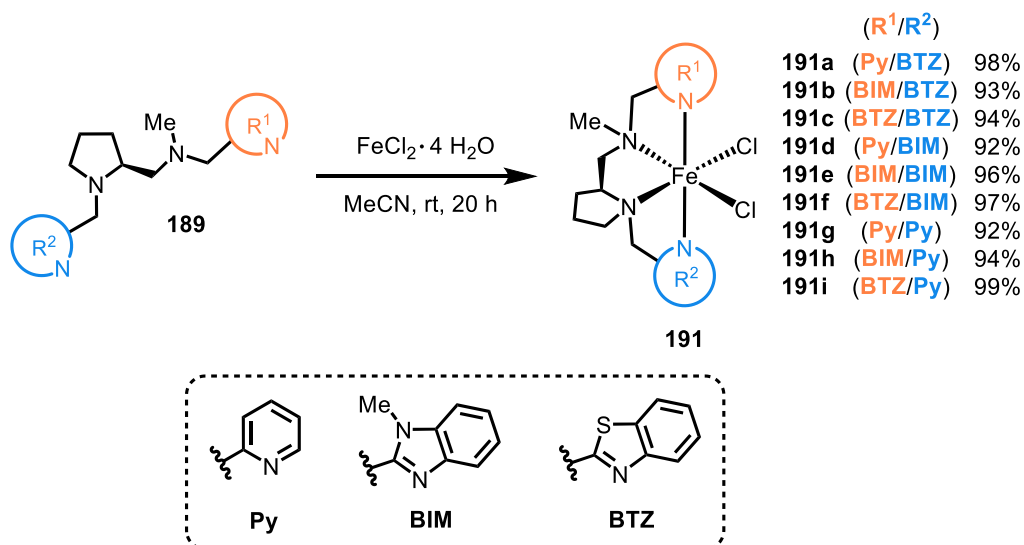


Scheme 52: General synthetic approach towards final, tetradentate ligands for non- C_2 -symmetric and pseudo- C_2 -symmetric compounds **189**. The nine possible ligands synthesized in the course of this work and the corresponding yields are depicted below.

With all nine ligands in hand, the complexation with Fe(II)-chloride tetrahydrate was investigated. Following a procedure by Sun *et al.*,^[92] all iron(II) complexes **191** were conveniently afforded in excellent yields (Scheme 53). Due to the high-spin nature of the obtained complexes,^[216,217] a thorough NMR spectroscopic analysis was not feasible. Therefore, the products were characterized

Results and Discussion

by elemental analysis and mass spectroscopy, which both confirmed the complexation while reassuring a high purity of the isolated complexes.^[215]



Scheme 53: Complexation of tetradentate ligands **189** with iron(II) chloride tetrahydrate to furnish octahedral complexes **191**.

In order to validate the coordination topology, a single crystal suitable for X-ray crystallographic analysis of complex **191a** was obtained. The structure of which is shown in Figure 29 and confirms the coordination in a *cis-α*-topology as well as a Λ -configuration of the stereogenic metal center.

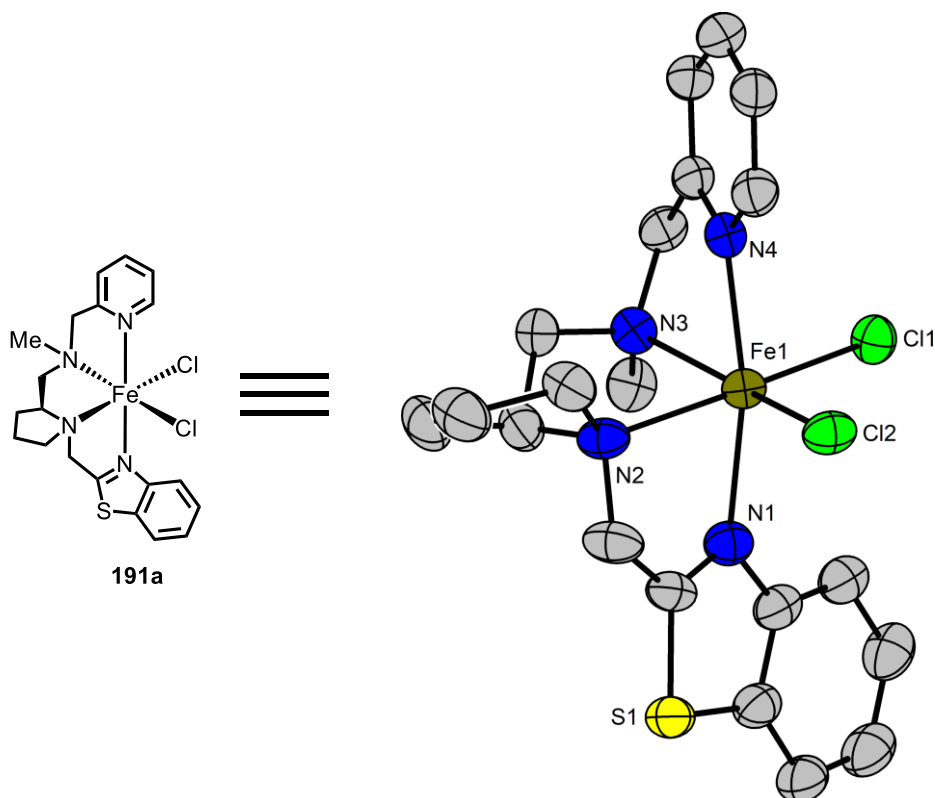


Figure 29: X-ray crystallographic structure of complex **191a** as an ORTEP drawing with 50% probability thermal ellipsoids. Solvent molecules are omitted for clarity.

Results and Discussion

Although complex **191a** exhibited high-spin characteristics, a paramagnetic ^1H NMR was measured for further insights into the structural integrity of the coordination mode in solution and the diastereoselectivity towards the *cis- α* topology. Performing the measurement under optimized parameters provided a conclusive spectrum indicating the presence of just one paramagnetic species in solution (Figure 30).

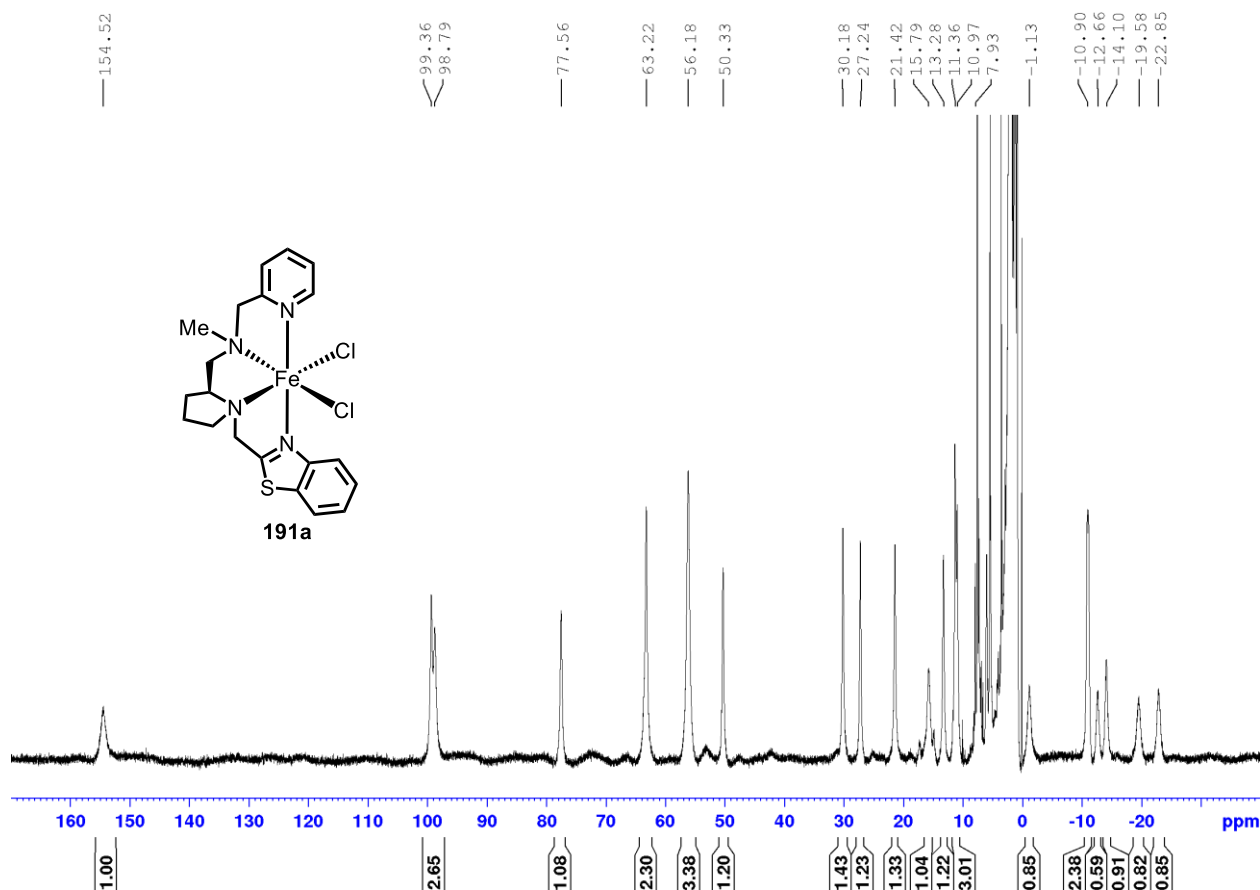
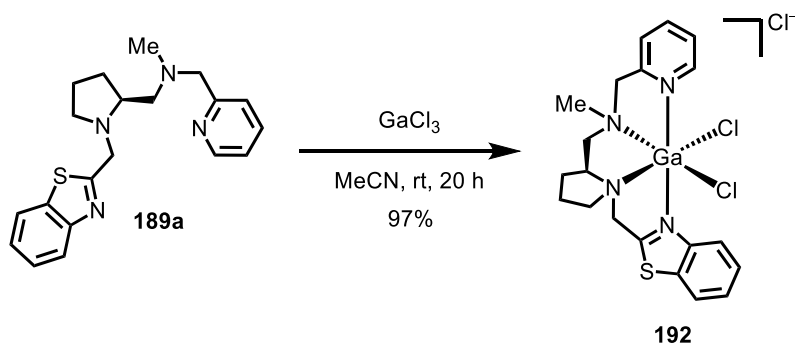


Figure 30: Paramagnetic ^1H NMR spectrum (CD_3CN , 500 MHz, rt) of complex **191a**. The integrated signals correspond to 24 protons assigned to the paramagnetic complex.

Moreover, a diamagnetic Ga(III)-analogue of complex **192** was synthesized with tetradentate ligand **189a**. The desired complex **192** was afforded in 97% yield according to the same procedure applied to obtain the iron complexes **191** (Scheme 54). In contrast to the high-spin character of complexes **191** hampering in-depth NMR spectroscopic analysis, gallium(III) enables the feasibility of such measurements due to its diamagnetic nature. Furthermore, Ga(III) has previously been applied to substitute iron in complexes with siderophores for a structure determination via NMR spectroscopic measurements.^[218–220]

Results and Discussion



Scheme 54: Complexation with ligand **189a** to furnish diamagnetic Ga(III)-complex **192**.

Subsequent ^1H NMR and ^{13}C NMR spectroscopic measurements of complex **192** showed only one set of signals indicating that just one species is present when dissolved (Figure 31).

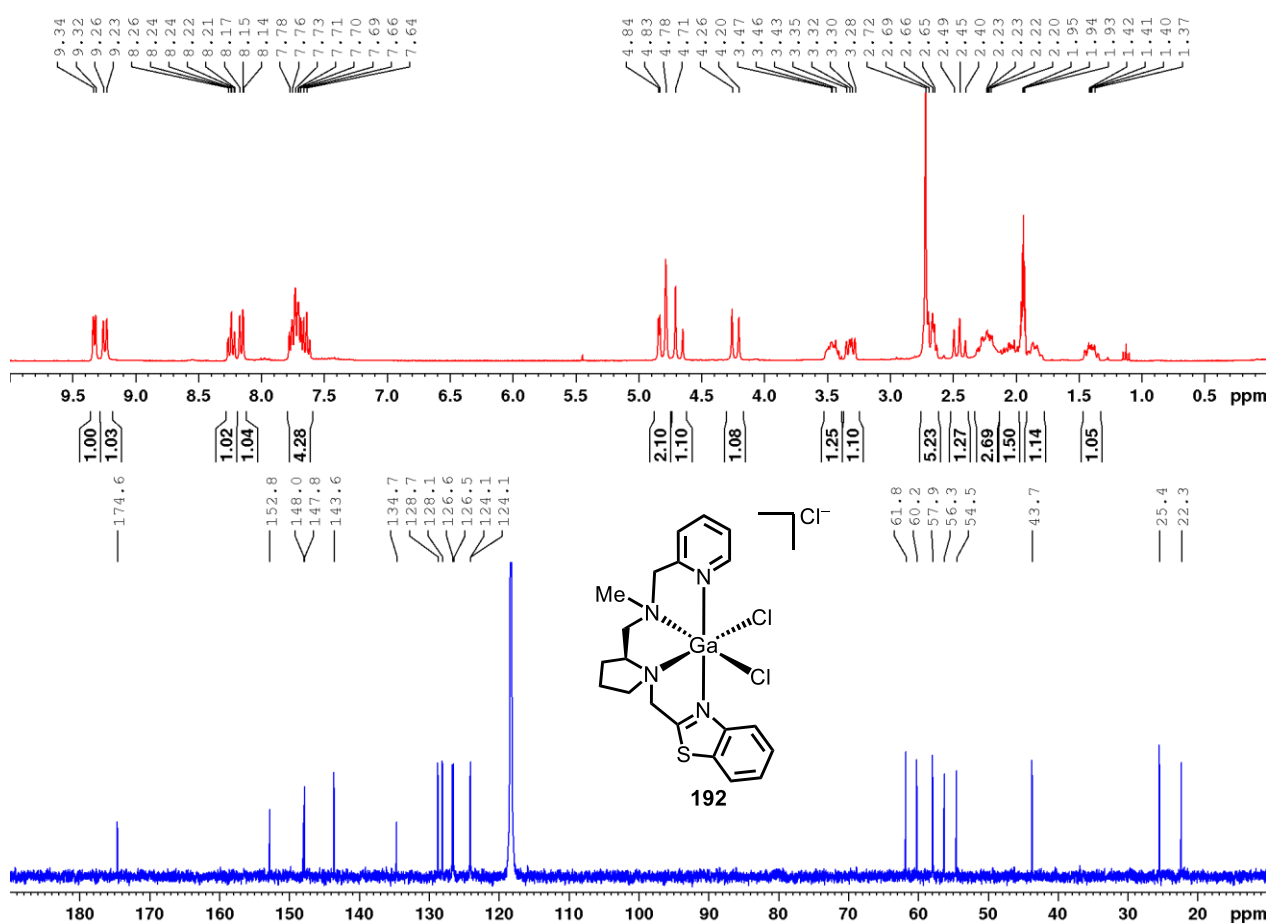


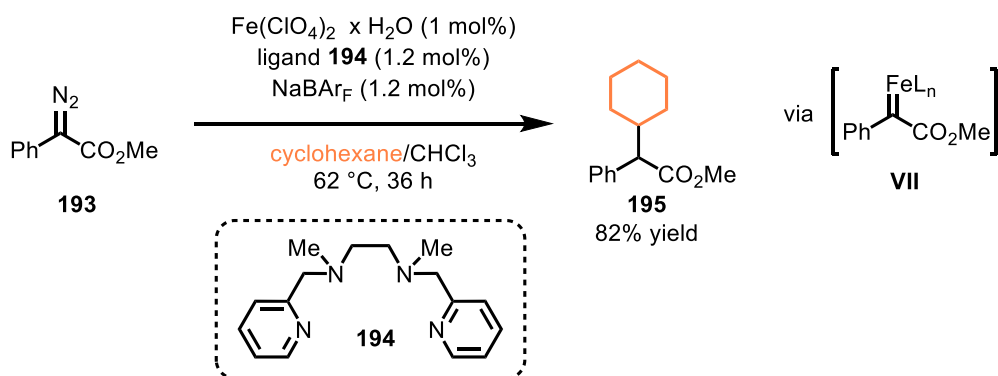
Figure 31: ^1H NMR (CD₃CN, rt, 300 MHz) and ^{13}C NMR (CD₃CN, rt, 75 MHz) spectrum of complex **192**.

After having established a convenient access towards Fe(II)-complexes with tetradentate, N₄-type ligands with the possibility of decreasing the overall symmetry and achieving the considered requirements, their efficacy in asymmetric catalysis was set to be corroborated.

3.4.3 Asymmetric Catalysis with the Non-C₂-Symmetric Iron Complexes

In terms of application in enantioselective reactions, iron complexes with tetradentate N₄-type ligands have mainly been employed in oxidative transformations involving C-O bond formations.^[79,221] Hence, the possibility of applying the complexes introduced in this work as catalysts in other reaction types was planned to be scrutinized.

The enantioselective formation of C-C bonds with chiral iron catalysts still represents an underdeveloped field in asymmetric catalysis.^[25,222] Therefore, the development of novel catalytic systems based on iron for such transformations is an enticing task. A convenient approach for realizing the formation of carbon-carbon bonds is the reaction of a metal carbene species via C-H insertion. Previously, iron salts and iron complexes have been extensively shown to facilitate carbene formation with diazo compounds for numerous transformations.^[223–225] Specifically, insertion into non-activated C(sp³)-H bonds with carbene intermediates to furnish chiral compounds is of particular interest and has been achieved, for example, by the group of Davies with rhodium catalysts.^[226,227] Pertinently, the Woo group reported an Fe(III)-porphyrin catalyzed C(sp³)-H insertion of an iron carbene with 2-phenyldiazoacetate (**193**) as carbene precursor and cyclohexane as reagent in 2008.^[228] This work was followed up in 2017 by Zhou *et al.* when they presented a C(sp³)-H bond insertion catalyzed by an *in situ* formed iron(II) complex.^[229] Intriguingly, a linear, tetradentate N₄ type ligand **194** was used in presence of sodium tetrakis[3,5-bis(trifluoromethyl)phenyl]borate (NaBAR_F) as additive. The reaction is depicted in Scheme 55.



Scheme 55: C(sp³)-H insertion with non-activated cyclohexane in presence of iron(II) catalyst comprising tetradentate ligand **194** as reported by Zhou.^[229]

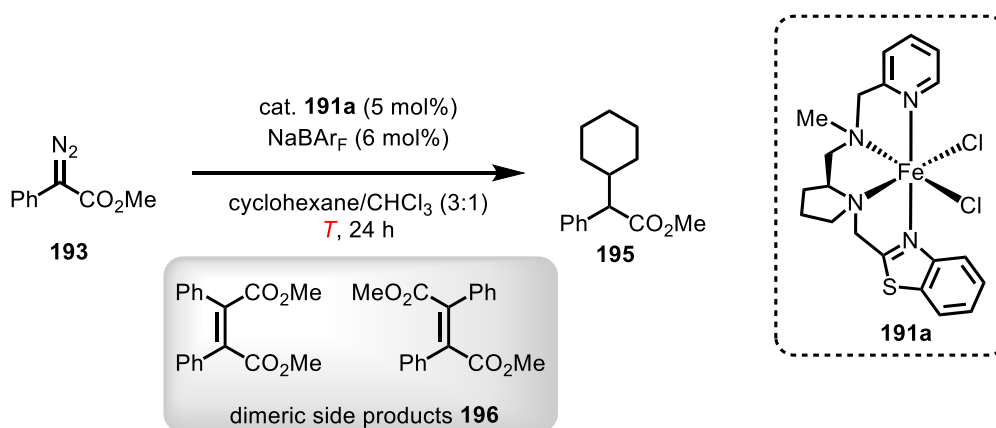
Due to ligand **194** strongly resembling the ligands **189** introduced in this work, a potential application of complexes **191** in this reaction was investigated regarding the possibility of furnishing an enantiomerically enriched product **195**. First attempts of evaluating the feasibility of this transformation are summarized in Table 9 and were conducted with complex **191a** as a standard catalyst due to its established synthesis. In addition to the desired product **195**, a possible side reaction

Results and Discussion

can lead to the formation of dimeric products **196**. At rt, no conversion to product **195** and formation of dimers **196** in traces was observed (Table 9, entry 1). When the temperature was increased to 70 °C, only traces of **195** were detected. However, NMR analysis of the crude reaction mixture showed a significant amount of the dimeric side products **196** in 24% yield (entry 2). Interestingly, when NaBAr_F was omitted, a higher yield of ester **195** (13%) with a low ee of 7% was observed while the yield of side products **196** significantly dropped to 7% (entry 3). In absence of catalyst **191a**, both, dimers **196** and product **195**, were only formed in traces (entry 4). When the reaction was performed without NaBAr_F and complex **191a**, a higher yield of 14% of desired compound **195** was afforded (entry 5). This result indicates on the one hand that a rather strong background reaction is occurring and on the other hand that the additive can impede the product formation. Furthermore, the possibility of applying visible light for activation of the catalytic system was examined. After irradiation of the reaction mixture with a compact fluorescent light (CFL) lamp for 24 h at rt, ester **195** was obtained in 27% yield with a low enantiomeric excess of 6% (entry 6). The low enantioselectivity can be rationalized by a rather strong background reaction in presence of irradiation by visible light which was confirmed by a control reaction without adding iron catalyst **191a** (entry 7). The undesired background reaction can be explained by a light-promoted photolysis of diazocompound **193** providing the free carbene that can subsequently be converted.^[230] Ultimately, the reaction was conducted with indane instead of cyclohexane (entry 8) due to an activated benzylic C(sp³)-H bond possibly facilitating the desired transformation. After reaction for 24 h at an elevated temperature, the indane C-H insertion product was only observed in traces. Therefore, further investigations on this reaction were discarded due to a low reactivity of the catalytic system and a strong background reaction leading to low enantioselectivities.

Results and Discussion

Table 9: Initial Feasibility Study of Carbene C(sp³)-H Insertion with Catalyst **191a**.

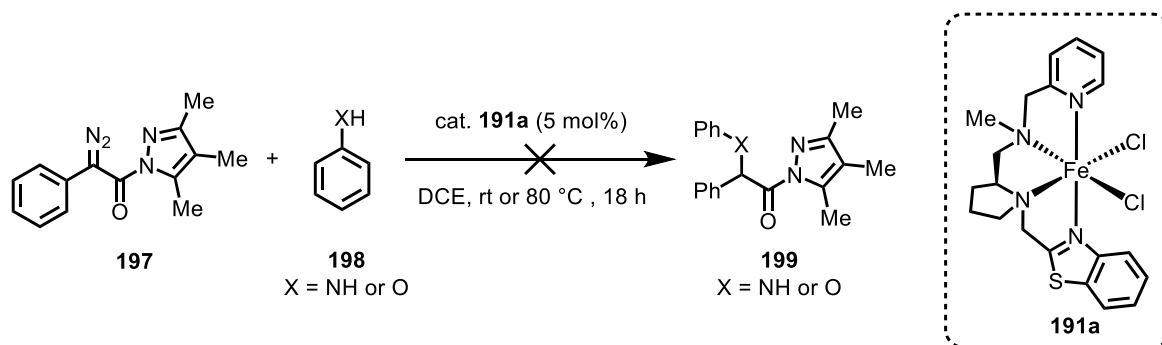


entry	<i>T</i> (°C)	yield dimers 196 (%) ^a	yield 191a (%) ^a	ee (%) ^b
1	rt	traces	none	–
2	70	24	traces	–
3^c	70	7	13	7
4^d	70	traces	traces	–
5^{c,d}	70	25	14	–
6^e	rt	traces	27	6
7^{d,e}	rt	traces	26	–
8^f	70	traces	traces	–

^aNMR yield with 1,1,2,2-tetrachlorethane as internal standard. ^bDetermined by HPLC analysis on a chiral stationary phase. ^cReaction performed without NaBARF. ^dReaction performed without catalyst **191a**. ^eReaction was irradiated with a CFL lamp. ^fReaction was performed with indane instead of cyclohexane.

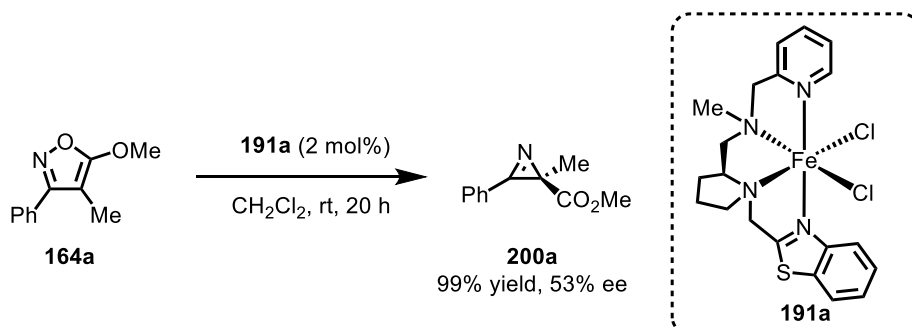
Subsequently, the feasibility of applying a bidentate carbene precursor substrate was tested due to the catalysts **191** comprising two labile reactive sites. In 2018, the group of Feng introduced a bidentate α -diazo pyrazoleamide substrate suitable for different metal carbenoid mediated asymmetric reactions.^[231–233] The bidentate coordination to the iron center of complex **191** could potentially provide the possibility of a stronger interaction with the substrate and, thus, lead to a higher selectivity to facilitate an enantioselective conversion. Accordingly, substrate **197** was reacted in presence of 5 mol% of catalyst **191a** with phenol or aniline (**198**) to evaluate a potential X-H (X = O or NH) insertion. The catalysis was conducted at rt and elevated temperature in DCE as solvent. Apparently, no conversion was observed for both reactions indicating that a formation of the required iron carbene species is not occurring. When the reactions were performed at higher temperatures, only low conversion was detected by NMR spectroscopic analysis which was attributed to decomposition of the starting material **197**. Analysis via mass spectroscopy showed no formation of the desired products **199** as shown in Scheme 56. Hence, the focus of applying the Fe(II)-complexes **191** in asymmetric catalysis was shifted towards other reactions.

Results and Discussion



Scheme 56: Carbenoid mediated X-H (X = NH or O) bond insertion with bidentate diazo compound **197** in presence of catalyst **191a**.

Due to the intriguing results observed for the ring contraction of isoxazoles to furnish *2H*-azirines with Fe(II)-catalysts comprising a pentadentate ligand (see Chapter 3.3), the application of the novel non- C_2 -symmetric complexes **191** as catalysts for this transformation was investigated. Initially, the reaction was conducted with 2 mol% of standard catalyst **191a** in methylene chloride at rt for 20 h. Pleasingly, full conversion was detected and the desired azirine **200** (for reasons of understandability, the azirines in this section will be given a separate number and isoxazoles **164** will be specified with separate letters) was obtained in quantitative yield exhibiting a moderate enantiomeric excess of 53% (Scheme 57). Moreover, this result indicates the possibility of applying the iron(II) dichloro complexes as catalysts without further activation by a ligand exchange. Commonly, such dichloro complexes are converted to more active catalysts by ligand exchange to enhance their reactivity. However, the synthetic access towards these catalysts often requires the application of expensive silver salts which renders the possibility of directly using the dichloro catalysts subsequent to complexation an attractive and convenient approach.

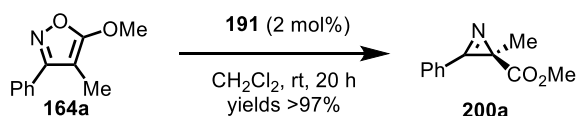


Scheme 57: Initial reaction of isoxazole **164a** with catalyst **191a** to afford chiral *2H*-azirine **200a** in quantitative yield with 53% ee. Complex **191a** comprising a chiral pentadentate ligand provided product **200a** in quantitative yield with an enantiomeric excess of 60% under comparable conditions.

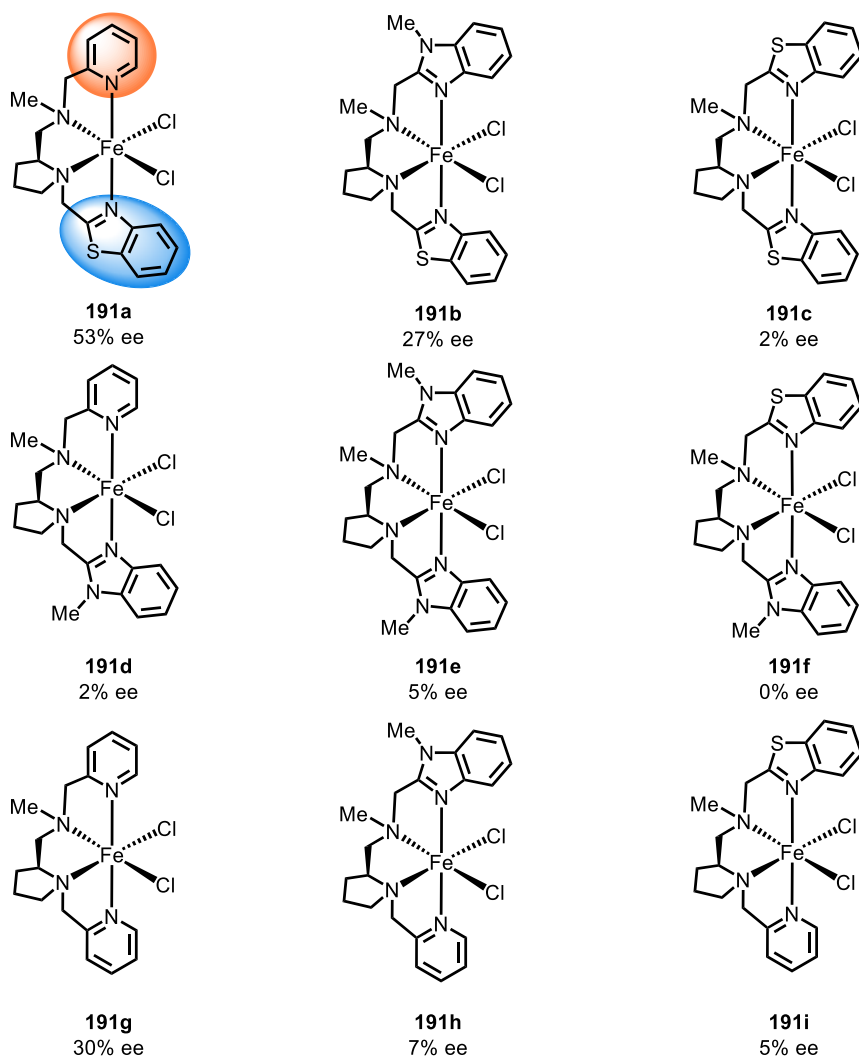
Afterwards, an initial catalyst screening with all nine synthesized complexes was conducted to evaluate the influence of their different properties and to provide further insights into the potential advantages of such a decrease regarding the overall symmetry (Scheme 58). Notably, all catalysts exhibited a high activity providing the desired azirine **200a** in virtually quantitative yields.

Results and Discussion

Interestingly, complex **191a** with the highest differentiation of the terminal coordinating aryl groups in regard to steric extension provided the highest enantioselectivity with 53% ee. When the reaction was conducted in presence of complex **191b**, in which the pyridyl ring of **191a** is replaced by a benzimidazole moiety, optically active product **200a** was obtained with 27% ee. Similarly, the pseudo- C_2 -symmetric Fe(II)-catalyst **191g** with two pyridine motifs furnished azirine **200a** with 30% ee. Conspicuously, the stereinduction of the other iron complexes was significantly lower and azirine **200a** was afforded in mostly very low enantioselectivities of less than 7% ee.^[215]



steric extension first ancillary arm



steric extension second ancillary arm

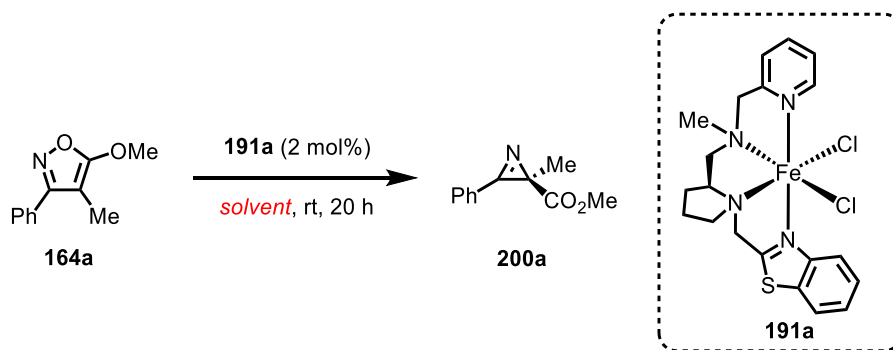
Scheme 58: Initial catalyst screening for ring contraction of isoxazole **164a** with chiral complexes **200a** comprising linear tetradentate ligands.

Results and Discussion

Ultimately, due to catalyst **191a** giving the best result in regard to enantioselectivity, an optimization of the reaction conditions was conducted in order to improve the enantiomeric excess as summarized in Table 10. First, various solvents were screened as summarized. All chlorinated solvents smoothly facilitated the reaction and azirine **200a** was obtained in quantitative yields (Table 10, entries 1–5). With chloroform (entry 2) and 1,1,2,2-tetrachloroethane (entry 3) as solvents a slightly improved enantioselectivity was observed and the desired product **200a** could be afforded with 59% ee and 58% ee, respectively. A reaction set-up with 1,2-DCE resulted in the formation of **200a** with a significantly improved ee of 75% (entry 4). When the catalysis was performed in 1,2-dichlorobenzene, 65% ee was observed (entry 5). In toluene, the catalyst showed a significantly lower activity as well as selectivity, consequently granting a reduced yield of 44% and 24% ee (entry 6). The reduced activity can be rationalized by a low solubility of iron complex **191a** in the solvent impeding the conversion. Acetonitrile had no disadvantageous effect on the yield (in contrast to pentadentate complex **150a**) However, *2H*-azirine **200a** was formed with a low enantioselectivity (5% ee, entry 7). Both, acetone (entry 8) and HFIP (entry 9), facilitated the reaction with quantitative yield granting an enantiomeric excess of 35% and 57%, respectively. Intriguingly, complex **191a** showed high robustness towards hydrolysis which is indicated by the result obtained when H₂O was used as solvent. The significantly lower yield compared to other solvents could be explained by solubility issues and a potential competing complexation of water molecules by the catalyst. Nevertheless, desired azirine **200a** could be isolated with 41% ee (entry 10). Finally, different alcohols were examined (entries 11–13). Gratifyingly, product **200a** was obtained in quantitative yield with a good enantioselectivity of 85% ee when the reaction was performed in MeOH (entry 11). Likewise, ethanol and isopropyl alcohol enabled an excellent conversion; however, the enantioselectivities were significantly lower when compared to methanol. Prior to further optimizations to enhance the enantiomeric excess, the effect of longer reaction times in MeOH in terms of racemization was investigated. Pleasingly, no racemization was detected even after stirring for 48 h rendering this solvent suitable for the catalysis (entry 14). Subsequently, the reaction was conducted in presence of various additives. Such compounds are regularly applied to enhance the catalytic performance by an *in situ* anion exchange to form a catalytically more reactive species.^[234] In accordance, the reaction was conducted in presence of different sodium salts. However, none of the applied additives had any effect on the stereoinduction and, thus, their usage was discarded (entries 15–17). Delightfully, the reaction was feasible without loss of activity or enantioselectivity under open flask conditions in presence of air, indicating a high robustness of catalyst **191a** towards oxidative decomposition (entry 18). Moreover, with open flask conditions a more convenient reaction set-up can be realized that further emphasizes the usefulness of the catalytic system.^[215]

Results and Discussion

Table 10: Initial Optimization for Ring Contraction of Isoxazole **164a** with Catalyst **191a**.^a



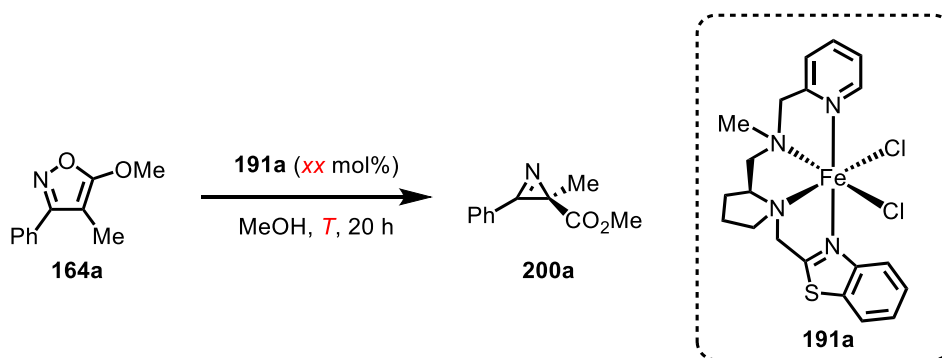
entry	solvent	yield 200a (%) ^b	ee (%) ^c
1	CH ₂ Cl ₂	99	53
2	CHCl ₃	99	59
3	1,1,2,2-tetrachloroethane	99	58
4	1,2-DCE	99	75
5	1,2-DCB ^d	99	65
6	toluene	44	24
7	MeCN	98	5
8	acetone	95	35
9	HFIP	99	57
10	H ₂ O ^e	39	41
11	MeOH	99	85
12	EtOH	99	60
13	<i>i</i> PrOH	99	57
14 ^f	MeOH	99	85
15 ^g	MeOH	99	85
16 ^h	MeOH	99	85
17 ⁱ	MeOH	99	85
18^j	MeOH	99	85

^aReaction conditions: Catalyst **191a** (2 mol%) was dissolved in the indicated solvent (0.2 M, 0.25 mL) under inert gas atmosphere. Subsequently, isoxazole **164a** was added and the resulting mixture was stirred for 20 h at rt. Afterwards, the reaction was diluted with EtOAc, filtered over a short plug of silica, the solvent was removed under vacuum, and crude ¹H NMR and HPLC spectra were measured. When the conversion was not complete, the crude product was submitted to column chromatography on silica gel to obtain pure 2H-azirine **200a** for HPLC analysis. ^bNMR yield with 1,1,2,2-tetrachloroethane as internal standard. ^cDetermined by HPLC analysis on a chiral stationary phase. ^dDue to the high boiling point of the solvent, an aliquot was taken for ¹H NMR analysis and the residual reaction mixture was directly submitted to column chromatography on silica gel. ^eAfter 20 h, the reaction mixture was extracted using CH₂Cl₂ (3x) prior to analysis and further purification. ^fReaction results obtained after stirring for 48 h. ^gReaction was performed with 4 mol% NaSbF₆. ^hReaction was performed with 4 mol% NaBARf. ⁱReaction was performed with 4 mol% NaOTf. ^jReaction was conducted under air.

Results and Discussion

Next, the influence of the reaction temperature as well as the catalyst loading in regard to enantioselectivity was determined (Table 11). Therefore, the catalysis was conducted at lower temperatures (Table 11, entries 2–4). By lowering the temperature to 4 °C, an increase of the enantioselectivity to up to 90% ee was observed while still affording azirine **200a** in quantitative yield (entry 2). A further decrease to –5 °C showed no beneficial effect on the stereoinduction, albeit the yield dropped to 92% (entry 3). Notably, when the reaction was performed at –20 °C, both, yield and enantiomeric excess, were significantly lower (entry 4). Hence, a temperature of 4 °C was chosen as the standard reaction temperature for further reactions. Subsequently, a decrease of the catalyst loading was considered. Conveniently, when the reaction was conducted in presence of just 1 mol% of catalyst **191a**, product **200a** could still be obtained in quantitative yield with 90% ee (entry 5). However, further lowering the amount of catalyst resulted in a significantly slower conversion providing azirine **200a** in 55% yield with 89% ee after a reaction time of 20 h (entry 6). As a note, the catalysis was also feasible when technical grade methanol was employed, again emphasizing the robustness of catalyst **191a**.

Table 11: Screening of Temperature and Catalyst Loading.^a



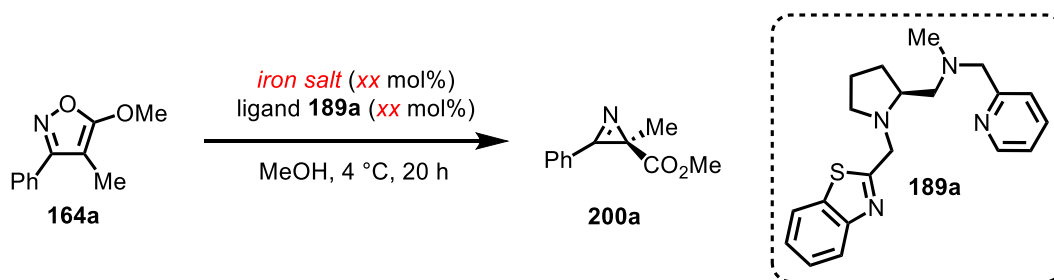
entry	<i>T</i> (°C)	catalyst loading (mol%)	yield 200a (%) ^b	ee (%) ^c
1	rt	2	99	85
2	4	2	99	90
3	–5	2	92	90
4	–20	2	70	71
5	4	1	99	90
6	4	0.5	55	89

^aReaction conditions: Catalyst **191a** (0.5–2 mol%) was dissolved in MeOH (0.2 M, 0.25 mL) under air. Subsequently, isoxazole **164a** (0.05 mmol) was added and the resulting mixture was stirred for 20 h at the stated temperature. Afterwards, the reaction was diluted with EtOAc, filtered over a short plug of silica, the solvent was removed under vacuum, and crude ¹H NMR and HPLC spectra were measured. When the conversion was not complete, the crude product was submitted to column chromatography on silica gel to obtain pure 2*H*-azirine **200a** for HPLC analysis. ^bNMR yield with 1,1,2,2-tetrachloroethane as internal standard. ^cDetermined by HPLC analysis on a chiral stationary phase.

Results and Discussion

Additionally, the feasibility of directly applying ligand **189a** and an iron salt for an *in situ* formation of the catalytically active species was evaluated (Table 12). First, iron(II) chloride tetrahydrate was applied as iron precursor due to its employment during the synthesis of catalyst **191a**. Thus, 2 mol% of the precursor and 3 mol% of ligand **189a** were used providing 2*H*-azirine **200a** in quantitative yield, albeit with a significantly lower enantioselectivity of 80% (Table 12, entry 1). Next, the catalysis was conducted with anhydrous FeCl₂ (entry 2) and FeBr₂ (entry 3) to evaluate the influence of the iron precursor. Product **200a** was afforded in 99% yield with all iron(II) salts, with FeCl₂ providing the best enantiomeric excess (83% ee). Subsequently, the amount and ratio of iron salt and ligand **189a** was altered. By increasing the amount of ligand **189a** to 6 mol%, an increase in enantioselectivity to 86% was observed (entry 4). Finally, employing 5 mol% of iron(II) chloride and 6 mol% of **189a** gave the best results in regard to enantiomeric excess furnishing chiral product **200a** with 87% ee (entry 5). These results show, that an isolation of the catalyst prior to this reaction is not necessary for a satisfactory result.

Table 12: Survey of Feasibility of an *in situ* Catalyst Formation.^a



entry	iron salt	amount of ligand (mol%)	yield 200a (%) ^b	ee (%) ^c
1	FeCl ₂ · 4 H ₂ O (2 mol%)	3	99	80
2	FeCl ₂ (2 mol%)	3	99	83
3	FeBr ₂ (2 mol%)	3	99	79
4	FeCl ₂ (2 mol%)	6	99	86
5	FeCl ₂ (5 mol%)	6	99	87

^aReaction conditions: The indicated Fe-salt and ligand **189a** were dissolved in MeOH (0.2 M, 0.25 mL) under air at 4 °C, prestirred for 5 min, and isoxazole **164a** (0.05 mmol) was added. The resulting mixture was stirred for 20 h at 4 °C. Afterwards, the reaction was diluted with EtOAc, filtered over a short plug of silica, the solvent was removed under vacuum, and crude ¹H NMR and HPLC were measured. ^bNMR yield with 1,1,2,2-tetrachloroethane as internal standard. ^cDetermined by HPLC analysis on a chiral stationary phase.

With optimized reaction conditions in hand, a concluding catalyst screening was conducted. The results of which are illustrated in Figure 32. Conspicuously, when the reaction was conducted under optimized conditions, significant differences regarding yield and enantioselectivity could be observed depending on the applied catalyst. Generally, implementation of a benzimidazolyl-motif into the ligand scaffold showed detrimental effects, especially on the stereoselectivity when compared to the

Results and Discussion

sterically similar benzothiazole-comprising ligands. Accordingly, all ligand scaffolds containing a benzimidazole group provided lower enantioselectivities than the corresponding pyridyl- or benzothiazolyl-ligands. Due to their similar steric extension, the different electronic properties seem to have a crucial influence. Thiazole exhibits a stronger π -electron withdrawing effect than imidazole,^[235] which appears to be beneficial during this catalytic transformation. Ultimately, complex **191a** furnished the highest enantioselectivity and activity. Interestingly, catalysts **191a** and its “inverted” derivative **191i**, which show the highest differentiation of the terminal coordinating aryl groups in regard to steric extension, furnished the best results when enantioselectivity as well as yield are considered. Nevertheless, there is a significant difference between the observed enantioselectivities for these two catalysts which could be attributed to the C_1 -symmetric topology of the diamine backbone that distinguishes the two terminal coordinating groups (similar to the example of the Sun group depicted in Scheme 46).^[215]

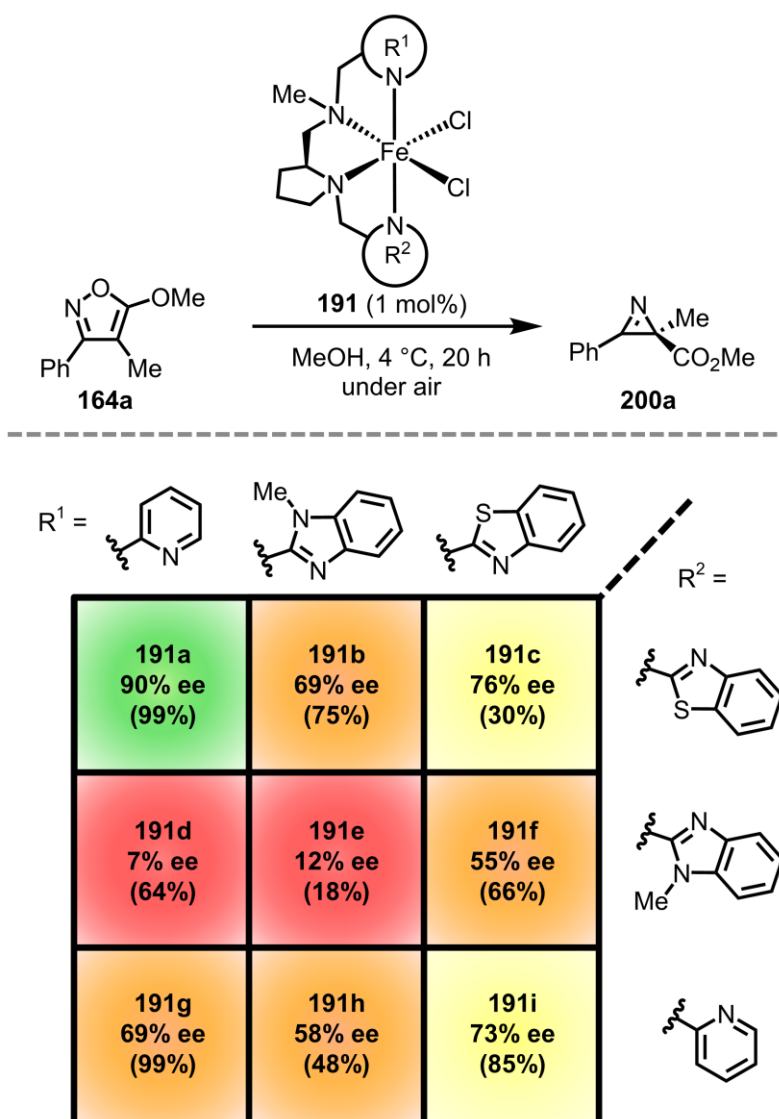
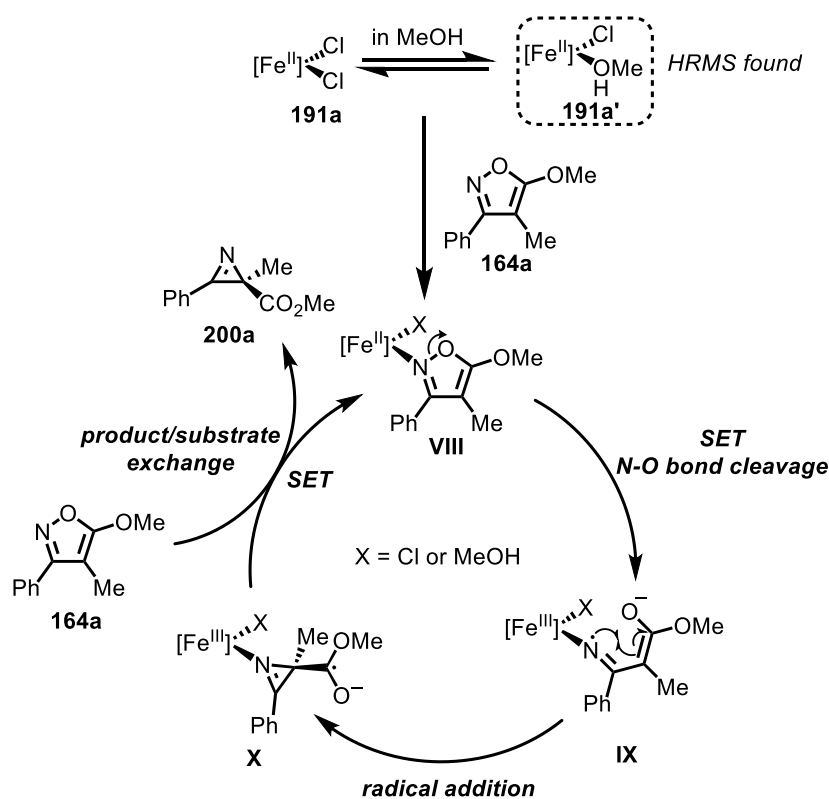


Figure 32: Concluding catalyst screening under optimized reaction conditions. Yields are stated in parentheses and the color of the squares are assigned according to the afforded enantioselectivities.

Results and Discussion

Based on previous reports by the groups of Majee and Auricchio,^[236,237] a proposed mechanism is shown in Scheme 59. The catalytic cycle commences with the coordination of azirine **164a** to one labile coordination site of the active catalytic species (**191a** or **191a'**) forming intermediate **VIII**. Subsequently, heterolytic N-O bond cleavage induced by a single electron transfer (SET) from the Fe-center furnishes the distonic iminyl radical anion intermediate **IX**. After stereocontrolled C-N bond formation by intramolecular radical addition, radical anion **X** is formed which can reduce the iron center back to Fe(II). Finally, product substrate exchange restarts another catalytic cycle. The higher efficiency of the catalyst in methanol regarding enantioselectivity could be rationalized by the formation of complex **191a'** comprising one MeOH ligand. This species was detected during mass spectroscopy and can potentially provide a stronger distinction between the heterotopic reaction sites, therefore facilitating the coordination of azirine **200a** in a site selective fashion. Moreover, the selectivity of the substrate coordination to the iron complex could explain the difference observed regarding enantioselectivities for isomeric complex pairs (Figure 32). The requirement of only one vacant coordination site for substrate **164a** and the heterotopic nature of the catalytically active site might have a crucial effect on the observed stereinduction.



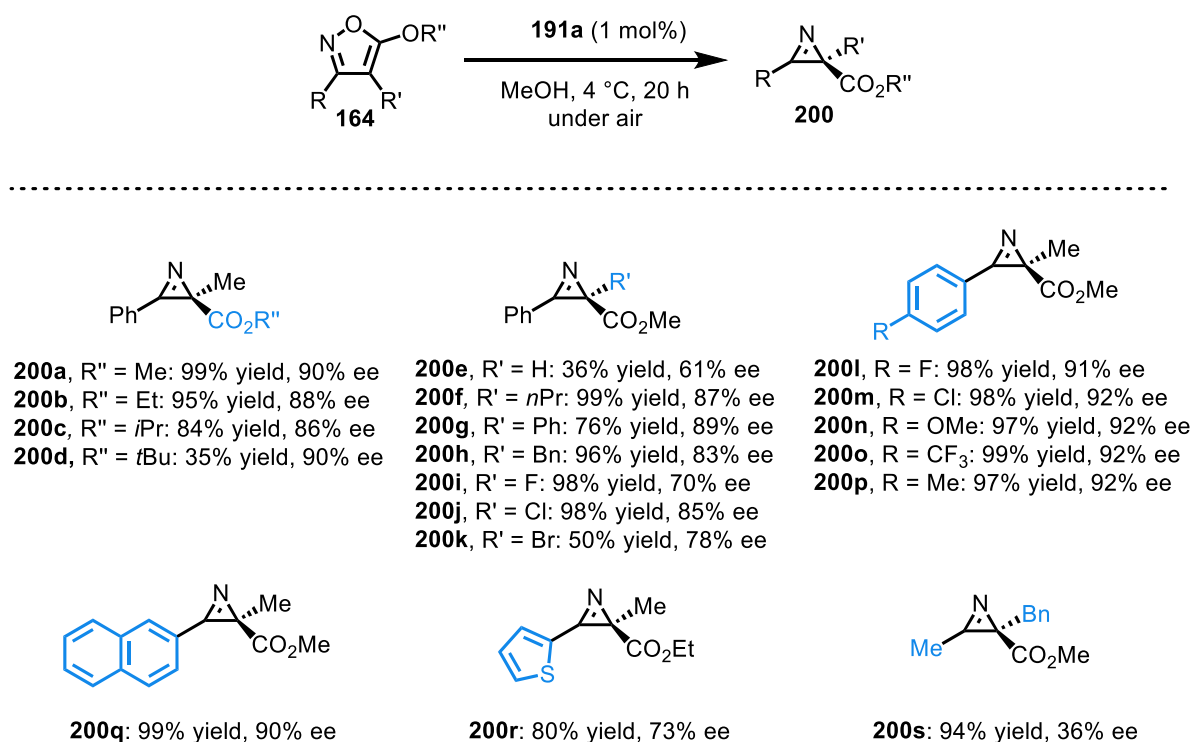
Scheme 59: Proposed mechanism of the asymmetric ring contraction of isoxazoles **164a** to afford chiral 2H-azirines **200a**.^[236,237]

After having established optimized reaction conditions and the most suitable catalyst, the applicability of this system was supposed to be demonstrated for a substrate scope of the asymmetric ring

Results and Discussion

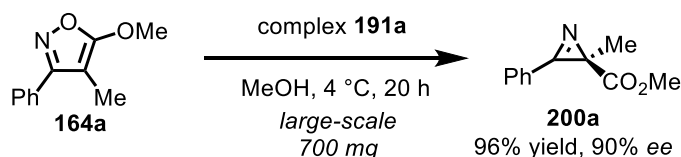
contraction to obtain chiral azirines **200** (Scheme 60). Initially, the alkoxy group of substrates **164** was varied (**164a–d**). When isoxazole **164b** with an ethoxy moiety was applied, corresponding product **200b** could be obtained in 95% yield with a slightly decreased ee of 88%. Additionally, the effect of sterically more demanding groups was investigated by implementation of an isopropoxide residue that provided product **200c** in a lower yield of 84% with a good enantioselectivity of 86% ee. *2H*-Azirine **200d** containing a bulky *Ot*Bu group was afforded in a significantly lower yield of 35%, albeit the enantiomeric excess proved to be high with 90% ee. The lower yield regarding this substrate could be rationalized by the steric demand of the *t*Bu-group leading to a reduced activity of catalyst **191a**. Subsequently, the methyl group at the 4-position of isoxazole **164** was substituted by other groups (**164e–k**). When **164e** with a hydrogen instead of the methyl residue was applied, corresponding azirine **200e** was obtained with a low yield of 36% and a moderate enantioselectivity of 61% ee. Propyl substituted derivative **164f** provided azirine **200f** with a satisfactory ee of 87% in quantitative yield. A decreased yield of 76% was observed for isoxazole **164g** with two phenyl residues while product **200g** was formed with 89% ee. Contrary, benzylic compound **200h** could be isolated in a significantly higher yield of 96% while the desired product exhibited an enantiomeric excess of 89%. Next, halogenated isoxazoles (**164i–k**) were tested with the introduced catalytic system. Accordingly, the results of the catalysis differ significantly depending on the incorporated halogen. Fluorinated (**200i**) and chlorinated (**200j**) products were afforded in quantitative yields but exhibited a big difference in enantioselectivity with 70% ee and 85% ee, respectively. When bromine was implemented, a modest yield of 50% and a moderate ee of 78% for azirine **200k** were observed. Afterwards, isoxazoles with different *para*-substituted moieties were scrutinized (**200l–p**). Fluorinated (**164l**) and chlorinated (**164m**) isoxazoles granted excellent yields with high enantioselectivities of 91% ee and 92% ee, respectively. An electron-donating (**200n**) as well as an electron-withdrawing (**200o**) group were tolerated and the corresponding azirines were obtained in high yields with a high enantiomeric excess of 92%. Likewise, *p*-tolyl azirine **200p** was afforded in an excellent yield with 92% ee. Sterically more demanding 2-naphthyl substrate **164q** was converted to product **200q** in quantitative yield with 90% ee. The introduction of 2-thiophenyl resulted in a significantly lower yield of 80% and a decreased ee of 73% of **200r** which could be explained by a competing coordination of sulfur to the Fe(II)-center of catalyst **191a**, thus deteriorating its catalytic efficacy. The implementation of an aliphatic methyl group instead of an aryl residue resulted in a significant drop of the detected enantioselectivity (36% ee) while *2H*-azirine **200s** could be afforded with a high yield of 94%. Ultimately, the substrate scope implies that the novel catalytic system is well suited for this enantioselective transformation providing the majority of the desired azirines **200** in excellent yields of up to 99% with good or high enantioselectivities (up to 92% ee).^[215]

Results and Discussion



Scheme 60: Substrate scope of enantioselective ring contraction with catalyst **191a** under optimized reaction conditions and in presence of air. Reactions were performed on a 0.10 mmol scale and the yields refer to isolated products after column chromatography.

In order to emphasize the utility of the novel catalytic system, a large-scale synthesis of azirine **200a** was set up and was conveniently feasible without any loss of enantioselectivity or activity when compared to the small-scale reactions (Scheme 61).

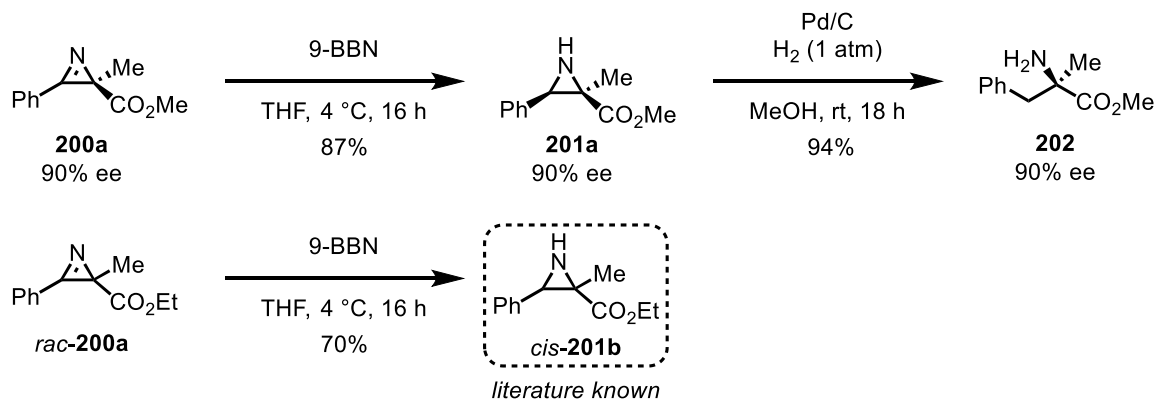


Scheme 61: Large-scale catalysis with complex **191a** and standard isoxazole **164a** under optimized conditions.

Furthermore, the versatility of *2H*-azirines **200** was set to be corroborated for an application in follow-up transformations.^[238] First, the possibility of reducing compound **200** to the corresponding aziridine **201a** was tested. By using 9-borabicyclo[3.3.1]nonane (9-BBN) as reducing agent at 4 °C the desired product **201a** could be afforded as a single diastereomer without any loss of enantioselectivity after a reaction time of 16 h in 87% yield (Scheme 62). For determining the relative configuration of aziridine **201a**, the reported compound **201b** was synthesized with racemic ethyl ester azirine **200b** via the same reduction procedure with 9-BBN. Comparison with reported data confirmed the *cis*-configuration. Such aziridines have been shown to represent valuable synthetic

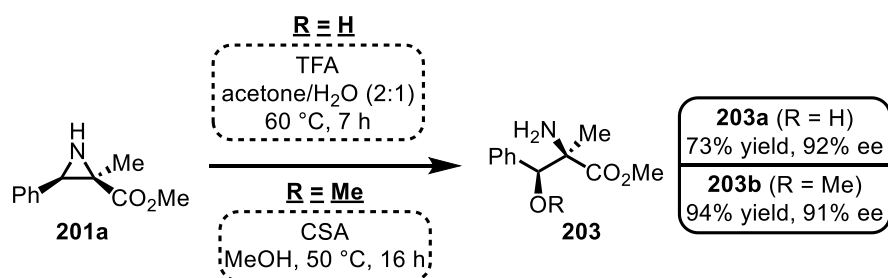
Results and Discussion

intermediates for numerous transformations.^[239–242] Hence, compound **201a** was subsequently converted to different α -methyl amino acid derivatives. When a ring opening via a Pd-catalyzed hydrogenation was conducted, α -methyl phenylalanine ester (**202**) was obtained in 94% yield with 90% ee as depicted in Scheme 62.



Scheme 62: Reduction of azirine **200a** with 9-BBN as reducing agent. Conveniently, aziridine **201a** was furnished as a single diastereomer without loss of enantioselectivity. Subsequent ring opening via hydrogenation provided α -methyl phenylalanine with 90% ee. The relative configuration of **201a** was determined by synthesis of ethyl ester aziridine **201b** and comparison with reported data.

Afterwards, ring opening reactions with nucleophiles were examined (Scheme 63). Conveniently, aziridine **201a** could be converted to the corresponding β -hydroxy (**203a**) and β -methoxy (**203b**) phenylalanine derivatives in 73% and 94% yield, respectively. Both products were formed with very high enantioselectivities and as the *threo*-isomer as validated by either comparison with the literature (for **203a**)^[243] or via NMR spectroscopic determination of the relative configuration (for **203b**, see Section 5.5.4). Such α -quaternary amino acid compounds are useful for the synthesis of peptidomimetics and are found in pharmaceuticals like methyl dopa and, thus, their synthetic access is of high interest.^[244–247]

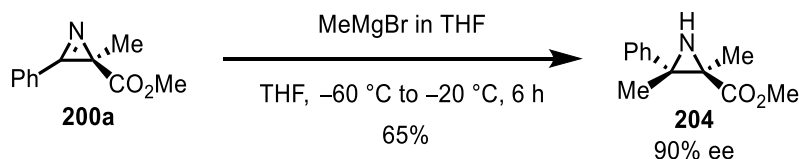


Scheme 63: Nucleophilic ring opening of aziridine **201a** to furnish the two β -substituted amino acid ester derivatives **203**. Both products were obtained as the *threo*-isomers.

Additionally, furnished *2H*-azirine **200a** was methylated by reaction with methyl magnesium bromide to afford aziridine **204** without any detectable isomerization as depicted in Scheme 64.

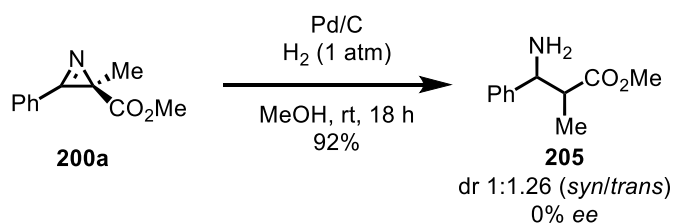
Results and Discussion

Intriguingly, this compound can serve as a valuable intermediate for the synthesis of α,β -dimethyl phenylalanine as reported by the Davis group.^[248]



Scheme 64: Methylation of azirine **200a** with methyl magnesium bromide to furnish aziridine **204**.

Ultimately, the feasibility of directly applying the hydrogenation protocol to chiral *2H*-azirine **200a** was evaluated to provide a more convenient access towards α -amino acid ester **202**. Azirines are usually converted into the corresponding aziridines via reduction or hydrogenation prior to the ring opening.^[249] Serendipitously, instead of the conversion towards α -amino acid ester **202**, the exclusive formation of β^2,β^3 -disubstituted amino acid product **205** was observed as depicted in Scheme 65. However, the chiral stereocenter completely racemized in the course of this reaction providing a diastereomeric mixture of compound **205** with a dr of 1:1.26 without any enantioselectivity. Interestingly, the reaction exhibited full conversion without the formation of side products. Previously, there has only been one report of a direct, palladium catalyzed hydrogenation for the ring opening of polyfunctionalized azirines to furnish an aminocoumarin derivative via ring enlargement.^[250] Enticingly, the direct access of such β -amino acid derivatives via hydrogenation of *2H*-azirines has never been reported before and could represent a convenient access to this intriguing class of compounds.^[215]



Scheme 65: Palladium catalyzed hydrogenation of *2H*-azirine **200a** to afford β^2,β^3 -disubstituted β -amino acid ester **205**. Noteworthy, no formation of aziridine **201a**, α -amino acid ester **202**, or remaining starting material was observed.

3.4.4 Concluding Remarks

In summary, an elegant synthetic pathway towards non-*C*₂-symmetric chiral iron(II) complexes based on a modular, chiral, tetradentate, N₄-type ligand system was established. The readily available, proline-based, chiral diamine backbone conveniently granted the feasibility of a tailored adjustment of electronic and steric properties. Three electronically and sterically distinct terminal coordinating

Results and Discussion

aryl moieties were chosen and complexes with all possible combinations synthesized. The diamine backbone exhibited the required high diastereoselectivity during complexation, forming the desired complexes with a *cis- α* -topology as confirmed by X-ray analysis of a single crystal for standard catalyst **191a**. Furthermore, NMR spectroscopic measurements of the paramagnetic Fe(II)-complex **191a** and of a diamagnetic gallium(III) derivative indicated the presence of only one diastereomer in solution. Subsequently, the catalytical efficacy of the newly synthesized complexes was evaluated for an asymmetric ring contraction of isoxazoles **164**. Remarkably, of all iron complexes applied, a derivative comprising one pyridine and one benzothiazole moiety exhibited the best performance in regard to enantioselectivity and activity when compared to other heteroaromatic ligand combinations. Hence, these results demonstrate the advantages offered by a modular ligand design with reduced symmetry. Moreover, the possibility of applying bench-stable dichloro-based catalysts erases the necessity of using expensive silver salts and the obtained complexes show a high robustness towards air and water enabling a convenient catalysis under open flask conditions. The performance of Fe(II)-catalyst **191a** was further evaluated during a substrate scope providing 19 chiral *2H*-azirines **164** with mostly good to very high enantioselectivities of up to 92% ee in good to excellent yields (up to 99% yield). Afterwards, the versatility of the obtained products was demonstrated by several follow-up reactions to obtain useful building blocks and α -amino acid derivatives without any loss of enantiomeric excess. Interestingly, an attempted hydrogenation of the ring contraction product provided an unprecedented reactivity to afford β -amino acid derivatives, albeit no enantioselectivity was observed. Nevertheless, the here presented novel access towards interesting β^2, β^3 -disubstituted β -amino acids could represent an enticing foundation for future work to facilitate this transformation under conditions enabling a sophisticated stereoinduction.

4. Summary and Outlook

4.1 Summary

The achievements realized in the course of this work represent valuable contributions to the field of asymmetric iron catalysis and complement preceding accomplishments in order to attain a more sustainable and economic synthesis of non-racemic chiral compounds. Moreover, the presented results intriguingly depict the attainment of previously untapped opportunities, albeit chiral iron complexes being successfully applied to transfer chiral information to substrates for nearly four decades. Hence, the design, development, synthesis, and application of novel catalytic systems is a timely and ongoing endeavor with yet to be uncovered chances and possibilities. Considering the aims of this work, the obtained observations further emphasize the importance of a sophisticated and well-tailored catalyst design regarding the access towards novel reactivities.

Development of Chiral-at-Metal Iron(II) Complexes with a Pentadentate Ligand. The design and synthesis of novel pentadentate ligands providing Fe(II)-complexes inheriting metal-centered stereogenicity was realized as presented in Chapter 3.1. Initially, the feasibility of applying an achiral pentadentate amido scaffold (1st generation) was scrutinized to furnish a chiral-at-iron complex as a racemic mixture (Figure 33). The complexation was analyzed by mass spectroscopy and elemental analysis, however, NMR measurements exhibited paramagnetic properties, consequently rendering the product insufficient for the purpose of this work. For the possibility of a comprehensive NMR spectroscopic analysis, a modified ligand (2nd generation) without amide motif was synthetically accessed. Fortunately, the altered framework facilitated the isolation of a chiral iron complex with diamagnetic properties, accordingly meeting the initially considered requirements. A subsequent separation of the enantiomers by exploiting chiral auxiliaries was shown to provide insufficient results and, thus, an alternative stereogenic-at-iron approach was investigated.

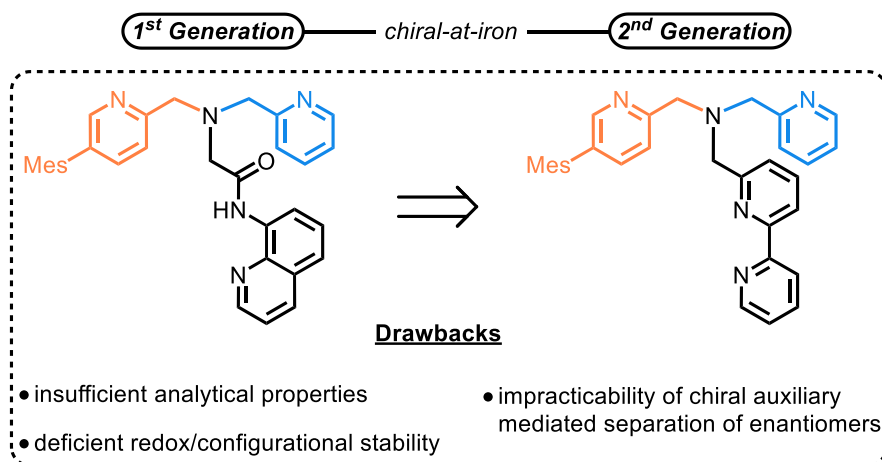


Figure 33: Evolution of the pentadentate ligand design for chiral octahedral iron complexes in this work.

Stereogenic-at-Iron Complexes with a Chiral Tripodal Pentadentate Ligand. A synthetic access towards chiral iron(II) complexes comprising pentadentate chiral ligands was established in Chapter 3.2. In order to enable the feasibility of isolating iron compounds with a well-defined metal-centered stereogenicity, a finely tailored pentadentate chiral ligand scaffold (3rd generation) was developed and synthesized. Subsequent complexation and analysis via NMR spectroscopic measurements showed that the corresponding complexes are diamagnetic and obtained as a mixture of diastereomers. Separation of the diastereomeric iron complexes by conventional methods such as column chromatography or precipitation were shown to provide unsatisfactory results. Gratifyingly, an interconversion due to the significantly different thermodynamic stabilities was discovered and a following examination confirmed the possibility of exploiting this behavior to furnish a diastereomerically pure (dr >20:1) complex. The circumvention of a laborious separation as well as the possibility of a virtually complete isomerization without decomposition render this approach an enticing and convenient method (Figure 34).

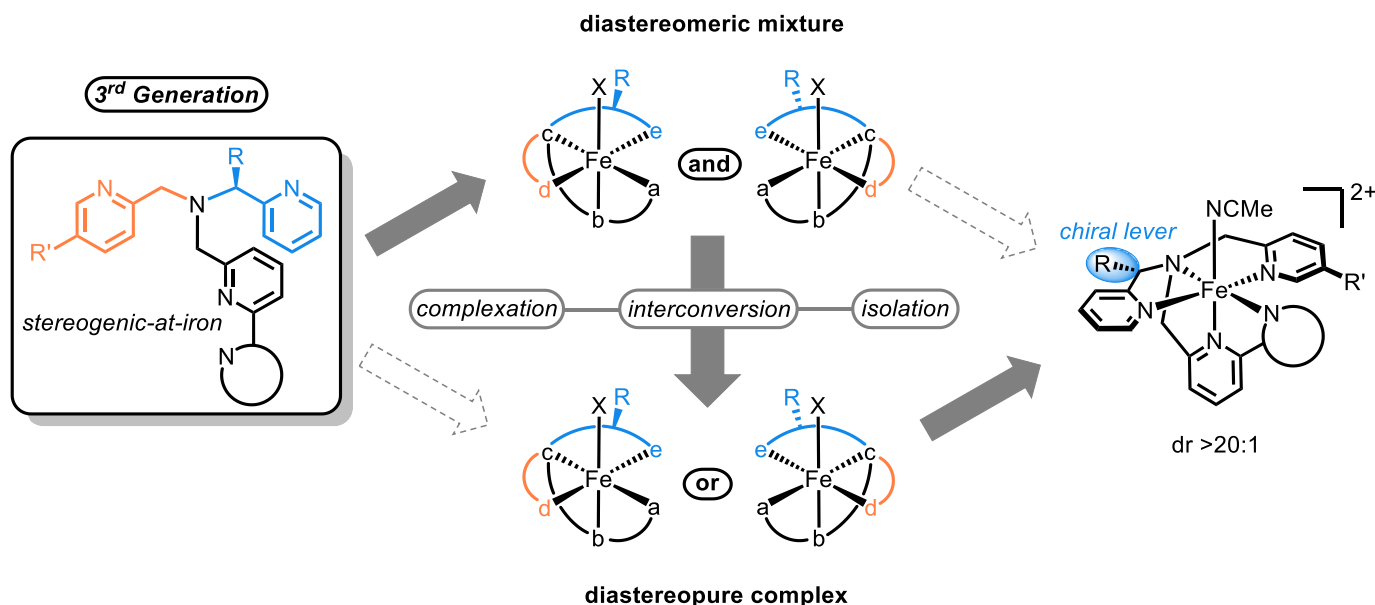


Figure 34: Schematic pathway facilitating the isolation of diastereomerically pure stereogenic-at-iron complexes by exploitation of a chiral lever.^[150]

By sterically enhancing the chiral lever of the ligand, a faster interconversion was achieved and subsequent modifications of the ligand scaffold further confirmed and established the applicability of the here introduced complex synthesis. Furthermore, the diamagnetic behavior facilitated an in-depth analysis of the structural features and dynamics by NMR spectroscopy of an isopropyl derivative. Ultimately, four different iron complexes were synthesized with alterations on different positions of the tripodal ligand scaffold and were accessible in very high yields after complexation and isomerization. Single crystals suitable for X-ray analysis of two iron compounds confirmed the

configurational topology and independently verified the structural elucidation by NMR spectroscopic analysis (Figure 35).

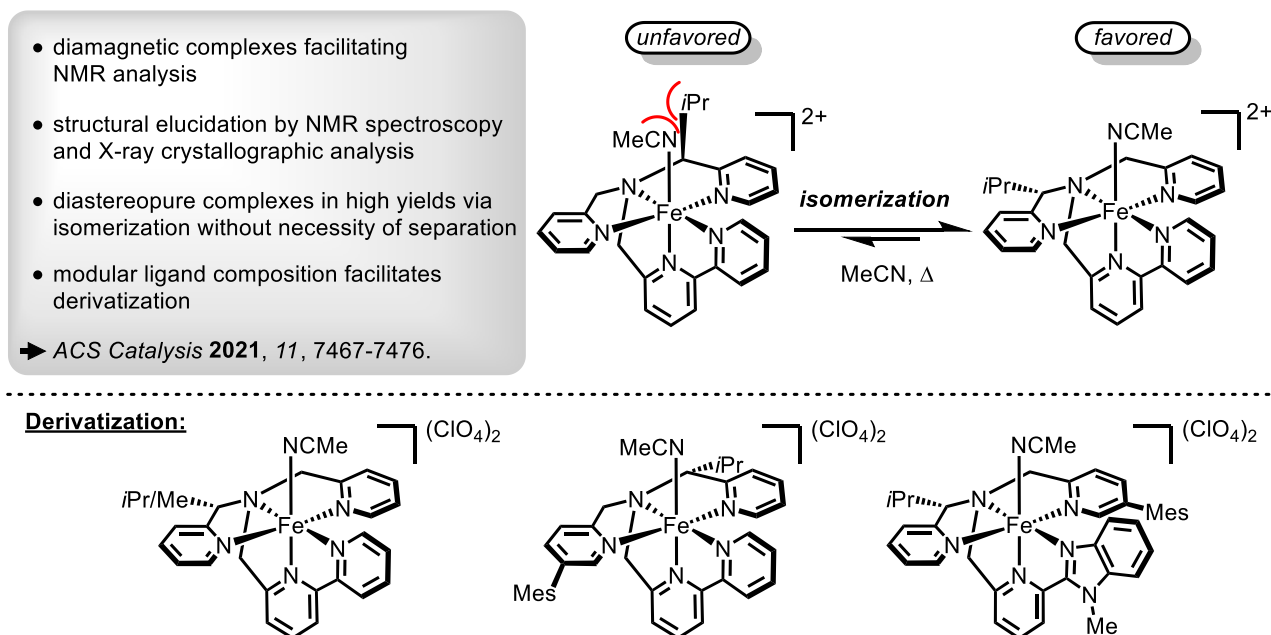
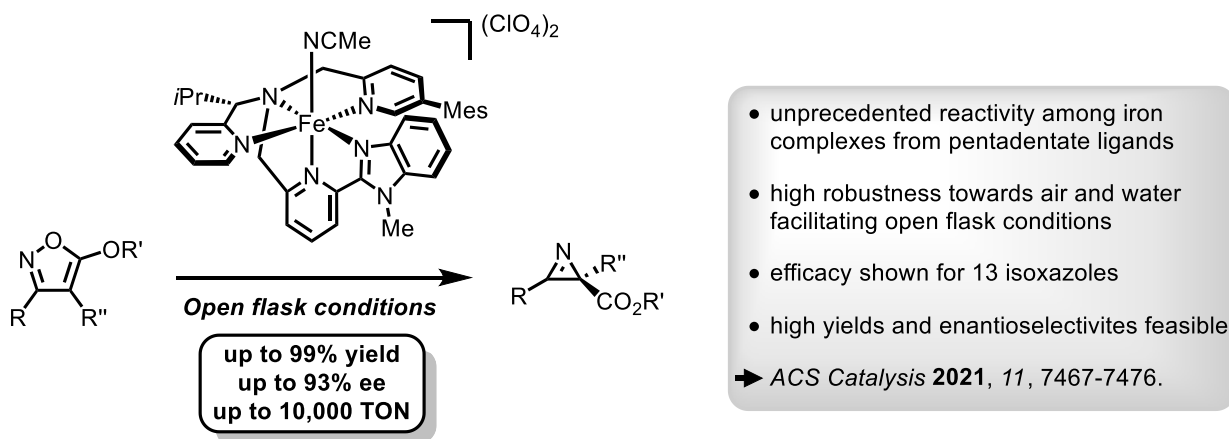


Figure 35: Synthetic access of diastereopure stereogenic-at-metal iron(II) complexes via isomerization erasing the necessity of the separation of diastereomers. The modular composition of the pentadentate ligands enables a convenient derivatization.^[150]

Application of Iron Complexes with a Chiral Pentadentate Ligand in Asymmetric Catalysis.

The feasibility of employing the novel chiral iron complexes in asymmetric catalysis was explored as described in Chapter 3.3. The catalysts showed an unprecedented activity for an asymmetric ring contraction of isoxazoles to afford chiral *2H*-azirines surpassing the reactivity of previously reported rhodium and ruthenium catalysts for this transformation. Impressively, turnover numbers of up to 10,000 were observed. An initial catalyst screening and subsequent optimization of the reaction conditions facilitated high enantioselectivities. Conveniently, the catalysts exhibited a high robustness towards oxidative decomposition or hydrolysis enabling this enantioselective transformation under open flask conditions. Furthermore, the efficacy of the catalytic system was demonstrated for 13 isoxazoles to furnish the corresponding products in up to 99% yield and with up to 93% ee. Previously reported iron catalysts comprising pentadentate ligands were mainly applied to oxidation reactions with mostly low to moderated enantioselectivities with only one exception of a sulfide oxidation reported by the Kaizer group.^[114] Hence, the reactivity and stereoselectivity achieved with the here described system are unprecedented among complexes derived from chiral pentadentate ligand scaffolds and highlight the ability of 3d-transition metals to not only substitute more noble transition metal catalysts but also surpass their performance in asymmetric transformations (Scheme 66).



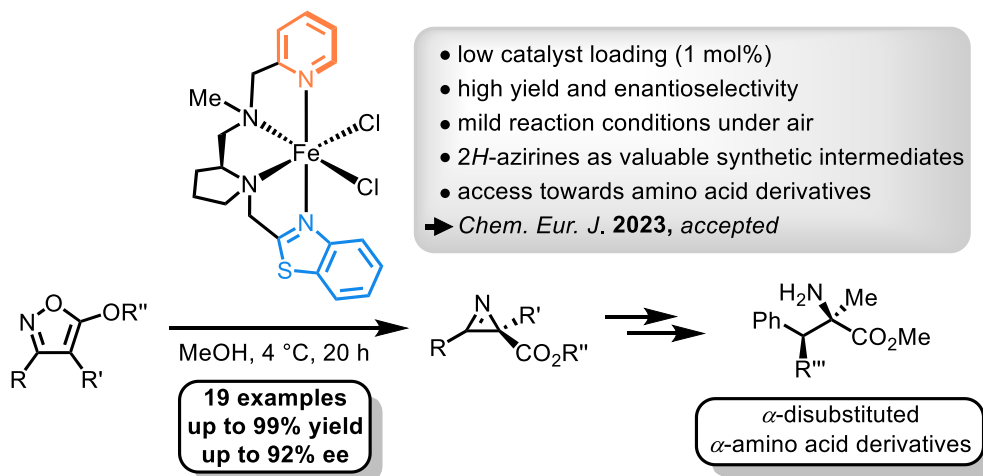
Scheme 66: Application of novel iron(II) complexes in asymmetric catalysis for the enantioselective ring contraction of isoxazoles to afford chiral 2*H*-azirines.^[150]

Expanding the Family of non-*C*₂-Symmetric, Linear, Tetradentate Ligands for Fe(II)-Catalysts.

Chapter 3.4 describes the development of novel non-*C*₂-symmetric N₄-type ligand scaffolds for a subsequent application in iron(II) complexes suitable for asymmetric catalysis. By employing a readily available proline-based chiral diamine backbone, an unsymmetric synthesis of tetradentate ligands exhibiting sterically and electronically different characteristics was successfully established. Moreover, the chiral backbone facilitated the predetermination of the metal-centered stereogenicity as well as an overall *cis-α* coordination topology of the obtained complexes. Subsequently, an evaluation of the catalytic performance of the iron compounds for an asymmetric ring contraction of isoxazoles provided insights into the advantages of decreasing the overall symmetry of the applied catalysts. Intriguingly, a derivative comprising a pyridine and a benzothiazole group as terminal coordinating moieties exhibited the best results in regard to activity and selectivity. Moreover, the convenient possibility of applying bench-stable dichloro complexes was successfully proven, erasing the necessity of using expensive silver salts for the catalyst synthesis. An optimization of the reaction conditions granted the feasibility of furnishing the desired product in high yield with a high enantiomeric excess under convenient open flask conditions. Subsequently, the performance of the catalytic system was demonstrated for a substrate scope of 19 isoxazoles. Accordingly, the desired 2*H*-azirines were formed with up to 92% ee in excellent yields of up to 99% with a low catalyst loading of 1 mol%. This represents a rare example in which a desymmetrization of the terminal coordinating groups in such a linear, tetradentate, N₄-type ligand provides a significantly better stereoinduction during homogeneous asymmetric catalysis. Furthermore, the versatility of the obtained products was shown for several follow-up reactions to furnish *α*-disubstituted *α*-amino acid derivatives without loss of enantiomeric excess. Surprisingly, during this investigation a novel transformation was found providing a direct access to *β*²,*β*³-amino acid derivatives in a single step

Summary and Outlook

via hydrogenation of an azirine derivative, albeit in a non-selective fashion in terms of stereoselectivity.



Scheme 67: Enantioselective ring contraction with non-C₂-symmetric Fe(II)-catalyst to obtain 2*H*-azirines in high yields with high enantioselectivities.^[215]

4.2 Outlook

The results presented in this work emphasize the significance of a sophisticated catalyst design and showcase the value of finely tailored ligands to achieve enantiomeric transformations. Moreover, the advantages that accompany scaffolds, that give rise to metal-centered stereogenicity, should be taken into account for future efforts of complementing asymmetric transition metal catalysts. Previously, especially the Meggers group highlighted the opportunities that considerations of the metal-centered chirality can provide. In order to develop novel catalytically active complexes based on 3d-transition metals, the results obtained in the course of this work can serve as a useful inspiration. For instance, modifications on different segments of the pentadentate ligand could be scrutinized in future projects to alter the steric and electronic properties of the corresponding iron complexes. The modular synthetic approach grants the possibility of conveniently synthesizing differently substituted arms of the tripodal scaffold. Moreover, the application of other metal precursors, such as cobalt or manganese, represents an interesting survey. These metals show similar complexation properties when compared to iron and catalysts coordinated by the here established pentadentate ligands are potentially able to provide novel and unique synthetic opportunities. The ideas for possible future projects are depicted in Figure 36.

Summary and Outlook

Other Metals & Ligand Modification

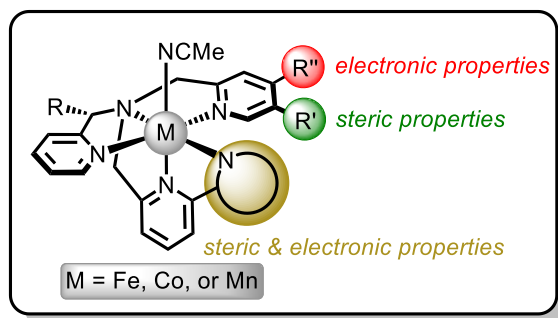


Figure 36: Considering the results obtained during this work for pentadentate stereogenic-at-iron complexes, future projects could include further modifications on the ligand framework or the application of other 3d-transition metals.

As depicted in Chapter 3.4, a decrease on the overall symmetry of octahedral complexes with a linear, tetradentate N₄-type ligand can provide enhanced catalytic properties in regard to selectivity and reactivity. The straightforward synthetic pathway towards the final ligands introduced in this work provides the feasibility of introducing other, sterically more demanding moieties into the scaffold to further differentiate the two labile reaction sites of the corresponding catalysts. For instance, implementation of a mesityl-substituted pyrazole motif could improve the shielding of the catalytically active site. A similar motif was recently shown by the Meggers group to improve the selectivity for a rhodium(III) catalyzed asymmetric α -fluorination and α -chlorination of 2-acyl imidazoles.^[108] Moreover, the influence of electronically different substituents would represent an interesting survey. In addition to altering the terminal coordinating aryl groups, the application of other chiral diamine backbones combined with the non- C_2 -symmetric ligand approach could be examined to evaluate their influence on the derived catalysts (Figure 37).

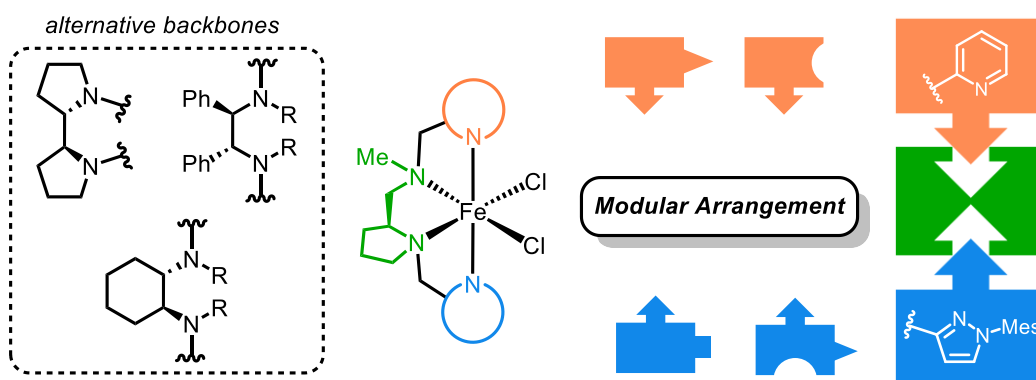


Figure 37: Potential adjustments of tetradentate, linear N₄-type ligand scaffolds to furnish non- C_2 -symmetric iron(II) complexes.

Additionally, by combining the experiences gained for the pentadentate and tetradentate ligand systems, a potential modification of the proline-based tetradentate scaffold could be envisioned to

furnish a chiral pentadentate ligand. Substitution of the methyl group on the nitrogen of the chiral diamine backbone by a coordinating methylene-bridged aryl group (for instance, benzimidazole) can provide interesting ligands to form novel iron(II) complexes (Figure 38). Similar ligands with all three coordinating aryl groups being identical have been reported by the group of Sun for the synthesis of manganese and iron complexes.^[202,251–253] However, by implementation of two different aryl rings, a distinct topology is feasible that can provide a unique and sophisticated chiral environment for asymmetric catalysis. In theory, two diastereomeric complexes can be formed that may evince different thermodynamic stabilities depending on the steric demand of the aryl groups and, hence, could either grant a diastereoselective complexation or the possibility of isomerization.

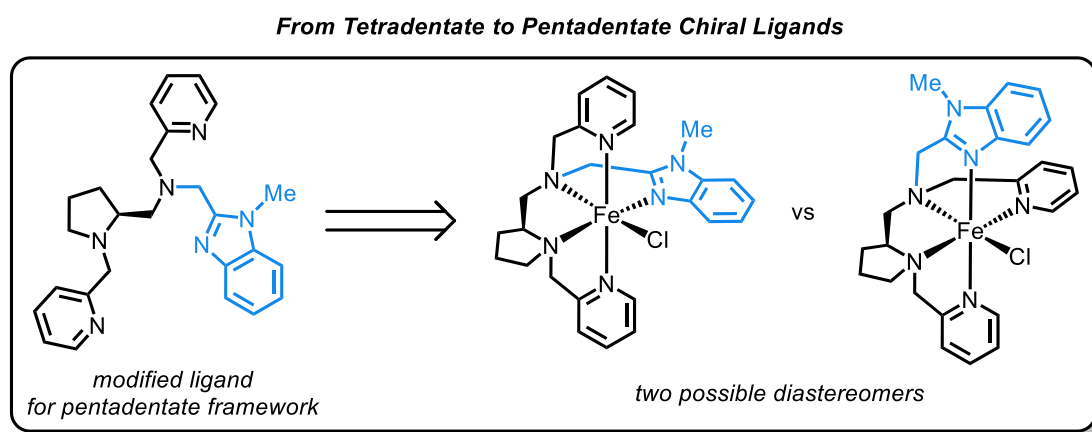
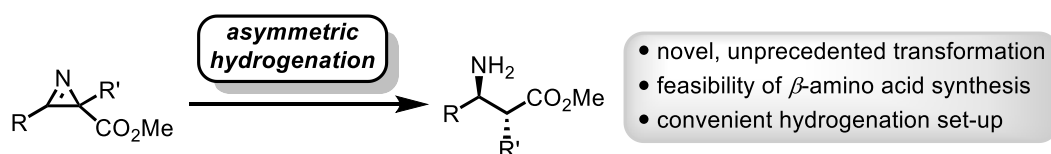


Figure 38: Modification of the chiral, tetradentate, proline-derived ligand to furnish a pentadentate scaffold by addition of a coordinating benzimidazole motif (blue).

Besides modifications regarding the ligand and catalyst design, a further investigation concerning the reactivity to facilitate novel transformations should be considered for future projects. As mentioned in Chapter 3.4, especially iron-catalyzed enantioselective C-C bond formations present and underdeveloped and enticing research topic. Noteworthy, a scrutiny of the β^2, β^3 -substituted amino acid synthesis via asymmetric hydrogenation of azirines could provide a convenient access towards this interesting class of compounds. By employing a suitable chiral catalyst system, the possibility of conducting the reaction with a sufficient stereoinduction could be realized. Due to the complete racemization observed, this transformation should in theory be feasible with racemic starting substrate (Scheme 68).



Scheme 68: Exploiting the transformation introduced in this work to furnish β -amino acid derivatives directly from azirines could provide a new access towards these intriguing compounds in an enantioselective fashion.

5. Experimental Part

5.1 General Methods

All reactions were carried out under inert nitrogen gas atmosphere in heat-gun dried (630 °C) glassware using Schlenk-technique unless stated otherwise. Commercially purchased reagents were used without further purification. Prior to usage, all solvents were purified by distillation on a rotary evaporator at 40 °C under reduced pressure to remove higher-boiling impurities. Solvents with HPLC grade quality were used without further purification or drying. Solvents for water-sensitive reactions were distilled under nitrogen atmosphere after drying over sodium/benzophenone (THF, Et₂O, toluene), calcium hydride (MeCN, CH₂Cl₂, MeOH), or phosphorus pentoxide (CHCl₃).

5.2 Materials and Instruments

Thin Layer Chromatography (TLC)

Monitoring of reactions was performed by using TLC plates (TLC Silica gel 60 F₂₅₄) coated on glass from Merck KGaA or by using TLC plates (ALUGRAM ALOX N / UV₂₅₄) coated on aluminum sheets from Macherey-Nagel. If not stated otherwise, R_f-values account for TLC analysis with silica gel coated TLC plates. Visualization of compounds was either realized by fluorescence quenching under UV-light ($\lambda = 254$ or 366 nm) or by staining the TLC plates with potassium permanganate solution (3 g KMnO₄, 20 g Na₂CO₃, and one NaOH pellet dissolved in 240 mL H₂O) or with a ninhydrin-solution (3 g ninhydrin dissolved in 200 mL of *n*-butanol and 6 mL acetic acid).

Flash Column Chromatography

Purification by column chromatography was performed with silica gel 60 M from Macherey-Nagel (irregular shaped, 230-400 mesh, pH 6.8, pore volume: 0.81 mL · g⁻¹, mean pore size: 66 Å, specific surface: 492 m² · g⁻¹, particle size distribution: 0.5% < 25 μm and 1.7% > 71 μm, water content: 1.6%), with neutral aluminum oxide from Macherey-Nagel (pH 7 ± 0.5, activity 1, particle size 50-200 μm, specific surface: 130 m² · g⁻¹), and with basic aluminum oxide either from Honeywell Fluka™ (pH 8.5–10.5, activated, Brockmann I, specific surface: 184.5–225.5 m² · g⁻¹, grain size: at least 95% between 0.04–0.30 mm) or from Sigma-Aldrich (pH 9.5 ± 0.5, activated, Brockmann I, mean pore size: 58 Å). Crude products were either transferred to the column in a minimum amount

Experimental Part

of solvent or they were first adsorbed onto a small amount of silica gel (dry-load). If not stated otherwise, samples were normally transferred while dissolved in a solvent.

Nuclear Magnetic Resonance Spectroscopy (NMR)

^1H NMR, $^{13}\text{C}\{^1\text{H}\}$ NMR, and $^{19}\text{F}\{^1\text{H}\}$ NMR spectra were recorded on a Bruker AV II 300 MHz or AV III HD 250 MHz spectrometer in automation or a Bruker AVIII HD 300 MHz, AV III 500 MHz, or AVII 600 MHz spectrometer by the NMR service department of the Philipps-Universität Marburg. Unless noted otherwise, measurements were conducted at an ambient temperature of 300 K. The chemical shift δ is listed in ppm referenced against tetramethylsilane (TMS, $\delta=0$ ppm) with the residual solvent signal as internal standard. Measurements were performed with CDCl_3 (^1H : $\delta=7.26$ ppm; ^{13}C : $\delta=77.16$ ppm), CD_2Cl_2 (^1H : $\delta=5.32$ ppm; ^{13}C : $\delta=53.84$ ppm), and CD_3CN (^1H : $\delta=1.94$ ppm; ^{13}C : $\delta=1.32/118.26$ ppm) as solvents.^[254] $^{19}\text{F}\{^1\text{H}\}$ NMR are were calibrated to trichlorofluoromethane (CFCl_3 , $\delta=0$ ppm) as external standard. The multiplicity of signals is described phenomenologically and, hence, does not describe the theoretically expected multiplicity. Multiplicities are abbreviated as follows: s = singlet, br s = broad singlet, d = doublet, t = triplet, q = quartet, m = multiplet, and combinations thereof. Coupling constants J are given in Hertz (Hz) and attribute to H-H couplings (^1H NMR) or C-F couplings (^{13}C NMR). All ^{13}C NMR signals are singlets and account for one carbon atom if not stated otherwise.

High-Performance Liquid Chromatography (HPLC)

Enantiomeric excess was measured by HPLC analysis on a chiral stationary phase with an Agilent 1200 or Agilent 1260 system. Daicel Chiralpak[®] and Daicel Chiralcel[®] columns were employed as chiral stationary phases. Detailed HPLC conditions are described in the analytical data for the individual compounds.

High-Resolution Mass Spectrometry (HRMS)

Mass spectra were recorded by the mass service department of the Philipps-Universität Marburg. High-resolution mass spectra were measured via electrospray-ionization-technique (ESI) or atmospheric pressure chemical ionization-technique (APCI) on a Finnigan LTQ-FT Ultra mass spectrometer from Thermo Fischer Scientific. The resolution was set 100.000. The ion masses m/z are given in units (u).

Elemental Analysis

Elemental analysis for carbon, hydrogen, nitrogen, and sulfur (CHN/S-analysis) was performed via combustion analysis with a vario Micro cube from Elementar in either CHN- or CHNS-mode.

Infrared Spectroscopy (IR)

Infrared spectra were acquired using a Bruker Alpha FT-IR spectrometer. The resulting absorption bands are listed as wavenumbers (cm^{-1}) and the correlating intensities are specified as follows: w = weak, m = medium, and s = strong.

Optical Rotation

Optical rotations were measured at 22 °C for the Na-D wavelength ($\lambda = 589 \text{ nm}$) on a Krüss P8000-T polarimeter with $[\alpha]_{\text{D}}^{22}$ values listed in degrees with concentrations reported in g/100 mL.

X-Ray Crystallography

Single crystal X-ray diffraction measurements were measured by members of the department for crystal structure analysis of the Philipps-Universität Marburg with a STOE STADIVARI or a Bruker AXS D8 Quest diffractometer. Obtained diffraction data were evaluated and the corresponding crystal structure resolved by Dr. (RUS) Sergei I. Ivlev.

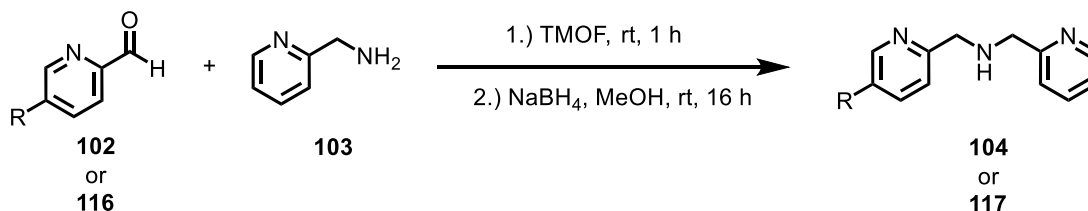
Microwave

Microwave reactions were performed in 10 mL microwave vials sealed with Sil/PTFE septa in a single-mode Discover System by CEM.

5.3 Synthesis of Pentadentate Ligands

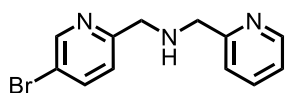
5.3.1 Synthesis of Pentadentate Amide Ligand **101** and Complex **108**

General Procedure A: Reductive Amination for Dipicolylamine Synthesis (GP A)



Following a procedure by Tilmans *et al.*,^[124] aldehyde **102** or **116** (1.20 eq.) was dissolved in trimethylorthoformate (0.25 M) and picolylamine (**103**, 1.00 eq.) was added while stirring. After stirring for 1 h at rt, the solvent was removed under reduced pressure and the resulting oil was redissolved in MeOH (0.25 M). NaBH₄ (2.10 eq.) was added in portions and the reaction mixture was subsequently stirred for 16 h at rt. Afterwards, the reaction was quenched and diluted with H₂O and the pH-value was adjusted to pH = 14 with 10 M aq. NaOH-solution. The aq. phase was extracted with Et₂O (3x) and the combined organic layers were washed with 0.5 M aq. NaOH-solution. Afterwards, the product was again drawn back into the aq. layer by extraction with 1 M aq. citric acid solution (3x). Subsequently, the pH-value was adjusted back to pH = 14 by using 10 M aq. NaOH-solution and the aq. layer again extracted with Et₂O (5x). The combined organic layers were washed with brine, dried over Na₂SO₄, and the solvent was removed under reduced pressure. After drying under vacuum, dipicolylamine **104** or **117** was obtained as a yellow oil and used without further purification.

1-(5-Bromopyridin-2-yl)-N-(pyridin-2-ylmethyl)methanamine (**104**)



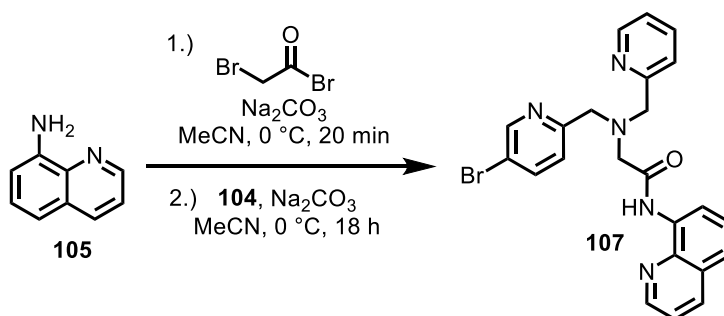
Following **GP A**, 2-formyl-5-bromopyridine (**102**, 1.03 g, 5.55 mmol, 1.20 eq.), picolylamine (**103**, 0.48 mL, 0.50 g, 4.62 mmol, 1.00 eq.), and NaBH₄ (0.37 g, 9.71 mmol, 2.10 eq.) were employed to obtain dipicolylamine **104** (1.26 g, 4.54 mmol, 98%) as a yellow oil.

Experimental Part

¹H NMR: (300 MHz, CD₂Cl₂) δ = 8.59 (d, J = 2.3 Hz, 1H), 8.52 (d, J = 5.0 Hz, 1H), 7.78 (dd, J = 8.3, 2.4 Hz, 1H), 7.65 (td, J = 7.7, 1.8 Hz, 1H), 7.35-7.29 (m, 2H), 7.16 (dd, J = 7.1, 4.9 Hz, 1H), 3.91 (s, 2H), 3.89 (s, 2H) ppm.

Analytical data were consistent with reported data.^[124]

2-(((5-Bromopyridin-2-yl)methyl)(pyridin-2-ylmethyl)amino)-*N*-(quinolin-8-yl)acet-amide (107)



According to a slightly modified procedure by Hitomi *et al.*,^[107] 8-aminoquinoline (**105**, 235 mg, 1.63 mmol, 1.00 eq.) and Na₂CO₃ (242 mg, 2.28 mmol, 1.40 eq.) were suspended in MeCN (4.5 mL, 0.35 M), cooled to 0 °C, and bromoacetyl bromide (0.17 mL, 395 mg, 1.96 mmol, 1.20 eq.) was added dropwise. After stirring for 20 min at 0 °C, the mixture was filtered over a short plug of Celite and the solvent was evaporated to give an orange solid. The residue was again dissolved in MeCN (9.0 mL, 0.18 M), the solution was cooled to 0 °C, and Na₂CO₃ (242 mg, 2.28 mmol, 1.40 eq.) and dipicolylamine **104** (544 mg, 1.96 mmol, 1.20 eq.) were added. The resulting mixture was stirred for 18 h at 0 °C after which filtration over a short plug of Celite gave the crude product that was further purified by column chromatography on neutral alumina (*n*-pentane/EtOAc 1:1 → EtOAc pure) to give **107** (510 mg, 1.10 mmol, 68%) as an off-white solid.

TLC: R_f = 0.45 (EtOAc, on neutral alumina).

¹H NMR: (300 MHz, CD₂Cl₂) δ = 11.51 (s, 1H), 8.94 (dd, J = 4.2, 1.7 Hz, 1H), 8.72 (dd, J = 6.3, 2.7 Hz, 1H), 8.56 (d, J = 1.9 Hz, 1H), 8.50 (dq, J = 4.9, 0.8 Hz, 1H), 8.23 (dd, J = 8.3, 1.7 Hz, 1H), 7.91 (d, J = 8.4 Hz, 1H), 7.87 (d, J = 7.9 Hz, 1H), 7.78 (dd, J = 8.4, 2.4 Hz, 1H), 7.65 (td, J = 7.7, 1.8 Hz, 1H), 7.58-7.52 (m, 3H), 7.16 (ddd, J = 7.5, 4.9, 0.9 Hz, 1H), 3.97 (s, 2H), 3.95 (s, 2H), 3.50 (s, 2H) ppm.

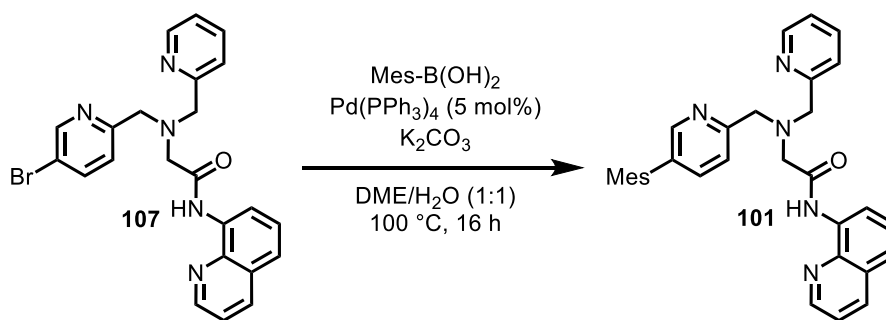
Experimental Part

¹³C NMR: (75 MHz, CD₂Cl₂) δ = 169.6, 158.5, 157.6, 150.4, 149.5, 148.7, 139.5, 139.2, 136.8, 136.7, 134.9, 128.6, 127.6, 125.3, 123.8, 122.7, 122.2, 122.0, 119.7, 116.5, 61.3, 60.8, 59.8 ppm.

IR: (neat): $\tilde{\nu}$ = 3295 (w), 3049 (w), 3008 (w), 2832 (w), 1680 (m), 1580 (w), 1519 (s), 1476 (m), 1427 (m), 1371 (m), 1323 (w), 1249 (w), 1120 (w), 1090 (w), 1056 (w), 1001 (m), 900 (w), 823 (m), 790 (m), 754 (s), 670 (w), 628 (w), 555 (w), 518 (w), 494 (w), 404 (w) cm⁻¹.

HRMS: (ESI+) m/z calcd. for C₂₃H₂₀BrN₅O₂Na [M+Na]⁺: 486.0726; found: 486.0709.

2-(((5-Mesitylpyridin-2-yl)methyl)(pyridin-2-ylmethyl)amino)-*N*-(quinolin-8-yl)acetamide (**101**)



According to a slightly modified procedure by Roy *et al.*,^[125] a Schlenk flask was charged with bromide **107** (3.20 g, 6.92 mmol, 1.00 eq.), mesitylboronic acid (1.36 g, 8.31 mmol, 1.20 eq.), Pd(PPh₃)₄ (0.40 g, 0.35 mmol, 0.05 eq.), K₂CO₃ (2.87 g, 20.8 mmol, 3.00 eq.), and 1,2-dimethoxyethane/H₂O (1/1 v%, 42 mL, 0.17 M). The resulting suspension was thoroughly degassed via freeze-pump-thaw for three cycles and subsequently stirred for 16 h at 100 °C. Afterwards, the reaction mixture was cooled to rt, diluted with EtOAc, and layers were separated. The aq. layer was extracted with EtOAc (3x), the combined organic layers were washed with brine, dried over Na₂SO₄, filtered, and the solvent was removed under reduced pressure. The crude product was purified by column chromatography on neutral alumina (*n*-pentane/EtOAc 1:1 → EtOAc) to obtain pure ligand **101** (3.34 g, 6.67 mmol, 96%) as a colorless solid.

TLC: R_f = 0.50 (EtOAc, on neutral alumina).

¹H NMR: (300 MHz, CD₂Cl₂) δ = 11.60 (s, 1H), 8.95 (dd, J = 4.3, 1.4 Hz, 1H), 8.73 (dd, J = 5.6, 3.5 Hz, 1H), 8.52 (d, J = 4.3 Hz, 1H), 8.27 (d, J = 1.4 Hz, 1H), 8.20 (dd, J = 8.2, 1.4 Hz, 1H), 8.00 (d, J = 7.9 Hz, 2H), 7.68 (td, J = 7.6, 1.6 Hz, 1H), 7.55-7.47 (m, 3H),

Experimental Part

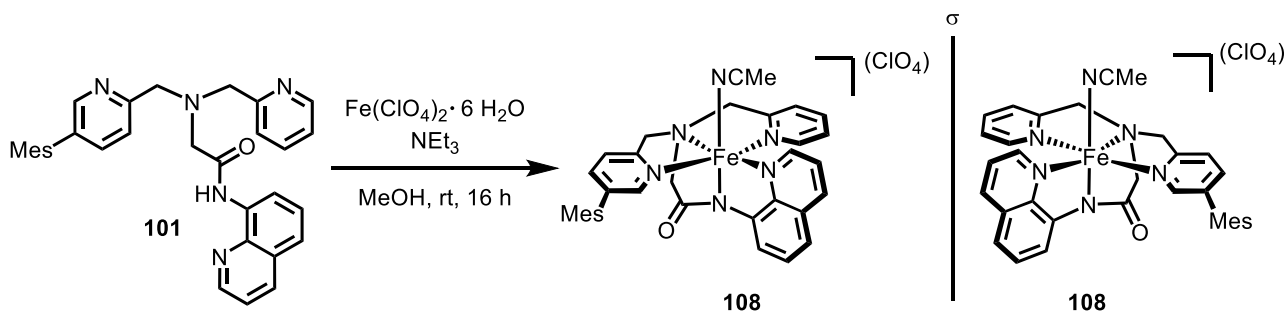
7.43 (dd, $J = 7.9, 2.1$ Hz, 1H), 7.16 (dd, $J = 7.6, 5.2$ Hz, 1H), 6.91 (s, 2H), 4.07 (s, 4H), 3.58 (s, 2H), 2.29 (s, 3H), 1.89 (s, 6H) ppm.

^{13}C NMR: (75 MHz, CD_2Cl_2) $\delta = 169.9, 159.0, 156.9, 149.9, 149.5, 148.7, 139.3, 137.9$ (2C), 137.7, 136.8, 136.7, 136.6 (2C), 135.6, 135.4, 135.1, 128.6, 128.5, 127.6, 123.8, 123.5, 122.7, 122.1, 121.9, 116.5, 61.8, 61.6, 60.0, 21.1, 20.9 (2C) ppm.

IR: (neat) $\tilde{\nu} = 3305$ (w), 2301 (w), 2266 (w), 2207 (w), 2146 (w), 2106 (w), 2023 (w), 1999 (w), 1956 (w), 1891 (w), 1686 (m), 1589 (w), 1522 (s), 1478 (m), 1428 (m), 1374 (w), 1324 (w), 1250 (w), 1126 (w), 976 (w), 849 (w), 828 (w), 790 (w), 758 (m), 574 (w), 518 (w), 453 (w), 418 (w) cm^{-1} .

HRMS: (ESI+) m/z calcd. for $\text{C}_{32}\text{H}_{31}\text{N}_5\text{O}$ $[\text{M}+\text{Na}]^+$: 524.2421; found: 524.2413.

Synthesis of Amido-Fe Complex 108



Following a slightly modified by procedure by Hitomi *et al.*,^[107] a Schlenk flask was charged with $\text{Fe}(\text{ClO}_4)_2 \cdot 6 \text{H}_2\text{O}$ (145 mg, 0.40 mmol, 1.00 eq.) and MeOH (2.0 mL). To this suspension was added a solution of ligand **101** (200 mg, 0.40 mmol, 1.00 eq.) in MeOH (2.0 mL, 0.1 M in total) and the resulting mixture was subsequently treated with NEt_3 (55 μL , 0.40 mmol, 1.00 eq.). The dark-red reaction was then stirred for 16 h at rt. Afterwards, the precipitate was filtered off, washed extensively with Et_2O , and dried under vacuum to obtain complex **108** (256 mg, 0.38 mmol, 95%) as a dark-red solid.

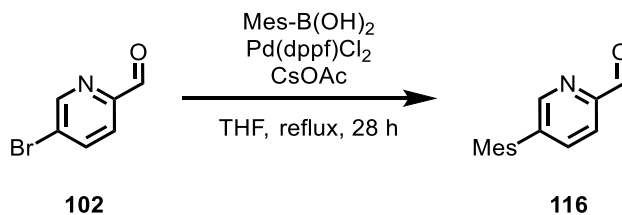
CHN: calcd. for $\text{C}_{32}\text{H}_{31}\text{ClFeN}_5\text{O}_6 \cdot \text{H}_2\text{O}$: C, 55.63; H, 4.81; N, 10.41; found: C, 55.02; H, 5.46; N, 9.81.

HRMS: (APCI+) m/z calcd. for $\text{C}_{32}\text{H}_{30}\text{FeN}_5\text{O}$ $[\text{M}]^+$: 556.1795, found: 556.1803.

IR: (neat) $\tilde{\nu} = 3518$ (w), 2387 (w), 2339 (w), 2263 (w), 2211 (w), 2178 (w), 2128 (w), 2082 (w), 2003 (w), 1959 (w), 1893 (w), 1450 (w), 1085 (s), 847 (w), 773 (m), 622 (m), 556 (m), 499 (w), 441 (m), 413 (m) cm^{-1} .

5.3.2 Synthesis of Pentadentate Ligand 115 and Complex 121

5-Mesitylpicolinaldehyde (116)



According to a slightly modified procedure by Wang *et al.*,^[132] a Schlenk flask was charged with 5-bromopyridine-2-carbaldehyde (**102**, 0.56 g, 3.01 mmol, 1.00 eq.), mesityl boronic acid (0.99 g, 6.02 mmol, 2.00 eq.), Pd(dppf)Cl₂ (0.22 g, 0.30 mmol, 0.10 eq.), and CsOAc (1.44 g, 7.53 mmol, 2.50 eq.). The vessel was put under vacuum and purged with nitrogen for three cycles. Afterwards, degassed THF (15 mL, 0.2 M) was added and the resulting mixture was stirred at 80 °C for 28 h under inert gas atmosphere. Afterwards, the mixture was allowed to reach rt and diluted with Et₂O. The organic phase was washed with sat. aq. NaHCO₃-solution and sat. aq. NaCl-solution, dried over Na₂SO₄, filtered, and the solvent was removed under reduced pressure. The crude product was purified by column chromatography on silica gel (*n*-pentane/EtOAc 30:1) to afford aldehyde **116** (0.43 g, 1.92 mmol, 64%) as a colorless solid.

TLC: $R_f = 0.55$ (*n*-pentane/EtOAc 8:1).

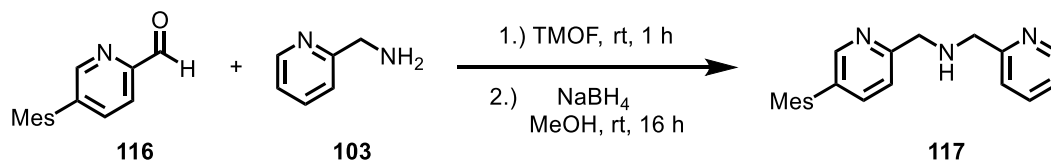
¹H NMR: (300 MHz, CDCl₃) $\delta = 10.14$ (d, $J = 0.6$ Hz, 1H), 8.60 (dd, $J = 2.0, 0.7$ Hz, 1H), 8.05 (dd, $J = 7.9, 0.7$ Hz, 1H), 7.70 (ddd, $J = 7.9, 2.0, 0.7$ Hz, 1H), 6.99 (s, 2H), 2.35 (s, 3H), 2.00 (s, 6H) ppm.

¹³C NMR: (75 MHz, CDCl₃) $\delta = 193.3, 151.5, 151.1$ (2C), 141.8, 138.3, 138.3, 135.9, 134.1, 128.7 (2C), 121.6, 21.2, 20.9 (2C) ppm.

IR: (neat) $\tilde{\nu} = 2974$ (w), 2917 (w), 2814 (w), 1773 (w), 1711 (s), 1606 (w), 1565 (w), 1457 (m), 1359 (w), 1283 (w), 1200 (m), 1112 (w), 1032 (w), 999 (m), 946 (w), 845 (s), 749 (w), 705 (m), 637 (w), 578 (m), 515 (w), 475 (w), 413 (m) cm⁻¹.

HRMS: (ESI⁺) m/z calcd. for C₁₅H₁₅NONa [M+Na]⁺: 248.1046, found: 248.1060.

1-(5-Mesitylpyridin-2-yl)-N-(pyridin-2-yl)methanamine (**117**)



Following **GP A**, aldehyde **116** (0.90 g, 4.00 eq., 1.20 eq.), picolylamine (**103**, 0.34 mL, 0.36 g, 3.33 mmol, 1.00 eq.), and NaBH₄ (0.26 g, 6.99 mmol, 2.10 eq.) were employed to obtain dipicolylamine **117** (1.03 g, 3.24 mmol, 97%) as a yellow oil.

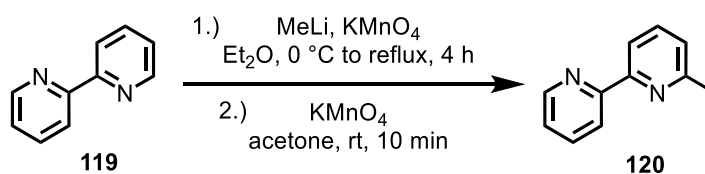
¹H NMR: (300 MHz, CDCl₃) δ = 8.58 (d, J = 4.8 Hz, 1H), 8.38-8.35 (m, 1H), 7.66 (td, J = 7.7, 1.8 Hz, 1H), 7.47-7.38 (m, 3H), 7.17 (dd, J = 7.5, 5.1 Hz, 1H), 6.96 (s, 2H), 4.05 (s, 2H), 4.04 (s, 2H), 2.33 (s, 3H), 2.00 (s, 6H), 1.85 (br s, 1H) ppm.

¹³C NMR: (75 MHz, CDCl₃) δ = 159.9, 158.0, 149.8, 149.4, 137.6, 137.5, 136.6, 136.5 (2C), 135.1, 135.0, 128.4 (2C), 122.4, 122.1, 122.0, 55.1, 54.8, 21.1, 21.0 (2C) ppm.

IR: (neat) $\tilde{\nu}$ = 3311 (w), 3006 (w), 2916 (w), 2854 (w), 1592 (m), 1466 (m), 1435 (m), 1367 (w), 1298 (w), 1226 (w), 12121 (w), 1041 (w), 999 (m), 946 (w), 847 (s), 753 (s), 631 (w), 574 (w), 515 (w), 406 (w) cm⁻¹.

HRMS: (ESI+) m/z calcd. for C₂₁H₂₄N₃ [M+H]⁺: 318.1965; found: 318.1956.

6-Methyl-2,2'-bipyridine (**120**)



According to a procedure by Bevilacqua *et al.*,^[134] a Schlenk flask was charged with 2,2'-bipyridine (**119**, 1.00 g, 6.40 mmol, 1.00 eq.) and Et₂O (35 mL, 0.16 M). The solution was cooled to 0 °C and MeLi (1.6 M solution in Et₂O, 4.00 mL, 6.40 mmol, 1.00 eq.) was added dropwise over the course of 30 min. After complete addition, the reaction was stirred at 40 °C until TLC showed full conversion. The mixture was cooled to rt, H₂O was added, and layers were separated. The aq. layer was extracted with Et₂O (3x), washed with brine (2x), dried over Na₂SO₄, filtered, and the solvent was removed under reduced pressure. To the residue was added a saturated solution of KMnO₄ in acetone (about 100 mL) and the suspension left standing for 10 min. Subsequently, filtration over Celite, rinsing with acetone, and removal of the solvent under reduced pressure gave a brown oil. The crude product was

Experimental Part

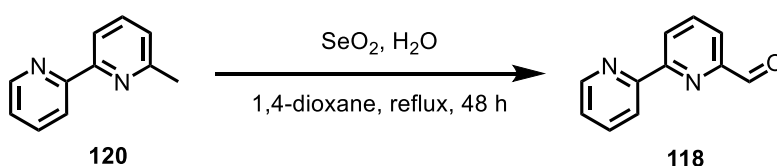
further purified by column chromatography on silica gel (*n*-pentane/EtOAc 5:1 → 3:1) to obtain **120** (0.70 g, 4.13 mmol, 65%) as a yellow oil.

TLC: $R_f = 0.60$ (*n*-pentane/EtOAc 1:1).

¹H NMR: (300 MHz, CDCl₃) $\delta = 8.67$ (d, $J = 4.7$ Hz, 1H), 8.40 (d, $J = 8.0$ Hz, 1H), 8.16 (d, $J = 7.8$ Hz, 1H), 7.80 (t, $J = 7.7$ Hz, 1H), 7.70 (t, $J = 7.7$ Hz, 1H), 7.29 (dd, $J = 7.2$, 5.0 Hz, 1H), 7.17 (d, $J = 7.6$ Hz, 1H), 2.64 (s, 3H) ppm.

Analytical data were consistent with reported data.^[134]

[2,2'-Bipyridine]-6-carbaldehyde (**118**)



Following a slightly modified procedure by Heitzler *et al.*,^[133] a flask was charged with methylated bipyridine **120** (0.70 g, 4.13 mmol, 1.00 eq.), SeO₂ (0.69 g, 6.20 mmol, 1.50 eq.), and 1,4-dioxane (18 mL, 0.23 M). The suspension was refluxed for 3 h after which the reaction was cooled to rt and another portion of SeO₂ (0.69 g, 6.20 mmol, 1.50 eq.) was added. Afterwards, the mixture was refluxed for 48 h while stirring. Subsequently, the hot mixture was filtered over Celite, rinsed with warm 1,4-dioxane (ca. 40 °C) and CH₂Cl₂, and the solvent was removed under reduced pressure. The crude product was purified by column chromatography on silica gel (CH₂Cl₂/EtOAc 15:1 → 6:1) to obtain pure aldehyde **118** (0.30 g, 1.63 mmol, 39%) as an off-white solid.

TLC: $R_f = 0.45$ (CH₂Cl₂/EtOAc 6:1).

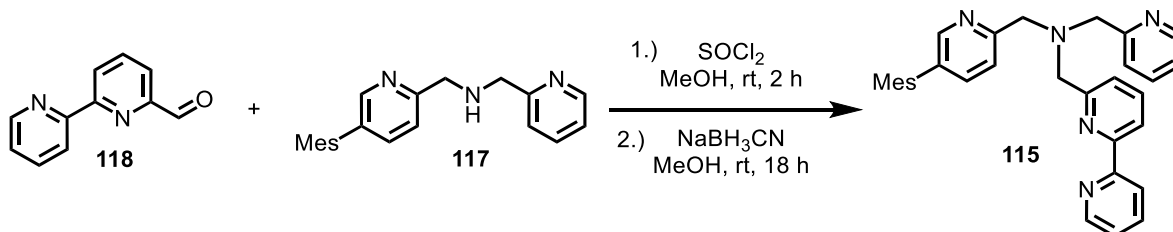
¹H NMR: (300 MHz, CDCl₃) $\delta = 10.16$ (s, 1H), 8.70 (d, $J = 4.6$ Hz, 1H), 8.65 (dd, $J = 6.2$, 2.9 Hz, 1H), 8.54 (d, $J = 8.0$ Hz, 1H), 8.01–7.95 (m, 2H), 7.86 (td, $J = 7.8$, 1.8 Hz, 1H), 7.35 (ddd, $J = 7.6$, 4.8, 1.1 Hz, 1H) ppm.

¹³C NMR: (75 MHz, CDCl₃) $\delta = 193.8$, 156.8, 155.1, 152.5, 149.5, 138.0, 137.2, 125.3, 124.4, 121.5, 121.4 ppm.

Analytical data were consistent with reported data.^[133]

Experimental Part

1-((2,2'-Bipyridin]-6-yl)-N-((5-mesitylpyridin-2-yl)methyl)-N-(pyridin-2-ylmethyl)-methanamine (115)



Following a slightly modified procedure by Wong *et al.*,^[128] a Schlenk flask was charged with aldehyde **118** (0.35 g, 1.90 mmol, 1.00 eq.), dipicolylamine **117** (0.67 g, 2.11 mmol, 1.11 eq.), and MeOH (30 mL, 0.06 M). Thionyl chloride (69.0 μ L, 0.11 g, 0.95 mmol, 0.50 eq.) was added dropwise and the reaction was stirred for 3 h at rt. Afterwards, NaBH₃CN (0.32 g, 5.04 mmol, 2.65 eq.) was added in portions and the resulting mixture was again stirred at rt for 18 h. Subsequently, the mixture was quenched carefully by adding conc. aq. HCl (12 M) dropwise (**caution**: highly toxic HCN can form during this workup!). When gas evolution ceased, the mixture was washed with Et₂O (2x) and the pH-value was adjusted to pH = 9 with conc. aq. NH₃-solution. The aq. layer was extracted with CH₂Cl₂ (3x), the combined organic layers were dried over Na₂SO₄, filtered, and the solvent was removed under reduced pressure to obtain ligand **115** (0.92 g, 1.89 mmol, >99%) as an off-white solid that was used without further purification.

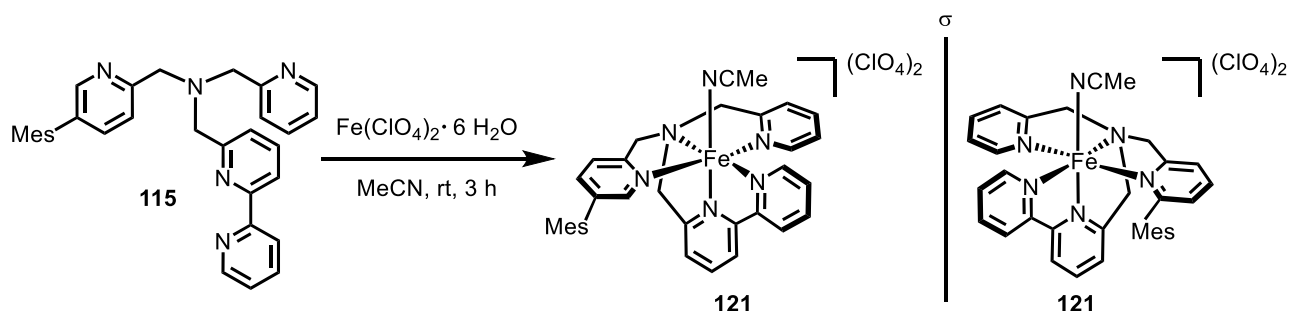
¹H NMR: (300 MHz, CDCl₃) δ = 8.66 (d, J = 4.5 Hz, 1H), 8.55 (d, J = 4.9 Hz, 1H), 8.46 (d, J = 8.0 Hz, 1H), 8.34 (d, J = 2.0 Hz, 1H), 8.26 (d, J = 7.7 Hz, 1H), 7.80 (t, J = 7.8 Hz, 2H), 7.71-7.66 (m, 3H), 7.60 (d, J = 7.5 Hz, 1H), 7.48-7.43 (m, 2H), 7.32-7.28 (m, 1H), 7.19-7.13 (m, 1H), 6.95 (s, 2H), 4.09-4.01 (m, 6H), 2.33 (s, 3H), 1.98 (s, 6H) ppm.

¹³C NMR: (75 MHz, CDCl₃) δ = 159.8, 158.9, 157.9, 155.6, 149.8, 149.6, 149.4, 149.2, 137.5, 137.5, 137.4, 137.0, 136.6, 136.5 (2C), 135.1, 135.0, 128.4 (2C), 123.7, 123.0, 122.5, 122.4, 122.1, 121.3, 119.4, 60.7, 60.5, 60.4, 21.1, 21.0 (2C) ppm.

IR: (neat) $\tilde{\nu}$ = 3056 (w), 3007 (w), 2917 (w), 2828 (w), 2145 (w), 1574 (m), 1467 (m), 1429 (s), 1366 (m), 1304 (w), 1254 (w), 1121 (w), 1086 (w), 1042 (w), 994 (m), 898 (w), 848 (m), 771 (s), 624 (w), 574 (w), 517 (w), 406 (w) cm⁻¹.

HRMS: (ESI⁺) m/z calcd. for C₃₂H₃₁N₅Na [M+Na]⁺: 508.2472; found: 508.2466.

Synthesis of Fe(II) Complex **121**



According to a slightly modified procedure by Wong *et al.*,^[128] a Schlenk flask was charged with $\text{Fe}(\text{ClO}_4)_2 \cdot 6 \text{H}_2\text{O}$ (55.3 mg, 0.15 mmol, 1.00 eq.) and MeCN (4.0 mL). A solution of ligand **115** (74.0 mg, 0.15 mmol, 1.00 eq.) in MeCN (2.0 mL, 0.025 M in total) was added and the resulting red mixture was stirred for 3 h at rt. Afterwards, the mixture was concentrated carefully under vacuum (to about half volume) and again stirred for 1 h. Subsequently, Et_2O was added and precipitation of a red solid was observed. For completion of precipitation, the mixture was stirred for an additional 30 min. The solid was filtered off, washed extensively with Et_2O and *n*-pentane, and dried under vacuum to obtain Fe-complex **121** (109 mg, 0.14 mmol, 92%) as a dark-red solid.

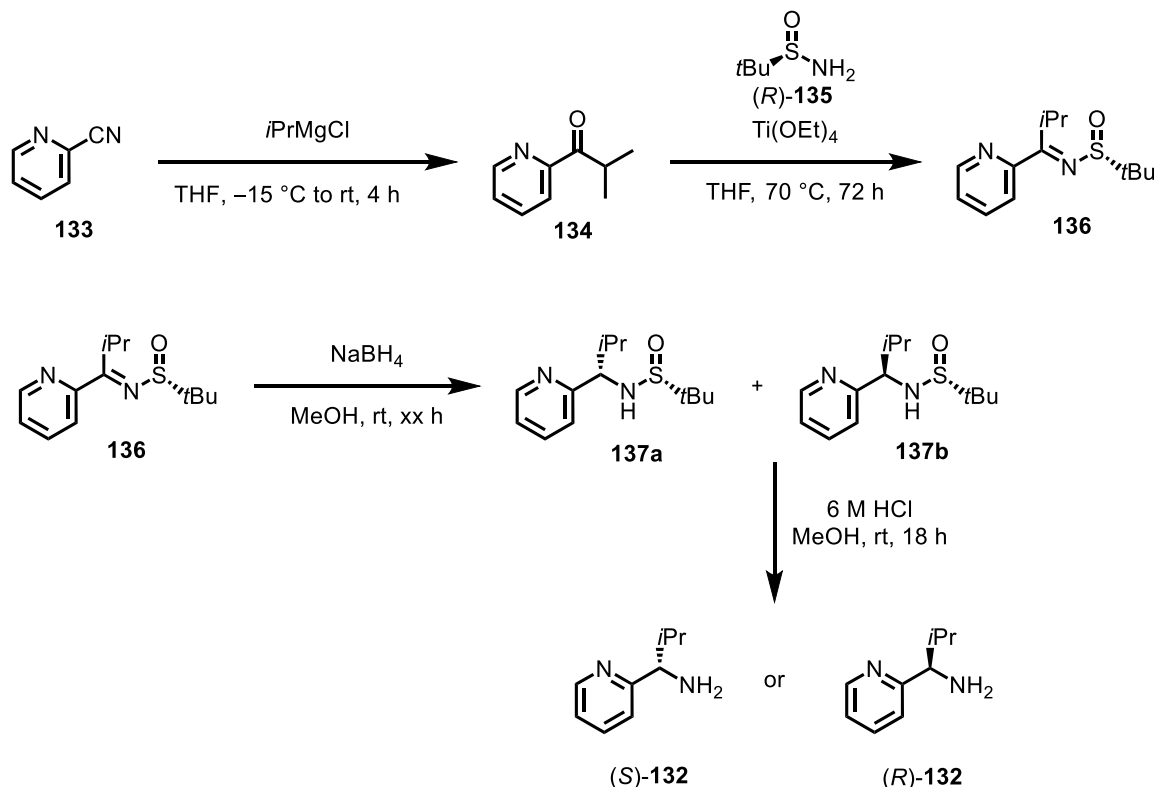
¹H NMR: (300 MHz, CD_3CN) δ = 9.07 (d, J = 5.3 Hz, 1H), 8.05 (d, J = 8.1 Hz, 1H), 8.31 (d, J = 8.0 Hz, 1H), 8.19 (td, J = 7.8, 1.3 Hz, 1H), 7.88 (t, J = 8.0 Hz, 1H), 7.78-7.70 (m, 2H), 7.55-7.47 (m, 2H), 7.44 (d, J = 7.8 Hz, 1H), 7.30 (d, J = 7.9 Hz, 1H), 7.02 (d, J = 6.5 Hz, 1H), 6.89-6.84 (m, 2H), 6.80 (s, 1H), 6.45 (s, 1H), 5.02 (dd, J = 15.6, 7.5 Hz, 2H), 4.90 (dd, J = 15.4, 7.0 Hz, 2H), 4.83-4.69 (m, 2H), 2.20 (s, 3H), 1.86 (s, 3H), 1.35 (s, 3H) ppm.

IR: (neat) $\tilde{\nu}$ = 2924 (w), 2181 (w), 1605 (w), 1448 (w), 1295 (w), 1242 (w), 1077 (s), 854 (w), 772 (m), 620 (m), 520 (w), 452 (w), 415 (w) cm^{-1} .

HRMS: (ESI+) m/z calcd. for $\text{C}_{32}\text{H}_{31}\text{FeN}_5\text{ClO}_4$ [$\text{M} - \text{ClO}_4^-$ and MeCN]⁺: 640.1409; found: 640.1406.

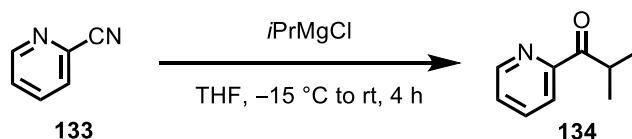
5.3.3 Synthesis of Chiral Pentadentate Ligands

Enantiopure chiral amines (*S*)-**132** and (*R*)-**132** were synthesized according to a reported procedure^[149] by starting from commercially available 2-cyanopyridine (**133**) as depicted in Scheme 69. Chiral sulfinamide (*R*)-**135** was purchased commercially.



Scheme 69: Synthetic pathway towards chiral picolyamine **132** starting from commercially available 2-cyanopyridine (**133**).

2-Methyl-1-(pyridin-2-yl)propan-1-one (**134**)



According to a procedure by Easmon *et al.*,^[255] a Schlenk flask was charged with 2-cyanopyridine (**133**, 2.00 g, 19.2 mmol, 1.00 eq.) and Et₂O (30 mL, 0.64 M). The resulting solution was cooled to -15 °C and a solution of *i*PrMgCl (2.0 M solution in THF, 11.5 mL, 23.1 mmol, 1.20 eq.) was added dropwise at this temperature over the course of 10 min. After complete addition, the reaction was stirred at -15 °C for another 60 min and subsequently for 3 h at rt. When TLC indicated full conversion, the mixture was quenched by addition of 2 M aq. HCl and stirring for another 20 min. The two phases were separated, the aq. phase adjusted to pH = 8 with 2 M aq. NaOH, and extracted

Experimental Part

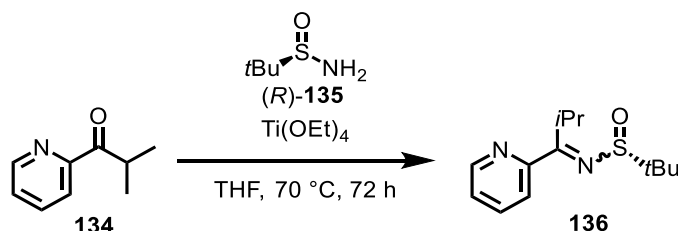
with CH₂Cl₂ (3x). The combined organic layers were washed with water and brine, dried over Na₂SO₄, filtered, and the solvent was removed under reduced pressure. The crude product was purified by column chromatography on silica gel (*n*-pentane/EtOAc) via dry-load to obtain pure ketone **134** (2.28 g, 15.3 mmol, 80%) as a colorless liquid.

TLC: $R_f = 0.34$ (*n*-pentane/EtOAc 10:1).

¹H NMR: (300 MHz, CDCl₃) $\delta = 8.68$ (d, $J = 4.7$ Hz, 1H), 8.04 (d, $J = 7.8$ Hz, 1H), 7.83 (t, $J = 7.7$ Hz, 1H), 7.45 (dd, $J = 7.5, 5.2$ Hz, 1H), 4.11 (m, $J = 6.9$ Hz, 1H), 1.21 (d, $J = 6.9$ Hz, 6H) ppm.

Analytical data were consistent with reported data.^[255]

(*R*)-2-Methyl-*N*-(2-methyl-1-(pyridin-2-yl)propylidene)propane-2-sulfinamide (**136**)



Following a procedure by Chelucci *et al.*,^[149] a Schlenk flask was charged with ketone **134** (1.50 g, 10.1 mmol, 1.00 eq.), chiral sulfinamide (*R*)-**135** (1.22 g, 10.1 mmol, 1.00 eq.), Ti(OEt)₄ (4.59 g, 20.1 mmol, 2.00 eq.), and THF (30 mL, 0.28 M). Subsequently, the mixture was stirred at 70 °C for 72 h after which the reaction was cooled to rt and the solvent was removed under reduced pressure. The residue was dissolved in EtOAc, brine was added slowly, and the suspension was stirred for 20 min at rt. Afterwards, filtration over Celite, drying over Na₂SO₄, filtration, and solvent evaporation gave the crude product which was further purified by column chromatography on silica gel (*n*-pentane/EtOAc 2:1 → 1:1) to obtain pure **136** (0.92 g, 3.66 mmol, 36%) as a yellow oil.

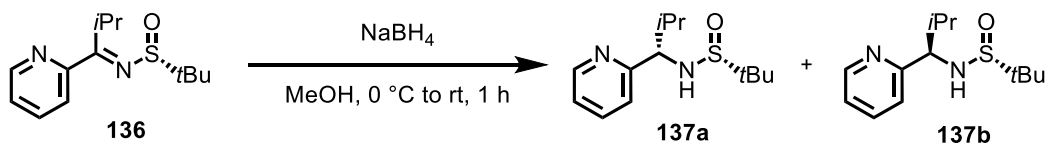
TLC: $R_f = 0.40$ (*n*-pentane/EtOAc 1:1).

¹H NMR: (300 MHz, CDCl₃) $\delta = 8.64$ (dt, $J = 4.8, 1.1$ Hz, 1H), 7.73 (td, $J = 7.8, 1.8$ Hz, 1H), 7.47 (br s, 1H), 7.30 (ddd, $J = 7.8, 4.8, 1.1$ Hz, 1H), 1.24 (s, 9H) ppm.

Analytical data were consistent with reported data.^[149]

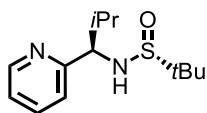
Experimental Part

(*R*)-2-Methyl-*N*-((*S*)-2-methyl-1-(pyridin-2-yl)propyl)propane-2-sulfinamide (**137a**) and (*R*)-2-methyl-*N*-((*R*)-2-methyl-1-(pyridin-2-yl)propyl)propane-2-sulfinamide (**137b**)



Following a procedure by Chelucci *et al.*,^[149] a Schlenk flask was charged with sulfinamide **136** (0.73 g, 2.89 mmol, 1.00 eq.) and MeOH (40 mL, 0.07 M). The solution was cooled to 0 °C, NaBH₄ (0.22 g, 5.79 mmol, 2.00 eq.) was added in portions, and the mixture was stirred for 1 h at rt. Afterwards, the reaction was quenched with aq. sat. NH₄Cl-solution and the crude product was extracted with EtOAc (3x). The combined organic layers were dried over Na₂SO₄, filtered, and the solvent was removed under reduced pressure to obtain a diastereomeric mixture (dr 1:1.4 (*R_S,R*)/(*R_S,S*)) as determined by ¹H NMR analysis. The crude product was purified by column chromatography on silica gel (CH₂Cl₂/MeOH 40:1 → 30:1) via dry-load to obtain the diastereomerically pure (dr > 20:1) sulfinamides (*R_S,R*)-**137b** (0.27 g, 1.06 mmol, 37%) as a colorless oil and (*R_S,S*)-**137a** (0.39 g, 1.53 mmol, 53%) as a colorless solid.

Analytical data for (*R_S,R*)-**137b**:

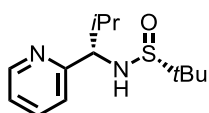


TLC: $R_f = 0.57$ (CH₂Cl₂/MeOH 10:1).

¹H NMR: (300 MHz, CDCl₃) $\delta = 8.53$ (d, $J = 4.3$ Hz, 1H), 7.61 (td, $J = 7.7, 1.7$ Hz, 1H), 7.20 (d, $J = 7.8$ Hz, 1H), 7.15 (ddd, $J = 7.5, 4.8, 1.0$ Hz, 1H), 5.05 (d, $J = 7.41$ Hz, 1H), 4.14 (dd, $J = 7.4, 6.1$ Hz, 1H), 2.04 (m, $J = 6.6$ Hz, 1H), 1.28 (s, 9H), 0.87 (d, $J = 6.7$ Hz, 3H), 0.86 (d, $J = 6.7$ Hz, 3H) ppm.

Analytical data were consistent with reported data.^[149]

Analytical data for (*R,S*)-**137a**:

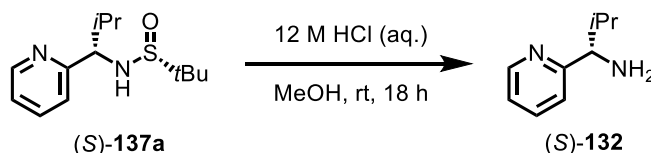


TLC: $R_f = 0.53$ ($\text{CH}_2\text{Cl}_2/\text{MeOH}$ 10:1).

$^1\text{H NMR}$: (300 MHz, CDCl_3) $\delta = 8.56$ (d, $J = 4.5$ Hz, 1H), 7.63 (td, $J = 7.7, 1.8$ Hz, 1H), 7.21-7.14 (m, 2H), 4.23 (d, $J = 3.6$ Hz, 2H), 2.23-2.12 (m, 1H), 1.15 (s, 9H), 0.98 (d, $J = 6.8$ Hz, 3H), 0.88 (d, $J = 6.8$ Hz, 3H) ppm.

Analytical data were consistent with reported data.^[149]

(*S*)-2-Methyl-1-(pyridin-2-yl)propan-1-amine (**132**)



To a solution of diastereomerically pure sulfinamide (*S*)-**137a** (0.50 g, 1.97 mmol, 1.00 eq.) in MeOH (13 mL, 0.15 M) was added a solution of aq. 12 M HCl in MeOH (50 vol% for HCl-solution, 13 mL) under air at rt and the reaction was stirred for 18 h. Afterwards, CH_2Cl_2 was added, the aq. layer was adjusted to pH = 8-9 with aq. 5 M NaOH-solution, and layers were separated. The aq. phase was extracted with CH_2Cl_2 (3x), the combined organic layers were dried over Na_2SO_4 , filtered, and the solvent was removed under reduced pressure. The crude product was further purified by column chromatography on silica gel ($\text{CH}_2\text{Cl}_2/\text{MeOH}$ 8:1 \rightarrow 5:1) to obtain pure amine **132** (0.27 g, 1.80 mmol, 91%) as a colorless liquid.

TLC: $R_f = 0.43$ ($\text{CH}_2\text{Cl}_2/\text{MeOH}$ 10:1).

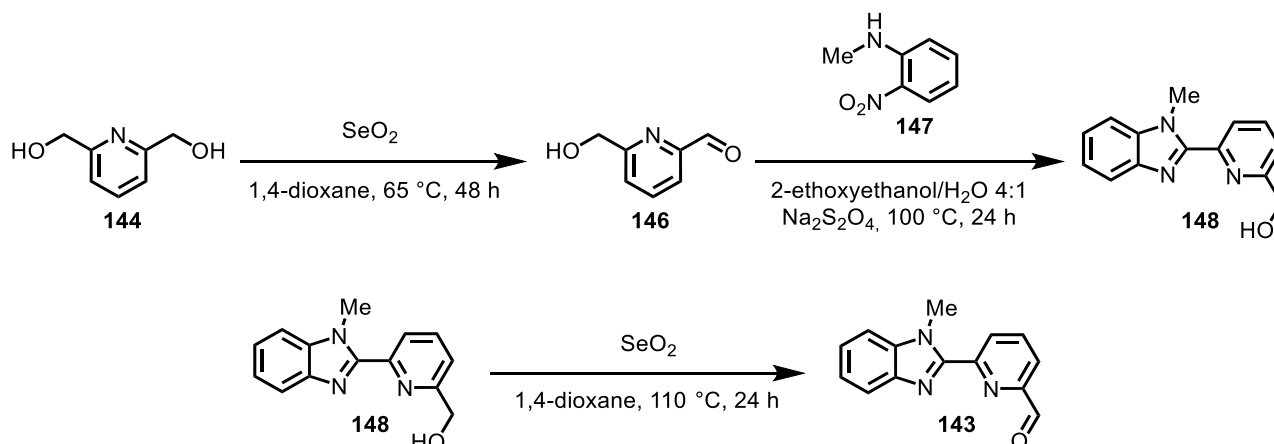
$^1\text{H NMR}$: (300 MHz, CDCl_3) $\delta = 8.53$ (d, $J = 4.4$ Hz, 1H), 7.61 (td, $J = 7.7, 1.6$ Hz, 1H), 7.22 (d, $J = 7.8$ Hz, 1H), 7.13 (dd, $J = 7.4, 5.0$ Hz, 1H), 3.74 (d, $J = 6.5$ Hz, 1H), 2.68 (s, 2H, NH_2), 2.04 (m, $J = 6.7$ Hz, 1H), 0.93 (d, $J = 6.7$ Hz, 3H), 0.81 (d, $J = 6.8$ Hz, 3H) ppm.

$^{13}\text{C NMR}$: (75 MHz, CDCl_3) $\delta = 164.2, 149.0, 136.1, 121.9, 121.7, 63.1, 34.9, 19.9, 18.1$ ppm.

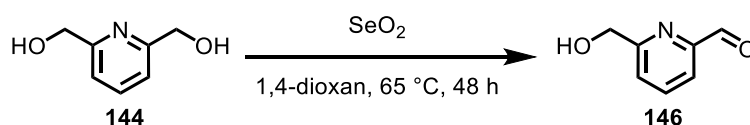
Compound (*R*)-**132** was prepared analogously. Analytical data were consistent with reported data.^[256]

Experimental Part

Benzimidazole aldehyde **143** was synthesized starting from commercially available 2,6-bis(hydroxymethyl)pyridine (**144**) as depicted in Scheme 70. *N*-Methyl-2-nitroaniline (**147**) was synthesized according to a published procedure.^[257]



6-(Hydroxymethyl)picolinaldehyde (**146**)



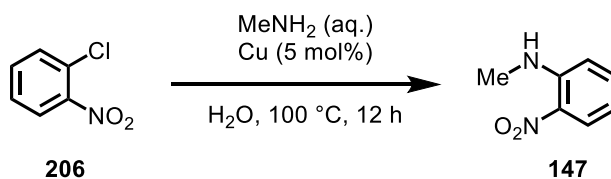
Following a procedure by Join *et al.*,^[151] a Schlenk flask was charged with 2,6-bis(hydroxymethyl)pyridine (**144**, 1.00 g, 7.19 mmol, 1.00 eq.) and SeO₂ (0.40 g, 3.59 mmol, 0.50 eq.). 1,4-dioxane (20 mL, 0.36 M) was added and the resulting suspension was stirred at 65 °C for 24 h. Afterwards, the mixture was cooled to rt, put into an ultra-sonic bath for 5 min, and subsequently again stirred at 65 °C for another 24 h. After cooling to rt, the mixture was diluted with CH₂Cl₂, filtered over Celite, and the solvent was removed under reduced pressure. The crude product was purified by column chromatography on silica gel (CH₂Cl₂/MeOH 40:1 → 20:1) to afford aldehyde **146** (0.78 g, 5.69 mmol, 79%) as an off-white solid.

TLC: R_f = 0.14 (CH₂Cl₂/MeOH 40:1).

¹H NMR: (300 MHz, CDCl₃) δ = 10.09 (s, 1H), 7.89 (d, *J* = 4.3 Hz, 2H), 7.52 (t, *J* = 4.3 Hz, 1H), 4.88 (s, 2H) ppm.

Analytical data were consistent with reported data.^[151]

N-Methyl-2-nitroaniline (147)



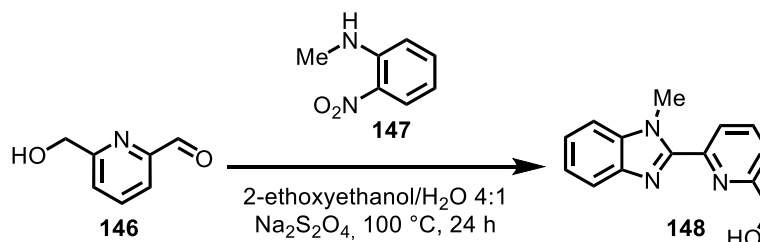
Following a procedure by Jiao *et al.*,^[257] a pressure tube was charged with 1-chloro-2-nitrobenzene (**206**, 0.50 g, 3.17 mmol, 1.00 eq.), copper powder (0.01 g, 0.16 mmol, 0.05 eq.), and methylamine (40 wt% in H₂O, 1.37 mL, 15.9 mmol, 5.00 eq.). Afterwards, the mixture was stirred at 100 °C for 12 h. The mixture was then allowed to cool to rt, EtOAc was added, and the layers were separated. The aq. phase was extracted with EtOAc (3x), the combined organic layers were dried over Na₂SO₄, filtered, and the solvent was removed under reduced pressure. The crude product was purified by column chromatography on silica gel (*n*-pentane/EtOAc 15:1) to obtain nitroaniline **147** (0.41 g, 2.68 mmol, 84%) as a red solid.

TLC: $R_f = 0.57$ (*n*-pentane/EtOAc 5:1).

¹H NMR: (300 MHz, CDCl₃) $\delta = 8.17$ (dd, $J = 8.6, 1.6$ Hz, 1H), 8.03 (br s, 1H), 7.46 (td, $J = 7.8, 1.4$ Hz, 1H), 6.84 (d, $J = 8.6$ Hz, 1H), 6.65 (td, $J = 7.7, 1.1$ Hz, 1H), 3.02 (d, $J = 5.1$ Hz, 3H) ppm.

Analytical data were consistent with reported data.^[258]

(6-(1-Methyl-1H-benzo[d]imidazol-2-yl)pyridin-2-yl)methanol (148)



Following a procedure by Join *et al.*,^[151] a Schlenk flask was charged with aldehyde **146** (0.44 g, 3.21 mmol, 1.00 eq.), nitroaniline **147** (0.49 g, 3.21 mmol, 1.00 eq.), and a mixture of ethoxyethanol/H₂O (4:1, 12 mL, 0.27 M). The solution was thoroughly degassed via freeze-pump-thaw for three cycles and stirred at 100 °C for 1 h. Afterwards, the reaction was cooled to rt, Na₂S₂O₄ (1.68 g, 9.63 mmol, 3.00 eq.) was added, and again stirred at 100 °C for 23 h. When TLC showed full conversion, the solvent was evaporated under reduced pressure, EtOAc and H₂O were added, and

Experimental Part

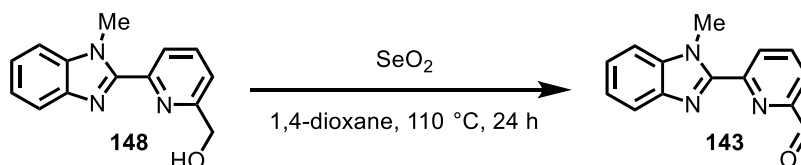
layers were separated. The aq. phase was extracted with EtOAc (3x), the combined organic layers were dried over Na₂SO₄, filtered, and the solvent was removed under reduced pressure. The crude product was purified by column chromatography on silica gel (CH₂Cl₂/MeOH 50:1 → 20:1) to obtain benzimidazole **148** (0.43 g, 1.81 mmol, 57%) as a pale-green solid.

TLC: $R_f = 0.27$ (CH₂Cl₂/MeOH 20:1)

¹H NMR: (300 MHz, CDCl₃) $\delta = 8.27$ (d, $J = 7.8$ Hz, 1H), 7.88-7.81 (m, 2H), 7.44 (dd, $J = 6.3, 1.9$ Hz, 1H), 7.39-7.29 (m, 3H), 4.87 (s, 2H), 4.22 (s, 3H) ppm with additional signals due to 2-ethoxyethanol.

Analytical data were consistent with reported data.^[151]

6-(1-Methyl-1H-benzo[d]imidazol-2-yl)picolinaldehyde (**143**)



Following a procedure by Join *et al.*,^[151] a Schlenk flask was charged with benzimidazole **148** (0.43 g, 1.81 mmol, 1.00 eq.), SeO₂ (0.22 g, 2.00 mmol, 1.10 eq.), and 1,4-dioxane (9.5 mL, 0.19 M). Afterwards, the resulting mixture was heated at 110 °C and stirred for 24 h. After cooling to rt, filtration over celite and removal of the solvent gave the crude product which was purified by column chromatography on silica gel (CH₂Cl₂/MeOH 30:1 → 20:1) to furnish aldehyde **143** (0.41 g, 1.73 mmol, 96%) as an off-white solid.

TLC: $R_f = 0.43$ (CH₂Cl₂/MeOH 20:1).

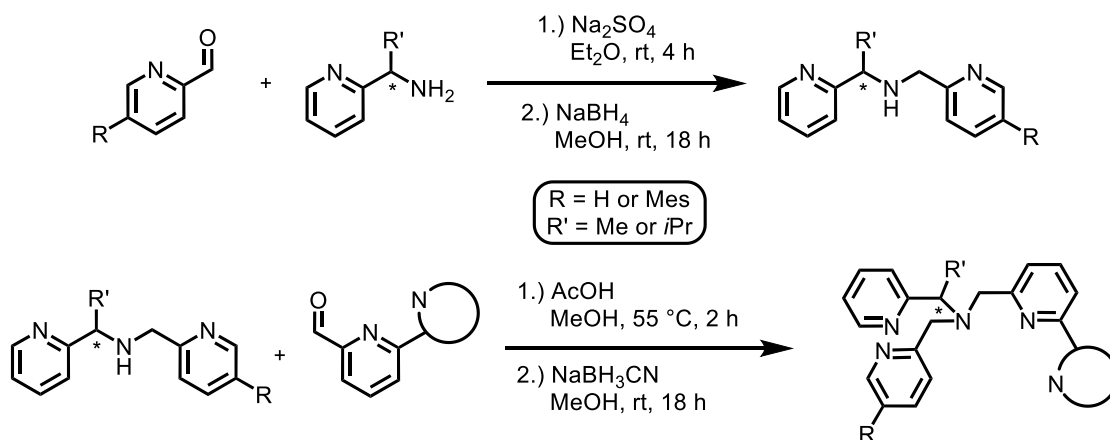
¹H NMR: (300 MHz, CDCl₃) $\delta = 10.17$ (s, 1H), 8.68 (dd, $J = 6.7, 2.2$ Hz, 1H), 8.08–7.98 (m, 2H), 7.85 (d, $J = 7.4$ Hz, 1H), 7.48 (d, $J = 7.9$ Hz, 1H), 7.42-7.31 (m, 2H), 4.38 (s, 3H) ppm.

¹³C NMR: (75 MHz, CDCl₃) $\delta = 192.9, 152.0, 151.5, 149.0, 142.7, 138.2, 137.5, 128.9, 124.0, 123.1, 121.6, 120.4, 110.2, 33.1$ ppm.

Analytical data were consistent with reported data.^[151]

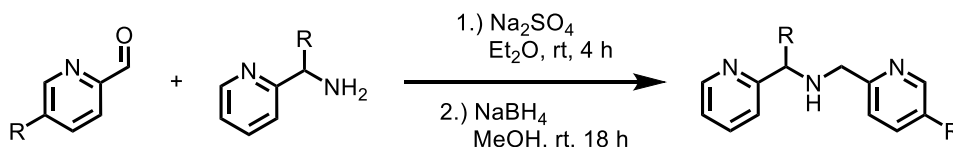
Experimental Part

The synthesis of the final chiral, pentadentate ligands was realized via two reductive aminations as depicted in Scheme 71. Chiral (*S*)-(pyridine-2-yl)ethan-1-amine (**128**) was purchased commercially and used without further purification.



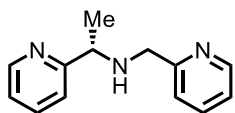
Scheme 71: Synthetic access towards final chiral, pentadentate ligands.

General Procedure B: Reductive Amination towards Chiral Dipicolylamines (GP B)



According to a slightly modified procedure by Brunner *et al.*,^[148] a Schlenk flask was charged with aldehyde (1.00 eq.), enantiopure picolylamine (1.00 eq.), and Et₂O (0.16 M). Na₂SO₄ (200 mg per 1 mmol aldehyde) was added and the mixture was stirred for 4 h at rt. Afterwards, Na₂SO₄ was filtered off and the solvent was evaporated. The residue was dissolved in MeOH (0.16 M) and NaBH₄ (2.50 eq.) was added in small portions. Subsequently, the mixture was stirred at rt for 18 h. Next, the solvent was removed under vacuum and the precipitate was treated with aq. HCl (2 M) to quench remaining NaBH₄. The solution was adjusted to pH = 8-9 with aq. NaOH (2 M) and the aq. layer was extracted with CH₂Cl₂ (3x). The combined organic layers were dried over Na₂SO₄, filtered, and the solvent was removed under reduced pressure to obtain dipicolylamines. If necessary, the crude product was purified by column chromatography on basic alumina (EtOAc → EtOAc/MeOH 20:1). However, yields dropped significantly when column chromatography was performed, possibly due to decomposition.

(S)-1-(Pyridin-2-yl)-N-(pyridin-2-ylmethyl)ethan-1-amine (130)



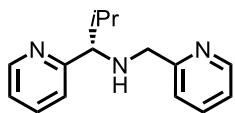
Following **GP B**, (*S*)-picolylamine **128** (100 mg, 0.82 mmol, 1.00 eq.), aldehyde **129** (78 μ L, 87.7 mg, 0.82 mmol, 1.00 eq.), and NaBH₄ (77.4 mg, 2.05 mmol, 2.50 eq.) were employed to obtain dipicolylamine **130** (160 mg, 0.75 mmol, 92%) as a yellow oil without further purification.

¹H NMR: (300 MHz, CDCl₃) δ = 8.55 (t, J = 5.2 Hz, 2H), 7.66 (dd, J = 7.6, 1.8 Hz, 1H), 7.59 (dd, 7.7, 1.8 Hz, 1H), 7.38 (d, J = 7.8 Hz, 1H), 7.30-7.24 (m, 1H), 7.18-7.10 (m, 2H), 3.95 (q, J = 6.7 Hz, 1H), 3.79 (s, 2H), 1.45 (d, J = 6.9 Hz, 3H) ppm.

¹³C NMR: (75 MHz, CDCl₃) δ = 164.6, 160.0, 149.4, 149.4, 136.7, 136.5, 122.3, 122.0, 121.9, 121.2, 59.4, 53.3, 23.0 ppm.

Analytical data were consistent with reported data.^[259]

(S)-2-Methyl-1-(pyridin-2-yl)-N-(pyridin-2-ylmethyl)propan-1-amine (138)



Following **GP B**, (*S*)-picolylamine **132** (52.0 mg, 0.35 mmol, 1.00 eq.), aldehyde **129** (33 μ L, 37.1 mg, 0.35 mmol, 1.00 eq.), and NaBH₄ (33.1 mg, 0.88 mmol, 2.50 eq.) were employed to obtain dipicolylamine **138** (83.0 mg, 0.34 mmol, 99%) as a colorless oil without further purification.

¹H NMR: (300 MHz, CDCl₃) δ = 8.56 (d, J = 4.8 Hz, 1H), 8.50 (d, J = 4.8 Hz, 1H), 7.64–7.55 (m, 2H), 7.32–7.27 (m, 2H), 7.15–7.07 (m, 2H), 3.75 (d, J = 14.4 Hz, 1H), 3.63 (d, J = 14.4 Hz, 1H), 3.46 (d, J = 6.9 Hz, 1H), 2.43 (s, 1H, NH), 2.03 (m, J = 6.8 Hz, 1H), 1.01 (d, J = 6.8 Hz, 3H), 0.78 (d, J = 6.8 Hz, 3H) ppm

¹³C NMR: (75 MHz, CDCl₃) δ = 163.1, 160.5, 149.3, 149.2, 136.4, 136.0, 123.0, 122.4, 121.9, 121.8, 70.1, 53.6, 34.1, 19.8, 19.4 ppm.

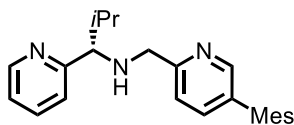
IR: (neat) $\tilde{\nu}$ = 3321 (w), 3061 (w), 3007 (w), 2959 (w), 2873 (w), 1693 (w), 1587 (m), 1467 (m), 1432 (m), 1365 (w), 1296 (w), 1222 (w), 1143 (w), 1113 (w), 1046 (w), 993 (w), 864 (w), 750 (s), 622 (w), 553 (w), 468 (w), 404 (w) cm⁻¹.

Experimental Part

HRMS: (ESI+) m/z calcd. for $C_{15}H_{20}N_3$ $[M+H]^+$: 242.1669, found: 242.1658.

$[\alpha]_D^{22}$: -46.0° ($c = 1.0$, CH_2Cl_2).

(*S*)-*N*-((5-Mesitylpyridin-2-yl)methyl)-2-methyl-1-(pyridin-2-yl)propan-1-amine (**142**)



Following **GP B**, (*R*)-picolyamine **132** (113 mg, 0.75 mmol, 1.00 eq.), aldehyde **116** (170 mg, 0.75 mmol, 1.00 eq.), and $NaBH_4$ (71.1 mg, 1.88 mmol, 2.50 eq.) were employed to obtain dipicolyamine **142** (270 mg, 0.75 mmol, >99%) as a colorless oil.

1H NMR: (300 MHz, $CDCl_3$) $\delta = 8.59$ (d, $J = 4.7$ Hz, 1H), 8.32 (d, $J = 1.6$ Hz, 1H), 7.64 (td, $J = 7.6, 1.8$ Hz, 1H), 7.43-7.34 (m, 3H), 7.15 (ddd, $J = 7.4, 4.8, 1.1$ Hz, 1H), 6.95 (s, 2H), 3.81 (d, $J = 14.3$ Hz, 1H), 3.73 (d, $J = 14.4$ Hz, 1H), 3.55 (d, $J = 6.8$ Hz, 1H), 2.42 (br, 1H, NH), 2.33 (s, 3H), 2.08 (m, $J = 6.8$ Hz, 1H), 1.99 (s, 3H), 1.98 (s, 3H), 1.04 (d, $J = 6.8$ Hz, 3H), 0.82 (d, $J = 6.8$ Hz, 3H) ppm.

^{13}C NMR: (75 MHz, $CDCl_3$) $\delta = 163.2, 158.6, 149.6, 149.3, 137.5, 137.4, 136.5, 136.5, 136.1, 135.2, 134.7, 128.4$ (2C), 123.0, 122.0, 121.9, 70.4, 53.6, 34.2, 21.1, 21.0, 21.0, 19.8, 19.4 ppm.

IR: (neat) $\tilde{\nu} = 2958$ (m), 2918 (m), 2868 (w), 1590 (m), 1466 (s), 1437 (m), 1369 (m), 1263 (w), 1103 (m), 1038 (w), 999 (m), 916 (w), 849 (m), 784 (w), 734 (s), 643 (w), 573 (w), 408 (w) cm^{-1} .

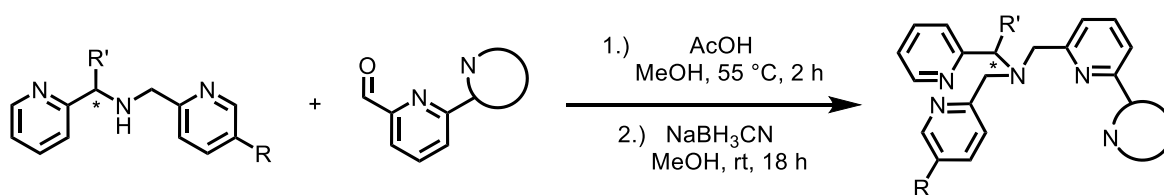
HRMS: (ESI+) m/z calcd. for $C_{24}H_{30}N_3$ $[M+H]^+$: 360.2434, found: 360.2440.

$[\alpha]_D^{22}$: -24.1° ($c = 1.0$, CH_2Cl_2).

The (*R*)-enantiomer of dipicolyamine **142** was synthesized analogously. Analytical data were consistent with the data listed for (*S*)-**142**.

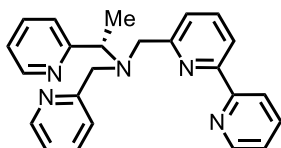
$[\alpha]_D^{22}$: $+24.2^\circ$ ($c = 1.0$, CH_2Cl_2) for (*R*)-**142**.

General Procedure C: Reductive Amination towards Chiral Pentadentate Ligands (GP C)



A Schlenk flask was charged with aldehyde (1.00 eq.) and dipicolylamine (1.30 eq.). MeOH (0.13 M) and AcOH (0.50 eq.) were added and the resulting mixture was stirred at 55 °C for 2 h. Afterwards, the reaction was cooled to 0 °C and NaBH₃CN (6.00 eq.) was added in small portions. The solution was then stirred for 18 h at rt after which aq. HCl-solution (2 M) was added until gas evolution stopped (**caution**: highly toxic HCN can form during this workup!). Afterwards, aq. NaOH (2 M) was used to adjust the solution to pH = 8–9 and the aq. phase was extracted with CH₂Cl₂ (3x). The combined org. layers were dried over Na₂SO₄, filtered, and the solvent was removed under reduced pressure. The crude product was subsequently purified by column chromatography on basic alumina (*n*-pentane/EtOAc) to afford pure ligands.

(S)-N-([2,2'-Bipyridin]-6-ylmethyl)-1-(pyridin-2-yl)-N-(pyridin-2-ylmethyl)ethan-1-amine (127)



Following **GP C**, aldehyde **118** (100 mg, 0.54 mmol, 1.00 eq.), dipicolylamine **130** (151 mg, 0.71 mmol, 1.30 eq.), AcOH (15.5 μL, 0.27 mmol, 0.50 eq.), and NaBH₃CN (205 mg, 3.26 mmol, 6.00 eq.) were employed to obtain pentadentate ligand **127** (91.4 mg, 0.24 mmol, 44%) as a yellow oil after column chromatography on basic alumina (*n*-pentane/EtOAc 2:1 → 1:2).

TLC: R_f = 0.41 (*n*-pentane/EtOAc 2:1, on neutral alumina).

¹H NMR: (300 MHz, CDCl₃) δ = 8.66 (d, J = 4.3 Hz, 1H), 8.58 (d, J = 4.3 Hz, 1H), 8.49 (d, J = 4.8 Hz, 1H), 8.42 (d, J = 7.9 Hz, 1H), 8.21 (d, J = 7.7 Hz, 1H), 7.80 (td, J = 7.8, 1.6 Hz, 1H), 7.75 (t, J = 7.8 Hz, 1H), 7.69–7.59 (m, 3H), 7.57 (d, J = 7.8 Hz, 1H), 7.52 (d, J = 7.6 Hz, 1H), 7.28 (ddd, J = 7.4, 4.8, 0.9 Hz, 1H), 7.18–7.07 (m, 2H), 4.18–3.99 (m, 3H), 3.87 (dd, J = 15.0, 4.7 Hz, 2H), 1.59 (d, J = 6.8 Hz, 3H) ppm.

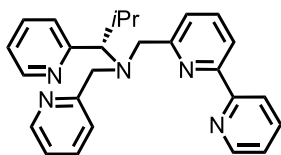
Experimental Part

¹³C NMR: (75 MHz, CDCl₃) δ = 160.9, 160.1, 156.6, 155.4, 154.9, 149.2, 149.0, 149.0, 137.3, 137.0, 136.4, 136.2, 123.7, 123.0, 122.9, 122.8, 122.0, 121.9, 121.3, 119.2, 60.6, 57.1, 56.8, 14.8 ppm.

IR: (neat) $\tilde{\nu}$ = 3058 (w), 2975 (w), 2926 (w), 2842 (w), 2424 (w), 2213 (w), 1734 (w), 1575 (m), 1466 (w), 1428 (m), 1370 (w), 1297 (w), 1250 (w), 1147 (w), 1087 (w), 1045 (w), 992 (w), 910 (w), 827 (w), 772 (s), 728 (s), 625 (w), 538 (w), 465 (w), 403 (w) cm⁻¹.

HRMS: (ESI+) m/z calcd. for C₂₄H₂₄N₅ [M+H]⁺: 381.1953, found: 381.1861.

(S)-N-([2,2'-Bipyridin]-6-ylmethyl)-2-methyl-1-(pyridin-2-yl)-N-(pyridin-2-ylmethyl)propan-1-amine (**139**)



Following **GP C**, aldehyde **118** (48.0 mg, 0.26 mmol, 1.00 eq.), dipicolylamine **138** (81.8 mg, 0.34 mmol, 1.30 eq.), AcOH (7.5 μ L, 0.13 mmol, 0.50 eq.), and NaBH₃CN (98.6 mg, 1.56 mmol, 6.00 eq.) were employed to obtain pentadentate ligand **139** (50.0 mg, 0.12 mmol, 47%) as a colorless solid after column chromatography on basic alumina (*n*-pentane/EtOAc 4:1 \rightarrow 2:1 \rightarrow 1:1). Enantiomeric excess was established by HPLC analysis on a chiral stationary phase: ee = 99%, HPLC conditions: Daicel Chiralcel[®] OD-H column, 250 x 4.6 mm, absorbance at 254 nm, *n*-hexane/isopropanol 98:2, isocratic flow, flow rate 1.0 mL/min, 25 °C, t_r (minor) = 26.1 min, t_r (major) = 29.4 min.

TLC: R_f = 0.60 (*n*-pentane/EtOAc 2:1, on neutral alumina).

¹H NMR: (300 MHz, CDCl₃) δ = 8.69 (d, J = 4.5 Hz, 1H), 8.65 (d, J = 4.5 Hz, 1H), 8.49 (d, J = 4.6 Hz, 1H), 8.42 (d, J = 8.0 Hz, 1H), 8.23 (d, J = 7.7 Hz, 1H), 7.81–7.57 (m, 6H), 7.30–7.24 (m, 1H), 7.21–7.08 (m, 3H), 4.18 (t, J = 14.1 Hz, 2H), 3.49 (d, J = 15.0 Hz, 2H), 3.28 (d, J = 10.6 Hz, 1H), 2.78–2.63 (m, 1H), 1.24 (d, J = 6.6 Hz, 3H), 0.61 (d, J = 6.5 Hz, 3H) ppm.

¹³C NMR: (75 MHz, CDCl₃) δ = 161.0, 160.2, 158.0, 156.6, 155.4, 149.5, 149.2, 148.9, 137.2, 136.9, 136.4, 135.6, 125.3, 123.6, 123.1, 123.0, 122.0, 121.8, 121.3, 119.1, 71.4, 56.9, 56.7, 28.4, 20.8, 20.7 ppm.

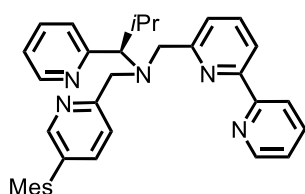
Experimental Part

IR: (neat) $\tilde{\nu}$ = 3059 (w), 2957 (w), 2923 (w), 2865 (w), 1727 (w), 1576 (m), 1466 (m), 1428 (s), 1370 (w), 1301 (w), 1258 (w), 1150 (w), 1085 (m), 1045 (w), 990 (m), 871 (w), 822 (w), 775 (s), 749 (s), 677 (s), 621 (w), 589 (w), 553 (w), 466 (w), 404 (w) cm^{-1} .

HRMS: (ESI+) m/z calcd. for $\text{C}_{26}\text{H}_{27}\text{N}_5\text{Na}$ $[\text{M}+\text{Na}]^+$: 432.2159, found: 432.2153.

$[\alpha]_{\text{D}}^{22}$: -83.0° ($c = 1.0$, CH_2Cl_2).

(*R*)-*N*-([2,2'-Bipyridin]-6-ylmethyl)-*N*-((5-mesitylpyridin-2-yl)methyl)-2-methyl-1-(pyridin-2-yl)propan-1-amine (**141**)



Following **GP C**, aldehyde **118** (18.0 mg, 0.10 mmol, 1.00 eq.), dipicolylamine **142** (45.7 mg, 0.13 mmol, 1.30 eq.), AcOH (2.8 μL , 0.05 mmol, 0.50 eq.), and NaBH_3CN (36.8 mg, 0.59 mmol, 6.00 eq.) were employed to furnish pentadentate ligand **141** (27.0 mg, 0.05 mmol, 52%) as a colorless solid after column chromatography on basic alumina (*n*-pentane/EtOAc 4:1 \rightarrow 2:1 \rightarrow 1:1). Enantiomeric excess was established by HPLC analysis on a chiral stationary phase: ee = 99%, HPLC conditions: Daicel Chiralpak[®] AD-H column, 250 x 4.6 mm, absorbance at 254 nm, *n*-hexane/isopropanol 99:1, isocratic flow, flow rate 1.0 mL/min, 25 $^\circ\text{C}$, t_{r} (minor) = 46.7 min, t_{r} (major) = 55.3 min.

TLC: R_{f} = 0.70 (*n*-pentane/EtOAc 2:1, on neutral alumina).

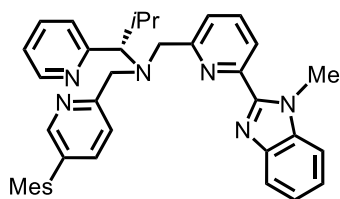
^1H NMR: (300 MHz, CDCl_3) δ = 8.71 (d, $J = 3.9$ Hz, 1H), 8.66 (d, $J = 4.0$ Hz), 8.44 (d, $J = 7.9$ Hz, 1H), 8.28 (s, 1H), 8.24 (d, $J = 7.7$ Hz, 1H), 7.82–7.60 (m, 5H), 7.42 (d, $J = 7.8$ Hz, 1H), 7.30–7.17 (m, 3H), 6.94 (s, 2H), 4.23 (d, $J = 14.9$ Hz, 2H), 3.58 (d, $J = 14.9$ Hz, 1H), 3.55 (d, 14.5 Hz, 1H), 3.36 (d, $J = 10.5$ Hz, 1H), 2.80–2.66 (m, 1H), 2.32 (s, 3H), 1.98 (s, 3H), 1.96 (s, 3H), 1.27 (d, $J = 6.6$ Hz, 3H), 0.64 (d, $J = 6.3$ Hz, 3H) ppm.

^{13}C NMR: (75 MHz, CDCl_3) δ = 160.3, 159.2, 158.2, 156.7, 155.4, 149.5, 149.3, 149.2, 137.5, 137.4, 137.3, 136.9, 136.6, 136.5, 135.6, 135.3, 134.6, 128.4 (2C), 125.3, 123.6, 123.3, 122.7, 122.0, 121.3, 119.2, 71.9, 57.1, 56.9, 28.4, 21.1, 21.0, 20.9, 20.9, 20.8 ppm.

Experimental Part

- IR:** (neat) $\tilde{\nu}$ = 3059 (w), 2957 (w), 2921 (w), 2863 (w), 1575 (m), 1466 (m), 1429 (m), 1370 (w), 1301 (w), 1259 (w), 1151 (w), 1093 (w), 1041 (w), 994 (w), 909 (w), 850 (w), 777 (m), 732 (s), 637 (w), 572 (w), 476 (w), 407 (w) cm^{-1} .
- HRMS:** (ESI+) m/z calcd. for $\text{C}_{35}\text{H}_{38}\text{N}_5$ $[\text{M}+\text{H}]^+$: 528.3122, found: 528.3118.
- $[\alpha]_{\text{D}}^{22}$:** -88.6° ($c = 1.0$, CH_2Cl_2).

(*S*)-*N*-((5-Mesitylpyridin-2-yl)methyl)-2-methyl-*N*-((6-(1-methyl-1*H*-benzo[*d*]imidazol-2-yl)pyridin-2-yl)methyl)-1-(pyridin-2-yl)propan-1-amine (**145**)



Following **GP C**, aldehyde **143** (64.0 mg, 0.27 mmol, 1.00 eq.), dipicolylamine **142** (126 mg, 0.35 mmol, 1.30 eq.), AcOH (7.7 μL , 0.14 mmol, 0.50 eq.), and NaBH_3CN (102 mg, 1.62 mmol, 6.00 eq.) were employed to furnish pentadentate ligand **145** (61.0 mg, 0.11 mmol, 39%) as a colorless solid after column chromatography on basic alumina (*n*-pentane/EtOAc 3:1 \rightarrow 1:1 \rightarrow EtOAc pure). Enantiomeric excess was established by HPLC analysis on a chiral stationary phase: ee = 99%, HPLC conditions: Daicel Chiralcel[®] OD-H column, 250 x 4.6 mm, absorbance at 254 nm, *n*-hexane/isopropanol 80:20, isocratic flow, flow rate 1.0 mL/min, 25 $^\circ\text{C}$, t_{r} (major) = 7.7 min, t_{r} (minor) = 10.3 min.

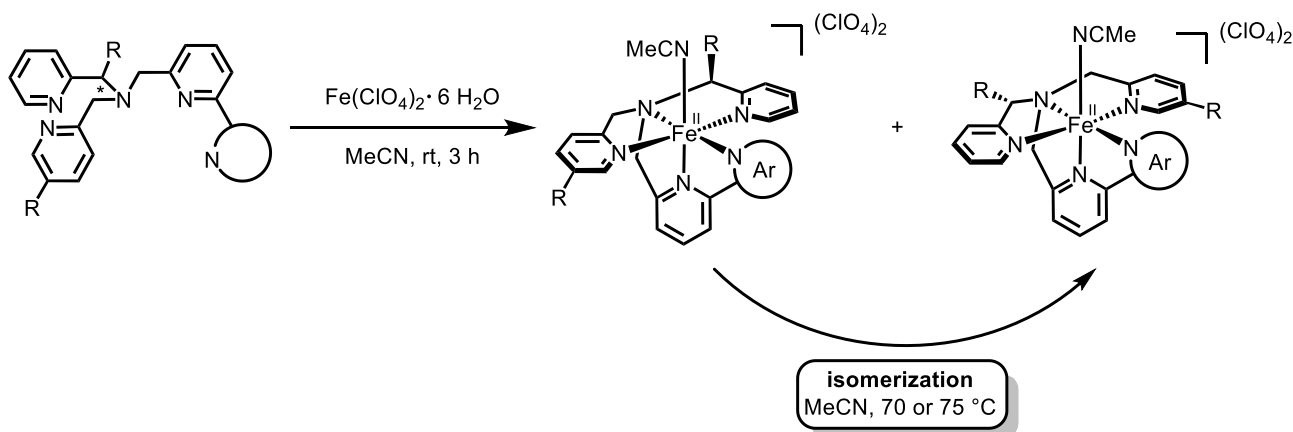
- TLC:** $R_f = 0.45$ (*n*-pentane/EtOAc 2:1, on neutral alumina).
- $^1\text{H NMR}$:** (300 MHz, CDCl_3) δ = 8.71 (d, $J = 4.3$ Hz, 1H), 8.30 (d, $J = 1.7$ Hz, 1H), 8.25 (d, $J = 7.7$ Hz, 1H), 7.86–7.80 (m, 2H), 7.71–7.65 (m, 3H), 7.47–7.40 (m, 2H), 7.37–7.29 (m, 2H), 7.28–7.15 (m, 2H), 6.95 (s, 2H), 4.28 (s, 3H), 4.28–4.25 (m, 1H), 4.23 (d, $J = 5.3$ Hz, 1H), 3.57 (d, $J = 14.9$ Hz, 1H), 3.56 (d, $J = 14.7$ Hz, 1H), 3.37 (d, $J = 10.6$ Hz, 1H), 2.80–2.65 (m, 1H), 2.32 (s, 3H), 1.98 (s, 6H), 1.28 (d, $J = 6.5$ Hz, 3H), 0.65 (d, $J = 6.4$ Hz, 3H) ppm.
- $^{13}\text{C NMR}$:** (75 MHz, CDCl_3) δ = 160.0, 158.9, 158.0, 150.6, 150.0, 149.5, 149.4, 142.7, 137.5 (2C), 137.4, 137.3, 136.5, 136.4, 135.7, 135.1, 134.8, 128.4, 128.4, 125.2, 123.4, 123.3, 123.0, 122.7, 122.6, 122.1, 120.1, 110.0, 71.9, 57.1, 56.9, 32.9, 28.5, 21.1, 21.0, 20.9, 20.9, 20.8 ppm.

Experimental Part

- IR:** (neat) $\tilde{\nu}$ = 3054 (w), 2954 (w), 2920 (w), 2863 (w), 1579 (m), 1466 (m), 1434 (m), 1378 (w), 1327 (w), 1262 (w), 1152 (w), 1082 (w), 1039 (w), 995 (w), 907 (w), 848 (w), 815 (w), 739 (s), 575 (w), 547 (w), 415 (w) cm^{-1} .
- HRMS:** (ESI+) m/z calcd. for $\text{C}_{38}\text{H}_{41}\text{N}_6$ $[\text{M}+\text{H}]^+$: 581.3379, found: 581.3381.
- $[\alpha]_{\text{D}}^{22}$:** -74.2° ($c = 1.0$, CH_2Cl_2).

5.3.4 Synthesis of Fe(II) Complexes with Chiral Pentadentate Ligands

General Procedure D: Complexation towards Stereogenic-at-Iron Complexes



A procedure by Wong *et al.*^[128] was slightly modified and used for the synthesis of Fe(II) complexes. A Schlenk flask was charged with iron(II) perchlorate hexahydrate (1.00 eq.) and MeCN was added. Subsequently, a solution of predissolved pentadentate ligand (1.00 eq.) in MeCN (0.02 M in total) was added providing a dark red reaction mixture that was stirred for 90 min. Afterwards, the solution was carefully concentrated under vacuum (about half volume) and again stirred for 1 h. Dry Et_2O was added and precipitation of the red complex was observed. For completion of precipitation, the mixture was stirred for another 30 min. Subsequently, the solid was filtered off, washed extensively with Et_2O and *n*-pentane, and dried under vacuum to obtain a diastereomeric mixture of complexes.

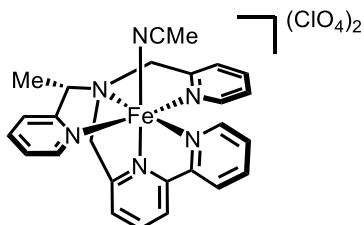
For isomerization, a Schlenk flask was charged with a diastereomeric mixture of complexes and MeCN (0.04 M). The solution was subsequently stirred for 16 h at 70 °C (complex **140**), 24 h at 75 °C (complexes **149** and **150**), or 5 d at 75 °C (complex **131**). Afterwards, the solvent was evaporated under reduced pressure and the solid dried under vacuum to afford pure complexes.

The stated NMR data refer to the thermodynamically more stable isomer after isomerization. NMR data of the second isomer will not be listed.

Experimental Part

For practical reasons it is noteworthy, that the obtained catalysts were stored under air at 4 °C for over two years without signs of decomposition due to air- or moisture-sensitivity as evaluated by ^1H NMR analysis.

Fe(II)-Complex 131a



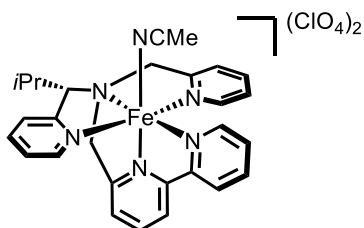
Following **GP D**, pentadentate ligand **127** (158 mg, 0.41 mmol, 1.00 eq.) and $\text{Fe}(\text{ClO}_4)_2 \cdot 6 \text{H}_2\text{O}$ (150 mg, 0.41 mmol, 1.00 eq.) were employed to provide complex **131a** (280 mg, 0.41 mmol, >99%) after isomerization as a dark-red solid.

^1H NMR: (600 MHz, CD_3CN) δ = 9.07 (d, J = 5.4 Hz, 1H), 8.57 (d, J = 7.9 Hz, 1H), 8.34-8.24 (m, 2H), 7.90-7.75 (m, 3H), 7.70 (t, J = 7.7 Hz, 1H), 7.40 (d, J = 7.7 Hz, 1H), 7.31 (d, J = 7.9 Hz, 1H), 7.22 (d, J = 7.8 Hz, 1H), 7.07-6.94 (m, 3H), 6.72 (d, J = 5.4 Hz, 1H), 5.16 (q, J = 6.7 Hz, 1H), 4.94 (d, J = 16.0 Hz, 1H), 4.82 (d, J = 16.0 Hz, 1H), 4.64 (d, J = 18.9 Hz, 1H), 4.36 (d, J = 18.9 Hz, 1H), 1.85 (d, J = 6.7 Hz, 3H) ppm.

IR: (neat) $\tilde{\nu}$ = 3676 (w), 3595 (w), 2434 (w), 2279 (w), 2241 (w), 2174 (m), 2140 (w), 2111 (w), 2049 (m), 2002 (w), 1973 (w), 1914 (w), 1076 (s), 912 (w), 766 (s), 617 (s), 538 (w), 444 (m), 412 (w) cm^{-1} .

HRMS: (ESI+) m/z calcd. for $\text{C}_{24}\text{H}_{23}\text{FeN}_5\text{ClO}_4$ [$\text{M} - \text{ClO}_4$ and MeCN] $^+$: 536.0783; found: 536.0800.

Fe(II)-Complex 140a



Following **GP D**, pentadentate ligand **139** (65.0 mg, 0.16 mmol, 1.00 eq.) and $\text{Fe}(\text{ClO}_4)_2 \cdot 6 \text{H}_2\text{O}$

Experimental Part

(57.6 mg, 0.16 mmol, 1.00 eq.) were employed to provide complex **140a** (110 mg, 0.16 mmol, 98%) after isomerization as a dark-red solid.

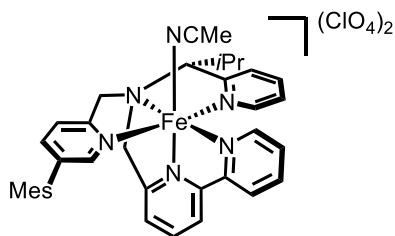
¹H NMR: (600 MHz, CD₃CN) δ = 9.02 (d, J = 5.3 Hz, 1H), 8.55 (d, J = 8.0 Hz, 1H), 8.31–8.26 (m, 2H), 7.86–7.81 (m, 2H), 7.79–7.75 (m, 1H), 7.70 (dt, J = 7.7, 1.4 Hz, 1H), 7.46 (d, J = 8.0 Hz, 1H), 7.42 (d, J = 7.8 Hz, 1H), 7.23 (d, J = 7.8 Hz, 1H), 7.05–7.01 (m, 2H), 6.99 (t, J = 6.6 Hz, 1H), 6.67 (d, J = 5.4 Hz, 1H), 5.19 (d, J = 16.0 Hz, 1H), 5.05 (d, J = 16.1 Hz, 1H), 4.72 (d, J = 18.6 Hz, 1H), 4.65 (d, J = 7.7 Hz, 1H), 4.61 (d, J = 18.6 Hz, 1H), 2.85–2.77 (m, J = 7.0 Hz, 1H), 1.54 (d, J = 7.0 Hz, 3H), 1.46 (d, J = 6.5 Hz, 3H) ppm (signals of labile MeCN ligand not visible).

¹³C NMR: (126 MHz, CD₃CN) δ = 166.3, 165.6, 165.5, 160.6, 158.9, 158.0, 154.9, 153.2, 139.4, 139.1, 139.1, 137.7, 128.3, 125.9, 125.0 (2C), 124.8, 123.1, 122.8, 121.3, 79.9, 69.8, 65.3, 31.4, 22.9, 21.4 ppm (signals of labile MeCN ligand not visible).

IR: (neat) $\tilde{\nu}$ = 3605 (w), 3085 (w), 2971 (w), 1603 (w), 1443 (w), 1297 (w), 1251 (w), 1168 (w), 1070 (s), 810 (w), 766 (m), 656 (w), 618 (m), 502 (w), 416 (w) cm⁻¹.

HRMS: (ESI+) m/z calcd. for C₂₆H₂₇FeN₅ClO₄ [M – ClO₄ and MeCN]⁺: 564.1079; found: 564.1096.

Fe(II) Complex 149a



Following **GP D**, pentadentate ligand **141** (86.0 mg, 0.16 mmol, 1.00 eq.) and Fe(ClO₄)₂ · 6 H₂O (59.1 mg, 0.16 mmol, 1.00 eq.) were employed to provide complex **149a** (132 mg, 0.16 mmol, 98%) after isomerization as a dark-red solid.

¹H NMR: (300 MHz, CD₃CN) δ = 8.98 (d, J = 5.3 Hz, 1H), 8.49 (d, J = 8.0 Hz, 1H), 8.28 (d, J = 8.0 Hz, 1H), 8.18 (dt, J = 7.8, 1.1 Hz, 1H), 7.87 (t, J = 8.0 Hz, 1H), 7.83–7.69 (m, 2H), 7.54–7.46 (m, 3H), 7.27 (d, J = 7.9 Hz, 1H), 7.05 (d, J = 4.3 Hz, 2H), 6.87 (s, 1H), 6.80 (s, 1H), 6.27 (s, 1H), 5.21 (d, J = 15.9 Hz, 1H), 5.08 (d, J = 15.9 Hz, 1H), 4.72 (d, J = 7.4 Hz, 1H), 4.67 (d, J = 4.3 Hz, 2H), 2.89–2.76 (m, J = 6.8 Hz, 1H), 2.21

Experimental Part

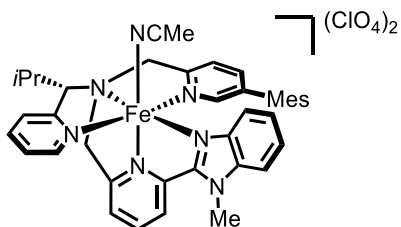
(s, 3H), 1.87 (s, 3H), 1.56 (d, $J=7.0$ Hz, 3H), 1.50 (d, $J=6.5$ Hz, 3H), 1.32 (s, 3H) ppm (signals of labile MeCN ligand not visible).

^{13}C NMR: (126 MHz, CD_3CN , -20 °C) $\delta=166.2, 165.4, 163.6, 160.1, 158.5, 157.9, 154.9, 152.7, 140.0, 139.2, 139.0, 138.9, 138.1, 137.4, 136.5, 136.1, 133.2, 129.2, 128.1, 125.7, 124.6, 122.7, 122.5, 121.1, 79.3, 69.2, 65.1, 31.3, 22.8, 21.0, 20.8, 20.6, 20.0$ ppm (signals of labile MeCN ligand not visible).

IR: (neat) $\tilde{\nu}=3081$ (w), 2966 (w), 1604 (w), 1446 (w), 1295 (w), 1246 (w), 1074 (s), 933 (w), 850 (w), 770 (m), 658 (m), 618 (w), 416 (w) cm^{-1} .

HRMS: (ESI+) m/z calcd. for $\text{C}_{35}\text{H}_{37}\text{FeN}_5\text{ClO}_4$ [$\text{M} - \text{ClO}_4$ and MeCN] $^+$: 682.1879; found: 682.1858.

Fe(II) Complex 150a



Following **GP D**, pentadentate ligand **145** (70.0 mg, 0.12 mmol, 1.00 eq.) and $\text{Fe}(\text{ClO}_4)_2 \cdot 6 \text{H}_2\text{O}$ (43.7 mg, 0.12 mmol, 1.00 eq.) were employed to provide complex **150a** (98.0 mg, 0.11 mmol, 93%) after isomerization as a dark-red solid.

^1H NMR: (500 MHz, CD_3CN , -20 °C) $\delta=8.35$ (d, $J=8.1$ Hz, 1H), 7.91 (t, $J=8.0$ Hz, 1H), 7.86 (d, $J=8.2$ Hz, 1H), 7.80 (d, $J=8.4$ Hz, 1H), 7.73 (t, $J=7.8$ Hz, 1H), 7.59 (t, $J=7.7$ Hz, 1H), 7.52–7.42 (m, 4H), 7.28 (d, $J=7.8$ Hz, 1H), 7.03 (d, $J=5.1$ Hz, 1H), 6.94 (t, $J=6.5$ Hz, 1H), 6.77 (s, 1H), 6.75 (s, 1H), 6.56 (s, 1H), 5.10 (d, $J=16.1$ Hz, 1H), 5.02 (d, $J=16.1$ Hz, 1H), 4.69 (d, $J=18.6$ Hz, 1H), 4.58 (d, $J=18.8$ Hz, 1H), 4.53 (d, $J=8.0$ Hz, 1H), 4.35 (s, 3H), 2.79–2.71 (m, 1H), 2.14 (s, 3H), 1.71 (s, 3H), 1.52 (d, $J=6.9$ Hz, 3H), 1.46–1.43 (m, 6H) ppm (signals of labile MeCN ligand not visible).

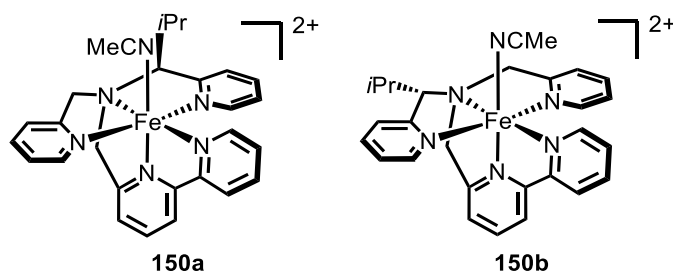
^{13}C NMR: (126 MHz, CD_3CN , -20 °C) $\delta=167.1, 166.2, 163.6, 155.5, 153.8, 153.2, 151.5, 143.5, 139.8, 138.9, 138.7, 138.6, 138.0, 137.3, 136.4, 136.3, 133.3, 129.1, 128.9, 126.7, 125.7, 125.5, 124.5, 123.8, 122.3, 120.8, 113.0, 79.1, 69.4, 65.0, 33.4, 31.2, 22.8, 21.0, 20.7, 20.5, 20.3$ ppm (signals of labile MeCN ligand not visible, one carbon signal may be overshadowed by solvent signal).

Experimental Part

IR: (neat) $\tilde{\nu}$ = 2962 (w), 1603 (w), 1480 (w), 1439 (w), 1298 (w), 1074 (s), 931 (w), 847 (w), 799 (w), 749 (m), 618 (m), 426 (w) cm^{-1} .

HRMS: (ESI+) m/z calcd. for $\text{C}_{38}\text{H}_{40}\text{FeN}_6$ [$\text{M} - 2 \text{ClO}_4^-$ and MeCN] $^{2+}$: 318.1327, found: 318.1334.

5.3.4.1 NMR Studies on Pentadentate Fe(II) Complex 140



General Information

Upon complexation of enantiomerically pure chiral ligand to the Fe(II) center, two diastereomers can be formed (**140a** and **140b**). Isomerization in CH_3CN showed that one of these diastereomers is thermodynamically favored probably due to steric repulsion of the isopropyl moiety on the pentadentate ligand. In this section, NMR experiments will be discussed which were conducted to evaluate the configuration of the thermodynamically favored diastereomer as well as to get insight into the kinetics of the complexation and isomerization. These studies were conducted in collaboration with Dr. Xiulan Xie who performed the NMR measurements and analyzed the obtained spectra.

For measurements on the dynamic of the labile acetonitrile ligand, about 8 mg of the complex after isomerization were dissolved in 0.5 mL of a mixture of $\text{CH}_3\text{CN}/\text{CD}_3\text{CN}$ (10% v/v of CD_3CN). Experiments were performed on a Bruker AVIII HD 500 MHz equipped with a 5 mm TBI probe with z-gradient at temperatures 300, 243 and 273 K and on a Bruker AVII 600 MHz spectrometer equipped with a TXI probe with z-gradient at temperatures 300 and 273 K. One-dimensional ^1H and two-dimensional ^1H , ^1H DQF-COSY, NOESY and ROESY spectra were recorded by using standard programs with solvent suppression.^[260] Solvent suppression was performed with the excitation sculpting method.^[261] NOESY spectra were taken at mixing times of 0.5, 1.5 and 3.0 s, while ROESY at 200 ms. Two-dimensional ^1H , ^{13}C HSQC and HMBC spectra were recorded with standard procedure.^[260] The sample for NMR spectra concerning the isomerization process contained about 16 mg of the diastereomeric mixture (**140a** + **140b**) in CD_3CN without thermal treatment. This sample was also used for measurements regarding the structural elucidation by measuring 2D spectra before

Experimental Part

and after isomerization. Next, about 15 mg of the diastereomeric mixture of complex **140** were dissolved in 0.5 mL of CD₂Cl₂ for further evaluation of the complex behavior in other solvents than acetonitrile. The 1D ¹H spectra at 298, 273 and 263 K and 2D HSQC, HMBC and ROESY spectra at 263 K were recorded on a Bruker AVIII 500 MHz equipped with a cryo probe Prodigy BBO and a temperature unit BCU II. Finally, 8 mg of the isomeric mixture were dissolved in 0.5 mL of a mixture of CD₂Cl₂/CH₃CN (4% v/v of CH₃CN) to get further insight into the kinetics of the ligand exchange. For this purpose, ROESY spectra with mixing times of 50 ms were recorded on AVIII 500 MHz at 263, 273, and 283 K. All NMR spectra were processed by Bruker program package Topspin 4.0.8. Chemical shifts of ¹H and ¹³C resonances were referenced internally to the solvent peaks.

Dynamics of Labile Solvent Ligand

¹H NMR spectra of the isolated complex after isomerization in CD₃CN showed no signal of the labile acetonitrile ligand attached to the metal center. Therefore, we assumed this group to be rather labile and that it is exchanged with deuterated solvent molecules quickly, preventing visibility in ¹H NMR spectra. Instead of using CD₃CN as solvent, we dissolved the sample in a mixture of CH₃CN/CD₃CN (10% v/v of CD₃CN) to prevent the exchange of the labile solvent with an invisible deuterated acetonitrile molecule. The dominant signal of CH₃CN was suppressed by using the excitation sculpting technique which was originally designed for the observation of amide-protons in protein-NMR measurements.^[261,262] By using this approach, a sharp ¹H peak at 2.55 ppm could be detected when the measurement was performed at -30 °C. However, the same peak became broader at 0 °C and disappeared completely at 27 °C (Figure 39). This experiment shows that the acetonitrile ligand is labile and is easily exchanged by other solvent molecules. Efforts towards detecting NOE contact signals between the iron-bound acetonitrile and the pentadentate ligand were unsuccessful. Both, NOESY and ROESY spectra at low temperatures (-30 °C and 0 °C) provided no cross peaks.

Experimental Part

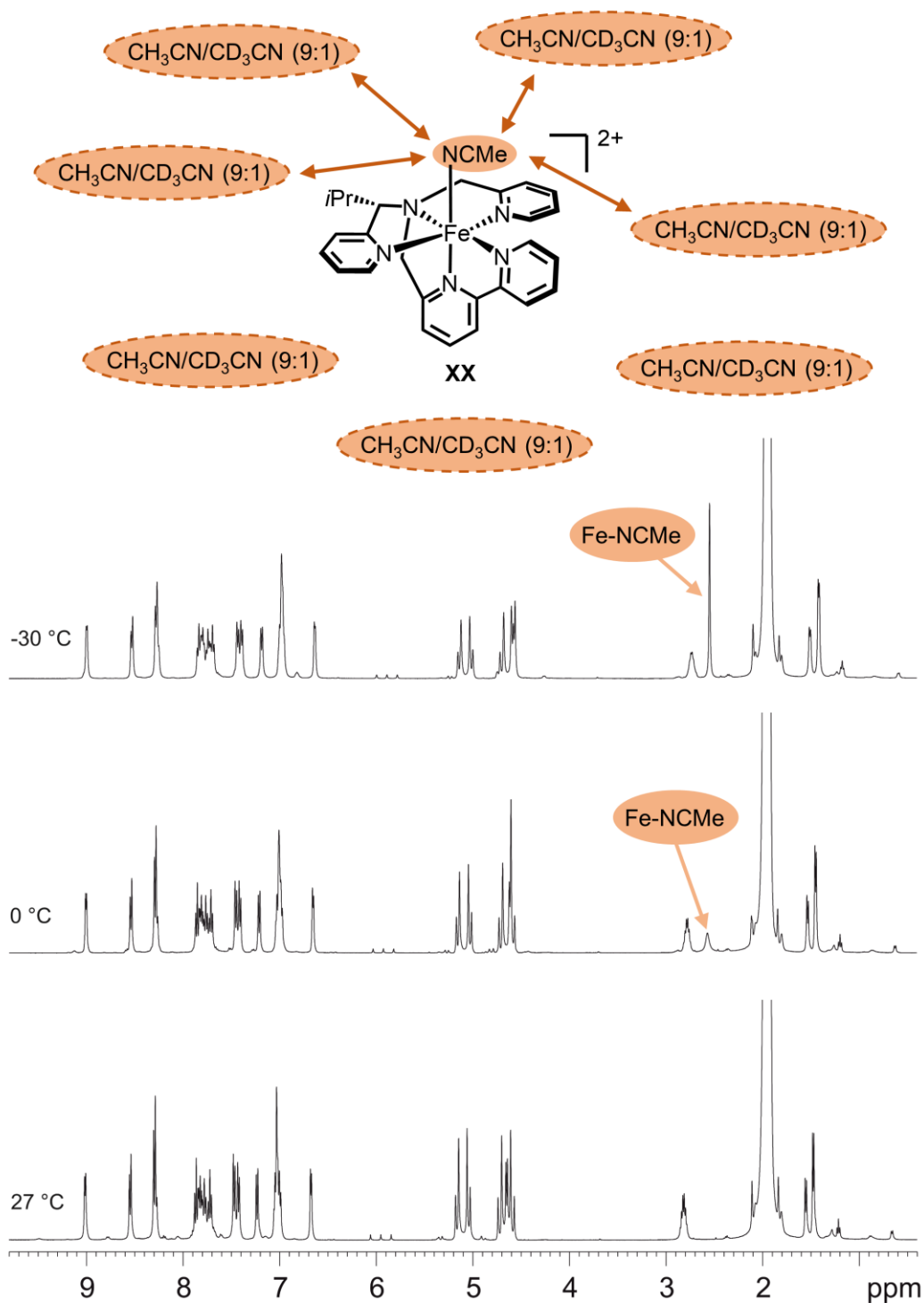


Figure 39: ¹H NMR spectra of diastereomer **140** in CH₃CN/CD₃CN (10% v/v of CD₃CN) measured on an AV-HD 500 at various temperatures.

Full Signal Assignment and Structural Determination

The diastereomerically pure complex was submitted to a full suite of measurements with DQF-COSY, TOCSY, NOESY, ¹H-¹³C HSQC and HMBC. For this purpose, the ligand was divided into

Experimental Part

three parts that are indicated by different colors. Analysis of the DQF-COSY and TOCSY spectra showed spin systems and connections within the individual parts of the ligand while an HMBC spectrum verified the long-range connectivity between them. A full assignment was conducted. The ^1H and ^{13}C chemical shifts of the isomerized complex are listed in Table 13.

Table 13: Chemical Shifts and HMBC Correlation of Complex 140a.

Position	$\delta_{13\text{C}}$ (ppm)	$\delta_{1\text{H}}$ (ppm) (multi: J (Hz))	HMBC correlation	
Py-1 (blue)	2	166.26	/	
	3	124.72	7.464 (d: 8.0)	H3 to C5, C1 ^{am}
	4	138.98	7.769 (td: 7.6, 2.2)	H4 to C2, C6
	5	125.82	7.038 (t: 6.3)	H5 to C3
	6	154.84	7.033 (d: 6.9)	H6 to C2, C4
Py-2 (red)	2	165.43	/	
	3	122.99	7.42 (d : 7.7)	H3 to C5, C1' ^{am}
	4	138.89	7.70 (td: 7.8, 1.5)	H4 to C2, C6
	5	125.83	6.99 (t: 6.6)	H5 to C3
	6	153.09	6.67 (5.3)	H6 to C2, C4
bpy	2	158.86	/	
	3	122.66	8.298 (d: 7.9)	H3 to C5, C2'
	4	137.53	7.84 (t: 7.9)	H4 to C2, C6
	5	121.17	7.232 (d: 7.7)	H5 to C3, C1 ^{ax}
	6	165.51	/	
	2'	160.44	/	
	3'	124.92	8.554 (d: 8.0)	H3' to C5', C2
	4'	139.28	8.279 (td: 7.7, 1.4)	H4' to C2', C6'
	5'	128.29	7.823 (ddd: 7.7, 5.5, 1.4)	H5' to C3'
	6'	157.97	9.023 (d: 5.3)	H6' to C2', C4'
	am	1 ^{am}	79.78	4.651 (d: 7.6)
2 ^{am}		31.26	2.810 (sept: 6.8)	H2 ^{am} to C3 ^{am} , C3' ^{am} , C2
3 ^{am}		21.30	1.542 (d: 6.8)	H3 ^{am} to C2 ^{am} , C1 ^{am} , C3' ^{am}
3' ^{am}		22.78	1.460 (d: 6.5)	H3' ^{am} to C2 ^{am} , C1 ^{am} , C3 ^{am}
1' ^{am}		69.75	5.19 (d:16.0); 5.05 (d:16.1)	H1' ^{am} to C1 ^{am} , C1 ^{ax} , C2, C3
1 ^{ax}		65.21	4.719 (d:18.7); 4.612 (d:18.8)	H1 ^{ax} to C1 ^{am} , C1' ^{am} , C5, C6
CH₃CN*	CH ₃	5.40	2.552 (s)	CH ₃ to CN
	CN	137.40	/	

On the basis of the complete assignment, unambiguous NOE interactions among the protons of the isopropyl group of the ligand, the methine, and the methylene groups at α -positions of the tertiary amine could be identified. Thus, strong NOE cross peaks between the protons of position 2^{am} and the methyl group at position 3^{am} and 2^{am}-3'^{am}, cross peaks of intermediate strength between positions 1^{am}-2^{am}, 1^{am}-3^{am}, 1^{am}-3'^{am}, 1^{am}-1'^{am} _{α} , 1'^{am} _{β} -1^{ax} _{β} , 1'^{am} _{α} -3^{am}, 1'^{am} _{β} -3^{am}, 1'^{am} _{α} -3'^{am}, 1'^{am} _{β} -3'^{am}, 1^{ax} _{α} -3^{am}, 1^{ax} _{α} -3'^{am}, and weak cross peaks between the positions 1'^{am} _{β} -2^{am} were

Experimental Part

observed. This pattern of NOE interactions can only be induced by the configuration of complex **140a**. The NOESY spectrum of the aliphatic region is shown in Figure 40.

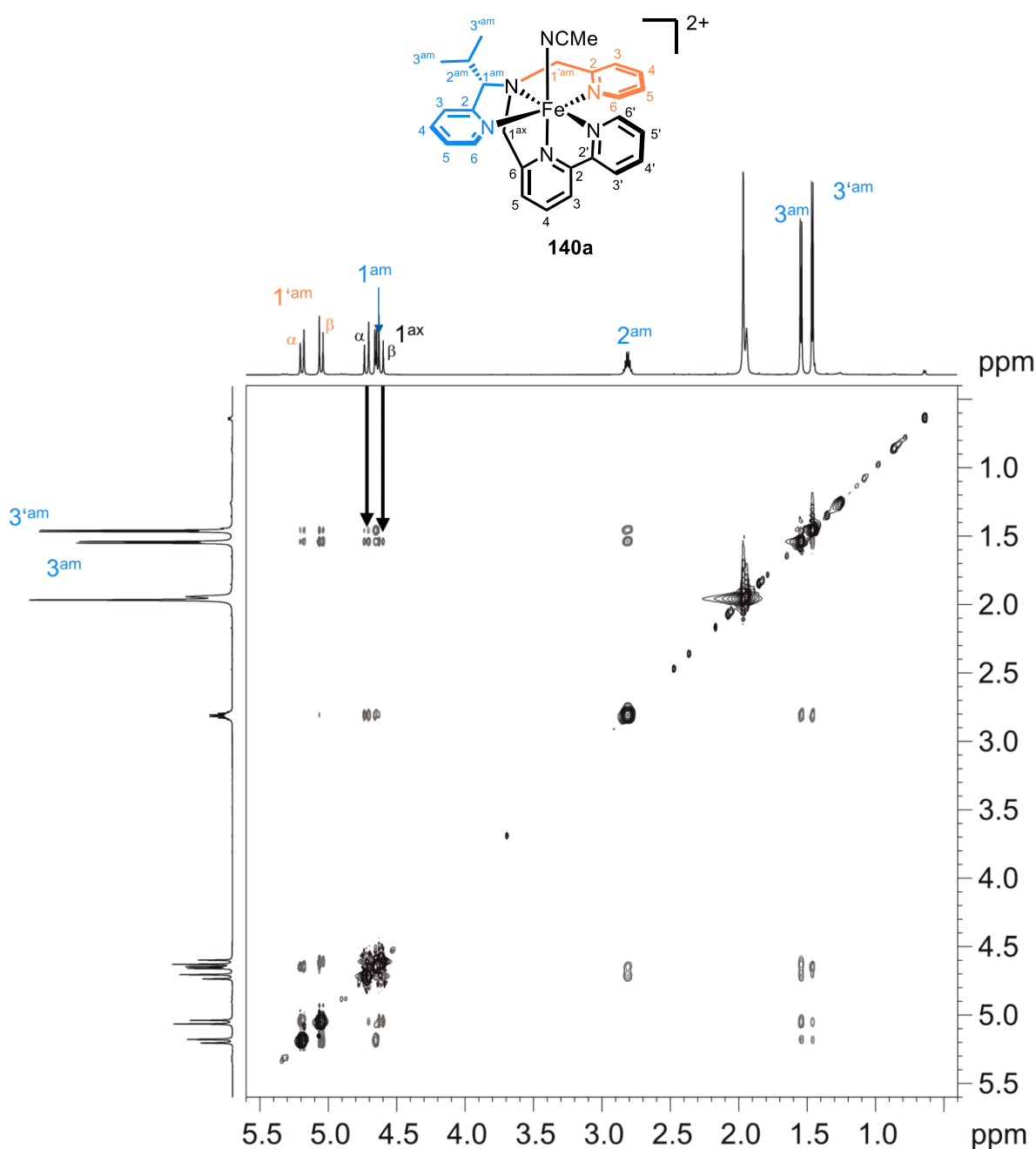


Figure 40: Section of the ^1H - ^1H NOESY spectrum showing interactions among the aliphatic fragments. The spectrum was recorded on an AV II 600 at 25 °C with a mixing time of 0.5 s.

The structure of the thermodynamically more favored diastereomer was further verified by an observation of the NOE interactions of the unfavored diastereomer. Since this isomer could not be isolated purely, NOESY measurements of the diastereomeric mixture were conducted (Figure 41). Fortunately, the ^1H NMR spectrum of the isomer mixture shortly after sample dissolution showed well resolved signals in the aliphatic region (0.5 – 5.5 ppm). Thus, the NOESY spectrum was

Experimental Part

recorded directly after sample dissolution and NOE cross peaks were carefully analyzed (signal assignments for the thermodynamically unfavored diastereomer **140b** are underlined for better understanding). The same NOE cross peaks as shown for the pure sample in Figure 40 were observed. Additionally, cross peaks of lower intensities could be detected and were assigned to be between $\underline{2}^{\text{am}} - \underline{3}^{\text{am}}$, $\underline{2}^{\text{am}} - \underline{3}^{\prime\text{am}}$, $\underline{1}^{\prime\text{am}}_{\alpha} - \underline{2}^{\text{am}}$, $\underline{1}^{\prime\text{am}}_{\alpha} - \underline{3}^{\text{am}}$, $\underline{1}^{\prime\text{ax}}_{\beta} - \underline{3}^{\text{am}}$ (very weak). No further NOE contact between the isopropyl moiety and the methylene on the axial position was detectable for **140b**. Therefore, the NOE pattern for the minor peaks agrees with the stereoconfiguration of diastereomer **140b**.

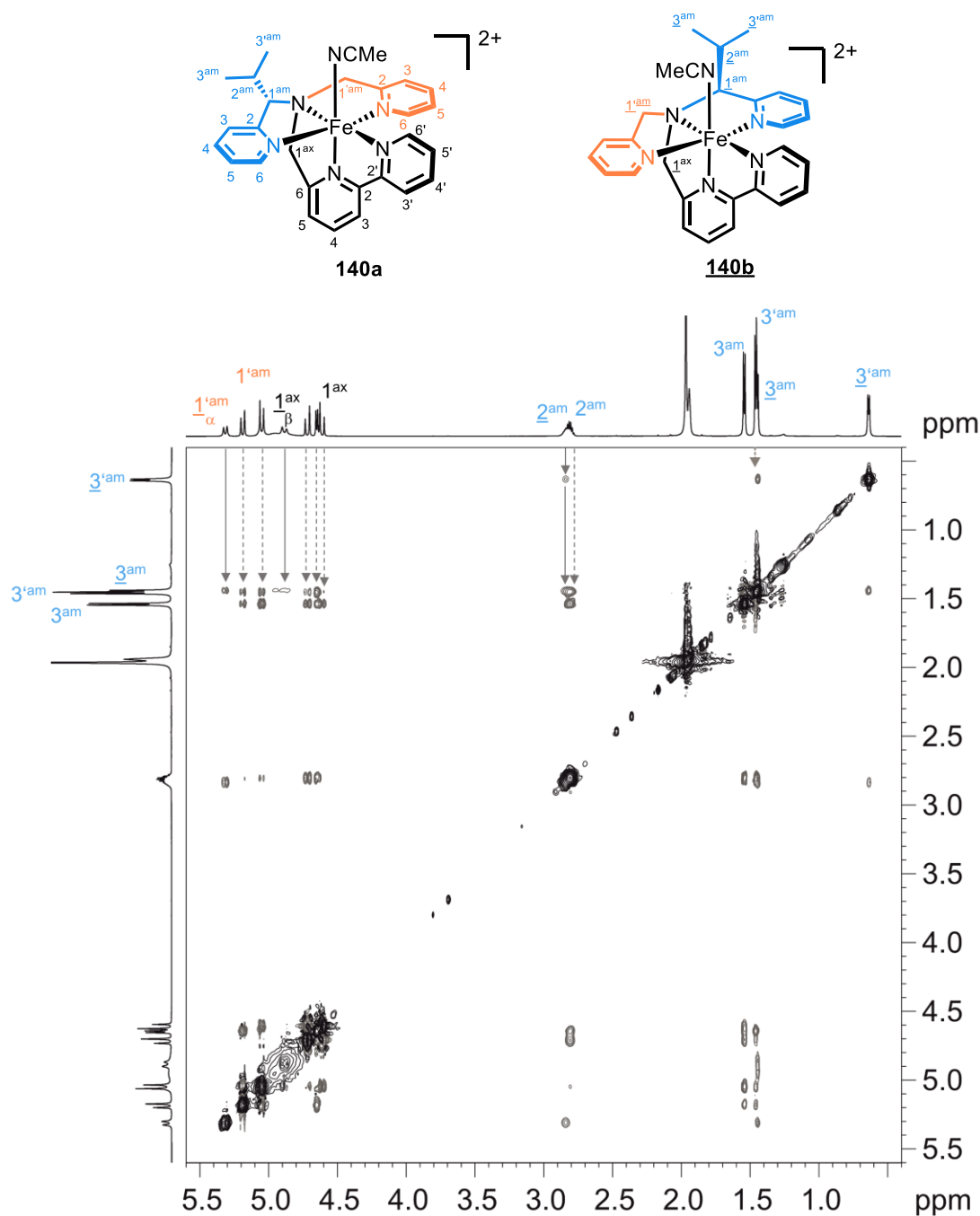


Figure 41: Section of the $^1\text{H} - ^1\text{H}$ NOESY spectrum showing interactions in the aliphatic region. The spectrum was recorded on an AVII 600 at 25 °C with a mixing time of 0.5 s. Signal assignments are shown along the 1D projections. Important cross peaks are highlighted with broken (**140a**) and straight (**140b**) lines.

Studies on the Kinetics of Labile Acetonitrile Ligand

Studies of the kinetics involving the labile solvent ligand of complex **140a** were realized by analyzing exchange peaks between coordinated and “free” MeCN in ROESY spectra with a mixing time of 50 ms.

The exchange rate between the two sites can easily be determined by measuring the intensities of the diagonal peaks and the cross peaks caused by the chemical exchange. The two-dimensional exchange spectroscopy (EXSY) is useful for the study of such exchanges, where the exchange time scales from milliseconds to seconds.^[262,263] The exchange rate k between two chemical sites A and B can be calculated with the following equations.^[264]

$$2k = \frac{1}{\tau_m} \ln \left(\frac{r + 1}{r - 1} \right) \quad (1)$$

$$r = \frac{4p_A p_B (I_{AA} + I_{BB})}{I_{AB} + I_{BA}} - (p_A - p_B)^2 \quad (2)$$

In these equations, p_A and p_B refer to the fractional population of A and B, τ_m is the mixing time of the EXSY experiment, I_{AA} and I_{BB} are the diagonal peaks, and I_{AB} and I_{BA} are the intensities of the cross peaks.

Although the mechanism of chemical exchange is rather different to that of the NOE, the two processes have the transfer of longitudinal magnetization in common so that they can be detected with the same NMR experiment. In fact, the NOESY/ROESY pulse sequences are applied for EXSY experiments to determine the rate constants.^[265] For non-small molecules the use of ROESY pulse sequences enables the differentiation of the chemical exchange and NOE interactions rather quickly. The cross peaks from NOE interactions are always positive whereas those caused by chemical exchanges are always negative.

This intrinsic dynamic behavior of acetonitrile as a coordinating ligand to the Fe(II)-center is expected to follow the Arrhenius law and can be described by the following Arrhenius equations:^[266]

$$k = \frac{RT}{hN_A} e^{-\frac{\Delta G^\ddagger}{RT}} \quad (3)$$

Equation (3) is often rearranged as

$$\ln\left(\frac{k}{T}\right) = \ln\left(\frac{R}{hN_A}\right) - \frac{\Delta G^\ddagger}{R} \frac{1}{T} \quad (4)$$

Experimental Part

where k is the exchange rate in Hz, R is the universal gas constant ($8.315 \text{ J} \cdot \text{K}^{-1}$), T is the absolute temperature in K, h Plank's constant ($6.626 \cdot 10^{-34} \text{ J} \cdot \text{s}$), N_A the Avogadro constant ($6.02 \cdot 10^{23} \text{ mol}^{-1}$) and the free energy of activation ΔG^\ddagger in $\text{kJ} \cdot \text{mol}^{-1}$. The free energy of activation can be substituted by using equation (5).

$$\Delta G^\ddagger = \Delta H^\ddagger - T\Delta S^\ddagger \quad (5)$$

When combining equations (4) and (5), the Eyring equation is formed and the Eyring plot follows:

$$\ln\left(\frac{k}{T}\right) = \left(23.76 + \frac{\Delta S^\ddagger}{R}\right) - \left(\frac{\Delta H^\ddagger}{R}\right)\frac{1}{T} \quad (6)$$

By measuring the exchange rate k at different temperatures and plotting $\ln\left(\frac{k}{T}\right)$ against $\left(\frac{10000}{T}\right)$, a linear regression is obtained whereby the intercept A reveals the values for ΔS^\ddagger ($=R(A-23.76)$) and the slope B the value for ΔH^\ddagger ($=-1000 RB$). In this way, the corresponding free energy of activation at each studied temperature can be calculated according to equation (3). The results are presented in Table 14. The obtained free enthalpy was $30.2 \text{ kJ} \cdot \text{mol}^{-1}$ and the free entropy was $-119.2 \text{ J} \cdot \text{K}^{-1} \text{ mol}^{-1}$.

Table 14: EXSY Results of Complex **140a** in $\text{CD}_2\text{Cl}_2/\text{MeCN}$ (4% v/v for MeCN).

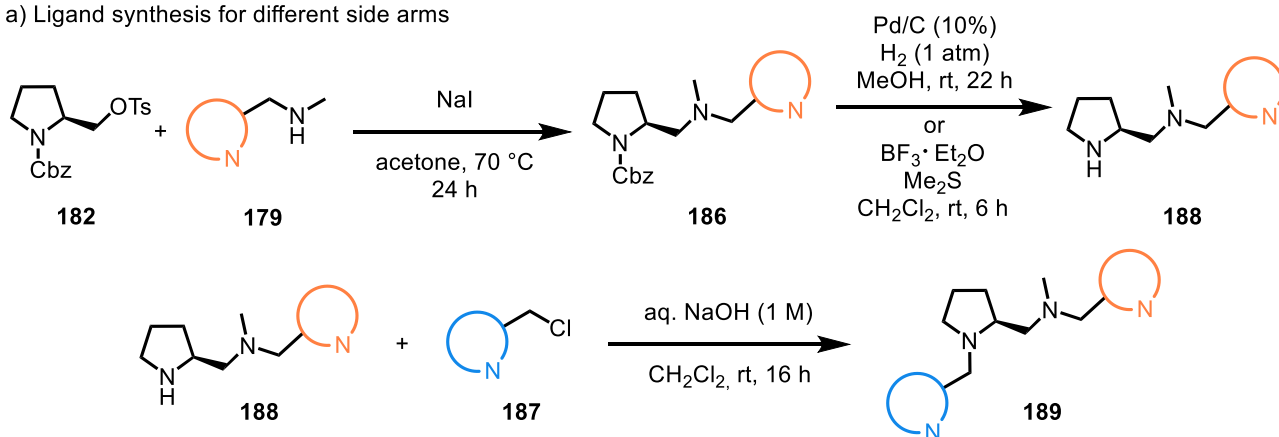
Temperature (K)	Exchange Rate k (s^{-1})	Free Energy ΔG^\ddagger (kJ/mol)
263	3.2	61.5
273	6.3	62.7
283	9.1	63.9

5.4 Synthesis of Tetradentate Complexes

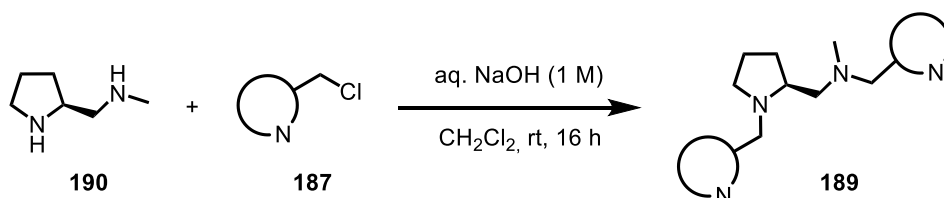
5.4.1 Synthesis of Chiral Tetradentate Ligands

The tetradentate, proline-based ligand scaffold was synthesized as depicted in Scheme 72 starting from commercially available (*S*)-prolinol (**183**) or diamine **190**. The synthesis of Cbz- and Ts-functionalized compound **182** was performed according to reported procedures.^[267,268] The synthetic access towards benzimidazole and benzothiazole amines **179b** and **179c** is described in the following section. *N*-Methyl-1-(pyridine-2-yl)methanamine (**179a**) was commercially purchased.

a) Ligand synthesis for different side arms

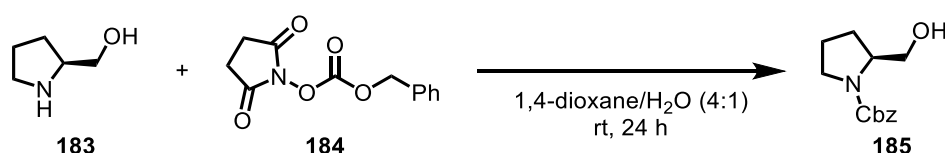


b) Ligand synthesis for identical side arms



Scheme 72: Synthetic access towards chiral, tetradentate ligand scaffold **189**.

Benzyl (*S*)-2-(hydroxymethyl)pyrrolidine-1-carboxylate (**185**)



Following a procedure by Calveras *et al.*,^[267] to a solution of (*S*)-prolinol (**183**, 1.50 mL, 1.54 g, 15.2 mmol, 1.00 eq.) in 1,4-dioxane/H₂O (4:1, 30 mL) was added dropwise a solution of succinimide **184** (3.64 g, 14.6 mmol, 0.96 eq.) in 1,4-dioxane/H₂O (4:1, 15 mL, 0.33 M in total) and

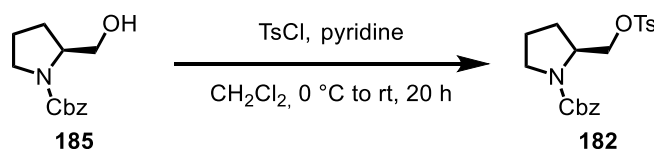
Experimental Part

the resulting mixture was stirred for 24 h at rt under air. Afterwards, the solvent was removed under reduced pressure and the residue was dissolved in EtOAc. The organic layer was washed with an aq. solution of citric acid (5 w%, 3x), saturated aq. NaHCO₃-solution (3x), and brine (2x). The organic layer was subsequently dried over Na₂SO₄, filtered, and the solvent was removed under reduced pressure to give **185** (3.24 g, 13.8 mmol, 91%) as an off-white solid that was used without further purification.

¹H NMR: (300 MHz, CDCl₃) δ = 7.40-7.29 (m, 5H), 5.15 (s, 2H), 4.06-3.96 (m, 1H), 3.73-3.50 (m, 3H), 3.45-3.35 (m, 1H), 2.02 (m, J = 6.6 Hz, 1H), 1.84 (m, J = 6.1 Hz, 2H), 1.66-1.54 (m, 1H) ppm.

Analytical data were consistent with reported data.^[269]

Benzyl (*S*)-2-((tosyloxy)methyl)pyrrolidine-1-carboxylate (**182**)



Following a modified procedure by Chu *et al.*,^[268] a Schlenk flask was charged with prolinol **185** (3.24 g, 13.8 mmol, 1.00 eq.), CH₂Cl₂ (27 mL, 0.5 M), and pyridine (8.33 mL, 8.16 g, 103 mmol, 7.50 eq.) and the solution was cooled to 0 °C. Afterwards, 4-toluenesulfonyl chloride (3.28 g, 17.2 mmol, 1.25 eq.) was added and the mixture was allowed to warm to rt and stirred for 20 h. Subsequently, the reaction was diluted with CH₂Cl₂ and the organic layer was washed with H₂O (2x), an aq. solution of citric acid (10 wt%, 2x), and brine (2x). The organic phase was dried over Na₂SO₄, filtered, and the solvent was removed under reduced pressure. The crude product was purified by column chromatography on silica gel (*n*-pentane/EtOAc 2:1) to obtain pure **182** (4.98 g, 12.8 mmol, 93%) as a colorless oil and mixture of isomers that solidified upon standing.

TLC: R_f = 0.34 (*n*-pentane/EtOAc 2:1).

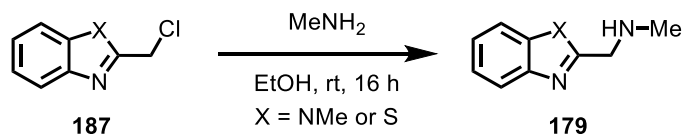
¹H NMR: (300 MHz, CDCl₃) δ = 7.76 (d, J = 7.8 Hz, 1H), 7.70 (d, J = 7.5 Hz, 1H), 7.39-7.24 (m, 7H), 5.12-4.95 (m, 2H), 4.23-3.88 (m, 3H), 3.46-3.30 (m, 2H), 2.42 (s, 3H), 2.00-1.76 (m, 4H) ppm.

¹³C NMR: (75 MHz, CDCl₃) δ = 170.4, 154.9, 154.6, 144.9, 136.7, 136.5, 133.0, 130.0, 128.6, 128.1, 128.0, 127.8, 70.0, 69.8, 67.1, 66.9, 56.3, 55.6, 47.2, 46.9, 28.6, 27.7, 24.0, 23.0, 21.7 ppm.

Experimental Part

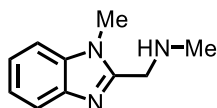
Analytical data were consistent with reported data.^[270]

General Procedure E: Synthesis of Methylamine Building Blocks 179 (GP E)



Following a slightly modified procedure by Butera *et al.*,^[271] the corresponding chloride **187** (1.00 eq.) was added to a stirred solution of MeNH₂ in ethanol (33 wt%, 0.3 M based on chloride) under air. The resulting mixture was stirred for 16 h at rt. Afterwards, water was added, the aq. layer was extracted with CH₂Cl₂ (3x), and the combined organic layers were dried over Na₂SO₄. After filtration, removal of the solvent, and drying under vacuum, the crude products were obtained and used without further purification. Analytical data of compounds **179** are listed below.

N-Methyl-1-(1-methyl-1H-benzo[d]imidazol-2-yl)methanamine (179b)



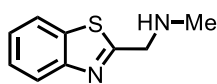
Following **GP E**, benzimidazole **187b** (0.50 g, 2.77 mmol, 1.00 eq.) was employed to furnish amine **186b** (0.48 g, 2.71 mmol, 98%) as a pale-yellow solid.

¹H NMR: (300 MHz, CDCl₃) δ = 7.78-7.72 (m, 1H), 7.37-7.24 (m, 3H), 4.04 (s, 2H), 3.83 (s, 3H), 2.55 (s, 3H), 1.80 (br s, 1H) ppm.

¹³C NMR: (75 MHz, CDCl₃) δ = 153.0, 142.5, 136.2, 122.5, 122.0, 119.6, 109.2, 48.5, 36.6, 29.9 ppm.

Analytical data were consistent with reported data.^[271]

1-(Benzo[d]thiazol-2-yl)-N-methylmethanamine (179c)



Following **GP E**, benzothiazole **187c** (1.00 g, 5.45 mmol, 1.00 eq.) was employed to furnish amine **179c** (0.97 g, 5.41 mmol, 99%) as a yellow solid.

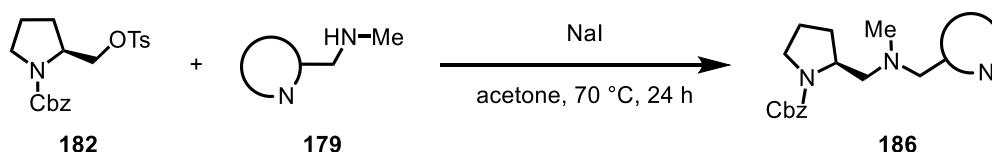
Experimental Part

¹H NMR: (300 MHz, CDCl₃) δ = 7.97 (d, J = 8.0 Hz, 1H), 7.87 (d, J = 7.9 Hz, 1H), 7.45 (t, J = 7.7 Hz, 1H), 7.35 (t, J = 7.8 Hz, 1H), 4.19 (s, 2H), 2.56 (s, 3H), 1.80 (br s, 1H) ppm.

¹³C NMR: (75 MHz, CDCl₃) δ = 173.3, 153.5, 135.2, 126.0, 124.9, 122.8, 121.9, 53.8, 36.5 ppm.

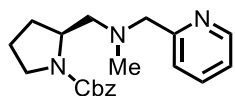
Analytical data were consistent with reported data.^[272]

General Procedure F: Nucleophilic Substitution of OTs (GP F)



Following a slightly modified procedure by Law *et al.*,^[213] a pressure tube was charged with tosylate **182** (1.00 eq.), the corresponding amine **179** (2.00 eq.), and acetone (0.5 M). Afterwards, sodium iodide (2.00 eq.) was added in one portion and the mixture was stirred at 70 °C under inert gas atmosphere for 24 h. After cooling to rt, the suspension was filtered over a short plug of celite, rinsed with acetone (3x), and the filtrate was evaporated under reduced pressure. The crude product was purified by column chromatography on silica gel (*n*-pentane/EtOAc) to obtain pure products as a mixture of isomers. ¹³C-NMR spectra are described phenomenologically and peaks are listed without a distinction.

Benzyl (*S*)-2-((methyl(pyridin-2-ylmethyl)amino)methyl)pyrrolidine-1-carboxylate (**186a**)



Following **GP F**, tosylate **182** (1.00 g, 2.57 mmol, 1.00 eq.), amine **179a** (0.63 mL, 0.63 g, 5.14 mmol, 2.00 eq.), and NaI (0.77 g, 5.14 mmol, 2.00 eq.) were employed to obtain tertiary amine **186a** (0.50 g, 1.47 mmol, 57%) as a brownish oil after column chromatography on silica gel (*n*-pentane/EtOAc 1:1 \rightarrow EtOAc pure).

TLC: R_f = 0.30 (EtOAc).

¹H NMR: (300 MHz, CDCl₃) δ = 8.53 (d, J = 4.3 Hz, 1H), 7.63 (t, J = 7.2 Hz, 1H), 7.44-7.27 (m, 6H), 7.14 (dd, J = 6.5, 5.2 Hz, 1H), 5.15 (d, J = 12.5 Hz, 1H), 5.09 (d, J = 12.4 Hz,

Experimental Part

1H), 4.11-3.90 (m, 1H), 3.85-3.68 (m, 1H), 3.66-3.46 (m, 1H), 3.43-3.28 (m, 2H), 2.70-2.45 (m, 1H), 2.40-2.18 (m, 4H), 1.99-1.65 (m, 4H) ppm.

¹³C NMR: (75 MHz, CDCl₃) δ = 159.6, 155.0, 149.2 (2C), 136.4, 128.5 (2C), 128.2, 128.0, 127.9, 123.2, 122.1, 67.0 and 66.6, 64.8, 60.3, 59.5, 56.3, 55.7, 46.7, 46.4, 43.3, 29.6, 28.8, 23.5, 22.7 ppm.

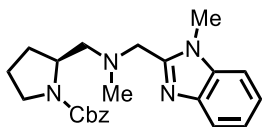
IR: (neat) $\tilde{\nu}$ = 2953 (w), 2879 (w), 2792 (w), 1694 (s), 1588 (w), 1409 (s), 1352 (m), 1274 (w), 1188 (w), 1096 (m), 1037 (w), 991 (w), 911 (w), 871 (w), 819 (w), 756 (s), 697 (m), 607 (w), 563 (w), 464 (w), 405 (w) cm⁻¹.

HRMS: (ESI+) m/z calcd. for C₂₀H₂₆N₃O₂ [M+H]⁺: 340.2020; found: 340.2019.

[α]_D²²: -83.5° (c = 1.0, CH₂Cl₂).

Analytical data were consistent with reported data.^[208]

Benzyl (*S*)-2-((methyl((1-methyl-1H-benzo[*d*]imidazol-2-yl)methyl)amino)methyl)pyrrolidine-1-carboxylate (**186b**)



Following **GP F**, tosylate **182** (0.40 g, 1.03 mmol, 1.00 eq.), amine **179b** (0.36 g, 2.05 mmol, 2.00 eq.), and NaI (0.31 g, 2.05 mmol, 2.00 eq.) were employed to obtain tertiary amine **186b** (0.18 g, 0.46 mmol, 45%) as a dark-yellow oil and a mixture of isomers after column chromatography on silica gel (*n*-pentane/EtOAc 1:1 → EtOAc pure).

TLC: R_f = 0.28 (EtOAc).

¹H NMR: (300 MHz, CDCl₃) δ = 7.72 (d, J = 7.5 Hz, 1H), 7.37-7.21 (m, 8H), 5.16-5.04 (m, 2H), 4.12-3.95 (m, 1H), 3.94-3.62 (m, 5H), 3.42-3.23 (m, 2H), 2.74-2.49 (m, 1H), 2.44-2.25 (m, 3H), 2.24-2.16 (m, 1H), 1.95-1.80 (m, 1H), 1.77-1.59 (m, 3H) ppm.

¹³C NMR: (75 MHz, CDCl₃) δ = 155.1, 152.1, 151.8, 142.3, 137.2, 136.8, 136.4, 128.6, 128.4, 128.2, 128.1, 127.9, 122.7, 122.0, 119.8, 109.2, 67.1, 66.7, 60.4, 59.7, 56.0, 55.5, 46.5, 46.2, 43.1, 43.0, 30.1, 29.8, 29.0, 23.5, 22.6 ppm.

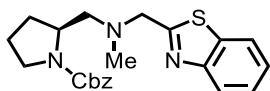
IR: (neat) $\tilde{\nu}$ = 3057 (w), 2950 (w), 2878 (w), 1692 (s), 1451 (m), 1407 (s), 1332 (m), 1284 (w), 1242 (w), 1187 (w), 1098 (m), 1030 (w), 975 (w), 912 (w), 859 (w), 818 (w), 740 (s), 697 (m), 601 (w), 562 (w), 490 (w), 436 (w) cm⁻¹.

Experimental Part

HRMS: (ESI+) m/z calcd. for $C_{23}H_{29}N_4O_2$ $[M+H]^+$: 393.2273; found: 393.2273.

$[\alpha]_D^{22}$: -91.4° ($c = 1.0$, CH_2Cl_2).

Benzyl (S)-2-(((benzo[d]thiazol-2-ylmethyl)(methyl)amino)methyl)pyrrolidine-1-carboxylate (186c)



Following **GP F**, tosylate **182** (0.37 g, 0.95 mmol, 1.00 eq.), amine **179c** (0.34 g, 1.90 mmol, 2.00 eq.), and NaI (0.28 g, 1.90 mmol, 2.00 eq.) were employed to obtain tertiary amine **186c** (0.15 g, 0.38 mmol, 40%) as a pale-yellow viscous oil and a mixture of isomers after column chromatography on silica gel (*n*-pentane/EtOAc 2:1 \rightarrow 1:1).

TLC: $R_f = 0.57$ (EtOAc).

1H NMR: (300 MHz, $CDCl_3$) $\delta = 7.96$ (d, $J = 7.9$ Hz, 1H), 7.86 (d, $J = 7.8$ Hz, 1H), 7.45 (td, $J = 7.6, 1.1$ Hz, 1H), 7.39-7.29 (m, 6H), 5.18-5.07 (m, 2H), 4.14-3.80 (m, 3H), 3.48-3.35 (m, 2H), 2.88-2.62 (m, 1H), 2.52-2.37 (m, 3H), 2.36-2.30 (m, 1H), 2.16-2.07 (m, 2H), 2.05-1.91 (m, 1H), 1.88-1.73 (m, 3H) ppm.

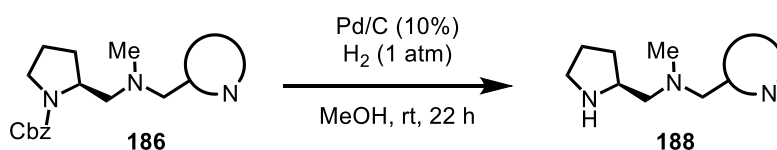
^{13}C NMR: (75 MHz, $CDCl_3$) $\delta = 173.3, 155.1, 153.4, 137.1, 136.7, 135.5, 128.6, 128.6, 128.2, 128.0, 127.9, 125.9, 124.9, 122.9, 121.8, 67.0, 66.8, 60.8, 60.6, 59.8, 56.4, 55.8, 46.8, 46.5, 43.5, 40.8, 30.1, 29.5, 28.6, 24.0, 23.7, 22.8$ ppm.

IR: (neat) $\tilde{\nu} = 3338$ (w), 3063 (w), 2952 (w), 2877 (w), 1694 (s), 1524 (w), 1410 (m), 1350 (m), 1244 (w), 1178 (w), 1102 (m), 1033 (w), 912 (w), 855 (w), 818 (w), 759 (s), 734 (m), 697 (m), 649 (w), 602 (w), 558 (w), 490 (w), 432 (w) cm^{-1} .

HRMS: (ESI+) m/z calcd. for $C_{22}H_{26}N_3O_2S$ $[M+H]^+$: 396.1746; found: 396.1737.

$[\alpha]_D^{22}$: -75.1° ($c = 1.0$, CH_2Cl_2).

General Procedure G: Cbz-Deprotection via Hydrogenation (GP G)

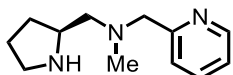


A round-bottom flask was charged with Cbz-protected amine **186** (1.00 eq.), Pd/C (10%, 0.10 eq.), and MeOH (0.1 M). Afterwards, the flask was purged with hydrogen (3x) and the resulting mixture

Experimental Part

was stirred at rt under hydrogen atmosphere (1 atm) for 22 h. Subsequently, the reaction was filtered over a short plug of celite for removal of the catalyst, the solvent was removed under reduced pressure, and the residue was dried under vacuum. The crude product was used without further purification.

(S)-N-Methyl-1-(pyridin-2-yl)-N-(pyrrolidin-2-ylmethyl)methanamine (188a)



Following **GP G**, Cbz-protected amine **186a** (0.22 g, 0.65 mmol, 1.00 eq.) and Pd/C (10 wt%, 69.0 mg, 0.10 eq.) were employed to obtain deprotected amine **188a** (0.13 g, 0.62 mmol, 97%) as a yellow oil.

¹H NMR: (300 MHz, CDCl₃) δ = 8.51 (d, J = 4.2 Hz, 1H), 7.64 (td, J = 7.6, 1.6 Hz, 1H), 7.40 (d, J = 7.8 Hz, 1H), 7.15 (dd, J = 6.7, 5.4 Hz, 1H), 3.75 (d, J = 14.1 Hz, 1H), 3.64 (d, J = 14.2 Hz, 1H), 3.38 (p, J = 6.9 Hz, 1H), 3.08 (br s, 1H, NH), 2.91 (t, J = 6.8 Hz, 2H), 2.43-2.37 (m, 1H), 2.31 (s, 3H), 1.95-1.84 (m, 1H), 1.79-1.68 (m, 2H), 1.45-1.25 (m, 2H) ppm.

¹³C NMR: (75 MHz, CDCl₃) δ = 159.6, 149.1, 136.6, 123.2, 122.1, 64.1, 62.5, 56.2, 45.7, 43.1, 29.6, 25.0 ppm.

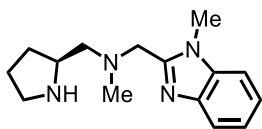
IR: (neat) $\tilde{\nu}$ = 3393 (w), 2937 (m), 2861 (m), 2793 (w), 1633 (w), 1591 (m), 1437 (m), 1329 (m), 1149 (w), 1091 (w), 1036 (m), 995 (w), 860 (w), 760 (s), 615 (m), 529 (w), 473 (w), 404 (w) cm⁻¹.

HRMS: (ESI+) m/z calcd. for C₁₂H₂₀N₃ [M+H]⁺: 206.1652; found: 206.1648.

[α]_D²²: +19.1° (c = 1.0, CH₂Cl₂).

Analytical data were consistent with reported data.^[208]

(S)-N-Methyl-1-(1-methyl-1H-benzo[d]imidazol-2-yl)-N-(pyrrolidin-2-ylmethyl)methanamine (188b)



Following **GP G**, Cbz-protected amine **186b** (0.19 g, 0.48 mmol, 1.00 eq.) and Pd/C (10 wt%, 51.5 mg, 0.10 eq.) were employed to obtain deprotected amine **188b** (0.13 g, 0.48 mmol, 98%) as an off-white solid and as a mixture of isomers as indicated by ^{13}C NMR spectrum. Signals of both isomers are listed.

^1H NMR: (300 MHz, CDCl_3) δ = 7.73-7.65 (m, 1H), 7.35-7.20 (m, 3H), 3.89-3.78 (m, 4H), 3.04 (br s, 1H, NH), 3.00-2.93 (m, 1H), 2.67-2.37 (m, 2H), 2.34 (s, 3H), 2.28-2.07 (m, 2H), 2.01-1.85 (m, 1H), 1.82-1.61 (m, 2H), 1.60-1.45 (m, 1H), 1.38-1.25 (m, 1H) ppm.

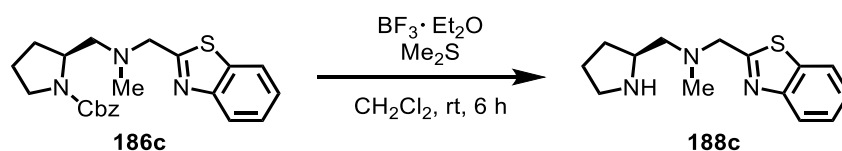
^{13}C NMR: (75 MHz, CDCl_3) δ = 152.1, 152.0, 142.4, 142.1, 136.5, 136.3, 122.7, 122.6, 122.2, 121.9, 109.2, 109.2, 63.8, 62.8, 62.3, 57.8, 56.6, 56.3, 55.5, 45.7, 43.0, 42.9, 41.4, 30.7, 30.3, 30.2, 29.6, 25.0, 22.4 ppm.

IR: (neat) $\tilde{\nu}$ = 3407 (w), 3051 (w), 2943 (w), 2847 (w), 2787 (w), 1687 (w), 1614 (w), 1513 (w), 1451 (m), 1397 (m), 1330 (m), 1286 (w), 1238 (w), 1126 (w), 1092 (w), 1027 (w), 974 (w), 916 (w), 855 (w), 741 (s), 663 (w), 579 (w), 540 (w), 493 (w), 435 (w) cm^{-1} .

HRMS: (ESI+) m/z calcd. for $\text{C}_{15}\text{H}_{23}\text{N}_4$ $[\text{M}+\text{H}]^+$: 259.1917; found: 259.1919.

$[\alpha]_{\text{D}}^{22}$: -9.7° ($c = 1.0$, CH_2Cl_2).

(S)-1-(Benzo[d]thiazol-2-yl)-N-methyl-N-(pyrrolidin-2-ylmethyl)methanamine (188c)



Following a slightly modified procedure by Yotapan *et al.*,^[214] a Schlenk flask was charged with protected amine **186c** (181 mg, 0.46 mmol, 1.00 eq.) and CH_2Cl_2 (0.1 M) under nitrogen atmosphere. Me_2S (2.34 mL, 32.0 mmol, 70 eq.) and $\text{BF}_3 \cdot \text{Et}_2\text{O}$ (0.58 mL, 4.58 mmol, 10 eq.) were added and the resulting mixture was stirred at rt for 3.5 h. Again, Me_2S (0.50 mL, 6.84 mmol, 14.9 eq.) was added and stirred for another 2.5 h. Subsequently, the reaction was quenched with aq. ammonia-solution

Experimental Part

(7%), layers were separated, and the aq. layer was extracted with CH₂Cl₂ (3x). The combined organic layers were dried over Na₂SO₄, filtered, and the solvent was removed under reduced pressure. The crude product was purified by column chromatography on silica gel (CH₂Cl₂/MeOH → CH₂Cl₂/MeOH + 1% conc. NH₃ (aq.)) to afford deprotected amine **188c** (94.0 mg, 0.36 mmol, 79%) as a yellow oil.

TLC: R_f = 0.33 (CH₂Cl₂/MeOH 10:1).

¹H NMR: (300 MHz, CDCl₃) δ = 7.94 (d, *J* = 8.0 Hz, 1H), 7.86 (d, *J* = 7.8 Hz, 1H), 7.45 (t, *J* = 7.6 Hz, 1H), 7.35 (d, *J* = 7.5 Hz, 1H), 4.05 (d, *J* = 15.6 Hz, 1H), 3.98 (d, *J* = 15.6 Hz, 1H), 3.47-3.22 (m, 2H), 3.05-2.91 (m, 2H), 2.60-2.48 (m, 2H), 2.45 (s, 3H), 2.00-1.88 (m, 1H), 1.82-1.70 (m, 2H), 1.45-1.34 (m, 1H) ppm.

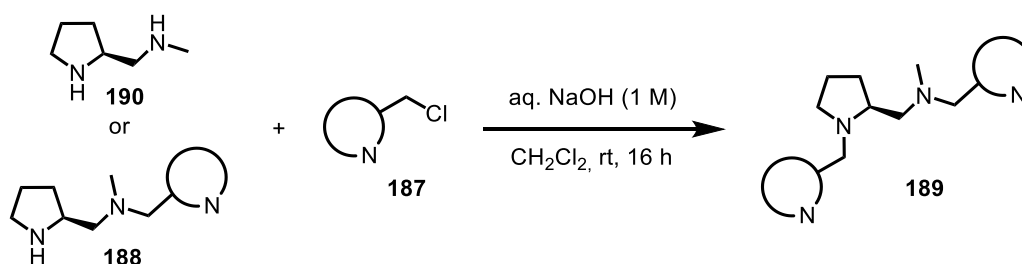
¹³C NMR: (75 MHz, CDCl₃) δ = 173.1, 153.3, 135.4, 126.0, 125.0, 122.8, 121.9, 62.5, 60.4, 56.4, 46.0, 43.4, 29.5, 25.0 ppm.

IR: (neat) $\tilde{\nu}$ = 3207 (w), 2955 (w), 2872 (w), 2799 (w), 1822 (w), 1650 (w), 1517 (w), 1439 (w), 1383 (w), 1347 (w), 1312 (w), 1280 (w), 1036 (s), 915 (w), 850 (w), 763 (m), 729 (m), 652 (w), 579 (w), 519 (w), 432 (w) cm⁻¹.

HRMS: (ESI+) *m/z* calcd. for C₁₄H₂₀N₃S [M+H]⁺: 262.1372; found: 262.1368.

[α]_D²²: -14.5° (*c* = 1.0, CH₂Cl₂).

General Procedure H: Nucleophilic Substitution towards Final Ligands (GP H)

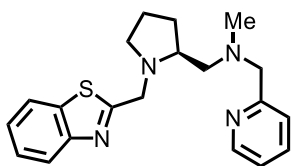


For non-C2-symmetric ligands: Following a slightly modified procedure by Ye *et al.*,^[89] a round bottom flask was charged with **188** (1.00 eq.) and CH₂Cl₂ (0.1 M). To this solution was added chloride **187** (1.10 eq.) and aq. NaOH (1 M, 1.00 eq.), and the mixture was stirred for 16 h under air. Afterwards, aq. NaOH-solution (1 M) and CH₂Cl₂ were added, layers were separated, and the aq. phase was extracted with CH₂Cl₂ (3x). The combined organic layers were dried over Na₂SO₄, filtered, and the solvent was removed under reduced pressure. The crude product was purified by column chromatography on silica gel (CH₂Cl₂/MeOH 30:1 → 10:1 → CH₂Cl₂/MeOH/conc. NH₃ (aq.) 10:1:0.1) to afford pure ligands **189**.

For pseudo-C₂-symmetric ligands (189c, 189e, and 189g): Following a slightly modified procedure by Ye *et al.*,^[89] a round bottom flask was charged with diamine **190** (1.00 eq.) and CH₂Cl₂ (0.1 M). To this solution was added chloride **187** (2.20 eq.) and aq. NaOH (1 M, 2.00 eq.), and the mixture was stirred for 16 h under air. Afterwards, aq. NaOH-solution (1 M) and CH₂Cl₂ were added, layers were separated, and the aq. phase was extracted with CH₂Cl₂ (3x). The combined organic layers were dried over Na₂SO₄, filtered, and the solvent was removed under reduced pressure. The crude product was purified by column chromatography on silica gel (CH₂Cl₂/MeOH 30:1 → 10:1 → CH₂Cl₂/MeOH/conc. NH₃ (aq.) 10:1:0.1) to afford pure ligands **189**.

For nucleophilic substitution reactions with picolyl chloride hydrochloride (**187a**), the equivalents of aq. NaOH-solution (1 M) were doubled accordingly.

(S)-1-(1-(Benzo[d]thiazol-2-ylmethyl)pyrrolidin-2-yl)-N-methyl-N-(pyridin-2-ylmethyl)-methanamine (189a)



Following **GP H**, amine **188a** (106 mg, 0.52 mmol, 1.00 eq.), chloride **187c** (104 mg, 0.57 mmol, 1.10 eq.), and aq. 1 M NaOH-solution (0.52 mL, 0.52 mmol, 1.00 eq.) were employed to obtain pentadentate ligand **189a** (114 mg, 0.32 mmol, 63%) as a yellow oil after column chromatography on silica gel.

TLC: $R_f = 0.33$ (CH₂Cl₂/MeOH 10:1).

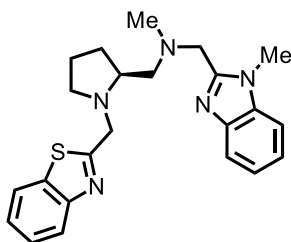
¹H NMR: (300 MHz, CDCl₃) $\delta = 8.49$ (d, $J = 4.2$ Hz, 1H), 7.95 (d, $J = 8.0$ Hz, 1H), 7.83 (d, $J = 7.9$ Hz, 1H), 7.53 (td, $J = 7.7, 1.6$ Hz, 1H), 7.43 (td, $J = 7.5, 1.2$ Hz, 1H), 7.40-7.30 (m, 2H), 7.09 (dd, $J = 6.6, 5.4$ Hz, 1H), 4.69 (d, $J = 15.6$ Hz, 1H), 3.96 (d, $J = 15.6$ Hz, 1H), 3.73 (d, $J = 14.0$ Hz, 1H), 3.67 (d, $J = 14.0$ Hz, 1H), 3.23-3.14 (m, 1H), 2.99-2.89 (m, 1H), 2.72 (dd, $J = 12.6, 5.9$ Hz, 1H), 2.50 (dd, $J = 12.6, 6.1$ Hz, 1H), 2.41 (q, $J = 8.6$ Hz, 1H), 2.30 (s, 3H), 2.06-1.96 (m, 1H), 1.83-1.70 (m, 2H), 1.68-1.56 (m, 1H) ppm.

¹³C NMR: (75 MHz, CDCl₃) $\delta = 174.4, 159.2, 153.5, 149.0, 136.6, 135.5, 125.8, 124.7, 123.3, 122.7, 122.1, 121.8, 64.7, 63.4, 61.7, 57.1, 55.4, 43.4, 30.2, 23.1$ ppm.

Experimental Part

- IR:** (neat) $\tilde{\nu}$ = 3061 (w), 2942 (w), 2797 (w), 1674 (w), 1589 (w), 1520 (w), 1434 (m), 1353 (w), 1312 (w), 1245 (w), 1126 (w), 1035 (w), 861 (w), 759 (s), 731 (m), 618 (w), 505 (w), 432 (w), 403 (w) cm^{-1} .
- HRMS:** (ESI+) m/z calcd. for $\text{C}_{20}\text{H}_{25}\text{N}_4\text{S}$ $[\text{M}+\text{H}]^+$: 353.1794; found: 353.1798.
- $[\alpha]_{\text{D}}^{22}$:** -36.3° ($c = 1.0$, CH_2Cl_2).

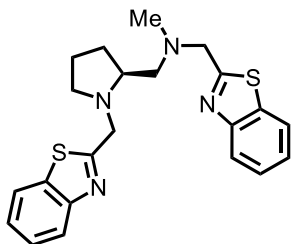
(S)-1-(1-(Benzo[d]thiazol-2-ylmethyl)pyrrolidin-2-yl)-N-methyl-N-((1-methyl-1H-benzo[d]imidazol-2-yl)methyl)methanamine (189b)



Following **GP H**, amine **188b** (62.0 mg, 0.24 mmol, 1.00 eq.), chloride **187c** (48.5 mg, 0.26 mmol, 1.10 eq.), and aq. 1 M NaOH-solution (0.24 mL, 0.24 mmol, 1.00 eq.) were employed to obtain pentadentate ligand **189b** (57.0 mg, 0.14 mmol, 59%) as a dark-yellow oil after column chromatography on silica gel.

- TLC:** $R_f = 0.40$ ($\text{CH}_2\text{Cl}_2/\text{MeOH}$ 10:1).
- $^1\text{H NMR}$:** (300 MHz, CDCl_3) $\delta = 7.93$ (d, $J = 8.1$ Hz, 1H), 7.76 (d, $J = 8.1$ Hz, 1H), 7.74-7.69 (m, 1H), 7.44 (t, $J = 7.9$ Hz, 1H), 7.34 (t, $J = 7.5$ Hz, 1H), 7.25-7.18 (m, 2H), 7.17-7.12 (m, 1H), 4.67 (d, $J = 15.6$ Hz, 1H), 3.93 (d, $J = 15.6$ Hz, 1H), 3.80 (s, 2H), 3.70 (s, 3H), 3.22-3.14 (m, 1H), 2.98-2.87 (m, 1H), 2.79 (dd, $J = 12.6, 6.3$ Hz, 1H), 2.52 (dd, $J = 12.6, 5.6$ Hz, 1H), 2.43-2.34 (m, 1H), 2.31 (s, 3H), 2.04-1.91 (m, 1H), 1.81-1.68 (m, 2H), 1.63-1.51 (m, 1H) ppm.
- $^{13}\text{C NMR}$:** (75 MHz, CDCl_3) $\delta = 174.1, 153.5, 151.7, 142.2, 136.4, 135.4, 125.9, 124.7, 122.7, 122.6, 122.0, 121.9, 119.7, 109.2, 63.3, 61.4, 57.0, 56.5, 55.5, 43.1, 30.1, 30.1, 23.0$ ppm.
- IR:** (neat) $\tilde{\nu}$ = 3418 (w), 3057 (w), 2943 (w), 2800 (w), 1619 (w), 1515 (w), 1446 (m), 1399 (w), 1326 (w), 1239 (w), 1122 (w), 1018 (w), 975 (w), 926 (w), 855 (w), 737 (s), 696 (w), 661 (w), 578 (w), 480 (w), 430 (w) cm^{-1} .
- HRMS:** (ESI+) m/z calcd. for $\text{C}_{23}\text{H}_{28}\text{N}_5\text{S}$ $[\text{M}+\text{H}]^+$: 406.2060; found: 406.2051.
- $[\alpha]_{\text{D}}^{22}$:** -26.7° ($c = 1.0$, CH_2Cl_2).

(S)-1-(Benzo[d]thiazol-2-yl)-N-((1-(benzo[d]thiazol-2-ylmethyl)pyrrolidin-2-yl)methyl)-N-methylmethanamine (189c)



Following **GP H**, diamine **190** (65.0 mg, 0.57 mmol, 1.00 eq.), chloride **187c** (230 mg, 1.20 mmol, 2.20 eq.), and aq. 1 M NaOH-solution (1.14 mL, 1.14 mmol, 2.00 eq.) were employed to obtain pentadentate ligand **189c** (143 mg, 0.35 mmol, 61%) as a yellow oil after column chromatography on silica gel.

TLC: $R_f = 0.66$ (CH₂Cl₂/MeOH 10:1).

¹H NMR: (300 MHz, CDCl₃) $\delta = 7.95$ (t, $J = 7.8$ Hz, 2H), 7.83 (d, $J = 7.8$ Hz, 1H), 7.77 (d, $J = 7.9$ Hz, 1H), 7.48-7.39 (m, 2H), 7.37-7.28 (m, 2H), 4.71 (d, $J = 15.5$ Hz, 1H), 4.08-3.93 (m, 3H), 3.26-3.17 (m, 1H), 3.02-2.91 (m, 1H), 2.80 (dd, $J = 12.6, 5.8$ Hz, 1H), 2.62 (dd, $J = 12.6, 6.0$ Hz, 1H), 2.47-2.37 (m, 1H), 2.41 (s, 3H), 2.11-1.98 (m, 1H), 1.87-1.69 (m, 3H) ppm.

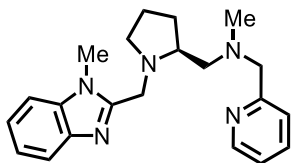
¹³C NMR: (75 MHz, CDCl₃) $\delta = 174.3, 173.1, 153.5, 153.3, 135.6, 135.5, 125.8, 125.8, 124.9, 124.7, 122.8, 122.8, 121.8, 121.8, 63.5, 61.9, 61.0, 57.3, 55.5, 43.7, 30.0, 23.2$ ppm

IR: (neat) $\tilde{\nu} = 3063$ (w), 2993 (w), 2926 (w), 2868 (w), 2795 (m), 1682 (w), 1592 (w), 1522 (m), 1433 (m), 1348 (w), 1313 (w), 1252 (w), 1127 (m), 1065 (w), 1023 (w), 968 (w), 851 (m), 757 (s), 726 (s), 692 (m), 654 (m), 618 (w), 512 (w), 467 (w), 428 (w) cm⁻¹.

HRMS: (ESI+) m/z calcd. for C₂₂H₂₄N₄S₂Na [M+Na]⁺: 431.1335; found: 431.1329.

[α]_D²²: -43.6° ($c = 1.0$, CH₂Cl₂).

(S)-N-Methyl-1-(1-((1-methyl-1*H*-benzo[*d*]imidazol-2-yl)methyl)pyrrolidin-2-yl)-N-(pyridin-2-ylmethyl)methanamine (189d)



Following **GP H**, amine **188a** (72.0 mg, 0.35 mmol, 1.00 eq.), chloride **187b** (69.7 mg, 0.39 mmol, 1.10 eq.), and aq. 1 M NaOH-solution (0.35 mL, 0.35 mmol, 1.00 eq.) were employed to obtain pentadentate ligand **189d** (82.3 mg, 0.24 mmol, 67%) as a yellow oil after column chromatography on silica gel.

TLC: $R_f = 0.31$ ($\text{CH}_2\text{Cl}_2/\text{MeOH}$ 10:1).

^1H NMR: (300 MHz, CDCl_3) $\delta = 8.54$ (d, $J = 4.3$ Hz, 1H), 7.75-7.68 (m, 1H), 7.62 (t, $J = 7.7$, 1.7 Hz, 1H), 7.40 (d, $J = 7.8$ Hz, 1H), 7.34-7.29 (m, 1H), 7.28-7.22 (m, 2H), 7.15 (dd, $J = 7.3$, 5.2 Hz, 1H), 4.59 (d, $J = 13.3$ Hz, 1H), 3.85 (s, 3H), 3.82-3.74 (m, 1H), 3.70 (s, 2H), 2.96-2.81 (m, 2H), 2.66 (dd, $J = 12.7$, 5.7 Hz, 1H), 2.52-2.40 (m, 2H), 2.29 (s, 3H), 2.08-1.99 (m, 1H), 1.76-1.56 (m, 3H) ppm.

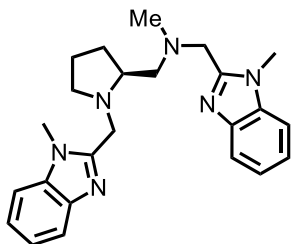
^{13}C NMR: (75 MHz, CDCl_3) $\delta = 159.2$, 152.6, 149.2, 142.4, 136.5, 136.4, 123.2, 122.5, 122.1, 121.9, 119.6, 109.2, 64.6, 63.4, 62.0, 55.2, 52.6, 43.3, 30.2, 30.2, 22.9 ppm.

IR: (neat) $\tilde{\nu} = 3398$ (w), 3056 (w), 2943 (w), 2799 (w), 1665 (w), 1591 (w), 1512 (w), 1468 (m), 1439 (m), 1399 (w), 1327 (m), 1286 (w), 1238 (w), 1123 (w), 1036 (w), 1001 (w), 919 (w), 962 (w), 740 (s), 617 (w), 575 (w), 528 (w), 436 (w), 405 (w) cm^{-1} .

HRMS: (ESI+) m/z calcd. for $\text{C}_{21}\text{H}_{28}\text{N}_5$ $[\text{M}+\text{H}]^+$: 350.2339; found 350.2336.

$[\alpha]_D^{22}$: -10.3° ($c = 1.0$, CH_2Cl_2).

(S)-N-Methyl-1-(1-methyl-1*H*-benzo[*d*]imidazol-2-yl)-N-((1-((1-methyl-1*H*-benzo[*d*]imidazol-2-yl)methyl)pyrrolidin-2-yl)methyl)methanamine (189e)



Following **GP H**, diamine **190** (25.0 mg, 0.22 mmol, 1.00 eq.), chloride **187b** (87.0 mg, 0.48 mmol, 2.20 eq.), and aq. 1 M NaOH-solution (0.44 mL, 0.44 mmol, 2.00 eq.) were employed to obtain pentadentate ligand **189e** (76.1 mg, 0.19 mmol, 85%) as an off-white solid after column chromatography on silica gel.

TLC: $R_f = 0.38$ (CH₂Cl₂/MeOH 10:1).

¹H NMR: (300 MHz, CDCl₃) $\delta = 7.77$ -7.71 (m, 1H), 7.71-7.65 (m, 1H), 7.31-7.20 (m, 6H), 4.37 (d, $J = 13.5$ Hz, 1H), 3.85-3.74 (m, 5H), 3.74-3.60 (m, 4H), 2.92 (br s, 2H), 2.67-2.56 (m, 1H), 2.54-2.38 (m, 2H), 2.31 (s, 3H), 2.11-1.99 (m, 1H), 1.79-1.60 (m, 2H), 1.59-1.47 (m, 1H) ppm.

¹³C NMR: (75 MHz, CDCl₃) $\delta = 151.8$, 151.6, 142.2, 142.1, 136.3, 136.2, 122.8, 122.6, 122.1, 122.0, 119.7, 119.6, 109.3, 109.2, 62.7, 62.3, 55.8, 54.9, 52.3, 43.4, 30.3, 30.1, 30.1, 22.9 ppm.

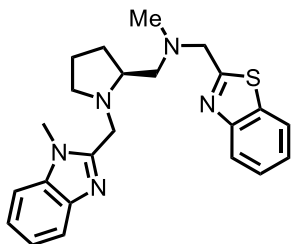
IR: (neat) $\tilde{\nu} = 3416$ (w), 3050 (w), 2948 (w), 2808 (w), 2133 (w), 1984 (w), 1614 (w), 1513 (w), 1463 (m), 1398 (w), 1327 (w), 1286 (w), 1236 (w), 1119 (w), 1021 (w), 923 (w), 855 (w), 738 (s), 575 (w), 433 (w) cm⁻¹.

HRMS: (ESI⁺) m/z calcd. for C₂₄H₃₁N₆ [M+H]⁺: 403.2616; found 403.2601.

[α]_D²²: -42.5° ($c = 1.0$, CH₂Cl₂).

Analytical data were consistent with reported data.^[209]

(S)-1-(Benzo[d]thiazol-2-yl)-N-methyl-N-((1-((1-methyl-1*H*-benzo[d]imidazol-2-yl)methyl)pyrrolidin-2-yl)methyl)methanamine (189f)



Following **GP H**, amine **188c** (50.0 mg, 0.19 mmol, 1.00 eq.), chloride **187b** (38.0 mg, 0.21 mmol, 1.10 eq.), and aq. 1 M NaOH-solution (0.19 mL, 0.19 mmol, 1.00 eq.) were employed to obtain pentadentate ligand **189f** (48.6 mg, 0.12 mmol, 63%) as a dark-yellow oil after column chromatography on silica gel.

TLC: $R_f = 0.40$ (CH₂Cl₂/MeOH 10:1).

¹H NMR: (300 MHz, CDCl₃) $\delta = 7.95$ (d, $J = 8.0$ Hz, 1H), 7.82 (d, $J = 7.9$ Hz, 1H), 7.76-7.70 (m, 1H), 7.44 (td, $J = 7.5, 1.2$ Hz, 1H), 7.38-7.28 (m, 2H), 7.27-7.20 (m, 2H), 4.58 (d, $J = 13.2$ Hz, 1H), 3.99 (d, $J = 15.6$ Hz, 1H), 3.93 (d, $J = 15.4$ Hz, 1H), 3.87 (s, 3H), 3.78 (d, $J = 13.2$ Hz, 1H), 2.91-2.81 (m, 2H), 2.66 (dd, $J = 12.3, 6.0$ Hz, 1H), 2.53 (dd, $J = 12.2, 6.4$ Hz, 1H), 2.48-2.40 (m, 1H), 2.37 (s, 3H), 2.13-1.98 (m, 1H), 1.78-1.62 (m, 3H) ppm.

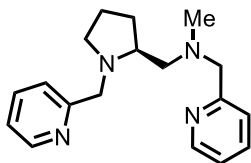
¹³C NMR: (75 MHz, CDCl₃) $\delta = 172.8, 153.3, 152.8, 142.3, 136.4, 135.4, 126.0, 125.0, 122.9, 122.5, 121.9, 121.9, 119.7, 109.2, 63.7, 62.0, 60.8, 55.3, 52.9, 43.6, 30.2, 30.2, 22.9$ ppm.

IR: (neat) $\tilde{\nu} = 3058$ (w), 2936 (w), 2803 (w), 2203 (w), 1676 (w), 1618 (w), 1517 (w), 1440 (m), 1440 (w), 1399 (w), 1327 (w), 1285 (w), 1238 (w), 1120 (w), 1032 (w), 913 (w), 854 (w), 731 (s), 647 (w), 576 (w), 527 (w), 433 (w) cm⁻¹.

HRMS: (ESI+) m/z calcd. for C₂₃H₂₈N₅S [M+H]⁺: 406.2060; found 406.2057.

[α]_D²²: -17.5° ($c = 1.0$, CH₂Cl₂).

(S)-N-Methyl-1-(pyridin-2-yl)-N-((1-(pyridin-2-ylmethyl)pyrrolidin-2-yl)methyl)methanamine (189g)



Following **GP H**, diamine **190** (50.0 mg, 0.44 mmol, 1.00 eq.), chloride **187a** (158.0 mg, 0.96 mmol, 2.20 eq.), and aq. 1 M NaOH-solution (1.84 mL, 1.84 mmol, 4.00 eq.) were employed to obtain pentadentate ligand **189g** (98.6 mg, 0.33 mmol, 76%) as a brown oil after column chromatography on silica gel.

TLC: $R_f = 0.27$ (CH₂Cl₂/MeOH 10:1).

¹H NMR: (300 MHz, CDCl₃) $\delta = 8.54$ -8.45 (m, 2H), 7.65-7.54 (m, 2H), 7.39 (t, $J = 8.0$ Hz, 2H), 7.14-7.07 (m, 2H), 4.32 (d, $J = 13.8$ Hz, 1H), 3.68 (d, $J = 14.1$ Hz, 1H), 3.61 (d, $J = 14.1$ Hz, 1H), 3.53 (d, $J = 13.7$ Hz, 1H), 3.01-2.91 (m, 1H), 2.85-2.73 (m, 1H), 2.60 (dd, $J = 12.4, 4.7$ Hz, 1H), 2.42 (dd, $J = 12.4, 7.5$ Hz, 1H), 2.31-2.21 (m, 4H), 2.10-1.94 (m, 1H), 1.75-1.56 (m, 3H) ppm.

¹³C NMR: (75 MHz, CDCl₃) $\delta = 159.9, 159.8, 149.1, 149.0, 136.4$ (2C), 123.2, 123.2, 122.0, 121.9, 64.8, 63.0, 62.3, 61.4, 55.0, 43.5, 30.2, 22.9 ppm.

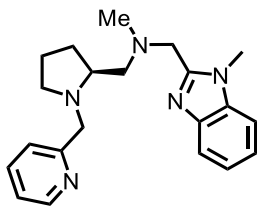
IR: (neat) $\tilde{\nu} = 3398$ (w), 3057 (w), 2949 (w), 2797 (w), 1662 (w), 1590 (m), 1469 (m), 1434 (m), 1361 (w), 1254 (w), 1145 (w), 1090 (w), 1039 (w), 995 (w), 856 (w), 759 (s), 616 (m), 468 (w), 404 (w) cm⁻¹.

HRMS: (ESI+) m/z calcd. for C₁₈H₂₅N₄ [M+H]⁺: 297.2074, found 297.2075.

[α]_D²²: -35.3° ($c = 1.0$, CH₂Cl₂).

Analytical data were consistent with reported data.^[210]

(S)-N-Methyl-1-(1-methyl-1H-benzo[d]imidazol-2-yl)-N-((1-(pyridin-2-ylmethyl)pyrrolidin-2-yl)methyl)methanamine (189h)



Following **GP H**, amine **188b** (40.0 mg, 0.16 mmol, 1.00 eq.), chloride **187a** (27.9 mg, 0.17 mmol, 1.10 eq.), and aq. 1 M NaOH-solution (0.31 mL, 0.31 mmol, 2.00 eq.) were employed to obtain pentadentate ligand **189h** (43.3 mg, 0.12 mmol, 80%) as an off-white solid after column chromatography on silica gel.

TLC: $R_f = 0.31$ (CH₂Cl₂/MeOH 10:1).

¹H NMR: (300 MHz, CDCl₃) $\delta = 8.50$ (d, $J = 4.7$ Hz, 1H), 7.72-7.67 (m, 1H), 7.58 (t, $J = 7.5$ Hz, 1H), 7.36 (d, $J = 7.6$ Hz, 1H), 7.30-7.20 (m, 3H), 7.16-7.11 (m, 1H), 4.37 (d, $J = 13.8$ Hz, 1H), 3.89-3.64 (m, 3H), 3.79 (s, 3H), 3.07 (bs, 2H), 2.83-2.69 (m, 1H), 2.50 (dd, $J = 12.1, 6.5$ Hz, 1H), 2.45-2.34 (m, 1H), 2.29 (s, 3H), 2.12-1.96 (m, 1H), 1.81-1.67 (m, 2H), 1.65-1.53 (m, 1H) ppm.

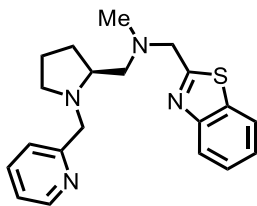
¹³C NMR: (75 MHz, CDCl₃) $\delta = 152.0, 149.1$ (2C), 142.1, 136.6, 136.3, 123.4, 122.6, 122.2, 122.0, 119.6, 109.2, 62.4 (2C), 61.1, 56.1, 54.8, 42.9, 30.2, 29.9, 22.9 ppm.

IR: (neat) $\tilde{\nu} = 2951$ (w), 2801 (w), 2764 (w), 1663 (w), 1589 (w), 1516 (w), 1470 (m), 1440 (m), 1395 (w), 1329 (m), 1238 (w), 1203 (w), 1129 (w), 1028 (m), 973 (w), 926 (w), 852 (m), 745 (s), 651 (w), 617 (w), 581 (w), 548 (w), 471 (w), 434 (w), 403 (w) cm⁻¹.

HRMS: (ESI+) m/z calcd. for C₂₁H₂₈N₅ [M+H]⁺: 350.2339, found 350.2331.

[α]_D²²: -59.2° ($c = 1.0$, CH₂Cl₂).

(S)-1-(Benzo[d]thiazol-2-yl)-N-methyl-N-((1-(pyridin-2-ylmethyl)pyrrolidin-2-yl)methyl)-methanamine (189i)



Following **GP H**, amine **188c** (88.0 mg, 0.34 mmol, 1.00 eq.), chloride **187a** (60.7 mg, 0.37 mmol, 1.10 eq.), and aq. 1 M NaOH-solution (0.34 mL, 0.34 mmol, 2.00 eq.) were employed to obtain pentadentate ligand **189i** (53.2 mg, 0.15 mmol, 45%) as a dark-yellow oil after column chromatography on silica gel.

TLC: $R_f = 0.32$ (CH₂Cl₂/MeOH 10:1).

¹H NMR: (300 MHz, CDCl₃) $\delta = 8.53$ (d, $J = 4.54$ Hz, 1H), 7.94 (d, $J = 8.1$ Hz, 1H), 7.83 (d, $J = 7.8$ Hz, 1H), 7.64 (t, $J = 7.8$ Hz, 1H), 7.49 (d, $J = 7.5$ Hz, 1H), 7.43 (t, $J = 7.5$ Hz, 1H), 7.34 (t, $J = 7.6$ Hz, 1H), 7.20-7.13 (m, 1H), 4.42 (d, $J = 13.6$ Hz, 1H), 4.01 (s, 2H), 3.90-3.70 (bs, 1H), 3.25-3.00 (bs, 2H), 2.95-2.75 (bs, 1H), 2.68-2.57 (m, 1H), 2.55-2.43 (bs, 1H), 2.38 (s, 3H), 2.15-2.02 (m, 1H), 1.90-1.73 (m, 3H) ppm.

¹³C NMR: (75 MHz, CDCl₃) $\delta = 173.0, 157.3, 153.3, 149.3, 136.7, 135.5, 125.9, 124.9, 123.9, 122.9, 122.5, 121.8, 62.8, 62.2, 60.9, 60.7, 54.9, 43.5, 29.8, 22.9$ ppm.

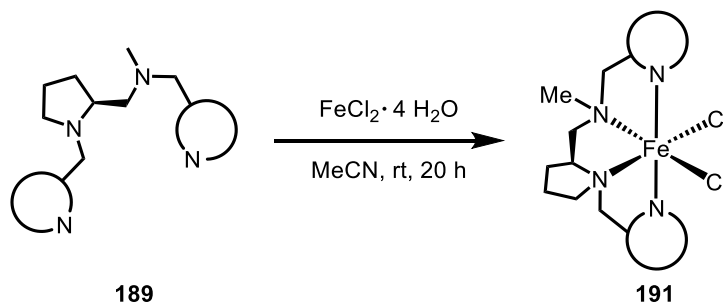
IR: (neat) $\tilde{\nu} = 3415$ (w), 3060 (w), 2947 (w), 2798 (w), 1590 (w), 1519 (w), 1439 (m), 1345 (w), 1120 (w), 1034 (w), 848 (w), 757 (s), 644 (w), 471 (w), 426 (w) cm⁻¹.

HRMS: (ESI+) m/z calcd. for C₂₀H₂₅N₄S [M+H]⁺: 353.1805, found 353.1790.

[α]_D²²: -33.9° ($c = 1.0$, CH₂Cl₂).

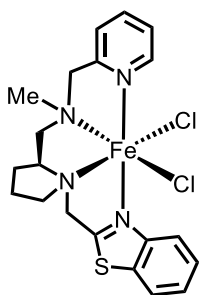
5.4.2 Synthesis of Complexes with Tetradentate Ligand Scaffold 189

General Procedure I: Synthesis of Fe(II) Complexes Comprising Tetradentate Ligands 189



Following a slightly modified procedure by Wang *et al.*,^[92] a flame-dried Schlenk flask was charged with tetradentate ligand **189** (1.05 eq.) and MeCN (0.1 M) under inert gas atmosphere. To this solution was added $\text{FeCl}_2 \cdot 4 \text{H}_2\text{O}$ (1.00 eq.) upon which precipitation of a fine solid occurred. The reaction was then stirred for 20 h at room temperature. Afterwards, Et_2O was added and further stirred for 90 min to achieve full precipitation of the complex. Stirring was stopped and the supernatant clear solution was carefully decanted. The precipitate was washed with Et_2O and again the supernatant solution was decanted. This process was repeated for a total of three times to remove any residual ligand. The solid was then suspended in Et_2O , transferred to another flask, and after removal of the solvent under reduced pressure, complexes **191** were dried under vacuum.

Complex 191a



Following **GP I**, ligand **189a** (99.6 mg, 0.28 mmol, 1.05 eq.) and $\text{FeCl}_2 \cdot 4 \text{H}_2\text{O}$ (53.5 mg, 0.27 mmol, 1.00 eq.) were employed to obtain complex **191a** (127 mg, 0.27 mmol, 98%) as a bright yellow solid.

CHNS: calcd. for $\text{C}_{20}\text{H}_{24}\text{FeN}_4\text{SCl}_2$: C, 50.12; H, 5.05; N, 11.69; S, 6.69; found: C, 49.96; H, 5.29; N, 11.44; S, 6.29.

IR: (neat) $\tilde{\nu}$ = 2170 (w), 2152 (w), 2042 (w), 1970 (w), 1602 (w), 1510 (w), 1439 (w), 1304 (w), 1142 (w), 1046 (m), 1017 (w), 985 (w), 885 (w), 765 (s), 731 (w), 510 (w),

Experimental Part

463 (w), 428 (w) cm^{-1} .

HRMS: (APCI+) m/z calcd. for $\text{C}_{20}\text{H}_{24}\text{FeN}_4\text{SCl} [\text{M}-\text{Cl}]^+$: 443.0755; found: 443.0753.

^1H NMR (500 MHz, CD_3CN): δ = 154.52, 99.36, 98.79, 77.56, 63.22, 56.18, 50.33, 30.18, 27.24, 21.42, 15.79, 13.28, 11.36, 10.97, 7.93, -1.13, -10.90, -12.66, -14.10, -19.58, -22.85 ppm.

Paramagnetic ^1H NMR measurement of complex **4a**

General Information. For the NMR measurements, about 5 mg of the complex were dissolved in 0.6 mL of CD_3CN . Experiments were performed on a Bruker AVIII HD 500 MHz spectrometer equipped with a 5 mm TXI probe with z-gradient. Paramagnetic ^1H NMR spectra were recorded with an optimized spectral width of 300 ppm, 128,000 data points, and 2048 transients. The relaxation delay was 0.5 s which resulted in an experimental time of 30 min per spectrum.

Results. The paramagnetic ^1H NMR spectra are shown in Figure 42. A rather strong temperature dependency of the chemical shift can be observed. The presence of only a single set of neat paramagnetic ^1H NMR signals verified a pure topological isomer of the complex in solution.

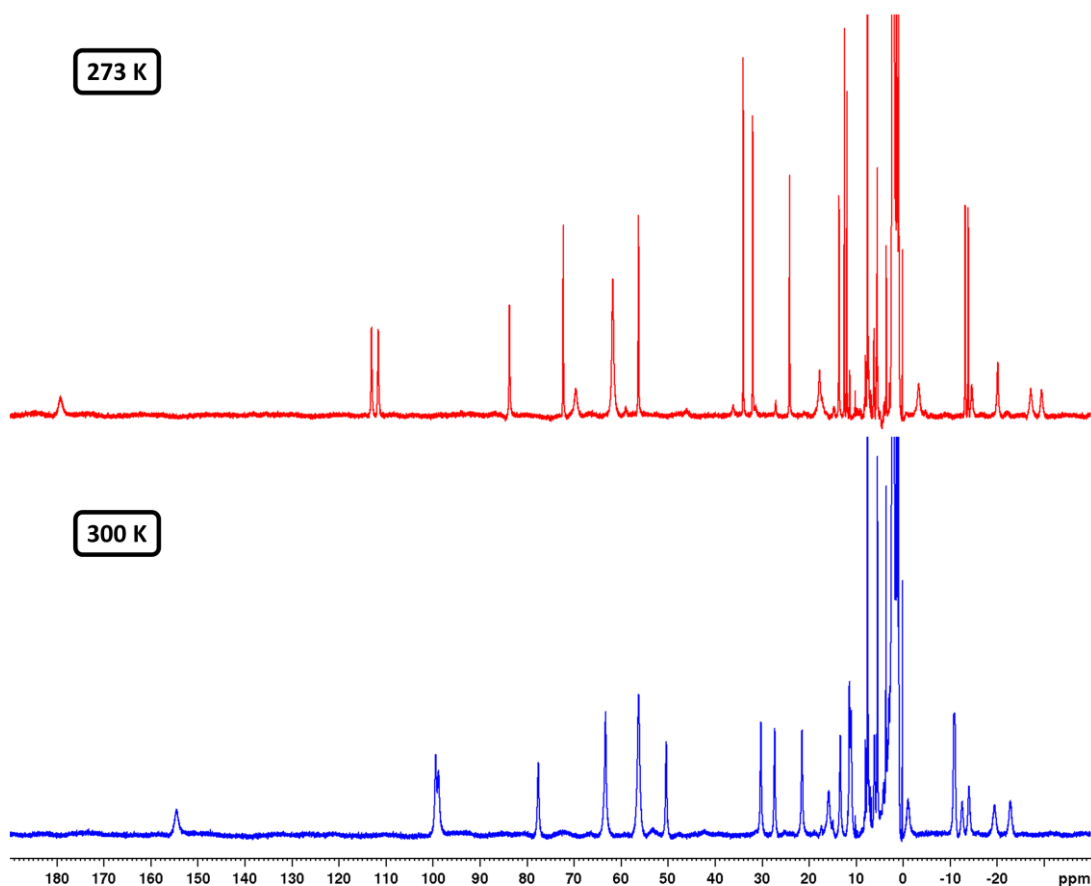
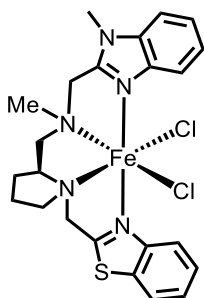


Figure 42: Paramagnetic ^1H NMR spectra of complex **191a** in CD_3CN at 273 and 300 K.

Complex 191b



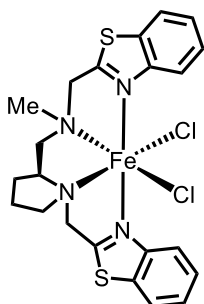
Following **GP I**, ligand **189b** (59.8 mg, 0.15 mmol, 1.05 eq.) and $\text{FeCl}_2 \cdot 4 \text{H}_2\text{O}$ (27.9 mg, 0.14 mmol, 1.00 eq.) were employed to obtain complex **191b** (69.7 mg, 0.13 mmol, 93%) as a dark-yellow solid.

CHNS: calcd. for $\text{C}_{23}\text{H}_{27}\text{FeN}_5\text{SCl}_2 \cdot \text{H}_2\text{O}$: C, 50.20; H, 5.31; N, 12.73; S, 5.83 found: C, 50.62; H, 5.01; N, 4.98; S, 5.75.

IR: (neat) $\tilde{\nu} = 3673$ (w), 2965 (w), 2213 (w), 2164 (w), 2093 (w), 2052 (w), 1995 (w), 1961 (w), 1621 (w), 1493 (m), 1456 (m), 1326 (w), 1292 (w), 1263 (w), 1142 (w), 1048 (w), 1015 (m), 986 (m), 888 (w), 830 (m), 758 (s), 699 (w), 618 (w), 562 (w), 527 (w), 482 (w), 432 (w) cm^{-1} .

HRMS: (ESI+) m/z calcd. for $\text{C}_{23}\text{H}_{27}\text{ClFeN}_5\text{S} [\text{M}-\text{Cl}]^+$: 496.1020; found: 496.1015.

Complex 191c



Following **GP I**, ligand **189c** (49.4 mg, 0.12 mmol, 1.05 eq.) and $\text{FeCl}_2 \cdot 4 \text{H}_2\text{O}$ (22.9 mg, 0.12 mmol, 1.00 eq.) were employed to obtain complex **191c** (57.8 mg, 0.11 mmol, 94%) as a yellow solid.

CHNS: calcd. for $\text{C}_{22}\text{H}_{24}\text{FeN}_4\text{S}_2\text{Cl}_2 \cdot \text{H}_2\text{O}$: C, 47.75; H, 4.74; N, 10.13; S, 11.59; found: C, 47.89; H, 4.51; N, 10.27; S, 11.24.

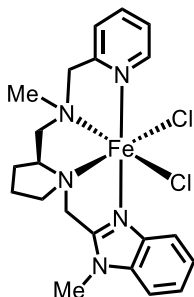
IR: (neat) $\tilde{\nu} = 2107$ (w), 2064 (w), 2000 (w), 1498 (w), 1431 (w), 1141 (w), 1062 (w),

Experimental Part

1011 (w), 980 (w), 880 (w), 776 (s), 735 (w), 669 (w), 569 (w), 483 (w), 433 (m) cm^{-1} .

HRMS: (ESI+) m/z calcd. for $\text{C}_{22}\text{H}_{24}\text{ClFeN}_4\text{S}_2$ $[\text{M}-\text{Cl}]^+$: 499.0475; found: 499.0468.

Complex 191d



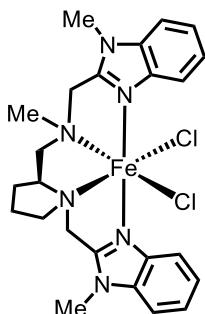
Following **GP I**, ligand **189d** (36.7 mg, 0.11 mmol, 1.05 eq.) and $\text{FeCl}_2 \cdot 4 \text{H}_2\text{O}$ (19.9 mg, 0.10 mmol, 1.00 eq.) were employed to obtain complex **191d** (43.9 mg, 0.09 mmol, 92%) as a dark-yellow solid.

CHN: calcd. for $\text{C}_{21}\text{H}_{27}\text{Cl}_2\text{FeN}_5 \cdot 4 \text{H}_2\text{O}$: C, 46.00; H, 6.43; N, 12.77; found: C, 45.53; H, 6.08; N, 12.54.

IR: (neat) $\tilde{\nu} = 3412$ (w), 2927 (w), 1608 (w), 1454 (m), 1330 (w), 1294 (w), 1155 (w), 1053 (w), 1016 (w), 933 (w), 842 (m), 753 (s), 691 (w), 644 (w), 472 (w), 427 (w) cm^{-1} .

HRMS: (ESI+) m/z calcd. for $\text{C}_{21}\text{H}_{27}\text{ClFeN}_5$ $[\text{M}-\text{Cl}]^+$: 440.1299; found: 440.1302.

Complex 191e



Following **GP I**, ligand **189e** (47.6 mg, 0.12 mmol, 1.05 eq.) and $\text{FeCl}_2 \cdot 4 \text{H}_2\text{O}$ (22.4 mg, 0.11 mmol, 1.00 eq.) were employed to obtain complex **191e** (57.0 mg, 0.11 mmol, 96%) as a dark-yellow solid.

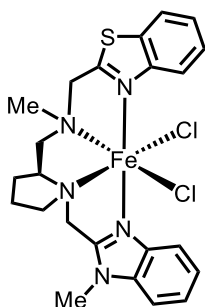
Experimental Part

CHN: calcd. for $C_{24}H_{30}Cl_2FeN_6 \cdot 2 H_2O$: C, 50.99; H, 6.06; N, 14.87; found: C, 50.70; H, 5.97; N, 14.48.

IR: (neat) $\tilde{\nu} = 2957$ (w), 1616 (w), 1493 (w), 1455 (m), 1330 (w), 1292 (w), 1259 (w), 1076 (w), 1015 (w), 932 (w), 824 (m), 751 (s), 692 (w), 611 (w), 525 (w), 481 (w), 430 (m) cm^{-1} .

HRMS: (ESI+) m/z calc. for $C_{24}H_{30}ClFeN_6 [M-Cl]^+$: 493.1565; found: 493.1560.

Complex 191f



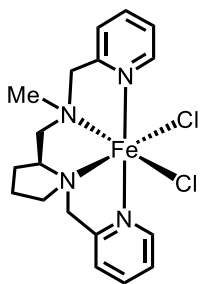
Following **GP I**, ligand **189f** (42.8 mg, 0.11 mmol, 1.05 eq.) and $FeCl_2 \cdot 4 H_2O$ (20.0 mg, 0.10 mmol, 1.00 eq.) were employed to obtain complex **191f** (52.2 mg, 0.10 mmol, 97%) as a yellow solid.

CHN: calcd. for $C_{23}H_{27}Cl_2FeN_5S \cdot 2 H_2O$: C, 48.61; H, 5.50; N, 12.32; found: C, 48.20; H, 5.77; N, 11.99.

IR: (neat) $\tilde{\nu} = 2922$ (w), 2099 (w), 2036 (w), 1495 (w), 1455 (m), 1326 (w), 1263 (w), 1130 (w), 1072 (w), 1015 (m), 983 (w), 882 (w), 756 (s), 688 (w), 560 (w), 482 (w), 435 (m) cm^{-1} .

HRMS: (ESI+) m/z calc. for $C_{23}H_{27}ClFeN_5S_1 [M-Cl]^+$: 496.1020; found: 496.1015.

Complex 191g



Following **GP I**, ligand **189g** (45.7 mg, 0.15 mmol, 1.05 eq.) and $FeCl_2 \cdot 4 H_2O$ (29.2 mg,

Experimental Part

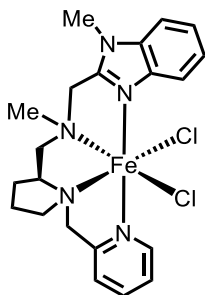
0.15 mmol, 1.00 eq.) were employed to obtain complex **191g** (57.4 mg, 0.14 mmol, 92%) as a bright yellow solid.

CHN: calcd. for $C_{18}H_{24}Cl_2FeN_4 \cdot 2 H_2O$: C, 47.08; H, 6.15; N, 12.20; found: C, 46.70; H, 5.76; N, 12.34.

IR: (neat) $\tilde{\nu} = 2961$ (w), 2234 (w), 2187 (w), 2140 (w), 2034 (w), 1970 (w), 1933 (w), 1650 (w), 1601 (w), 1567 (w), 1473 (w), 1438 (m), 1376 (w), 1345 (w), 1299 (w), 1262 (w), 1048 (w), 1017 (m), 985 (w), 927 (w), 878 (w), 851 (w), 778 (s), 733 (w), 638 (w), 576 (w), 537 (w), 484 (w), 418 (w) cm^{-1} .

HRMS: (ESI+) m/z calc. for $C_{18}H_{24}ClFeN_4 [M-Cl]^+$: 387.1034; found: 387.1028.

Complex 191h



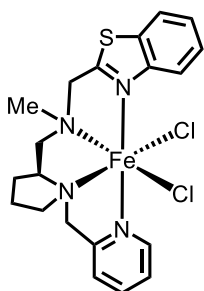
Following **GP I**, ligand **189h** (43.6 mg, 0.13 mmol, 1.05 eq.) and $FeCl_2 \cdot 4 H_2O$ (23.6 mg, 0.12 mmol, 1.00 eq.) were employed to obtain complex **191h** (53.0 mg, 0.11 mmol, 94%) as a yellow solid.

CHN: calcd. for $C_{21}H_{27}Cl_2FeN_5 \cdot 2 H_2O$: C, 49.24; H, 6.10; N, 13.67; found: C, 48.82; H, 5.68; N, 13.28.

IR: (neat) $\tilde{\nu} = 2958$ (w), 2278 (w), 2189 (w), 2119 (w), 1993 (w), 1903 (w), 1608 (w), 1489 (w), 1453 (m), 1330 (w), 1295 (w), 1260 (w), 1051 (w), 1017 (m), 985 (w), 932 (w), 888 (w), 841 (s), 800 (m), 757 (s), 698 (w), 644 (w), 613 (w), 568 (w), 530 (w), 484 (w), 423 (w) cm^{-1} .

HRMS: (ESI+) m/z calc. for $C_{21}H_{27}ClFeN_5 [M-Cl]^+$: 440.1299; found: 440.1293.

Complex 191i



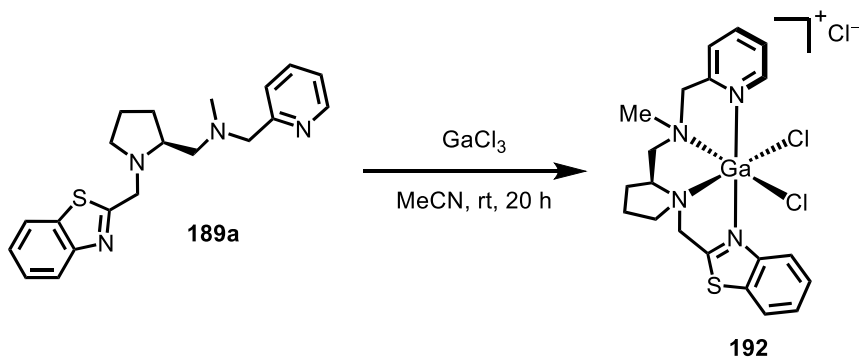
Following **GP I**, ligand **189i** (37.2 mg, 0.11 mmol, 1.05 eq.) and $\text{FeCl}_2 \cdot 4 \text{H}_2\text{O}$ (20.0 mg, 0.10 mmol, 1.00 eq.) were employed to obtain complex **191i** (47.7 mg, 0.10 mmol, 99%) as a yellow solid.

CHN: calcd. for $\text{C}_{20}\text{H}_{24}\text{Cl}_2\text{FeN}_4\text{S} \cdot 3 \text{H}_2\text{O}$: C, 45.04; H, 5.67; N, 10.51; found: C, 45.49; H, 5.22; N, 10.88.

IR: (neat) $\tilde{\nu} = 3058$ (w), 2960 (w), 2924 (w), 1603 (w), 1441 (m), 1375 (w), 1306 (w), 1261 (m), 1049 (m), 1015 (s), 851 (m), 799 (s), 765 (s), 727 (w), 638 (w), 574 (w), 482 (w), 430 (w) cm^{-1} .

HRMS: (ESI+) m/z calc. for $\text{C}_{20}\text{H}_{24}\text{ClFeN}_4\text{S}_1$ $[\text{M}-\text{Cl}]^+$: 443.0755; found: 443.0750.

Synthesis of Ga(III) Complex 192



Following **GP I**, ligand **189a** (37.0 mg, 0.11 mmol, 1.05 eq.) and GaCl_3 (17.6 mg, 0.10 mmol, 1.0 eq.) were employed to obtain Ga-complex **192** (51.0 mg, 0.10 mmol, 97%) as a pale-yellow solid.

^1H NMR: (300 MHz, CD_3CN) $\delta = 9.33$ (d, $J = 5.4$ Hz, 1H), 9.24 (d, $J = 8.3$ Hz, 1H), 8.24 (td, $J = 7.7, 1.5$ Hz, 1H), 8.12 (dd, $J = 7.9, 1.2$ Hz, 1H), 7.79-7.61 (m, 4H), 4.81 (d, $J = 17.4$ Hz, 1H), 4.80 (d, $J = 15.6$ Hz, 1H), 4.68 (d, $J = 17.3$ Hz, 1H), 4.23 (d, $J = 16.1$ Hz, 1H), 3.53-3.40 (m, 1H), 3.31 (dd, $J = 12.8, 7.7$ Hz, 1H), 2.74-2.68 (m,

Experimental Part

4H), 2.67-2.62 (m, 1H), 2.45 (t, $J = 13.4$ Hz, 1H), 2.32-2.09 (m, 3H), 2.08-1.98 (m, 1H), 1.91-1.79 (m, 1H), 1.46-1.34 (m, 1H) ppm.

^{13}C NMR: (75 MHz, CD_3CN) $\delta = 174.6, 152.8, 148.0, 147.8, 143.6, 134.7, 128.7, 128.1, 126.6, 126.5, 124.1, 124.1, 61.8, 60.2, 57.9, 56.3, 54.5, 43.7, 25.4, 22.3$ ppm.

IR: (neat) $\tilde{\nu} = 2243$ (w), 2197 (w), 2163 (w), 2118 (w), 2074 (w), 2027 (w), 1995 (w), 1951 (w), 1610 (w), 1455 (w), 1301 (w), 1263 (w), 1160 (w), 1102 (w), 1016 (w), 941 (w), 890 (w), 798 (m), 763 (s), 727 (m), 647 (m), 577 (m), 517 (m), 477 (s), 422 (s) cm^{-1} .

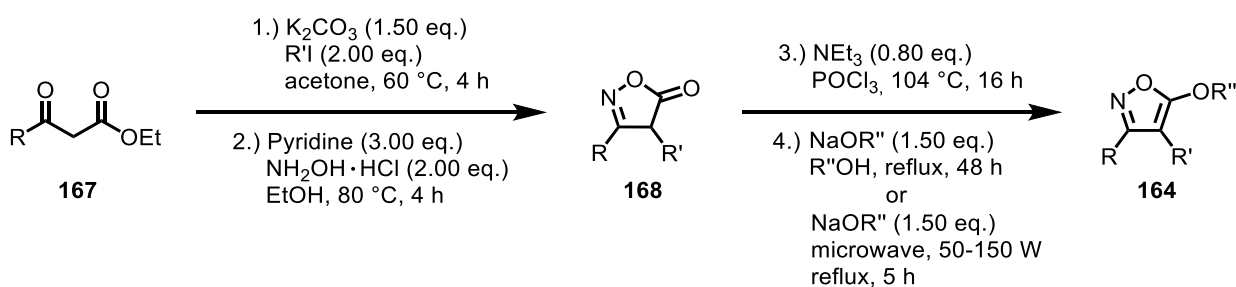
HRMS: (ESI+) m/z calcd. for $\text{C}_{20}\text{H}_{24}\text{Cl}_2\text{GaN}_4\text{S}$ $[\text{M}-\text{Cl}]^+$: 493.0331; found: 493.0322.

5.5 Asymmetric Ring Contraction of Isoxazoles towards Chiral 2*H*-Azirines

5.5.1 Synthesis of Substrates and Analytical Data

Substrates **164** for the asymmetric ring contraction were synthesized according to reported procedures. The general synthetic access towards isoxazoles **164** is depicted in Scheme 73 and described below. The identification numbers for the substrates are in accordance with section 3.3.2.

General Procedure J: Synthetic Pathway towards Isoxazole Substrates 164 (GP J)



Scheme 73: Synthesis of isoxazoles **164** for asymmetric ring contraction reaction.

Step 1: A round-bottom flask was charged with β -ketoester **167** (1.00 eq.), K_2CO_3 (1.50 eq.), $\text{R}'\text{I}$ (2.00 eq.), and acetone (0.9 M). The reaction was then stirred and refluxed under air for 4 h. After cooling to rt, the mixture was filtered over a short plug of Celite and concentrated under vacuum. The crude product was used without further purification.

Step 2: To a round-bottom flask were added crude alkylated β -ketoester (1.00 eq.), $\text{NH}_2\text{OH} \cdot \text{HCl}$ (1.50 eq.), pyridine (1.50 eq.), and ethanol (1.0 M). The mixture was then refluxed under air for 4 h and subsequently stirred for 16 h at rt. Afterwards, the mixture was cooled to rt, filtered over a short plug of Celite and rinsed with MeOH. The crude product was purified by column chromatography on silica gel (*n*-pentane/EtOAc) to afford pure isoxazolones.

Step 3: A flame dried Schlenk flask was charged with isoxazolone **168** (1.00 eq.), Net_3 (0.80 eq.) and POCl_3 (1.0 M). The resulting mixture was stirred for 16 h at 104 °C under inert gas atmosphere. Afterwards, the mixture was cooled to rt and poured to a cooled aq. sat. NaHCO_3 -solution. The aq. layer was extracted with EtOAc (3x), the combined organic layers were dried over Na_2SO_4 , filtered and the solvent was removed under reduced pressure. The crude product was purified by column chromatography on silica gel (*n*-pentane/EtOAc) to afford pure product.

Step 4: To a flame dried Schlenk flask were added chlorinated isoxazole (1.00 eq.), sodium alkoxide (1.50 eq.), and alcohol (1 M). Subsequently the mixture was refluxed under inert gas atmosphere for

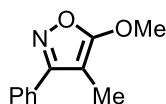
Experimental Part

48 h. After cooling to rt, filtration of the precipitate and removal of the solvent, the crude product was purified by column chromatography on silica gel (*n*-pentane/EtOAc) to afford pure isoxazole substrates **164**.

Alternatively, for Step 4: An oven-dried microwave tube was charged with chlorinated isoxazole (1.00 eq.), sodium alkoxide (1.50 eq.), and alcohol (1 M). The resulting suspension was placed in a microwave and stirred at reflux while irradiated with microwaves (for MeOH, EtOH, and *i*PrOH: 50 W; for *t*BuOH: 150 W). Afterwards, the mixture was filtered, the filtrate was concentrated, and the crude product was purified by column chromatography on silica gel (*n*-pentane/EtOAc) to afford pure isoxazole substrates **164**.

¹H NMR and ¹³C NMR data for reported substrates are stated below. Due to the broader substrate scope, the molecule numbers for the substrate will be according to Chapter 3.4.

5-Methoxy-4-methyl-3-phenylisoxazole (164a)



Colorless oil.

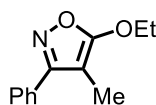
TLC: $R_f = 0.57$ (*n*-pentane/EtOAc 5:1).

¹H NMR: (300 MHz, CDCl₃) $\delta = 7.68$ -7.61 (m, 2H), 7.50–7.42 (m, 3H), 4.12 (s, 3H), 1.96 (s, 3H) ppm.

¹³C NMR: (75 MHz, CDCl₃) $\delta = 169.7, 164.9, 130.4, 129.6, 128.8$ (2C), 127.9 (2C), 86.6, 57.9, 6.6 ppm.

Analytical data were consistent with reported data.^[180]

5-Ethoxy-4-methyl-3-phenylisoxazole (164b)



Colorless oil.

TLC: $R_f = 0.67$ (*n*-pentane/EtOAc 5:1).

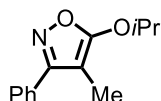
¹H NMR: (300 MHz, CDCl₃): $\delta = 7.68$ -7.62 (m, 2H), 7.49-7.42 (m, 3H), 4.45 (q, $J = 7.1$ Hz, 2H), 1.96 (s, 3H), 1.46 (t, $J = 7.1$ Hz, 3H) ppm.

Experimental Part

¹³C NMR: (75 MHz, CDCl₃): δ = 169.5, 164.7, 130.5, 129.5, 128.8 (2C), 127.9 (2C), 87.3, 67.5, 15.2, 6.7 ppm.

Analytical data were consistent with reported data.^[180]

5-(Isopropoxy)-4-methyl-3-phenylisoxazole (164c)



Pale-yellow oil.

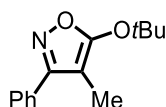
TLC: R_f = 0.75 (*n*-pentane/EtOAc 5:1).

¹H NMR: (300 MHz, CDCl₃) δ = 7.69-7.62 (m, 2H), 7.50-7.41 (m, 3H), 4.94 (septet, J = 6.1 Hz, 1H), 1.96 (s, 3H), 1.43 (d, J = 6.1 Hz, 6H) ppm.

¹³C NMR: (75 MHz, CDCl₃) δ = 169.3, 164.5, 130.6, 129.5, 128.8 (2C), 127.8 (2C), 88.6, 76.0, 22.7 (2C), 6.8 ppm.

Analytical data were consistent with reported data.^[180]

5-(*tert*-Butoxy)-4-methyl-3-phenylisoxazole (164d)



Off-white solid.

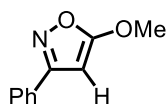
TLC: R_f = 0.28 (*n*-pentane/EtOAc 20:1).

¹H NMR: (300 MHz, CDCl₃) δ = 7.71-7.64 (m, 2H), 7.50-7.41 (m, 3H), 1.98 (s, 3H), 1.51 (s, 9H) ppm.

¹³C NMR: (75 MHz, CDCl₃) δ = 169.1, 163.8, 130.7, 129.5, 128.8 (2C), 127.7 (2C), 93.6, 85.4, 29.0, 7.5 ppm.

Analytical data were consistent with reported data.^[174]

5-Methoxy-3-phenylisoxazole (164e)



Colorless oil.

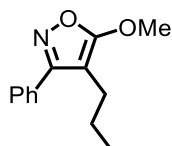
TLC: $R_f = 0.52$ (*n*-pentane/EtOAc 5:1).

¹H NMR: (300 MHz, CDCl₃): $\delta = 7.78\text{--}7.72$ (m, 2H), 7.47–7.41 (m, 3H), 5.53 (s, 1H), 4.05 (s, 3H) ppm.

¹³C NMR: (75 MHz, CDCl₃): $\delta = 174.6, 164.4, 130.2, 129.7, 128.9$ (2C), 126.6 (2C), 75.5, 58.9 ppm.

Analytical data were consistent with reported data.^[273]

5-Methoxy-3-phenyl-4-propylisoxazole (164f)



Colorless oil.

TLC: $R_f = 0.59$ (*n*-pentane/EtOAc 5:1).

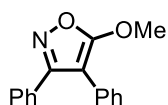
¹H NMR: (300 MHz, CDCl₃) $\delta = 7.63\text{--}7.56$ (m, 2H), 7.49–7.41 (m, 3H), 4.11 (s, 3H), 2.34 (t, $J = 7.6$ Hz, 2H), 1.47 (sext, $J = 7.5$ Hz, 2H), 0.86 (t, $J = 7.3$ Hz, 3H) ppm.

¹³C NMR: (75 MHz, CDCl₃) $\delta = 169.9, 165.1, 130.6, 129.5, 128.8$ (2C), 128.0 (2C), 91.7, 57.9, 23.3, 22.7, 13.8 ppm.

Analytical data were consistent with reported data.^[180]

5-Methoxy-3,4-diphenylisoxazole (164g)

The α -phenyl- β -ketoester intermediate for this substrate was synthesized according to a reported procedure.^[274]



Colorless solid.

Experimental Part

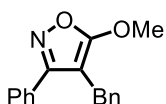
TLC: $R_f = 0.51$ (*n*-pentane/EtOAc 5:1).

¹H NMR: (300 MHz, CDCl₃) $\delta = 7.48$ (d, $J = 7.1$ Hz, 2H), 7.42-7.20 (m, 8H), 4.18 (s, 3H) ppm.

¹³C NMR: (75 MHz, CDCl₃) $\delta = 169.1, 163.8, 129.8, 129.7, 129.3, 129.2$ (2C), 128.7 (2C), 128.6 (2C), 128.5 (2C), 127.0, 93.7, 58.2 ppm.

Analytical data were consistent with reported data.^[180]

4-Benzyl-5-methoxy-3-phenylisoxazole (164h)



Colorless oil.

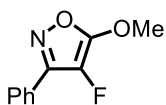
TLC: $R_f = 0.55$ (*n*-pentane/EtOAc 5:1).

¹H NMR: (300 MHz, CDCl₃): $\delta = 7.54$ -7.47 (m, 2H), 7.43-7.35 (m, 3H), 7.30-7.23 (m, 2H), 7.20 (d, $J = 6.6$ Hz, 1H), 7.17-7.10 (m, 2H), 4.13 (s, 3H), 3.73 (s, 2H) ppm.

¹³C NMR: (75 MHz, CDCl₃) $\delta = 170.4, 165.3, 139.8, 130.0, 129.7, 128.8$ (2C), 128.6 (2C), 128.1 (2C), 128.0 (2C), 126.4, 90.2, 58.0, 27.1 ppm.

Analytical data were consistent with reported data.^[180]

4-Fluoro-5-methoxy-3-phenylisoxazole (164i)



Fluorinated substrate **164i** was synthesized according to a published procedure.^[180]

Colorless oil.

TLC: $R_f = 0.58$ (*n*-pentane/EtOAc 5:1).

¹H NMR: (300 MHz, CDCl₃) $\delta = 7.88$ -7.80 (m, 2H), 7.51-7.44 (m, 3H), 4.20 (s, 3H) ppm.

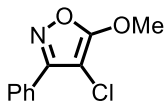
¹³C NMR: (75 MHz, CDCl₃) $\delta = 159.1$ (d, $J = 19.5$ Hz), 154.7 (d, $J = 7.8$ Hz), 130.6, 129.0 (2C), 127.4 (d, $J = 3.8$ Hz), 126.9 (d, $J = 3.4$ Hz, 2C), 123.8 (d, $J = 244.7$ Hz), 58.9 (d, $J = 2.0$ Hz) ppm.

¹⁹F NMR: (282 MHz, CDCl₃) $\delta = -196.6$ ppm.

Experimental Part

Analytical data were consistent with reported data.^[180]

4-Chloro-5-methoxy-3-phenylisoxazole (164j)



Chlorinated substrate **164j** was synthesized according to a published procedure.^[180]

Colorless solid.

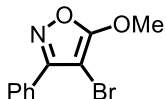
TLC: $R_f = 0.65$ (*n*-pentane/EtOAc 5:1).

¹H NMR: (300 MHz, CDCl₃) $\delta = 7.87$ - 7.81 (m, 2H), 7.51 - 7.45 (m, 3H), 4.20 (s, 3H) ppm.

¹³C NMR: (75 MHz, CDCl₃) $\delta = 168.0$, 161.6 , 130.4 , 128.8 (2C), 128.1 , 127.8 (2C), 83.1 , 58.6 ppm.

Analytical data were consistent with reported data.^[180]

4-Bromo-5-methoxy-3-phenylisoxazole (164k)



Brominated substrate **164k** was synthesized according to a published procedure.^[180]

Dark-yellow solid.

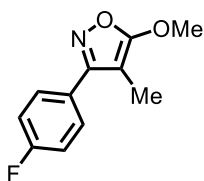
TLC: $R_f = 0.63$ (*n*-pentane/EtOAc 5:1).

¹H NMR: (300 MHz, CDCl₃) $\delta = 7.86$ - 7.80 (m, 2H), 7.51 - 7.44 (m, 3H), 4.20 (s, 3H) ppm.

¹³C NMR (75 MHz, CDCl₃) $\delta = 169.4$, 162.6 , 130.4 , 128.7 (2C), 128.4 , 128.0 (2C), 66.9 , 58.6 ppm.

Analytical data were consistent with reported data.^[180]

3-(4-Fluorophenyl)-5-methoxy-4-methylisoxazole (164l)



Colorless solid.

TLC: $R_f = 0.41$ (*n*-pentane/EtOAc 5:1).

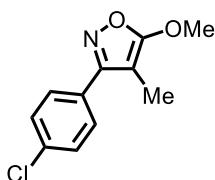
¹H NMR: (300 MHz, CDCl₃) $\delta = 7.67$ - 7.60 (m, 2H), 7.19 - 7.11 (m, 2H), 4.12 (s, 3H), 1.94 (s, 3H) ppm.

¹³C NMR: (75 MHz, CDCl₃) $\delta = 169.8$, 164.0 , 163.6 (d, $J = 249.3$ Hz, 2C), 129.8 (d, $J = 8.5$ Hz), 126.6 (d, $J = 3.4$ Hz), 115.9 (d, $J = 21.8$ Hz, 2C), 86.5 , 58.0 , 6.6 ppm.

¹⁹F NMR: (282 MHz, CDCl₃) $\delta = -111.4$ ppm.

Analytical data were consistent with reported data.^[174]

3-(4-Chlorophenyl)-5-methoxy-4-methylisoxazole (164m)



Colorless solid.

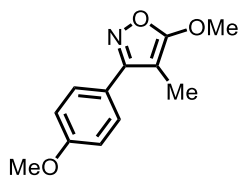
TLC: $R_f = 0.63$ (*n*-pentane/EtOAc 5:1).

¹H NMR: (300 MHz, CDCl₃) $\delta = 7.59$ (d, $J = 8.4$ Hz, 2H), 7.43 (d, $J = 8.4$ Hz, 2H), 4.12 (s, 3H), 1.94 (s, 3H) ppm.

¹³C NMR: (75 MHz, CDCl₃) $\delta = 169.9$, 163.8 , 135.7 , 129.1 (2C), 129.1 (2C), 128.9 , 86.6 , 58.0 , 6.6 ppm.

Analytical data were consistent with reported data.^[174]

5-Methoxy-3-(4-methoxyphenyl)-4-methylisoxazole (164n)



Colorless solid.

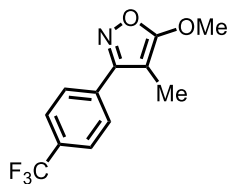
TLC: $R_f = 0.32$ (*n*-pentane/EtOAc 5:1).

$^1\text{H NMR}$: (300 MHz, CDCl_3) $\delta = 7.59$ (d, $J = 8.7$ Hz, 2H), 6.98 (d, $J = 8.7$ Hz, 2H), 4.11 (s, 3H), 3.85 (s, 3H), 1.95 (s, 3H) ppm.

$^{13}\text{C NMR}$: (75 MHz, CDCl_3) $\delta = 169.6$, 164.5, 160.7, 129.2 (2C), 122.9, 114.3 (2C), 86.5, 57.9, 55.5, 6.8 ppm.

Analytical data were consistent with reported data.^[174]

5-Methoxy-4-methyl-3-(4-(trifluoromethyl)phenyl)isoxazole (164o)



Colorless solid.

TLC: $R_f = 0.65$ (*n*-pentane/EtOAc 5:1).

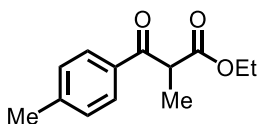
$^1\text{H NMR}$: (300 MHz, CDCl_3) $\delta = 7.79$ (d, $J = 8.5$ Hz, 2H), 7.72 (d, $J = 8.4$ Hz, 2H), 4.14 (s, 3H), 1.97 (s, 3H) ppm.

$^{13}\text{C NMR}$: (75 MHz, CDCl_3) $\delta = 170.1$, 163.6, 134.0, 131.6 (d, $J = 32.6$ Hz), 128.2 (2C), 125.8 (q, $J = 3.7$ Hz, 2C), 122.3, 86.8, 58.1, 6.6 ppm.

$^{19}\text{F NMR}$: (282 MHz, CDCl_3) $\delta = -62.8$ ppm.

Analytical data were consistent with reported data.^[174]

Ethyl 2-methyl-3-oxo-3-(*p*-tolyl)propanoate (207)



Following **GP J**, compound **207** (1.11 g, 5.04 mmol, >99%) was obtained as a colorless oil and the crude product was used without further purification.

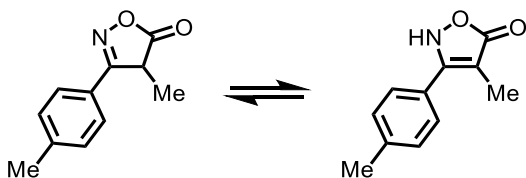
¹H NMR: (300 MHz, CDCl₃) δ = 7.87 (d, J = 8.2 Hz, 2H), 7.26 (d, J = 8.2 Hz, 2H), 4.34 (q, J = 7.1 Hz, 1H), 4.13 (q, J = 7.1 Hz, 2H), 2.40 (s, 3H), 1.47 (d, J = 7.1 Hz, 3H), 1.16 (t, J = 7.1 Hz, 3H) ppm.

¹³C NMR: (75 MHz, CDCl₃) δ = 195.6, 171.1, 144.4, 133.5, 129.5 (2C), 128.8 (2C), 61.4, 48.4, 21.8, 14.1, 13.9 ppm.

IR: (neat) $\tilde{\nu}$ = 2985 (w), 2940 (w), 1735 (s), 1682 (s), 1606 (m), 1571 (w), 1453 (w), 1408 (w), 1374 (w), 1329 (w), 1295 (m), 1227 (m), 1181 (s), 1084 (m), 1031 (m), 961 (m), 829 (w), 740 (w), 688 (w), 603 (w), 570 (w), 484 (w) cm⁻¹.

HRMS: (ESI⁺) m/z calcd. for C₁₃H₁₆O₃Na [M+Na]⁺: 243.0992; found: 243.0994.

4-Methyl-3-(*p*-tolyl)isoxazol-5(4*H*)-one (168p)



Following **GP J**, compound **168p** (0.75 g, 3.98 mmol, 73%) was obtained as an orange solid after column chromatography on silica gel (*n*-pentane/EtOAc 4:1 → 1:1) and as a mixture of imine and enamine (2:1) as determined by ¹H NMR analysis.

TLC: R_f = 0.33 (*n*-pentane/EtOAc 1:1).

¹H NMR: (300 MHz, CDCl₃) δ = 7.55 (d, J = 8.2 Hz, 2H), 7.46 (d, J = 8.1 Hz, 2H, enamine), 7.33-7.26 (m, 2H), 7.33-7.26 (m, 2H, enamine), 3.81 (q, J = 7.9 Hz, 1H), 2.41 (s, 3H), 1.99 (s, 3H, enamine), 1.55 (d, J = 7.9 Hz, 3H) ppm.

¹³C NMR: (75 MHz, CDCl₃) δ = 179.0, 174.4 (enamine), 167.3, 161.9 (enamine), 142.7, 141.8 (enamine), 130.1 (2C), 130.1 (2C, enamine), 127.4 (2C, enamine), 127.0 (2C), 124.6,

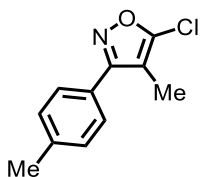
Experimental Part

99.3 (enamine), 39.7, 29.8 (enamine), 24.6 (enamine), 21.7, 21.6 (enamine), 14.8, 7.8 (enamine) ppm.

IR: (neat) $\tilde{\nu}$ = 3060 (w), 2917 (w), 2840 (w), 1800 (w), 1672 (s), 1594 (s), 1512 (w), 1472 (m), 1375 (w), 1286 (w), 1244 (w), 1185 (w), 1066 (m), 990 (m), 896 (w), 817 (m), 756 (m), 697 (m), 614 (m), 572 (m), 484 (m) cm^{-1} .

HRMS: (ESI+) m/z calcd. for $\text{C}_{11}\text{H}_{11}\text{NO}_2\text{Na}$ $[\text{M}+\text{Na}]^+$: 212.0682, found: 212.0684.

5-Chloro-4-methyl-3-(*p*-tolyl)isoxazole (208)



Following **GP J**, compound **208** (0.71 g, 3.41 mmol, 92%) was obtained as a yellow solid after column chromatography on silica gel (*n*-pentane/EtOAc 20:1).

TLC: R_f = 0.32 (*n*-pentane/EtOAc 20:1).

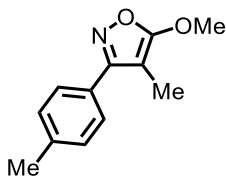
^1H NMR: (300 MHz, CDCl_3) δ = 7.55 (d, J = 8.1 Hz, 2H), 7.29 (d, J = 8.0 Hz, 2H), 2.42 (s, 3H), 2.11 (s, 3H) ppm.

^{13}C NMR: (75 MHz, CDCl_3) δ = 163.9, 151.9, 140.3, 129.7 (2C), 127.8 (2C), 126.2, 108.5, 21.5, 8.3 ppm.

IR: (neat) $\tilde{\nu}$ = 3031 (w), 2973 (w), 2861 (w), 1916 (w), 1661 (w), 1612 (m), 1569 (w), 1449 (s), 1412 (m), 1376 (m), 1238 (w), 1175 (m), 1092 (m), 1040 (w), 1008 (w), 888 (m), 818 (s), 726 (m), 702 (w), 700 (w), 549 (m), 508 (m), 460 (w), 404 (w) cm^{-1} .

HRMS: (ESI+) m/z calcd. for $\text{C}_{11}\text{H}_{11}\text{ClNO}$ $[\text{M}+\text{H}]^+$: 208.0524, found: 208.0527.

5-Methoxy-4-methyl-3-(*p*-tolyl)isoxazole (164p)



Following **GP J**, isoxazole **164p** (117 mg, 0.62 mmol, 43%) was obtained as a colorless solid after purification by column chromatography on silica gel (*n*-pentane/EtOAc 20:1).

Experimental Part

TLC: $R_f = 0.46$ (*n*-pentane/EtOAc 5:1).

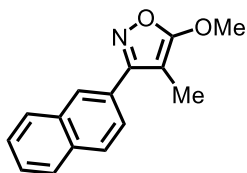
$^1\text{H NMR}$: (300 MHz, CDCl_3) $\delta = 7.54$ (d, $J = 8.1$ Hz, 2H), 7.26 (d, $J = 8.0$ Hz, 2H), 4.11 (s, 3H), 2.40 (s, 3H), 1.95 (s, 3H) ppm.

$^{13}\text{C NMR}$: (75 MHz, CDCl_3) $\delta = 169.6$, 164.8, 139.6, 129.5 (2C), 127.8 (2C), 86.6, 57.9, 21.5, 6.7 ppm.

IR: (neat) $\tilde{\nu} = 2947$ (w), 2862 (w), 1642 (s), 1572 (w), 1481 (m), 1408 (m), 1312 (w), 1225 (w), 1164 (m), 997 (m), 931 (w), 878 (w), 825 (m), 793 (w), 729 (m), 660 (w), 569 (w), 506 (m), 423 (w) cm^{-1} .

HRMS: (ESI+) m/z calcd. for $\text{C}_{12}\text{H}_{13}\text{NO}_2\text{Na}$ [$\text{M}+\text{Na}^+$]: 226.0838, found: 226.0842.

5-Methoxy-4-methyl-3-(naphthalen-2-yl)isoxazole (164q)



Colorless solid.

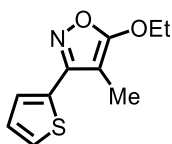
TLC: $R_f = 0.46$ (*n*-pentane/EtOAc 5:1).

$^1\text{H NMR}$: (300 MHz, CDCl_3) $\delta = 8.13$ (s, 1H), 7.96-7.85 (m, 3H), 7.79 (dd, $J = 8.5$, 1.6 Hz, 1H), 7.57-7.50 (m, 2H), 4.15 (s, 3H), 2.05 (s, 3H) ppm.

$^{13}\text{C NMR}$: (75 MHz, CDCl_3) $\delta = 169.9$, 164.8, 133.8, 133.3, 128.6, 128.6, 127.9 (2C), 127.6, 127.0, 126.6, 125.1, 86.9, 58.0, 6.9 ppm.

Analytical data were consistent with reported data.^[174]

5-Ethoxy-4-methyl-3-(thiophen-2-yl)isoxazole (164r)



Colorless oil.

TLC: $R_f = 0.59$ (*n*-pentane/EtOAc 5:1).

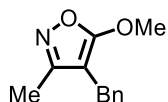
Experimental Part

¹H NMR: (300 MHz, CDCl₃) δ = 7.67-7.63 (m, 1H), 7.49 (d, J = 5.0 Hz, 1H), 7.40 (dd, J = 5.0, 2.9 Hz, 1H), 4.43 (q, J = 7.1 Hz, 2H), 2.00 (s, 3H), 1.44 (t, J = 7.1 Hz, 3H) ppm.

¹³C NMR: (75 MHz, CDCl₃) δ = 169.4, 160.3, 131.3, 126.4, 126.2, 124.7, 87.0, 67.5, 15.2, 6.8 ppm.

Analytical data were consistent with reported data.^[174]

4-Benzyl-5-methoxy-3-methylisoxazole (164s)



Colorless oil.

TLC: R_f = 0.50 (*n*-pentane/EtOAc 5:1).

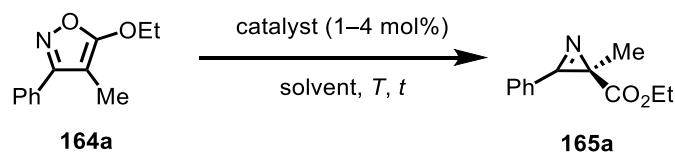
¹H NMR: (300 MHz, CDCl₃) δ = 7.32-7.24 (m, 2H), 7.22 (d, J = 6.6 Hz, 1H), 7.18-7.12 (m, 2H), 4.07 (s, 3H), 3.57 (s, 2H), 2.06 (s, 3H) ppm.

¹³C NMR: (75 MHz, CDCl₃) δ = 169.3, 163.0, 139.5, 128.6 (2C), 128.1 (2C), 126.3, 90.7, 57.8, 26.9, 11.3 ppm.

Analytical data were consistent with reported data.^[174]

5.5.2 Asymmetric Ring Contraction Catalyzed by Fe(II)-Complexes with a Chiral Pentadentate Ligand and Product Characterization

General Procedure K: Optimization of Reaction Conditions (GP K)



A flame dried Schlenk flask was charged with catalyst (1-4 mol%) under inert gas atmosphere and the indicated solvent (0.1 or 0.2 M) was added. The resulting solution was stirred at the stated temperature for at least 10 min. Subsequently, isoxazole (0.05 mmol) was added and the reaction mixture was stirred for the indicated time. Afterwards, the solvent was removed under reduced pressure and crude $^1\text{H NMR}$ and crude HPLC on a chiral stationary phase were measured to determine NMR yield and enantiomeric excess. For reactions involving temperatures of $-50\text{ }^\circ\text{C}$ or lower, the reaction was quenched with 2,2'-bipyridine after the indicated time. Afterwards, crude NMR and crude HPLC were measured.

The identification numbers for the azirine products are in accordance with section 3.3.2.

Table 15: Survey of Catalyst and Catalyst Loading.^a

Entry	Catalyst (mol%)	<i>t</i> (min)	Yield (%) ^b	ee (%) ^c
1	131a [4.0]	1	99	6
2	140a [4.0]	1	99	16
3	149a [4.0]	1	99	32
4	150a [4.0]	1	99	66
5	150a [1.0]	2	99	66

^aReaction conditions: Following **GP K**, the catalyst (1 or 4 mol%) was dissolved in CH_2Cl_2 (0.1 M, 0.5 mL) and the solution was cooled to $0\text{ }^\circ\text{C}$. Isoxazole **164a** (0.05 mmol) was added and the reaction was stirred until complete conversion of the starting material was observed. Afterwards, the solvent was removed under vacuum and crude $^1\text{H NMR}$ and HPLC were measured. ^bNMR yield with 1,1,2,2-tetrachloroethane as reference.

^cDetermined by HPLC analysis on a chiral stationary phase.

Experimental Part

Table 16: Survey of Solvents.^a

Entry	Solvent	<i>t</i> (min)	Yield (%) ^b	ee (%) ^c
1	CH ₂ Cl ₂	2	99	66
2	CDCl ₃	2	99	63
3	MeOH	50	98	62
4	Acetone	5	98	48
5	MeCN	180	96	49
6	1,2-Dichlorobenzene	8	98	70
7 ^d	1,2-Dichlorobenzene	45	97	72

^aReaction conditions: Following **GP K**, catalyst **150a** (1 mol%) was dissolved in the indicated solvent (0.1 M, 0.5 mL) and the solution was cooled to 0 °C. Isoxazole **164a** (0.05 mmol) was added and the reaction was stirred until complete conversion of the starting material was observed. Afterwards, the solvent was removed under vacuum and crude ¹H NMR and HPLC were measured. ^bNMR yield with 1,1,2,2-tetrachloroethane as reference. ^cDetermined by HPLC analysis on a chiral stationary phase. ^dReaction was conducted at -15 °C.

Table 17: Survey of Temperature and Final Optimization.^a

Entry	<i>T</i> (°C)	Cat. Loading (mol%)	<i>c</i> (mol/L)	<i>t</i> (h)	Yield (%) ^b	ee (%) ^c
1	0	1	0.1	2 min	99	66
2	-50	1	0.1	36	74	88
3	-60	1	0.1	36	48	89
4	-60	2	0.2	20	99	89
5	-75	2	0.2	20	50	92

^aReaction conditions: Following **GP K**, catalyst **150a** (1 or 2 mol%) was dissolved in CH₂Cl₂ (0.1 or 0.2 M) under inert gas atmosphere and the solution was cooled to the indicated temperature. After 15 min of stirring, isoxazole **164a** (0.05 mmol) was added and the reaction mixture was stirred for the stated time. Afterwards, 2,2'-bipyridine (5.0 eq.) were added to the solution at the reaction temperature and further stirred for at least 30 min to complete quenching of the catalyst. Afterwards, crude ¹H NMR and crude HPLC were measured to determine NMR yield and enantiomeric excess. ^bNMR yield with 1,1,2,2-tetrachloroethane as reference. ^cDetermined by HPLC analysis on a chiral stationary phase.

Experimental Part

Table 18: Control Reactions.^a

Entry	Variations form Standard Procedure	Yield (%) ^b	ee (%) ^c
1^d	none	99 (98)	89 (89)
2	under air	99	89
3	with 5.0 eq. H ₂ O	94	89
4	with 5.0 eq. 2,2'-bipyridine	traces	–
5^e	with 5.0 eq. 2,2'-bipyridine	traces	–

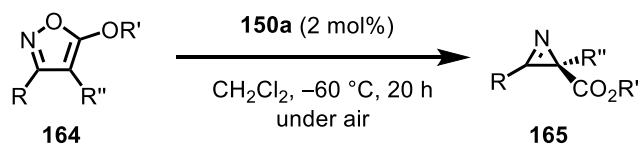
^aStandard procedure: A flame dried Schlenk flask was charged with catalyst **150a** (2 mol%) and dissolved in CH₂Cl₂ (0.25 mL) under inert gas atmosphere. The solution was cooled to –60 °C and stirred for 15 min at this temperature. Afterwards, isoxazole **164a** (0.05 mmol) was added and the reaction mixture was stirred at –60 °C for 20 h under inert gas atmosphere. The reaction was quenched with 2,2'-bipyridine (5.0 eq.) and stirred for at least 30 min. Next, the solvent was removed under reduced pressure and ¹H NMR and HPLC of the crude product were measured. ^bNMR yield. ^cDetermined by HPLC analysis on a chiral stationary phase. ^dBrackets give the results for yield and ee of isolated product after column chromatography on silica gel. ^eReaction was performed at rt. First, catalyst **150a** (2 mol%) was dissolved in CH₂Cl₂ (0.2 M) and 2,2'-bipyridine (5.0 eq.) was added. The mixture was stirred for 5 min and isoxazole **164a** (0.05 mmol) was given to the reaction. After stirring at rt for 24 h, the solvent was removed under vacuum and the precipitate was submitted to ¹H NMR measurement.

Table 19: Results of TON Screening.^a

Entry	Cat. Loading (mol%)	<i>t</i>	Yield (%) ^b	ee (%) ^c
1	1	2 min	99	60
2^d	0.1	30 min	99	60
3^{d,e}	0.01	18 h	99	59

^aReaction conditions: Following **GP K**, catalyst **150a** (0.01–1 mol%) was dissolved in CH₂Cl₂ (0.2 M) under air. Isoxazole **164a** (0.05 mmol) was added at rt and the resulting solution was stirred until complete conversion of the starting material was observed. Afterwards, crude ¹H NMR and crude HPLC were measured to determine NMR yield and enantiomeric excess. ^bNMR yield with 1,1,2,2-tetrachloroethane as reference. ^cDetermined by HPLC analysis on a chiral stationary phase. ^dA freshly prepared stock solution of catalyst **150a** (1.00 mg in 1.00 mL CH₂Cl₂) was used for catalyst addition. ^e Reaction was conducted under inert gas atmosphere.

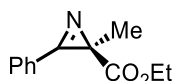
General Procedure L: Asymmetric Ring Contraction with Pentadentate Catalyst 150a under Optimized Conditions (GP L)



An oven dried flask was charged with catalyst **150a** (1.76 mg, 2 mol%) and CH₂Cl₂ (0.5 mL, 0.2 M). The red solution was cooled to –60 °C and stirred for at least 15 min before isoxazole **164** (0.10 mmol, 1.00 eq.) was added. The reaction mixture was stirred for 20 h at –60 °C in presence of air. Afterwards, the reaction was quenched with 2,2'-bipyridine (5.00 eq.) and stirred for another 30 min at –60 °C. The solvent was removed under reduced pressure and the precipitate was submitted to column chromatography on silica gel (*n*-pentane/EtOAc) to afford pure 2*H*-azirines **165**. Column chromatography for more polar products has to be performed carefully due to eluting 2,2'-bipyridine.

The absolute configuration of the products was determined by comparison of the HPLC traces and optical rotation values with reported data.^[174,180]

Ethyl (*R*)-2-methyl-3-phenyl-2*H*-azirine-2-carboxylate (165a**)**



Following **GP L**, compound **165a** (19.6 mg, 0.10 mmol, 98%) was obtained as a colorless oil after column chromatography on silica gel (*n*-pentane/EtOAc 5:1). Enantiomeric excess was established by HPLC analysis on a chiral stationary phase: ee = 89%, HPLC conditions: Daicel Chiralcel[®] OD-H column, 250 x 4.6 mm, absorbance at 254 nm, *n*-hexane/isopropanol = 98:2, isocratic flow, flow rate 1 mL/min, 25 °C, t_r (major) = 7.5 min, t_r (minor) = 8.0 min.

TLC: R_f = 0.45 (*n*-pentane/EtOAc 5:1).

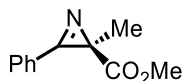
¹H NMR: (300 MHz, CDCl₃) δ = 7.86–7.81 (m, 2H), 7.66–7.53 (m, 3H), 4.15 (q, *J* = 7.1 Hz, 2H), 1.62 (s, 3H), 1.20 (t, *J* = 7.1 Hz, 3H) ppm.

¹³C NMR: (75 MHz, CDCl₃) δ = 173.2, 163.8, 133.7, 130.2 (2C), 129.5 (2C), 122.8, 61.5, 35.7, 17.9, 14.3 ppm.

[α]_D²²: –138.8° (*c* = 1.0, CH₂Cl₂).

Analytical data are in agreement with published data.^[174]

Methyl (*R*)-2-methyl-3-phenyl-2*H*-azirine-2-carboxylate (165b**)**



Following **GP L**, compound **165b** (18.7 mg, 0.10 mmol, 98%) was obtained as a colorless oil after column chromatography on silica gel (*n*-pentane/EtOAc 5:1). Enantiomeric excess was established by HPLC analysis on a chiral stationary phase: ee = 88%, HPLC conditions: Daicel Chiralcel[®] OD -H column, 250 x 4.6 mm, absorbance at 254 nm, *n*-hexane/isopropanol = 98:2, isocratic flow, flow rate 1 mL/min, 25 °C, *t_r* (major) = 8.4 min, *t_r* (minor) = 9.7 min.

TLC: $R_f = 0.36$ (*n*-pentane/EtOAc 5:1).

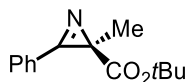
¹H NMR: (300 MHz, CDCl₃) $\delta = 7.84$ (d, $J = 7.4$ Hz, 2H), 7.66–7.54 (m, 3H), 3.68 (s, 3H), 1.63 (s, 3H) ppm.

¹³C NMR: (75 MHz, CDCl₃) $\delta = 173.7, 163.7, 133.8, 130.3$ (2C), 129.5 (2C), 122.7, 52.6, 35.6, 17.9 ppm.

$[\alpha]_D^{22}$: -111.6° ($c = 1.0$, CH₂Cl₂).

Analytical data are in agreement with published data.^[174]

***tert*-Butyl (*R*)-2-methyl-3-phenyl-2*H*-azirine-2-carboxylate (**165c**)**



Following **GP L** with 4 mol% of catalyst **150a**, compound **165c** (11.5 mg, 0.05 mmol, 50%) was obtained as an off-white solid after column chromatography on silica gel (*n*-pentane/EtOAc 30:1 → 20:1). Enantiomeric excess was established by HPLC analysis on a chiral stationary phase: ee = 27%, HPLC conditions: Daicel Chiralcel[®] OD-H column, 250 x 4.6 mm, absorbance at 254 nm, *n*-hexane/isopropanol = 99:1, isocratic flow, flow rate 0.6 mL/min, 25 °C, *t_r* (minor) = 14.4 min, *t_r* (major) = 16.0 min.

TLC: $R_f = 0.17$ (*n*-pentane/EtOAc 20:1).

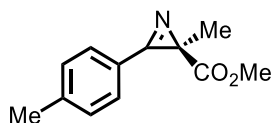
¹H NMR: (300 MHz, CDCl₃) $\delta = 7.86$ –7.79 (m, 2H), 7.65–7.53 (m, 3H), 1.58 (s, 3H), 1.41 (s, 9H) ppm.

¹³C NMR: (75 MHz, CDCl₃) $\delta = 172.5, 164.2, 133.5, 130.0$ (2C), 129.4 (2C), 123.2, 81.4, 36.5, 28.1 (3C), 17.9 ppm.

$[\alpha]_D^{22}$: -15.8° ($c = 1.0$, CH₂Cl₂).

Analytical data are in agreement with published data.^[174]

Methyl (*R*)-2-methyl-3-(*p*-tolyl)-2*H*-azirine-2-carboxylate (165d)



Following **GP L**, compound **165d** (20.1 mg, 0.10 mmol, 99%) was obtained as a colorless oil after column chromatography on silica gel (*n*-pentane/EtOAc 5:1). Enantiomeric excess was established by HPLC analysis on a chiral stationary phase: ee = 88%, HPLC conditions: Daicel Chiralcel[®] OD-H column, 250 x 4.6 mm, absorbance at 254 nm, *n*-hexane/isopropanol = 98:2, isocratic flow, flow rate 1 mL/min, 25 °C, *t_r* (minor) = 8.2 min, *t_r* (major) = 9.1 min.

TLC: R_f = 0.40 (*n*-pentane/EtOAc 5:1).

¹H NMR: (300 MHz, CDCl₃) δ = 7.73 (d, *J* = 8.0 Hz, 2H), 7.37 (d, *J* = 7.9 Hz, 2H), 3.67 (s, 3H), 2.45 (s, 3H), 1.61 (s, 3H) ppm.

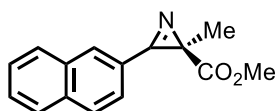
¹³C NMR: (75 MHz, CDCl₃) δ = 173.8, 163.2, 144.8, 130.3 (2C), 130.2 (2C), 119.8, 52.5, 35.2, 22.0, 17.9 ppm.

IR: (neat) $\tilde{\nu}$ = 2960 (w), 2925 (w), 2854 (w), 1722 (s), 1606 (w), 1506 (w), 1441 (m), 1381 (w), 1265 (s), 1174 (w), 1121 (s), 1018 (m), 949 (w), 853 (w), 816 (s), 795 (s), 739 (w), 707 (w), 612 (w), 550 (w), 515 (m), 461 (w), 401 (w) cm⁻¹.

HRMS: (ESI⁺) *m/z* calcd. for C₁₂H₁₃NO₂Na₁ [M+Na⁺]: 226.0838; found: 226.0841.

[α]_D²²: -135.8° (*c* = 1.0, CH₂Cl₂).

Methyl (*R*)-2-methyl-3-(naphthalen-2-yl)-2*H*-azirine-2-carboxylate (165e)



Following **GP L**, compound **165e** (23.2 mg, 0.10 mmol, 97%) was obtained as a colorless solid after column chromatography on silica gel (*n*-pentane/EtOAc 5:1). Enantiomeric excess was established by HPLC analysis on a chiral stationary phase: ee = 82%, HPLC conditions: Daicel Chiralcel[®] OD-H column, 250 x 4.6 mm, absorbance at 254 nm, *n*-hexane/isopropanol = 98:2, isocratic flow, flow rate 1 mL/min, 25 °C, *t_r* (minor) = 10.6 min, *t_r* (major) = 12.4 min.

TLC: R_f = 0.35 (*n*-pentane/EtOAc 5:1).

Experimental Part

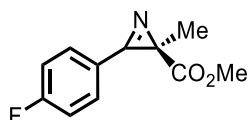
¹H NMR: (300 MHz, CDCl₃) δ = 8.25 (s, 1H), 8.05–7.88 (m, 4H), 7.70–7.55 (m, 2H), 3.70 (s, 3H), 1.70 (s, 3H) ppm.

¹³C NMR: (75 MHz, CDCl₃) δ = 173.8, 163.8, 135.9, 132.9, 132.4, 129.6, 129.3, 129.1, 128.3, 127.5, 124.9, 120.0, 52.6, 35.8, 18.0 ppm.

$[\alpha]_D^{22}$: –129.9° (*c* = 1.0, CH₂Cl₂).

Analytical data are in agreement with published data.^[174]

Methyl (*R*)-3-(4-fluorophenyl)-2-methyl-2*H*-azirine-2-carboxylate (**165f**)



Following **GP L**, compound **165f** (20.0 mg, 0.10 mmol, 97%) was obtained as a colorless oil after column chromatography on silica gel (*n*-pentane/EtOAc 5:1). Enantiomeric excess was established by HPLC analysis on a chiral stationary phase: ee = 88%, HPLC conditions: Daicel Chiralcel[®] OD-H column, 250 x 4.6 mm, absorbance at 254 nm, *n*-hexane/isopropanol = 98:2, isocratic flow, flow rate 1 mL/min, 25 °C, *t_r* (minor) = 9.0 min, *t_r* (major) = 10.1 min.

TLC: *R_f* = 0.37 (*n*-pentane/EtOAc 5:1).

¹H NMR: (300 MHz, CDCl₃) δ = 7.89–7.82 (m, 2H), 7.27 (t, *J* = 8.5 Hz, 2H), 3.68 (s, 3H), 1.62 (s, 3H) ppm.

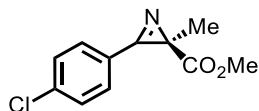
¹³C NMR: (75 MHz, CDCl₃) δ = 173.5, 166.0 (d, *J* = 256.5 Hz), 162.8, 132.7 (d, *J* = 9.4 Hz, 2C), 119.1 (d, *J* = 3.2 Hz), 117.1 (d, *J* = 22.5 Hz, 2C), 52.7, 35.7, 17.8 ppm.

¹⁹F NMR: (282 MHz, CDCl₃) δ = –103.0 ppm.

$[\alpha]_D^{22}$: –135.9° (*c* = 1.0, CH₂Cl₂).

Analytical data are in agreement with published data.^[174]

Methyl (*R*)-3-(4-chlorophenyl)-2-methyl-2*H*-azirine-2-carboxylate (165g)



Following **GP L**, compound **165g** (20.1 mg, 0.09 mmol, 91%) was obtained as a colorless oil after column chromatography on silica gel (*n*-pentane/EtOAc 8:1). Enantiomeric excess was established by HPLC analysis on a chiral stationary phase: ee = 82% ee; HPLC conditions: Daicel Chiralcel[®] OD-H column, 250 x 4.6 mm, absorbance at 254 nm, *n*-hexane/isopropanol = 98:2, isocratic flow, flow rate 1 mL/min, 25 °C, *t_r* (minor) = 7.8 min, *t_r* (major) = 9.1 min.

TLC: $R_f = 0.50$ (*n*-pentane/EtOAc 5:1).

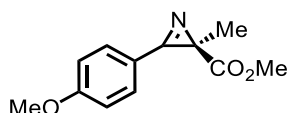
¹H NMR: (300 MHz, CDCl₃) $\delta = 7.78$ (d, $J = 8.4$ Hz, 2H), 7.55 (d, $J = 8.3$ Hz, 2H), 3.68 (s, 3H), 1.62 (s, 3H) ppm.

¹³C NMR: (75 MHz, CDCl₃) $\delta = 173.4$, 163.1, 140.2, 131.4 (2C), 130.0 (2C), 121.2, 52.7, 35.8, 17.8 ppm.

$[\alpha]_D^{22}$: -148.5° ($c = 1.0$, CH₂Cl₂).

Analytical data are in agreement with published data.^[174]

Methyl (*R*)-3-(4-methoxyphenyl)-2-methyl-2*H*-azirine-2-carboxylate (165h)



Following **GP L**, compound **165h** (21.0 mg, 0.10 mmol, 95%) was obtained as a colorless solid after column chromatography on silica gel (*n*-pentane/EtOAc 5:1). Enantiomeric excess was established by HPLC analysis on a chiral stationary phase: ee = 88%; HPLC conditions: Daicel Chiralcel[®] OD-H column, 250 x 4.6 mm, absorbance at 254 nm, *n*-hexane/isopropanol = 98:2, isocratic flow, flow rate 1 mL/min, 25 °C, *t_r* (minor) = 17.4 min, *t_r* (major) = 19.5 min.

TLC: $R_f = 0.20$ (*n*-pentane/EtOAc 5:1).

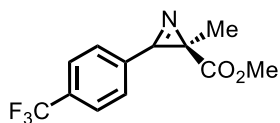
¹H NMR: (300 MHz, CDCl₃) $\delta = 7.78$ (d, $J = 8.8$ Hz, 2H), 7.05 (d, $J = 8.8$ Hz, 2H), 3.89 (s, 3H), 3.67 (s, 3H), 1.60 (s, 3H) ppm.

¹³C NMR: (75 MHz, CDCl₃) $\delta = 174.0$, 164.0, 162.3, 132.3 (2C), 115.0 (2C), 114.9, 55.7, 52.5, 35.1, 17.9 ppm.

$[\alpha]_D^{22}$: -162.7° ($c = 1.0$, CH₂Cl₂).

Analytical data are in agreement with published data.^[174]

Methyl (*R*)-2-methyl-3-(4-(trifluoromethyl)phenyl)-2*H*-azirine-2-carboxylate (165i)



Following **GP L**, compound **165i** (23.5 mg, 0.09 mmol, 91%) was obtained as a colorless solid after column chromatography on silica gel (*n*-pentane/EtOAc 5:1). Enantiomeric excess was established by HPLC analysis on a chiral stationary phase: ee = 85%; HPLC conditions: Daicel Chiralcel[®] OD-H column, 250 x 4.6 mm, absorbance at 254 nm, *n*-hexane/isopropanol = 98:2, isocratic flow, flow rate 1 mL/min, 25 °C, *t_r* (minor) = 7.0 min, *t_r* (major) = 8.8 min.

TLC: $R_f = 0.54$ (*n*-pentane/EtOAc 5:1).

¹H NMR: (300 MHz, CDCl₃) $\delta = 7.97$ (d, $J = 8.1$ Hz, 2H), 7.84 (d, $J = 8.2$ Hz, 2H), 3.70 (s, 3H), 1.65 (s, 3H) ppm.

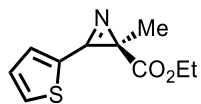
¹³C NMR: (75 MHz, CDCl₃) $\delta = 173.1$, 163.8, 135.2 (q, $J = 33.1$ Hz), 130.5 (2C), 126.5 (q, $J = 3.7$ Hz, 2C), 126.1, 123.5 (q, $J = 273.2$ Hz, signal almost not visible due to background noise), 52.8, 36.3, 17.8 ppm.

¹⁹F NMR: (282 MHz, CDCl₃) $\delta = -63.3$ ppm.

[α]_D²²: -86.2° ($c = 1.0$, CH₂Cl₂).

Analytical data are in agreement with published data.^[174]

Ethyl (*R*)-2-methyl-3-(thiophen-2-yl)-2*H*-azirine-2-carboxylate (165j)



Following **GP L**, compound **165j** (13.6 mg, 0.07 mmol, 65%) was obtained as a colorless solid after column chromatography on silica gel (*n*-pentane/EtOAc 15:1). Enantiomeric excess was established by HPLC analysis on a chiral stationary phase: ee = 74%; HPLC conditions: Daicel Chiralcel[®] OD-H column, 250 x 4.6 mm, absorbance at 254 nm, *n*-hexane/isopropanol = 90:10, isocratic flow, flow rate 1 mL/min, 25 °C, *t_r* (major) = 6.1 min, *t_r* (minor) = 6.7 min.

TLC: $R_f = 0.47$ (*n*-pentane/EtOAc 5:1).

Experimental Part

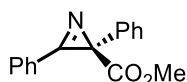
¹H NMR: (300 MHz, CDCl₃) δ = 7.97 (dd, J = 3.0, 1.0 Hz, 1H), 7.59 (dd, J = 5.2, 1.1 Hz, 1H), 7.51 (dd, J = 5.1, 2.9 Hz, 1H), 4.15 (q, J = 7.1 Hz, 2H), 1.59 (s, 3H), 1.21 (t, J = 7.1 Hz, 3H) ppm.

¹³C NMR: (75 MHz, CDCl₃) δ = 173.2, 158.2, 133.4, 128.1, 127.2, 124.7, 61.5, 35.2, 17.9, 14.3 ppm.

$[\alpha]_D^{22}$: -168.4° (c = 1.0, CH₂Cl₂).

Analytical data are in agreement with published data.^[174]

Methyl (*R*)-2,3-diphenyl-2*H*-azirine-2-carboxylate (**165k**)



Following **GP L**, compound **165k** (24.7 mg, 0.10 mmol, 98%) was obtained as a colorless solid after column chromatography on silica gel (*n*-pentane/EtOAc 5:1). Enantiomeric excess was established by HPLC analysis on a chiral stationary phase: ee = 93%; HPLC conditions: Daicel Chiralcel[®] OD-H column, 250 x 4.6 mm, absorbance at 254 nm, *n*-hexane/isopropanol = 98:2, isocratic flow, flow rate 1 mL/min, 25 °C, t_r (major) = 10.7 min, t_r (minor) = 12.9 min.

TLC: R_f = 0.34 (*n*-pentane/EtOAc 5:1).

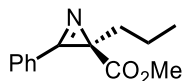
¹H NMR: (300 MHz, CDCl₃) δ = 7.92 (d, J = 7.9 Hz, 2H), 7.67–7.53 (m, 3H), 7.49 (d, J = 7.4 Hz, 2H), 7.35–7.23 (m, 3H), 3.74 (s, 3H) ppm.

¹³C NMR: (75 MHz, CDCl₃) δ = 171.8, 160.9, 136.3, 134.0, 130.6 (2C), 129.6 (2C), 128.4 (2C), 128.3 (2C), 127.9, 122.2, 52.8, 41.2 ppm.

$[\alpha]_D^{22}$: $+76.1^\circ$ (c = 1.0, CH₂Cl₂).

Analytical data are in agreement with published data.^[180]

Methyl (*R*)-3-phenyl-2-propyl-2*H*-azirine-2-carboxylate (**165l**)



Following **GP L**, compound **165l** (21.0 mg, 0.10 mmol, 97%) was obtained as a colorless solid after column chromatography on silica gel (*n*-pentane/EtOAc 10:1). Enantiomeric excess was established by HPLC analysis on a chiral stationary phase: ee = 73%; HPLC conditions: Daicel Chiralcel[®] OD-H

Experimental Part

column, 250 x 4.6 mm, absorbance at 254 nm, *n*-hexane/isopropanol = 98:2, isocratic flow, flow rate 1 mL/min, 25 °C, t_r (major) = 6.8 min, t_r (minor) = 7.9 min.

TLC: R_f = 0.51 (*n*-pentane/EtOAc 5:1).

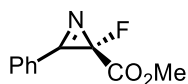
^1H NMR: (300 MHz, CDCl_3) δ = 7.85 (d, J = 7.8 Hz, 2H), 7.65–7.52 (m, 3H), 3.66 (s, 3H), 2.14–1.96 (m, 2H), 1.35–1.22 (m, 2H), 0.89 (t, J = 7.3 Hz, 3H) ppm.

^{13}C NMR: (75 MHz, CDCl_3) δ = 173.4, 163.1, 133.7, 130.2 (2C), 129.4 (2C), 123.2, 52.5, 39.8, 32.9, 19.7, 14.1 ppm.

$[\alpha]_D^{22}$: -104.1° (c = 1.0, CH_2Cl_2).

Analytical data are in agreement with published data.^[180]

Methyl (*S*)-2-fluoro-3-phenyl-2*H*-azirine-2-carboxylate (**165m**)



Following **GP L**, compound **165m** (19.2 mg, 0.10 mmol, 99%) was obtained as a colorless oil after column chromatography on silica gel (*n*-pentane/EtOAc 10:1). Enantiomeric excess was established by HPLC analysis on a chiral stationary phase: ee = 68%; HPLC conditions: Daicel Chiralcel[®] OD-H column, 250 x 4.6 mm, absorbance at 254 nm, *n*-hexane/isopropanol = 90:10, isocratic flow, flow rate 1 mL/min, 25 °C, t_r (major) = 6.1 min, t_r (minor) = 7.4 min.

TLC: R_f = 0.36 (*n*-pentane/EtOAc 5:1).

^1H NMR: (300 MHz, CDCl_3) δ = 7.96 (d, J = 7.2 Hz, 2H), 7.77–7.68 (m, 1H), 7.66–7.59 (m, 2H), 3.86 (s, 3H) ppm.

^{13}C NMR: (75 MHz, CDCl_3) δ = 67.2 (d, J = 43.5 Hz), 166.2 (d, J = 11.4 Hz), 135.2, 130.9 (2C), 129.8 (2C), 120.4, 78.2 (d, J = 264.1 Hz), 53.5 ppm.

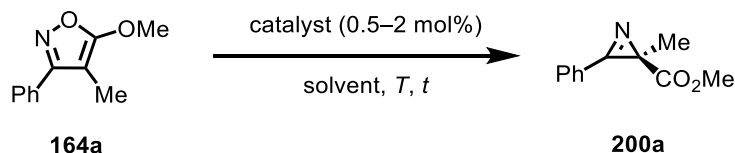
^{19}F NMR: (282 MHz, CDCl_3) δ = -155.20 ppm.

$[\alpha]_D^{22}$: -141.1° (c = 1.0, CH_2Cl_2).

Analytical data are in agreement with published data.^[180]

5.5.3 Asymmetric Ring Contraction with Tetradentate Complexes and Product Characterization

General Procedure M: Optimization of Reaction Conditions (GP M)



An oven-dried Schlenk flask was charged with Fe(II)-catalyst **191** (0.5–2 mol%) under inert gas atmosphere and the indicated solvent (0.2 M) was added. The resulting mixture was stirred at the stated temperature, isoxazole **164a** (0.05 mmol, 1.00 eq.) was added, and the reaction mixture was stirred for the indicated time, after which dilution with EtOAc and filtration over a short plug of silica to remove the complex gave the crude product. Yields were determined via ¹H-NMR spectra of the crude products using 1,1,2,2-tetrachloroethane as the internal standard. When conversion was not complete, the crude product was further purified on silica gel (*n*-pentane/EtOAc 10:1) for HPLC analysis on a chiral stationary phase to determine enantiomeric excess. When conversion was complete, enantiomeric excess was determined with the crude product.

The identification numbers for the azirine products are in accordance with section 3.4.3.

Table 20: Initial Catalyst Screening.^a

Entry	Catalyst (2 mol%)	Yield (%) ^b	ee (%) ^c
1	191a	99	53
2	191b	98	27
3	191c	98	2
4	191d	99	2
5	191e	97	5
6	191f	98	0
7	191g	97	30
8	191h	97	7
9	191i	99	5

^aReaction conditions: Following GP M, catalyst **191** (2 mol%) was dissolved in CH₂Cl₂ (0.2 M, 0.25 mL) and isoxazole **164a** (0.05 mmol) was added. The resulting mixture was stirred for 20 h at rt. Afterwards, the reaction was diluted with EtOAc, filtered over a short plug of silica, the solvent was removed under vacuum, and crude ¹H NMR and HPLC were measured. ^bNMR yield with 1,1,2,2-tetrachloroethane as internal standard.

^cDetermined by HPLC analysis on a chiral stationary phase.

Experimental Part

Table 21: Survey of Solvents.^a

Entry	Solvent	Yield (%) ^b	ee (%) ^c
1	CH ₂ Cl ₂	99	53
2	CHCl ₃	99	59
3	1,2-dichloroethane	99	75
4	1,2-dichlorobenzene ^d	99	65
5	1,1,2,2-tetrachloroethane	99	58
6	Toluene	44	24
7	MeCN	98	5
8	Acetone	95	35
9	H ₂ O ^e	39	41
10	MeOH	99	85
11	EtOH	99	60
12	<i>i</i> PrOH	99	57
13	HFIP	99	57

^aReaction conditions: Following **GP M**, catalyst **191a** (2 mol%) was dissolved in the indicated solvent (0.2 M, 0.25 mL) and isoxazole **164a** (0.05 mmol) was added. The resulting mixture was stirred for 20 h at rt. Afterwards, the reaction was diluted with EtOAc, filtered over a short plug of silica, the solvent was removed under vacuum, and crude ¹H NMR and HPLC were measured. When conversion was not complete, the crude mixture was submitted to column chromatography on silica gel (*n*-pentane/EtOAc 10:1) to obtain pure 2*H*-azirine **200a** for HPLC analysis. ^bNMR yield with 1,1,2,2-tetrachloroethane as internal standard. ^cDetermined by HPLC analysis on a chiral stationary phase. ^dDue to the high boiling point of the solvent, an aliquot was taken for ¹H NMR analysis and the residual reaction mixture was directly submitted to column chromatography on silica gel (*n*-pentane/EtOAc 10:1). ^eAfter 20 h, the reaction mixture was extracted using CH₂Cl₂ (3x) before analysis and further purification.

Experimental Part

Table 22: Survey of Reaction Time and Possible Racemization.^a

Entry	<i>t</i> [h]	Yield (%) ^b	ee (%) ^c
1	6	58	85
2	13	97	85
3	18	99	85
4	24	99	85
5	48	99	85

^aReaction conditions: Following **GP M**, catalyst **191a** (2 mol%) was dissolved in MeOH (0.2 M, 0.25 mL) and isoxazole **164a** (0.05 mmol) was added. The resulting mixture was stirred for the indicated time at rt. Afterwards, the reaction was diluted with EtOAc, filtered over a short plug of silica, the solvent was removed under vacuum, and crude ¹H NMR and HPLC were measured. When conversion was not complete, the crude mixture was submitted to column chromatography on silica gel (*n*-pentane/EtOAc 10:1) to obtain pure 2*H*-azirine **200a** for HPLC analysis. ^bNMR yield with 1,1,2,2-tetrachloroethane as internal standard. ^cDetermined by HPLC analysis on a chiral stationary phase.

Table 23: Survey of Additives.^a

Entry	Additives (4 mol%)	Yield (%) ^b	ee (%) ^c
1	–	99	85
2	NaPF ₆	98	85
3	NaSbF ₆	99	85
4	NaBArF	99	85
5	NaOTf	99	85

^aReaction conditions: Following **GP M**, catalyst **191a** (2 mol%) and additive (4 mol%) were dissolved in MeOH (0.2 M, 0.25 mL) and isoxazole **164a** (0.05 mmol) was added. The resulting mixture was stirred for 20 h at rt. Afterwards, the reaction was diluted with EtOAc, filtered over a short plug of silica, the solvent was removed under vacuum, and crude ¹H NMR and HPLC were measured. ^bNMR yield with 1,1,2,2-tetrachloroethane as internal standard. ^cDetermined by HPLC analysis on a chiral stationary phase.

Experimental Part

Table 24: Survey of Temperature and Catalyst Loading.^a

Entry	<i>T</i> (°C)	Catalyst Loading (mol%)	Yield (%) ^b	ee (%) ^c
1	25	2	99	85
2	4	2	99	90
3	-5	2	92	90
4	-20	2	70	71
5	4	1	99	90
6	4	0.5	55	89

^aReaction conditions: Following **GP M**, catalyst **191a** (0.5–2 mol%) was dissolved in MeOH (0.2 M, 0.25 mL) at the indicated temperature and isoxazole **164a** (0.05 mmol) was added. The resulting mixture was stirred for 20 h at the stated temperature. Afterwards, the reaction was diluted with EtOAc, filtered over a short plug of silica, the solvent was removed under vacuum, and crude ¹H NMR and HPLC were measured. When conversion was not complete, the crude mixture was submitted to column chromatography on silica gel (*n*-pentane/EtOAc 10:1) to obtain pure 2*H*-azirine **200a** for HPLC analysis. ^bNMR yield with 1,1,2,2-tetrachloroethane as internal standard. ^cDetermined by HPLC analysis on a chiral stationary phase.

Table 25: Control Reactions.^a

Entry	Variations from Standard Procedure	Yield (%) ^b	ee (%) ^c
1	none	99	90
2	under air	99	90
3	with 10 eq. H ₂ O	99	90
4	technical grade MeOH	99	90
5	FeCl ₂ · 4 H ₂ O as catalyst	40	–

^aReaction conditions: Following **GP M**, catalyst **191a** (1 mol%) was dissolved in MeOH (0.2 M, 0.25 mL) at 4 °C and isoxazole **164a** (0.05 mmol) was added. The resulting mixture was stirred for 20 h at 4 °C. Afterwards, the reaction was diluted with EtOAc, filtered over a short plug of silica, the solvent was removed under vacuum, and crude ¹H NMR and HPLC were measured. ^bNMR yield with 1,1,2,2-tetrachloroethane as internal standard. ^cDetermined by HPLC analysis on a chiral stationary phase.

Experimental Part

Table 26: Survey for *in situ* Catalyst Formation.^a

Entry	Fe-Precursor (mol% Fe/mol% ligand 189a)	Yield (%) ^b	ee (%) ^c
1	FeCl ₂ · 4 H ₂ O (2/3)	99	80
2	FeCl ₂ (2/3)	99	83
3	FeBr ₂ (2/3)	99	79
4	FeCl ₂ (2/2)	97	84
5	FeCl ₂ (2/4)	99	85
6	FeCl ₂ (2/6)	99	86
7	FeCl ₂ (2/8)	99	85
8	FeCl₂ (5/6)	99	87
9	FeCl ₂ (3/2)	99	85

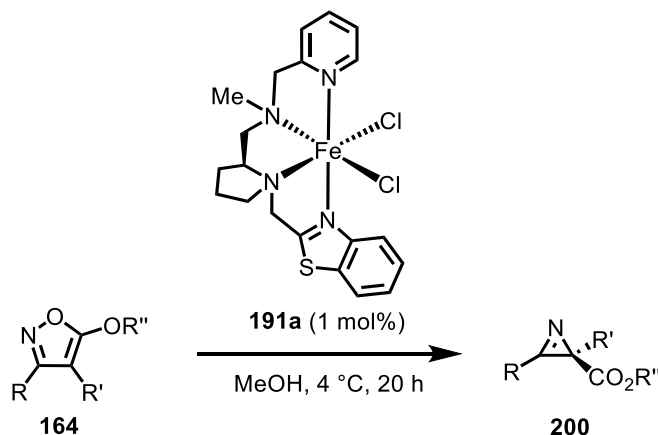
^aReaction conditions: The indicated Fe-salt and ligand **189a** were dissolved in MeOH (0.2 M, 0.25 mL) at 4 °C, prestirred for 5 min, and isoxazole **164a** (0.05 mmol) was added. The resulting mixture was stirred for 20 h at 4 °C. Afterwards, the reaction was diluted with EtOAc, filtered over a short plug of silica, the solvent was removed under vacuum, and crude ¹H NMR and HPLC were measured. ^bNMR yield with 1,1,2,2-tetrachloroethane as internal standard. ^cDetermined by HPLC analysis on a chiral stationary phase.

Table 27: Concluding Catalyst Screening.^a

Entry	Catalyst (1 mol%)	Yield (%) ^b	ee (%) ^c
1	191a	99	90
2	191b	75	69
3	191c	30	76
4	191d	64	7
5	191e	18	12
6	191f	66	55
7	191g	99	69
8	191h	48	58
9	191i	85	73

^aReaction conditions: Following **GP M**, catalyst **191** (1 mol%) was dissolved in MeOH (0.2 M, 0.25 mL) at 4 °C and isoxazole **164a** (0.05 mmol) was added. The resulting mixture was stirred for 20 h at 4 °C. Afterwards, the reaction was diluted with EtOAc, filtered over a short plug of silica, the solvent was removed under vacuum, and crude ¹H NMR and HPLC were measured. When conversion was not complete, the crude mixture was submitted to column chromatography on silica gel (*n*-pentane/EtOAc 10:1) to obtain pure 2*H*-azirine **200** for HPLC analysis. ^bNMR yield with 1,1,2,2-tetrachloroethane as internal standard. ^cDetermined by HPLC analysis on a chiral stationary phase.

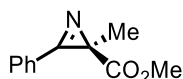
General Procedure N: Asymmetric Ring Contraction with Pentadentate Catalyst **191a under Optimized Conditions (GP N)**



A vial was charged with Fe(II)-catalyst **191a** (1 mol%) and MeOH (0.50 mL, 0.2 M) under air. The solution was cooled to 4 °C, isoxazole **164** (0.10 mmol, 1.00 eq.) was added, and the reaction mixture was stirred for 20 h at 4 °C. Afterwards, the mixture was diluted with EtOAc and filtered over a short plug of silica gel to remove the catalyst. The crude product was subsequently purified by column chromatography on silica gel (*n*-pentane/EtOAc) to obtain pure 2*H*-azirines **200**.

The absolute configuration of the products was determined by comparison of the HPLC traces and optical rotation values with the literature.^[174,180]

Methyl (*R*)-2-methyl-3-phenyl-2*H*-azirine-2-carboxylate (200a**)**



Following **GP N**, compound **200a** (18.7 mg, 0.10 mmol, 99%) was obtained as a colorless oil after column chromatography on silica gel (*n*-pentane/EtOAc 10:1). Enantiomeric excess was established by HPLC analysis on a chiral stationary phase: ee = 90%, HPLC conditions: Daicel Chiralcel[®] OJ-H column, 250 x 4.6 mm, absorbance at 254 nm, *n*-hexane/*i*PrOH 80:20, isocratic flow, flow rate 1.0 mL/min, 25 °C, *t_r* (minor) = 9.1 min, *t_r* (major) = 12.1 min.

TLC: *R_f* = 0.36 (*n*-pentane/EtOAc 5:1).

¹H NMR: (300 MHz, CDCl₃) δ = 7.84 (d, *J* = 7.4 Hz, 2H), 7.66–7.54 (m, 3H), 3.68 (s, 3H), 1.63 (s, 3H) ppm.

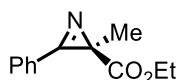
¹³C NMR: (75 MHz, CDCl₃) δ = 173.7, 163.7, 133.8, 130.3 (2C), 129.5 (2C), 122.7, 52.6, 35.6, 17.9 ppm.

Experimental Part

$[\alpha]_D^{22}$: -114.3° ($c = 1.0$, CH_2Cl_2).

Analytical data were consistent with reported data.^[174]

Ethyl (*R*)-2-methyl-3-phenyl-2*H*-azirine-2-carboxylate (**200b**)



Following **GP N**, compound **200b** (19.6 mg, 0.10 mmol, 98%) was obtained as a colorless oil after column chromatography on silica gel (*n*-pentane/EtOAc 10:1). Enantiomeric excess was established by HPLC analysis on a chiral stationary phase: ee = 88%, HPLC conditions: Daicel Chiralcel[®] OJ-H column, 250 x 4.6 mm, absorbance at 254 nm, *n*-hexane/*i*PrOH 80:20, isocratic flow, flow rate 1.0 mL/min, 25 °C, t_r (minor) = 6.4 min, t_r (major) = 9.0 min.

TLC: $R_f = 0.45$ (*n*-pentane/EtOAc 5:1).

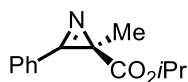
¹H NMR: (300 MHz, CDCl_3) $\delta = 7.86\text{--}7.81$ (m, 2H), 7.66–7.53 (m, 3H), 4.15 (q, $J = 7.1$ Hz, 2H), 1.62 (s, 3H), 1.20 (t, $J = 7.1$ Hz, 3H) ppm.

¹³C NMR: (75 MHz, CDCl_3) $\delta = 173.2$, 163.8, 133.7, 130.2 (2C), 129.5 (2C), 122.8, 61.5, 35.7, 17.9, 14.3 ppm.

$[\alpha]_D^{22}$: -135.6° ($c = 1.0$, CH_2Cl_2).

Analytical data were consistent with reported data.^[174]

Isopropyl (*R*)-2-methyl-3-phenyl-2*H*-azirine-2-carboxylate (**200c**)



Following **GP N**, compound **200c** (18.2 mg, 0.08 mmol, 84%) was obtained as a colorless solid after column chromatography on silica gel (*n*-pentane/EtOAc 20:1). Enantiomeric excess was established by HPLC analysis on a chiral stationary phase: ee = 86%, HPLC conditions: Daicel Chiralcel[®] OJ-H column, 250 x 4.6 mm, absorbance at 254 nm, *n*-hexane/*i*PrOH 92:8, isocratic flow, flow rate 1.0 mL/min, 25 °C, t_r (minor) = 6.1 min, t_r (major) = 7.6 min.

TLC: $R_f = 0.58$ (*n*-pentane/EtOAc 5:1).

¹H NMR: (300 MHz, CDCl_3) $\delta = 7.86\text{--}7.80$ (m, 2H), 7.66–7.53 (m, 3H), 5.02 (sept, $J = 6.3$ Hz, 1H), 1.61 (s, 3H), 1.21 (d, $J = 6.3$ Hz, 3H), 1.16 (d, $J = 6.2$ Hz, 3H) ppm.

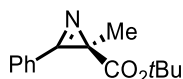
Experimental Part

¹³C NMR: (75 MHz, CDCl₃) δ = 172.8, 163.9, 133.6, 130.2 (2C), 129.4 (2C), 122.9, 69.0, 35.9, 21.9, 21.9, 17.9 ppm.

$[\alpha]_D^{22}$: -194.9° ($c = 1.0$, CH₂Cl₂).

Analytical data were consistent with reported data.^[180]

***tert*-Butyl (*R*)-2-methyl-3-phenyl-2*H*-azirine-2-carboxylate (**200d**)**



Following **GP N**, compound **200d** (8.1 mg, 0.04 mmol, 35%) was obtained as a colorless solid after column chromatography on silica gel (*n*-pentane/EtOAc 30:1). Enantiomeric excess was established by HPLC analysis on a chiral stationary phase: ee = 90%, HPLC conditions: Daicel Chiralcel[®] OJ-H column, 250 x 4.6 mm, absorbance at 254 nm, *n*-hexane/*i*PrOH 97:3, isocratic flow, flow rate 1.0 mL/min, 25 °C, t_r (minor) = 6.2 min, t_r (major) = 7.0 min.

TLC: $R_f = 0.17$ (*n*-pentane/EtOAc 20:1).

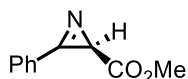
¹H NMR: (300 MHz, CDCl₃) δ = 7.86–7.79 (m, 2H), 7.65–7.53 (m, 3H), 1.58 (s, 3H), 1.41 (s, 9H) ppm.

¹³C NMR: (75 MHz, CDCl₃) δ = 172.5, 164.2, 133.5, 130.0 (2C), 129.4 (2C), 123.2, 81.4, 36.5, 28.1 (3C), 17.9 ppm.

$[\alpha]_D^{22}$: -54.1° ($c = 1.0$, CH₂Cl₂).

Analytical data were consistent with reported data.^[174]

Methyl (*R*)-3-phenyl-2*H*-azirine-2-carboxylate (200e**)**



Following **GP N**, compound **200e** (6.3 mg, 0.04 mmol, 36%) was obtained as a colorless oil after column chromatography on silica gel (*n*-pentane/EtOAc 10:1). Enantiomeric excess was established by HPLC analysis on a chiral stationary phase: ee = 61%, HPLC conditions: Daicel Chiralcel[®] OJ-H column, 250 x 4.6 mm, absorbance at 254 nm, *n*-hexane/*i*PrOH 80:20, isocratic flow, flow rate 1.0 mL/min, 25 °C, t_r (minor) = 10.3 min, t_r (major) = 13.6 min.

TLC: $R_f = 0.51$ (*n*-pentane/EtOAc 5:1).

Experimental Part

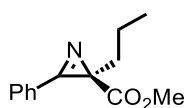
¹H NMR: (300 MHz, CDCl₃) δ = 7.92-7.85 (m, 2H), 7.68-7.54 (m, 3H), 3.74 (s, 3H), 2.86 (s, 1H) ppm.

¹³C NMR: (75 MHz, CDCl₃) δ = 172.2, 158.7, 134.1, 130.6 (2C), 129.5 (2C), 122.4, 52.4, 29.6 ppm.

$[\alpha]_D^{22}$: -101.5° ($c = 1.0$, CH₂Cl₂).

Analytical data were consistent with reported data.^[275]

Methyl (*R*)-3-phenyl-2-propyl-2*H*-azirine-2-carboxylate (**200f**)



Following **GP N**, compound **200f** (21.7 mg, 0.10 mmol, 99%) was obtained as a colorless solid after column chromatography on silica gel (*n*-pentane/EtOAc 10:1). Enantiomeric excess was established by HPLC analysis on a chiral stationary phase: ee = 87%, HPLC conditions: Daicel Chiralcel[®] OJ-H column, 250 x 4.6 mm, absorbance at 254 nm, *n*-hexane/*i*PrOH 90:10, isocratic flow, flow rate 1.0 mL/min, 25 °C, t_r (minor) = 6.7 min, t_r (major) = 8.3 min.

TLC: $R_f = 0.51$ (*n*-pentane/EtOAc 5:1).

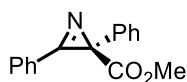
¹H NMR: (300 MHz, CDCl₃) δ = 7.85 (d, $J = 7.8$ Hz, 2H), 7.65–7.52 (m, 3H), 3.66 (s, 3H), 2.14–1.96 (m, 2H), 1.35–1.22 (m, 2H), 0.89 (t, $J = 7.3$ Hz, 3H) ppm.

¹³C NMR: (75 MHz, CDCl₃) δ = 173.4, 163.1, 133.7, 130.2 (2C), 129.4 (2C), 123.2, 52.5, 39.8, 32.9, 19.7, 14.1 ppm.

$[\alpha]_D^{22}$: -123.3° ($c = 1.0$, CH₂Cl₂).

Analytical data were consistent with reported data.^[180]

Methyl (*R*)-2,3-diphenyl-2*H*-azirine-2-carboxylate (**200g**)



Following **GP N**, compound **200g** (19.0 mg, 0.08 mmol, 76%) was obtained as a colorless solid after column chromatography on silica gel (*n*-pentane/EtOAc 10:1). Enantiomeric excess was established by HPLC analysis on a chiral stationary phase: ee = 89%, HPLC conditions: Daicel Chiralcel[®] OJ-H

Experimental Part

column, 250 x 4.6 mm, absorbance at 254 nm, *n*-hexane/*i*PrOH 80:20, isocratic flow, flow rate 1.0 mL/min, 25 °C, t_r (minor) = 18.4 min, t_r (major) = 23.6 min.

TLC: R_f = 0.34 (*n*-pentane/EtOAc 5:1).

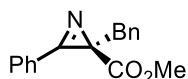
^1H NMR: (300 MHz, CDCl_3) δ = 7.92 (d, J = 7.9 Hz, 2H), 7.67–7.53 (m, 3H), 7.49 (d, J = 7.4 Hz, 2H), 7.35–7.23 (m, 3H), 3.74 (s, 3H) ppm.

^{13}C NMR: (75 MHz, CDCl_3) δ = 171.8, 160.9, 136.3, 134.0, 130.6 (2C), 129.6 (2C), 128.4 (2C), 128.3 (2C), 127.9, 122.2, 52.8, 41.2 ppm.

$[\alpha]_D^{22}$: +74.1° (c = 1.0, CH_2Cl_2).

Analytical data were consistent with reported data.^[180]

Methyl (*R*)-2-benzyl-3-phenyl-2*H*-azirine-2-carboxylate (**200h**)



Following **GP N**, compound **200h** (25.5 mg, 0.10 mmol, 96%) was obtained as a colorless oil after column chromatography on silica gel (*n*-pentane/EtOAc 10:1). Enantiomeric excess was established by HPLC analysis on a chiral stationary phase: ee = 83%, HPLC conditions: Daicel Chiralcel[®] OJ-H column, 250 x 4.6 mm, absorbance at 254 nm, *n*-hexane/*i*PrOH 80:20, isocratic flow, flow rate 1.0 mL/min, 25 °C, t_r (minor) = 14.2 min, t_r (major) = 21.8 min.

TLC: R_f = 0.47 (*n*-pentane/EtOAc 5:1).

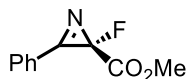
^1H NMR: (300 MHz, CDCl_3) δ = 7.60 (d, J = 7.7 Hz, 2H), 7.54 (d, J = 7.0 Hz, 1H), 7.45 (t, J = 7.2 Hz, 2H), 7.21–7.13 (m, 5H), 3.68 (s, 3H), 3.68 (d, J = 14.5 Hz, 1H), 3.13 (d, J = 14.7 Hz, 1H) ppm.

^{13}C NMR: (75 MHz, CDCl_3) δ = 173.1, 162.6, 137.7, 133.6, 130.3 (2C), 129.9 (2C), 129.2 (2C), 128.5 (2C), 126.6, 122.8, 52.7, 40.7, 37.8 ppm.

$[\alpha]_D^{22}$: –48.3° (c = 1.0, CH_2Cl_2).

Analytical data were consistent with reported data.^[174]

Methyl (S)-2-fluoro-3-phenyl-2H-azirine-2-carboxylate (200i)



Following **GP N**, compound **200i** (19.0 mg, 0.10 mmol, 98%) was obtained as a colorless oil after column chromatography on silica gel (*n*-pentane/EtOAc 10:1). Enantiomeric excess was established by HPLC analysis on a chiral stationary phase: ee = 70%, HPLC conditions: Daicel Chiralcel[®] OJ-H column, 250 x 4.6 mm, absorbance at 254 nm, *n*-hexane/*i*PrOH 80:20, isocratic flow, flow rate 1.0 mL/min, 25 °C, *t_r* (minor) = 11.0 min, *t_r* (major) = 23.7 min.

TLC: $R_f = 0.36$ (*n*-pentane/EtOAc 5:1).

¹H NMR: (300 MHz, CDCl₃) $\delta = 7.96$ (d, $J = 7.2$ Hz, 2H), 7.77–7.68 (m, 1H), 7.66–7.59 (m, 2H), 3.86 (s, 3H) ppm.

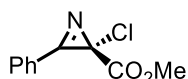
¹³C NMR: (75 MHz, CDCl₃) $\delta = 67.2$ (d, $J = 43.5$ Hz), 166.2 (d, $J = 11.4$ Hz), 135.2, 130.9 (2C), 129.8 (2C), 120.4, 78.2 (d, $J = 264.1$ Hz), 53.5 ppm.

¹⁹F NMR: (282 MHz, CDCl₃) $\delta = -155.20$ ppm.

$[\alpha]_D^{22}$: -144.7° ($c = 1.0$, CH₂Cl₂).

Analytical data were consistent with reported data.^[180]

Methyl (S)-2-chloro-3-phenyl-2H-azirine-2-carboxylate (200j)



Following **GP N**, compound **200j** (20.6 mg, 0.10 mmol, 98%) was obtained as a pale-yellow oil after column chromatography on silica gel (*n*-pentane/EtOAc 10:1). Enantiomeric excess was established by HPLC analysis on a chiral stationary phase: ee = 85%, HPLC conditions: Daicel Chiralcel[®] OJ-H column, 250 x 4.6 mm, absorbance at 254 nm, *n*-hexane/*i*PrOH 80:20, isocratic flow, flow rate 1.0 mL/min, 25 °C, *t_r* (minor) = 11.3 min, *t_r* (major) = 21.0 min.

TLC: $R_f = 0.40$ (*n*-pentane/EtOAc 5:1).

¹H NMR: (300 MHz, CDCl₃) $\delta = 7.98$ -7.92 (m, 2H), 7.73 (td, $J = 7.4, 1.4$ Hz, 1H), 7.66-7.60 (m, 2H), 3.82 (s, 3H) ppm.

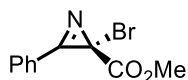
¹³C NMR: (75 MHz, CDCl₃) $\delta = 168.0, 163.8, 135.2, 131.0$ (2C), 129.8 (2C), 119.9, 54.1, 54.0 ppm.

$[\alpha]_D^{22}$: $+22.9^\circ$ ($c = 1.0$, CH₂Cl₂).

Experimental Part

Analytical data were consistent with reported data.^[180]

Methyl (*S*)-2-bromo-3-phenyl-2*H*-azirine-2-carboxylate (**200k**)



Following **GP N**, compound **200k** (12.8 mg, 0.05 mmol, 50%) was obtained as a yellow oil after column chromatography on silica gel (*n*-pentane/EtOAc 10:1). Enantiomeric excess was established by HPLC analysis on a chiral stationary phase: ee = 78%, HPLC conditions: Daicel Chiralcel[®] OJ-H column, 250 x 4.6 mm, absorbance at 254 nm, *n*-hexane/*i*PrOH 80:20, isocratic flow, flow rate 1.0 mL/min, 25 °C, *t_r* (minor) = 13.3 min, *t_r* (major) = 22.8 min.

TLC: $R_f = 0.38$ (*n*-pentane/EtOAc 5:1).

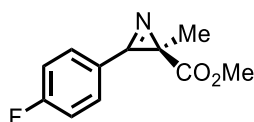
¹H NMR: (300 MHz, CDCl₃) $\delta = 7.99\text{--}7.93$ (m, 2H), 7.74 (td, $J = 7.4, 1.4$ Hz, 1H), 7.67–7.60 (m, 2H), 3.81 (s, 3H) ppm.

¹³C NMR: (75 MHz, CDCl₃) $\delta = 167.4, 164.6, 135.3, 131.1$ (2C), 129.8 (2C), 119.9, 54.3, 43.9 ppm.

$[\alpha]_D^{22}$: +20.4° ($c = 1.0$, CH₂Cl₂).

Analytical data were consistent with reported data.^[180]

Methyl (*R*)-3-(4-fluorophenyl)-2-methyl-2*H*-azirine-2-carboxylate (**200l**)



Following **GP N**, compound **200l** (20.3 mg, 0.10 mmol, 98%) was obtained as a yellow oil after column chromatography on silica gel (*n*-pentane/EtOAc 10:1). Enantiomeric excess was established by HPLC analysis on a chiral stationary phase: ee = 91%, HPLC conditions: Daicel Chiralcel[®] OJ-H column, 250 x 4.6 mm, absorbance at 254 nm, *n*-hexane/*i*PrOH 80:20, isocratic flow, flow rate 1.0 mL/min, 25 °C, *t_r* (minor) = 7.8 min, *t_r* (major) = 11.1 min.

TLC: $R_f = 0.37$ (*n*-pentane/EtOAc 5:1).

¹H NMR: (300 MHz, CDCl₃) $\delta = 7.89\text{--}7.82$ (m, 2H), 7.27 (t, $J = 8.5$ Hz, 2H), 3.68 (s, 3H), 1.62 (s, 3H) ppm.

Experimental Part

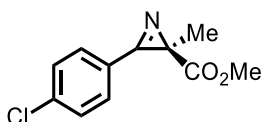
¹³C NMR: (75 MHz, CDCl₃) δ = 173.5, 166.0 (d, J = 256.5 Hz), 162.8, 132.7 (d, J = 9.4 Hz, 2C), 119.1 (d, J = 3.2 Hz), 117.1 (d, J = 22.5 Hz, 2C), 52.7, 35.7, 17.8 ppm.

¹⁹F NMR: (282 MHz, CDCl₃) δ = -103.0 ppm.

$[\alpha]_D^{22}$: -141.3° (c = 1.0, CH₂Cl₂).

Analytical data were consistent with reported data.^[174]

Methyl (*R*)-3-(4-chlorophenyl)-2-methyl-2*H*-azirine-2-carboxylate (**200m**)



Following **GP N**, compound **200m** (22.0 mg, 0.10 mmol, 98%) was obtained as a colorless oil after column chromatography on silica gel (*n*-pentane/EtOAc 10:1). Enantiomeric excess was established by HPLC analysis on a chiral stationary phase: ee = 92%, HPLC conditions: Daicel Chiralcel[®] OJ-H column, 250 x 4.6 mm, absorbance at 254 nm, *n*-hexane/*i*PrOH 80:20, isocratic flow, flow rate 1.0 mL/min, 25 °C, t_r (minor) = 7.1 min, t_r (major) = 9.7 min.

TLC: R_f = 0.50 (*n*-pentane/EtOAc 5:1).

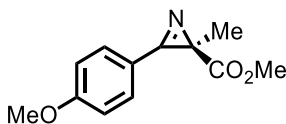
¹H NMR: (300 MHz, CDCl₃) δ = 7.78 (d, J = 8.4 Hz, 2H), 7.55 (d, J = 8.3 Hz, 2H), 3.68 (s, 3H), 1.62 (s, 3H) ppm.

¹³C NMR: (75 MHz, CDCl₃) δ = 173.4, 163.1, 140.2, 131.4 (2C), 130.0 (2C), 121.2, 52.7, 35.8, 17.8 ppm.

$[\alpha]_D^{22}$: -165.9° (c = 1.0, CH₂Cl₂).

Analytical data were consistent with reported data.^[174]

Methyl (*R*)-3-(4-methoxyphenyl)-2-methyl-2*H*-azirine-2-carboxylate (**200n**)



Following **GP N**, compound **200n** (21.2 mg, 0.10 mmol, 97%) was obtained as a colorless solid after column chromatography on silica gel (*n*-pentane/EtOAc 5:1). Enantiomeric excess was established by HPLC analysis on a chiral stationary phase: ee = 92%, HPLC conditions: Daicel Chiralcel[®] OJ-H

Experimental Part

column, 250 x 4.6 mm, absorbance at 254 nm, *n*-hexane/*i*PrOH 80:20, isocratic flow, flow rate 1.0 mL/min, 25 °C, t_r (minor) = 12.2 min, t_r (major) = 16.7 min.

TLC: R_f = 0.20 (*n*-pentane/EtOAc 5:1).

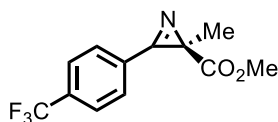
^1H NMR: (300 MHz, CDCl_3) δ = 7.78 (d, J = 8.8 Hz, 2H), 7.05 (d, J = 8.8 Hz, 2H), 3.89 (s, 3H), 3.67 (s, 3H), 1.60 (s, 3H) ppm.

^{13}C NMR: (75 MHz, CDCl_3) δ = 174.0, 164.0, 162.3, 132.3 (2C), 115.0 (2C), 114.9, 55.7, 52.5, 35.1, 17.9 ppm.

$[\alpha]_D^{22}$: -170.1° (c = 1.0, CH_2Cl_2).

Analytical data were consistent with reported data.^[174]

Methyl (*R*)-2-methyl-3-(4-(trifluoromethyl)phenyl)-2*H*-azirine-2-carboxylate (**200o**)



Following **GP N**, compound **200o** (25.5 mg, 0.10 mmol, 99%) was obtained as a colorless solid after column chromatography on silica gel (*n*-pentane/EtOAc 10:1). Enantiomeric excess was established by HPLC analysis on a chiral stationary phase: ee = 92%, HPLC conditions: Daicel Chiralcel[®] OJ-H column, 250 x 4.6 mm, absorbance at 254 nm, *n*-hexane/*i*PrOH 80:20, isocratic flow, flow rate 1.0 mL/min, 25 °C, t_r (minor) = 5.7 min, t_r (major) = 6.7 min.

TLC: R_f = 0.54 (*n*-pentane/EtOAc 5:1).

^1H NMR: (300 MHz, CDCl_3) δ = 7.97 (d, J = 8.1 Hz, 2H), 7.84 (d, J = 8.2 Hz, 2H), 3.70 (s, 3H), 1.65 (s, 3H) ppm.

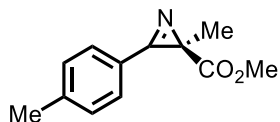
^{13}C NMR: (75 MHz, CDCl_3) δ = 173.1, 163.8, 135.2 (q, J = 33.1 Hz), 130.5 (2C), 126.5 (q, J = 3.7 Hz, 2C), 126.1, 123.5 (q, J = 273.2 Hz, signal almost not visible due to background noise), 52.8, 36.3, 17.8 ppm.

^{19}F NMR: (282 MHz, CDCl_3) δ = -63.3 ppm.

$[\alpha]_D^{22}$: -94.0° (c = 1.0, CH_2Cl_2).

Analytical data were consistent with reported data.^[174]

Methyl (*R*)-2-methyl-3-(*p*-tolyl)-2*H*-azirine-2-carboxylate (200p**)**



Following **GP N**, compound **200p** (19.7 mg, 0.10 mmol, 97%) was obtained as a colorless solid after column chromatography on silica gel (*n*-pentane/EtOAc 10:1). Enantiomeric excess was established by HPLC analysis on a chiral stationary phase: ee = 92%, HPLC conditions: Daicel Chiralcel[®] OJ-H column, 250 x 4.6 mm, absorbance at 254 nm, *n*-hexane/*i*PrOH 80:20, isocratic flow, flow rate 1.0 mL/min, 25 °C, *t_r* (minor) = 7.9 min, *t_r* (major) = 12.1 min.

TLC: $R_f = 0.40$ (*n*-pentane/EtOAc 5:1).

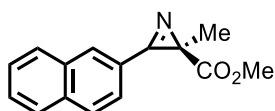
¹H NMR: (300 MHz, CDCl₃) $\delta = 7.73$ (d, $J = 8.0$ Hz, 2H), 7.37 (d, $J = 7.9$ Hz, 2H), 3.67 (s, 3H), 2.45 (s, 3H), 1.61 (s, 3H) ppm.

¹³C NMR: (75 MHz, CDCl₃) $\delta = 173.8$, 163.2, 144.8, 130.3 (2C), 130.2 (2C), 119.8, 52.5, 35.2, 22.0, 17.9 ppm.

$[\alpha]_D^{22}$: -144.8° ($c = 1.0$, CH₂Cl₂).

Analytical data are consistent with the data described in Chapter 5.5.2.

Methyl (*R*)-2-methyl-3-(naphthalen-2-yl)-2*H*-azirine-2-carboxylate (200q**)**



Following **GP N**, compound **200q** (23.7 mg, 0.10 mmol, 99%) was obtained as a colorless solid after column chromatography on silica gel (*n*-pentane/EtOAc 10:1). Enantiomeric excess was established by HPLC analysis on a chiral stationary phase: ee = 90%, HPLC conditions: Daicel Chiralcel[®] OD-H column, 250 x 4.6 mm, absorbance at 254 nm, *n*-hexane/*i*PrOH 99:1, isocratic flow, flow rate 1.0 mL/min, 25 °C, *t_r* (minor) = 17.7 min, *t_r* (major) = 20.9 min.

TLC: $R_f = 0.35$ (*n*-pentane/EtOAc 5:1).

¹H NMR: (300 MHz, CDCl₃) $\delta = 8.25$ (s, 1H), 8.05–7.88 (m, 4H), 7.70–7.55 (m, 2H), 3.70 (s, 3H), 1.70 (s, 3H) ppm.

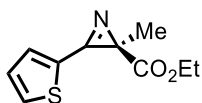
¹³C NMR: (75 MHz, CDCl₃) $\delta = 173.8$, 163.8, 135.9, 132.9, 132.4, 129.6, 129.3, 129.1, 128.3, 127.5, 124.9, 120.0, 52.6, 35.8, 18.0 ppm.

$[\alpha]_D^{22}$: -140.5° ($c = 1.0$, CH₂Cl₂).

Experimental Part

Analytical data were consistent with reported data.^[174]

Ethyl (*R*)-2-methyl-3-(thiophen-2-yl)-2*H*-azirine-2-carboxylate (**200r**)



Following **GP N**, compound **200r** (16.9 mg, 0.08 mmol, 80%) was obtained as a colorless solid after column chromatography on silica gel (*n*-pentane/EtOAc 15:1). Enantiomeric excess was established by HPLC analysis on a chiral stationary phase: ee = 73%, HPLC conditions: Daicel Chiralcel[®] OJ-H column, 250 x 4.6 mm, absorbance at 254 nm, *n*-hexane/*i*PrOH 80:20, isocratic flow, flow rate 1.0 mL/min, 25 °C, *t_r* (minor) = 7.9 min, *t_r* (major) = 12.8 min.

TLC: $R_f = 0.47$ (*n*-pentane/EtOAc 5:1).

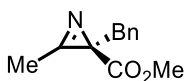
¹H NMR: (300 MHz, CDCl₃) $\delta = 7.97$ (dd, $J = 3.0, 1.0$ Hz, 1H), 7.59 (dd, $J = 5.2, 1.1$ Hz, 1H), 7.51 (dd, $J = 5.1, 2.9$ Hz, 1H), 4.15 (q, $J = 7.1$ Hz, 2H), 1.59 (s, 3H), 1.21 (t, $J = 7.1$ Hz, 3H) ppm.

¹³C NMR: (75 MHz, CDCl₃) $\delta = 173.2, 158.2, 133.4, 128.1, 127.2, 124.7, 61.5, 35.2, 17.9, 14.3$ ppm.

$[\alpha]_D^{22}$: -165.3° ($c = 1.0, \text{CH}_2\text{Cl}_2$).

Analytical data were consistent with reported data.^[174]

Methyl (*R*)-2-methyl-3-phenyl-2*H*-azirine-2-carboxylate (**200s**)



Following **GP N**, compound **200s** (19.0 mg, 0.09 mmol, 94%) was obtained as a colorless oil after column chromatography on silica gel (*n*-pentane/EtOAc 10:1). Enantiomeric excess was established by HPLC analysis on a chiral stationary phase: ee = 36%, HPLC conditions: Daicel Chiralcel[®] OJ-H column, 250 x 4.6 mm, absorbance at 254 nm, *n*-hexane/*i*PrOH 85:15, isocratic flow, flow rate 1.0 mL/min, 25 °C, *t_r* (major) = 12.8 min, *t_r* (minor) = 13.8 min.

TLC: $R_f = 0.37$ (*n*-pentane/EtOAc 5:1).

¹H NMR: (300 MHz, CDCl₃) $\delta = 7.29$ -7.17 (m, 3H), 7.11 (d, $J = 7.5$ Hz, 2H), 3.69 (s, 3H), 3.61 (d, $J = 15.0$ Hz, 1H), 3.00 (d, $J = 14.9$ Hz, 1H), 2.19 (s, 3H) ppm.

Experimental Part

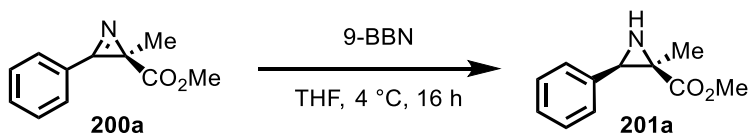
¹³C NMR: (75 MHz, CDCl₃) δ = 173.4, 163.1, 137.4, 129.8 (2C), 128.6 (2C), 126.6, 52.6, 38.8, 37.1, 12.4 ppm.

[α]_D²²: -17.0° (*c* = 1.0, CH₂Cl₂).

Analytical data were consistent with reported data.^[174]

5.5.4 Follow-Up Conversion of 2*H*-Azirines

Methyl (2*R*,3*R*)-2-methyl-3-phenylaziridine-2-carboxylate (**201a**)



A Schlenk flask was charged with azirine **200a** (75.0 mg, 0.40 mmol, 1.00 eq.) and THF (0.1 M) under inert gas atmosphere. The resulting solution was cooled to 0 °C and 9-BBN (0.5 M in THF, 1.19 mL, 0.60 mmol, 1.50 eq.) was added dropwise. Afterwards, the reaction was stirred for 16 h at 4 °C. Subsequently, the mixture was quenched with H₂O, diluted with CH₂Cl₂, layers were separated, and the aq. phase was extracted with CH₂Cl₂ (3x). The combined org. layers were washed with 2 M aq. NaOH-solution (3x) and brine, dried over Na₂SO₄, filtered, and the solvent was removed under reduced pressure. The crude product was purified by column chromatography on silica gel (*n*-pentane/EtOAc 5:1 → 3:1) to obtain pure aziridine **201a** (66.0 mg, 0.35 mmol, 87%) as a colorless oil and as a single diastereomer. Enantiomeric excess was established by HPLC analysis on a chiral stationary phase: ee = 90%, HPLC conditions: Daicel Chiralpak[®] IA column, 250 x 4.6 mm, absorbance at 220 nm, *n*-hexane/*i*PrOH 97:3, isocratic flow, flow rate 1.0 mL/min, 25 °C, *t_r* (major) = 14.2 min, *t_r* (minor) = 17.9 min.

TLC: *R_f* = 0.15 (*n*-pentane/EtOAc 5:1).

¹H NMR: (300 MHz, CDCl₃) δ = 7.34-7.25 (m, 5H), 3.48 (s, 3H), 3.23 (s, 1H), 1.67 (s, 3H) ppm.

¹³C NMR: (75 MHz, CDCl₃) δ = 171.4, 135.5, 128.2 (2C), 127.6, 127.3 (2C), 52.3, 47.7, 43.2, 20.5 ppm.

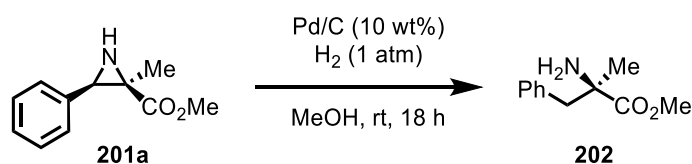
IR: (neat) $\tilde{\nu}$ = 3298 (w), 3030 (w), 2954 (w), 1726 (s), 1603 (w), 1498 (w), 1450 (m), 1339 (w), 1300 (w), 1259 (w), 1204 (s), 1166 (s), 1085 (m), 1015 (w), 976 (w), 918 (w), 878 (w), 843 (w), 806 (w), 775 (w), 737 (s), 696 (m), 609 (w), 571 (w), 533 (w) cm⁻¹.

HRMS: (ESI+) *m/z* calcd. for C₁₁H₁₄N₁O₂ [M+H]⁺ 192.1025, found 192.1017.

[α]_D²²: -2.9° (*c* = 1.0, CH₂Cl₂).

For determination of the relative configuration, *rac*-ethyl ester azirine **200b** was submitted to the same reduction procedure as described above to obtain aziridine **201b** (15.0 mg, 0.08 mmol, 70%) as a colorless oil and a single diastereomer. Comparison with this literature known compound indicates the formation of *cis*-isomer.^[276]

Methyl (*R*)-2-amino-2-methyl-3-phenylpropanoate (202)



A flask was charged with aziridine **201a** (20.0 mg, 0.11 mmol, 1.00 eq.), Pd on carbon (10 wt%, 11.1 mg, 0.10 mmol, 0.10 eq.), and MeOH (1.05 mL, 0.10 M). The vessel was put under hydrogen atmosphere (1 atm) and stirred vigorously for 20 h at rt. Afterwards, the mixture was filtered over Celite, the solvent was removed under reduced pressure, and the crude product dried under vacuum to obtain pure α -methyl phenylalanine derivative **202** (19.0 mg, 0.10 mmol, 94%) as a colorless solid. Enantiomeric excess was established by HPLC analysis on a chiral stationary phase: ee = 90%, HPLC conditions: Daicel Chiralcel[®] OD-H column, 250 x 4.6 mm, absorbance at 220 nm, *n*-hexane/*i*PrOH 95:5, isocratic flow, flow rate 1.0 mL/min, 25 °C, *t_r* (major) = 8.6 min, *t_r* (minor) = 10.4 min.

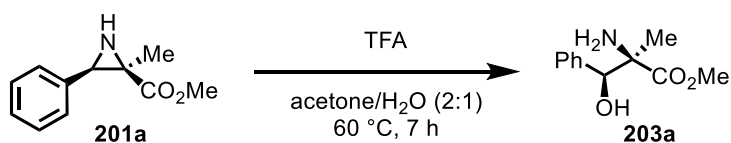
¹H NMR: (300 MHz, CDCl₃) δ = 7.32-7.22 (m, 3H), 7.14 (d, *J* = 7.1 Hz, 2H), 3.70 (s, 3H), 3.13 (d, *J* = 13.1 Hz, 1H), 2.80 (d, *J* = 13.2 Hz, 1H), 1.60 (br s, 2H), 1.39 (s, 3H) ppm.

¹³C NMR: (75 MHz, CDCl₃) δ = 177.7, 136.7, 130.1 (2C), 128.5 (2C), 127.1, 59.0, 52.2, 47.1, 26.8 ppm.

$[\alpha]_D^{22}$: +20.8° (*c* = 0.5, CH₃Cl).

Analytical data were consistent with reported data.^[277]

Methyl (2*R*,3*S*)-2-amino-3-hydroxy-2-methyl-3-phenylpropanoate (203a)



According to a modified procedure by Huang *et al.*,^[278] a round-bottom flask was charged with aziridine **201a** (20.0 mg, 0.11 mmol, 1.00 eq.) and acetone/H₂O (2:1 v/v, 1.05 mL, 0.1 M). The mixture was cooled to 0 °C and trifluoroacetic acid (8.1 μ L, 11.9 mg, 0.11 mmol, 1.00 eq.) was added slowly. Subsequently, the mixture was stirred at 60 °C for 7 h, after which the reaction was quenched with saturated aq. NaHCO₃-solution. The aq. layer was extracted using CH₂Cl₂ (3x), the combined organic layers were dried over Na₂SO₄, filtered, and the solvent was removed under reduced pressure. ¹H-NMR spectrum of the crude product was measured to determine the diastereomeric ratio

Experimental Part

(dr >20:1) and it was subsequently purified by column chromatography on silica gel (CH₂Cl₂/MeOH 20:1 → 10:1) to obtain compound **203a** (16.0 mg, 0.08 mmol, 73%) as a colorless oil. Enantiomeric excess was established by HPLC analysis on a chiral stationary phase: ee = 92%, HPLC conditions: Daicel Chiralcel[®] OJ-H column, 250 x 4.6 mm, absorbance at 220 nm, *n*-hexane/*i*PrOH 90:10, isocratic flow, flow rate 1.0 mL/min, 25 °C, *t_r* (major) = 17.9 min, *t_r* (minor) = 22.4 min.

TLC: *R_f* = 0.30 (CH₂Cl₂/MeOH 20:1).

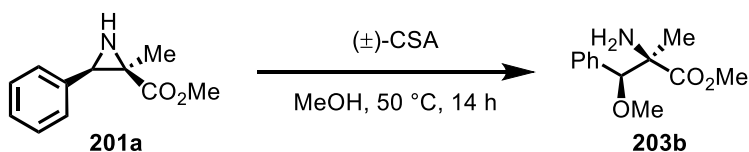
¹H NMR: (300 MHz, CDCl₃) δ = 7.37-7.27 (m, 5H), 4.89 (s, 1H), 3.77 (s, 3H), 1.91 (br s, 2H), 1.14 (s, 3H) ppm.

¹³C NMR: (75 MHz, CDCl₃) δ = 176.7, 139.3, 128.2, 128.1 (2C), 127.6 (2C), 77.6, 62.1, 52.7, 23.1 ppm.

[α]_D²²: -26.8° (*c* = 0.5, CH₂Cl₂).

Analytical data were consistent with reported data.^[243]

Methyl (2*R*,3*S*)-2-amino-3-methoxy-2-methyl-3-phenylpropanoate (**203b**)



According to a slightly modified procedure by Jat *et al.*,^[279] a Schlenk flask was charged with aziridine **201a** (21.0 mg, 0.11 mmol, 1.00 eq.) and MeOH (1.1 mL, 0.1 M) under inert gas atmosphere. The mixture was cooled to 0 °C and (±)-camphersulfonic acid (25.5 mg, 0.11 mmol, 1.00 eq.) was added while stirring. Afterwards, the mixture was stirred at 50 °C for 14 h. When TLC showed full conversion, the reaction was cooled to rt, diluted with H₂O and CH₂Cl₂, and the aq. layer was adjusted to pH = 8-9 by using 1 M aq. NaOH-solution. Layers were separated, the aq. phase was extracted with CH₂Cl₂ (3x), and the combined organic layers were washed with brine and dried over Na₂SO₄. After filtration, removal of the solvent under reduced pressure, and drying under vacuum, compound **203b** (23.0 mg, 0.10 mmol, 94%) was obtained as a colorless solid and a single diastereomer without further purification. Enantiomeric excess was established by HPLC analysis on a chiral stationary phase: ee = 91%, HPLC conditions: Daicel Chiralpak[®] IG column, 250 x 4.6 mm, absorbance at 220 nm, *n*-hexane/*i*PrOH 90:10, isocratic flow, flow rate 1.0 mL/min, 25 °C, *t_r* (major) = 12.9 min, *t_r* (minor) = 16.6 min.

Experimental Part

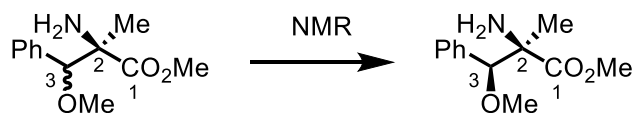
- ¹H NMR:** (300 MHz, CDCl₃) δ = 7.740-7.30 (m, 5H), 4.53 (s, 1H), 3.79 (s, 3H), 3.20 (s, 3H), 1.76 (br s, 2H), 1.07 (s, 3H) ppm.
- ¹³C NMR:** (75 MHz, CDCl₃) δ = 176.9, 136.3, 128.8 (2C), 128.4, 128.1 (2C), 84.8, 62.4, 57.4, 52.6, 23.5 ppm.
- IR:** (neat) $\tilde{\nu}$ = 3392 (w), 2985 (w), 2935 (w), 2825 (w), 1732 (m), 1600 (w), 1492 (w), 1450 (m), 1370 (w), 1229 (m), 1098 (s), 982 (w), 875 (w), 817 (w), 763 (m), 704 (s), 618 (w), 521 (w), 476 (w), 428 (w) cm⁻¹.
- HRMS:** (ESI+) *m/z* calcd. for C₁₂H₁₈N₁O₃ [M+H]⁺ 224.1281, found 224.1276.
- [α]_D²²:** +41.0° (*c* = 1.0, CH₂Cl₂).

Determination of Relative Configuration

Experimental: About 15 mg of the substance was dissolved in 0.60 mL of CDCl₃. Experiments were performed on a Bruker AVII 600 MHz spectrometer equipped with a 5 mm TBI probe with z-gradient. NOESY experiments were performed with mixing times of 0.5 s and 1.5 s. Furthermore, DQF-COSY, ¹H-¹³C HSQC and ¹H-¹³C HMBC spectra were recorded for an unambiguous signal assignment. The ¹H and ¹³C chemical shifts were referenced to the solvent signals at 7.24 ppm and 77.0 ppm, respectively. Spectra were processed with Bruker program package Topspin 4.0.8.

Results and Discussion: The proposed structure is shown in Scheme 74. Given the chirality at C-2 known, chirality at C-3 was identified by determining the relative configuration along C-2 and C-3 of the molecule. Since the molecular backbone contains just one methane group, there is no ³J_{HH} coupling constant available for the determination of torsion angles within the backbone of the molecule. Therefore, we have to rely just on the NOE contacts among the substituents. Fortunately, we observed clear pattern of NOE contacts, which led us to an unambiguous determination of the relative configuration along C-2 and C-3. Thus, at a mixing time of 1.5 s, Strong NOE contacts were observed between H-3 (4.50 ppm) and Me-2 (1.05 ppm), Ph^{ortho} (7.31-7.32 ppm) and Me-2 (1.05 ppm), Ph^{ortho} (7.31-7.32 ppm) and NH₂-2 (1.81 ppm), medium contact between OMe-3 (3.17) and COOMe-1 (3.76 ppm), whereas weak contact was observed between H-3 and NH₂-2. Further NOE contacts are medium between H-3 and OMe-3 and medium between Me-2 and COOMe-1. This pattern of NOE interactions among H-3, Ph^{ortho}, Me-2 and NH₂-2 confirmed a *syn* configuration between H-3 and Me-2. The key NOE contacts, which led to the determined stereo structure shown in Scheme 74, are presented in Table 28. The ¹H, ¹³C, NOESY, the ¹H-¹³C HSQC and HMBC spectra, with which the signal assignment was fulfilled, are shown in Figure 43–Figure 47.

Experimental Part



Scheme 74: Structure determination of **203b**.

Table 28: Key NOESY Cross Peaks Observed in CDCl₃.

No.	Positions	Strength	No.	Positions	Strength
1	H-3 – Me-2	strong	6	Me-2 – NH ₂ -2	strong
2	Ph ^{ortho} – Me-2	strong	7	Ph ^{ortho} – H-3	medium
3	Ph ^{ortho} – NH ₂ -2	strong	8	Ph ^{ortho} – OMe-3	medium
4	H-3 – NH ₂ -2	weak	9	H-3 – OMe-3	medium
5	COOMe-1 – OMe-3	medium	10	Me-2 – COOMe-1	medium

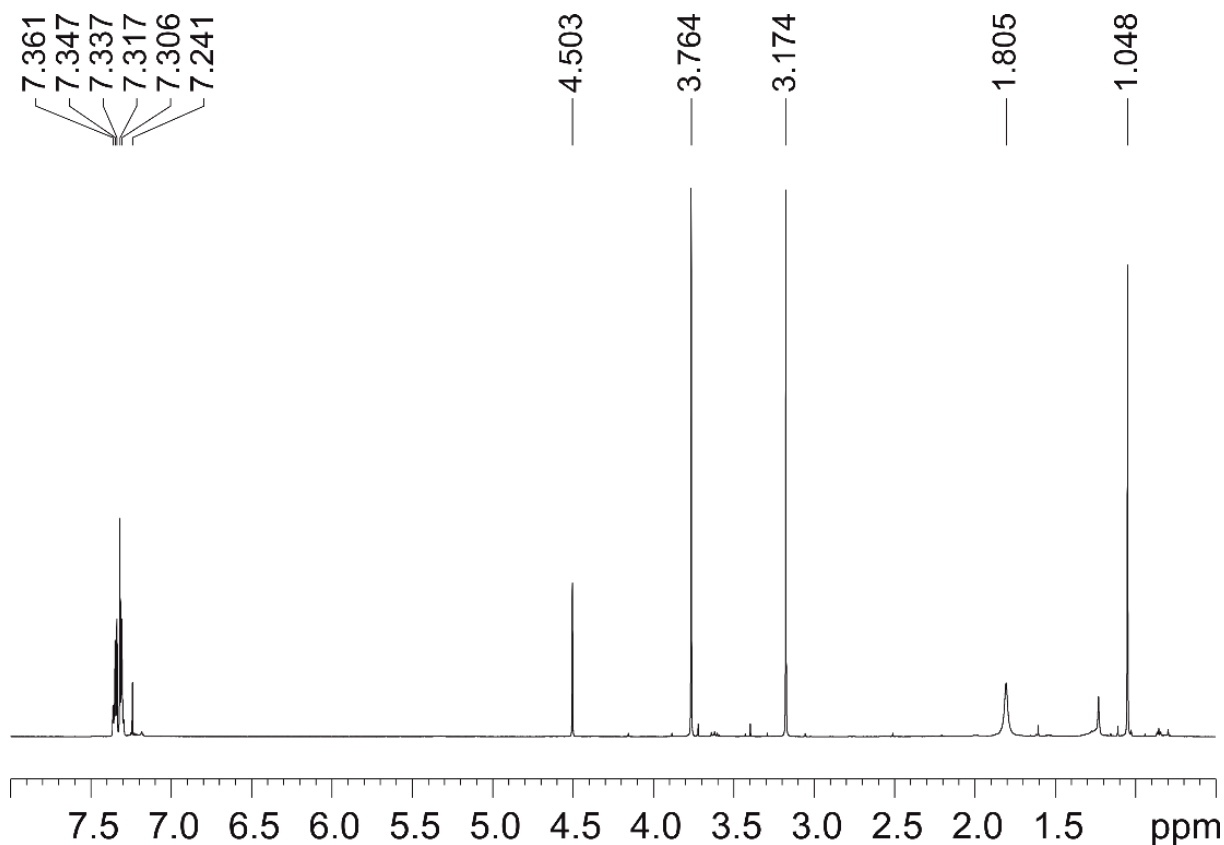


Figure 43: ¹H NMR-spectrum (600 MHz) of **203b** in CDCl₃.

Experimental Part

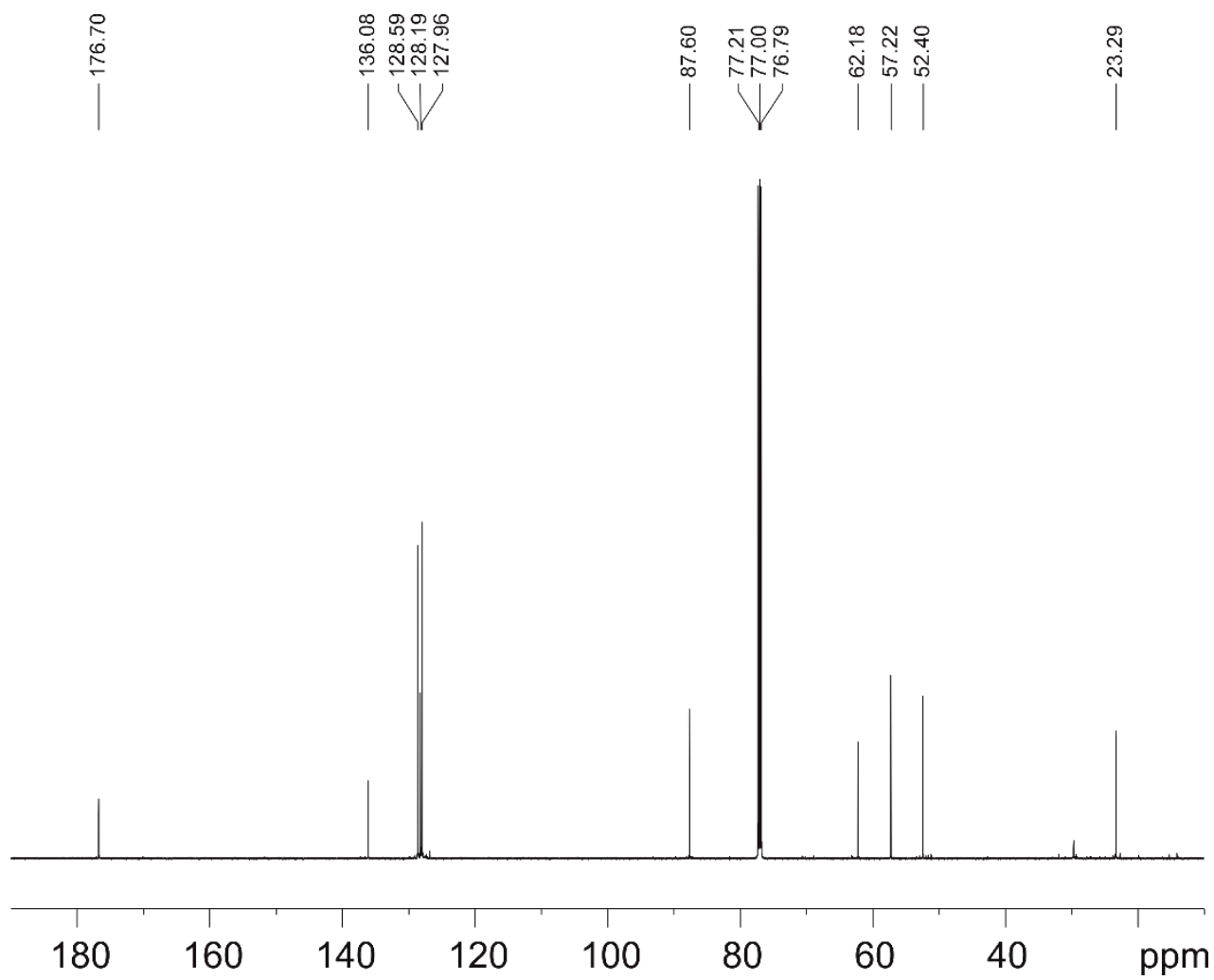


Figure 44: ^{13}C NMR-spectrum (150 MHz) of **203b** in CDCl_3 .

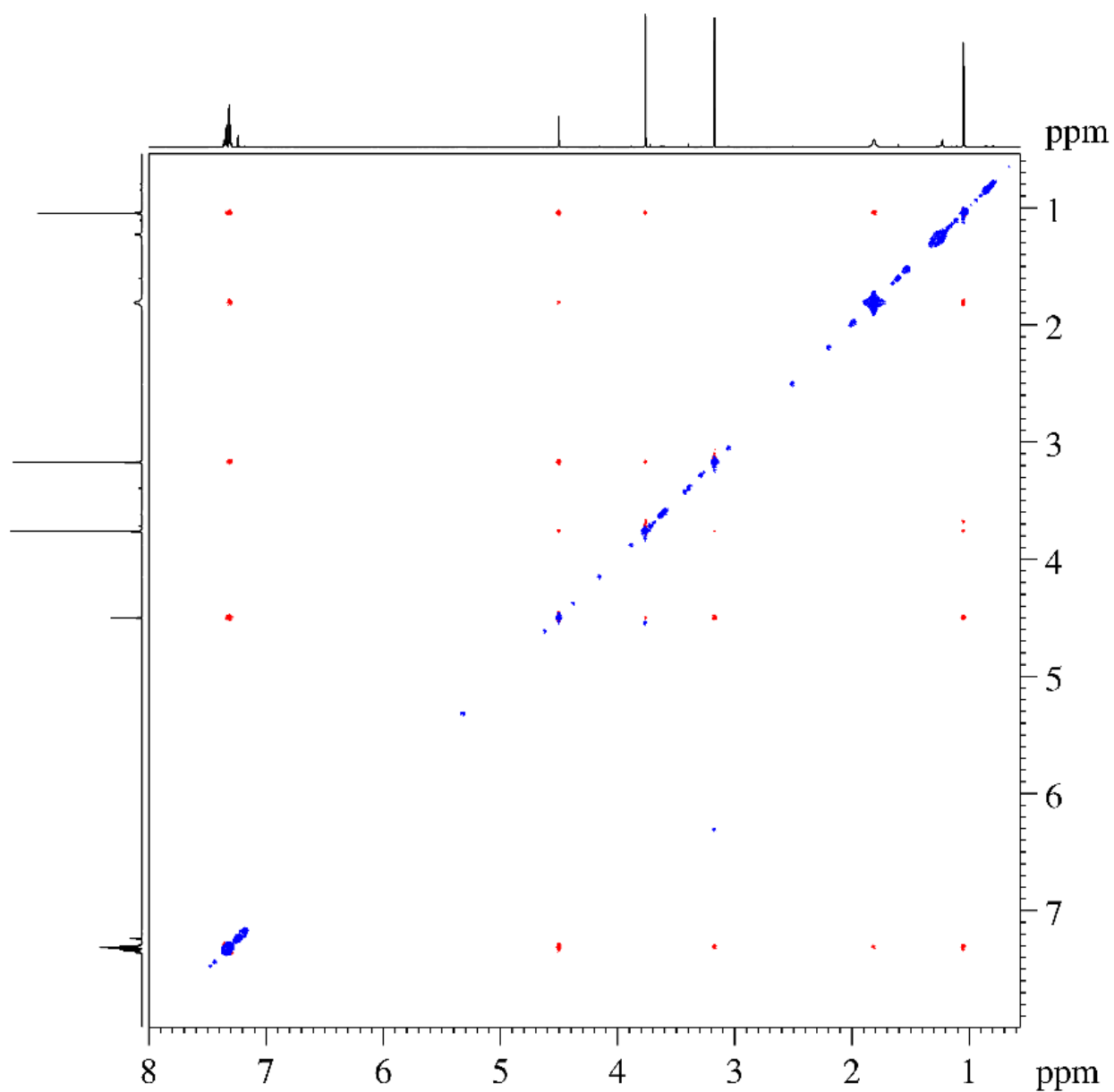


Figure 45: NOESY spectrum (600 MHz) of **203b** in CDCl₃, mixing time 1.5 s.

Experimental Part

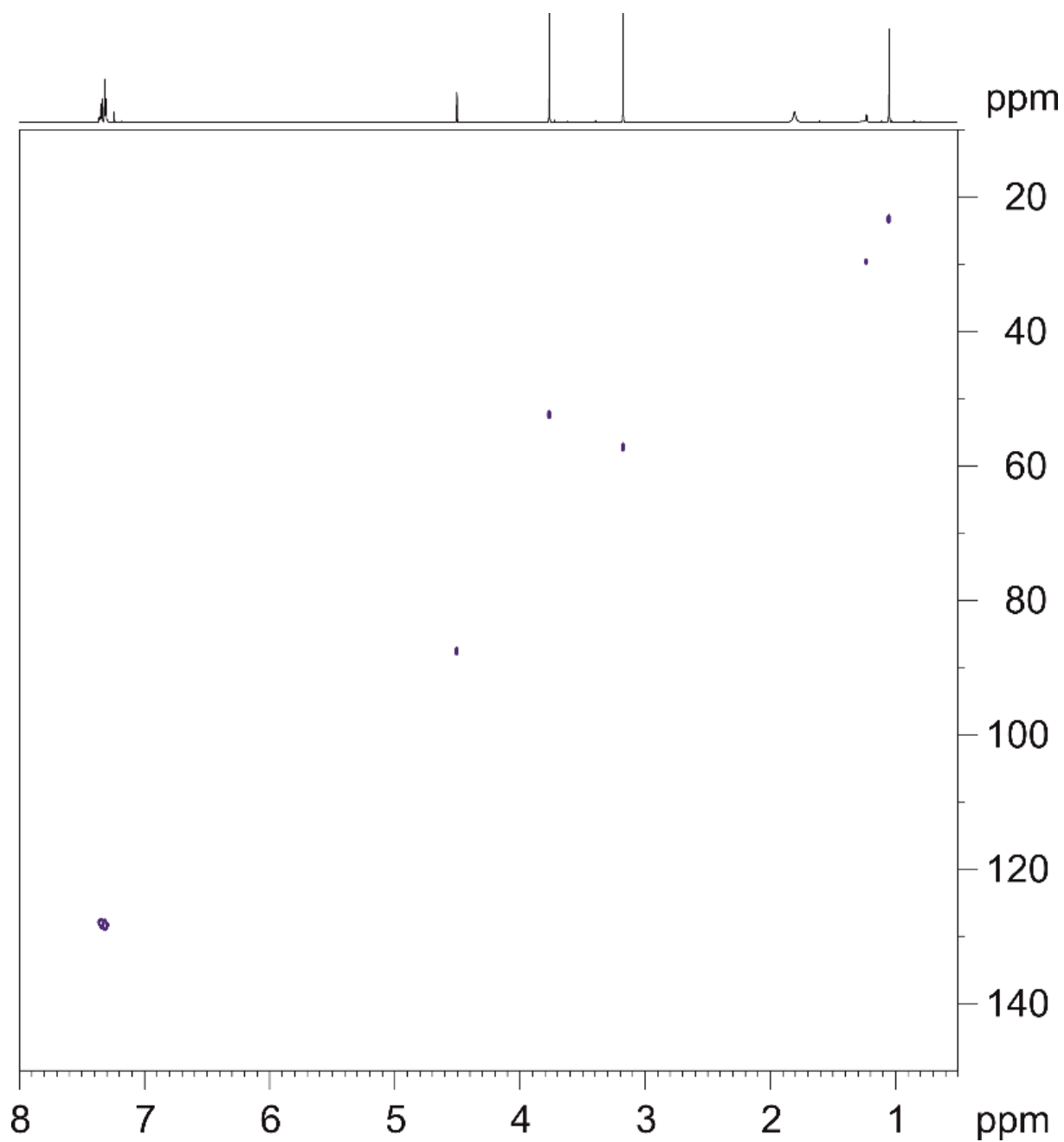


Figure 46: ^1H - ^{13}C HSQC spectrum of **203b** in CDCl_3 .

Experimental Part

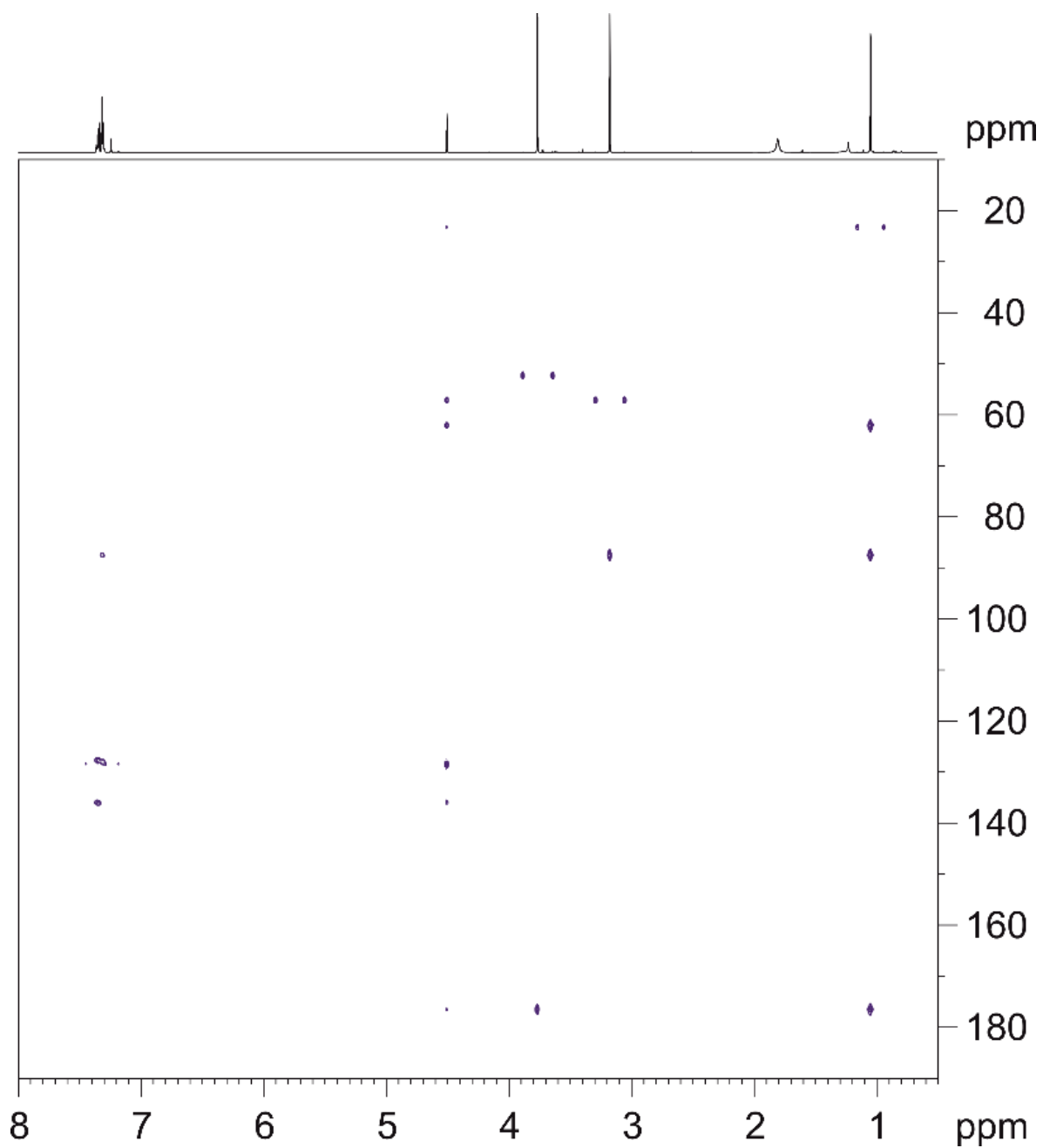
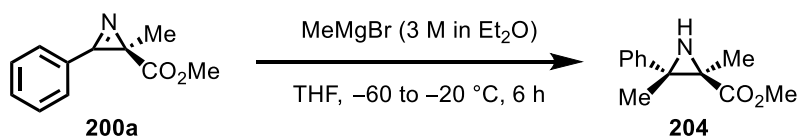


Figure 47: ^1H - ^{13}C HMBC spectrum of **203b** in CDCl_3 .

Methyl (2*R*,3*S*)-2,3-dimethyl-3-phenylaziridine-2-carboxylate (**204**)



According to a slightly modified procedure by Davis *et al.*,^[248] a Schlenk flask was charged with azirine **200a** (20.0 mg, 0.11 mmol, 1.00 eq.) and THF (1.1 mL, 0.1 M) under nitrogen atmosphere. The solution was cooled to -60 °C and a solution of MeMgBr in Et₂O (3 M, 0.18 mL, 0.53 mmol, 5.00 eq.) was added dropwise. The resulting reaction was stirred at -60 °C for 4 h and subsequently allowed to warm to -20 °C. After additional stirring at -20 °C for 2 h, the reaction was quenched with H₂O and extracted with EtOAc (3x). The combined organic layers were washed with brine, dried over Na₂SO₄, filtered, and the solvent was removed under reduced pressure. The crude product was purified by column chromatography on silica gel (*n*-pentane/EtOAc 5:1 → 3:1) to obtain aziridine **204** (14.0 mg, 0.07 mmol, 65%) as a colorless oil. Enantiomeric excess was established by HPLC analysis on a chiral stationary phase: ee = 90%, HPLC conditions: Daicel Chiralpak[®] IG column, 250 x 4.6 mm, absorbance at 220 nm, *n*-hexane/*i*PrOH 98:2, isocratic flow, flow rate 1.0 mL/min, 25 °C, *t_r* (major) = 10.2 min, *t_r* (minor) = 16.3 min.

TLC: *R_f* = 0.33 (*n*-pentane/EtOAc 5:1).

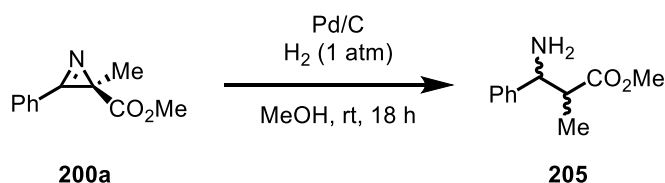
¹H NMR: (300 MHz, CDCl₃) 7.40-7.29 (m, 4H), 7.28-7.21 (m, 1H), 3.83 (s, 3H), 1.58 (s, 3H), 1.04 (s, 3H) ppm.

¹³C NMR: (75 MHz, CDCl₃) δ = 173.7, 141.2, 128.4 (2C), 127.7 (2C), 127.2, 52.8, 48.6, 46.1, 21.9, 17.6 ppm.

[α]_D²²: -99.5° (*c* = 0.5, CH₂Cl₂).

Analytical data were consistent with reported data.^[248]

Methyl 3-amino-2-methyl-3-phenylpropanoate (**205**)



A flask was charged with 2*H*-azirine **200a** (40.0 mg, 0.21 mmol, 1.00 eq.), Pd on carbon (10 wt%, 22.5 mg, 0.02 mmol, 0.10 eq.), and MeOH (2.1 mL, 0.1 M). The flask was purged with hydrogen

Experimental Part

(3x) and the reaction was stirred for 18 h at rt under an atmosphere of hydrogen (1 atm). Afterwards, the mixture was filtered over a short plug of celite and the solvent was removed under reduced pressure. After drying under vacuum, β -amino acid ester **205** (37.5 mg, 0.19 mmol, 92%) was obtained as a colorless oil as a diastereomeric mixture (*syn/trans* 1:1.26) as determined via ¹H-NMR analysis. Enantiomeric excess was evaluated by HPLC analysis on a chiral stationary phase. No enantioselectivity was observed. HPLC conditions: Daicel Chiralcel[®] OJ-H column, 250 x 4.6 mm, absorbance at 220 nm, *n*-hexane/*i*PrOH 90:10, isocratic flow, flow rate 1.0 mL/min, 25 °C, t_{r1} = 9.5 min, t_{r2} = 11.5 min, t_{r3} = 13.3 min, t_{r4} = 16.4 min.

¹H NMR: (300 MHz, CDCl₃) 7.36-7.22 (m, 10H), 4.28 (d, J = 5.7 Hz, 1H), 4.02 (d, J = 9.5 Hz, 1H), 3.72 (s, 3H), 3.57 (s, 3H), 2.82-2.66 (m, 2H), 2.01 (br s, 4H), 1.16 (d, J = 7.0 Hz, 3H), 0.94 (d, J = 7.1 Hz, 3H) ppm.

¹³C NMR: (75 MHz, CDCl₃) δ = 176.4, 175.5, 143.5, 143.4, 128.7 (2C), 128.5 (2C), 127.7, 127.4, 127.1 (2C), 126.7 (2C), 59.2, 57.5, 51.8, 51.7, 48.0, 47.3, 15.5, 12.1 ppm.

Analytical data were consistent with reported data.^[280,281]

6. Appendix

6.1 Representative NMR Spectra

This section will include all ^1H NMR and ^{13}C NMR spectra of final ligands, complexes, and newly synthesized, unpublished compounds.

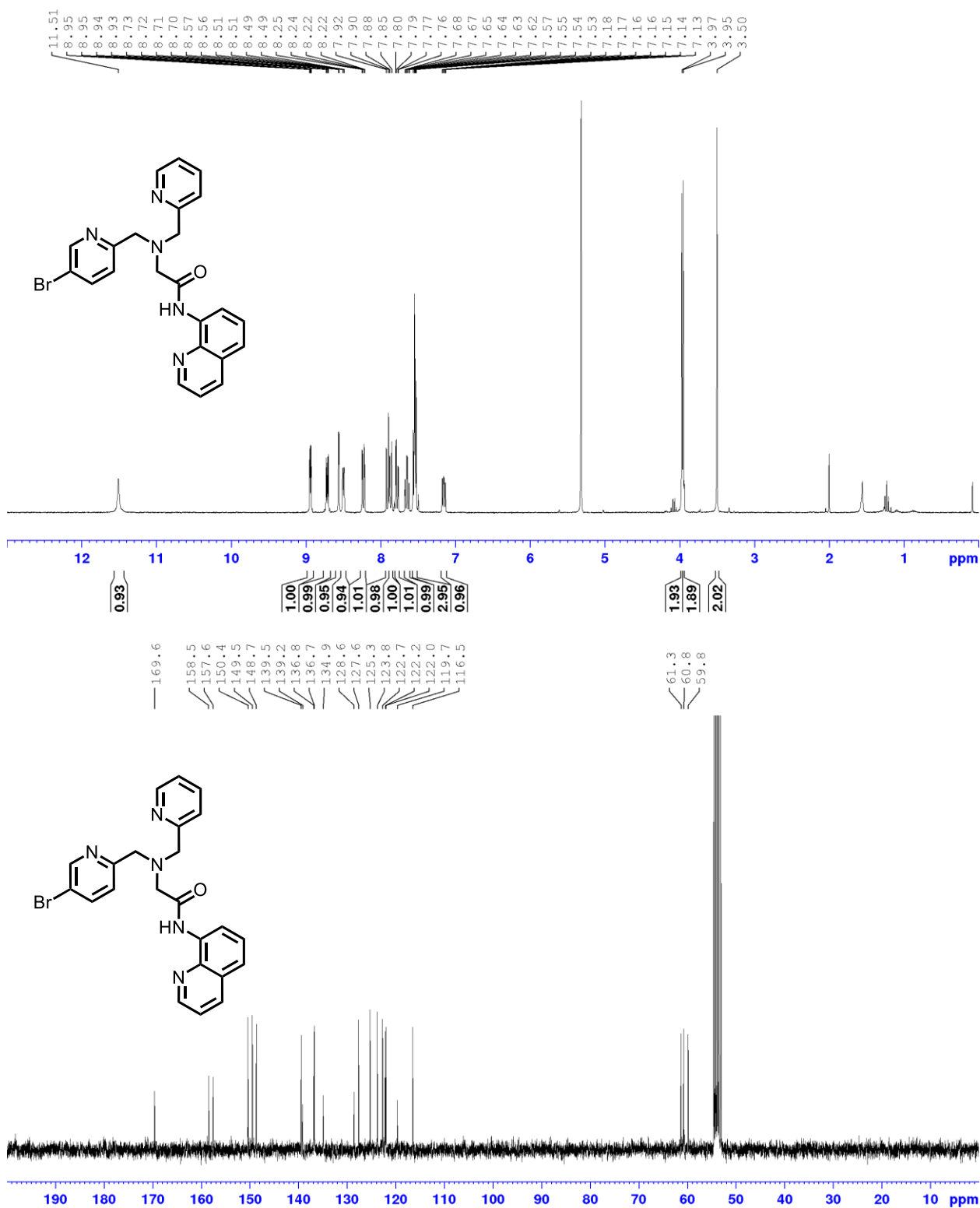


Figure 48: ^1H NMR (300 MHz) and ^{13}C NMR (75 MHz) spectrum of **107** in CDCl_3 .

Appendix

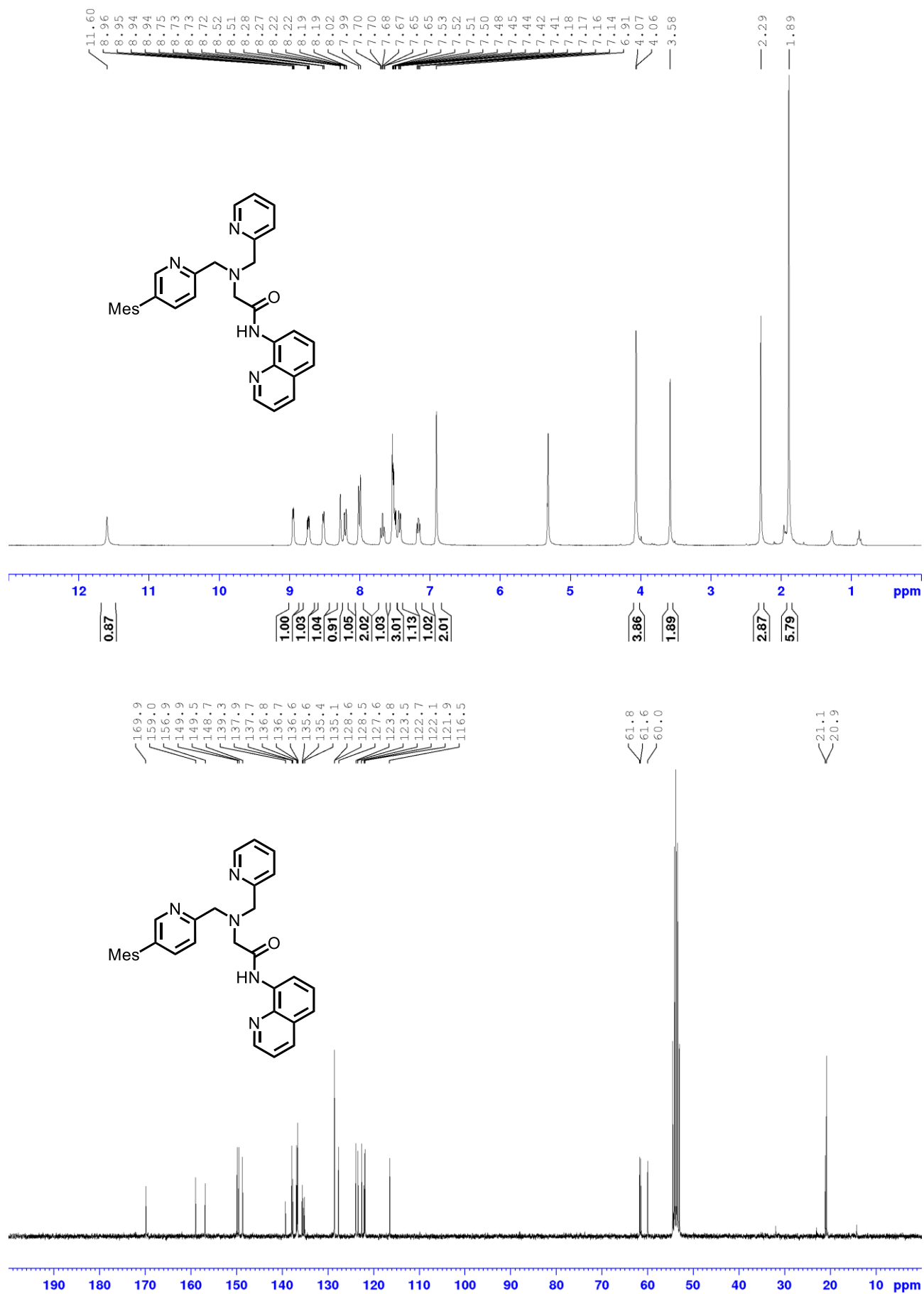


Figure 49: ¹H NMR (300 MHz) and ¹³C NMR (75 MHz) spectrum of **101** in CDCl₃.

Appendix

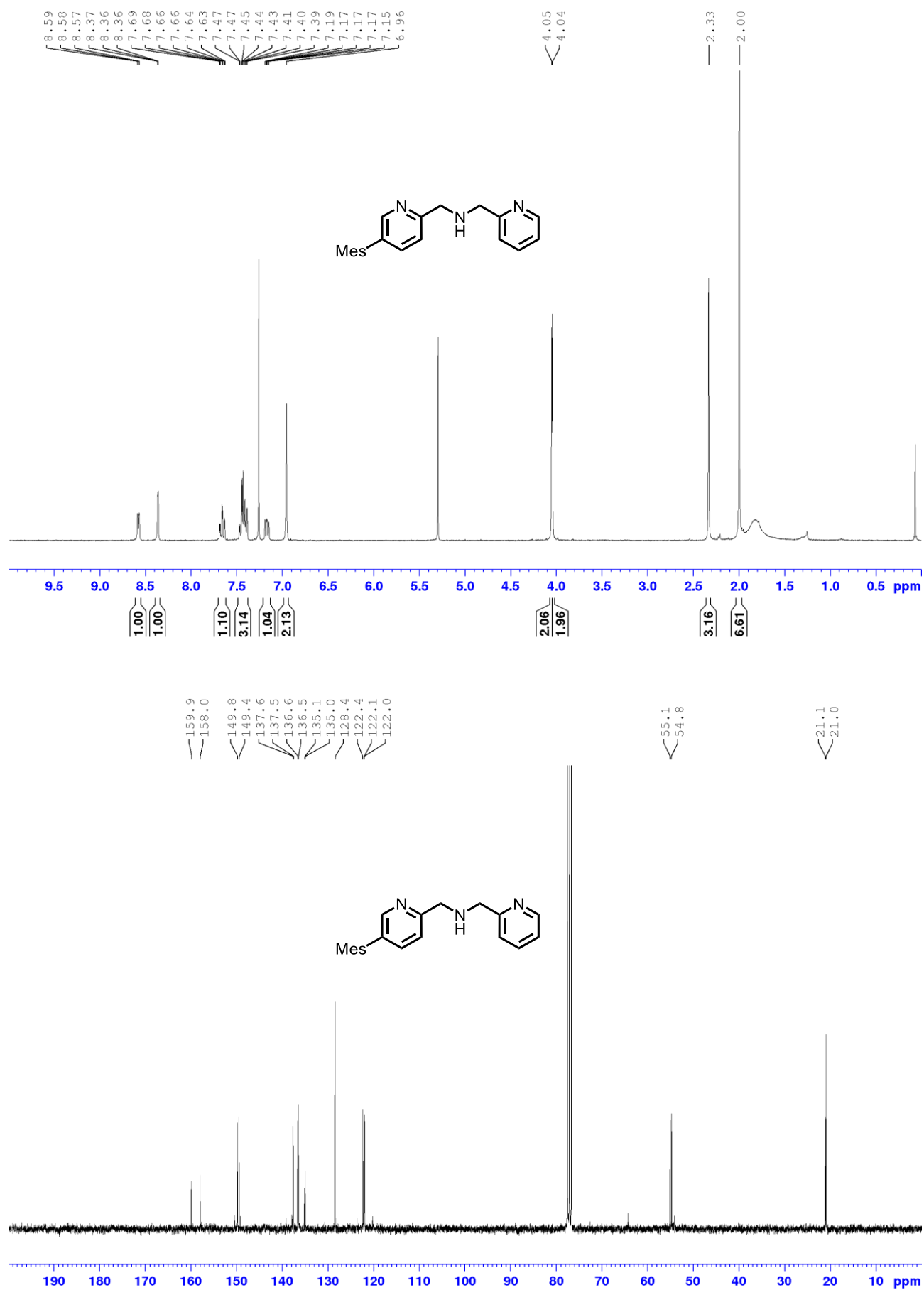


Figure 50: ^1H NMR (300 MHz) and ^{13}C NMR (75 MHz) spectrum of **117** in CDCl_3 .

Appendix

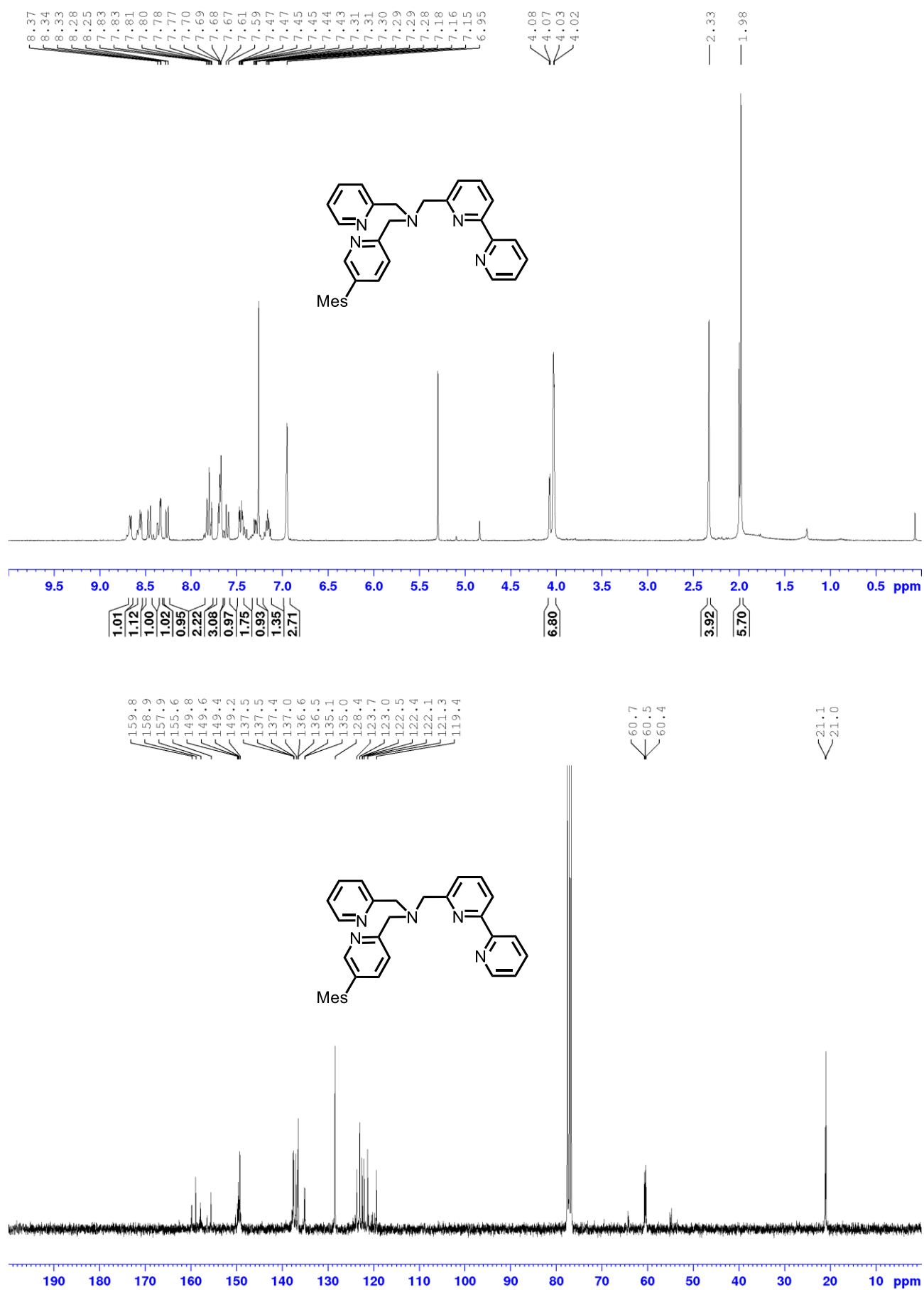


Figure 51: ¹H NMR (300 MHz) and ¹³C NMR (75 MHz) spectrum of **115** in CDCl₃.

Appendix

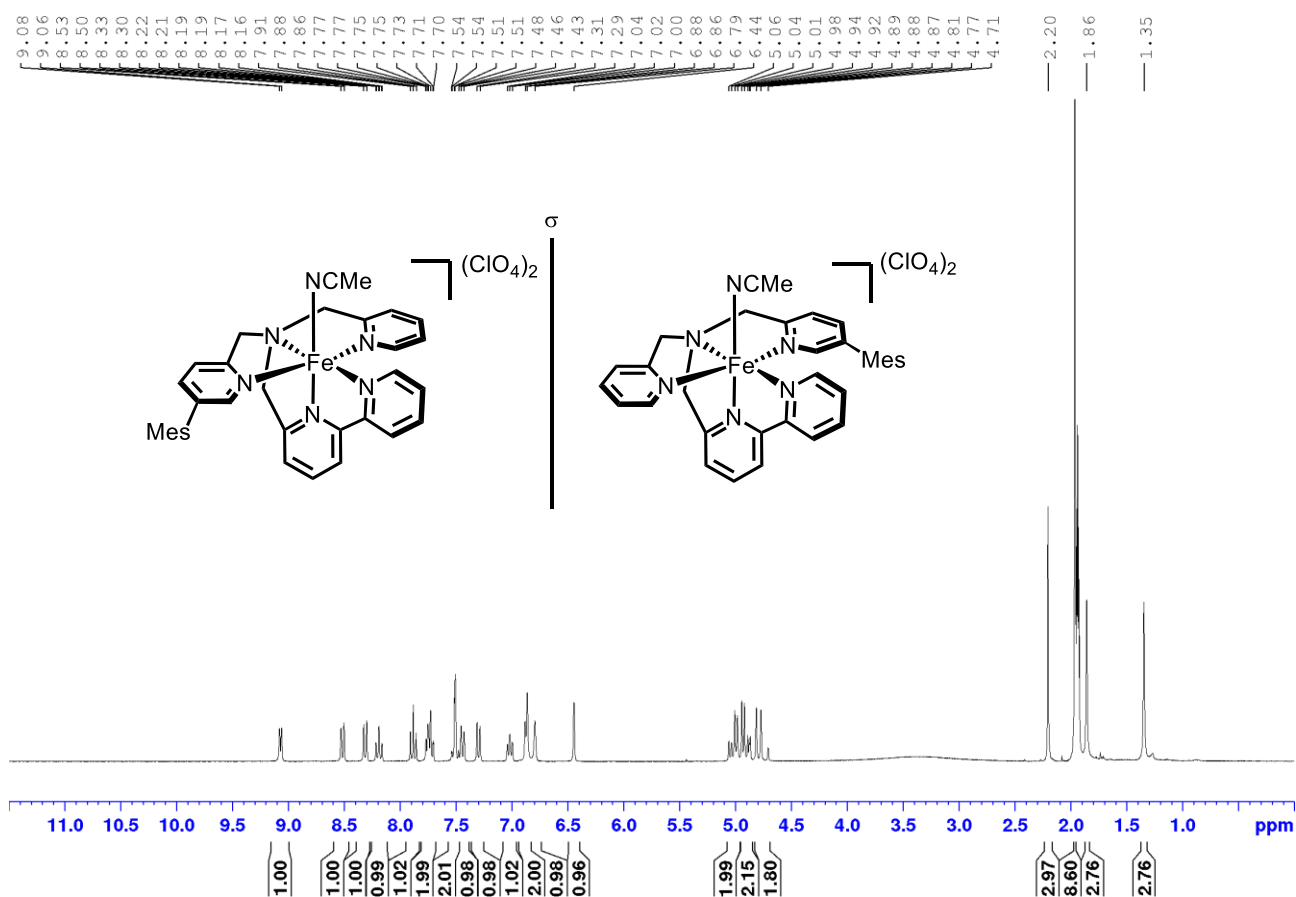
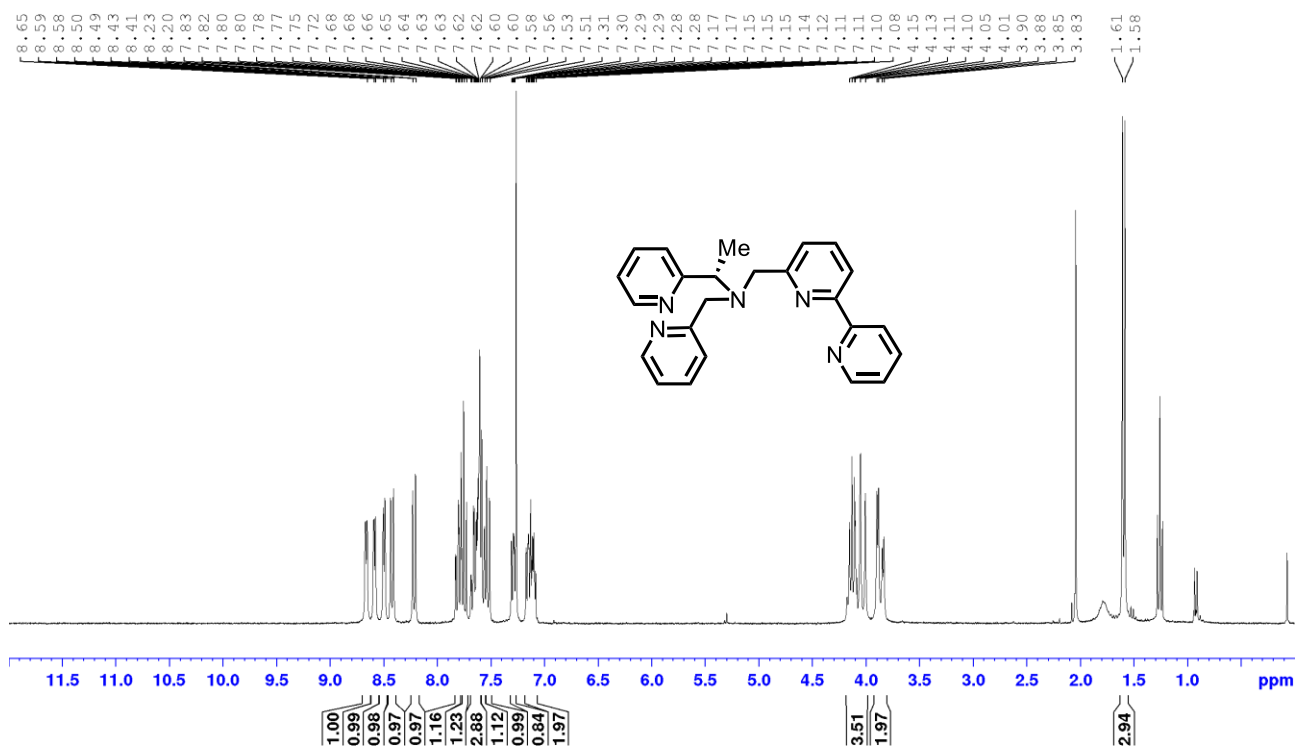


Figure 52: ^1H NMR spectrum (300 MHz) of complex 121 in CD_3CN .



Appendix

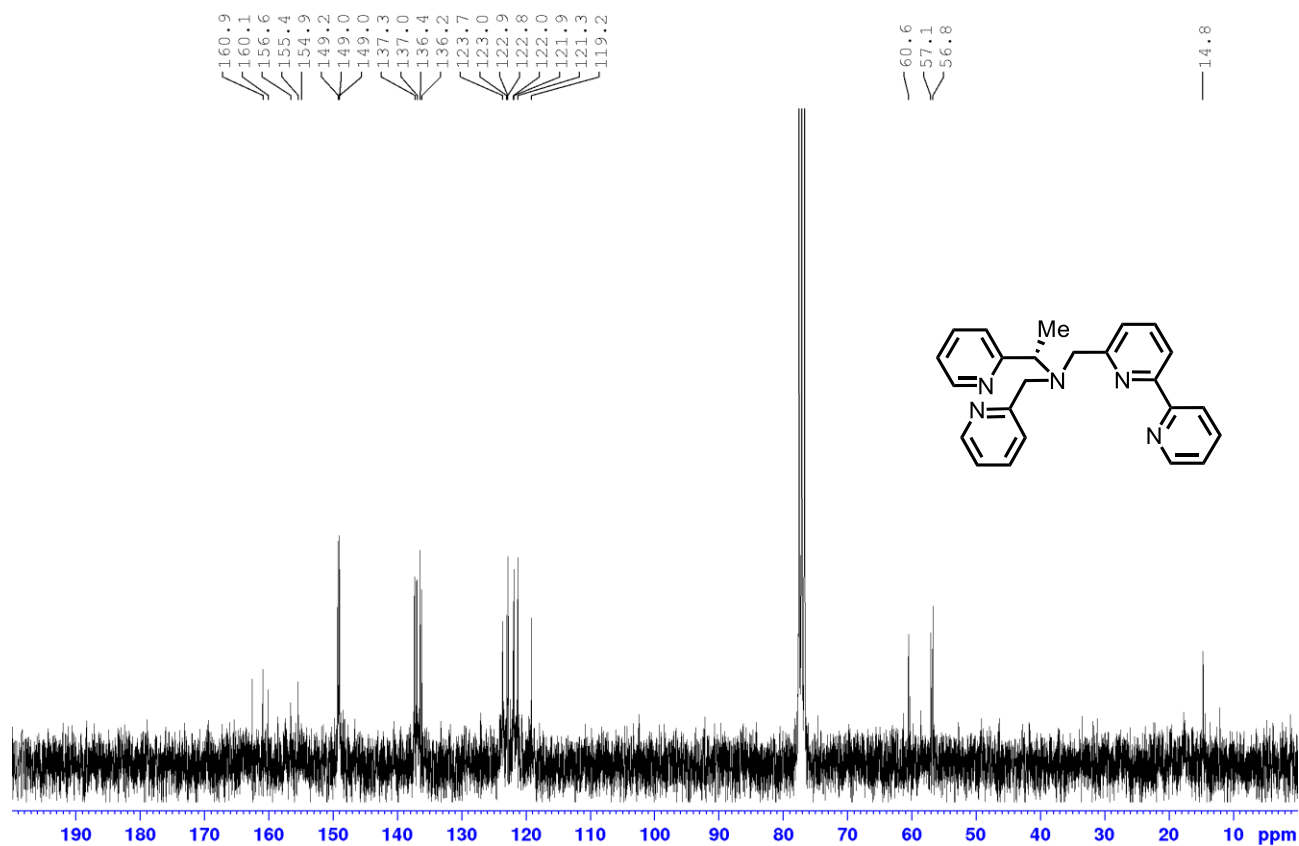
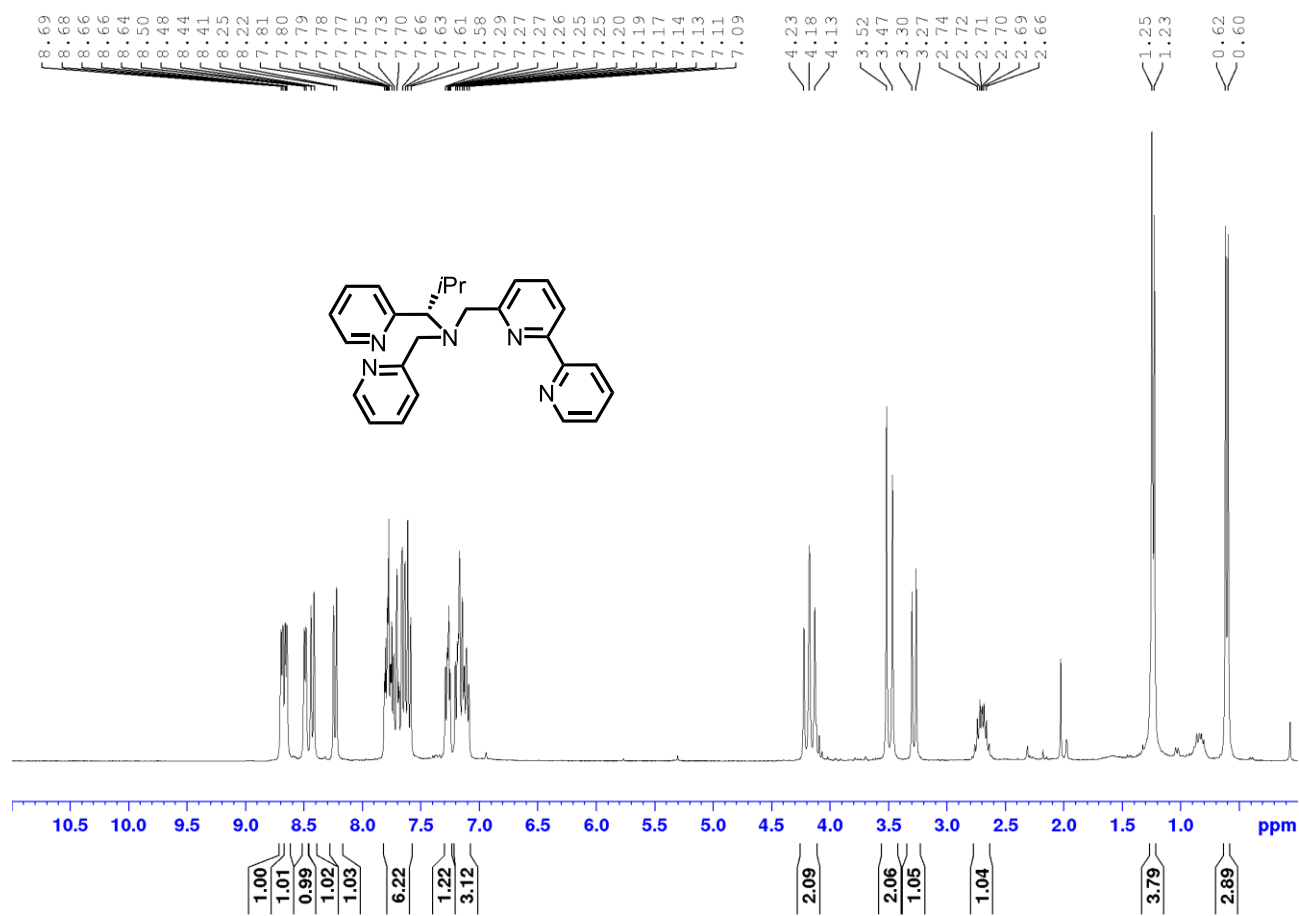


Figure 53: ¹H NMR (300 MHz) and ¹³C NMR (75 MHz) spectrum of 127 in CDCl₃.



Appendix

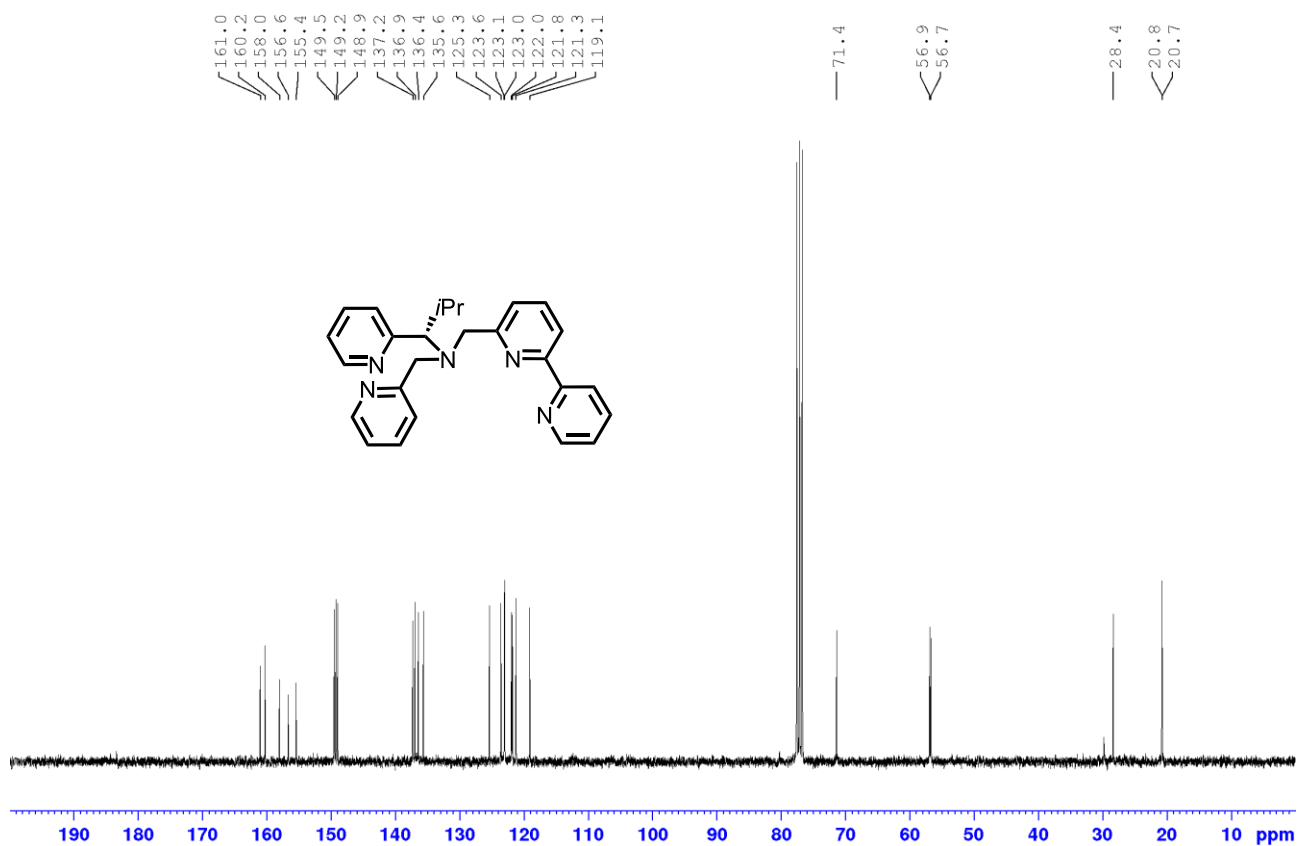
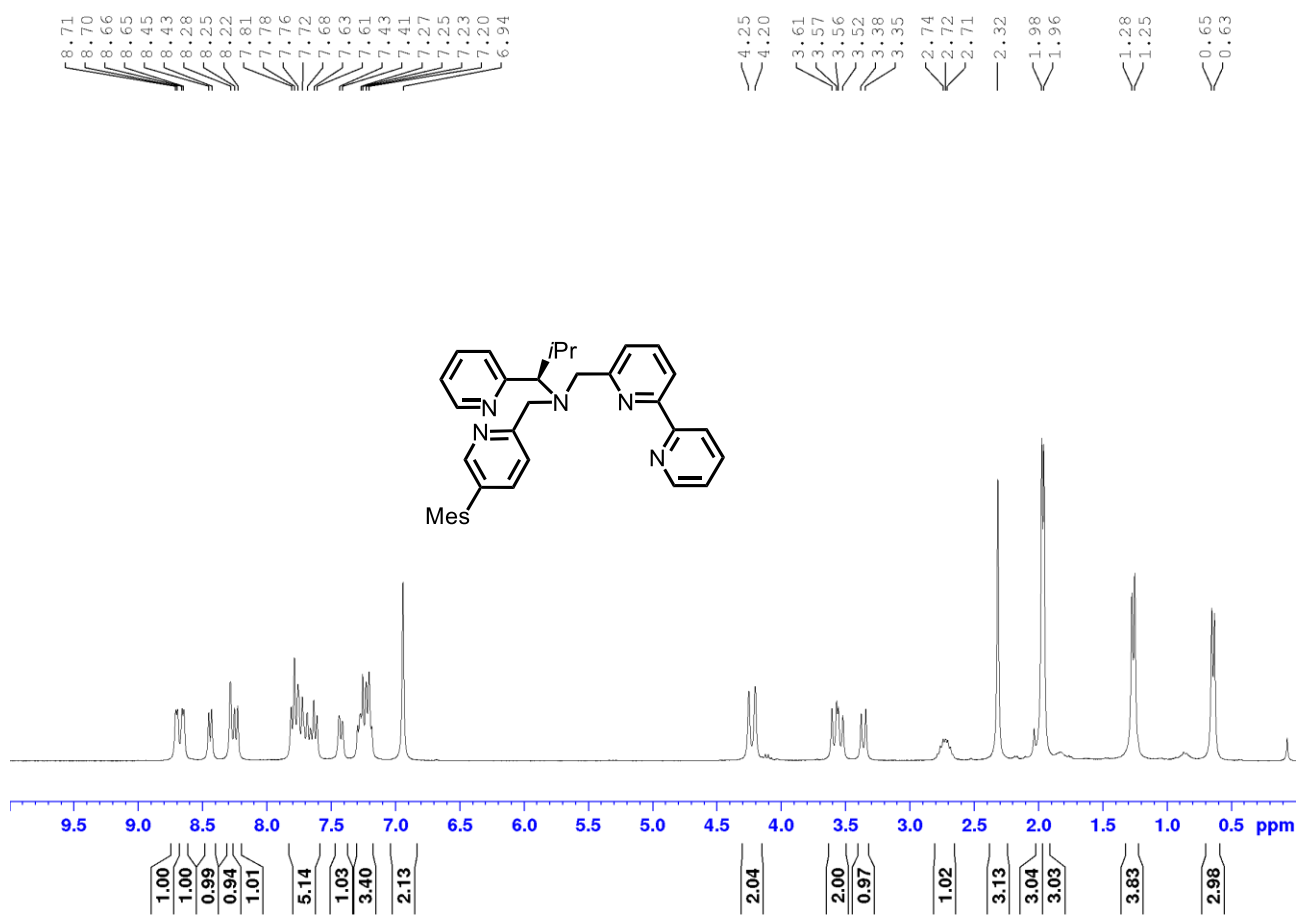


Figure 54: ¹H NMR (300 MHz) and ¹³C NMR (75 MHz) spectrum of **139** in CDCl₃.



Appendix

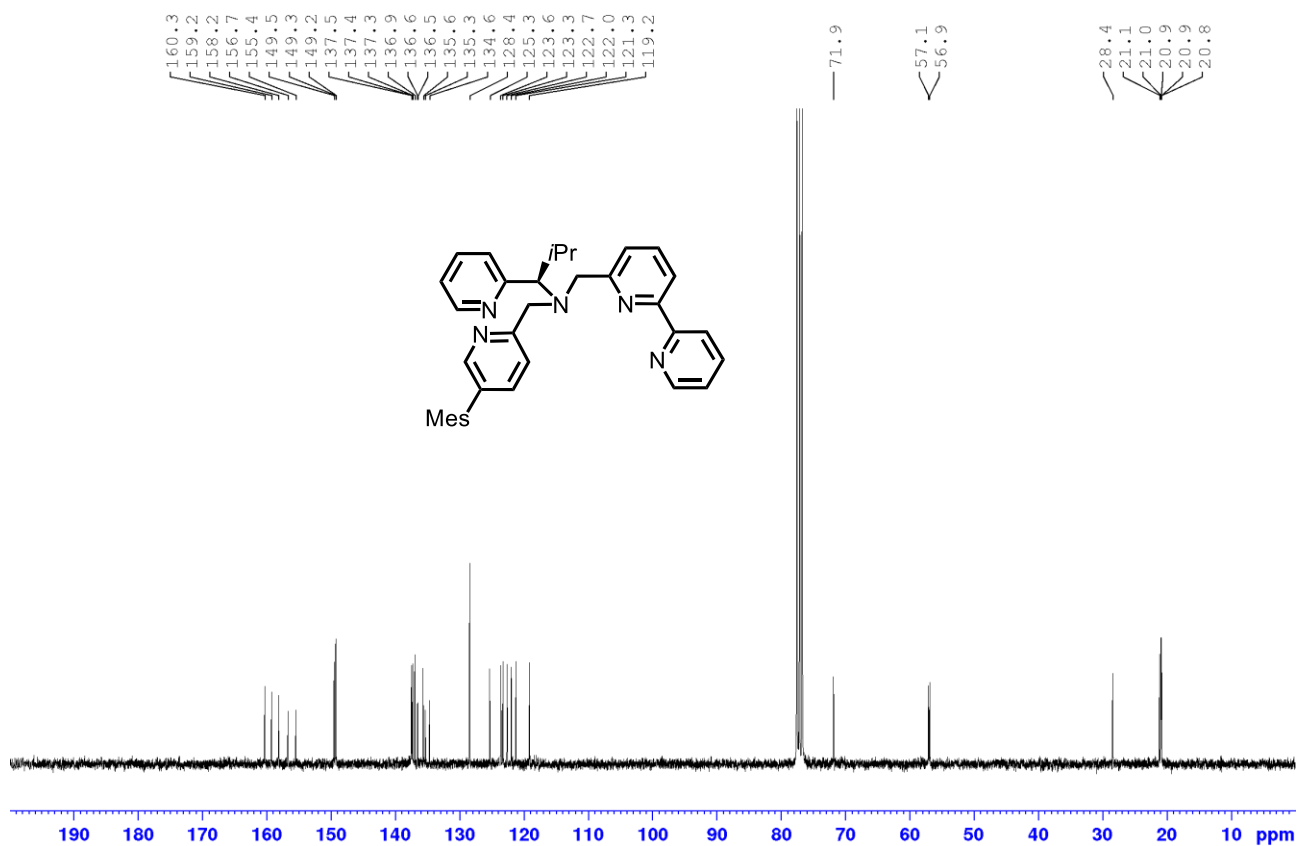
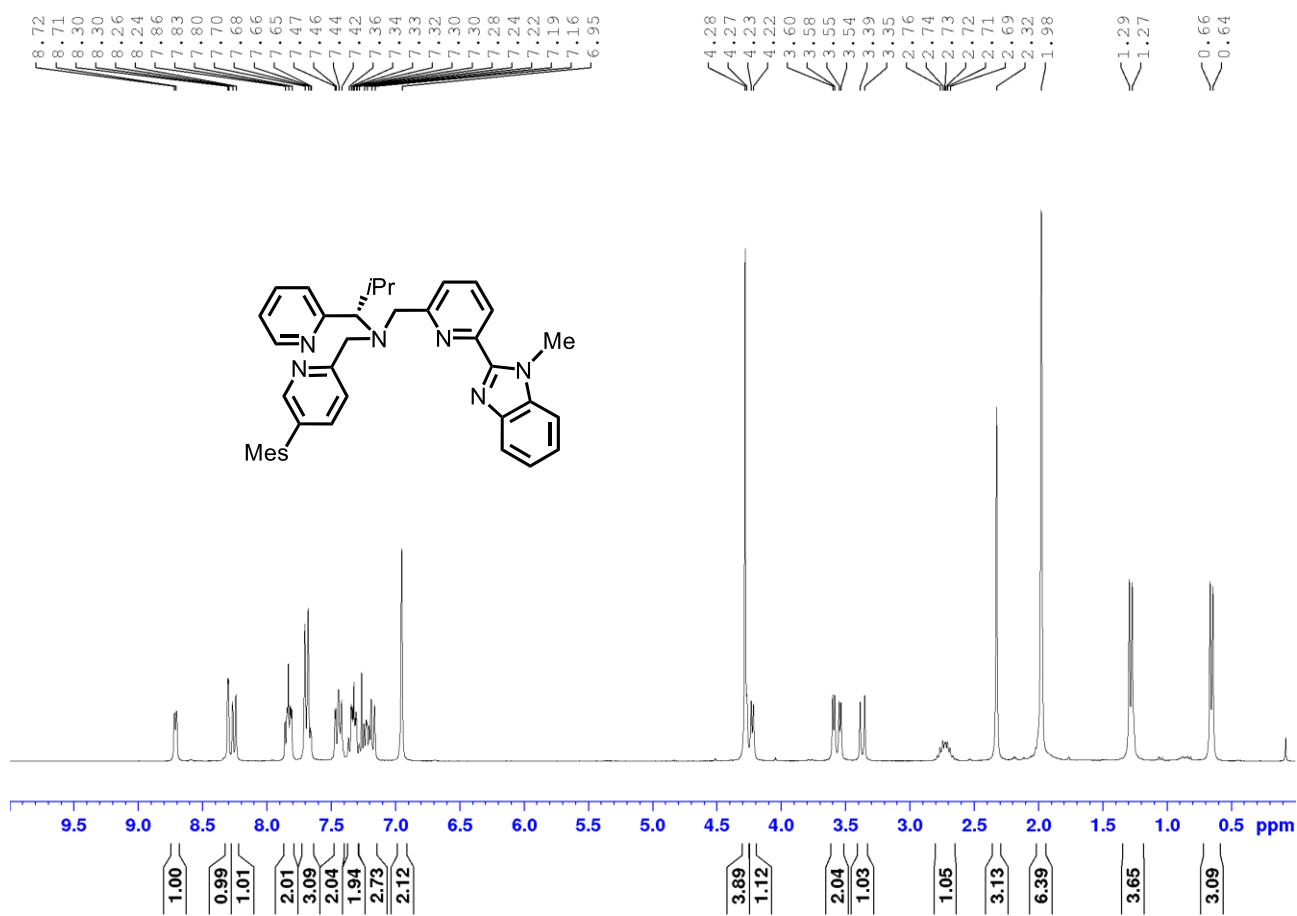


Figure 55: ¹H NMR (300 MHz) and ¹³C NMR (75 MHz) spectrum of **141** in CDCl₃.



Appendix

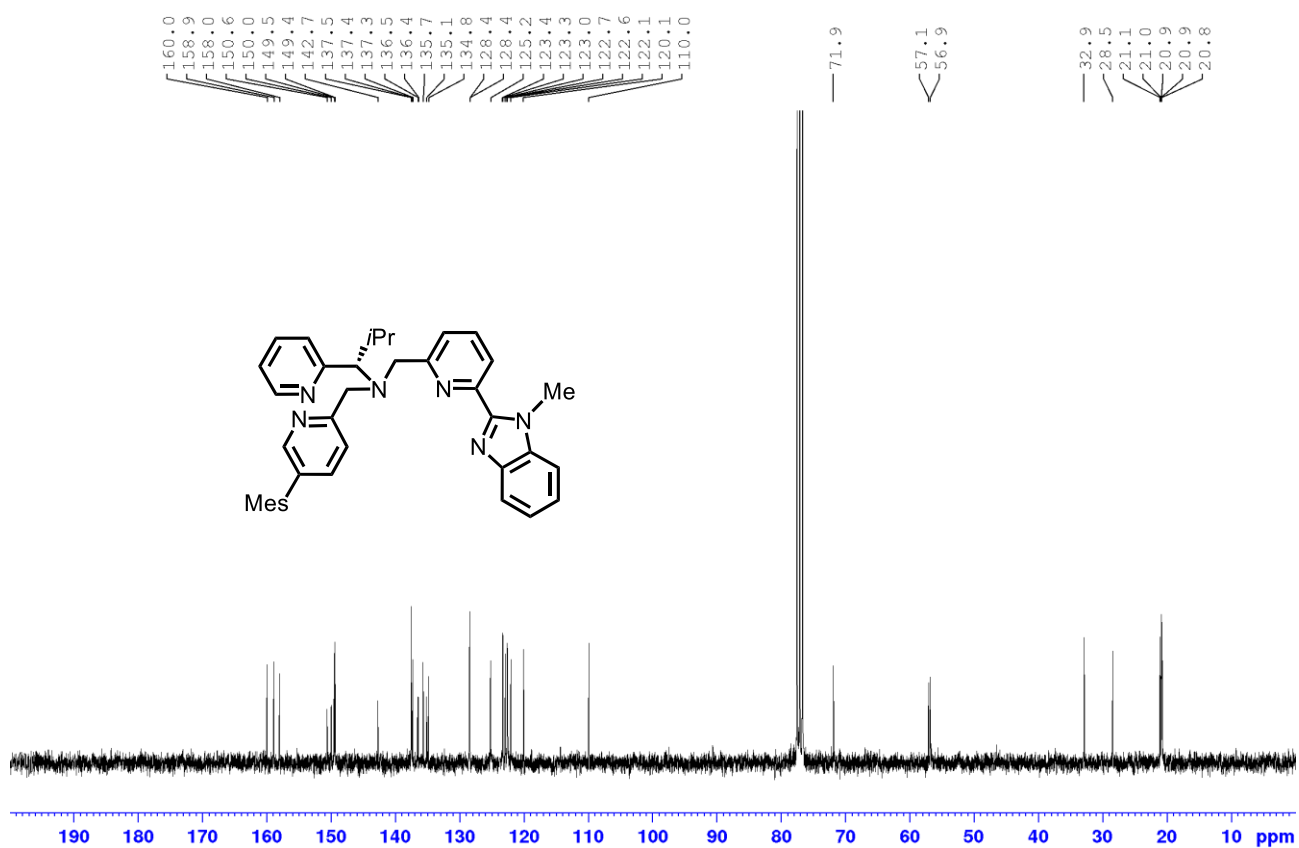


Figure 56: ¹H NMR (300 MHz) and ¹³C NMR (75 MHz) spectrum of **145** in CDCl₃.

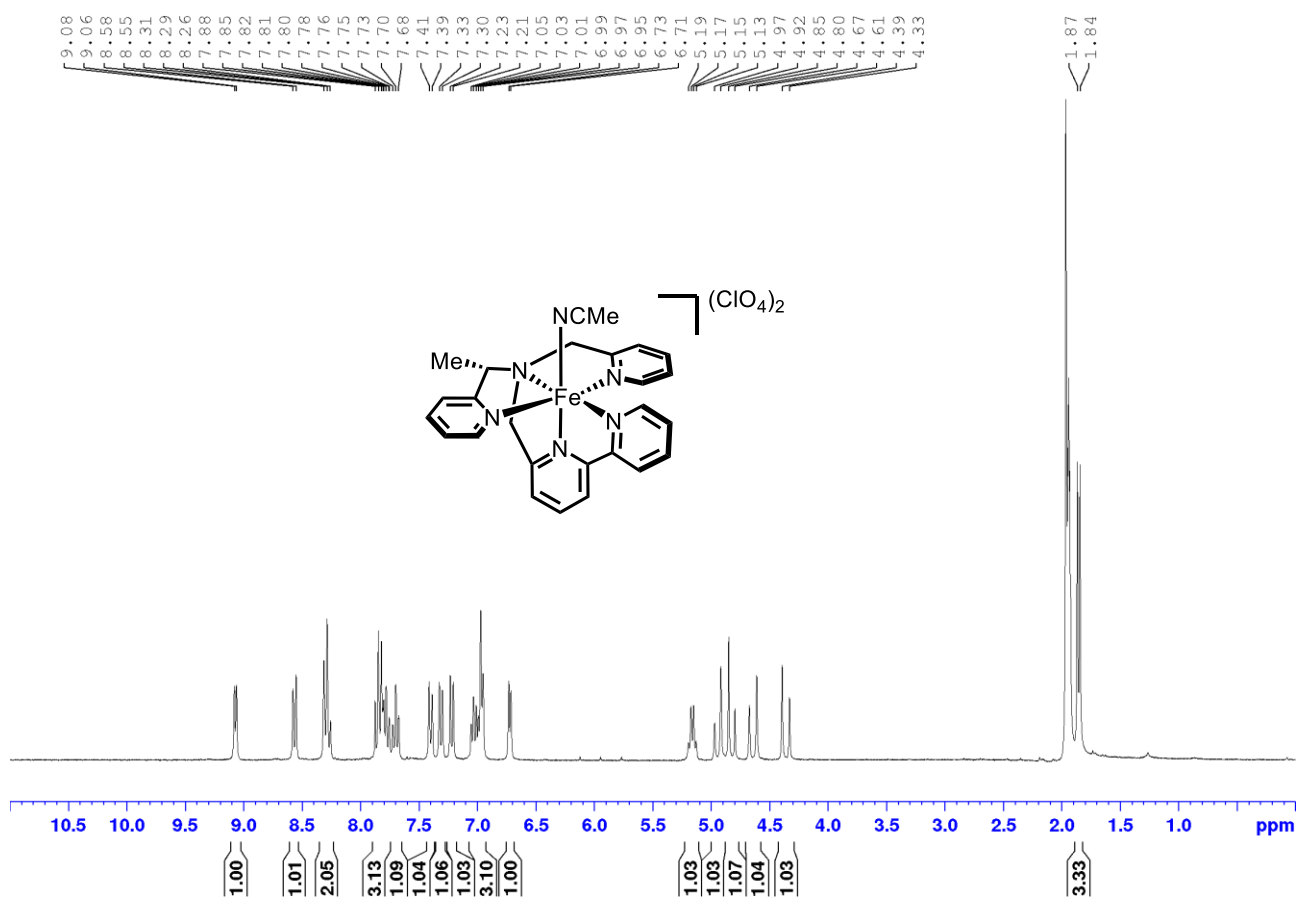


Figure 57: ¹H NMR spectrum (300 MHz) of complex **131a** in CD₃CN.

Appendix

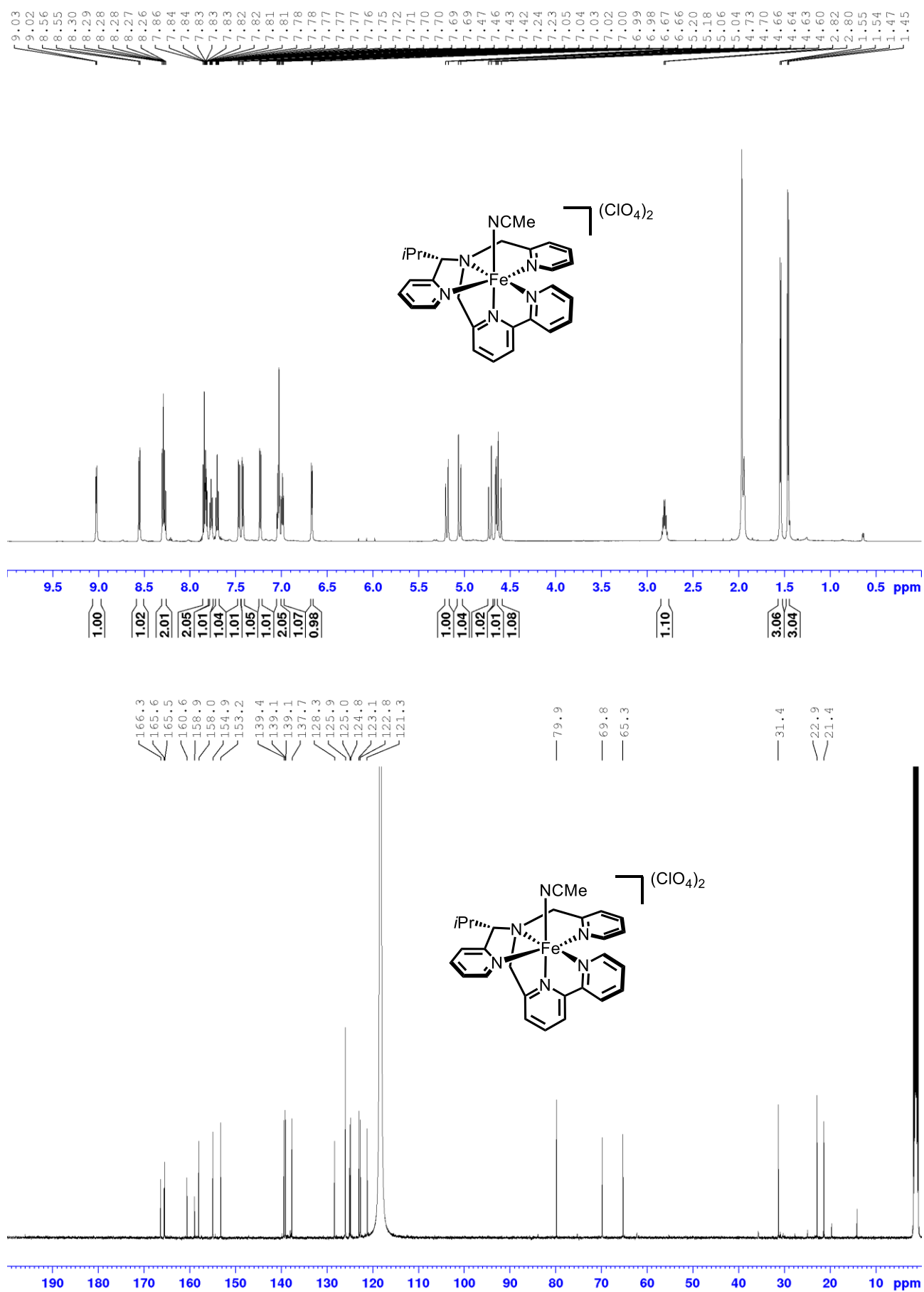


Figure 58: ¹H NMR (600 MHz) and ¹³C NMR (126 MHz) spectrum of complex **140a** in CD₃CN.

Appendix

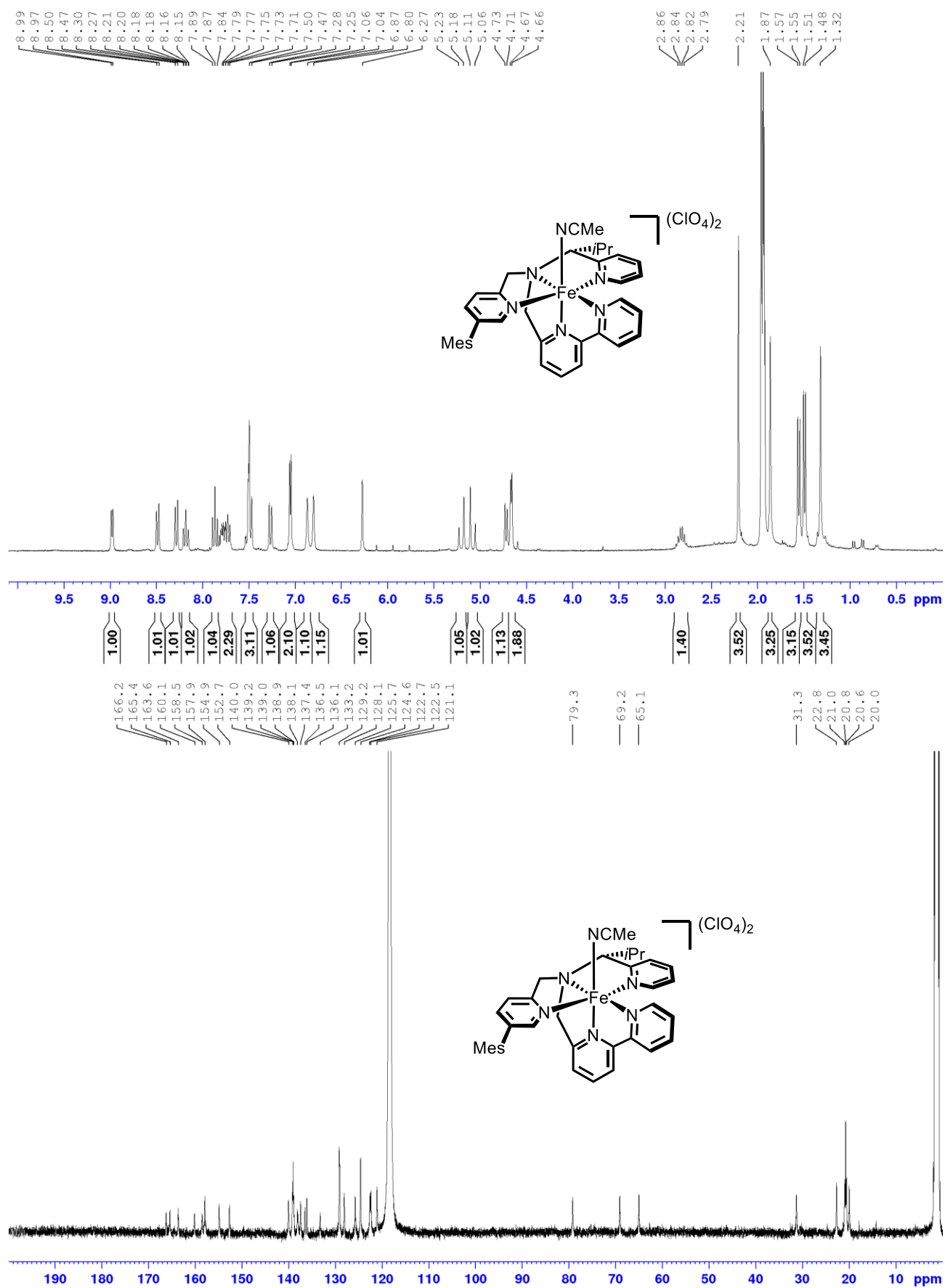


Figure 59: ¹H NMR (300 MHz) and ¹³C NMR (126 MHz, -20 °C) spectrum of complex **149a** in CD₃CN.

Appendix

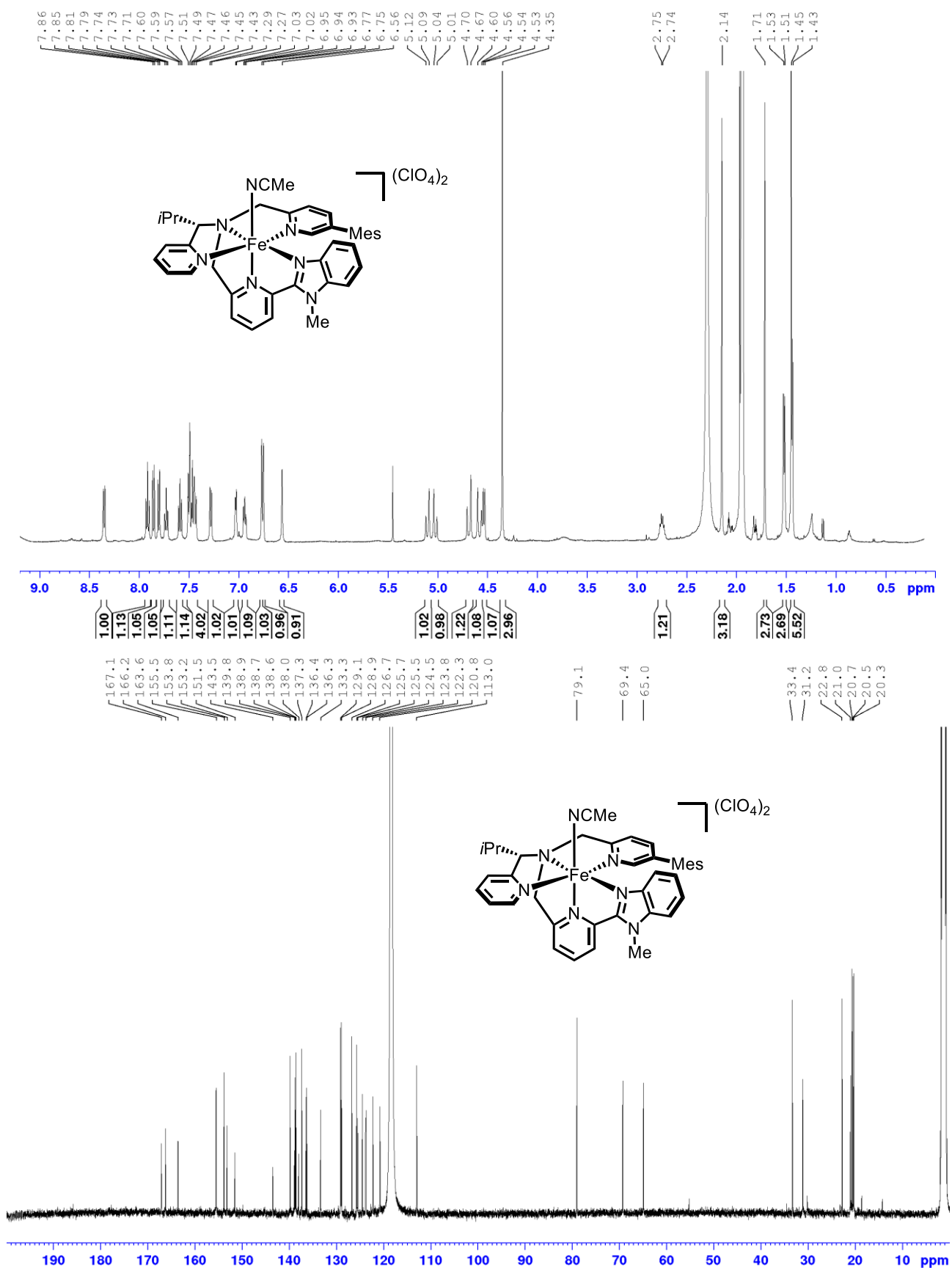


Figure 60: ¹H NMR (500 MHz, -20 °C) and ¹³C NMR (126 MHz, -20 °C) spectrum of complex **150a** in CD₃CN.

Appendix

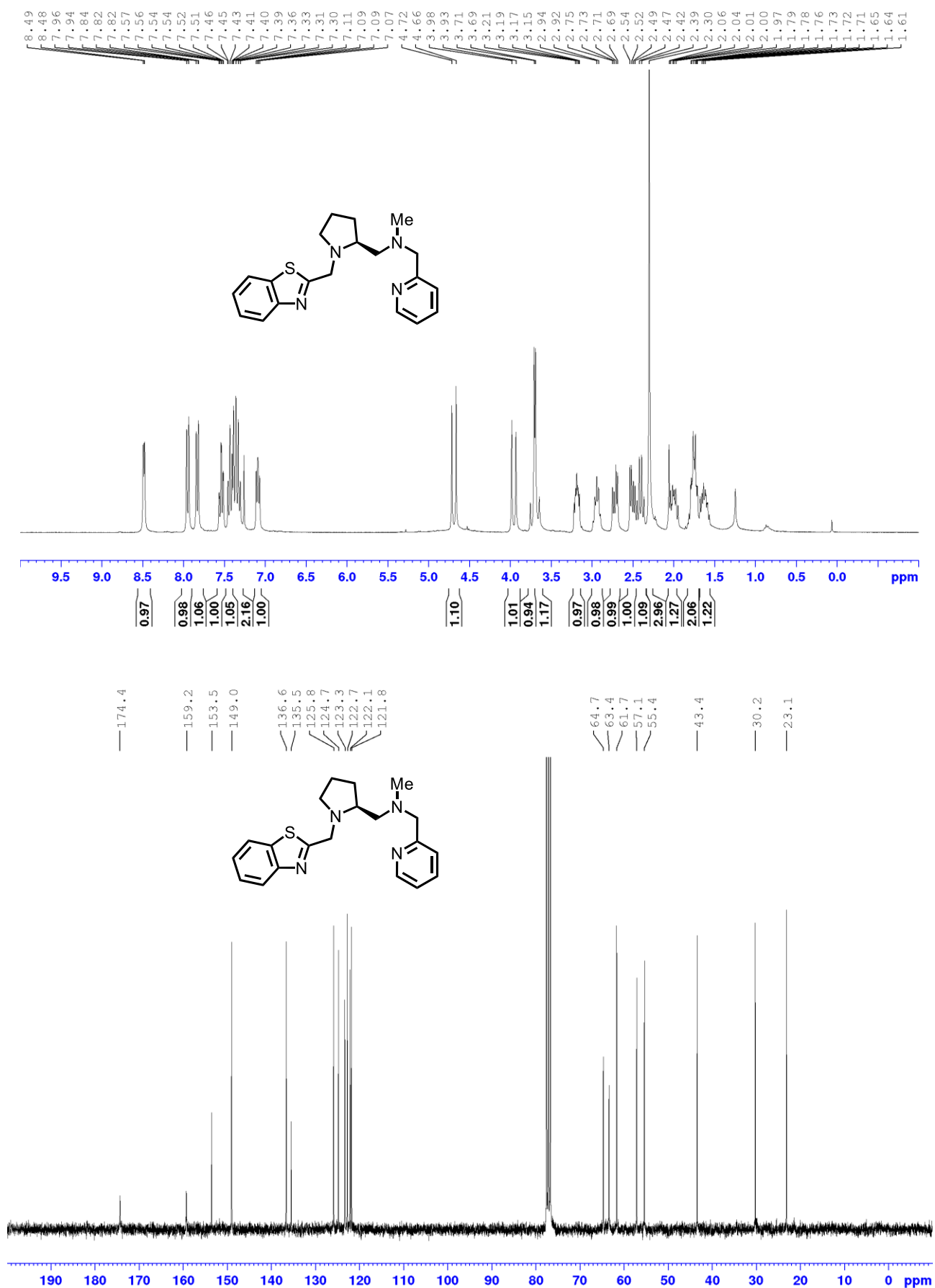


Figure 61: ¹H NMR (300 MHz) and ¹³C-NMR (75 MHz) spectra of **189a** in CDCl₃.

Appendix

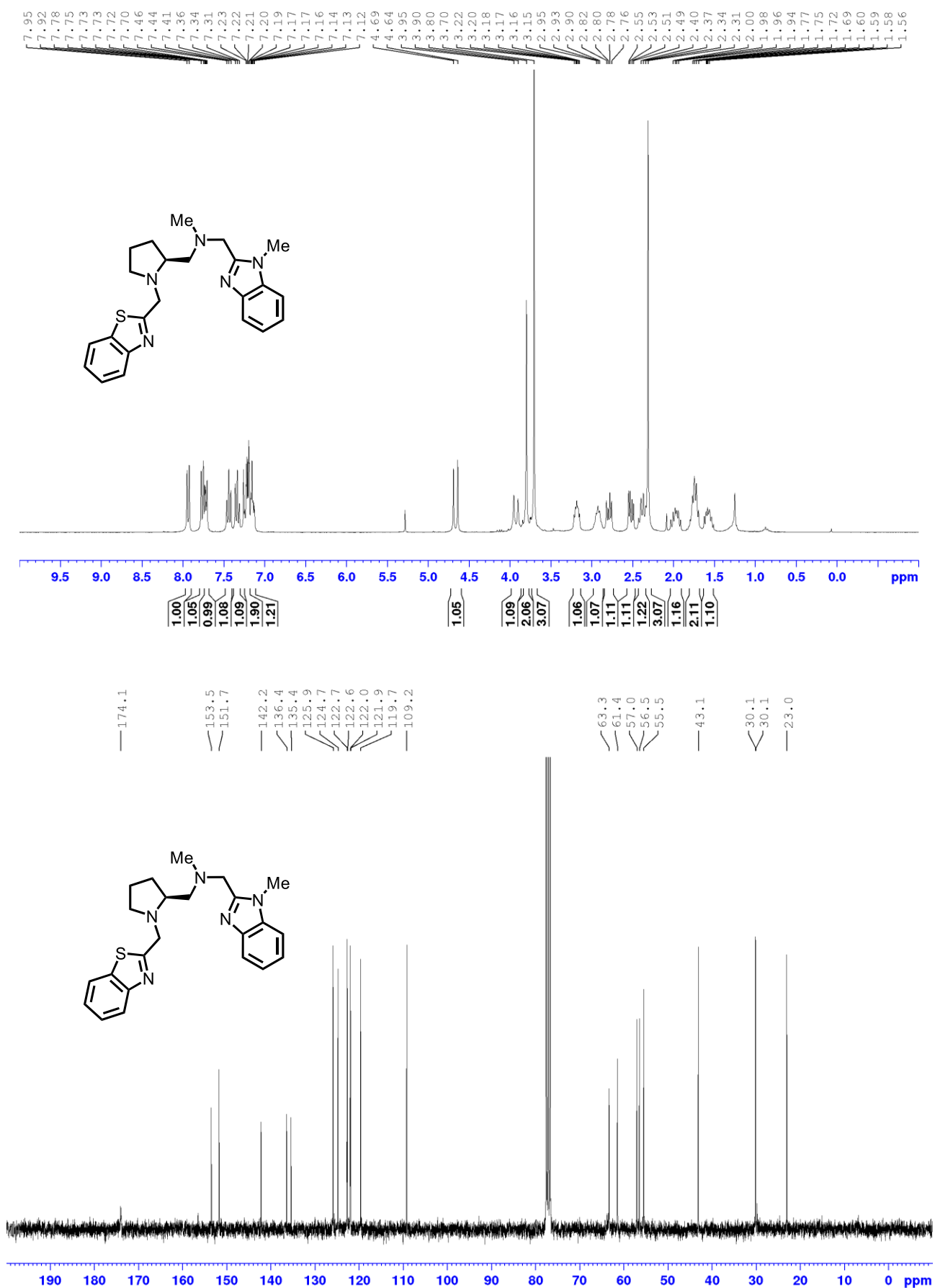


Figure 62: ¹H NMR (300 MHz) and ¹³C-NMR (75 MHz) spectra of **189b** in CDCl₃.

Appendix

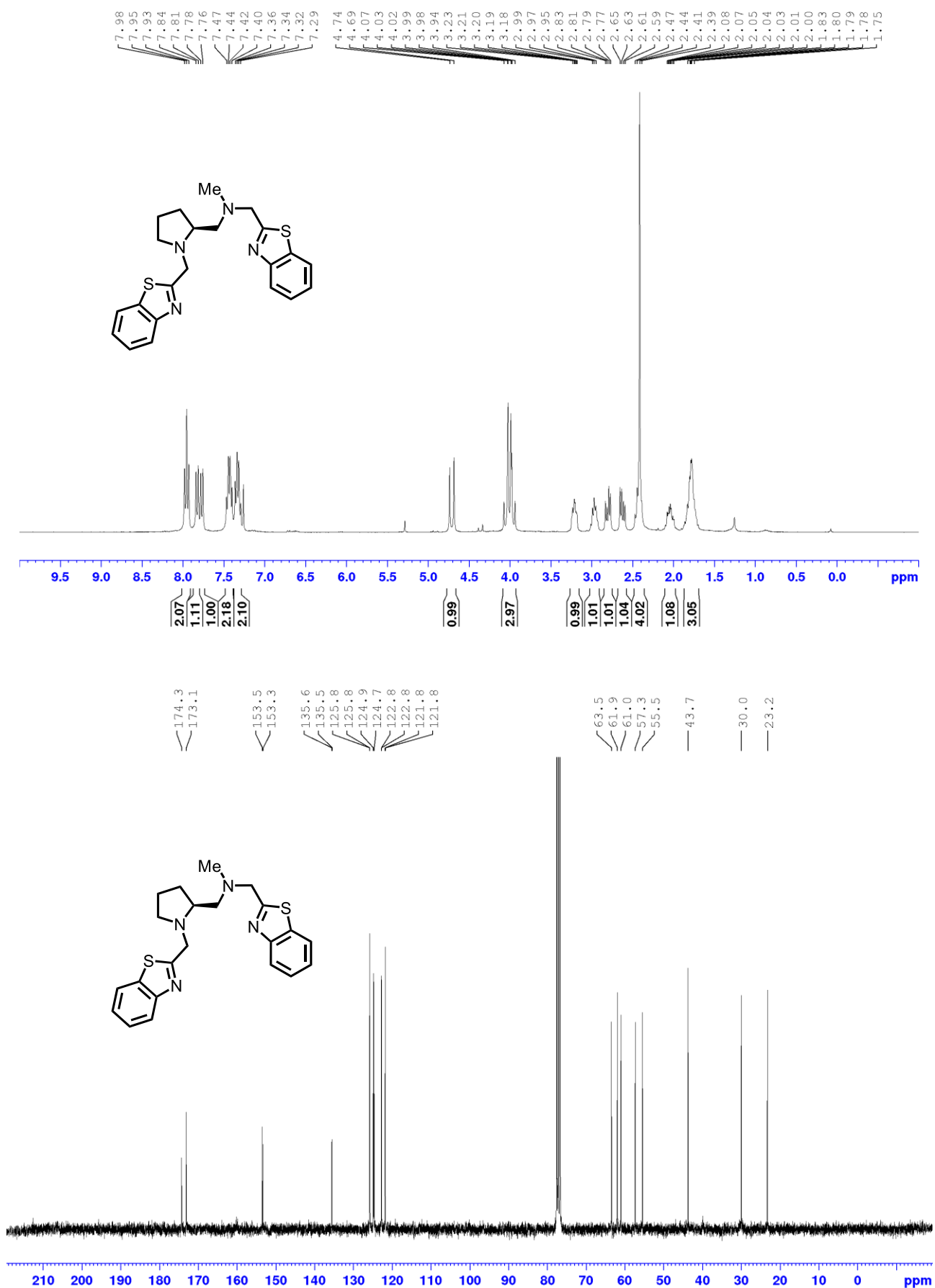


Figure 63: ¹H NMR (300 MHz) and ¹³C-NMR (75 MHz) spectra of **189c** in CDCl₃.

Appendix

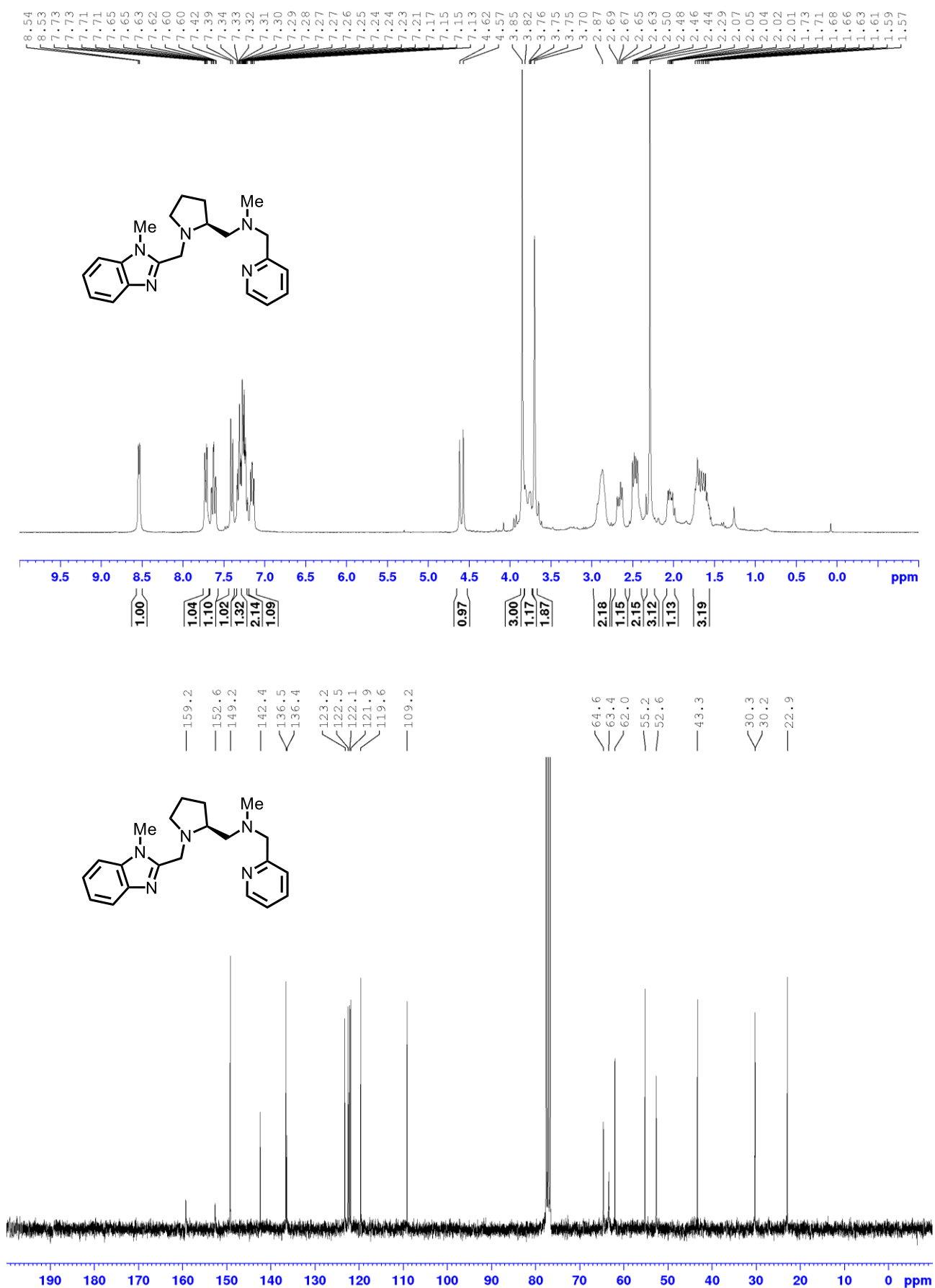


Figure 64: ¹H NMR (300 MHz) and ¹³C-NMR (75 MHz) spectra of **189d** in CDCl₃.

Appendix

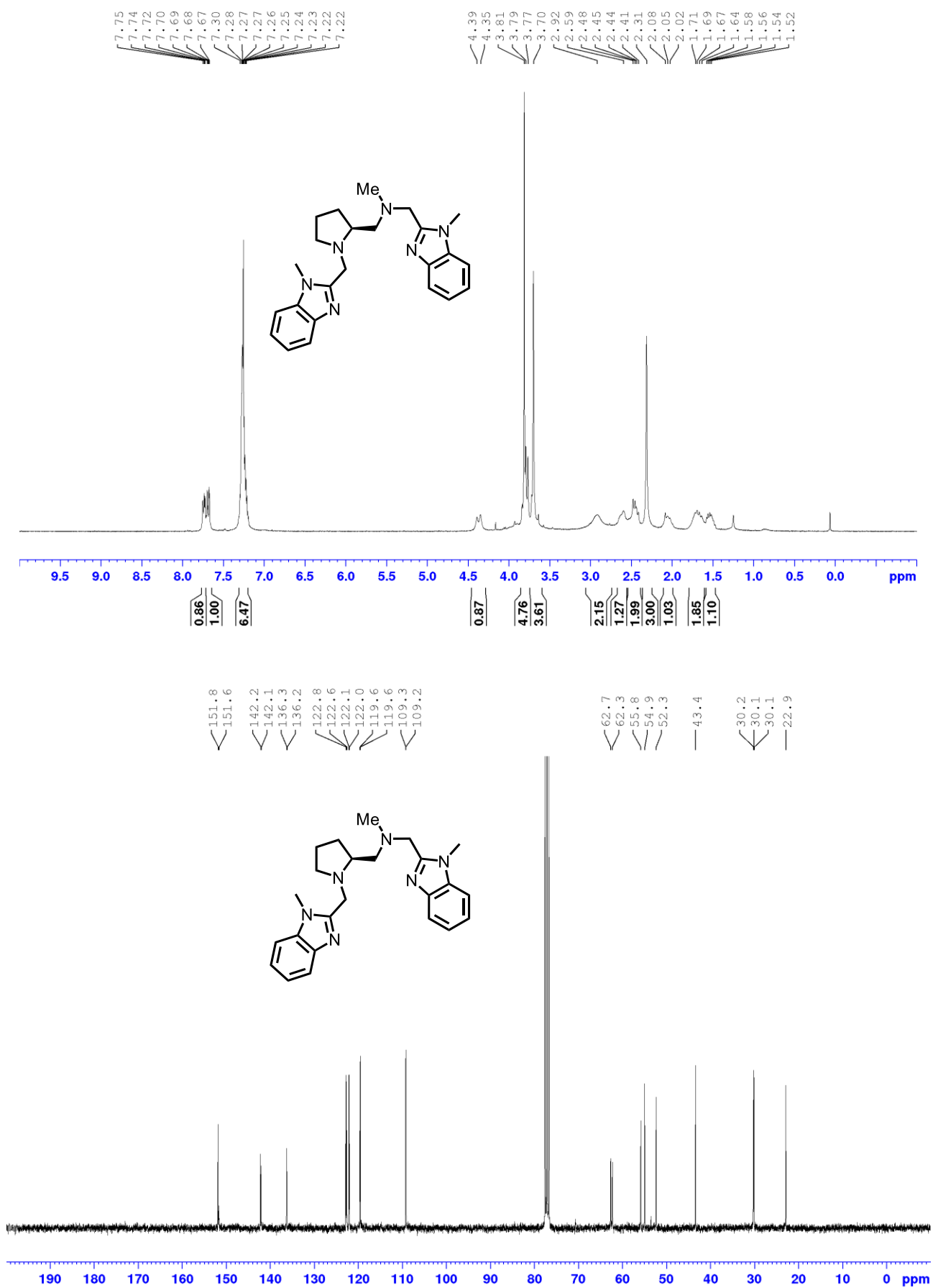


Figure 65: ¹H NMR (300 MHz) and ¹³C-NMR (75 MHz) spectra of **189e** in CDCl₃.

Appendix

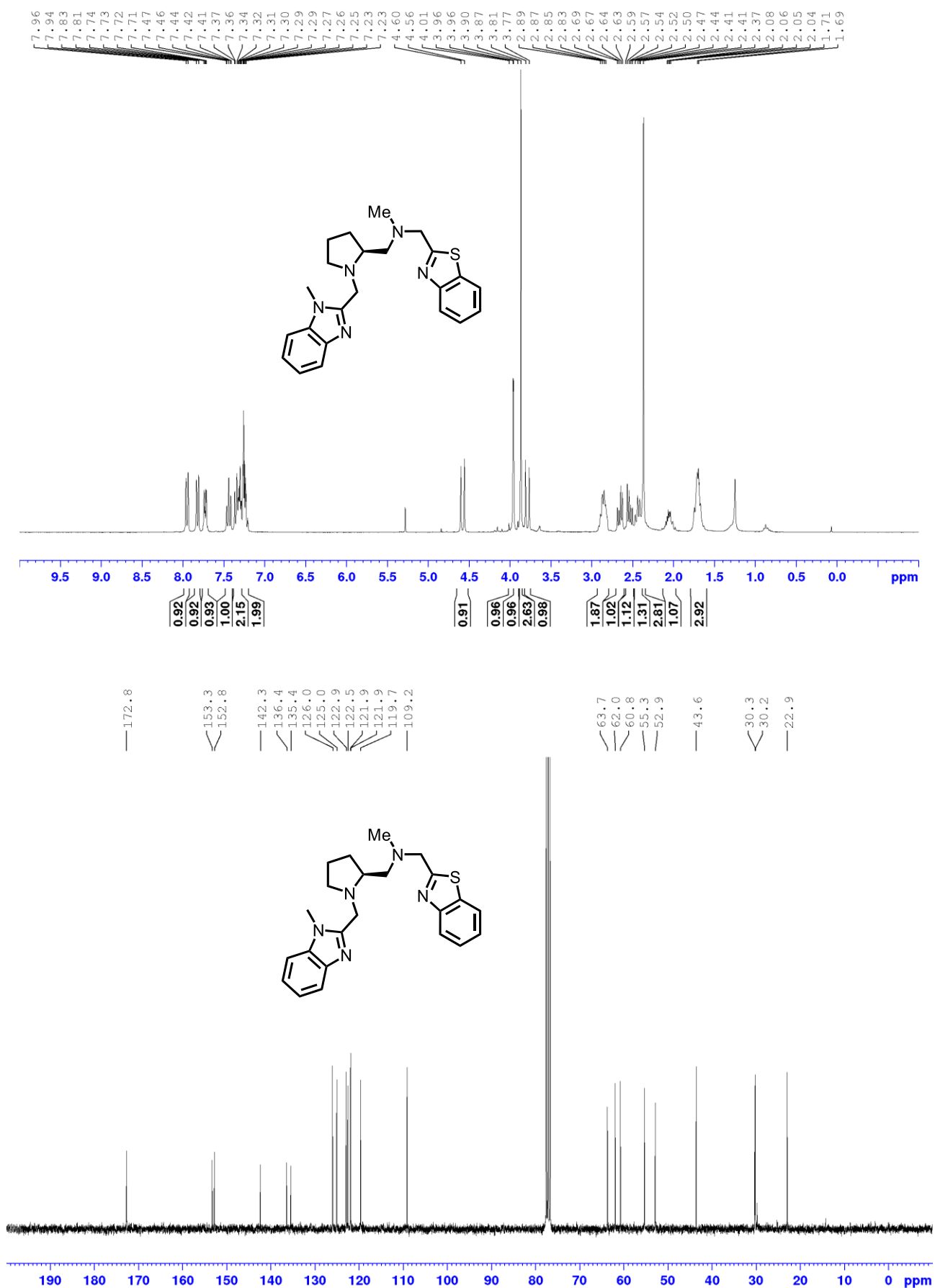


Figure 66: ¹H NMR (300 MHz) and ¹³C-NMR (75 MHz) spectra of **189f** in CDCl₃.

Appendix

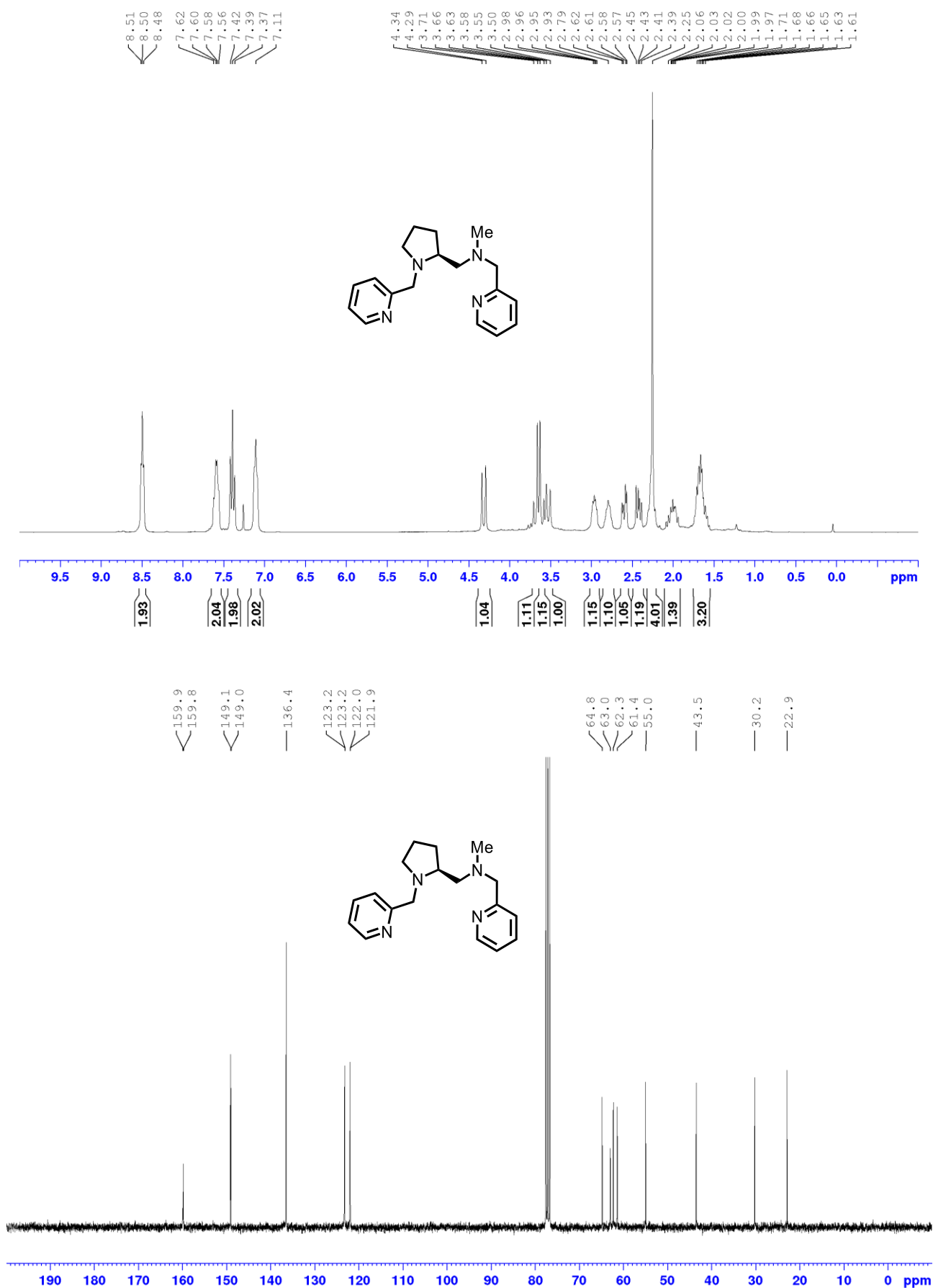


Figure 67: ¹H NMR (300 MHz) and ¹³C-NMR (75 MHz) spectra of **189g** in CDCl₃.

Appendix

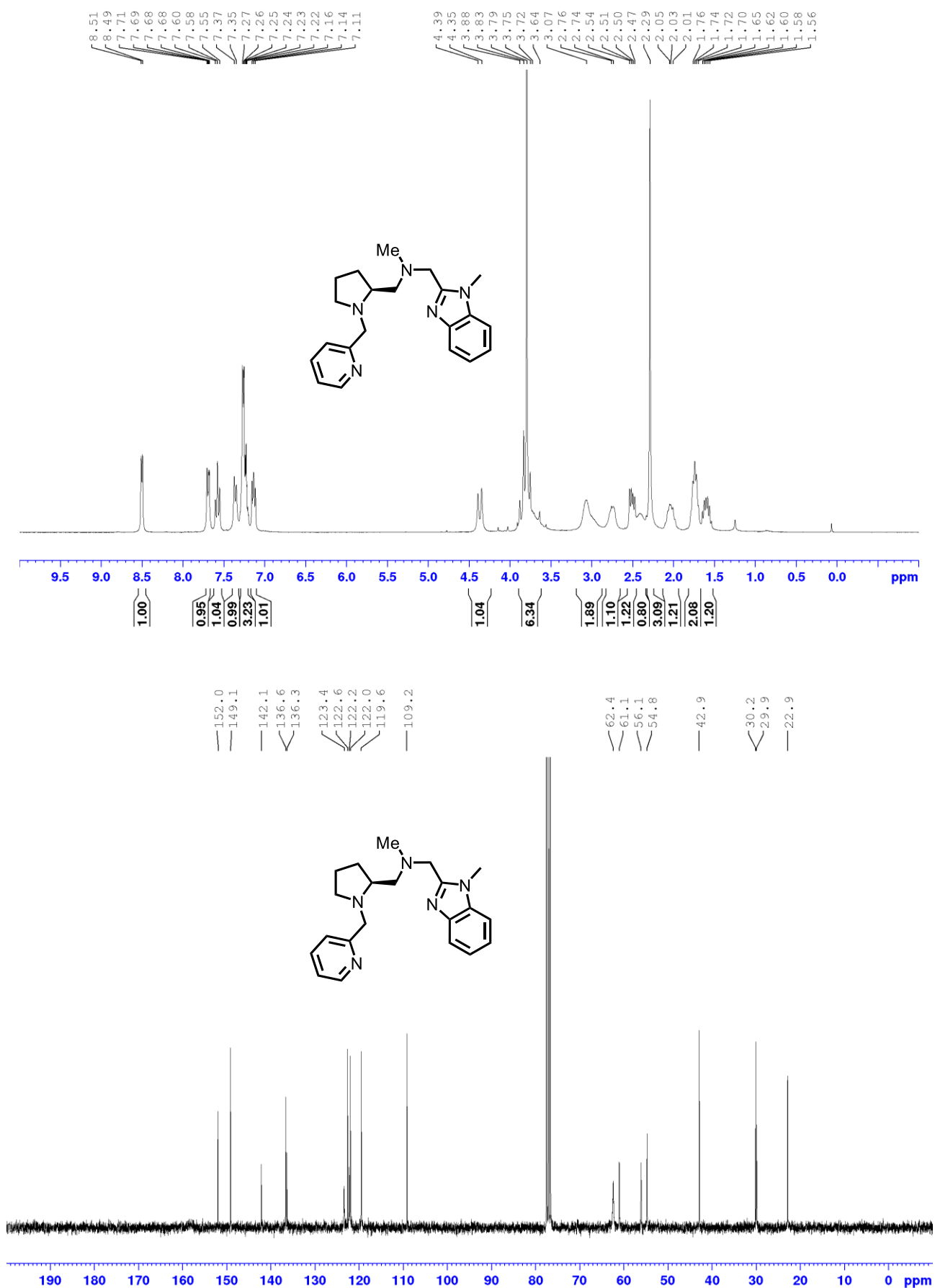


Figure 68: ¹H NMR (300 MHz) and ¹³C-NMR (75 MHz) spectra of **189h** in CDCl₃.

Appendix

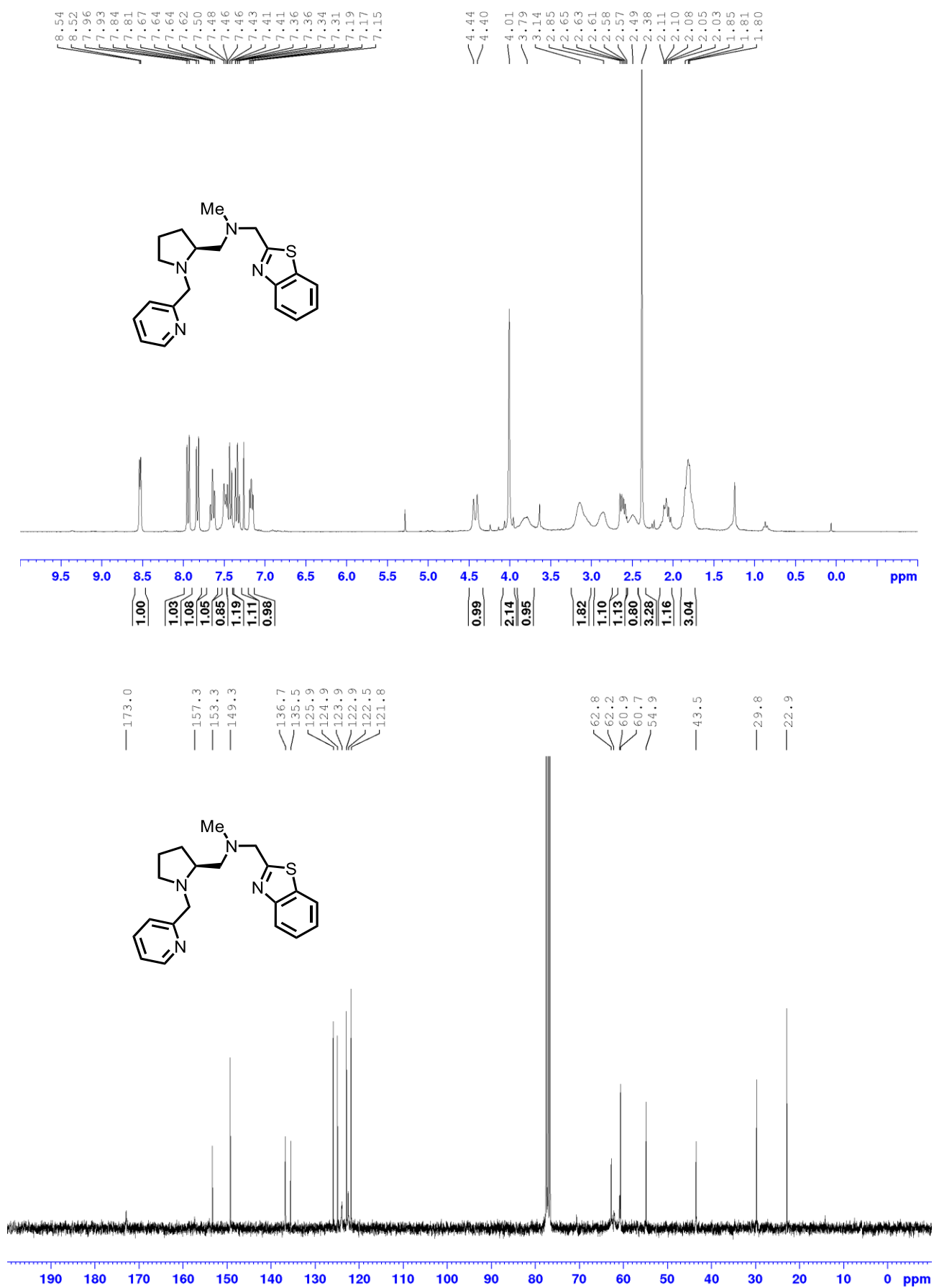


Figure 69: ¹H NMR (300 MHz) and ¹³C-NMR (75 MHz) spectra of **189i** in CDCl₃.

Appendix

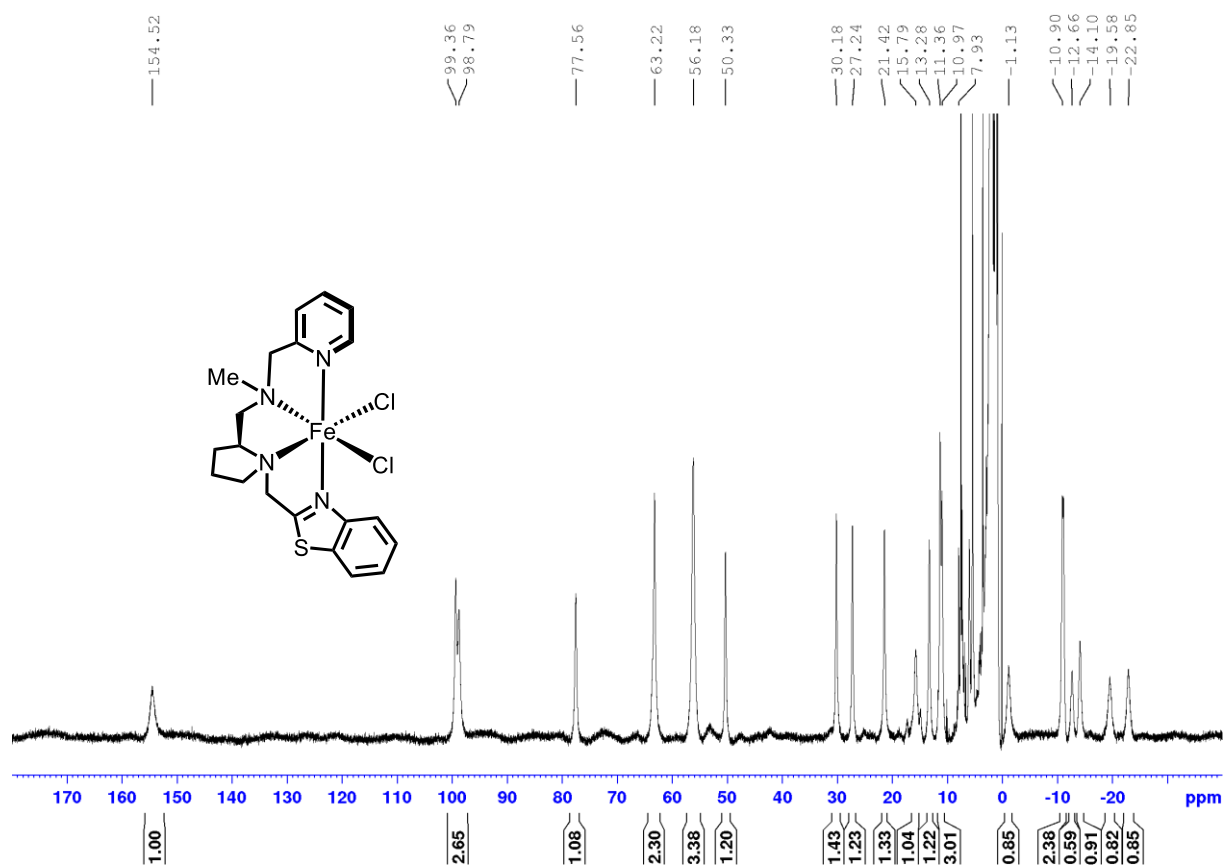
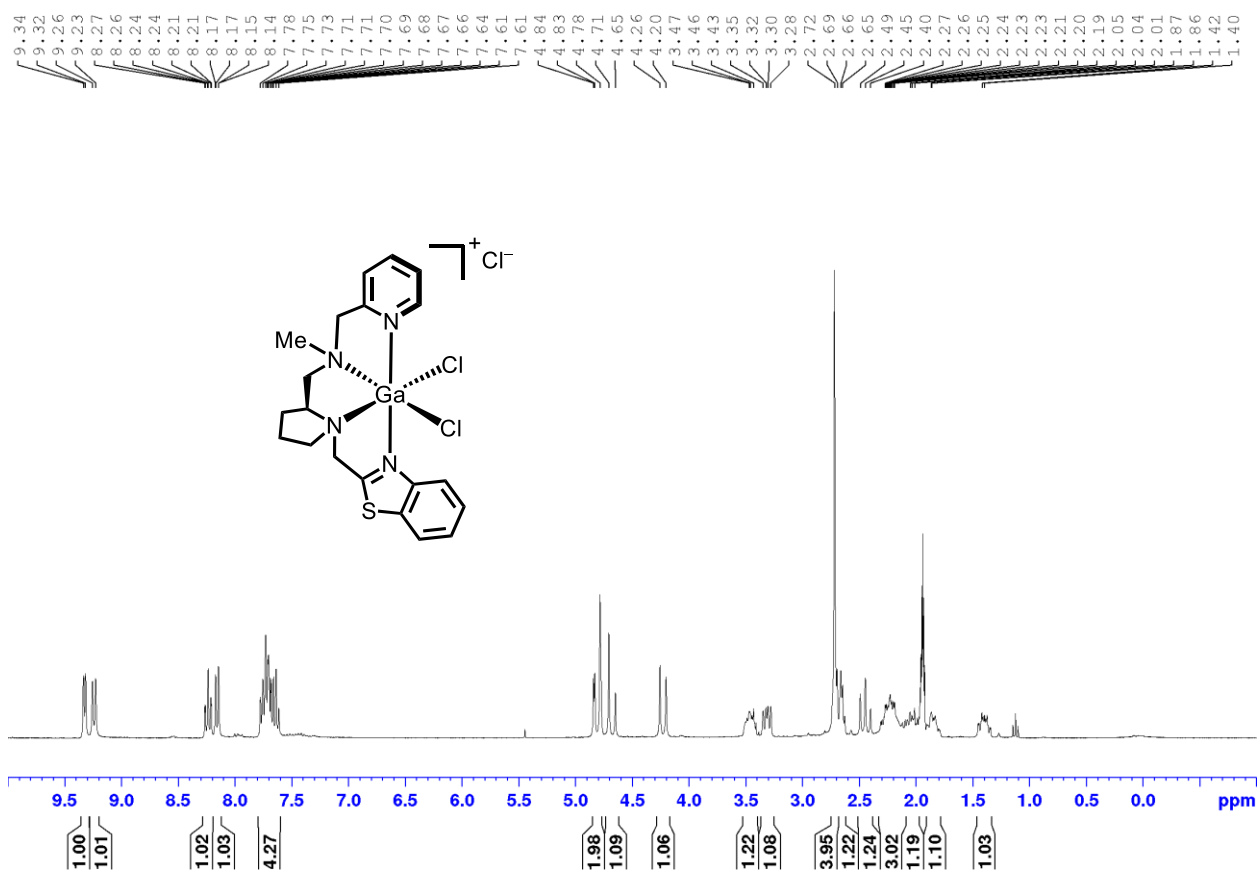


Figure 70: Paramagnetic ^1H NMR spectrum (500 MHz, rt) of complex **191a** in CD_3CN .



Appendix

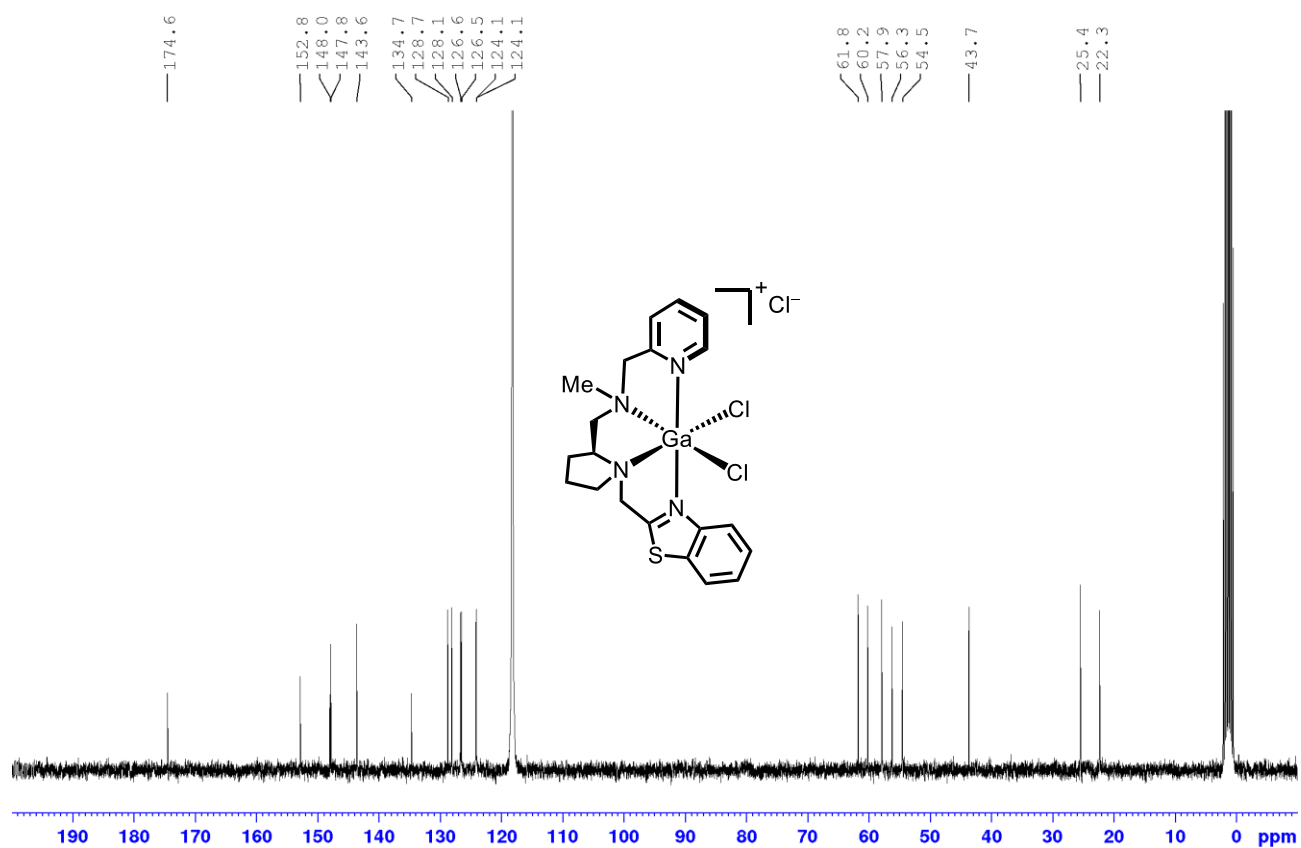


Figure 71: ¹H NMR (300 MHz) and ¹³C-NMR (75 MHz) spectra of complex **192** in CD₃CN.

6.2 Chiral HPLC Traces

This chapter will contain HPLC traces of chiral ligands (Chapter 5.3.3) and chiral products that are related to the follow-up chemistry of 2*H*-azirines (Chapter 5.5.4). HPLC traces of enantiopure 2*H*-azirines **165** and **200** can be found in the Supporting Information of the corresponding publications.^[150,215]

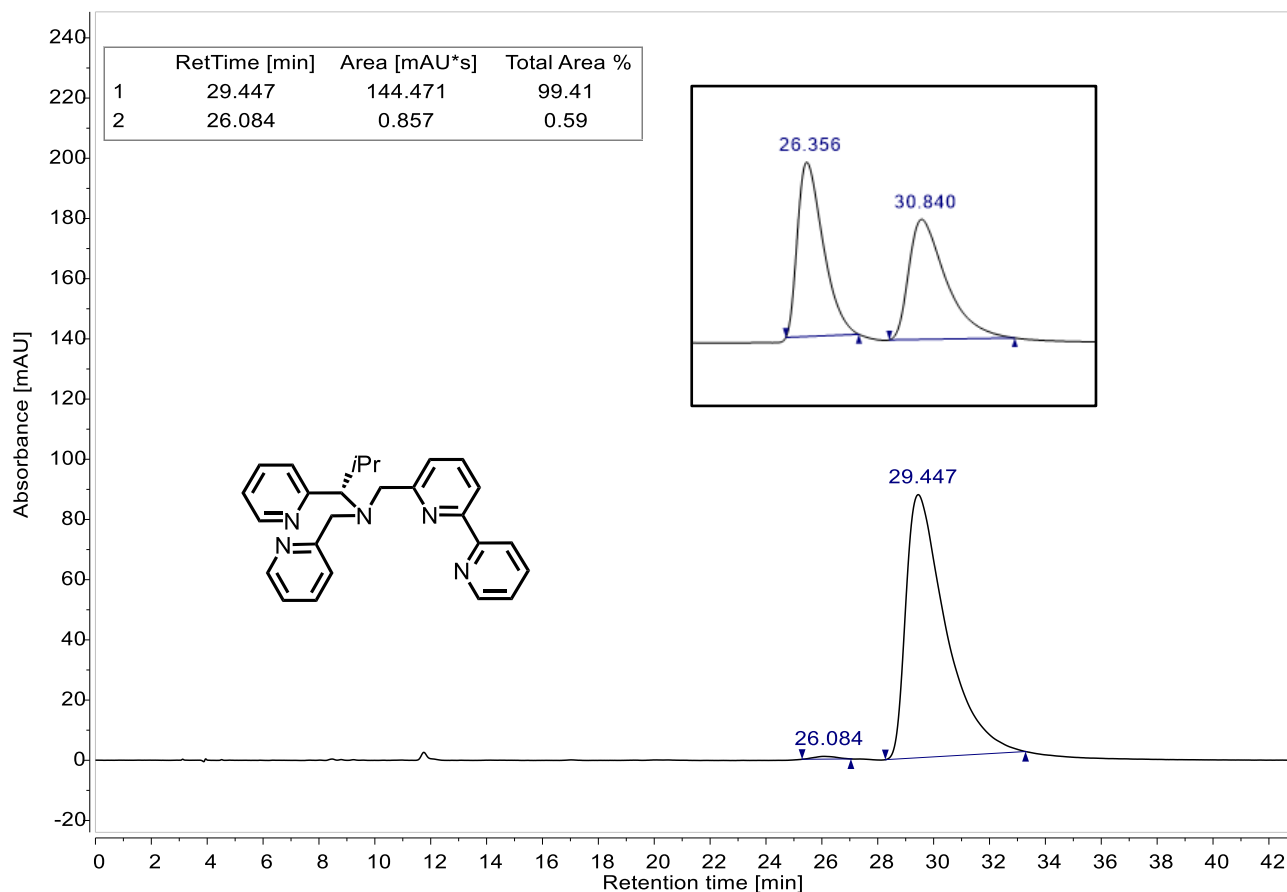


Figure 72: HPLC traces of enantiopure and *rac*-139.

Appendix

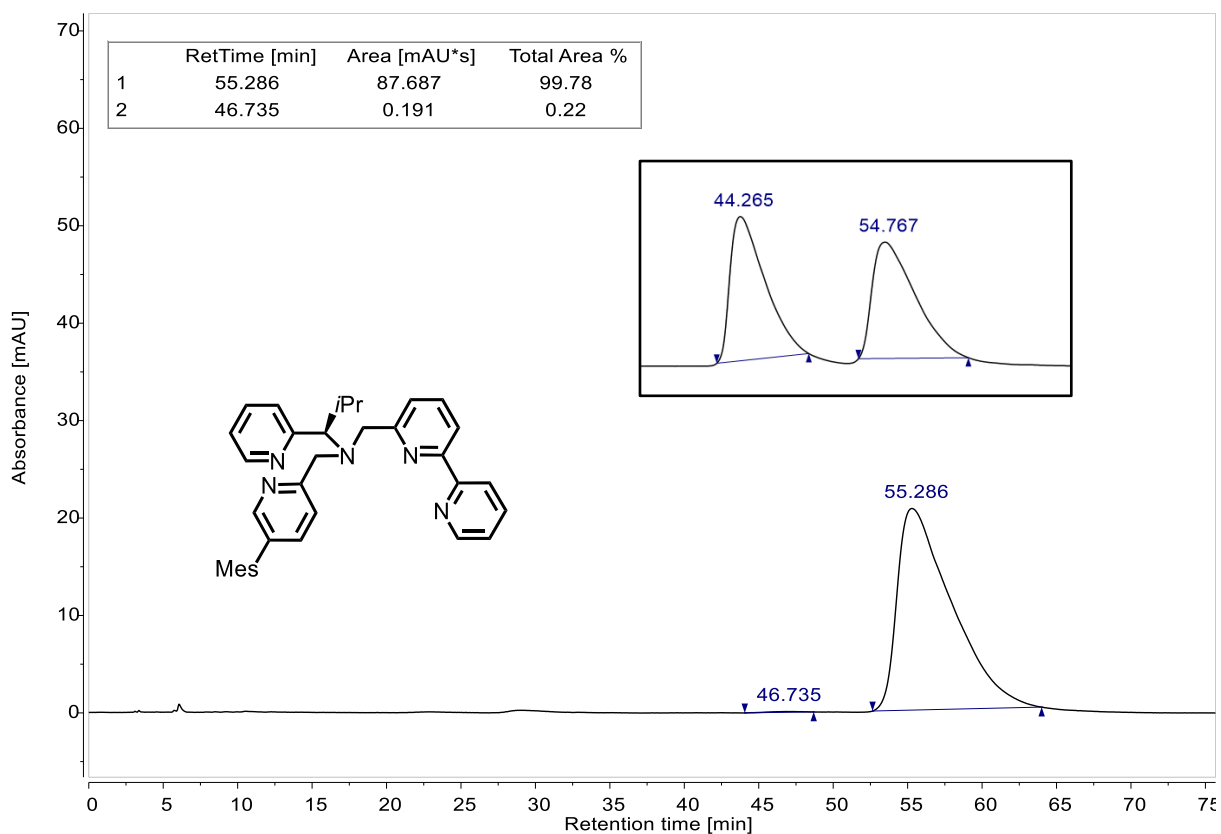


Figure 73: HPLC traces of enantiopure and *rac*-141.

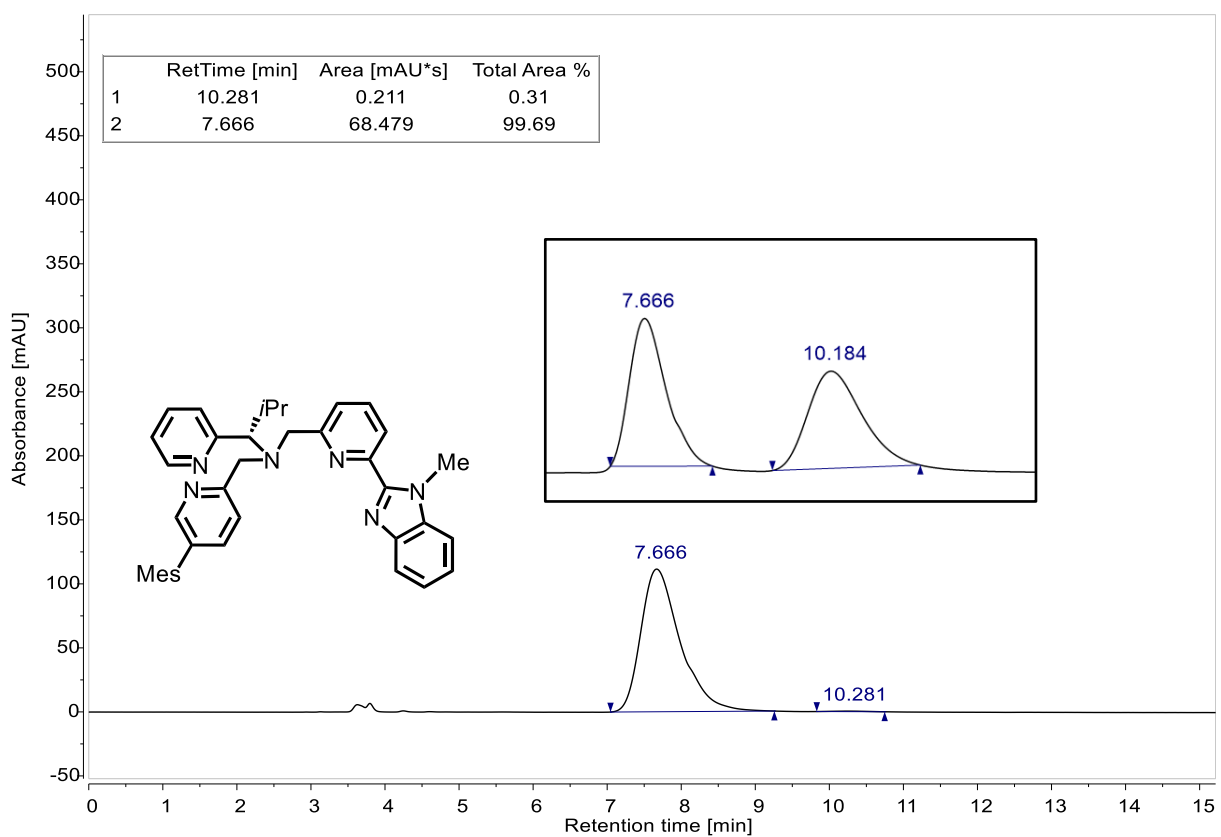


Figure 74: HPLC traces of enantiopure and *rac*-145.

Appendix

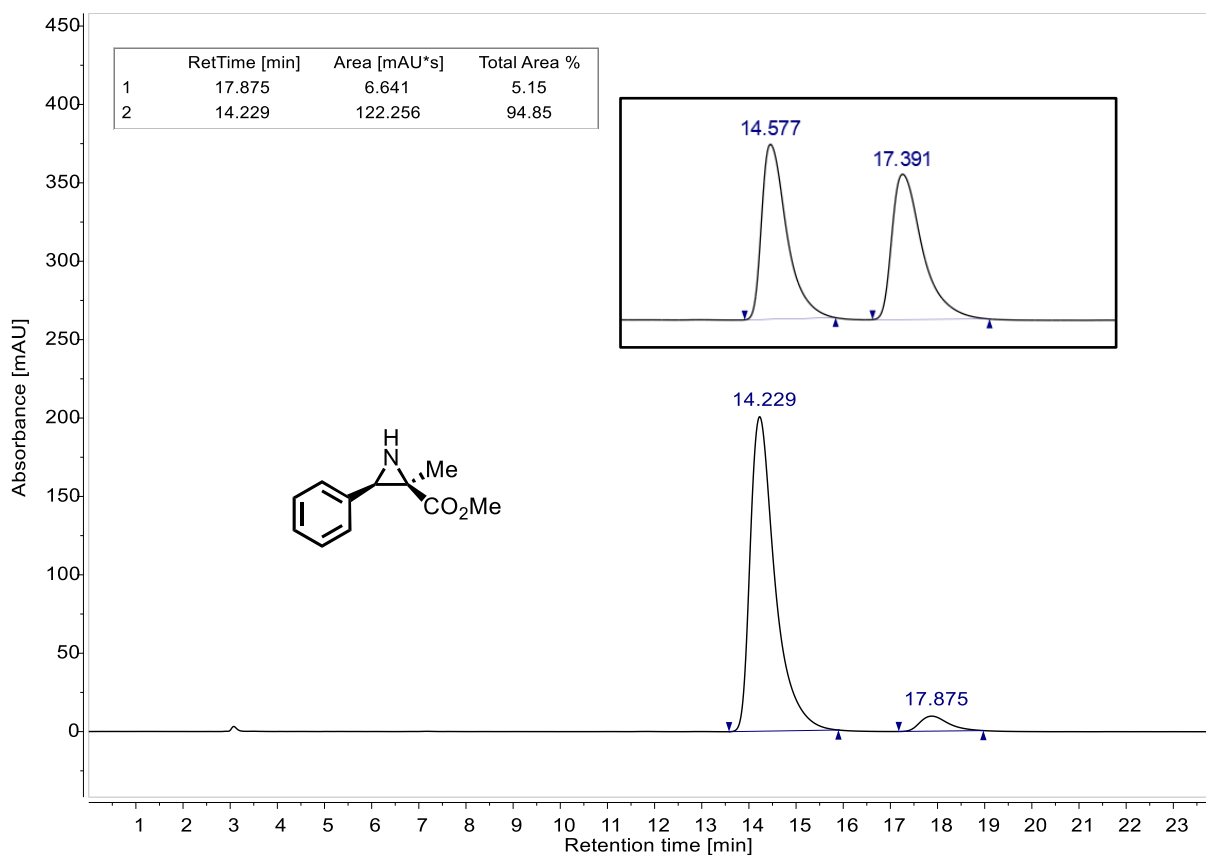


Figure 75: HPLC traces of enantiopure and *rac*-201a.

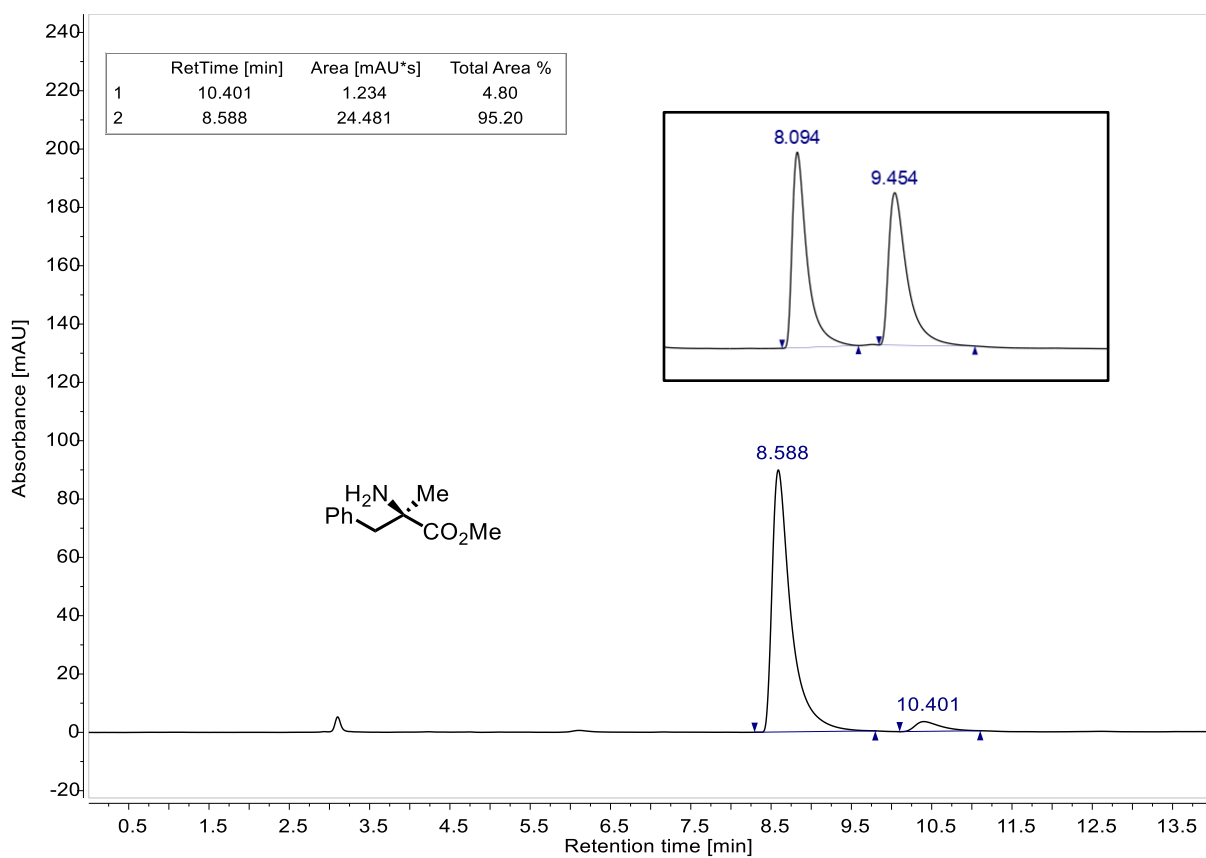


Figure 76: HPLC traces of enantiopure and *rac*-202.

Appendix

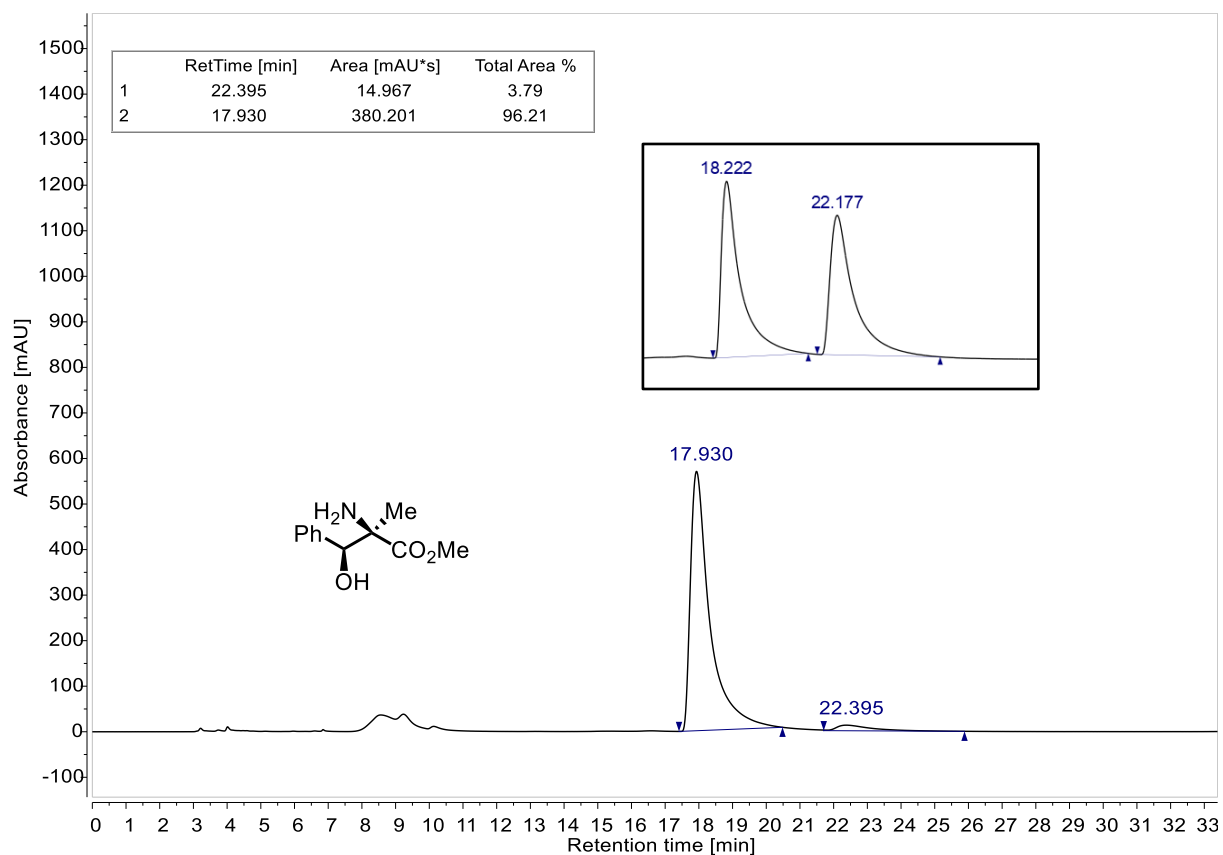


Figure 77: HPLC traces of enantiopure and *rac*-203a.

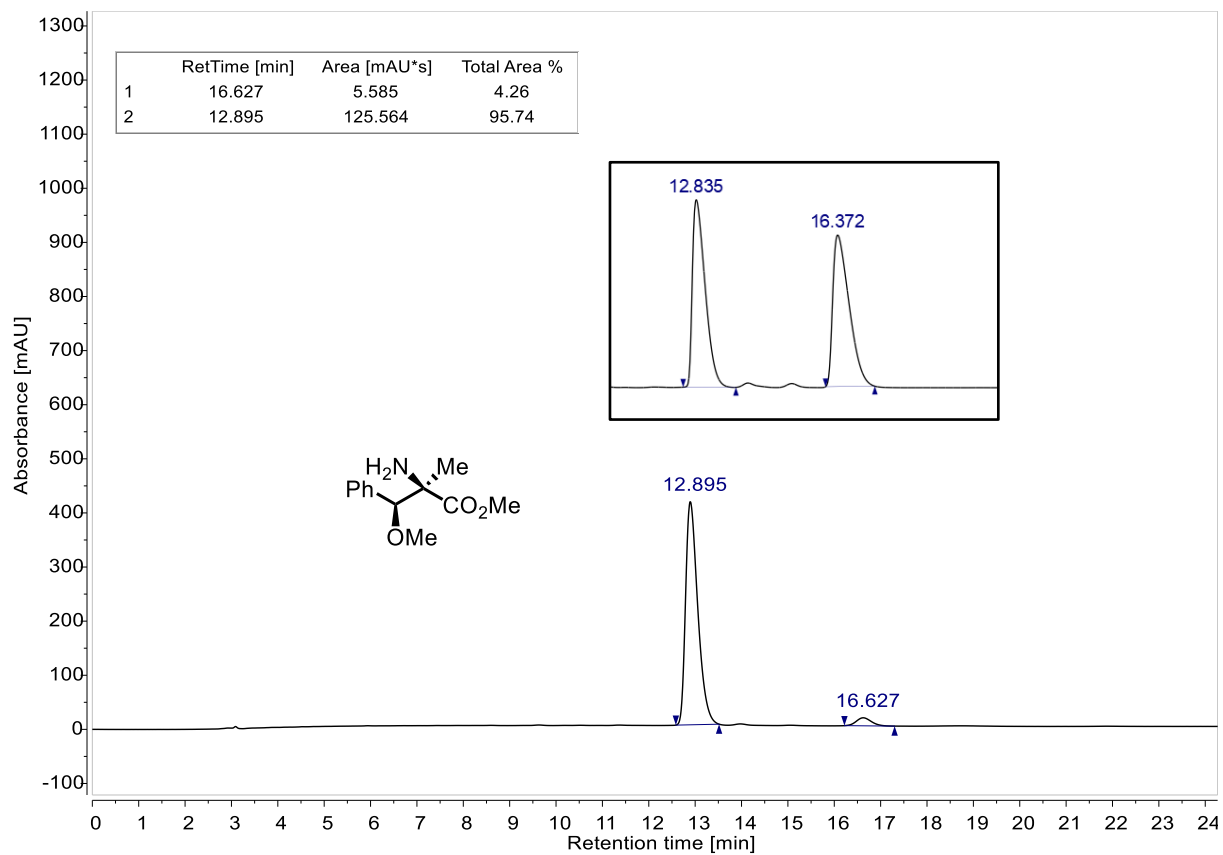


Figure 78: HPLC traces of enantiopure and *rac*-203b.

Appendix

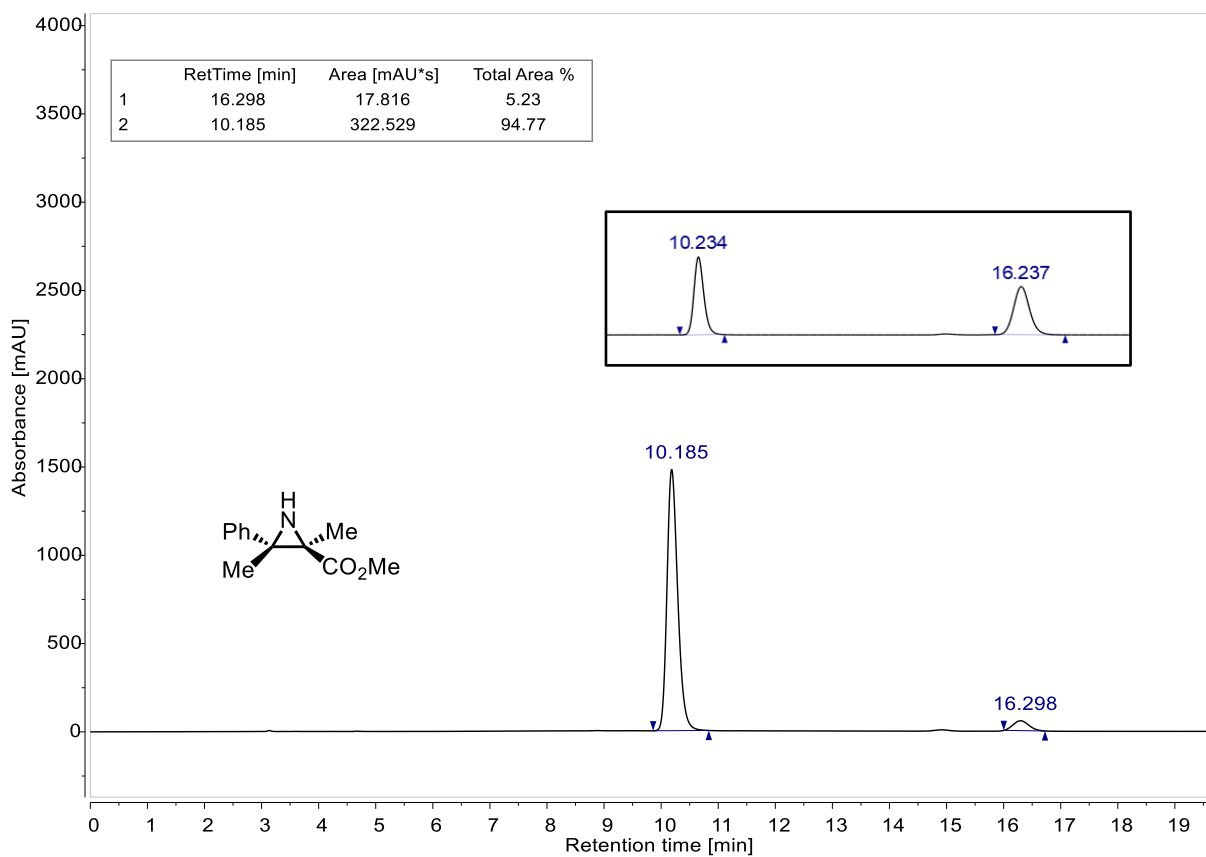


Figure 79: HPLC traces of enantiopure and *rac*-204.

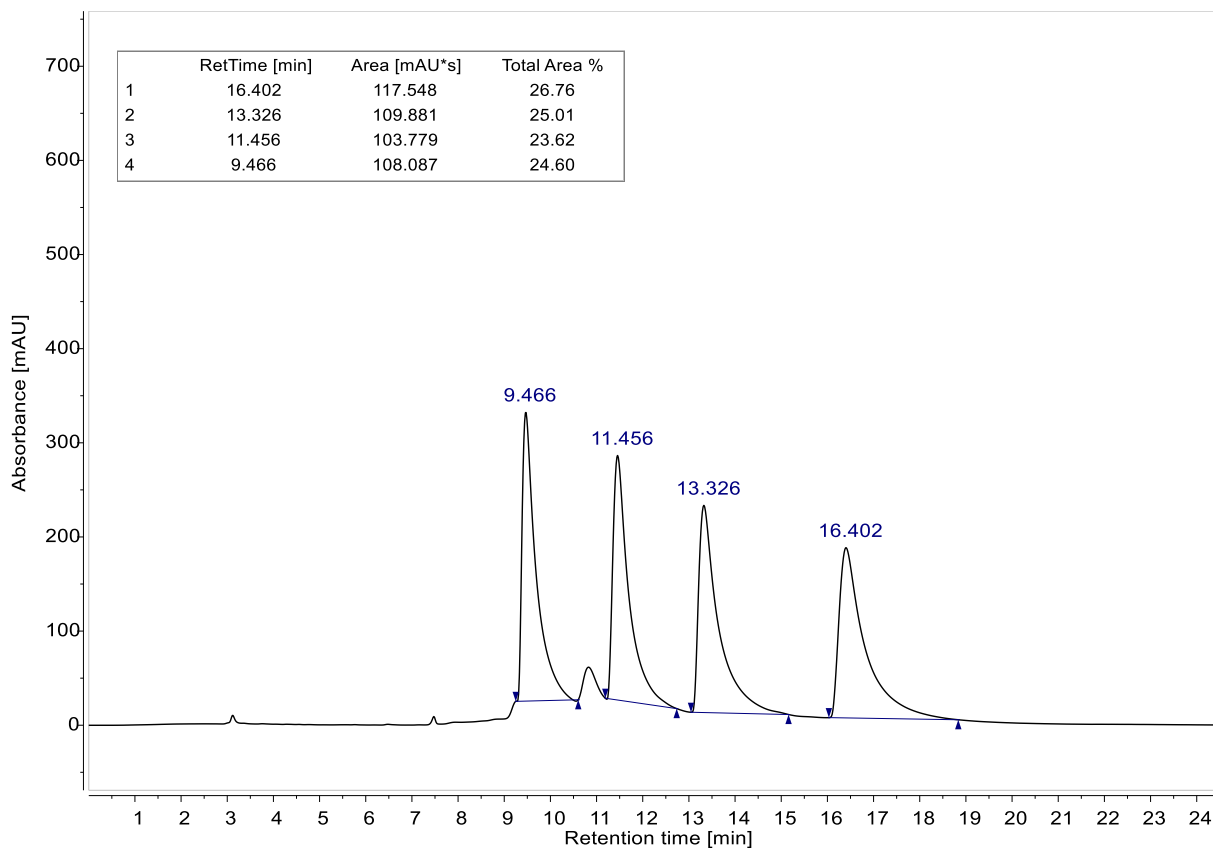


Figure 80: HPLC trace of *rac*-205.

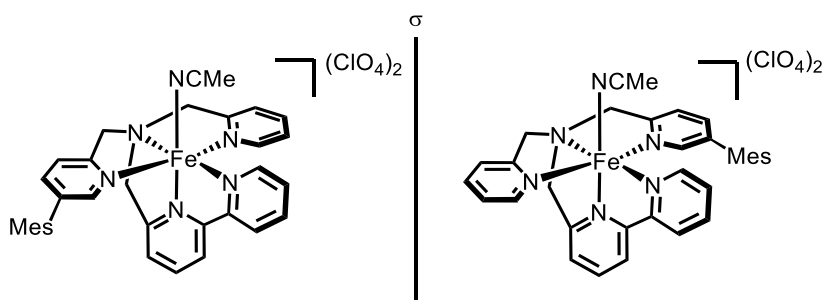
6.3 X-Ray Crystallographic Data

Measurements of single crystals suitable for X-ray crystallographic diffraction were performed by the members of the department for X-ray crystallography at the Philipps-Universität Marburg. Crystal structures of Fe(II)-complexes **121**, **140a**, **149a**, and **191a** were analyzed and evaluated by Dr. (RUS) Sergei I. Ivlev.

Details of growing the single crystals, the crystallographic data, and details of the measurements for structure determination are stated for each crystal structure.

Structures that are part of publications were deposited to the Cambridge Crystallographic Data Centre (CCDC) and can be accessed free of charge via www.cdc.cam.ac.uk/structures.

Single Crystal Structure Determination of Complex **121**



Single crystals of Fe(II)-complex **121** suitable for X-ray crystallographic diffraction were obtained by crystal growth in an NMR tube via slow diffusion. For this purpose, about 3 mg of complex **121** were dissolved in MeCN (ca. 0.2 mL). THF (two drops) was added and the solution was carefully layered with Et₂O. The sample was stored at rt for several days until formation of single crystals was observed.

A suitable crystal of C₃₄H₃₄FeN₆(ClO₄)₂ · C₂H₃N was selected under inert oil and mounted using a MiTeGen loop. Intensity data of the crystal were recorded with a D8 Quest diffractometer (Bruker AXS). The diffractometer was operated with Mo-K α radiation (0.71073 Å, microfocus source) and equipped with a PHOTON 100 detector. Evaluation, integration, and reduction of the diffraction data was carried out using the Bruker APEX 3 software suite.^[282] Multi-scan and numerical absorption corrections were applied using the SADABS program.^[283,284] The structure was solved using dual-space methods (SHELXT-2014/5) and refined against F^2 (SHELXL-2018/3).^[285,286] All non-hydrogen atoms were refined with anisotropic displacement parameters. The hydrogen atoms were refined using the “riding model” approach with isotropic displacement parameters 1.2 times (1.5 times for the methyl groups) of that of the preceding carbon atom.

Appendix

One $[\text{ClO}_4]^-$ anions showed signs of orientation and position disorder and, therefore, its atoms were split in two positions with complementary refined occupancies, restrained bond lengths, and anisotropic displacement parameters. The disordered acetonitrile molecule was refined using the same approach. The solved crystal structure is depicted in Figure 81. Details of the structure determination and selected crystallographic data are listed in Table 29.

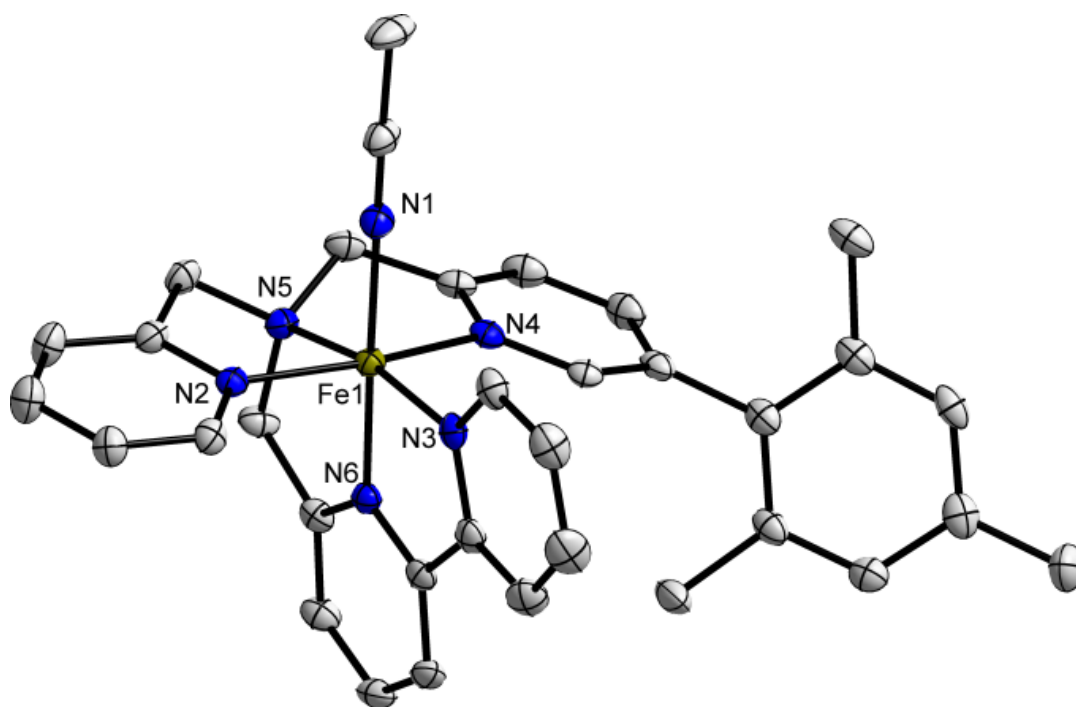


Figure 81: Crystal structure of rac Fe(II)-complex **121** as an ORTEP drawing with 50% probability thermal ellipsoids. Solvent molecules and perchlorate counterions are omitted for clarity.

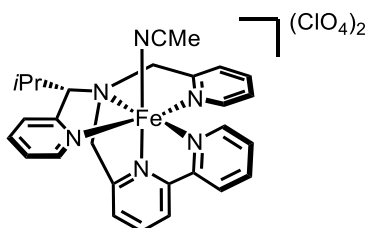
Table 29: Selected Crystallographic Data and Details of Structure Determination for Fe(II)-Complex **121**.

Identification code	mferPS103
Empirical formula	$\text{C}_{36}\text{H}_{37}\text{Cl}_2\text{FeN}_7\text{O}_8$
Molar mass / $\text{g}\cdot\text{mol}^{-1}$	1043.78
Space group (No.)	$P2_1/c$ (14)
a / \AA	10.9616(7)
b / \AA	11.0844(7)
c / \AA	30.8405(19)
β / $^\circ$	94.157(2)
V / \AA^3	3737.3(4)
Z	4
$\rho_{\text{calc.}}$ / $\text{g}\cdot\text{cm}^{-3}$	1.462
μ / mm^{-1}	0.608

Appendix

Color	red
Crystal habitus	block
Crystal size / mm ³	0.291 x 0.242 x 0.119
<i>T</i> / K	100
λ / Å	0.71073 (Mo-K α)
θ range / °	2.206 to 28.373
	$-13 \leq h \leq 13$
Range of Miller indices	$-16 \leq k \leq 13$
	$-53 \leq l \leq 53$
Absorption correction	multi-scan and numerical
<i>T</i> _{min} , <i>T</i> _{max}	0.8769, 0.9513
<i>R</i> _{int} , <i>R</i> σ	0.0500, 0.0296
Completeness of the data set	0.999
No. of measured reflections	85082
No. of independent reflections	9319
No. of parameters	549
No. of restraints	33
No. of constrains	0
<i>S</i> (all data)	1.127
<i>R</i> (<i>F</i>) (<i>I</i> \geq 2 σ (<i>I</i>), all data)	0.0499, 0.0673
<i>wR</i> (<i>F</i> ²) (<i>I</i> \geq 2 σ (<i>I</i>), all data)	0.1040, 0.1104
Extinction coefficient	not refined
$\Delta\rho_{\max}$, $\Delta\rho_{\min}$ / e \cdot Å ⁻³	0.810, -0.538

Single Crystal Structure Determination of Complex 140a



Single crystals of Fe(II)-complex **140a** suitable for X-ray crystallographic diffraction were obtained by crystal growth in an NMR tube via slow diffusion. For this purpose, about 3 mg of complex **140a** were dissolved in MeCN (ca. 0.2 mL) and the solution was carefully layered with Et₂O. The sample was stored at rt for several days until formation of single crystals was observed.

A suitable crystal of C₂₈H₃₀FeN₆ · 2 ClO₄ was selected under inert oil and mounted using a MiTeGen loop. Intensity data of the crystal was recorded with a STADIVARI diffractometer (Stoe & Cie). The diffractometer was operated with Cu-K α radiation (1.54186 Å, microfocus source) and equipped with a Dectris PILATUS 300K detector. Evaluation, integration, and reduction of the diffraction data was

Appendix

carried out using the X-Area software suite.^[287] Multi-scan and numerical absorption corrections were applied with the LANA and X-RED32 modules of the X-Area software suite.^[288,289] The structures were solved using dual-space methods (SHELXT-2018/2) and refined against F^2 (SHELXL-2018/3 using ShelXle interface).^[285,286,290] All non-hydrogen atoms were refined with anisotropic displacement parameters. The hydrogen atoms were refined using the “riding model” approach with isotropic displacement parameters 1.2 times (1.5 times for the methyl groups) of that of the preceding carbon atom.

Two of the four $[\text{ClO}_4]^-$ were refined using a split model in order to account for disorder. One of the two cations in the asymmetric unit has an isopropyl group disordered between two positions, which was refined accordingly. The crystal structure contains two small solvent accessible voids with weak peaks on the Fourier difference map. It was not possible to unambiguously distinguish between real small molecule (e.g. water) or an artifact, therefore, this peak was eliminated using the SQUEEZE algorithm implemented in the PLATON software.^[291] CCDC 2061419 contains the supplementary crystallographic data for this structure. These data can be obtained free of charge from The Cambridge Crystallographic Data Centre via www.ccdc.cam.ac.uk/structures. The solved crystal structure is depicted in Figure 82. Details of the structure determination and selected crystallographic data are listed in Table 30.

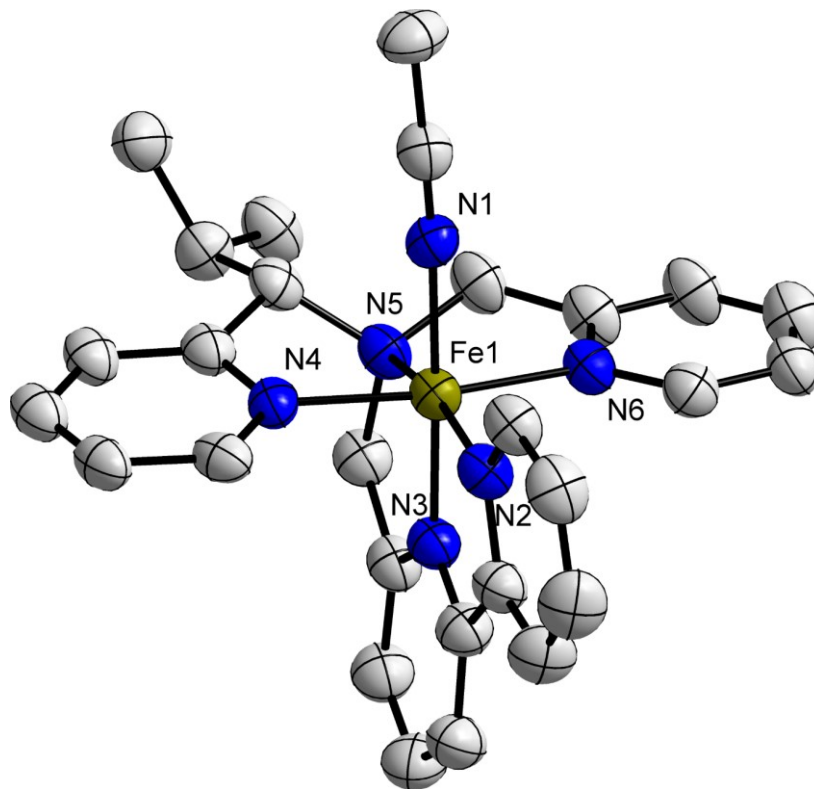
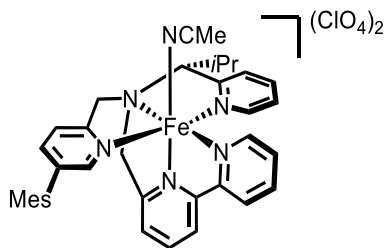


Figure 82: Crystal structure of Fe(II)-complex **140a** as an ORTEP drawing with 50% probability thermal ellipsoids. Solvent molecules and perchlorate counterions are omitted for clarity.

Appendix

Table 30: Selected Crystallographic Data and Details of Structure Determination for Fe(II)-Complex **140a**.

Identification code	mferPS174
Empirical formula	C ₂₈ H ₃₀ Cl ₂ FeN ₆ O ₈
Molar mass / g·mol ⁻¹	705.33
Space group (No.)	<i>P</i> 2 ₁ (4)
<i>a</i> / Å	17.6340(5)
<i>b</i> / Å	10.0115(2)
<i>c</i> / Å	17.9621(6)
β / °	106.724(2)
<i>V</i> / Å ³	3036.95(15)
<i>Z</i>	4
$\rho_{calc.}$ / g·cm ⁻³	1.543
μ / mm ⁻¹	6.123
Color	red
Crystal habitus	plate
Crystal size / mm ³	0.202 x 0.099 x 0.036
<i>T</i> / K	100
λ / Å	1.54186 (Cu-K α)
θ range / °	3.095 to 75.361
	$-22 \leq h \leq 21$
Range of Miller indices	$-12 \leq k \leq 12$
	$-12 \leq l \leq 22$
Absorption correction	multi-scan and numerical
<i>T</i> _{min} , <i>T</i> _{max}	0.0829, 0.6562
<i>R</i> _{int} , <i>R</i> _{σ}	0.0461, 0.0441
Completeness of the data set	0.999
No. of measured reflections	57121
No. of independent reflections	12116
No. of parameters	903
No. of restraints	492
<i>S</i> (all data)	1.147
<i>R</i> (<i>F</i>) (<i>I</i> ≥ 2σ(<i>I</i>), all data)	0.0759, 0.0899
<i>wR</i> (<i>F</i> ²) (<i>I</i> ≥ 2σ(<i>I</i>), all data)	0.2122, 0.2212
Extinction coefficient	not refined
Flack parameter <i>x</i>	-0.025(5)
$\Delta\rho_{max}$, $\Delta\rho_{min}$ / e·Å ⁻³	0.774, -0.569

Single Crystal Structure Determination of Complex **149a**

Single crystals of Fe(II)-complex **149a** suitable for X-ray crystallographic diffraction were obtained by crystal growth in an NMR tube via slow diffusion. For this purpose, about 3 mg of complex **149a** were dissolved in MeCN (ca. 0.2 mL) and the solution was carefully layered with Et₂O. The sample was stored at rt for several days until formation of single crystals was observed.

A suitable crystal of C₃₇H₄₀FeN₆(ClO₄)₂ · 2 C₂H₃N was selected under inert oil and mounted using a MiTeGen loop. Intensity data of the crystal was recorded with a STADIVARI diffractometer (Stoe & Cie). The diffractometer was operated with Cu-K_α radiation (1.54186 Å, microfocus source) and equipped with a Dectris PILATUS 300K detector. Evaluation, integration, and reduction of the diffraction data was carried out using the X-Area software suite.^[287] Multi-scan and numerical absorption corrections were applied with the LANA and X-RED32 modules of the X-Area software suite.^[288,289] The structures were solved using dual-space methods (SHELXT-2018/2) and refined against *F*² (SHELXL-2018/3 using ShelXle interface).^[285,286,290] All non-hydrogen atoms were refined with anisotropic displacement parameters. The hydrogen atoms were refined using the “riding model” approach with isotropic displacement parameters 1.2 times (1.5 times for the methyl groups) of that of the preceding carbon atom.

The [ClO₄][−] anion lying on the special position (2-fold rotation axis) showed signs of disorder, however, no significant model improvement could be achieved either by moving the Cl atom away from the special position or by twin refinement in the space group *C*1 (*P*1). The residual electron density in the solvent-accessible voids could not be satisfactorily modelled and was eliminated using the SQUEEZE algorithm in the PLATON software.^[291,292] CCDC 2063648 contains the supplementary crystallographic data for this paper. These data can be obtained free of charge from The Cambridge Crystallographic Data Centre via www.ccdc.cam.ac.uk/structures. The solved crystal structure is depicted in Figure 83. Details of the structure determination and selected crystallographic data are listed in Table 31.

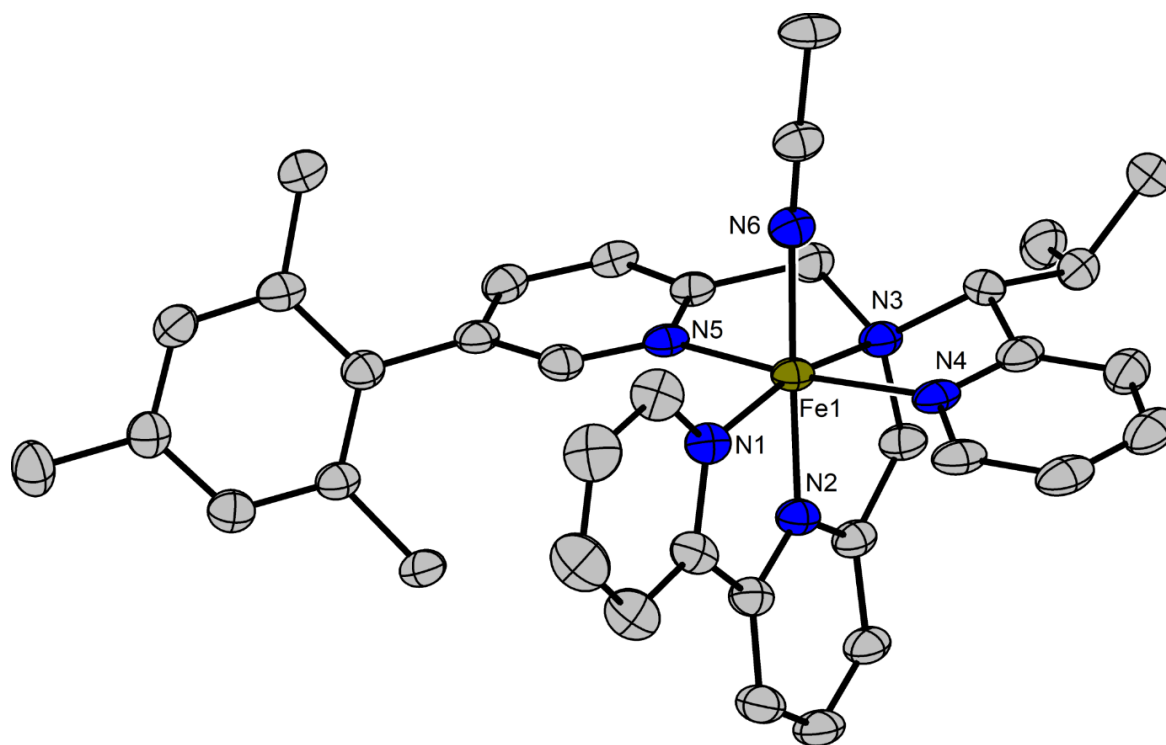


Figure 83: Crystal structure of Fe(II)-complex **149a** as an ORTEP drawing with 50% probability thermal ellipsoids. Solvent molecules and perchlorate counterions are omitted for clarity.

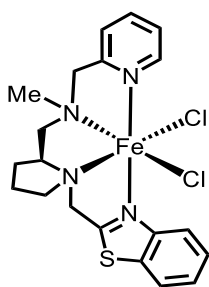
Table 31: Selected Crystallographic Data and Details of Structure Determination for Fe(II)-Complex **149a**.

Identification code	PS200
Empirical formula	C ₄₁ H ₄₆ Cl ₂ FeN ₈ O ₈
Molar mass / g·mol ⁻¹	905.61
Space group (No.)	C2 (5)
<i>a</i> / Å	33.3550(5)
<i>b</i> / Å	15.0190(2)
<i>c</i> / Å	8.92030(10)
β / °	90.7160(10)
<i>V</i> / Å ³	4468.35(10)
<i>Z</i>	4
$\rho_{calc.}$ / g·cm ⁻³	1.346
μ / mm ⁻¹	4.298
Color	red
Crystal habitus	needle
Crystal size / mm ³	0.256 x 0.097 x 0.045
<i>T</i> / K	100
λ / Å	1.54186 (Cu-K α)
θ range / °	4.949 to 75.438
	-41 ≤ <i>h</i> ≤ 41
Range of Miller indices	-18 ≤ <i>k</i> ≤ 18
	-5 ≤ <i>l</i> ≤ 10

Appendix

Absorption correction	multi-scan and numerical
T_{\min} , T_{\max}	0.406, 0.830
R_{int} , R_{σ}	0.0410, 0.0344
Completeness of the data set	0.997
No. of measured reflections	50540
No. of independent reflections	9025
No. of parameters	550
No. of restraints	1
S (all data)	1.093
$R(F)$ ($I \geq 2\sigma(I)$, all data)	0.0418, 0.0479
$wR(F^2)$ ($I \geq 2\sigma(I)$, all data)	0.1079, 0.1107
Extinction coefficient	not refined
Flack parameter x	-0.010(3)
$\Delta\rho_{\max}$, $\Delta\rho_{\min}$ / $\text{e} \cdot \text{\AA}^{-3}$	0.581, -0.555

Single Crystal Structure Determination of Complex **191a**



Single crystals of Fe(II)-complex **191a** suitable for X-ray crystallographic diffraction were obtained by crystal growth in an NMR tube via slow diffusion. For this purpose, about 3 mg of complex **191a** were dissolved in MeCN (ca. 0.2 mL) and the solution was carefully layered with Et₂O. The sample was stored at rt for several days until formation of single crystals was observed.

A suitable crystal of C₂₀H₂₄FeN₄SCl₂ was selected under inert oil and mounted using a MiTeGen loop. Intensity data of the crystal were recorded with a STADIVARI diffractometer (Stoe & Cie). The diffractometer was operated with Cu-K α radiation (1.54186 Å, microfocus source) and equipped with a Dectris PILATUS 300K detector. Evaluation, integration and reduction of the diffraction data was carried out using the X-Area software suite.^[287] Multi-scan and numerical absorption corrections were applied with the LANA and X-RED32 modules of the X-Area software suite.^[288,289] The structure was solved using dual-space methods (SHELXT-2018/2) and refined against F^2 (SHELXL-2019/1 using ShelXle interface).^[285,286,290] All non-hydrogen atoms were refined with anisotropic displacement parameters. The hydrogen atoms were refined using the “riding model” approach with isotropic displacement parameters 1.2 times (1.5 times for the methyl groups) of that of the preceding

Appendix

carbon atom. CCDC 2237550 contains the supplementary crystallographic data for this paper. These data can be obtained free of charge from The Cambridge Crystallographic Data Centre via www.ccdc.cam.ac.uk/structures. The solved crystal structure is depicted in Figure 84. Details of the structure determination and selected crystallographic data are listed in Table 32.

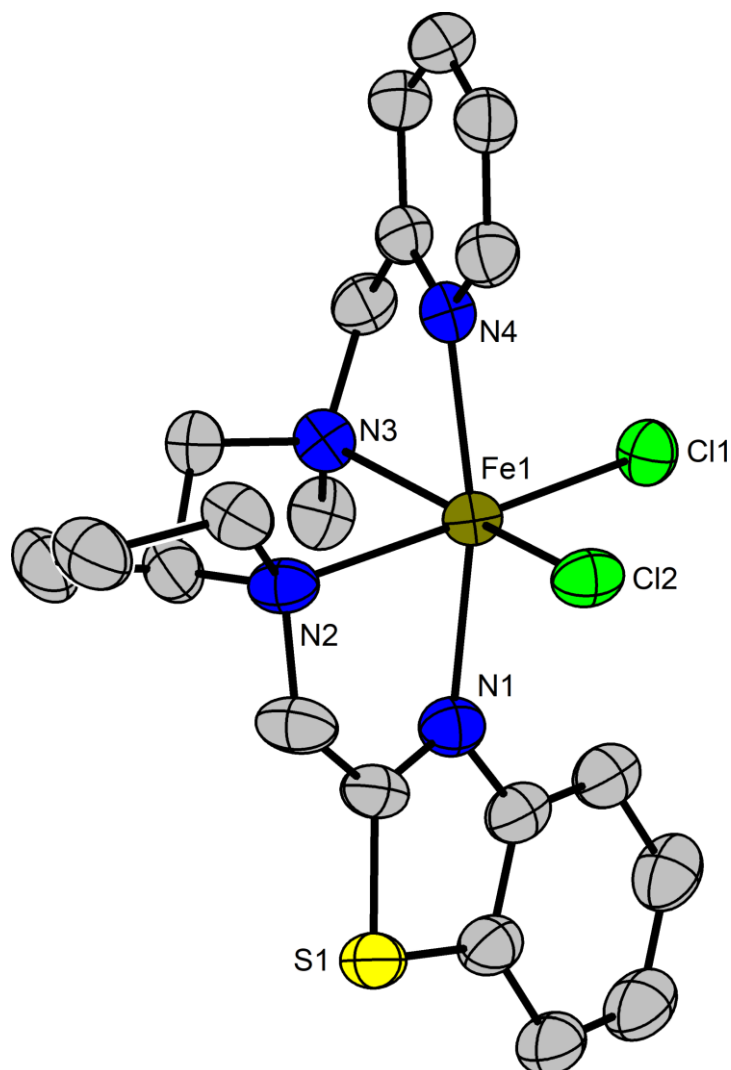


Figure 84: Crystal structure of Fe(II)-complex **191a** as an ORTEP drawing with 50% probability thermal ellipsoids. Solvent molecules and perchlorate counterions are omitted for clarity.

Table 32: Selected Crystallographic Data and Details of Structure Determination for Fe(II)-Complex **191a**.

Identification code	PS1274
Empirical formula	C ₂₀ H ₂₄ Cl ₂ FeN ₄ S
Molar mass / g·mol ⁻¹	479.24
Space group (No.)	<i>P</i> 2 ₁ 2 ₁ 2 ₁ (19)
<i>a</i> / Å	9.3857(2)
<i>b</i> / Å	13.5917(2)
<i>c</i> / Å	16.3490(4)

Appendix

$V / \text{\AA}^3$	2085.60(7)
Z	4
$\rho_{\text{calc.}} / \text{g}\cdot\text{cm}^{-3}$	1.526
μ / mm^{-1}	9.197
Color	yellow
Crystal habitus	plate
Crystal size / mm^3	0.072 x 0.048 x 0.015
T / K	100
$\lambda / \text{\AA}$	1.54186 (Cu- K_{α})
θ range / $^{\circ}$	4.230 to 76.093
	$-5 \leq h \leq 11$
Range of Miller indices	$-17 \leq k \leq 16$
	$-19 \leq l \leq 20$
Absorption correction	multi-scan and numerical
$T_{\text{min}}, T_{\text{max}}$	0.5204, 0.8707
$R_{\text{int}}, R_{\sigma}$	0.0460, 0.0298
Completeness of the data set	0.999
No. of measured reflections	24051
No. of independent reflections	4310
No. of parameters	254
No. of restraints	0
S (all data)	1.049
$R(F)$ ($I \geq 2\sigma(I)$, all data)	0.0436, 0.0533
$wR(F^2)$ ($I \geq 2\sigma(I)$, all data)	0.1050, 0.1121
Extinction coefficient	not refined
Flack parameter x	-0.017(4)
$\Delta\rho_{\text{max}}, \Delta\rho_{\text{min}} / \text{e}\cdot\text{\AA}^{-3}$	0.304, -0.334

7. Abbreviations and Symbols

{ ¹ H}	proton decoupled	Cp*	1,2,3,4,5-pentamethylcyclopentadienyl
δ	chemical shift	1,2-DCB	1,2-dichlorobenzene
λ	wavelength	1,2-DCE	1,2-dichloroethane
Λ	absolute stereochemical descriptor: left-handed propeller	DET	Diethyl tartrate
Δ	absolute stereochemical descriptor: right-handed propeller	DMBA	2,2-dimethylbutanoic acid
$\tilde{\nu}$	wavenumber	DiPAMP	1,2-bis[(2-methoxyphenyl)(phenyl)phosphanyl]ethane
σ	mirror plane	DMAP	4-(dimethylamino)pyridine
τ _m	mixing time	DMF	<i>N,N</i> -dimethylformamide
Ac	acyl	DMSO	dimethylsulfoxid
AcOH	acetic acid	DQF-COSY	double-quantum filtered correlation spectroscopy
APCI	atmospheric pressure chemical ionization	d.r.	diastereomeric ratio
aq.	aqueous	DVB	divinylbenzene
aux	auxiliary	E _{1/2}	half wave potential or redox potential
BAr _F	Tetrakis(3,5-bis(trifluoromethyl)phenyl)borate	ee	enantioemeric excess
9-BBN	9-borabicyclo(3.3.1)nonane	2-eha	2-ethylhexanoic acid
BINAP	2,2'-bis(diphenylphosphino)-	<i>e.g.</i>	<i>exempli gratia</i> (“example given”)
BINOL	1,1'-binaphthyl	eq.	equivalents
Bn	benzyl	ESI	electrospray ionization
Boc	<i>tert</i> -butyloxycarbonyl	Et	ethyl
bopa	bis(oxazolinyphenyl)amine	<i>et al.</i>	<i>et alii</i> (“and others”)
BOX	bis(oxazoline)	Et ₂ O	diethylether
brine	saturated aqueous NaCl-solution	EtOAc	ethylacetate
BuLi	butyllithium	EtOH	ethanol
calcd.	calculated	FT-IR	Fourier transform infrared spectroscopy
cat.	catalyst or catalytic	<i>G</i>	Gibbs-energy
Cbz	Benzyloxycarbonyl	<i>H</i>	enthalpy
CCDC	Cambridge Crystallographic Data Centre	· HCl	hydrochloride salt

Abbreviations and Symbols

H ₂ O	water	Ph	Phenyl
HFIP	1,1,1,2,2,2-hexafluoro- <i>iso</i> -propanol	ppm	parts per million
HMBC	heteronuclear multiple bond correlation	Py	pyridine
HPLC	high performance liquid chromatography	Pr	propyl
HRMS	high resolution mass spectrometry	PyBOX	pyridine bis(oxazoline)
HSQC	heteronuclear single quantum coherence	quant.	quantitative
<i>i</i> -	<i>iso</i> -	R	residue
<i>i</i> -PrOH	2-propanol	<i>R</i>	universal gas constant
IPO	Iminopyridine-oxazoline	R _f	retardation factor
<i>J</i>	coupling constant	ROESY	rotating-frame nuclear Overhauser effect correlation spectroscopy
k	exchange rate	r _t	retention time
K	Kelvin	rt	room temperature
KOtBu	potassium <i>tert</i> -butoxide	sat.	saturated
M	molarity (of solutions) or molar mass	SET	single electron transfer
<i>m</i> -	<i>meta</i> -	<i>t</i>	<i>tert</i>
Me	methyl	<i>T</i>	entropy
MeCN	acetonitrile	T	temperature
MeOH	methanol	TBAC	tributyl 2-(acetyloxy)propane-1,2,3-tricarboxylate
m/z	mass-to-charge ratio	1,1,2,2-TCE	1,1,2,2-tetrachlorethane
Mes	mesityl (2,4,6-trimethylphenyl)	THF	tetrahydrofuran
mol%	molar percentage	TLC	thin layer chromatography
MS	molecular sieves	TMOF	trimethyl orthoformate
N _A	Avogadro constant	TOCSY	total correlation spectroscopy
NMR	Nuclear magnetic resonance	TOF	turnover frequency
NOE	nuclear Overhauser effect	TON	turnover number
NOESY	nuclear Overhauser enhancement spectroscopy	tol	Tolyl or toluene
<i>o</i> -	<i>ortho</i> -	Troc	trichloroethoxycarbonyl
<i>p</i> -	<i>para</i> -	UV	ultraviolet

8. References

- [1] S. H. A. M. Leenders, R. Gramage-Doria, B. de Bruin, J. N. H. Reek, *Chem. Soc. Rev.* **2015**, *44*, 433–448.
- [2] C. A. Busacca, D. R. Fandrick, J. J. Song, C. H. Senanayake, Transition Metal Catalysis in the Pharmaceutical Industry, in *Applications of transition metal catalysis in drug discovery and development: An industrial perspective*, John Wiley & Sons, Hoboken, New Jersey, USA, **2012**; pp 1-24.
- [3] H. Yorimitsu, M. Kotora, N. T. Patil, *Chem. Rec.* **2021**, *21*, 3335–3337.
- [4] R. A. Sheldon, I. Arends, U. Hanefeld, *Green Chemistry and Catalysis*, WILEY-VCH, Weinheim, Germany, **2007**; pp 1-47.
- [5] P. Gandeepan, T. Müller, D. Zell, G. Cera, S. Warratz, L. Ackermann, *Chem. Rev.* **2019**, *119*, 2192–2452.
- [6] B. Klein Gebbink, M.-E. Moret (Eds.) *Non-noble metal catalysis. Molecular approaches and reactions*, WILEY-VCH, Weinheim, Germany, **2019**.
- [7] P. Ahlberg, *Advanced Information on the Nobel Prize in Chemistry 2001*. The Royal Swedish Academy of Sciences, Stockholm, Sweden, **2001**, can be found under <https://www.nobelprize.org/prizes/chemistry/2001/advanced-information/> (1st Jan. 2023).
- [8] J. Halpern, B. M. Trost, *Proc. Natl. Acad. Sci. USA* **2004**, *101*, 5347.
- [9] P. J. Walsh, M. C. Kozlowski, *Fundamentals of asymmetric catalysis*, Univ. Science Books, Sausalito, California, USA, **2009**.
- [10] J. Loup, U. Dhawa, F. Pesciaioli, J. Wencel-Delord, L. Ackermann, *Angew. Chem. Int. Ed.* **2019**, *58*, 12803–12818.
- [11] W. S. Knowles, *Angew. Chem. Int. Ed.* **2002**, *41*, 1998–2007.
- [12] R. Noyori, *Angew. Chem. Int. Ed.* **2002**, *41*, 2008–2022.
- [13] K. B. Sharpless, *Angew. Chem. Int. Ed.* **2002**, *41*, 2024–2032.
- [14] H. B. Kagan, *Pure Appl. Chem.* **1975**, *43*, 401–421.
- [15] W. M. Haynes (Ed.), *CRC Handbook of Chemistry and Physics. A Ready-Reference Book of Chemical and Physical Data*. 97th Edition, CRC Press, Boca Raton (Florida), USA, **2017**, chapter 14, p. 17.
- [16] N. Abbaspour, R. Hurrell, R. Kelishadi, *J. Res. Med. Sci.* **2014**, *19*, 164–174.
- [17] P. Aisen, C. Enns, M. Wessling-Resnick, *Int. J. Biochem. Cell Biol.* **2001**, *33*, 940–959.

References

- [18] A. Sigel, H. Sigel, R. K. O. Sigel (Eds.) *The Ubiquitous Roles of Cytochrome P450 Proteins. Volume 3*, John Wiley & Sons, Chichester, England, **2007**.
- [19] C. J. C. Whitehouse, S. G. Bell, L.-L. Wong, *Chem. Soc. Rev.* **2012**, *41*, 1218–1260.
- [20] C. G. Acevedo-Rocha, F. Hollmann, J. Sanchis, Z. Sun, *ACS Catal.* **2020**, *10*, 15123–15139.
- [21] Y. Yang, F. H. Arnold, *Acc. Chem. Res.* **2021**, *54*, 1209–1225.
- [22] Y. Wang, P. Xue, M. Cao, T. Yu, S. T. Lane, H. Zhao, *Chem. Rev.* **2021**, *121*, 12384–12444.
- [23] M. L. Crawley, B. M. Trost (Eds.) *Applications of transition metal catalysis in drug discovery and development. An industrial perspective*, John Wiley & Sons, Hoboken, N.J, **2012**.
- [24] H. Pellissier, *Coord. Chem. Rev.* **2019**, *386*, 1–31.
- [25] K. Gopalaiah, *Chem. Rev.* **2013**, *113*, 3248–3296.
- [26] H. Nozaki, H. Takaya, S. Moriuti, R. Noyori, *Tetrahedron* **1968**, *24*, 3655–3669.
- [27] R. E. Lowenthal, A. Abiko, S. Masamune, *Tetrahedron Lett.* **1990**, *31*, 6005–6008.
- [28] G. Desimoni, G. Faita, K. A. Jørgensen, *Chem. Rev.* **2006**, *106*, 3561–3651.
- [29] C. Moberg, *Angew. Chem. Int. Ed.* **1998**, *37*, 248–268.
- [30] E. J. Corey, N. Imai, H. Y. Zhang, *J. Am. Chem. Soc.* **1991**, *113*, 728–729.
- [31] M. P. Sibi, S. Manyem, H. Palencia, *J. Am. Chem. Soc.* **2006**, *128*, 13660–13661.
- [32] K. S. Williamson, T. P. Yoon, *J. Am. Chem. Soc.* **2012**, *134*, 12370–12373.
- [33] G.-S. Liu, Y.-Q. Zhang, Y.-A. Yuan, H. Xu, *J. Am. Chem. Soc.* **2013**, *135*, 3343–3346.
- [34] C.-L. Zhu, J.-S. Tian, Z.-Y. Gu, G.-W. Xing, H. Xu, *Chem. Sci.* **2015**, *6*, 3044–3050.
- [35] B. Liu, S.-F. Zhu, L.-X. Wang, Q.-L. Zhou, *Tetrahedron: Asymmetry* **2006**, *17*, 634–641.
- [36] T. Ollevier, *Catal. Sci. Technol.* **2016**, *6*, 41–48.
- [37] S.-F. Zhu, Y. Cai, H.-X. Mao, J.-H. Xie, Q.-L. Zhou, *Nat. Chem.* **2010**, *2*, 546–551.
- [38] Y. Nishikawa, H. Yamamoto, *J. Am. Chem. Soc.* **2011**, *133*, 8432–8435.
- [39] Y. Hong, L. Jarrige, K. Harms, E. Meggers, *J. Am. Chem. Soc.* **2019**, *141*, 4569–4572.
- [40] H. Nishiyama, H. Sakaguchi, T. Nakamura, M. Horihata, M. Kondo, K. Itoh, *Organometallics* **1989**, *8*, 846–848.
- [41] H. Usuda, A. Kuramochi, M. Kanai, M. Shibasaki, *Org. Lett.* **2004**, *6*, 4387–4390.

References

- [42] Y. Shimizu, S.-L. Shi, H. Usuda, M. Kanai, M. Shibasaki, *Angew. Chem. Int. Ed.* **2010**, *49*, 1103–1106.
- [43] J. Jankowska, J. Paradowska, J. Mlynarski, *Tetrahedron Lett.* **2006**, *47*, 5281–5284.
- [44] J. Jankowska, J. Paradowska, B. Rakiel, J. Mlynarski, *J. Org. Chem.* **2007**, *72*, 2228–2231.
- [45] D.-F. Lu, C.-L. Zhu, J. D. Sears, H. Xu, *J. Am. Chem. Soc.* **2016**, *138*, 11360–11367.
- [46] D.-F. Lu, G.-S. Liu, C.-L. Zhu, B. Yuan, H. Xu, *Org. Lett.* **2014**, *16*, 2912–2915.
- [47] J. Chen, T. Xi, X. Ren, B. Cheng, J. Guo, Z. Lu, *Org. Chem. Front.* **2014**, *1*, 1306–1309.
- [48] L. Zhang, Z. Zuo, X. Wan, Z. Huang, *J. Am. Chem. Soc.* **2014**, *136*, 15501–15504.
- [49] R. Connon, B. Roche, B. V. Rokade, P. J. Guiry, *Chem. Rev.* **2021**, *121*, 6373–6521.
- [50] J. Chen, T. Xi, Z. Lu, *Org. Chem. Front.* **2018**, *5*, 247–253.
- [51] J. Chen, T. Xi, Z. Lu, *Org. Lett.* **2014**, *16*, 6452–6455.
- [52] J. Chen, B. Cheng, M. Cao, Z. Lu, *Angew. Chem. Int. Ed.* **2015**, *54*, 4661–4664.
- [53] J. Guo, Z. Cheng, J. Chen, X. Chen, Z. Lu, *Acc. Chem. Res.* **2021**, *54*, 2701–2716.
- [54] P. Lu, X. Ren, H. Xu, D. Lu, Y. Sun, Z. Lu, *J. Am. Chem. Soc.* **2021**, *143*, 12433–12438.
- [55] S. Song, S.-F. Zhu, S. Yang, S. Li, Q.-L. Zhou, *Angew. Chem. Int. Ed.* **2012**, *51*, 2708–2711.
- [56] S. F. Oon, M. Nallappan, T. T. Tee, S. Shohaimi, N. K. Kassim, M. S. F. Sa'ariwijaya, Y. H. Cheah, *Cancer Cell Int.* **2015**, *15*, 100.
- [57] H. A. McManus, P. J. Guiry, *J. Org. Chem.* **2002**, *67*, 8566–8573.
- [58] H. A. McManus, S. M. Barry, P. G. Andersson, P. J. Guiry, *Tetrahedron* **2004**, *60*, 3405–3416.
- [59] H. Nishiyama, A. Furuta, *Chem. Commun.* **2007**, 760–762.
- [60] T. Inagaki, T. Le Phong, A. Furuta, J. Ito, H. Nishiyama, *Chem. Eur. J.* **2010**, *16*, 3090–3096.
- [61] M. Inoue, T. Suzuki, M. Nakada, *J. Am. Chem. Soc.* **2003**, *125*, 1140–1141.
- [62] T. Niwa, M. Nakada, *J. Am. Chem. Soc.* **2012**, *134*, 13538–13541.
- [63] Q.-H. Deng, H. Wadepohl, L. H. Gade, *Chem. Eur. J.* **2011**, *17*, 14922–14928.
- [64] Q.-H. Deng, T. Bleith, H. Wadepohl, L. H. Gade, *J. Am. Chem. Soc.* **2013**, *135*, 5356–5359.
- [65] S. Shaw, J. D. White, *Chem. Rev.* **2019**, *119*, 9381–9426.

References

- [66] E. Rose, B. Andrioletti, S. Zrig, M. Quelquejeu-Ethève, *Chem. Soc. Rev.* **2005**, *34*, 573–583.
- [67] S. Hiroto, Y. Miyake, H. Shinokubo, *Chem. Rev.* **2017**, *117*, 2910–3043.
- [68] J. T. Groves, R. S. Myers, *J. Am. Chem. Soc.* **1983**, *105*, 5791–5796.
- [69] J. T. Groves, T. E. Nemo, R. S. Myers, *J. Am. Chem. Soc.* **1979**, *101*, 1032–1033.
- [70] J. T. Groves, P. Viski, *J. Org. Chem.* **1990**, *55*, 3628–3634.
- [71] G. Simonneaux, P. Le Maux, *Coord. Chem. Rev.* **2002**, *228*, 43–60.
- [72] M. P. Doyle, *Angew. Chem. Int. Ed.* **2009**, *48*, 850–852.
- [73] I. Nicolas, T. Roisnel, P. Le Maux, G. Simonneaux, *Tetrahedron Lett.* **2009**, *50*, 5149–5151.
- [74] R. L. Halterman, S. T. Jan, *J. Org. Chem.* **1991**, *56*, 5253–5254.
- [75] P. Le Maux, G. Simonneaux, *Chem. Commun.* **2011**, *47*, 6957–6959.
- [76] O. Cussó, X. Ribas, M. Costas, *Chem. Commun.* **2015**, *51*, 14285–14298.
- [77] G. Olivo, O. Cussó, M. Borrell, M. Costas, *J. Biol. Inorg. Chem.* **2017**, *22*, 425–452.
- [78] J. England, G. J. P. Britovsek, N. Rabadia, A. J. P. White, *Inorg. Chem.* **2007**, *46*, 3752–3767.
- [79] W. Sun, Q. Sun, *Acc. Chem. Res.* **2019**, *52*, 2370–2381.
- [80] R. R. Fenton, F. S. Stephens, R. S. Vagg, P. A. Williams, *Inorg. Chim. Acta* **1991**, *182*, 67–75.
- [81] M. Costas, A. K. Tipton, K. Chen, D. H. Jo, L. Que, *J. Am. Chem. Soc.* **2001**, *123*, 6722–6723.
- [82] C. Zang, Y. Liu, Z.-J. Xu, C.-W. Tse, X. Guan, J. Wei, J.-S. Huang, C.-M. Che, *Angew. Chem. Int. Ed.* **2016**, *55*, 10253–10257.
- [83] J. Wei, B. Cao, C.-W. Tse, X.-Y. Chang, C.-Y. Zhou, C.-M. Che, *Chem. Sci.* **2019**, *11*, 684–693.
- [84] S. Hong, Y.-M. Lee, K.-B. Cho, K. Sundaravel, J. Cho, M. J. Kim, W. Shin, W. Nam, *J. Am. Chem. Soc.* **2011**, *133*, 11876–11879.
- [85] M. S. Chen, M. C. White, *Science* **2007**, *318*, 783–787.
- [86] K. Suzuki, P. D. Oldenburg, L. Que, *Angew. Chem. Int. Ed.* **2008**, *47*, 1887–1889.
- [87] O. Cussó, I. Garcia-Bosch, X. Ribas, J. Lloret-Fillol, M. Costas, *J. Am. Chem. Soc.* **2013**, *135*, 14871–14878.
- [88] R. Mas-Ballesté, L. Que, *J. Am. Chem. Soc.* **2007**, *129*, 15964–15972.

References

- [89] C.-X. Ye, X. Shen, S. Chen, E. Meggers, *Nat. Chem.* **2022**, *14*, 566–573.
- [90] R. R. Fenton, F. S. Stephens, R. S. Vagg, P. A. Williams, *Inorg. Chim. Acta* **1992**, *197*, 233–242.
- [91] B. Wang, C. Miao, S. Wang, C. Xia, W. Sun, *Chem. Eur. J.* **2012**, *18*, 6750–6753.
- [92] B. Wang, S. Wang, C. Xia, W. Sun, *Chem. Eur. J.* **2012**, *18*, 7332–7335.
- [93] J. Tian, J. Lin, J. Zhang, C. Xia, W. Sun, *Adv. Synth. Catal.* **2022**, *364*, 593–600.
- [94] T. P. Yoon, E. N. Jacobsen, *Science* **2003**, *299*, 1691–1693.
- [95] K. Muñoz, C. Bolm, *Chem. Eur. J.* **2000**, *6*, 2309–2316.
- [96] P. S. Steinlandt, L. Zhang, E. Meggers, Metal Stereogenicity in Asymmetric Transition Metal Catalysis, *Chem. Rev.* **2023**, DOI: 10.1021/acs.chemrev.2c00724.
- [97] A. Werner, *Ber. Dtsch. Chem. Ges.* **1911**, *44*, 1887–1898.
- [98] M. Chavarot, S. Ménage, O. Hamelin, F. Charnay, J. Pécaut, M. Fontecave, *Inorg. Chem.* **2003**, *42*, 4810–4816.
- [99] J. Hartung, R. H. Grubbs, *J. Am. Chem. Soc.* **2013**, *135*, 10183–10185.
- [100] L. Zhang, E. Meggers, *Chem. Asian J.* **2017**, *12*, 2335–2342.
- [101] L. Song, L. Gong, E. Meggers, *Chem. Commun.* **2016**, *52*, 7699–7702.
- [102] H. Huo, X. Shen, C. Wang, L. Zhang, P. Röse, L.-A. Chen, K. Harms, M. Marsch, G. Hilt, E. Meggers, *Nature* **2014**, *515*, 100–103.
- [103] L. Hu, S. Lin, S. Li, Q. Kang, Y. Du, *ChemCatChem* **2020**, *12*, 118–121.
- [104] L. Feng, X. Dai, E. Meggers, L. Gong, *Chem. Asian J.* **2017**, *12*, 963–967.
- [105] G.-Q. Xu, H. Liang, J. Fang, Z.-L. Jia, J.-Q. Chen, P.-F. Xu, *Chem. Asian J.* **2016**, *11*, 3355–3358.
- [106] J. Gong, K. Li, S. Qurban, Q. Kang, *Chin. J. Chem.* **2016**, *34*, 1225–1235.
- [107] Y. Hitomi, K. Arakawa, T. Funabiki, M. Kodera, *Angew. Chem. Int. Ed.* **2012**, *51*, 3448–3452.
- [108] Y. Grell, X. Xie, S. I. Ivlev, E. Meggers, *ACS Catal.* **2021**, *11*, 11396–11406.
- [109] Z. Zhou, S. Chen, Y. Hong, E. Winterling, Y. Tan, M. Hemming, K. Harms, K. N. Houk, E. Meggers, *J. Am. Chem. Soc.* **2019**, *141*, 19048–19057.
- [110] A. G. Blackman, *Polyhedron* **2019**, *161*, 1–33.

References

- [111] A. Grohmann, *Dalton Trans.* **2010**, 39, 1432–1440.
- [112] A. Suga, T. Sugiyama, M. Otsuka, M. Ohno, Y. Sugiura, K. Maeda, *Tetrahedron* **1991**, 47, 1191–1204.
- [113] S. Gosiewska, M. Lutz, A. L. Spek, R. J. Klein Gebbink, *Inorg. Chim. Acta* **2007**, 360, 405–417.
- [114] D. Lakk-Bogáth, R. Csonka, G. Speier, M. Réglíer, A. J. Simaan, J.-V. Naubron, M. Giorgi, K. Lázár, J. Kaizer, *Inorg. Chem.* **2016**, 55, 10090–10093.
- [115] M. Di Berto Mancini, A. Del Gelsomino, S. Di Stefano, F. Fratelloreto, A. Lapi, O. Lanzalunga, G. Olivo, S. Sajeva, *ACS Omega* **2021**, 6, 26428–26438.
- [116] M. R. Bukowski, P. Comba, A. Lienke, C. Limberg, C. Lopez de Laorden, R. Mas-Ballesté, M. Merz, L. Que, *Angew. Chem. Int. Ed.* **2006**, 45, 3446–3449.
- [117] R. Y. N. Ho, G. Roelfes, B. L. Feringa, L. Que, *J. Am. Chem. Soc.* **1999**, 121, 264–265.
- [118] G. Roelfes, M. Lubben, S. W. Leppard, E. P. Schudde, R. M. Hermant, R. Hage, E. C. Wilkinson, L. Que, B. L. Feringa, *J. Mol. Catal. A: Chem.* **1997**, 117, 223–227.
- [119] M. Lubben, A. Meetsma, E. C. Wilkinson, B. Feringa, L. Que, *Angew. Chem. Int. Ed.* **1995**, 34, 1512–1514.
- [120] D. Lakk-Bogáth, N. P. Juraj, B. I. Meena, B. Perić, S. I. Kirin, J. Kaizer, *Molecules* **2021**, 26, 3220.
- [121] B. I. Meena, D. Lakk-Bogáth, B. Kripli, G. Speier, J. Kaizer, *Polyhedron* **2018**, 151, 141–145.
- [122] R. Turcas, D. Lakk-Bogáth, G. Speier, J. Kaizer, *Inorg. Chem. Commun.* **2018**, 92, 141–144.
- [123] D. Lakk-Bogáth, B. Kripli, B. I. Meena, G. Speier, J. Kaizer, *Inorg. Chem. Commun.* **2019**, 104, 165–170.
- [124] N. P. Tilmans, C. J. Krusemark, P. A. B. Harbury, *Bioconjugate Chem.* **2010**, 21, 1010–1013.
- [125] S. Roy, S. K. Das, B. Chattopadhyay, *Angew. Chem. Int. Ed.* **2018**, 57, 2238–2243.
- [126] J. M. Rowland, M. Olmstead, P. K. Mascharak, *Inorg. Chem.* **2001**, 40, 2810–2817.
- [127] A. K. Patra, M. M. Olmstead, P. K. Mascharak, *Inorg. Chem.* **2002**, 41, 5403–5409.
- [128] E. Wong, J. Jeck, M. Grau, A. J. P. White, G. J. P. Britovsek, *Catal. Sci. Technol.* **2013**, 3, 1116–1122.
- [129] M. E. de Vries, R. M. La Crois, G. Roelfes, H. Kooijman, A. L. Spek, R. Hage, B. L. Feringa, *Chem. Commun.* **1997**, 1549–1550.

References

- [130] G. Roelfes, V. Vrajmasu, K. Chen, R. Y. N. Ho, J.-U. Rohde, C. Zondervan, R. M. La Crois, E. P. Schudde, M. Lutz, A. L. Spek et al., *Inorg. Chem.* **2003**, *42*, 2639–2653.
- [131] G. Roelfes, M. Lubben, K. Chen, R. Y. N. Ho, A. Meetsma, S. Genseberger, R. M. Hermant, R. Hage, S. K. Mandal, V. G. Young et al., *Inorg. Chem.* **1999**, *38*, 1929–1936.
- [132] B. Wang, H.-X. Sun, Z.-H. Sun, *Eur. J. Org. Chem.* **2009**, *2009*, 3688–3692.
- [133] F. R. Heirtzler, M. Neuburger, M. Zehnder, E. C. Constable, *Liebigs Ann./Recl.* **1997**, 297–301.
- [134] V. Bevilacqua, M. King, M. Chaumontet, M. Nothisen, S. Gabillet, D. Buisson, C. Puente, A. Wagner, F. Taran, *Angew. Chem. Int. Ed.* **2014**, *53*, 5872–5876.
- [135] L. Gong, M. Wenzel, E. Meggers, *Acc. Chem. Res.* **2013**, *46*, 2635–2644.
- [136] M. Helms, Z. Lin, L. Gong, K. Harms, E. Meggers, *Eur. J. Inorg. Chem.* **2013**, *2013*, 4164–4172.
- [137] E. Meggers, *Chem. Eur. J.* **2010**, *16*, 752–758.
- [138] Y. Hong, T. Cui, S. Ivlev, X. Xie, E. Meggers, *Chem. Eur. J.* **2021**, *27*, 8557–8563.
- [139] J. Ma, X. Zhang, X. Huang, S. Luo, E. Meggers, *Nat. Protoc.* **2018**, *13*, 605–632.
- [140] A. D. Read, R. E. Bentley, S. L. Archer, K. J. Dunham-Snary, *Redox Biol.* **2021**, *47*, 102164.
- [141] J. C. Crack, J. Green, A. J. Thomson, N. E. Le Brun, *Acc. Chem. Res.* **2014**, *47*, 3196–3205.
- [142] W. Chen, S. Li, X. Li, C. Zhang, X. Hu, F. Zhu, G. Shen, F. Feng, *Chem. Sci.* **2019**, *10*, 2179–2185.
- [143] A. C. Brown, N. B. Thompson, D. L. M. Suess, *J. Am. Chem. Soc.* **2022**, *144*, 9066–9073.
- [144] I. Méndez, C. Ferrer, R. Rodríguez, F. J. Lahoz, P. García-Orduña, D. Carmona, *ACS Omega* **2020**, *5*, 27978–27989.
- [145] D. Carmona, M. P. Lamata, F. Viguri, R. Rodríguez, L. A. Oro, F. J. Lahoz, A. I. Balana, T. Tejero, P. Merino, *J. Am. Chem. Soc.* **2005**, *127*, 13386–13398.
- [146] D. Carmona, M. P. Lamata, F. Viguri, R. Rodríguez, T. Fischer, F. J. Lahoz, I. T. Dobrinovitch, L. A. Oro, *Adv. Synth. Catal.* **2007**, *349*, 1751–1758.
- [147] D. Carmona, C. Cativiela, R. García-Correas, F. J. Lahoz, M. P. Lamata, J. A. López, M. P. L.-R. de Víu, L. A. Oro, E. S. José, F. Viguri, *Chem. Commun.* **1996**, 1247–1248.
- [148] H. Brunner, M. Niemetz, *Monatshfte fuer Chemie* **2002**, *133*, 115–126.

References

- [149] G. Chelucci, S. Baldino, S. Chessa, G. A. Pinna, F. Soccolini, *Tetrahedron: Asymmetry* **2006**, *17*, 3163–3169.
- [150] P. S. Steinlandt, X. Xie, S. Ivlev, E. Meggers, *ACS Catal.* **2021**, *11*, 7467–7476.
- [151] B. Join, K. Möller, C. Ziebart, K. Schröder, D. Gördes, K. Thurow, A. Spannenberg, K. Junge, M. Beller, *Adv. Synth. Catal.* **2011**, *353*, 3023–3030.
- [152] M. M. Heravi, V. Zadsirjan, *RSC advances* **2020**, *10*, 44247–44311.
- [153] N. Kerru, L. Gummidi, S. Maddila, K. K. Gangu, S. B. Jonnalagadda, *Molecules* **2020**, *25*.
- [154] A. Fanourakis, B. D. Williams, K. J. Paterson, R. J. Phipps, *J. Am. Chem. Soc.* **2021**, *143*, 10070–10076.
- [155] H. Hayashi, T. Uchida, *Eur. J. Org. Chem.* **2020**, *2020*, 909–916.
- [156] J. Jeong, H. Jung, D. Kim, S. Chang, *ACS Catal.* **2022**, *12*, 8127–8138.
- [157] E. Lee, Y. Hwang, Y. B. Kim, D. Kim, S. Chang, *J. Am. Chem. Soc.* **2021**, *143*, 6363–6369.
- [158] K. M. Nakafuku, Z. Zhang, E. A. Wappes, L. M. Stateman, A. D. Chen, D. A. Nagib, *Nat. Chem.* **2020**, *12*, 697–704.
- [159] Z. Zhou, Y. Tan, X. Shen, S. Ivlev, E. Meggers, *Sci. China Chem.* **2021**, *64*, 452–458.
- [160] Z. Zhou, Y. Tan, T. Yamahira, S. Ivlev, X. Xie, R. Riedel, M. Hemming, M. Kimura, E. Meggers, *Chem* **2020**, *6*, 2024–2034.
- [161] S. Y. Hong, Y. Park, Y. Hwang, Y. B. Kim, M.-H. Baik, S. Chang, *Science* **2018**, *359*, 1016–1021.
- [162] Y. Park, S. Chang, *Nat Catal* **2019**, *2*, 219–227.
- [163] H. Wang, Y. Park, Z. Bai, S. Chang, G. He, G. Chen, *J. Am. Chem. Soc.* **2019**, *141*, 7194–7201.
- [164] Q. Xing, C.-M. Chan, Y.-W. Yeung, W.-Y. Yu, *J. Am. Chem. Soc.* **2019**, *141*, 3849–3853.
- [165] L. Jarrige, Z. Zhou, M. Hemming, E. Meggers, *Angew. Chem. Int. Ed.* **2021**, *60*, 6314–6319.
- [166] N. W. Goldberg, A. M. Knight, R. K. Zhang, F. H. Arnold, *J. Am. Chem. Soc.* **2019**, *141*, 19585–19588.
- [167] L. Zhang, L. Deng, *Chin. Sci. Bull.* **2012**, *57*, 2352–2360.
- [168] A. J. South, A. M. Geer, L. J. Taylor, H. R. Sharpe, W. Lewis, A. J. Blake, D. L. Kays, *Organometallics* **2019**, *38*, 4115–4120.

References

- [169] P. F. Kuijpers, J. I. van der Vlugt, S. Schneider, B. de Bruin, *Chem. Eur. J.* **2017**, *23*, 13819–13829.
- [170] Y.-D. Du, C.-Y. Zhou, W.-P. To, H.-X. Wang, C.-M. Che, *Chem. Sci.* **2020**, *11*, 4680–4686.
- [171] X. Li, L. Dong, Y. Liu, *Inorg. Chem.* **2020**, *59*, 1622–1632.
- [172] B. Plietker, A. Röske, *Catal. Sci. Technol.* **2019**, *9*, 4188–4197.
- [173] D.-Q. Wu, Z.-Y. Guan, Y. Peng, J. Sun, C. Zhong, Q.-H. Deng, *Adv. Synth. Catal.* **2018**, *360*, 4720–4725.
- [174] L. Li, F. Han, X. Nie, Y. Hong, S. Ivlev, E. Meggers, *Angew. Chem. Int. Ed.* **2020**, *59*, 12392–12395.
- [175] K. Lang, S. Torker, L. Wojtas, X. P. Zhang, *J. Am. Chem. Soc.* **2019**, *141*, 12388–12396.
- [176] H. Jiang, K. Lang, H. Lu, L. Wojtas, X. P. Zhang, *Angew. Chem. Int. Ed.* **2016**, *55*, 11604–11608.
- [177] M. Ichinose, H. Suematsu, Y. Yasutomi, Y. Nishioka, T. Uchida, T. Katsuki, *Angew. Chem. Int. Ed.* **2011**, *50*, 9884–9887.
- [178] H. Lu, H. Jiang, L. Wojtas, X. P. Zhang, *Angew. Chem. Int. Ed.* **2010**, *49*, 10192–10196.
- [179] Y. Yang, I. Cho, X. Qi, P. Liu, F. H. Arnold, *Nat. Chem.* **2019**, *11*, 987–993.
- [180] K. Okamoto, A. Nanya, A. Eguchi, K. Ohe, *Angew. Chem. Int. Ed.* **2018**, *57*, 1039–1043.
- [181] A. Pfaltz, W. J. Drury, *Proc. Natl. Acad. Sci. USA* **2004**, *101*, 5723–5726.
- [182] K. Zhang, L.-Q. Lu, Y. Jia, Y. Wang, F.-D. Lu, F. Pan, W.-J. Xiao, *Angew. Chem. Int. Ed.* **2019**, *58*, 13375–13379.
- [183] A. Call, M. Cianfanelli, P. Besalú-Sala, G. Olivo, A. Palone, L. Vicens, X. Ribas, J. M. Luis, M. Bietti, M. Costas, *J. Am. Chem. Soc.* **2022**, *144*, 19542–19558.
- [184] L. Vicens, M. Bietti, M. Costas, *Angew. Chem. Int. Ed.* **2021**, *60*, 4740–4746.
- [185] R. V. Ottenbacher, V. I. Kurganskiy, E. P. Talsi, K. P. Bryliakov, *Adv. Synth. Catal.* **2021**, *363*, 2778–2782.
- [186] E. Masferrer-Rius, F. Li, M. Lutz, R. J. M. Klein Gebbink, *Catal. Sci. Technol.* **2021**, *11*, 7751–7763.
- [187] K. Feng, R. E. Quevedo, J. T. Kohrt, M. S. Oderinde, U. Reilly, M. C. White, *Nature* **2020**, *580*, 621–627.
- [188] R. V. Ottenbacher, E. P. Talsi, K. P. Bryliakov, *J. Catal.* **2020**, *390*, 170–177.

References

- [189] E. P. Talsi, D. G. Samsonenko, R. V. Ottenbacher, K. P. Bryliakov, *ChemCatChem* **2017**, *9*, 4580–4586.
- [190] Y. Popowski, I. Goldberg, M. Kol, *Chem. Commun.* **2016**, *52*, 7932–7934.
- [191] J. Lin, F. Wang, J. Tian, J. Zhang, Y. Wang, W. Sun, *Chinese Chemical Letters* **2022**, *33*, 1515–1518.
- [192] M. Milan, M. Bietti, M. Costas, *Org. Lett.* **2018**, *20*, 2720–2723.
- [193] M. Milan, M. Bietti, M. Costas, *ACS Cent. Sci.* **2017**, *3*, 196–204.
- [194] W. Wang, Q. Sun, D. Xu, C. Xia, W. Sun, *ChemCatChem* **2017**, *9*, 420–424.
- [195] D. Shen, B. Qiu, D. Xu, C. Miao, C. Xia, W. Sun, *Org. Lett.* **2016**, *18*, 372–375.
- [196] N. C. Maity, P. Kumar Bera, D. Ghosh, S. H. R. Abdi, R. I. Kureshy, N. H. Khan, H. C. Bajaj, E. Suresh, *Catal. Sci. Technol.* **2014**, *4*, 208–217.
- [197] J. Wei, J.-S. Huang, C.-M. Che, *Org. Lett.* **2021**, *23*, 6993–6997.
- [198] J. Wei, L. Wu, H.-X. Wang, X. Zhang, C.-W. Tse, C.-Y. Zhou, J.-S. Huang, C.-M. Che, *Angew. Chem. Int. Ed.* **2020**, *59*, 16561–16571.
- [199] M. Tretbar, C. B. W. Stark, *Eur. J. Org. Chem.* **2017**, *2017*, 6942–6946.
- [200] Q. Sun, W. Sun, *Org. Lett.* **2020**, *22*, 9529–9533.
- [201] B. Qiu, D. Xu, Q. Sun, J. Lin, W. Sun, *Org. Lett.* **2019**, *21*, 618–622.
- [202] J. Du, C. Miao, C. Xia, Y.-M. Lee, W. Nam, W. Sun, *ACS Catal.* **2018**, *8*, 4528–4538.
- [203] B. Qiu, D. Xu, Q. Sun, C. Miao, Y.-M. Lee, X.-X. Li, W. Nam, W. Sun, *ACS Catal.* **2018**, *8*, 2479–2487.
- [204] W. Wang, Q. Sun, C. Xia, W. Sun, *Chin. J. Catal.* **2018**, *39*, 1463–1469.
- [205] O. Cussó, M. Cianfanelli, X. Ribas, R. J. M. Klein Gebbink, M. Costas, *J. Am. Chem. Soc.* **2016**, *138*, 2732–2738.
- [206] L. Vicens, G. Olivo, M. Costas, *Angew. Chem. Int. Ed.* **2022**, *61*, e202114932.
- [207] B. Wang, J. Lin, Q. Sun, C. Xia, W. Sun, *ACS Catal.* **2021**, *11*, 10964–10973.
- [208] B. Wang, C.-X. Miao, S.-F. Wang, F. E. Kühn, C.-G. Xia, W. Sun, *J. Organomet. Chem.* **2012**, *715*, 9–12.
- [209] D. Shen, C. Miao, S. Wang, C. Xia, W. Sun, *Org. Lett.* **2014**, *16*, 1108–1111.

References

- [210] R. V. Ottenbacher, D. G. Samsonenko, E. P. Talsi, K. P. Bryliakov, *Org. Lett.* **2012**, *14*, 4310–4313.
- [211] R. Singh, M. K. Parai, S. Mondal, G. Panda, *Synthetic Communications* **2013**, *43*, 253–259.
- [212] H. Zhao, A. Thurkauf, *Synlett* **1999**, *1999*, 1280–1282.
- [213] J. A. Law, N. M. Bartfield, J. H. Frederich, *Angew. Chem. Int. Ed.* **2021**, *60*, 14360–14364.
- [214] N. Yotapan, A. Paptchikhine, M. Bera, S. K. Avula, T. Vilaivan, P. G. Andersson, *Asian J. Org. Chem.* **2013**, *2*, 674–680.
- [215] P. S. Steinlandt, M. Hemming, X. Xie, S. I. Ivlev, E. Meggers, Trading Symmetry for Stereoinduction in Tetradentate, non-C₂-Symmetric Fe(II)-Complexes for Asymmetric Catalysis, *Chem. Eur. J.* **2023**, *accepted*.
- [216] J. Huang, R. Xie, Y. Hu, S. Lei, Q. Li, *Chem. Phys. Lett.* **2020**, *758*, 137925.
- [217] X. Yu, T. Y. Chen, Y. S. Ye, X. Bao, *J. Phys. Condens. Matter* **2020**, *32*, 174001.
- [218] O. Lazos, M. Tosin, A. L. Slusarczyk, S. Boakes, J. Cortés, P. J. Sidebottom, P. F. Leadlay, *Chem. Biol.* **2010**, *17*, 160–173.
- [219] R. A. Atkinson, A. L. Salah El Din, B. Kieffer, J. F. Lefèvre, M. A. Abdallah, *Biochemistry* **1998**, *37*, 15965–15973.
- [220] G. Mohn, P. Koehl, H. Budzikiewicz, J. F. Lefèvre, *Biochemistry* **1994**, *33*, 2843–2851.
- [221] L. Vicens, G. Olivo, M. Costas, *ACS Catal.* **2020**, *10*, 8611–8631.
- [222] A. Casnati, M. Lanzi, G. Cera, *Molecules* **2020**, *25*.
- [223] P. Kaur, V. Tyagi, *Adv. Synth. Catal.* **2021**, *363*, 877–905.
- [224] V. Carreras, N. Tanbouza, T. Ollevier, *Synthesis* **2021**, *53*, 79–94.
- [225] V. F. Batista, D. C. G. A. Pinto, A. M. S. Silva, *ACS Catal.* **2020**, *10*, 10096–10116.
- [226] H. M. L. Davies, K. Liao, *Nat. Rev. Chem.* **2019**, *3*, 347–360.
- [227] W. Liu, Z. Ren, A. T. Bosse, K. Liao, E. L. Goldstein, J. Bacsá, D. G. Musaev, B. M. Stoltz, H. M. L. Davies, *J. Am. Chem. Soc.* **2018**, *140*, 12247–12255.
- [228] H. M. Mbuvi, L. K. Woo, *Organometallics* **2008**, *27*, 637–645.
- [229] Q.-Q. Cheng, J.-M. Yang, H. Xu, S.-F. Zhu, *Synlett* **2017**, *28*, 1327–1330.
- [230] I. D. Jurberg, H. M. L. Davies, *Chem. Sci.* **2018**, *9*, 5112–5118.

References

- [231] X. Lin, M. Pu, X. Sang, S. Li, X. Liu, Y.-D. Wu, X. Feng, *Angew. Chem. Int. Ed.* **2022**, *61*, e202201151.
- [232] X. Lin, W. Yang, W. Yang, X. Liu, X. Feng, *Angew. Chem. Int. Ed.* **2019**, *58*, 13492–13498.
- [233] X. Lin, Y. Tang, W. Yang, F. Tan, L. Lin, X. Liu, X. Feng, *J. Am. Chem. Soc.* **2018**, *140*, 3299–3305.
- [234] L. Hong, W. Sun, D. Yang, G. Li, R. Wang, *Chem. Rev.* **2016**, *116*, 4006–4123.
- [235] A. Abbotto, S. Bradamante, G. A. Pagani, *J. Org. Chem.* **1996**, *61*, 1761–1769.
- [236] A. De, A. Majee, *Journal of Heterocyclic Chem* **2022**, *59*, 422–448.
- [237] S. Auricchio, A. Bini, E. Pastormerlo, A. M. Truscello, *Tetrahedron* **1997**, *53*, 10911–10920.
- [238] F. Palacios, A. M. O. de Retana, E. M. de Marigorta, J. M. de los Santos, *Eur. J. Org. Chem.* **2001**, *2001*, 2401–2414.
- [239] G. S. Singh, S. Sudheesh, N. Keroletswe, *Arkivoc* **2019**, *2018*, 50–113.
- [240] S. Stanković, M. D'hooghe, S. Catak, H. Eum, M. Waroquier, V. van Speybroeck, N. de Kimpe, H.-J. Ha, *Chem. Soc. Rev.* **2012**, *41*, 643–665.
- [241] J. B. Sweeney, *Chem. Soc. Rev.* **2002**, *31*, 247–258.
- [242] W. McCoull, F. A. Davis, *Synthesis* **2000**, *2000*, 1347–1365.
- [243] U. Schöllkopf, U. Groth, W. Hartwig, *Liebigs Ann. Chem.* **1981**, 2407–2418.
- [244] P. Ji, J. Chen, X. Meng, F. Gao, Y. Dong, H. Xu, W. Wang, *J. Org. Chem.* **2022**, *87*, 14706–14714.
- [245] I. Netz, M. Kucukdisli, T. Opatz, *J. Org. Chem.* **2015**, *80*, 6864–6869.
- [246] C. Cativiela, M. D. Díaz-de-Villegas, *Tetrahedron: Asymmetry* **2007**, *18*, 569–623.
- [247] C. Toniolo, F. Formaggio, B. Kaptein, Q. Broxterman, *Synlett* **2006**, *2006*, 1295–1310.
- [248] F. A. Davis, C.-H. Liang, H. Liu, *J. Org. Chem.* **1997**, *62*, 3796–3797.
- [249] P. Roth, P. G. Andersson, P. Somfai, *Chem. Commun.* **2002**, 1752–1753.
- [250] S. Ueda, S. Naruto, T. Yoshida, T. Sawayama, H. Uno, *J. Chem. Soc., Perkin Trans. I* **1988**, 1013.
- [251] J. Du, D. Xu, C. Zhang, C. Xia, Y. Wang, W. Sun, *Dalton Trans.* **2016**, *45*, 10131–10135.
- [252] J. Du, C. Miao, C. Xia, W. Sun, *Chinese Chemical Letters* **2018**, *29*, 1869–1871.

References

- [253] J. Du, J. Zhang, J. Zhu, C. Xia, W. Sun, *New J. Chem.* **2018**, *42*, 8315–8319.
- [254] G. R. Fulmer, A. J. M. Miller, N. H. Sherden, H. E. Gottlieb, A. Nudelman, B. M. Stoltz, J. E. Bercaw, K. I. Goldberg, *Organometallics* **2010**, *29*, 2176–2179.
- [255] J. Easmon, G. Pürstinger, K.-S. Thies, G. Heinisch, J. Hofmann, *J. Med. Chem.* **2006**, *49*, 6343–6350.
- [256] G. Alvaro, P. Pacioni, D. Savoia, *Chem. Eur. J.* **1997**, *3*, 726–731.
- [257] J. Jiao, X.-R. Zhang, N.-H. Chang, J. Wang, J.-F. Wei, X.-Y. Shi, Z.-G. Chen, *J. Org. Chem.* **2011**, *76*, 1180–1183.
- [258] O. A. Mukhina, D. M. Kuznetsov, T. M. Cowger, A. G. Kutateladze, *Angew. Chem. Int. Ed.* **2015**, *54*, 11516–11520.
- [259] S. Mundinger, U. Jakob, P. Bichovski, W. Bannwarth, *J. Org. Chem.* **2012**, *77*, 8968–8979.
- [260] S. Berger, S. Braun, *200 and more NMR experiments. A practical course*, WILEY-VCH, Weinheim, **2011**.
- [261] T. L. Hwang, A. J. Shaka, *J. Magn. Reson. A* **1995**, *112*, 275–279.
- [262] A. Bax, D. G. Davis, *J. Magn. Reson.* **1985**, *65*, 355–360.
- [263] C. L. Perrin, T. J. Dwyer, *Chem. Rev.* **1990**, *90*, 935–967.
- [264] J. N. S. Evans, *Biomolecular NMR spectroscopy*. 3rd Edition, Oxford University Press, Oxford, England, **1995**; pp 48–50.
- [265] T. D. W. Claridge, *High-resolution NMR techniques in organic chemistry*. 2nd Edition, Elsevier, Amsterdam, The Netherlands, **2009**; pp 295–313.
- [266] H. Günther, *NMR Spectroscopy. Basic Principles, Concepts, and Applications in Chemistry*. 3rd Edition, WILEY-VCH, Weinheim, Germany, **2013**; pp 501–556.
- [267] J. Calveras, J. Casas, T. Parella, J. Joglar, P. Clapés, *Adv. Synth. Catal.* **2007**, *349*, 1661–1666.
- [268] W. Chu, J. Zhang, C. Zeng, J. Rothfuss, Z. Tu, Y. Chu, D. E. Reichert, M. J. Welch, R. H. Mach, *J. Med. Chem.* **2005**, *48*, 7637–7647.
- [269] S. Dei, C. Bellucci, M. Buccioni, M. Ferraroni, F. Gualtieri, L. Guandalini, D. Manetti, R. Matucci, M. N. Romanelli, S. Scapecchi et al., *Biorg. Med. Chem.* **2003**, *11*, 3153–3164.
- [270] D. J. Morris, A. S. Partridge, C. V. Manville, D. T. Racys, G. Woodward, G. Docherty, M. Wills, *Tetrahedron Lett.* **2010**, *51*, 209–212.
- [271] J. A. Butera, W. Spinelli, V. Anantharaman, N. Marcopulos, R. W. Parsons, I. F. Moubarak, C. Cullinan, J. F. Bagli, *J. Med. Chem.* **1991**, *34*, 3212–3228.

References

- [272] R. Ueno, Y. Ikeda, E. Shirakawa, *Eur. J. Org. Chem.* **2017**, 2017, 4188–4193.
- [273] I. A. Smetanin, M. S. Novikov, A. V. Agafonova, N. V. Rostovskii, A. F. Khlebnikov, I. V. Kudryavtsev, M. A. Terpilowski, M. K. Serebriakova, A. S. Trulioff, N. V. Goncharov, *Org. Biomol. Chem.* **2016**, 14, 4479–4487.
- [274] P. Drouhin, R. J. K. Taylor, *Eur. J. Org. Chem.* **2015**, 2333–2336.
- [275] Q. Peng, D. Guo, B. Zhang, L. Liu, J. Wang, *Chem. Commun.* **2020**, 56, 12427–12430.
- [276] A. P. Patwardhan, Z. Lu, V. R. Pulgam, W. D. Wulff, *Org. Lett.* **2005**, 7, 2201–2204.
- [277] P. Page, G. Parkes, B. Buckley, J. Wailes, *Synlett* **2011**, 3005–3007.
- [278] M.-T. Huang, H.-Y. Wu, R.-J. Chein, *Chem. Commun.* **2014**, 50, 1101–1103.
- [279] J. L. Jat, M. P. Paudyal, H. Gao, Q.-L. Xu, M. Yousufuddin, D. Devarajan, D. H. Ess, L. Kürti, J. R. Falck, *Science* **2014**, 343, 61–65.
- [280] K. Sato, M. Isoda, S. Ohata, S. Morita, A. Tarui, M. Omote, I. Kumadaki, A. Ando, *Adv. Synth. Catal.* **2012**, 354, 510–514.
- [281] S. Kobayashi, J. Kobayashi, H. Ishiani, M. Ueno, *Chem. Eur. J.* **2002**, 8, 4185–4190.
- [282] *APEX3*. Bruker AXS Inc., Madison, Wisconsin, USA, **2018**.
- [283] *SADABS*. Bruker AXS Inc., Madison, Wisconsin, USA, **2018**.
- [284] L. Krause, R. Herbst-Irmer, G. M. Sheldrick, D. Stalke, *J. Appl. Crystallogr.* **2015**, 48, 3–10.
- [285] G. M. Sheldrick, *Acta Crystallogr. Sect. A: Found. Adv.* **2015**, 71, 3–8.
- [286] G. M. Sheldrick, *Acta Crystallogr. Sect. C: Struct. Chem.* **2015**, 71, 3–8.
- [287] *X-Area*. STOE & Cie GmbH, Darmstadt, Germany, **2018**.
- [288] *X-RED32*. STOE & Cie GmbH, Darmstadt, Germany, **2018**.
- [289] *LANA - Laue Analyzer*. STOE & Cie GmbH, Darmstadt, Germany, **2019**.
- [290] C. B. Hübschle, G. M. Sheldrick, B. Dittrich, *J. Appl. Crystallogr.* **2011**, 44, 1281–1284.
- [291] A. L. Spek, *PLATON - A Multipurpose Crystallographic Tool*, Utrecht University, Utrecht, The Netherlands, **2019**.
- [292] A. L. Spek, *Acta Crystallogr. Sect. C: Struct. Chem.* **2015**, 71, 9–18.

Erklärung

Ich erkläre, dass eine Promotion noch an keiner anderen Hochschule als der Philipps-Universität Marburg, Fachbereich Chemie, versucht wurde.

Hiermit versichere ich, dass ich die vorliegende Dissertation

***“Design and Synthesis of Stereogenic-at-Iron
Complexes with Multidentate Ligands and Application in Asymmetric Catalysis”***

selbstständig, ohne unerlaubte Hilfe Dritter angefertigt und andere als die in der Dissertation angegebenen Hilfsmittel nicht benutzt habe. Alle Stellen, die wörtlich oder sinngemäß aus veröffentlichten oder unveröffentlichten Schriften entnommen sind, habe ich als solche kenntlich gemacht. Dritte waren an der inhaltlich-materiellen Erstellung der Dissertation nicht beteiligt; insbesondere habe ich hierfür nicht die Hilfe eines Promotionsberaters in Anspruch genommen. Kein Teil dieser Arbeit ist in einem anderen Promotions- oder Habilitationsverfahren verwendet worden. Mit dem Einsatz von Software zur Erkennung von Plagiaten bin ich einverstanden.

Ort/Datum

Unterschrift (Vor- und Nachname)